

IntechOpen

Nuclear Power

Edited by Pavel Tsvetkov



Nuclear Power

edited by

Pavel V. Tsvetkov

Nuclear Power

<http://dx.doi.org/10.5772/263>

Edited by Pavel Tsvetkov

© The Editor(s) and the Author(s) 2010

The moral rights of the and the author(s) have been asserted.

All rights to the book as a whole are reserved by INTECH. The book as a whole (compilation) cannot be reproduced, distributed or used for commercial or non-commercial purposes without INTECH's written permission.

Enquiries concerning the use of the book should be directed to INTECH rights and permissions department (permissions@intechopen.com).

Violations are liable to prosecution under the governing Copyright Law.



Individual chapters of this publication are distributed under the terms of the Creative Commons Attribution 3.0 Unported License which permits commercial use, distribution and reproduction of the individual chapters, provided the original author(s) and source publication are appropriately acknowledged. If so indicated, certain images may not be included under the Creative Commons license. In such cases users will need to obtain permission from the license holder to reproduce the material. More details and guidelines concerning content reuse and adaptation can be found at <http://www.intechopen.com/copyright-policy.html>.

Notice

Statements and opinions expressed in the chapters are those of the individual contributors and not necessarily those of the editors or publisher. No responsibility is accepted for the accuracy of information contained in the published chapters. The publisher assumes no responsibility for any damage or injury to persons or property arising out of the use of any materials, instructions, methods or ideas contained in the book.

First published in Croatia, 2010 by INTECH d.o.o.

eBook (PDF) Published by IN TECH d.o.o.

Place and year of publication of eBook (PDF): Rijeka, 2019.

IntechOpen is the global imprint of IN TECH d.o.o.

Printed in Croatia

Legal deposit, Croatia: National and University Library in Zagreb

Additional hard and PDF copies can be obtained from orders@intechopen.com

Nuclear Power

Edited by Pavel Tsvetkov

p. cm.

ISBN 978-953-307-110-7

eBook (PDF) ISBN 978-953-51-5940-7

We are IntechOpen, the world's leading publisher of Open Access books Built by scientists, for scientists

4,200+

Open access books available

116,000+

International authors and editors

125M+

Downloads

151

Countries delivered to

Our authors are among the
Top 1%

most cited scientists

12.2%

Contributors from top 500 universities



WEB OF SCIENCE™

Selection of our books indexed in the Book Citation Index
in Web of Science™ Core Collection (BKCI)

Interested in publishing with us?
Contact book.department@intechopen.com

Numbers displayed above are based on latest data collected.
For more information visit www.intechopen.com



Meet the editor

Dr. Tsvetkov is an Associate Professor in the Department of Nuclear Engineering, Texas A&M University. He has Ph.D. in Nuclear Engineering from Texas A&M University and M.S. in Nuclear Engineering from Moscow State Engineering Physics Institute (TU), Russia. His research program is focused on novel energy systems meeting global growing needs in sustainable resources. System design and optimization methods for complex engineered systems enable development of advanced sustainable nuclear energy technologies towards \environmentally benign\ system design and deployment. The integrated systems approach of Dr. Tsvetkov's research program makes it possible to optimize choices for the system. Dr. Tsvetkov is a member of ANS, ASME, ASEE, Alpha Nu Sigma and Phi Kappa Phi. Dr. Tsvetkov and his students published over 340 papers in peer reviewed journals, conference proceedings, technical reports, books.

Contents

Preface XI

- Chapter 1 **Nuclear power generation as a reasonable option for energy strategies 1**
Tamás János Katona
- Chapter 2 **The Dead Fish Option for Australia's future electricity generation technologies: Nuclear Power 17**
Lucas Skoufa
- Chapter 3 **Advanced Magnetic-Nuclear Power Systems for Reliability Demanding Applications Including Deep Space Missions 31**
Pavel V. Tsvetkov and Troy L. Guy
- Chapter 4 **Construction, Decommissioning, and Replacement of Nuclear Power Plants under Uncertainty 49**
Ryuta Takashima
- Chapter 5 **Artificial Intelligence Methods Applied to the In-Core Fuel Management Optimization 63**
Anderson Alvarenga de Moura Meneses, Alan Miranda Monteiro de Lima and Roberto Schirru
- Chapter 6 **Certification of software in safety-critical I&C systems of nuclear power plants 79**
Lic. Tech. Risto Nevalainen, M.Sc. (Eng) Juha Halminen, Lic. Tech. Hannu Harju and M.Sc. (Eng) Mika Johansson
- Chapter 7 **Pressure sensing line diagnostics in nuclear power plants 97**
Kang Lin and Keith E. Holbert
- Chapter 8 **Probabilistic Safety Assessment and Risk-Informed Decision-Making 123**
Marko Čepin
- Chapter 9 **Current status of fire risk assessment for nuclear power plants 141**
Heinz Peter Berg and Marina Röwekamp

- Chapter 10 **Application of Probabilistic Methods to the Structural Integrity Analysis of RBMK Reactor Critical Structures** 163
G. Dundulis, R. Kulak, R. Alzbutas and E. Uspuras
- Chapter 11 **Biofouling and its control in seawater cooled power plant cooling water system - a review** 191
K.K. Satpathy, A.K. Mohanty, Gouri Sahu, S. Biswas and M. Sivanayagam
- Chapter 12 **Atmospheric corrosion studies in a decommissioned nuclear power plant** 243
Manuel Morcillo, Eduardo Otero, Belén Chico and Daniel de la Fuente
- Chapter 13 **Stochastic wind profiles determination for radioactive substances released from nuclear power plants** 267
Kelen Berra de Mello, Marco Túllio de Vilhena and Bardo E.J. Bodmann
- Chapter 14 **Carbon-14 in Terrestrial and Aquatic Environment of Ignalina Nuclear Power Plant: Sources of Production, Releases and Dose Estimates** 293
Jonas Mazeika
- Chapter 15 **Impact of radionuclide discharges from Temelín Nuclear Power Plant on the Vltava River (Czech Republic)** 311
Eduard Hanslík, Diana Ivanovová
- Chapter 16 **Fatigue, sleep disorders, and excessive sleepiness: important factors for nuclear power shift workers** 337
Marco Túllio de Mello
- Chapter 17 **Benchmark modeling and analysis** 349
Hangbok Choi
- Chapter 18 **Nuclear Plants and Emergency Virtual Simulations based on a Low-cost Engine Reuse** 367
Carlos Alexandre F. Jorge, Antônio Carlos A. Mól and Pedro Mól Couto

Preface

The world of the twenty first century is an energy consuming society. Due to increasing population and living standards, each year the world requires more energy and new efficient systems for delivering it. Furthermore, the new systems must be inherently safe and environmentally benign. These realities of today's world are among the reasons that lead to serious interest in deploying nuclear power as a sustainable energy source. Today's nuclear reactors are safe and highly efficient energy systems that offer electricity and a multitude of co-generation energy products ranging from potable water to heat for industrial applications.

Nuclear reactors are incredibly complex engineered systems. This book consists of 18 chapters covering a collection of research and development topics including:

- Energy strategies with conventional reactors (chapters 1 and 2),
- National programs and decisions (chapter 2),
- Advanced nuclear energy systems for reliability demanding applications (chapter 3),
- Life cycle of nuclear power plants (chapters 4 and 12),
- Fuel management optimisation (chapter 5),
- Instrumentation and control (chapter 6),
- Diagnostics (chapter 7),
- Safety evaluation methods (chapters 6, 8, 9 and 10),
- Environment and nuclear power plants (chapters 11 - 15),
- Human factors (chapter 16),
- Software development and benchmarking for nuclear engineering applications (chapters 17 and 18).

With all diversity of topics in 18 chapters, the integrated systematics is the common thread that is easily identifiable in all chapters of our book. The "system-thinking" approach allows synthesising the entire body of provided information into a consistent integrated picture of the real-life complex engineering system - nuclear power system - where everything is working together. Integrated system design and optimisation methods for complex engineered systems enable development of advanced sustainable nuclear energy systems towards "environmentally benign" long-term scenarios.

The goal of the book is to show the current state-of-the-art in the covered technical areas as well as to demonstrate how general engineering principles and methods can be applied to nuclear power systems. The book shows applications of - Artificial intelligence methods (chapter 5), - Probabilistic methods (chapters 8 and 10), - Risk assessment methods (chapter 9), - Stochastic methods (chapter 13) in research and development efforts for nuclear power systems.

The book targets all students, researchers and practitioners, who are interested to learn about nuclear power and explore its technical areas and related fields. The idea is to facilitate intellectual cross-fertilisation between field experts and non-field experts taking advantage of methods and tools developed by both groups. The book inspires future efforts by stimulating ideas and identifying methods and tools. The broad range of the covered topics adds elements of a handbook.

We hope our readers will enjoy the book and will find it both interesting and useful.

Editor

Pavel V. Tsvetkov

*Department of Nuclear Engineering
Texas A&M University
United States of America
E-mail: Tsvetkov@tamu.edu*

Nuclear power generation as a reasonable option for energy strategies

Tamás János Katona
Nuclear Power Plant Paks Ltd.
Hungary

1. Introduction

Main challenge of the 21st century is to find the ways of sustainable development for the world's growing population. The development of world economy, the energy need of growing population in developing countries, rapid increase of consumption of emerging economies result in 40% increase of energy consumption by 2030, which reflects both the impact of the recent economic crisis and of new government policies introduced over the last years (IEA, 2009). Increase of energy consumption, which is essential for global development, affects the environment and the climate irreversibly and adversely. The World Energy Outlook (IAEA, 2009) sets out a timetable of actions needed to limit the long-term concentration of greenhouse gases in the atmosphere to 450 parts per million of carbon-dioxide equivalent and to keep the global temperature rise to around 2° Celsius. This goal might be achieved by enormous investments into energy sector, by increasing the effectiveness of energy utilisation and deployment of emission-free technologies, using of renewable and nuclear energy. Because of the complexity of the issue complex energy strategies have to be developed on country, region and global level.

The global concern is expressed in the establishment of United Nations Framework Convention on Climate Change (UNFCCC), which is the international environmental treaty aimed at fighting global warming. The global policy is expressed in Kyoto Protocol, (UNFCCC, 1998) continuation of which is endorsed by the Copenhagen Accord in 2009, (UNFCCC, 2009). The European Union is committed to achieve at least a 20% reduction of greenhouse-gas emission by 2020, while the primary energy use should be decreased by 20% and utilisation of renewable energy sources increased also by 20%, (European Commission, 2007). Nuclear power generation is accepted by the EU policy as one of low-emission technologies. The US energy policy is also targeted on reduction of greenhouse gas emission and emphasises the role of nuclear energy, see (DoE EIA, 2009). China and the emerging economies are also intending to develop nuclear power generation for covering the rapidly growing needs of their economy. Although growing energy consumption drives the development of these countries, the environmental and climate protection goals are also respected, (DoE EIA, 2009). Energy import dependence and security of the supply became also a serious issue for many countries and regions. In case of European Union the reliance

on imports of gas is expected to increase from 57% to 84% by 2030, (European Commission, 2007).

Representative studies highlight the effective solutions for avoiding severe climate change, while also enhancing energy security. Essential contribution should come from energy efficiency, while the role of low carbon technologies will also be critical (IEA, 2006; IEA, 2008; IAEA, 2009). The studies show that the use of renewable sources is one, but not the only solution due to the low energy density, large land demand on the one hand, and immaturity of some technologies and operating limitations of electrical grid system on the other hand. Clean coal is a secure source for long term. However the deployment of clean technologies and industrial implementation of CO₂ capture have to be waited for quite a long time.

One of possible option for clean generation of electricity is the utilisation of nuclear energy. According to the International Atomic Energy Agency data, currently 436 nuclear power reactors in operation in the world with a total net installed capacity of 370.407 GW(e), which provide the half of CO₂ emission-free production of electricity; 56 nuclear power units are under construction (IAEA PRIS, 2009). In 2009 construction of 13 units were started and two new units have been connected to the grid. Nuclear power plants provided 13.8% of generation worldwide and 21.4% in OECD countries in 2007 (IEA, 2009).

The status of development of nuclear power generation industry worldwide might be characterized by the following:

1. The existing nuclear power plants will be kept in operation as long as safe and economically reasonable (for example operational licence of more than half of plants operated in the U.S. are already renewed and extended for 20 years in addition to the 40 years of licensed term).
2. New nuclear power plants are under construction or preparation. In majority of OECD countries - in addition to utilisation of renewable sources - the use of nuclear energy is considered as acceptable emission-free electricity production methods for the future, see e.g. (UK, 2007). Moreover in some countries, such as in the USA, the same preferences are given to nuclear as the other emission-free technologies (US, 2005). Germany seems to be the only exception, where the phase-out of nuclear is still in force, while in some other countries like Italy radical changes of the political and public opinion could be observed.
3. Development of new nuclear reactors have been restarted in the vendor countries (Canada, France, Japan, Russia, South Korea and the USA); other countries like China and India are intensively developing own industrial capacities;
4. Some 60 countries worldwide that do not yet operate nuclear power plants have expressed an interest in including nuclear in the future energy mix, and more than 30 countries lunched programmes for developing national infrastructure or are preparing national nuclear programmes.

Energy policy and the strategy of development of energy sector is subject of public interest. Although the views are changing in positive direction regarding nuclear energy, the use of nuclear energy is a matter of public debates in connection with sustainable development (Eurobarometer, 2008; OECD NEA, 2010). The critical opinion on nuclear power generation is mainly linked to controversial views on generating technologies, misleading representation of benefits of some technologies, which have deceiving effects on public opinion.

A quite detailed but rather simple assessment of nuclear power generation is attempted below, which demonstrates that the nuclear power generation should be part of the solution for ensuring the energy needs of a sustainable development and it should be accounted in the definition of the strategy for development of the power generating capacity mix.

2. Comparative assessment of power generation technologies

Adequate decision on the energy strategy and composition of energy mix of a country has to be based on realistic assessment of available technologies. Large number of studies has been published on the future perspectives of the nuclear power generation referring to or based on complex comparison of generating options; see for example the most recent publications (OECD NEA, 2008; IAEA, 2009; MIT, 2009).

OECD NEA Nuclear Energy Outlook (OECD, 2008) covered the following aspects of nuclear power generation:

- Nuclear power's current status and projected trends;
- Environmental impacts;
- Uranium resources and security of supply;
- Costs, safety and regulation;
- Radioactive waste management and decommissioning;
- Non-proliferation and security;
- Legal frameworks;
- Infrastructure;
- Stakeholder engagement;
- Advanced reactors and advanced fuel cycles.

The study of Massachusetts Institute of Technology (MIT, 2009) covers practically the same areas as above, with main message regarding economic chances of nuclear power generation:

- Status of nuclear power deployment;
- Nuclear generation economics;
- Government incentives and regulations;
- Safety;
- Waste management;
- Fuel cycle issues;
- Non-proliferation;
- Technology opportunities and R&D needs.

Other studies assess the environmental impact of nuclear power generation comparing with other generating technologies. Life cycle emissions and environmental impact of utilisation of different energy sources and generating technologies have been studied which demonstrate the environmental advantages of nuclear power generation (IAEA, 1999) and (Vattenfall, 1999). A comprehensive life cycle assessment (LCA) for the whole energy sector is given in (WEC, 2004). More recent and comprehensive study on sustainability of utilisation of nuclear energy is given in (ISA, 2006). This type of analyses of sustainability with respect to complex and "cradle-to-grave" approach is supported by standards ISO 14040:2006 and 14044:2006, which standardize the LCA methodology for complex assessment of different production activities. Recently a new update of LCA methodology has been published for complex assessment of production and generation activities

(Goedkoop, M. et al., 2009). This method provides a synthesis of the baseline LCA and the “eco-indicator 99” endpoint approach and assess the midpoint level impact, like climate change, human toxicity, land use, mineral resources depletion, etc to three endpoint category: damage to human health, ecosystem and resource availability.

The mentioned above studies and methods are comprehensive and providing very valuable results. However for justification of decisions regarding energy strategy and composition of energy mix of power generation industry aggregation of some characteristics might be needed on one hand, and on the other, the analysis should be extended to some new features.

The methodology outlined and applied below is an integration of approaches with focus on decision on energy strategy and integration of capacities into energy system. The logics of this approach is based on the study of OECD NEA titled as ‘Risks and Benefits of Nuclear Energy’ (OECD NEA, 2007) and is an amendment of the method applied in (Katona, 2008).

In the method followed below, attributes of production technologies are aggregated into three main endpoints or areas of consideration/judgement: economical, environmental and social.

Decision on energy strategy and long-term plans for development of energy mix should not be considered as a decision on an isolated investment project, it should be based on considerations on integration and co-operation of technologies in energy system. Therefore it might need two further areas of consideration/judgement: what kind features, limitations should be taken into account while integrating that technology into the energy system and what is the development potential of a given technology in long term.

Considerations regarding possibility and limitations for integration of a generation technology into energy system should be an obligatory part of energy strategy development and establishment of an optimum capacity mix with respect to primary sources, technologies, etc. Integration has several aspects: integration into energy market, integration regarding grid stability and integration various technologies together into the system for ensuring its diversity which decrease the vulnerability against diversity of disturbances. These aspects are usually not considered in representative studies mentioned above. Technical aspects and limitations for integration of a generation technology into the energy system is a typical issue of countries with relative small total capacity of electric energy system or pour cross-border integration and co-operation. These aspects might be very important for developing countries. Policy measures intervening into the industry for ensuring diversity of energy system are also not emphasised in the representative studies: they seem to be inadequate in a deregulated market economy, although preferences and non-preferences exist like clean-air policy and CO₂ penalties.

The listed five areas of judgement are complex, integrating several features and considerations. The assessment of technologies in each area is dominated by certain parameter. Nevertheless for the comprehensive assessment all related to the area features have to be accounted. The areas of judgement could not be separated completely, there are interactions between the areas, which should be identified and analysed from all relevant aspects.

There are features of generating technologies, which become importance only if they cross some level (e.g. the share of wind generating capacities in an energy system, or the maximum unit size). In the decision on the composition of energy production capacities of a country the features with scale effect might be also identified and analysed. Some of the

indicators for characterising the different generation technologies are qualitative, which might be and have to be assessed and compared without exact measures and still very realistic.

3. Features of nuclear power generation

3.1 Economic dimension

Regarding economic area, first attribute to be considered is the competitiveness, which is defined by the costs of nuclear power generation. A nuclear power plant is the most investment demanding technology, with high operation and maintenance cost and very low fuel cost. The nuclear power generation costs are dominated by high up-front capital costs. Comparison of cost structure of different generation technologies is given in Table 1. (Hydroelectric power plants are not included in the table; they need also very high investment costs like the nuclear.)

Cost contributor, %	Nuclear	Gas/CCGT	Coal	Wind
Investment	50-60	15-20	40-50	80-85
Operational and maintenance	30-35	5-10	15-20	10-15
Fuel	15-20	70-80	35-40	0

Table 1. Cost components of electricity generation technologies (WEC, 2007)

The study (IEA, 2006) estimated the average specific construction costs of nuclear power plant as 1500 USD/kW (10% interest rate and 5-year construction period) and gave the cost range as 1300-2000 USD/kW, where the upper limit is the price of demonstrations/prototypes. The range of investment cost estimation is much higher recently. Nevertheless even a relative small 'penalty' imposed due to CO₂ emissions or encouragement of emission-free electricity generation will make new nuclear power plants far competitive against the gas-fired ones. The (IEA, 2006) study estimated the operational costs as 0.021-0.031 USD/kWh, assuming 5% interest rate, 50% investment, 30% operational and maintenance, and 20% fuel components. As maximum values of the estimation, assuming 10% interest rate, 70% investment, 20% operational and maintenance, and 10% fuel components the operational costs were estimated for 0.03-0.05 USD/kWh. Consequently, nuclear power plants were assessed to be competitive compared with gas-fired plants, if the gas price is higher than 5.70 USD/MBtu or the oil price is higher than 40-45 USD/barrel. This was one of the reasons of the recent break-through in development of nuclear power generation.

According to the MIT update study the levelized cost might be considered as an integrating characteristic with respect of costs and competitiveness (MIT, 2009).

Since the up-front capital costs are dominating in the cost structure the levelized cost varies very sensitive with discount rate and with the risk-premium associated to nuclear investments. With respect to the possibility of reduction of penalising rates, the experience of preparation and implementation of new nuclear projects is controversial: In the US improvement of the assurance of investors is expected due to rationalised regulatory requirements and governmental loan guaranty. In case of Finland Olkilouto Unit 3 the changing regulatory practice together with improper project preparation and management

lead to delay and costs overruns, which seems to be a justification of investment risk of nuclear projects. There are only a few positive examples for implementation of nuclear projects in time and budget (Japan, South-Korea), which might change the opinion of the financial sector. As it is stated in (MIT, 2009) avoiding only the risk premium to capital cost would make the nuclear option competitive even without emission penalty. Recently the ranges of levelized costs of electricity from natural gas, coal and nuclear sources largely overlap between 2 to 9 US cents/kWh. Besides the risk premium and emission penalty the preferences of particular countries depend on local circumstances, such as the lack or availability of cheap domestic fossil resources. Similar conclusions have been made earlier in (OECD NEA, 2005).

Recent study of World Nuclear Association on economics of nuclear power is investigating the capital, finance and operating costs (WNA, 2010). The study demonstrates the generating price advantage of nuclear power compared for majority of countries. There is an obvious strong dependence of the generating costs on discount rate, construction time and operational lifetime. Increase of the discount rate from 5% to 10% may increase of generating costs of nuclear power by nearly 50%. The shorten construction time (5 versus 7 years) and the longer operation lifetime (40 versus 60years) also may decrease the generation cost about 20%. The bare plant costs (i.e. the engineering, procurement and construction costs) are very much depending on the country of supply and where the plant is built. It may vary between 1500-4000USD/kW; see also (OECD NEA, 2005).

There are features of the nuclear power generation, which have economic nature and not covered by levelized costs. These are the following:

- effect on the security of supply,
- stabilisation of the market - low price volatility due to low fuel price dependence,
- geopolitical aspect of accessibility of fuel,
- long-term availability of the fuel.

Nuclear power generation has an overwhelming advantage compared to other conventional generation technologies with respect to the security of supply. In short term any disturbances in fuel supply can be managed by stockpiling of fresh fuel. Stockpiling of the fresh fuel at the nuclear power plants ensuring quite long period of operation is feasible due to the high energy-concentration of fuel. For generation 1GWyear of electricity 2.5 million tons of coal, 1.6 million tons of oil and 3.9 million tons of natural gas would be required approximately. The same amount of electricity requires about 20 tons of nuclear fuel. In some countries stockpiling of fresh fuel sufficient for two years of operation is obligatory. Import dependent countries established alternative fuel supply for fresh nuclear fuel.

Low fuel cost sensibility of nuclear power generation ensures stable market position for nuclear and it affect also the stability of the electricity market; production cost increments less than 10%, if the fuel price will double.

The availability and accessibility of nuclear fuel generates issues of technical, economical and geopolitical nature. It is rather obvious that any limitations on the availability and accessibility of fuel will increase the generation costs and destabilize the market. The geopolitical aspects of accessibility are part of social area. However the geopolitical aspect of accessibility of fuel has direct impact on the economy; any limitation of the accessibility of fuel will cause economical uncertainty, price-increase (and political tensions). From geopolitical point of view the nuclear fuel seems to be much less critical compared to oil and gas due to distribution of Uranium resources over the world.

The long-term availability of nuclear fuel might become a more critical issue. The identified uranium reserves being used in the existing light-water reactors are sufficient just for less than one hundred years. In these reactors about one percent of the fissile isotopes burns up and the remaining fissile part can be reprocessed. Establishing a system with fast breeder reactors and closed fuel cycle, the known conventional Uranium reserves will be sufficient for more than three thousand years (more than twenty thousand years if the non-conventional resources are accounted), see e.g. (OECD NEA, 2008).

There are advantages of nuclear power generation compared to the other generation technologies, which are not or not explicitly addressed by levelized cost.

Assessments of the role of a given technology in the energy system, ideally, should be based upon comparisons of full costs to society. Therefore some other costs are also worth to consider while assessing the economic area, e.g.

- the external costs,
- the relative societal cost for greenhouse gas (GHG) saving,
- need for subsidies for research and development, deployment or operation.

Comprehensive analysis of external costs of different power generating technologies has been performed in the frame of ExternE research project of the European Commission. Summary and comparison of generating technologies regarding external costs is given in (WEC, 2004). The study demonstrates that nuclear power is favourable compared with other technologies. Most health and environmental costs of nuclear power generation are already internalised. It may take more than 20% of production costs. If these costs were included, the European Union price of electricity from coal would double and that from gas would increase 30%. These are without attempting to include the external costs of global warming, which might be considered as delayed penalty for the uncontrolled emission from fossil fuel use. All studies on the subject agree that the nuclear power generation is the least cost solution for reduction of GHG emission (IAEA, 2009).

Research and development, deployment (sometimes also the operation) of low-emission technologies need state subsidies. Nuclear power generation is a mature low-emission technology, which does not need state subsidies. In the same time the state has very important role with respect to the development of nuclear industry, but it is limited to establishment of stable regulatory framework and equal to other low-emission technologies treatment of the nuclear electricity generation. It has to be underlined, that the low-emission technologies might be subsidised only within the capability of society, i.e. even the very developed countries could not afford today a replacement of conventional power generation technologies with emissions-free one.

Considering the existing nuclear power plants, they represent major corporate assets. The reason for long-term operating the existing nuclear power plants is economic triviality, since they are not imposed by capital costs and still operable for a long time (totally about 60 years), considered as the cheapest and most reliable producers (load factor 85÷93%), competitiveness might be improved by power up-rates, see (IAEA-TECDOC-1309, 2002). Business evaluation of nuclear power plants has been done for example in (EPRI, 2001).

3.2 Environmental dimension

The environmental impact of different technologies has to be considered with respect to the following main aspects:

- real and potential environmental impact of operation,

- waste issue, waste management,
- natural resource management.

It is an unquestionable fact that negative environmental effects exist in the case of all energetic technologies, even in the case of the so-called green technologies.

Regarding real environmental impact, today the 439 operating nuclear power plants provide the half of GHG emission-free electricity generation. In comparison to other technologies, the GHG emission of nuclear power plants is negligible, even if the whole life cycle, including uranium mining, is taken into account. It is hardly believable but a fact that generation of one kWh electricity in a photovoltaic or wind power plant results in more greenhouse gas (GHG) emissions than in nuclear power plants, if the whole life cycle (manufacturing, operation, decommissioning) is included, see (OECD NEA 2008; ISA, 2009). The regional environmental impacts caused by nuclear power plants are neutral or fully negligible. In majority of cases the only reportable environmental load during normal operation is the heat load due to cooling to air or aquatic environment. All types of effluents to the environment are controlled under strict norms at nuclear power plants.

Waste is generated unavoidable during electricity production. In nuclear power plants considerably less industrial wastes are produced per kWh than in other power plants. Waste management practice of nuclear industry is based on the principle of 'collect, control and confine' contrary to the 'dilute and release' practice of other technologies. Techniques for management and final disposal of radioactive wastes are available; existing problems in this field are of political and social nature.

Considering the potential impact, safety of power generation has been essentially improved during last twenty years. The probability of early large release of radioactive substances to the environment due to accidents is less than 10^{-6} /years. It means that the risk of nuclear power generation should be more than an order of magnitude less compared to any other industrial activity.

Further improvements of safety features are in progress in case of newly designed Generation III and III+ reactors, due to implementation of high quality, and reliability components and proven techniques. The Generation IV reactors will have very high safety level due to principally new design features based on passive and inherently safe solutions.

Nuclear power plants are high unit power production capacities with operational lifetime 60 years and the capacity factor about 86-92%. These parameters of nuclear power plants essentially affect all characteristics, which are related to the total energy produced during operational lifetime, e.g. (1) the energy intensity coefficient, which is equal to the ratio of total energy needed for construction, operation, decommissioning, etc. to the produced by the plant energy during the whole lifetime; (2) use of resources per unit power (MW) or for the total production (MWh), e.g. materials (steel, concrete, copper, etc.), land etc.

Mentioned above parameters are adequate also for comparison of rational use of resources. With this respect nuclear is the most favourable technology compared to any other, including technologies utilising renewable energy sources. This statement is justified in all representative studies (ISA, 2009; WEC, 2004).

3.3 Social dimension

Development any energy strategy should start with evaluation of the needs and expectations of the society and with the social impact of the strategy when implemented. Evaluation of generating technologies in the social dimension is very complex. Practically all

features mentioned above characterising economical and environmental acceptability of technologies have social connotation.

In the social dimension the technologies have to be evaluated from point of view of direct risk (mortality under normal operation) and potential risk, i.e. frequency of incidents and their consequences (fatality), including risk due to severe accidents.

Contrary to the public opinion frequency of severe accidents is the lowest at nuclear power plants; it is less than 10^{-6} /years. After TMI accident and the severe Chernobyl accident safety reviews have performed at all nuclear power plants in the world and significant safety improvements programs have been implemented. For example at Paks NPP, Hungary the core damage probability has been improved by more than one order of magnitude (i.e. the probability of core damage decreased) due to safety improvement measures. This value is $\sim 10^{-5}$ /year now, as illustrated in Fig. 1. It has been a typical tendency at each nuclear power plant for the last two decades.

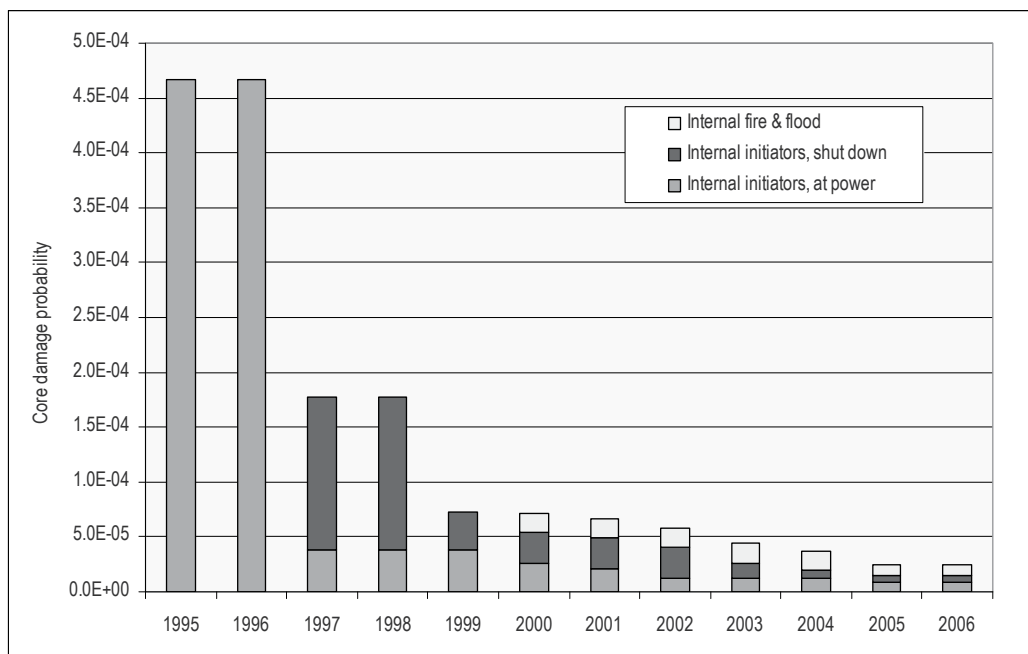


Fig. 1. Decrease of core damage probability at Paks NPP as a consequence of safety upgrading measures

The risk of serious accidents at nuclear power plants accompanied by health effects is negligible; its frequency is less than 10^{-7} /year.

Concerning the mortality under normal operation nuclear power generation has better statistics compared to the traditional generating technologies. This can be easily understood since the operation and maintenance of nuclear power plants require high level of generic technical and safety culture, the operational processes are formalized, licensed and controlled in accordance with the regulatory requirements.

Waste generation, use of land and other resources, security of supply, availability and accessibility of primary sources, and also the public conceptions on these aspects of energy

system affect the acceptance of energy strategy with different composition of primary energy sources and generating capacities in it.

In the social dimension the responsibility of the society regarding waste management has to be considered. The responsibility of society is specific in case of nuclear power generation due to necessity of safe and long-time isolation of radioactive waste from the environment. In the case of low- and medium-level radioactive wastes this time-span is 600 years (at least 20 half-times, when the activity of dominating isotopes will decline to the level of natural background).

In the case of high-level radioactive wastes the halftime of isotopes can be very long. The researches launched for disposal of high-level radioactive wastes and the current international practice have clearly justified that disposal of radioactive wastes and spent fuel can be implemented technically with maximal safety of the society and environment. The current ongoing researches promise to provide more effective methods for management and disposal of spent fuel and radioactive wastes. Technologies suitable for burning actinides exist and are currently under development, which will be discussed in connection with the development potential of nuclear generation later. The high-level radioactive wastes (not spent fuel, which can be reprocessed) can be finally disposed in deep geologic storage facilities.

Accessibility of resources and the possible geopolitical tensions might be conflicting with social interests from both economical and security point of view. Land use is not only an environmental issue, but can be the source of serious social conflicts. Given that the size of crop lands and food production may decrease due to the climate change, while the global population will increase, then starving people will compete for the croplands with biomass and bio fuel producers.

The social dimension covers for example the human capital, institutional framework, non-proliferation, public participation and political aspects. Nuclear energy is one of the great scientific discoveries of the 20th century. It constitutes achievements of the state-of-the-art scientific and technical development, and requires highly developed technical-scientific background, high-level professional and safety culture and complex institutional infrastructure. The nuclear power plant operating countries have effective and independent regulation, backed by strong legislation. It ensures that the nuclear energy activities are carried out in compliance with high safety and radiation protection standards.

Like waste issue the proliferation issue requires high social responsibility. Obviously, nuclear power generation should not contribute to the proliferation of nuclear weapons on one hand and renouncing nuclear energy would not eliminate the risk of nuclear weapon proliferation on the other.

Policies for sustainable development require not only public support, but also certain immolation of the society. Financial support required for deployment nuclear power generation technologies is negligible small compared to other clean technologies; it is mainly limited for establishment of scientific support and developing safety related researches for regulatory institutions. However, the regulation should recognise the emission-savings due to nuclear power generation and should not apply different from other environmental-friendly technologies policy. There are already positive examples for the balanced policy, see (US, 2005).

For nuclear energy most concerns arise from the public perceptions of the risks involved. Recent developments in many countries, e.g. Sweden, Italy, UK, Germany data show the

improving acceptance of nuclear power due to better communication and greater participation by the public. However a better demonstration of benefits of nuclear in comparison with other technologies seems to be needed. For example, the promotion programs for renewable energy technologies do not even mention that hazardous wastes generating during the whole lifecycle of wind or solar energy production have to be managed in a similar way than radioactive wastes of nuclear power plants. It is not even discussed under the topic of the social issues. Because of the low shear of such technologies in the whole system, the issue is not recognised by the society and does not alert social concern.

4. Integration into energy system

The electricity market is a deregulated competitive market. Contrary to this, the competing electricity producers are integrated into an energy system, which is linking the producers together and forcing them to co-operate, otherwise the stability of supply could not be ensured from the point of view of operation of the electrical distribution system. There are technical conditions and limitations for the integration into the electrical grid. While comparing the technologies and integrating each technology into the system of energy supply the effects of introduction of the new capacity on the stability of the electricity grid has to be considered. For example the maximum rated power of a new capacity should be fitted to the total capacity and structure of the whole system. An optimum size of new capacity exists from technical point of view (similar to the optimum size from business point of view), which depends on the total grid capacity, level of regional, cross-border integration, reserving in the system, types of co-operating capacities. This issue might be marginal, if such technologies are present in the system with a small weight, but it might be essential, when the contribution of a technology approaches a certain limit, and the stability of the system is endangered.

Considering the nuclear power generation, integration into the grid might be difficult in case of countries with small system capacity since the rated power of Generation III and III+ reactors is over 1000MWe. For ensuring the required system back-up capacities pumping storage hydroelectric plants might be very appropriate, they may essentially improve the system quality and they are really emissions-free solutions. Similar problem may arise, while incorporating wind power plants into the electrical system. The predictability of availability of wind plants is limited therefore the system backup capability will limit the shear of wind capacities in the system.

Configuration of a diverse energy system seems to be an important aspect of energy strategies. An optimal energy system should be divers regarding technologies, sources of primary energy, import markets. The diversity decreases the system vulnerability to technical disturbances. Diversity of energy system might be important also for those countries, which have essential fossil resources (for example United Arab Emirates).

5. Development potential of nuclear power generation

The current needs for nuclear construction are satisfied by the so-called Generation III and III+ reactor types, which have been developed using the design, manufacturing and operational experiences gained during the previous decades. They represent high-level

safety and availability due to proven solutions. Some inherent safe characteristics appear, which use gravitation drive and natural circulation cooling to the safety functions, and do not require actuating resources. There are design features for management of some classes of beyond design base accidents and mitigation of their consequences (design base extension). Reactor containment buildings are designed to be impervious to catastrophes. Nuclear power plants containment structures have been designed to withstand the impact of hurricanes, tornadoes, floods, missiles and large aircraft impacts. The plants can be operated in load follow regime. Fuel burn-up is high compared to Generation 2 reactors, which results in relatively lower radioactive waste production per kWh and per kg of fresh fuel. Operational lifetime of these plants is >60 years. The load factor is around 90%. Standardised design and manufacturing will decrease the construction time and costs. For example, the Advanced Boiling Water Reactors (ABWR), European Pressurised Water Reactors (EPR), the US designed AP-1000 and the Russian designed AES-2006, the South Korean designed APR-1400 pressurised water reactors represent the Generation III reactors. These reactors are mature for the market.

The innovative, new trends in reactor technology are represented by the Generation IV nuclear reactors, which are under intensive development; see for example (DoE, 2002). They will represent the state-of-the-art in XXI. Century.

According to (DoE, 2002) the goals of development of Generation IV reactors are as follows:

- The Generation IV systems will provide sustainable energy generation with respect to minimum life cycle GHG emission, effective use of fuel and other resources, while generation of waste will be minimized and the long-term stewardship burden notably reduced, thereby improving protection for the public health and the environment.
- The Generation IV nuclear energy systems will have a clear lifecycle cost advantage over other energy sources and business as usual financial risk.
- The Generation IV nuclear energy systems shall have very high reliability and safety with a very low likelihood and degree of reactor core damage without any need for offsite emergency response.
- The Generation IV systems shall have proliferation resistance and physical protection capability.

Large variety of types of reactors is under development:

- Sodium-cooled fast reactors (SFR)
- Very high temperature reactors (VHTR)
- High temperature gas-cooled fast reactors (GFR)
- Lead-cooled fast reactors (LFR)
- Molten salt reactors (MSR)
- Supercritical water-cooled reactors (SCWR)

Development potential of new generation of nuclear reactors can be demonstrated by the diversity of applications. Diversity of the reactor and power plant types being under development is extremely remarkable.

The Generation IV reactors cover a very wide range of features:

- Considering the unit size: they are small (a few hundred) to very large (2000 MW) plants: The LFR might have power level less than 100MW, the GFR, SFR, VHTR might be medium and also large size, the SCWR is a large size reactor.

- With respect of the reactor temperature: they are of moderate temperature for conventional steam-turbine power generation (SCWR and SFR) to very high supercritical temperatures and also with parameters applicable for Hydrogen energy system (GFR, LFR, MSR, VHTR).
- With respect to the neutron physics the types vary from thermal to fast-neutron reactors, with fuel breeding or even actinides burning
- Regarding fuel cycle the types vary from reactors with open fuel cycle (VHTR) like the recent light water reactors (Generation II, III and III+), to different types of fast breeders and reactors able to burn the actinides (GFR, MFR, LFR, SFR).

This is shown in Fig. 2 where the versatility of utilisation of Generation IV reactors is illustrated in the dimensions of neutron-physics, i.e. capability of reactor to work in closed fuel cycle, or even to burn actinides, reactor rated power from small to huge capacity plants, producing electricity or Hydrogen.

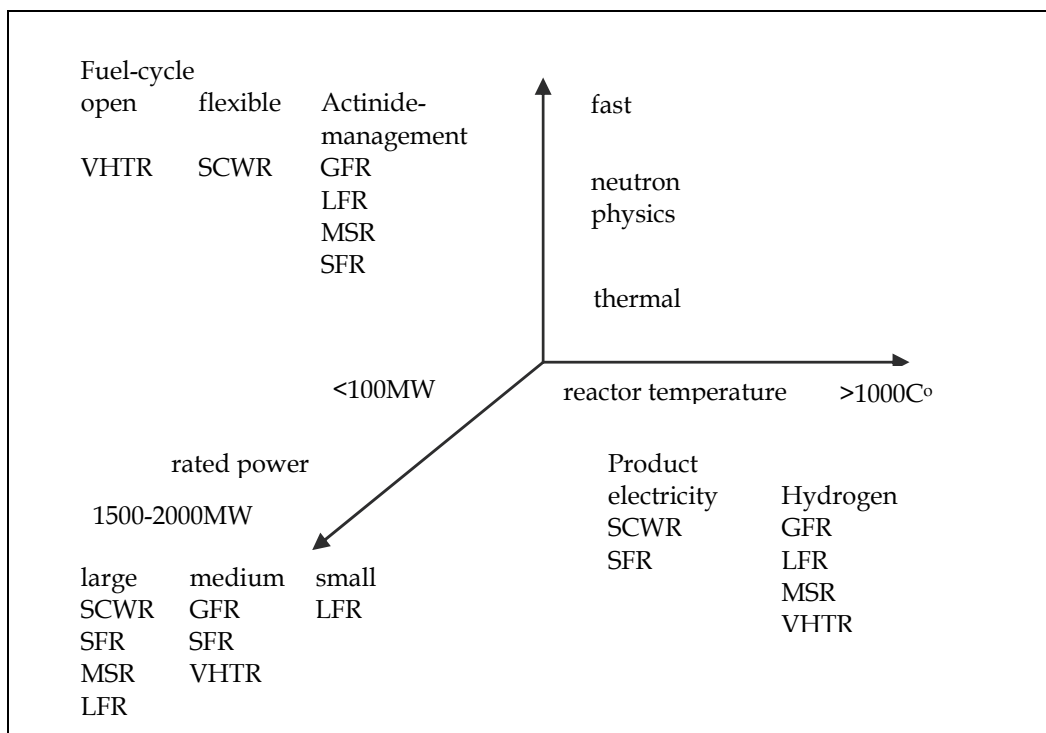


Fig. 2. Development potential of the fourth generation of nuclear power plants

Such a versatile energetic technology can be easily adjusted to a modern energy supply system, where the plants utilising renewable sources and nuclear energy can be used for electricity generation and hydrogen production. Hydrogen is a new fuel for transport, and oxygen can be used for modern burning of coal with CO₂ capture. This high variety of types may cover wide spectrum of needs of future costumers and allow integration of nuclear power generation into the complex frame of industrial technologies. However the highest efficiency of nuclear power can be achieved not in electron-Hydrogen but in electron-economy, where for example the electrical energy is directly used in transportation.

Development potential of new generation of nuclear reactors can be demonstrated by the viability of deployment of new types. It is worth mentioning also the time of industrial application of the new types, which is expected to be between 2015 (sodium-cooled fast reactors) and 2025 (gas, molten salt or lead-cooled fast reactors and supercritical water-cooled reactors). Some intermediate types like the gas-cooled pebble-bed reactors might be constructed within coming decade.

7. Conclusion

Decision on the development of power generation industry has to be derived from the visions of a country regarding own overall development perspectives and goals. It requires consideration and assessment of economical and ecological benefit from development of different generation technologies manifesting in security of supply and emission saving. Financial and technical aspect of feasibility of different development options and also the expected generation costs are decisive as well as the total societal costs. However for the development of an optimal power generating system adjusted to the condition of a country configuration of a diverse production capacity mix is needed, which is divers regarding technologies, sources of primary energy, import markets. There are technical conditions and limitations for the integration into the electrical grid, which define the size of generating units as well as the optimum contribution of each technology from the point of view of the stability of the electrical grid. While assessing the role and contribution of different generating technologies in the production mix also the development potential of different technologies has to be considered. Comparative studies based on assessment of complexity of aspects show that the nuclear energy is a clean, safe and affordable alternative to other power generating technologies including those using renewable energy sources.

8. References

- IEA (2009). *World Energy Outlook 2009*, International Energy Agency, ISBN 978-92-64-06130-9, Paris
- UNFCCC (1998). *Kyoto Protocol to the United Nations Framework Convention on Climate Change*, United Nations, 1998,
<http://unfccc.int/resource/docs/convkp/kpeng.pdf>,
- UNFCCC (2009). *Copenhagen Accord United Nations Framework Convention on Climate Change*, 2009, Copenhagen, <http://unfccc.int/resource/docs/2009/cop15/eng/107.pdf>
- Commission of the European Communities (2007) *Communication from the Commission to the European Council and the European Parliament – An Energy Policy for Europe*, Brussels, 10.1.2007, COM(2007)
- DoE EIA (2009). *International Energy Outlook – 2009*, U.S. Department of Energy, Energy Information Administration, 2009
- IEA (2006). *Energy Technology Perspectives 2006 - Scenarios & Strategies to 2050*, OECD IEA, ISBN: 92-64-10982-X-2006, Paris
- WNA (2010). *The Economics of Nuclear Power*, World Nuclear Association, <http://www.world-nuclear.org/info/inf02.html>
- IAEA (2009). *Climate Change and Nuclear Power 2009*, International Atomic Energy Agency, ISBN 978-92-0-1123-9-1, Vienna

- IAEA PRIS (2009). *PRIS database*, International Atomic Energy Agency, 2009, Vienna
<http://www.iaea.org/programmes/a2/>
- UK (2007). *Meeting the Energy Challenge, White Paper on Energy*, HM Government, TSO, ISBN 978-0-10-171242-2, London
- US (2005). *Energy Policy Act of 2005*, 119 STAT. 594, Public Law 109-58-AUG.8, 2005
www.epa.gov/oust/fedlaws/publ_109-058.pdf
- Eurobarometer (2008). *Attitudes towards radioactive waste, Special Eurobarometer 297*, European Commission, http://ec.europa.eu/public_opinion/archives/ebs/ebs_297_en.pdf
- OECD NEA (2010). *Public Attitudes to Nuclear Power*, Nuclear Energy Agency, ISBN 978-92-64-99111-8, Paris
- OECD NEA (2008). *Nuclear Energy Outlook*, Nuclear Energy Agency, ISBN: 9789264054103, Paris
- MIT (2009). *Update of the MIT Future of 2003 Nuclear Power: An Interdisciplinary MIT Study*, Massachusetts Institute of Technology, Cambridge, MA (2009),
<http://web.mit.edu/nuclearpower/pdf/nuclearpower-update2009.pdf>
- OECD NEA (2005). *Projected Costs of Generating Electricity, 2005 Update*, Nuclear Energy Agency, ISBN 92-64-00826-8, Paris
- IAEA (1999). *Health and Environmental Impacts of Electricity Generation Systems: Procedures for Comparative Assessment, Technical Reports Series No. 394*, International Atomic Energy Agency, ISBN 92-0-102999-3, Vienna
- Vattenfall (1999). *Vattenfall's Life Cycle Studies of Electricity*, VATTENFALL, 16287 Stockholm, Sweden, www.vattenfall.se
- WEC (2004). *Comparison of energy systems using life cycle assessment*, World Energy Council, ISBN 0 946121 16 8, London
- ISA (2006). *Life_cycle Energy Balance and Greenhouse Gas Emissions of Nuclear Energy in Australia*, ISA, The University of Sydney, <http://www.isa.org.usyd.edu.au>
- Goedkoop, M. et al. (2009). *ReCiPe 2008, A life cycle impact assessment method which comprises harmonised category indicators at the midpoint and the endpoint level*, Ministry of Housing, Spatial Planning and Environment, Netherlands, <http://www.lcia-recipe.net/>
- OECD NEA (2007). *Risks and Benefits of Nuclear Energy*, (OECD Nuclear Energy Agency, 2007, Paris, NEA No. 6242
- Katona T. (2008). Role of nuclear energy in sustainable development, *Nukleon*, HU ISSN, 1789-9613, www.nuklearis.hu, 1. évf, 3. szám, 2008. szeptember, I. évf. (2008) 17, in Hungarian
- WEC (2007). *The Role of Nuclear Power in Europe*, January 2007, World Energy Council, ISBN 0 946121 23 0, London
- IAEA-TECDOC-1309 (2002). *Cost drivers for the assessment of nuclear power plant life extension*, International Atomic Energy Agency, ISBN 92-0-114402-4, Vienna
- EPRI (2001). *Nuclear Power Financial Indicators for a Competitive Market*, EPRI, Palo Alto, CA: 2001. 1003050, www.epri.com
- DoE (2002). *A Technology Roadmap for Generation IV Nuclear Energy Systems*, Issued by the U.S. DOE Nuclear Energy Research Advisory Committee and the Generation IV International Forum, GIF-002-00,
http://gif.inel.gov/roadmap/pdfs/gen_iv_roadmap.pdf

The Dead Fish Option for Australia's future electricity generation technologies: Nuclear Power

Lucas Skoufa

*The University of Queensland, St. Lucia
Queensland, Australia, 4072*

1. Introduction

The discussion of the use of nuclear power in Australia has been ongoing since the late 1960s, the first large-scale reactor was supposed to be built near the Royal Australian Naval College on the coast of southern New South Wales. When the author was a Naval Officer under training at the college he remembers the early morning winter runs to the site! The site was not developed as a nuclear power station due to increasing concerns at that time about the operating safety of these plants and how the waste would be disposed of safely given that radioactive levels last for millennia. Although in a recent study (Macintosh, 2007) the site was amongst many suggested if nuclear power would be adopted in Australia, this is a politically contentious issue at this time in Australia even with concerns about climate change damage.

There has been a range of recent material on the issue of uranium and nuclear power in Australia (see Gittus, 2006; Commonwealth of Australia, 2006; Owen, 2006; Falk, Green and Mudd, 2006; Macintosh, 2007; Skoufa and Tamaschke, 2008). In addition there have been several studies on the merits of implementing an emissions trading scheme in Australia, which is known as the Carbon Pollution Reduction Scheme (CPRS). In April 2010, the legislation was postponed until 2013 due to the Australian Federal government's concerns about its lack of support in the Senate (ABC, 2010). One of the background studies considered in the Australian government's formulation of the CPRS was the 2008 *Garnaut Climate Change Review*. The Garnaut (2008) study centred on what needed to be done by Australia in the face of growing concerns about the potential for future climate change damage. Another recent study in Australia also considered the effects of the hidden costs of power generation in Australia (Biegler, 2009) and was based on the European Union's ExterneE project. Climate change issues and power generation technologies remain important issues in Australia. This book chapter attempts to take these previous works and other studies from abroad, into account to state that the use of nuclear power is not a dead-fish option for Australia.

This book chapter will cover the following. First, a review of the literature (academic and industry) will look at the major material published from not only an Australian perspective but also of American and other global sources. Second, this chapter will discuss the merits

of using the various power generation technologies available for use in Australia, included in this will be discussion about centralised generation and distributed generation systems. Third and finally, the chapter will make a recommendation that nuclear power is in general a viable power generation technology in Australia.

2. Review of Ideas and Key Points

A perusal of recent literature (IEA, 2003; MIT, 2003; Gittus, 2006; Commonwealth of Australia, 2006; Kruger, 2006; Rothwell and Graber, 2010) suggests there are four realistic ways over the next few decades of reducing greenhouse gas emissions from electricity generation:

1. Increased efficiency in electricity generation and its use;
2. Expand the use of renewable sources such as wind, solar, biomass, and geothermal;
3. Capture carbon dioxide emissions from fossil fuelled plants (especially coal) and permanently sequester the carbon dioxide; and
4. Increase the use of nuclear power.

It is felt that Australia is well on the way to implementing the first three options shown above. If we consider option (4), Australia has major uranium deposits, which includes 38 percent of the world's low-cost uranium deposits according to a Commonwealth of Australia (2006) study on uranium mining and nuclear power. Presently Australia is almost exclusively involved in the mining and milling part of the uranium fuel cycle (Commonwealth of Australia, 2006). Australia also has experience with three small nuclear reactors and this is covered later in the book chapter. Australian society seems to be increasingly Climate Change proactive (e.g., see Commonwealth of Australia, 2006). If nuclear power becomes viable in the eyes of the general public and can supply part of the base-load section of electricity generation it would thereby displace some increasingly uncompetitive, and highly polluting, coal-fired and older gas-fired plants from the supply curve. At present coal-fired and gas-fired technologies are able to hold the base-load section of electricity generation due to their overwhelming cost competitiveness compared to nuclear plants. This is mainly due to the fact that externalities such as greenhouse gas emissions have not as yet been internalised into the cost structure for fossil fuel plants.

Australia is a nation that is fossil fuel rich, possessing large amounts of relatively cheap and easily accessible reserves of coal, gas and uranium that could be utilised for power generation purposes. Coal has been the primary fuel for power generation in Australia due to its abundance, low cost and government support (Kellow, 1996; Naughten, 2003; Thomis, 1987). It has taken several decades post World War 2 to build and then operate the large scale fossil fuel dominated electricity system infrastructure in Australia. Thus, to modify the system to accommodate climate change policy, in the form of an emission trading scheme or other instrument/s, will also need time for the existing infrastructure to adjust. Amongst many, one key issue/question is how current and potential new electricity generation firms will adjust? That is, with the experience and know-how they have can they change their dominant power generation technology mindset? Australia is quite large in area and its population is concentrated in coastal areas in mainly the eastern/south-eastern part of the continent. The electricity supply industry in Australia operates the longest interconnected system on the planet, a distance of some 5000 kilometres (AEMO, 2009). These long distances place a strain on the high-voltage transmission network since the locations of large

power stations may be hundred of kilometres from large load centres (e.g., large cities such as Sydney and Melbourne). Some think that Distributed Generation (DG) could be one solution to this problem. Instead of investing large funds into new large scale power plants and long distance transmission lines a local point of consumption DG system can accommodate for demand growth and at the same time not increase overall greenhouse gas emissions. With regard to the centralised generation versus distributed generation issue the range of technologies available (fossil and renewable) can be implemented for both systems, the only real exception is that of nuclear power (Rukes and Taud, 2004:1855). Apart from technical criteria such as high reliability, high efficiency, and low emissions a low as possible life-cycle costs is a requirement for any power plant technology (Rukes and Taud, 2004).

Having considered the above it is also pertinent to note that two major energy challenges facing the world are (1) replacing oil consumption and (2) reducing greenhouse gas emissions (Forsberg, 2009). Even though Forsberg (2009) did not directly mention an easy path to reduce greenhouse gas emissions (GHG) newer power generation technologies are now more likely to be gas- instead of coal-fired. However, gas-fired power generation technologies still have GHG emissions, around one-third to one-half that of coal-fired, their use as a larger scale base load source of power whilst being limited a few years ago will increase. Other options can be to move towards distributed power generation, that is generating power at or very close to the point of consumption. This allows for the use of renewable technologies such as solar photovoltaic (PV) and wind. For all of these options there are social and institutional barriers that need to be overcome or convinced of the benefits of switching to lower or zero carbon power generation technologies. Indeed the CEO of the US Electric Power Research Institute (EPRI) recently stated that in the USA to achieve an 80% reduction in GHG emission by 2050 it would be wrong to prematurely classify any technology as a winner or loser; CCS and nuclear must not be discarded (Specker, 2009). A similar outlook must be held for Australia's desire to reduce GHG emissions.

The latest Intergovernmental Panel on Climate Change (IPCC) Report published in 2007, the Fourth Assessment Report on Climate Change stated there is no "one size fits all solution" to the global issue of climate change and the need to reduce GHG emissions (Barker et al., 2007:27). The solutions to this global issue will be regional, or country specific especially if we consider Australia, an "isolated" island continent. The role of technologies is important to the solutions that will be needed (Barker et al., 2007). Switching fossil fuel from coal-fired to gas-fired reduces CO₂ emissions, gas-fired power plants have 40% - 45% of the emissions intensity of black coal power plants, as expressed in t CO₂/MWh (Chappin, Dijkema, de Vries, 2009). The electricity sector possesses significant mitigation potential across a range of power generation technologies combined with end-use energy conservation and efficiency (Barker, et al., 2007).

In all of the debate on climate change and GHG emission reductions the continued use of fossil fuels for power generation has been a major issue. Globally the electricity sector contributes 41% of global energy related CO₂ emissions. (IEA, 2008a) and this is mainly due to the heavy reliance on the burning of fossil fuels. For the next twenty years to 2030 world population growth combined with vast reserves of fossil fuels suggests that this dependency must inevitably continue, particularly for the generation of base-load electrical energy supplied through centrally controlled and coordinated networks (IEA, 2008a). There have

been recent arguments for and against the continued dominant use of fossil fuels for electricity (power) generation. The "... plans for the end of the fossil-fuel economy are now being laid" proclaimed *The Economist* (2008:13). However, such plans might need to convince a sceptical portion of the general population that feels indifferent to the benefits of a cleaner source of electricity. The International Energy Agency (IEA) *World Energy Outlook 2008* highlights that coal will remain as the leading fuel input for power generation to the year 2030 (IEA, 2008b). Announcements in 2009 such as the plan for a low-carbon future for the UK, the 'Desertec' Industrial Initiative in northern Africa, a possible nuclear power expansion in the EU, and calls for increasing the use of distributed generation suggest that a new look electricity sector is coming. Of course these changes will need time, money and some impetus to overcome several barriers to the uptake of these next technologies (Jamashb, Nuttall, Pollitt, Maratou, 2008). 'Decarbonisation' is the key to achieving the goals of large GHG emissions reductions by 2050. The product of two factors can be used to express decarbonisation (1) carbon emissions per unit of energy consumption and (2) the energy requirements per unit of value added, often known as energy intensity (Nakicenovic, 1996:99).

The climate change debate and its relation to the electricity supply industry can be thought of as having the following major elements (Grubb, Jamashb and Pollitt, 2008):

1. Establishing emission and technology targets. The setting of emission targets should come with an emission trading scheme that is adopted in Australia. The Carbon Pollution Reduction Scheme (CPRS) as it is known is the centre-piece of a suite of policies aimed at reducing Australia's GHG emissions in line with Kyoto Protocol obligations.
2. Incorporating the externalities of conventional and alternative generation sources in electricity prices. This area has seen an increase in publications/studies, calculating a reasonable price for such externalities is always going to be difficult.
3. Expedite energy efficiency improvements. An area that has been under-promoted in Australia until recently.
4. Support the use of alternative fuel sources for power generation. There are some support mechanisms for this in Australia, the Federal government's Renewable Energy Target, essentially guarantees a market for high-cost new power generation technologies that have greatly reduced or zero GHG emission intensities.

3. Nuclear Power and Centralised Power Generation Technologies

From a regional perspective it is prudent to investigate what can be done to mitigate greenhouse gas emissions in a high per capita emission country such as Australia. Is it just the case that technology will simply change from coal- to gas-fired, or for Carbon Capture and Storage (CCS) to become the dominant design? Can we utilise the solar energy striking the surface of Australia's vast tracts of land? And what social and institutional barriers will be present that hamper technological change? Implementing low-carbon technologies can be impeded by the lack of human and instructional capacity (IPCC, 2007); the marketplace left to its own devices will just keep selecting the cheapest technological options for power generation and not consider the costs of the damage caused by using such technologies. Normally the cheaper options are coal-fired and in some cases gas-fired technologies. Within the developing world the use of coal- and gas-fired power generation technologies

will continue unabated as these countries further industrialise and move toward developed status; the demand for coal for power generation use is expected to double by 2030 (IPCC, 2007).

Most modern technologies display increasing returns to adoption in that more adoption means more experience and consequently improvements occur (Arthur, 1989). A technology used in an industry that has an early lead may eventually corner the market and 'lock-out' other technologies (Arthur, 1989); this had been the general case for coal-fired power generation technologies until the reform/restructuring process began in the mid-1990s. So, those technologies that are locked-out cannot gain a foothold in the marketplace due not only cost competitiveness but also technical competitiveness or other issues. For example, hydro-electric power can become more costly as dam sites become scarcer and less suitable (Arthur, 1989).

The latest IPCC Fourth Assessment Report on Climate Change (Barker, et al., 2007) stresses that the multitude of GHG emission scenarios all assume that technological changes occur during this 21st century. The electricity/power generation sector globally contributes 41% of energy related global GHG emissions per year at present (IEA, 2008). In Australia the electricity/power generation sector contributes 35% of the country's total yearly GHG emissions (Garnaut, 2008). Australia's per capita GHG emissions are amongst the highest of OECD nations and around the globe as a matter of fact (Garnaut, 2008). And Australia's share of global GHG emissions in 2005 was 1.5% of the total (Garnaut, 2008). Thus, one could argue that it does not matter if Australia progresses towards a low-carbon power generation sector.

Australia's traditional ties with the United Kingdom (UK) did in part see both countries' ESIs resemble each other since the end of the Second World War. Both countries established large centralised systems based primarily on coal-fired power plants. The onset of privatisation/reform for the UK ESI in 1990 then saw similar reform process being followed in the various Australian state based ESIs. The UK has embarked on a Low-Carbon future; various goals have been identified for the UK in the quest for this to occur (Grubb, Jamasb and Pollit, 2008). Australia's position on a low-carbon future has been clouded by the delay in the passage of legislation that introduces a nationwide emissions trading scheme. As previously mentioned the passage of this legislation has now been postponed until 2013.

Whatever the outcome for Australia with respect to nuclear power, it is still unclear what the best method is to dispose of nuclear waste and how this 'externality' can be costed. In a way this is similar to how the costs of greenhouse gas emissions shape the social costs and competitiveness of fossil fuel stations. Nuclear power plants need large amounts of water for cooling purposes so the location of these plants on the eastern Australia seaboard would be a major challenge for any potential new project. In addition there is not a vast supply of nuclear qualified engineering/technical staff residing in Australia so this would have to be developed quickly if nuclear power was approved. For Australia nuclear power is currently not an option as the Australian Labor Party (which is in government federally and in nearly all states) prohibits the development of a nuclear power industry (Rudd, 2009). This sentiment was reinforced by the Australian Climate Change Minister who ruled out the possibility of the current Labour Government wanting to have nuclear power generation in Australia (Bloomberg New Energy Finance, 2010). As part of this statement the Minister said that Australia should concentrate on renewable energy and also the storage of emissions from coal-fired plants (Bloomberg New Energy Finance, 2010). So, where does this

leave the issue of using nuclear power in Australia as part of a suite of zero/low-carbon power generation technologies to meet ambitious greenhouse gas emission reductions by 2050?

Another recent media report highlighted that coal mining and coal-fired power station emissions of dust particles and noxious gases has caused increased health problems for some 40,000 resident in the Hunter Valley of New South Wales Australia (ABC, 2010). The issue of human health damage effects from the mining and combustion of coal is very important, but seems to have taken a back-seat to the greenhouse gas emissions issue. One comprehensive study that explored the issue of human health damage costs was that by the Australian Academy of Technological Sciences and Engineering (ATSE) (2009). This study was a follow on from the European ExternE study (2005) which mainly explored the externalities of the energy sector in Europe.

A recent presentation by Angwin (2010) and commentary by Toohey (2010) suggests that for nuclear power to be adopted:

1. Australia has infrastructure support for the mining, processing, power generation, and disposal of waste components of the uranium life cycle.
2. For Australia the decision to adopt nuclear power needs:
 - a) Political support from Federal and State governments. At present the level of support for nuclear power is ambivalent at best.
 - b) Financial support from the federal government. This follows on from recent US news that the latest 3rd generation Light Water Reactors to be approved for construction in the United States cost more than expected and the Obama administration has offered loan guarantees for the power companies investing in these plants. These guarantees amount to a considerable part of the initial capital cost. For example, for a 2200 MW expansion of an existing plant that will at present cost \$US14.5 billion the US government's loan guarantee amounts to \$US8.3 billion.
 - c) People with the necessary skills and training in the operation of nuclear power plants. Australia does have limited experience with smaller nuclear reactors, the Australian Nuclear Science and Technology Organisation (ANSTO) operated a 10kW reactor (then expanded to 100kW) from 1961 to 1995 (Reztsov, 2010), and a 10MW reactor was shut down in 2007 after almost 50 years service. ANSTO now operates a 20MW reactor (ANSTO, 2010a). These three reactors have been used mainly for producing isotopes for medical and industrial use, materials science research, and for irradiating silicon ingots which are subsequently used in electronic semiconductor devices. And ANSTO and selected contractor staff have now had not only operational experience but also decommissioning experience. Therefore there might be a perceived lack of necessary skills in Australia but this is not justified.
 - d) A comprehensive regulatory framework to cover the various components of the uranium life cycle. Because of the small nuclear reactors located at the ANSTO facility the Australian government has established the Australian Radiation Protection and Nuclear Safety Authority (ANSTO, 2010b). This authority regulates nuclear facilities in Australia via the *Australian Radiation Protection and Nuclear Safety Act 1998* (ANSTO, 2010b). However, the establishment of large scale nuclear reactors in Australia will necessitate much further and more stringent regulation than presently established.

- e) A good business case for investors. The business case for investment into power generation plants has been around since the privatisation of the United Kingdom's electricity supply industry in 1990. The main factor that would differentiate the decision to adopt nuclear power for large scale application (e.g., 1000MW) is the appropriate level of risk premium. Nuclear power investment is not really possible without government support.
- f) Public support is a crucial issue on whether or not to adopt nuclear power and is discussed in the last section of this chapter.

With regards to the business case for power generation investment discussion on the restructuring of electricity supply is now presented. Before climate change became a major issue the power generation sector was part of a vertically integrated government owned monopoly electricity supply industry. The reform process that began in the 1980s had a major assumption that restructuring and liberalisation of these industries would result in greater economic efficiency (Skoufa, 2006; Skoufa and Tamaschke, 2008). The three major forces that drove change within utility industries such as electricity supply (and electricity generation) included (Weiner, Nohria, Hickman, Smith, 1997; Lomi and Larsen, 1999):

1. Market Change - liberalisation, that is, the establishment of competition introduced consumer choice, price and product differentiation, asymmetric information between firms and regulators, and new entrants trying to capture capacity share from incumbents.
2. Regulatory and Political change - the objectives of the regulator (seen as 'watchdogs') and the regulated (profit or shareholder maximising firms) tended to become less co-operative in some instances.
3. Technological Change - technological change ended the traditional advantage of having economies of scale derived from possessing large-scale coal-fired generation plants. For example, coal-fired plants that were scale efficient at approximately 1000MW were replaced with gas-fired combined-cycle plants with scale efficiency at approximately 400MW.

These forces are still relevant in other ways for the power generation sector. Some lessons and suggestions for Australia's power generation sector can be learned from the experiences of the European Union's Emissions Trading Scheme (EU ETS); although the United States has had an ETS for SO₂ emissions since the 1970s (Klaassen, 1996). The EU ETS was launched in January 2005 and has become a reference point for greenhouse gas (GHG) emissions trading schemes in other parts of the world including Australia. If nothing else the EU ETS is a start at trying to address the potentially damaging effects of climate change. As three years have now passed published work on the effectiveness of the EU ETS has grown in volume within the areas of economic analysis and policy issues. From a business perspective Egenhofer (2007) identified that up to now the EU ETS has not encouraged investment into new and low-carbon power generation technologies due to various uncertainties. One of these uncertainties is the international indecision on what will replace the Kyoto Protocol which expires at the end of 2012.

Electricity supply has the unique distinction of being classed as an essential service and security of supply (i.e., keep the lights on at all costs) is of paramount importance (AEMO, 2009). However, to guarantee security of supply cost effectiveness and environmental criteria may be comprised (Sims, et al., 2007).

According to Dyner, Larsen and Lomi (2003) there are three broad categories of risk facing companies involved with electricity supply (specifically the generation sector); *organisational risks*, *market risks*, and *regulatory risks*. *Organisational risks* are those mainly associated with inertia within an organisation, that is, the tendency of established companies to resist change (both the content of the change and the process by which it is done). *Market risks* are those related to issues brought on by competition such as customer choice, price volatility, asymmetric information, new and possibly aggressive new entrants to the industry, and variable rates of return. *Regulatory risks* come about because even after restructuring and deregulation regulatory body/bodies have been established to oversee the electricity supply industry. Regulatory bodies have to choose how to balance controls on such issues as prices, anti-competitive behaviour and now with climate change and greenhouse gas emissions being of importance there will be uncertainty in policy and regulations and thus increased risk. Another way to view the major risks facing investors in power generation sectors is shown below in Figure 1.

Plant Risk	Market Risk	Regulatory Risk	Policy Risk
Construction costs	Fuel cost	Market design	Environmental standards
Lead time	Demand	Regulation of competition	CO ₂ constraints
Operational cost	Competition	Regulation of transmission	Support for specific technologies (renewables, nuclear, CCS)
Availability/performance	Electricity price	Licensing and approval	Energy efficiency

Fig. 1. Major Risk Factors for Investors in Power Generation

Source: Nguyen, Stridbaek, and van Hulst, 2007, *Tackling Investment Challenges in Power Generation*, p. 134

Even if the technical and economic criteria make a generation technology viable the level of support for adopting these technologies; by governments, generation companies, or the public is a strong component to be considered. Technological choices are shaped in part by social political factors (Jamasp, et al., 2008). To 'decarbonise' the electricity generation sector multiple dimensions of technical, economic, social and political are needed to be addressed (Pfaffenberger, 2010). Additionally various barriers to the adoption of various power generation technologies has been identified for the UK ESI (Jamasp, et al., 2008). These five barriers should also apply to the situation facing Australia, if a low-carbon electricity system is to be established. The five barriers are:

1. Technical – an obvious factor for both large scale (coal, nuclear) and distributed generation (DG). It is suggested that a wide adoption of DG systems in Australia

would present control, voltage and power flows issue for the current centralised system. If the systems are considered separately then the issue of fuel availability is a factor of high importance. Australia has vast reserves of coal, gas, uranium and its solar intensity is one of the highest in the world.

2. Regulatory – the Australian Renewable Energy Target encourages the use of new, higher cost renewable sources of power generation and these can be implemented in both centralised and DG systems. This is seen to be a barrier to the continued dominance of coal-fired technology and to some extent the gas-fired technology. An emissions trading scheme would also present itself as a barrier to coal-fired technologies as the short-run and long-run costs would be increased, quite significantly for the high CO₂ emitting brown-coal fired power stations in Victoria.
3. Existing planning and approval procedures – for example the current Queensland State Government has stipulated that no new coal-fired power stations would be approved for Queensland unless (1) the proposed station uses the world's best practice low emissions technology, and (2) it is CCS ready and can fit that technology within five years of CCS becoming commercially viable (Queensland Office of Climate Change, 2009). For a region with a plentiful supply of coal reserves this could see problems in the future if older large-scale coal-fired plant is not replaced by other technologies that provide similar scale. Obviously with no nuclear power industry in Australia the planning and approval procedures would have to be established and most likely follow that of the United States system of procedures.
4. Lack of standards – this is more applicable to nuclear power and small scale DG technologies in Australia at this time. For instance, standards need to be in place for safe operation of nuclear power plants and then for subsequent radioactive waste disposal and storage. The selection of sites for disposal would have to be heavily regulated via appropriate standards.
5. Public opposition/lack of awareness – especially relevant for nuclear power stations in Australia; the Not In My Back Yard (NIMBY) feeling amongst the public is strong. However this can also occur for other technologies like wind power (the large tall turbines), coal-fired power stations, and solar (PV and/or concentrated).

Rothwell and Graber (2010) state that for nuclear power to have a significant role in global GHG mitigation four countries that already have nuclear power are crucial; China, India, the United States and Russia. It is foreseen that if these four countries build substantial numbers of new nuclear power stations then GHG emission reduction could also be substantial. So where does this leave Australia? It is envisaged that this would delay or cancel out the nuclear power option for Australia, the fission option anyway. For nuclear fusion only time will tell.

In 2009 MIT updated its 2003 *The Future of Nuclear Power* study. The main conclusions of what has changed between 2003 and 2009 were (MIT, 2009):

1. That nuclear power will diminish as a viable generation technology in the quest to reduce GHG emissions. This is due to the lack of support for the technology from the US Government. However, in March 2010 President Obama pledged funding, reportedly \$US 8 billion, for underwriting new investment into nuclear power stations.
2. The renewed interest in the United States for using nuclear power stems from the fact that the average capacity factor of these plants in the US has been around 90%. Also, the US public support has increased since 2003.

3. US government support via such instruments as financial funding is comparable to those given to wind and solar technologies. Such support can bring nuclear more into line with coal- and gas-fired technologies on a long-run marginal cost (LRMC) basis. And this is before carbon pricing is included in LRMC calculations.

Australia's position on the use of nuclear power has been mired in controversy for several decades. The latest data shows that Australia is the country with the highest proportion of identified uranium reserves, this was at 23% in 2007 (OECD, 2008). The key advantages and disadvantages of currently available electricity generation technologies for use within Australia's NEM are summarised in Table 1.

Technology	Generating Cost (US c/kWh)- Based on AUD/USD 0.9093 average for 2010	CO ₂ Emissions (g/kWh) (Lifecycle)	Major Advantages	Major Disadvantages
Coal	3-5 (no carbon price) 6-8 (for a carbon price of USD18/tCO ₂)	900 average - for brown and black coal plants	Abundant reserves in Australia Clean coal technologies are being developed but 10-15 years from commercialisation Lower operating (private) costs relative to gas	Relatively high emissions and emission control (social) costs (use of CO ₂ scrubbers, carbon sequestration) Location problems for new plants Takes 8-48 hours to bring online for dispatch from cold
Natural Gas	4-6 (no carbon price) 5-8 (for a carbon price of USD18/tCO ₂)	450 average (combined and open cycle)	Abundant reserves in Australia Low construction cost Lower environmental damage relative to coal (lower social cost) Takes 20 minutes to bring online for dispatch from cold Coal Seam Methane can be used for power generation (with potential Greenhouse Gas Credits to be paid)	Higher fuel (private) cost than coal Export market demand has driven up prices recently, and will do so in the future Can drive up gas prices for other non-electricity users
Nuclear	3-7 (Probably closer to 7 based on 2010 capital costs estimates for new plants in the USA)	65	Australia has 38% of global low-cost uranium deposit No air pollutants Low operating (private) costs Non-sensitive to world oil prices Proven technology 40 - 60 year lifetime, possibly 100 years with appropriate maintenance	Safety concerns (operational plants) High capacity (investment) cost with long construction time Approval process expected to be protracted Potential severe public backlash at its introduction in Australian and ultimate location of plant (on coastline for large amounts of water for cooling) Disposal of waste (where and also potential for

				weapons use)
Hydro-electric	4-20	45-200 (large and small hydro plants)	No air pollutants Low economic costs Takes 1 minute to bring online for dispatch from cold	Limited capacity expansion Volatile and increasingly scarce availability of water in Australia
Renewable(e.g. solar, wind, geothermal)	3-20 (wind is generally cheapest, then geothermal and then solar)	65-200 (inclusive of manufacturing emissions)	Minimal fuel-price risk Environmentally benign (low social costs) Stable or decreasing costs	Intermittent and other reliability concerns High economic capital costs

Table 1. Characteristics of different generation technologies for use in Australia's NEM

Based on: Commonwealth of Australia (2006); Costello (2005); Gittus (2006); Graham and Williams (2003); Lenzen (2009); Mollard, et al. (2006); Naughten (2003); NEMMCO (2007); Rothwell and Graber (2010); Rukes and Taud (2004); Sims, et al. (2003)

4. Is It Possible in Australia?

One previous study (Macintosh, 2007) looked at several criteria for the siting of nuclear power plants in Australia. In that study Macintosh (2007) proposed 19 locations in four Australian states. These locations were basically all coastal, the need for seawater cooling as opposed to freshwater cooling is important given Australia's relatively dry climate. Apart from the need for a coastal location other criteria such as minimal ecology disruption, closeness to the current transmission grid, appropriate distance away from populated areas, and earthquake activity were amongst several criteria considered by Macintosh (2007).

Recent public opinion polls in Australia on nuclear power were published by The Sydney Morning Herald (2009) and Newspoll (2007). The 2009 poll found that 49% of the survey said they would support using nuclear power as a means of reducing carbon pollution and 43% said they did not support using nuclear power for reducing carbon pollution (The Sydney Morning Herald, 2009). The 2007 poll found that whilst 45% of the survey favoured the use of nuclear power for reducing greenhouse gas emissions only 25% of the survey was in favour of a nuclear power plant being built in their local area (Newspoll, 2007). In general the NIMBY feeling remains strong in Australia, it is suggested this is in part due to the fact that large scale major coal-fired power stations are well away from major cities such as Sydney, Melbourne and Brisbane. Similarly the public attitudes to nuclear power reflect those of Australian surveys in the United States, Germany France and Japan to name a few (Rothwell and Graber, 2010). Maybe half the population might support using nuclear power plants to reduce/mitigate GHG emissions, but less would accommodate those plants in their local area. By way of some contrast there is some government support, mainly in from China and the United States, for using nuclear power in a clean energy scenario (World Nuclear News, 2010).

It might be easy to reject the use of nuclear power in Australia due to 'competition' from other sources of power generation such as coal-fired, gas-fired and renewables (solar, wind, geothermal, and so on). Interestingly enough Australia generally has abundant supplies of all 'fuel sources' for power generation. However, in Australia the abundance of uranium ore and of thorium (which is increasingly another fuel option for nuclear) may mean that

when a breakthrough comes along that greatly reduces the radioactive danger for nuclear fission the apparent Australia myopia in not establishing a nuclear power industry might turn out to be a big misguided fallacy. In other words, Australian has not until now fully considered the merits of using nuclear power.

5. References

- ABC, 2010, *Four Corners Programme - 'A Dirty Business'*, 12 April, viewed 13 April, <<http://www.abc.net.au/4corners/content/2010/s2870687.htm>>
- ABC, 2010a, *Labor shelves emissions scheme*, 27 April, viewed 29 April, <<http://www.abc.net.au/news/stories/2010/04/27/2883282.htm>>
- ACIL Tasman, 2005, *Report on NEM generator costs (Part 2)*, Canberra
- Angwin, M., 2010, *Economic growth, global energy and Australian uranium*, Conference Presentation to Energy Security and Climate Change, 16 March, Brisbane
- Biegler, 2009, *The Hidden Costs of Electricity: Externalities of Power Generation in Australia*, The Australian Academy of Technological Sciences and Engineering, Melbourne
- Australian Financial Review, 2006, *Howard's nuclear vision generates heat*, 22 November
- Australian Financial Review, 2010, *Time to forget about nuclear power*, 1 - 5 April
- Australian Nuclear Science and Technology Organisation (ANSTO), 2010a, *ANSTO's research reactor*, ANSTO, viewed 27 April, 2010, <http://www.ansto.gov.au/discovering_ansto/anstos_research_reactor>
- Australian Nuclear Science and Technology Organisation (ANSTO), 2010a, *Regulations governing ANSTO*, ANSTO, viewed 27 April, 2010, viewed 27 April, <http://www.ansto.gov.au/discovering_ansto/institute_of_environmental_research/safety_management/regulations_governing_ansto>
- Arthur, W.B., 1989, *Competing Technologies, Increasing Returns, and Lock-In by Historical Events*, *The Economic Journal*, 99, pp. 116-131
- Bloomberg New Energy Finance, 2010, *Australian Climate Minister Rejects Nuclear Power*, viewed 12 April, <http://www.bernama.com/bernama/v5/newsworld.php?id=489834&utm_source=newsletter&utm_medium=email&utm_campaign=sendNuclearHeadlines>
- Bunn, D.W. and Larsen, E.R., 1994, *Assessment of the uncertainty in future UK electricity investment using an industry simulation model*, *Utilities Policy*, 4(3), pp. 229-236
- Chappin, E. J. L., Dijkema, G.P.J., de Vries, L.J., 2010, *Carbon Policies: Do They Deliver in the Long Run?* in Sioshansi, F.P. (Editor), *Generating Electricity in a Carbon-Constrained World*, Academic Press (Elsevier), Burlington, Massachusetts, USA
- Commonwealth of Australia 2006, *Uranium Mining, Processing and Nuclear Energy – Opportunities for Australia?*, Report to the Prime Minister by the Uranium Mining, Processing and Nuclear Energy Review Taskforce, December
- Costello, K., 2005, *A Perspective on Fuel Diversity*, *The Electricity Journal*, 18 (4), pp. 28-47
- Dyner, I., Larsen, E.R. and Lomi, A., 2003, *Simulation for Organisational Learning in Competitive Electricity Markets* in Ku, A. (Editor), *Risk and Flexibility in Electricity: Introduction to the Fundamentals and Techniques*, Risk Books, London
- ExternE, 2005, *ExternE: Externalities of Energy, Methodology 2005 Update*, EUR21951, Bickel, P. and Friedrich, R. (Editors), European Communities, Luxembourg
- Falk, J., Green, J., and Mudd, G., 2006, *Australia, uranium and nuclear power*, *International Journal of Environmental Studies*, 63(6), pp. 845-857

- Garnaut, R. (2008), *The Garnaut Climate Change Review: Final Report*, Cambridge University Press: Melbourne
- Gittus, J.H., 2006, *Introducing Nuclear Power to Australia: An Economic Comparison*, Australian Nuclear Science and Technology Organisation, Sydney
- Graham, P.W. and Williams, D.J., 2003, *Optimal technological choices in meeting Australian energy policy goals*, *Energy Economics*, 25, pp. 691-712
- Grubb, M., Jamasb, T., Pollitt, M.G., 2008, *A low-carbon electricity sector for the UK: issues and options* in Grubb, M., Jamasb, T., Pollitt, M.G. (Editors), *Delivering a Low-Carbon Electricity System*, Cambridge University Press: Cambridge, UK
- International Energy Agency (IEA), 2003, *Power Generation Investment in Electricity Markets*, OECD/IEA, Paris
- International Energy Agency (IEA), 2006, *Energy Technology Perspectives: Scenario & Strategies to 2050*, OECD/IEA, Paris
- International Energy Agency (IEA) (2008a), *CO₂ Capture and Storage: A key carbon abatement option*, OECD/IEA: Paris
- International Energy Agency (IEA) (2008b), *World Energy Outlook 2008*, OECD/IEA: Paris
- Jamasb, T., Nuttall, W.J., Pollitt, M.G. and Maratou, A.M. (2008), *Technologies for a low-carbon electricity system: an assessment of the UK's issues and options* in Grubb, M., Jamasb, T., Pollitt, M.G. (Editors), *Delivering a Low-Carbon Electricity System*, Cambridge University Press: Cambridge, UK
- Kamerschen, D.R., and Thompson, H.G., 1993, *Nuclear and Fossil Fuel Steam Generation of Electricity: Differences and Similarities*, *Southern Economic Journal*, 60 (1), pp. 14-27
- Kellow, A. (1996), *Transforming Power: The Politics of Electricity Planning*, Cambridge University Press: Melbourne
- Klaassen, G., 1996, *Acid Rain and Environmental Degradation: The Economics of Emission Trading*, Edward Elgar, Cheltenham, UK
- Kruger, P., 2006, *Alternative Energy Resources: The Quest for Sustainable Energy*, John Wiley & Sons, Inc., Hoboken, New Jersey
- Lenzen, M., 2009, *Current state of development of electricity-generating technologies – a literature review*, *Integrated Sustainability Analysis*, The University of Sydney, Sydney
- Lomi, A. and Larsen, E., 1999, *Learning Without Experience: Strategic Implications of Deregulation and Competition in the Electricity Industry*, *European Management Journal*, 17(2), pp. 151-163
- Macintosh, A., 2007, *Siting Nuclear Power Plants in Australia: Where would they go?*, The Australia Institute, Research Paper No. 40, Canberra
- Massachusetts Institute of Technology (MIT), 2003, *The Future of Nuclear Power: An Interdisciplinary Study*, MIT, Boston
- MIT, 2009, *Update of the MIT 2003 Future of Nuclear Power*, MIT, Boston
- Mollard, W.S., Rumley, C., Penney, K. and Curtotti, R., 2006, *Uranium, Global Market Developments and Prospects for Australian Exports*, ABARE Research Report 06.21, Australian Bureau of Agricultural and Resource Economics, Canberra
- Nakicenovic, N., 1996, *Freeing Energy from Carbon*, *Daedalus*, 125(3); pp. 95-112
- Naughten, B. (2003), 'Economic assessment of combined cycle gas turbines in Australia: Some effects of microeconomic reform and technological change', *Energy Policy*, 31, 225-245
- Newspoll, 2007, *Nuclear power poll*, 6 March, viewed 28 April, <http://www.newspoll.com.au/image_uploads/0301%20Nuclear%20power.pdf>

- Nguyen, F., Stridbaek, U., van Hulst, N., 2007, *Tackling Investment Challenges in Power Generation: In IEA Countries*, OECD/IEA, Paris
- OECD-NEA/IAEA, 2008, *Uranium 2007: Resources, Production and Demand*, OECD-NEA No. 6345 (Red Book), Paris
- Owen, A., 2006, *Nuclear Power for Australia?*, *Agenda*, 13(3), pp. 195-210
- Reztsov, K., 2010, *Gentle fire goes out*, *The Journal of Engineers Australia*, 82(4), pp. 26-30
- Rothwell, G. and Gomez, T., 2003, *Electricity Economics: Regulation and Deregulation*, IEEE Press, Hoboken, New Jersey
- Rothwell, G. and Graber, R., 2010, *The Role of Nuclear Power in Climate Change Mitigation in Sioshansi*, F.P. (Editor), *Generating Electricity in a Carbon-Constrained World*, Academic Press (Elsevier), Burlington, Massachusetts, USA
- Rudd, K. (2009), *Rudd ridicules Opposition's nuclear push*, ABC News, 23 July
- Rukes, B. and Taud, R., 2004, *Status and perspectives of fossil power generation*, *Energy*, 29, pp. 1853-1874
- Sims, R.E.H., Rogner, H-H., and Gregory, K., 2003, *Carbon emissions and mitigation cost comparisons between fossil fuel, nuclear and renewable energy resources for electricity generation*, *Energy Policy*, 31, pp. 1315-1326
- Sims, R.E.H., Schock, R.N., Adegbululge, A., Fenhann, J., Konstantinaviciute, I., Moomaw, W., Nimir, H.B., Schlamadinger, B., Torres-Martínez, J., Turner, C., Uchiyama, Y., Vuori, S.J.V., Wamukonya, N., Zhang, X. (2007), *Energy supply. In Climate Change 2007: Mitigation. Contribution of Working Group III to the Fourth Assessment Report of the Intergovernmental Panel on Climate Change*, Metz, B., Davidson, O.R., Bosch, P.R., Dave, R., Meyer, L.A., (Editors), Cambridge University Press: Cambridge, UK
- Skoufa, L.A., 2006, *A strategic management framework for reformed electricity generation firms in Eastern Australia*, Unpublished PhD Thesis, The University of Queensland, Brisbane, Australia
- Skoufa, L.A. and Tamaschke, R., 2008, *Impact of environmental costs on competitiveness of Australian electricity generation technologies: is there a role for nuclear power?*, *Australasian Journal of Environmental Management*, 15(June), pp. 84-92
- Specker, S., 2009, *Viewpoint: The Prism in Action*, Electric Power Research Institute (EPRI) Journal, EPRI, Fall 2009, pp. 2-3
- The Economist, 2005, *The atomic elephant*, 375(8424), 30 April, p. 47
- The Sydney Morning Herald, 2009, *One in two favours using nuclear power to reduce pollution*, 13 October, viewed 28 April, <<http://www.smh.com.au/environment/one-in-two-favours-using-nuclear-power-to-reduce-pollution-20091012-gtyq.html>>
- Thomis, M.I. (1987), *A history of the Electricity Supply Industry in Queensland; Volume II: 1938-1988*, Boolarong Publications: Brisbane
- Toohy, B., 2010, *Time to forget about nuclear power*, *The Australian Financial Review*, 1 April, p. 79
- Weinberg, A.M., 2004, *On "immortal" nuclear power plants*, *Technology in Society*, vol. 26, pp. 447-453
- Weiner, M.; Nohria, N.; Hickman, A.; Smith, H., 1997, *Value Networks - The Future of the U.S. Electric Utility Industry*, *Sloan Management Review*, 38(4), pp. 21-34
- World Nuclear News, 2010, *Chu calls for direction on energy and climate*, 29 April, viewed 30 April, <http://www.world-nuclear-news.org/EE_Chu_calls_for_direction_on_energy_and_climate_2904102.html>

Advanced Magnetic-Nuclear Power Systems for Reliability Demanding Applications Including Deep Space Missions

Pavel V. Tsvetkov¹ and Troy L. Guy²

¹*Dept. Nucl. Eng., Texas A&M University, MS 3133, College Station, TX, 77843*

²*Lockheed Martin, 2400 NASA Parkway, Houston, Texas 77058*

1. Introduction

Deep space exploration has captured the imagination of the human spirit for thousands of years. Advanced deep space and interstellar propulsion concepts are critical to advancing future exploration, both locally in our solar system and in exosolar applications. Investigation of interstellar space regions have yet to be achieved beyond 200 astronomical units (AU), where one AU is the average distance between Earth and the Sun (approximately 150 million km). Pristine interstellar matter is expected to exist in this region. Advanced missions currently without a viable, robust mechanism for exploration include: Stellar probes, interstellar probes, Kuiper belt rendezvous vehicles, Oort cloud explorers and nearest-star targets. Outer edge solar system planets, atmospheres and planetary moon systems may hold insights into the physics of the early universe, yet they too have been largely unexplored. Terrestrial visits to Mars polar caps and Jupiter's icy moon oceans have been identified as future missions requiring advanced power and propulsion techniques. Despite overwhelming scientific interest and over 50 years of research, a robust mechanism for rapid space and interstellar exploration remains elusive. Propulsion and power technology applicable to deep space missions has generally fallen into four classes: chemical, fission, fusion, and exotic physics-based concepts. Despite persistent research in novel high-energy molecular chemical fuels and advanced bipropellant rocket engine concepts, chemical propulsion systems are limited to about 480 seconds of specific impulse, a value much too low to successfully meet deep space propulsion requirements (Liou, 2008). Owing to relatively low power per unit mass of ejected matter ratios and inherently limited chemical reaction energetics, chemical propulsion systems appear inadequate as primary fuel sources for interstellar or extended solar system edge missions. Fission reactors have long been proposed to address power and propulsion requirements. Essentially all solid, liquid and gas fission reactors fundamentally operate by converting kinetic energy from fission reactions into heat through a working fluid. Nuclear fusion holds tremendous potential for future space exploration initiatives. Inertial confinement, magnetic confinement, gas dynamic and magnetized target fusion concepts have been proposed (Kirkpatrick, 2002). Specific impulses on the order of 10^3 seconds are theoretically possible. Unfortunately, nuclear fusion ignition, confinement of hot

dense plasma and extreme heat management continue to be enormous obstacles for even mid-term fusion-based propulsion and power systems. Exotic physics-based concepts are varied in nature. Antimatter, solar sails, magnetic sails, beamed energy and fusion ramjets have been proposed for advanced propulsion. Limited technological developments appear to have restricted near-term deployment in space propulsion or power applications. This is evident in perhaps the most exciting exotic space propulsion candidate, antimatter. Matter-antimatter has excellent atomic reaction properties including converted mass fractions of 1.0 and energy releases of 9×10^{16} joules per kilogram in the case of proton-antiproton reactions (as compared to 2×10^8 joules per kilogram for atomic hydrogen and 3.4×10^{14} joules per kilogram for Deuterium-Deuterium or Deuterium-Helium-3 fusion fuels) (Borowski, 1987). Antimatter candidates have theoretical specific impulses of 10^5 - 10^6 seconds. Despite these highly attractive theoretical merits, antimatter candidate fuels have significant technological barriers such as the production and storage of antimatter. In addition, antimatter must be directed for thrust, a grand challenge yet to be mastered.

Propulsion and power systems developed for space exploration have historically focused on developing three types of systems: nuclear thermal propulsion (NTP), nuclear electric propulsion (NEP) and radioisotope thermoelectric generators (RTGs). NTP systems generate heat in a reactor which heats gas to very high temperatures. The heated gas expands and is ejected through a nozzle to create power and thrust. NEP systems use heat-to-electrical energy conversion mechanisms for generating electric power from heat provided by the reactor core. In general, NTP produces medium-to-high thrust with Isp levels on the order of 1000 s, while NEP systems typically provide higher Isp but much lower thrust levels (El-Wakil, 1992). Radioisotope power systems benefit from the direct radioactive decay of isotopes to generate electric power, but require a thermoelectric energy conversion process. Heat is converted to electricity using thermocouples. In the 1950's a study was initiated by the United States Air Force with the goal of designing and testing nuclear rockets (Gunn, 2001). The ROVER program was created as a succession of nuclear reactor tests. A major focus of this program was to demonstrate that a nuclear reactor could be used to heat a gas to very high temperatures, which would then expand and be directed through a nozzle to create thrust. In 1959 a series of reactors under the ROVER program were developed known as the Kiwi series. Highlights of this series include the Kiwi-A, Kiwi-B and Kiwi-B4E reactors. Kiwi-A utilized gaseous hydrogen for propellant, while Kiwi-B used liquid hydrogen and was designed to be 10-times the power of Kiwi-A. Kiwi-A and Kiwi-B successfully proved that a nuclear reactor could operate with high temperature fuels and utilize hydrogen (gaseous and liquid). The Kiwi series of tests ended with Kiwi-B4E. A second series of reactors developed in the 1960's under the ROVER program were known as the Phoebus series. The Phoebus 1 reactor was designed for up to 2.2×10^5 N of thrust and 1500 MW power. Phoebus 2A was designed for up to 5000 MW of power and up to 1.1×10^6 N of thrust. Phoebus 2A is the most powerful reactor ever built with actual record power and thrust levels of 4100 MW and 9.3×10^5 N of power and thrust, respectively (Durham, 1991). In addition to the Kiwi and Phoebus series of reactors, two other reactors under the NERVA (Nuclear Engine for Rocket Vehicle Application) program were the Pewee and Nuclear Furnace. Pewee was developed to demonstrate nuclear propulsion in space. The fuel selected for the Pewee reactor was niobium carbide (NbC) zirconium carbide (ZrC). In 1972, the Nuclear Furnace reactor was successful in demonstrating carbide-graphite composite fuel with a zirconium-carbide outer fuel layer that could be used as fuel. The

ROVER/NERVA program successfully demonstrated that graphite reactors and liquid hydrogen propellants could be used for space propulsion and power, with thrust capabilities up to 1.1×10^6 N and specific impulse of up to 850 seconds (Lawrence, 2005). However, NTP research has been minimal since these periods. In the 1950's a study was initiated under the Atomic Energy Commission which developed a series of reactors. This series was termed the Systems for Nuclear Auxiliary Power (SNAP) program. While multiple reactors were researched and developed (SNAP-series), the SNAP-10A reactor, flown in 1965, became the only United States fission reactor ever to be launched into space. The core consisted of enriched uranium-zirconium-hydride (U-ZrH) fuel, a beryllium (Be) reflector, a NaK coolant loop and a 1° per 300 second rotating control drum (Johnson, 1967). After reaching orbit and operating for 43 days, the SNAP-10A was shut down due to a failure in a non-nuclear regulator component. Currently, the SNAP-10A is in a 4000 year parking orbit. In the former USSR, more than 30 space power reactors were built and flown in space between 1970-1988. For example, the BUK thermoelectric uranium-molybdenum (U-Mo) fueled, sodium-potassium (NaK) cooled reactor was designed to provide power for low altitude spacecraft in support of marine radar observations (El-Genk, 2009). The BUK core consisted of 37 fuel rods and operated with a fast neutron spectrum. In 1987 the Russian TOPAZ reactor operated in space for 142 days and consisted of 79 thermionic fuel elements (TFE's) and a NaK coolant system. Two flights of the TOPAZ reactor were conducted. TOPAZ-1 was launched in 1987 and operated for 142 days. TOPAZ-II was launched in 1987 and operated for 342 days. Project Prometheus, a program initiated in 2003 by NASA, was established to explore deep space with long duration, highly reliable technology. Under the Prometheus charter, the Jupiter Icy Moons Orbiter (JIMO) project was conceived to explore three Jovian icy moons: Callisto, Ganymede and Europa. These moons were selected due to their apparent water, chemical, energy and potential life supporting features (Bennett, 2002). The selected reactor would operate for 10-15 years and provide approximately 200 kWe of electric power (Schmitz, 2005). Five reactor designs were studied as part of a selection process: low temperature liquid sodium reactor (LTLRS), liquid lithium cooled reactor with thermoelectric (TE) energy conversion, liquid lithium cooled reactor with Brayton energy conversion, gas reactor with Brayton energy conversion and a heat pipe cooled reactor with Brayton energy conversion. A gas reactor, with Brayton energy conversion, was chosen as the highest potential to support the JIMO deep space mission. Radioisotope thermoelectric generators (RTG) function by the radioactive decay process of nuclear material, such as Plutonium-238 (Pu-238), Strontium-90 (Sr-90), Curium-244 (Cu-244) or Cobalt-60 (Co-60). Many isotopes have been considered and are evaluated as potential power sources based, in part, on mechanical (form factor, melting point, production, energy density) and nuclear (half-life, energy density per unit density, decay modes, decay energy, specific power and density) properties. Heat is produced by radioactive decay and then converted to electric power by a thermoelectric generator, which is a direct energy conversion process based on the Seebeck Effect. In 1961, the first United States RTG was launched with one radioisotope source to produce a power of 2.7 We (Danchik, 1998). The Transit 4A spacecraft successfully reached orbit and was used for naval space navigation missions. RTG's have provided power for extended duration spacecraft missions over the past 40 years, including Apollo (moon mission), Viking (Mars mission), Voyager (outer planets and solar system edge missions), Galileo (Jupiter mission), Cassini (Saturn mission) and Pluto New Horizons (Pluto mission) (Kusnierkiewicz, 2005). In total,

there have been over 45 RTGs developed and operated by the US for space power (Marshall, 2008). Early RTG spacecraft operated with system efficiencies around 6%. An advanced version of the RTG, termed the Advanced Stirling Radioisotope Generator (ASRG) is being considered which is expected to increase efficiency and reduce the required amount of Pu-238 carried into space, with a predicted performance of up to 155 We and efficiency near 30% (Chan, 2007). A third type of radioisotope generator has been proposed. The Multi-Mission Radioisotope Thermoelectric Generator (MMRTG) is under development by the Department of Energy (DOE) and the National Aeronautics and Space Administration (NASA) and is expected to provide 2000 W of thermal power using plutonium dioxide fuel. This design will support a Mars surface laboratory, operating both in space and in the Martian atmosphere (Abelson, 2005).

This chapter is focused on a concept that utilizes the fission process but is fundamentally different than thermal or fast spectrum fission reactors and may offer a viable solution to stringent propulsion and power requirements related to deep space. The objective is to evaluate higher actinides beyond uranium that are capable of supporting power and propulsion requirements in robotic deep space and interstellar exploration. The possibility of developing a high efficiency MAGnetic NUClear System (MAGNUS) for space applications is discussed (Tsvetkov et al., 2006). The concept is based on a fission fragment magnetic collimator reactor (FFMCR) that has emerged from the DOE-NERI Direct Energy Conversion (DEC) Program as a feasible, highly efficient terrestrial power system. The central technology is based on utilizing advanced actinides for direct fission fragment energy conversion coupled with magnetic collimation. In the MAGNUS unit, the basic power/propulsion source is the kinetic energy of fission fragments (FFs). After FFs exit the fuel, they are captured by a magnetic field and directed out of the core. The energetic FFs flow has a high specific impulse and allows efficient power production and propulsion. The terrestrial application analysis indicated that direct energy conversion (DEC) efficiencies up to 90% are potentially achievable. Multiple studies demonstrated a potential for developing MAGNUS units for space applications. Absence of high temperatures and pressures, low fuel inventory, long-term operation, chemical propellant absence, highly efficient power generation, high specific impulse, and integral direct energy conversion without mechanical components provide an opportunity for exploration of the solar system and deep space. Interstellar missions of reasonable duration may be possible. Critical fission configurations are explored which are based on fission fragment energy conversion utilizing a nano-scale layer of the metastable isotope ^{242m}Am coated on carbon fibers. A 3D computational model of the reactor core is developed and neutron properties are presented. Fission neutron yield, exceptionally high thermal fission cross sections, high fission fragment kinetic energy and relatively low radiological emission properties are identified as promising features of ^{242m}Am as a fission fragment source. The isotopes ^{249}Cf and ^{251}Cf are found to be promising candidates for future studies. Conceptual system integration, deep space mission applicability and recommendations for future experimental development are introduced.

2. Reliability-Demanding Applications and Deep Space Missions

Deep space environments are often harsh and present significant challenges to instrumentation, components, spacecraft and people. Earth's moon will complete one full cycle every 29.53 days, creating extended cold temperatures during lunar night.

Temperature can range from 403 K to pre-dawn temperatures of 93 K (Fix, 2001). The moon's ultra thin atmosphere creates a dark sky during most of the lunar day. Thus, a highly reliable power source must be available for long-term exploration and human habitation. In addition, robust energy systems will enable in- depth terrestrial surveys of the far side and poles of the Moon. At a distance of 1.524 AU, Mars has seasonal weather patterns, which give rise to temperatures between 133 K and 294 K. Weather patterns observed from the Viking Lander observed daily temperature fluctuations of 315 K. In addition, temperatures have been found to change 277 K within minutes. Dust storms have been measured to travel up to 0.028 km/s, which often distribute dust over the majority of Mars' atmosphere. Solar energy flux is reduced by a half at Mars (relative to Earth) and dust storms can further reduce solar flux by up to 99%. Exploration of potential trapped H₂O on Mars polar caps will require reliable power sources for transport vehicles, drilling platforms, autonomous boring machines and supporting bases, seismic measuring stations spread across planetary surfaces and atmospheric-based satellite vehicles. In the interest of searching for pre-biotic chemistry, space exploration to the Jovian moon system has been proposed. Europa, Io, Ganymede and Callisto are planet-sized satellites of Jupiter (Bennett, 2002). Some of these moons are thought to contain ice or liquid water. In particular, Europa is predicted to contain oceans of liquid below its icy surface. Europa's ocean seafloors are thought to contain undersea volcanoes, a potential source of energy. Probes designed to dive into sub-surface regions require critical onboard instruments to function undersea and must be driven by robust power or propulsion sources. The Alpha Centauri star system, the closest star to Earth except the sun, is located at 200,000 AU. Proxima Centauri, one of three stars in the Alpha Centari system is the focus of advanced interstellar propulsion concepts with speculation of the existence of exoplanets. Proxima Centauri is a prohibitive destination with current state-of-the-art propulsion and power sources. For example, advanced chemical systems propelling a small robotic probe to Alpha Centari at a theoretical maximum speed of 0.001c (where c is the speed of light) would take approximately 4000 years. Conversely, a robotic probe propelled to 0.1c would take 40 years. Data could be returned at light speed to Earth in 4 years after arrival. Additionally, a star observer system outside 200 AU could return images and information about Earth's solar system never observed before. Interstellar mission requirements force high reliability constraints on power sources, which will require many years of constant operation.

3. Nuclear-Driven Direct Energy Converters

In conventional nuclear reactors, fission energy is harnessed from a working fluid. Nuclear fission releases a distribution of particles and corresponding energies as shown in Table 1 (Lamarsh, 2001). The largest fraction (81.16%) of energy released in the fission process goes to the kinetic energy of FFs which is then dissipated into heat and removed from the reactor core by a coolant such as sodium, carbon dioxide or helium. The heat removed is then used to produce energy through electromechanical energy conversion. Conventional heat engines are subject to Carnot efficiency limitations. In nuclear-driven direct energy conversion (NDDEC) FF kinetic energy is collected before it is turned into heat. Because intermediate energy conversion stages are eliminated, significant increases in efficiencies are possible. Figure 1 shows the difference between conventional nuclear power and the FFDEC concept.

Energy Release in Fission, by component	Energy (MeV)	Fraction (%)
<ul style="list-style-type: none"> ▪ Kinetic Energy of Fission Fragments (FF) ▪ Kinetic Energy of Fission Neutrons ▪ Energy of Prompt γ-rays ▪ Total Energy of β-particles ▪ Energy of Delayed γ-rays ▪ Energy of Neutrinos 	<p style="text-align: center;">168</p> <p style="text-align: center;">5</p> <p style="text-align: center;">7</p> <p style="text-align: center;">8</p> <p style="text-align: center;">7</p> <p style="text-align: center;">12</p>	<p style="text-align: center;">81.16</p> <p style="text-align: center;">2.42</p> <p style="text-align: center;">3.38</p> <p style="text-align: center;">3.86</p> <p style="text-align: center;">3.38</p> <p style="text-align: center;">5.80</p>
Total Energy released per Nuclear Fission Event	207	100.00

Table 1. Component energies in neutron-induced fission of ^{235}U .

The fundamental concept of producing electric power from charged particles via nuclear reactions was proposed by H. G. C. Moseley and J. Harling in 1913 (Tsvetkov et al., 2003). In these experiments, it was shown that charged particles could experimentally be utilized for creating high voltage. Direct fission fragment energy conversion (DFFEC) is the general process by which charged particles generated from nuclear fission are collected and directly used for energy generation or propulsion. Early studies of the DEC concept utilizing kinetic energy from FFs were initially proposed by E. P. Wigner in 1944 (El-Wakil, 1992). In 1957, G. M. Safonov performed the first theoretical study (Safonov, 1957). Experiments validated the basic physics of the concept, but a variety of technical challenges limited the observed efficiencies.

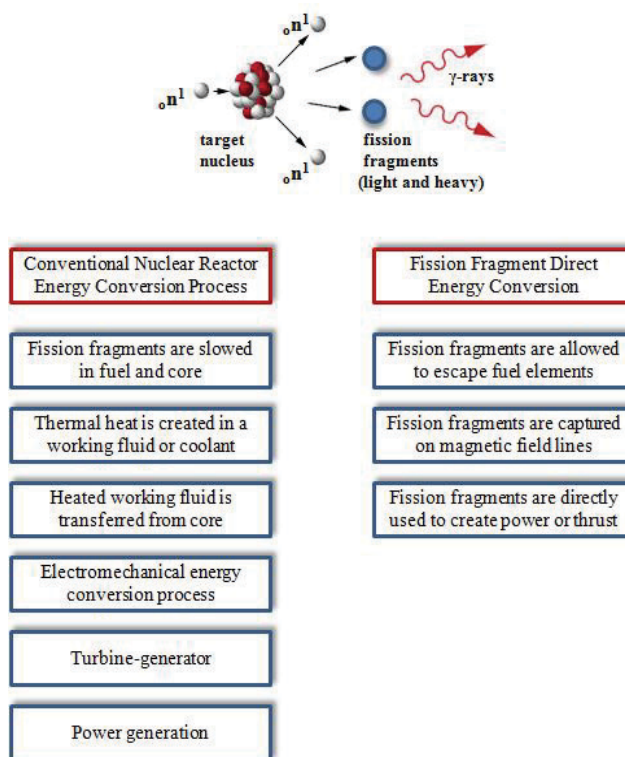


Fig. 1. Conventional nuclear reactor and direct energy conversion processes.

Further studies were conducted in which the core was in a vacuum and fissile material was inserted in the reactor core on very thin films (Chapline, 1988). Previous work by Ronen demonstrated the minimal fuel element thickness and the energy of the fission products emerging from these fuel elements, an element central to this concept. It was found that it is possible to design a nuclear reactor with a cylindrical fuel element with a thickness of less than 1 μm of $^{242\text{m}}\text{Am}$. In such a fuel element, 90% of the fission products can escape (Ronen, 2000). Further, Ronen showed that relatively low enrichments of $^{242\text{m}}\text{Am}$ are enough to assure nuclear criticality. In recent studies, as part of the United States Department of Energy Nuclear Energy Research Initiative Direct Energy Conversion (DOE NERI DEC) Project, the fission fragment magnetic collimator reactor (FFMCR) concept was identified as a promising technological concept for planetary power and interstellar propulsion applications (Tsvetkov et al., 2006). In the proposed concept, FFs exit the fuel element and are then directed out of the reactor core and through magnetic collimators by an external magnetic field to direct collectors located outside of the reactor core. This approach has the advantage of separating (in space) the generation and collection of FFs. In addition, achieving and maintaining criticality of the neutron chain reaction is easier for the FFMCR concept, as the metallic collection components can be located outside the nuclear reactor core. A feasibility study of this concept has been completed in which the basic power source is the kinetic energy of FFs that escape from a very thin fuel layer. The reactor core consists of a lattice of fuel-coated nano or micro-sized fibers utilizing graphite. After FFs exit the fuel element, they are captured on magnetic field lines and are directed out of the core and through magnetic collimators to produce thrust for space propulsion, electricity or to be used for a variety of applications. In previously proposed concepts, the basic reactor fuel is a pure $^{242\text{m}}\text{Am}$ fuel layer coated on graphite fiber rods. The FFMCR concept provides distinct fuel advantages for deep space, high-reliability applications (Tsvetkov, 2002). Some advantages include:

- Elimination of thermal-to-electric energy conversion stages,
- Very high efficiency,
- Very high specific impulse,
- Long-term operational capability,
- Reactor core with no moving parts,
- Low fuel inventory,
- Reduced Beginning of Mission (BOM) mass and volume,
- Propellant is not required,
- Significantly shorter probe transient times.

4. Potential Actinides for Deep Space Applications

Current concepts for extended deep space power sources are based on plutonium or uranium actinides. For example, the NASA Advanced Stirling Radioisotope Generator (ASRG) is expected to use a plutonium dioxide (PuO_2) fuel to heat Stirling converters and the Lunar Surface Fission Power (LSFP) source is expected to utilize uranium-based fuels such as uranium dioxide (UO_2) or uranium zirconium hydride (UZrH) (NASA, 2008). Uranium and plutonium, the most commonly proposed energy sources for space nuclear power, will serve as baseline reference actinides for comparison and analysis against higher actinides. Fuels for the FFMCR concept should have a half-life long enough to continually

produce power over all mission phases. In addition, the fuel should be able to produce optimal power to preclude having thousands of years of life that require extraneous and costly attention beyond the end-of-mission (EOM) timeline. Essentially, an ideal energy source would have a half-life to cover the mission and then safely decay within a reasonable timeframe after the EOM has been closed.

Baseline Actinides:	Isotopes
Uranium	^{235}U
Plutonium	^{238}Pu , ^{239}Pu , ^{241}Pu
Selected Actinides:	
Uranium	^{232}U
Americium	^{241}Am , $^{242\text{m}}\text{Am}$
Curium	^{243}Cm , ^{244}Cm
Californium	^{249}Cf , ^{251}Cf

Table 2. Baseline and selected candidate higher actinides.

In practical spacecraft development design, the specific activity of select nuclides should be kept as low as possible while maintaining the required power requirements from decay. Nuclides that decay and emit strong radiation fields will pose hazards to spacecraft equipment, scientific payloads and personnel.

Property	Metric
$T_{1/2}$: Half-Life	18 - 900 years
A: Specific Activity	< 50 curies per gram
P: Specific Power	< 1 watt per gram
η : Neutron production	> 2.6 neutrons per neutron absorbed
σ_F : Fission Cross Section	> U, Pu baseline actinides
ff_{KE} : FF Kinetic Energy	> U, Pu baseline actinides
γ -ray: Prompt γ -ray radiation	< U, Pu baseline actinides
Φ : Energy/Charge ratio	< 5 MV stopping power

Table 3. Metrics for determining nuclide viability for FF Reactor Cores.

Advanced actinides for the FFMCR should have minimal radiological activity. Specific power, the power produced per time and mass, is an important factor in determining heat shield and material requirements. Ideally, specific power should be kept as low as possible to create a technically viable space probe utilizing selected nuclides. If a nuclide exhibits a very high specific power, material margins may become serious limitations to the usefulness of the select actinide as a fuel candidate. Neutron induced fission is the process by which the FFMCR will be started. However, when bombarding target nuclei, the probability of interaction between the projectile and target nucleus is a quantum mechanical statistical process. In other words, there is no guarantee that a neutron projected at a target nucleus will produce a desired nuclear reaction. The successful higher actinide isotope will have a high thermal neutron cross section and, for

purposes of this discussion, have a higher thermal neutron fission cross section relative to baseline actinides. The probability of fission should be maximized. In the evaluation of nuclear reactor core performance, neutron production and absorption parameters must be considered per actinide isotope. Neutrons are released during fission, with some captured by absorption reactions with surrounding nuclei. A measurement of a nuclide's ability to produce neutrons will determine the ability to create and sustain a neutron-nucleus chain reaction and ultimately the ability of the nuclide to produce energy and power. The desire is to identify a nuclide which will produce more neutrons than are lost relative to baseline actinides listed in Table 2. For deep space power to be viable, robust and effective candidate isotopes must inherently contain suitable parameters. Candidate isotopes are analyzed according to the metrics summarized in Table 3.

The initial matrix criterion for acceptability was that the actinide isotope should have a half-life between 18 to 900 years. It is recognized that some isotopes on the lower range of this spectrum may not provide optimal mission timeline power or propulsion sources, but were included for completeness and comparison. Isotopes with half-life between 18 to 900 years are listed in Table 4. Associated decay constants and specific activities are given. Baseline Uranium and Plutonium isotopes are included for comparison.

Isotope	Half-Life, $T_{1/2}$ [yr]	Decay Constant, λ [yr ⁻¹]	Specific Activity, \bar{A} [Ci/g]
²³² U	68.9	0.01006	22
²³⁵ U	704×10^6	9.8×10^{-10}	2.2×10^{-6}
²³⁸ Pu	87.7	0.00790	17
²³⁹ Pu	24×10^3	2.8×10^{-05}	6.3×10^{-2}
²⁴¹ Pu	14.35	0.04830	100
²⁴¹ Am	432.2	0.00160	3.5
^{242m} Am	141	0.00491	9.8
²⁴³ Cm	29.1	0.02381	52
²⁴⁴ Cm	18.1	0.03829	82
²⁴⁹ Cf	351	0.00197	4.1
²⁵¹ Cf	900	0.00077	1.6

Table 4. Properties of relevant actinides.

Analysis of the nuclear data for actinides of interest shows that for thermal spectrum neutron reactions, ²⁴⁹Cf, ²⁴³Cm and ^{242m}Am produce the highest η (number of neutrons produced per neutron absorbed). Conversely, ²⁴¹Am, ²³⁸Pu and ²⁴⁴Cm appear to produce less than unity η in the thermal neutron spectrum. In the fast fission spectrum, the highest η produced occurs from the ²⁵¹Cf isotope and the lowest η produced is from ²³⁵U; η above approximately 106 eV grows exponentially with incident neutron energy. The ability to sustain a fission chain reaction with a given fuel element is hindered for actinide isotopes having η less than unity. Therefore, in this discussion, ²⁴¹Am, ²³⁸Pu and ²⁴⁴Cm will be discarded as potential candidates for energy sources. Additionally, ²³²U shows marginal ability for chain reaction sustainment and will also be eliminated from further consideration.

The requirements for deep space power or propulsion drive the search for acceptable actinide-based energy sources. For long term operation, successful actinide candidates must have half-life properties that support beginning-of-mission (BOM) to end-of-mission (EOM) power requirements. For deep space or interstellar operation, this generally translates to life-time properties greater than 20 years. In this survey of higher actinides ^{241}Pu and ^{244}Cm are excluded from further consideration based on half-lives of 14.35 and 18.1 years, respectively. In addition, for pre-launch operations, ^{241}Pu and ^{244}Cm post significant radiological hazards compared to other isotopes. The specific activity of ^{241}Pu is 100 Ci/g and that of ^{244}Cm is approximately 82 Ci/g. The next highest specific activity is ^{243}Cm at 52 Ci/g. Although excluded for half-life and high specific activity, it is notable that ^{244}Cm has the lowest thermal fission cross section of the surveyed actinides, also making it undesirable for deep space applications. The highest thermal fission cross section of the surveyed isotopes is $^{242\text{m}}\text{Am}$, followed by ^{251}Cf and ^{249}Cf . As noted previously, $^{242\text{m}}\text{Am}$ has a significantly higher (see Figure 4) thermal fission cross section than baseline isotopes ^{238}Pu , ^{239}Pu , ^{241}Pu or ^{235}U . The very high thermal fission cross section property of $^{242\text{m}}\text{Am}$ is attractive for energy production. Actinides ^{251}Cf and ^{249}Cf also have attractive fission cross section properties. The requirement for the reactor core to feasibly sustain a chain reaction is dependent upon a fuel's ability to produce extra neutrons from fission. The number of neutrons produced per neutron absorbed for $^{242\text{m}}\text{Am}$ is found to be superior to any other actinide. Conversely, η is less than unity for ^{241}Am , ^{238}Pu and ^{244}Cm . These isotopes cannot maintain criticality and are not adequate for satisfying deep space power or energy source requirements. Uranium-232 is also found to have only marginal values for η and is therefore not suited as an innovative energy source. High FF kinetic energies are desired for thrust and energy production. Particles captured by magnetic field lines should be highly energetic and have significant recoverable energy. Compared to baseline isotopes, $^{242\text{m}}\text{Am}$ and ^{243}Cm have the highest FF kinetic energy and recoverable energy release from thermal neutron induced nuclear fission. Charges in motion, the most fundamental definition of current, can be obtained using high ionic charges. Data indicate that higher charges are possible with $^{242\text{m}}\text{Am}$ and ^{243}Cm , slightly higher than what may be obtained from the baseline uranium and plutonium actinides. Curium is not found naturally and is produced from nuclear reactors through neutron capture reactions from plutonium or americium. The isotope ^{243}Cm has a relatively low half-life of 29 years and a medium grade specific activity of 52 Ci/g. In addition, ^{243}Cm produces significant amounts of prompt γ -ray radiation. For example, 6.92 MeV prompt γ -rays are emitted from ^{243}Cm , while 1.2 MeV prompt γ -rays are emitted from $^{242\text{m}}\text{Am}$. In addition, higher energy prompt neutrons are emitted from ^{243}Cm ; thus, ^{243}Cm should not be implemented as a majority fuel element in designing the reactor core.

The $^{242\text{m}}\text{Am}$ isomer exhibits one of the highest known thermal neutron fission cross sections. The thermal neutron cross section of $^{242\text{m}}\text{Am}$ is approximately 6000 barns. The $^{242\text{m}}\text{Am}$ thermal capture cross section is low relative to other actinides. In addition, the number of neutrons produced per fission is high compared to uranium, plutonium and other actinides. These properties, coupled with a half-life of 141 years, provide strong support for investigating novel uses of this isotope, including advanced deep space power and energy sources. The major disadvantage of $^{242\text{m}}\text{Am}$ is its availability. The world-wide production rate of $^{242\text{m}}\text{Am}$ is approximately 2.74 kg (6.04 lbs) per year. One reaction which creates $^{242\text{m}}\text{Am}$ arises from the plutonium decay from spent nuclear fuel in light water reactors

(LWR). Specifically, ^{242m}Am can be produced from ^{241}Pu . After ^{241}Am is created from decay of ^{241}Pu , the isomer ^{242m}Am can be produced from the neutron or radiative capture reaction $^{241}\text{Am}(n,\gamma)^{242m}\text{Am}$. Several methods to produce ^{242m}Am have been proposed in previous literature including particle accelerators and nuclear reactors. In order to maintain a viable deep space power program based on ^{242m}Am fuel, a production and manufacturing system must be executed. The set of higher actinides for implementation as a FFMCR fuel concept has been down-selected to three isotopes (^{242m}Am , ^{249}Cf and ^{251}Cf).

5. Energy System Design

The most critical component in examining the viability of the FFMCR concept design is the fuel element. The fuel element is a graphite fiber with a nano layer of fuel. The distance between fuel elements is 0.017 cm. The fuel layers are stacked on a fuel sub-assembly frame in a cylindrical assembly configuration. Neutron multiplicity is enhanced by using multiple layers of reflector material. The FFMCR design parameters are shown in Tables 5. The vacuum vessel, reflector layers and fuel assembly are shown in Fig. 2. The final whole-core 3-D reactor design is shown in Fig. 3. One unique feature of the FFMCR design is that both ends of the reactor core act as particle collectors, creating multiple points for propulsive force or power generation.

<i>Nuclear Reactor Core:</i>		
Outer Core Radius	414.5 cm	
Outer Core Length	740.0 cm	
Total Number of Fuel Assemblies	83	
Total Number of Sub-Assemblies	139440	
Total Number of Fuel Elements	1.39×10^{10}	
Total Fuel Loading	24 kg (approximately)	
<i>Fuel Assembly Design:</i>		
Geometry	Cylindrical	
Outer Fuel Assembly Length	140.0 cm	
Outer Fuel Assembly Radius	60.0 cm	
<i>Fuel Sub-Assembly Design:</i>		
Geometry	Rectangular Frame - Fuel Coated Fibers	
Outer Fuel Sub-Assembly Length		
Outer Sub-Assembly Width		20.0 cm
Outer Sub-Assembly Depth		5.0 cm
Number of Fuel Elements per Sub Assembly		1.0 cm
		1×10^5
<i>Fuel Element Design:</i>		
<i>Fuel Layer</i>	Fuel Coated Graphite Layer	
Fuel Thickness	100% (^{242m}Am) 0.0001 cm	
<i>Graphite Fiber</i>		
Radius	0.00015 cm	
Active Length	1.0 cm	
Burnable Absorber Doping	20.0 %	
Fuel Loading per Element	1.722×10^6 g	

Table 5. FFMCR core design components.

Multiple reflector regions have been added to provide room for expansion and potentially superconducting magnetic installation. The reflector region may be changed pending desired power level outputs and neutron confinement.

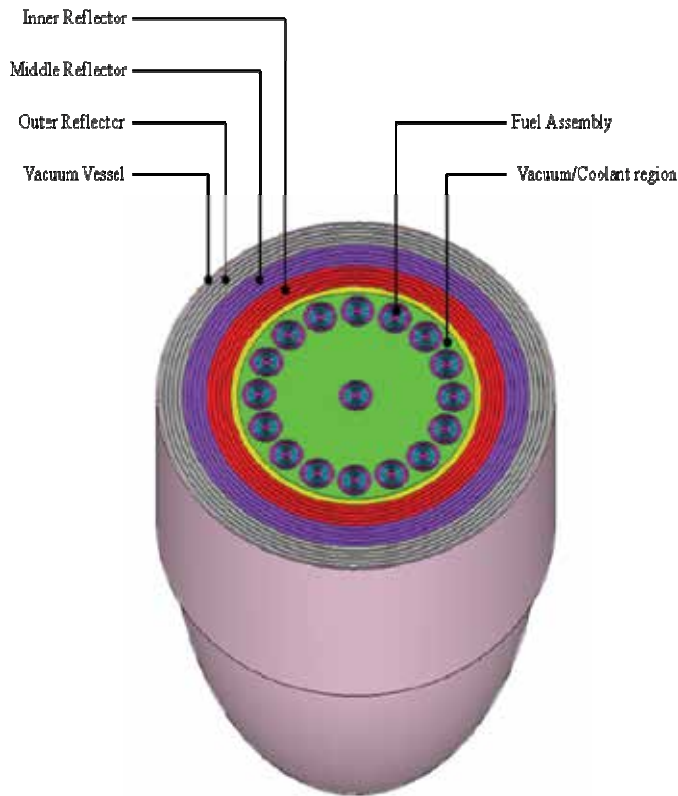
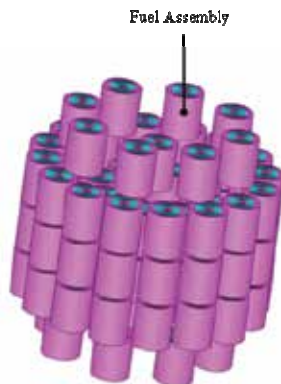


Fig. 2. Internal components of the FFMCR system.

Fuel lifetime can potentially be extended if burnable neutron absorbing additives are utilized to reduce beginning of life (BOL) excess reactivity of the fuel. In this case, a subsequent slow discharge during operation to compensate fuel depletion effects can be obtained.



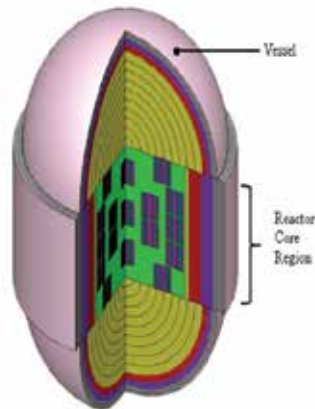


Fig. 3. Layout of the FFMCR system.

6. Deep Space Missions and the FFMCR with Advanced Actinide Fuels

Practical implementation of the FFMCR concept utilizing higher actinides may be accomplished using state-of-the-art material, nanotechnology, compact pulsed power, superconducting magnets and other COTS components. One example of how fission fragment particles can be deployed for propulsion is shown in Fig. 4.

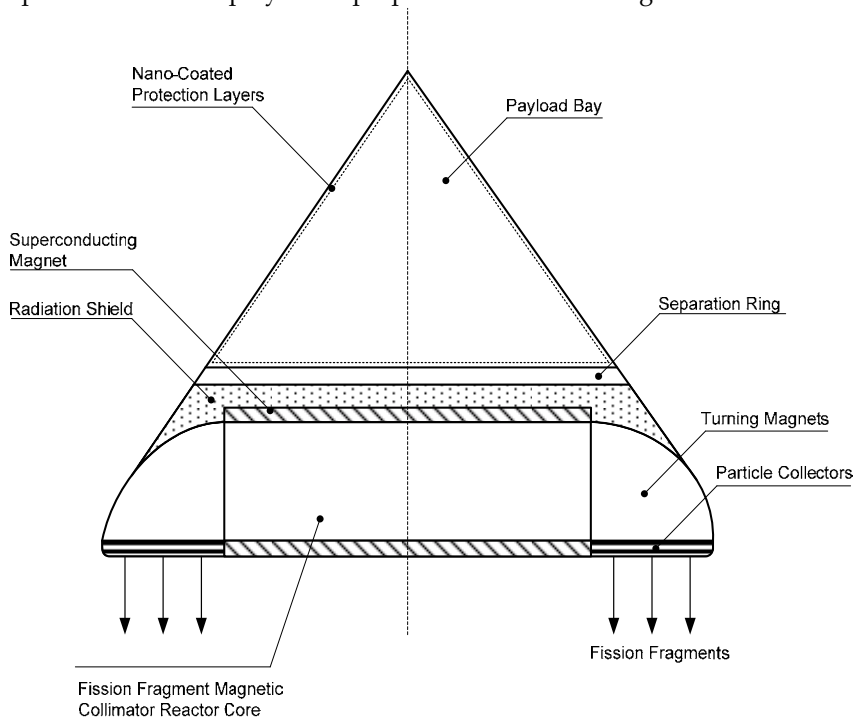


Fig. 4. Conceptual implementation of the FFMCR configuration.

In this concept, the FFMCR is oriented horizontally with high energy fission fragments born in the bottom of the vehicle. Ions created in the core are focused and collimated by magnetic field lines using superconducting magnets. Bidirectional ions are guided through 90° sector magnets toward exit collectors. High energy fission fragments are finally directed out the bottom of the spacecraft to create very high specific impulses at very high efficiency.

Radiation protection is accomplished using a thin layer of lightweight neutron, gamma and ion attenuation material. Deep space and interstellar mission scenarios may require separation of the payload bay from the entire FFMCR subsystem, which may be executed using a separation ring mechanism similar to existing spacecraft. Advanced light weight nano metamaterials may be applied to the outer cone region for extreme deep space protection from micrometeoroids.

It is acknowledged that the spacecraft concept proposed in Fig. 4 relies on multiple low technical readiness level (TRL) technologies, which increases developmental risks; however, the concept of using the fission fragment reactor for propulsion is demonstrated.

7. Conclusions

The MAGNUS concept, which is based on the FFMCR approach, offers space power and propulsion technology with a number of unique characteristics such as:

- Direct FF energy conversion is uniquely suitable for space operation;
- High efficiency DEC promises reduced thermal control and radiators;
- High specific impulse allows short trip times and extends exploration to the outer reaches of the solar system and beyond;
- Achievability of long-term operation assures power for missions within the solar system and for interstellar missions;
- Absence of chemical propellant and intermediate thermal energy conversion components allows minimization of weight;
- Low fuel inventory core without moving components assures inherent safety;
- Integral conversion and propulsion without moving components promises reliability;
- System modularity assures simplicity of integration with other components.

The meta-stable isomer ^{242m}Am , coated on graphite fibers, is found to have superior properties (relative to uranium and plutonium baseline isotopes), which when combined with magnetic collimation may provide a novel solution in high-reliability demanding environments. Key advantages of using ^{242m}Am are summarized below.

- ^{242m}Am has a half-life of 141 years (applicable to most mission profile requirements).
- ^{242m}Am has a low specific activity of 9.8 Ci/g (for improved radiological safety) and low specific power of 0.002 W/g (for practical material integration).
- The ^{242m}Am actinide has one of the highest known thermal fission cross sections and produces a high neutron yield per neutron absorbed.
- The fission fragment kinetic energy of ^{242m}Am is approximately 10-15 MeV above baseline uranium and plutonium fragments.
- Prompt neutron and γ -ray emission is lowest for ^{242m}Am , potentially adding addition safety margins relative to uranium or plutonium.
- Heavy ion fragments appear to be controllable using voltages greater than 5 MV.

- A 1-2 micron thick ^{242m}Am fuel layer allows most fission fragments to escape for magnetic focusing.
- Three-dimensional Monte Carlo analysis of baseline and higher actinides indicates that, given the FFMCR configuration in this work, criticality can be achieved using ^{242m}Am , ^{249}Cf , and ^{251}Cf . System criticality is not achievable for ^{235}U , ^{239}Pu or ^{241}Pu .
- Burnable absorbers can be mixed with higher actinides to reduce criticality at high fuel loadings, with the largest effect due to ^{135}Xe and ^{157}Gd .
- Limited production and availability of ^{242m}Am reduces its potential as a fuel for power and propulsion; however, it is recognized that select plutonium isotopes suffer from similar production and availability limitations.

Americium-242m is clearly established as a promising fuel for reliability-demanding applications, and ^{249}Cf and ^{251}Cf isotopes appear to hold similar promising properties such as high neutron yield, low specific activities, large fission fragment masses and applicable radioactive half-life. Recommendations for future work include:

- Detailed analysis of higher actinide fuels such as ^{249}Cf and ^{251}Cf to quantify potential benefits when used in propulsion or power applications.
- Proof-of-principle experimental nanofabrication of ^{242m}Am , ^{249}Cf and ^{251}Cf fuels to examine commercialization and implementation viability.
- Studies to demonstrate experimental systems integration utilizing pulsed power, magnets and heavy ion beam focusing should be initiated or continued.

The MAGNUS concept for space applications is an innovative approach that allows direct conversion of fission energy to electricity and thrust. It is anticipated that these systems should allow the achievement of high efficiencies with a minimum of energy wasted as heat. The terrestrial application analysis indicated that direct energy conversion efficiencies up to 90% are potentially achievable.

Absence of high temperatures and pressures, low fuel inventory, long-term operation, absence of chemical propellant, highly efficient power generation, high specific impulse, and integral direct energy conversion without mechanical components provide an opportunity for exploration of the solar system and deep space. Interstellar missions of reasonable duration may be possible.

In comparison with conventional thermal energy converters, the needs for thermal control and radiators are expected to be minimal in the MAGNUS units. The absence of intermediate conversion stages provides the potential for significant design simplifications. Given the theoretically more straightforward design of a direct conversion reactor, it is conceivable that safety system design will also be more straightforward. Furthermore, since the MAGNUS concept eliminates the need for chemical propellants, significant improvements in weight, volume, and specific impulse performance are anticipated over conventional chemical systems and nuclear thermal converters.

To assure fast development and to mitigate needs for scientific breakthroughs in the relevant fields of materials research, nuclear technologies, and electromagnetic technologies, the MAGNUS concept must be founded on and evolve from existing technologies and materials.

8. Nomenclature

ASRG	Advanced Stirling Radioisotope Generator
AU	Astronomical Unit
BOM	Beginning of Mission
COTS	Commercial Off The Shelf
DEC	Direct Energy Conversion
DFFEC	Direct Fission Fragment Energy Conversion
DOE	Department of Energy
ENDF	Evaluated Nuclear Data Files
EOM	End of Mission
FF	Fission Fragment
FFDEC	Fission Fragment Direct Energy Conversion
FFMCR	Fission Fragment Magnetic Collimator Reactor
JANIS	Java-based Nuclear Information Software
JIMO	Jupiter Icy Moons Orbiter
LWR	Light Water Reactor
MAGNUS	MAGnetic NUclear System
NASA	National Aeronautics and Space Administration
NDDEC	Nuclear Driven Direct Energy Conversion
NEP	Nuclear Electric Propulsion
NERI	Nuclear Energy Research Initiative
NERVA	Nuclear Engine for Rocket Vehicle Application
NTP	Nuclear Thermal Propulsion
RTG	Radioisotope Thermoelectric Generator
SCALE	Standardized Computer Analysis for Licensing Evaluation
SNAP	Systems for Nuclear Auxiliary Power
SRIM	Stopping and Range of Ions in Matter
STK	Satellite Tool Kit
TFE	Thermionic Fuel Elements
TRL	Technology Readiness Level

9. References

- Abelson, R. (2005). Expanding Frontiers with Standard Radioisotope Power Systems, JPL/CALTECH, JPL D-28902, NASA Jet Propulsion Laboratory, Pasadena, California.
- Bennett, J. (2002). *The Cosmic Perspective*, Addison-Wesley, San Francisco, California.
- Borowski, S. (1987). Comparison of Fusion/Antiproton Propulsion Systems for Interplanetary Travel, NASA/TM 107030, Lewis Research Center, Cleveland, Ohio.
- Chan, J. (2007). Development of Advanced Stirling Radioisotope Generator for Space Exploration, NASA/TM-2007-214806, NASA Glenn Research Center, Cleveland, Ohio.
- Chapline, G.; Dickson, P. & Schtzler, B. (1988). Fission Fragment Rockets - a Potential Breakthrough, EGG-M-88285, Lawrence Livermore National Laboratory, California (1988).

- Danchik, R. (1998). An Overview of Transit Development, *Johns Hopkins APL Technical Digest*, 19, 18-25.
- Durham, F. (1991). Review of the Los Alamos Effort in the Development of Nuclear Rocket Propulsion, LA-UR-91-2295, AIAA/NASA Conference on Advanced SEI Technologies, Cleveland, Ohio.
- El-Genk, M. (2009). Deployment History and Design Considerations for Space Reactor Power Systems, *Acta Astronautica*, 64, 833-850.
- El-Wakil, M. (1992). *Nuclear Energy Conversion*, American Nuclear Society, LaGrange Park, Illinois.
- Fix, J. (2001). *Astronomy: Journey to the Cosmic Frontier*, McGraw-Hill, Boston, Massachusetts.
- Gunn, S. (2001). Nuclear Propulsion – A Historical Perspective, *Space Policy*, 17, 291-300.
- Johnson, R. (1967). Design, Ground Test and Flight Test of SNAP-10A First Reactor in Space, *Atomics International, Nuclear Engineering and Design*, 5, 7-21.
- Kirkpatrick, R. (2002). Magnetized Target Fusion and Fusion Propulsion, *Proceedings of Space Technology and Applications International Forum-STAIIF*, American Institute of Physics, Albuquerque, New Mexico.
- Kusnierkiewicz, D. (2005). A Description of the Pluto-bound New Horizons Spacecraft, *Acta Astronautica*, 57, 136-137.
- Lamarsh, J. (2001). *Introduction to Nuclear Engineering*, Prentice-Hall, Upper Saddle River, New Jersey.
- Lawrence, T. (2005). Nuclear Thermal Rocket Propulsion Systems, IAA White Paper, International Academy of Aeronautics, Paris, France.
- Liou, L. (2008). Advanced Chemical Propulsion for Science Missions, NASA/TM-2008-215069, Glenn Research Center, Cleveland, Ohio.
- Marshall, A. (2008). *Space Nuclear Safety*, Krieger Publishing Company, Malabar, Florida.
- NASA (2008). Fission Surface Power System Technology for NASA Exploration Missions, <http://www.ne.doe.gov>.
- Ronen, Y. & Shwageraus, E. (2000). Ultra-thin ^{242m}Am Fuel Elements in Nuclear Reactors, *Nuclear Instruments and Methods in Physics Research A*, 455, 442-450.
- Safonov, G. (1957). Direct Conversion of Fission to Electric Energy in Low Temperature Reactors, RM-1870, Science and Technology Program, RAND Corporation, Santa Monica, California.
- Schmitz, P. (2005). Feasibility Study of a Nuclear-Stirling Power Plant for the Jupiter Icy Moons Orbiter, *Proceedings of Space Technology and Applications International Forum – STAIIF*, American Institute of Physics, Albuquerque, New Mexico.
- Tsvetkov, P. (2002). Direct Fission Fragment Energy Conversion Utilizing Magnetic Collimation, *Ph.D. Dissertation*, Texas A&M University, College Station, Texas.
- Tsvetkov, P.; Hart, R.; King, D. & Parish, T. (2006). Planetary Surface Power and Interstellar Propulsion Using Fission Fragment Magnetic Collimator Reactor, *Proceedings of Space Technology and Applications Forum-STAIIF*, American Institute of Physics, Albuquerque, New Mexico, 813, 803-812.
- Tsvetkov, P.; Hart, R. & Parish, T. (2003). Highly Efficient Power System Based on Direct Fission Fragment Energy Conversion Utilizing Magnetic Collimation, *Proceedings of the 11th International Conference on Nuclear Engineering (ICONE 11)*, Tokyo, Japan.

Construction, Decommissioning, and Replacement of Nuclear Power Plants under Uncertainty

Ryuta Takashima

Department of Risk Science in Finance and Management, Chiba Institute of Technology

1. Introduction

Currently, there exist 54 commercial nuclear power plants, which have a total capacity of 48.85 GW, in Japan. These power plants that have been operating for more than 40 years emerge in 2010 and onward. The framework for the nuclear energy policy describes the measures to be followed for aging nuclear power plants and the enhancement of safety under the assumption of a nuclear power plant operating for 60 years (AEC, 2006). The Tokai Nuclear Power Plant of the Japan Atomic Power Company, and units 1 and 2 of the Hamaoka Nuclear Power Plant of the Chubu Electric Power Company are currently under decommissioning, and this decommissioning can be decided at the discretion of the electric power supplier. In the future, it is also likely that the firm will determine the decommissioning of aging nuclear power plants, taking into account the economics of the plant. Moreover, it is necessary to make decisions not only regarding decommissioning but also regarding the replacement. In this context, although decommissioning and replacement as well as new construction have become important problems, there exist many factors that need to be solved, such as large costs, electricity demand, that is, profit of electric power selling and electricity deregulation.

Deregulation of electricity markets has occurred in several countries, including the United Kingdom, the United States, Nordic countries, and Japan. In the deregulated market, the electricity price is determined by supply and demand, rather than by the cost of generating electricity. Because of the electricity price uncertainty, market deregulation could introduce a new type of risk for power companies. Investment in power plants is planned based on long-term demand forecasts, and it becomes difficult to plan schedules for constructing plants based on only the demand forecast because there is no guarantee of cost recovery. In addition, since the replacement of nuclear power plants requires a great amount of capital investment, a proper method is necessary for valuation and decision making regarding projects considering uncertainty in the electricity price.

For one of economic analysis methods for investment projects under uncertainty, real options analysis has recently attracted growing attention (Dixit and Pindyck, 1994; Trigeorgis, 1996). Using this approach, the investment and operation of power plants has been studied by several research groups. Especially, several studies have examined various investment problems involving nuclear power plants (Gollier et al., 2005; Naito et al., 2010; Pindyck, 1993; Rothwell, 2006; Takashima et al., 2007; Takizawa et al., 2001).

In this chapter, we focus on real options models for analyzing construction, decommissioning, and replacement problems of nuclear power plants under electricity price uncertainty. The models of construction and decommissioning problems are basic models, and in real options studies, correspond to investment option and abandonment option, respectively. The model of replacement problem is an extended model, which combines construction and decommissioning options (Naito et al., 2010). For three models, we show how uncertainty and cost affect decisions of construction, decommissioning, and replacement.

The remainder of this chapter is organized as follows. In Section 2, we describe the model for analyzing construction, decommissioning, and replacement of nuclear power plants. Section 3 derives the solution by numerical calculations and provides some results of numerical analysis. Finally, Section 5 concludes the chapter.

2. The Model

In this section we describe the setting and the assumption of the model, and then derive economic evaluation models for construction, decommissioning, and replacement of nuclear power plants.

2.1 Model setup

The risk factor and uncertainty in the investment of nuclear power plants include construction cost, fuel cost, electricity price, decommissioning cost, litigation, unplanned shutdown, and regulatory change. In this chapter, we consider the model in which uncertainties with respect to profitability are reflected in the electricity prices, and other risks are reflected in a discount rate.

Suppose that the firm is a price taker, and, its actions have no influence on the dynamics of the electricity price. Thus, for a straightforward description of uncertainty, we assume that the electricity price follows the geometric Brownian motion:

$$dP_t = \mu P_t dt + \sigma P_t dW_t, \quad P_0 = p, \quad (1)$$

where μ is the instantaneous expected growth rate of P_t , and σ is the instantaneous volatility of P_t . W_t is a standard Brownian motion. The capacity factor, taking into account a decreasing due to the aging, is assumed to be expressed by the following equation:

$$\alpha_t = \alpha_0 e^{-\delta t}, \quad (2)$$

where δ is the decreasing rate. From these equations, the profit flow function of a nuclear power plant can be represented as follows:

$$\begin{aligned} \pi_t &\equiv \pi(P_t; \delta, C) = \alpha_t P_t - C, \\ &= \alpha_0 e^{-\delta t} P_t - C, \end{aligned} \quad (3)$$

where C is the operating cost that is composed of the fuel cost as well as operating and maintenance costs. To obtain the analytical solution, let us change the variable $P_t e^{-\delta t}$ to X_t :

$$X_t := P_t e^{-\delta t}. \quad (4)$$

Then, from Eqs. (1) and (4), the dynamics of X_t can be written as

$$dX_t = (\mu - \delta) X_t dt + \sigma X_t dW_t. \quad (5)$$

In this model, we consider this variable, X_t , as a state variable.

2.2 Construction option

In this section, we describe the model of Gollier et al. (2005) that extends the model of McDonald and Siegel (1986) deriving the investment timing and its option value by introducing fixed construction time and project lifetime. The firm starts operating a nuclear power plant by incurring investment cost I . The value of the investment opportunity is:

$$F(x) \equiv \sup_{\tau \in \mathcal{V}_i} \mathbb{E}_x \left[\int_{\tau+T}^{\tau+T+L} e^{-\rho t} \pi_t dt - e^{-\rho \tau} I \right], \quad (6)$$

where \mathbb{E}_x is expectation with respect to the probability law of X_t given an initial value x , τ is the investment time, \mathcal{V} is the set of stopping times of the filtration generated by the dynamics of X_t , and $\rho > 0$ is an arbitrary discount rate. We must have $\rho > \mu$ in order to ensure that the firm's value is finite for $L \rightarrow \infty$. Given the investment threshold, X^* , the optimal investment time, τ^* , has the following form:

$$\tau^* = \inf \{t \geq 0 \mid X_t \geq X^*\}. \quad (7)$$

Prior to determining X^* and $F(x)$, we calculate the now-or-never expected NPV, $V(x)$, of a nuclear power plant.

$$\begin{aligned} V(x) &= \mathbb{E}_x \left[\int_T^{T+L} e^{-\rho t} (\alpha_0 X_t - C) dt - I \right] = \int_T^{T+L} e^{-\rho t} \alpha_0 \mathbb{E}_x[X_t] - C dt - I \\ &= \int_T^{T+L} e^{-\rho t} \alpha_0 x e^{(\mu-\delta)t} - C dt - I = A_1 \frac{\alpha_0 x}{\rho - \mu + \delta} - A_2 \frac{C}{\rho} - I \end{aligned} \quad (8)$$

where $A_1 = e^{-(\rho-\mu+\delta)T} (1 - e^{-(\rho-\mu+\delta)L})$ and $A_2 = e^{-\rho T} (1 - e^{-\rho L})$. The following differential equation, which is satisfied by the investment value, is derived from the Bellman equation (See, for example, (Dixit and Pindyck, 1994)),

$$\frac{1}{2} \sigma x^2 F''(x) + (\mu - \delta) x F'(x) - \rho F(x) = 0, \quad (9)$$

where the primes denote derivatives, that is, $F'(x) = \frac{dF(x)}{dx}$ and $F''(x) = \frac{d^2F(x)}{dx^2}$. The investment value must satisfy the following boundary conditions:

$$F(0) = 0, \quad (10)$$

$$F(X^*) = V(X^*), \quad (11)$$

$$F'(X^*) = V'(X^*). \quad (12)$$

Condition (10) requires that the investment option becomes zero if the cash flow is close to zero. Conditions (11) and (12) are the value-matching and smooth-pasting conditions, respectively. The value-matching condition means that when the level of X_t is X^* , the firm exercises the construction option, and then can obtain the net value of $V(X^*)$. Additionally, the smooth-pasting condition means that if the construction at X^* is indeed optimal, the differentiation of the value function must be continuous at X_t . From these conditions, we can obtain the investment value as follows,

$$F(x) = \left(\frac{x}{X^*} \right)^{\beta_1} V(X^*), \quad (13)$$

where β_1 is the positive root of the characteristic equation $\frac{1}{2}\sigma^2\beta(\beta - 1) + (\mu - \delta)\beta - \rho = 0$, that is,

$$\beta_1 = \frac{1}{2} - \frac{\mu - \delta}{\sigma^2} + \sqrt{\left(\frac{\mu - \delta}{\sigma^2} - \frac{1}{2}\right)^2 + \frac{2\rho}{\sigma^2}} > 1. \quad (14)$$

The investment threshold is given by,

$$X^* = \frac{\beta_1}{\beta_1 - 1} \frac{\rho - \mu + \delta}{A_1\alpha_0} \left(\frac{A_2C}{\rho} + I \right) \quad (15)$$

By contrast, the now-or-never investment threshold is $X_{npv} = \frac{\rho - \mu + \delta}{A_1\alpha_0} \left(\frac{A_2C}{\rho} + I \right) < X^*$, i.e., having the deferral option provides a value to waiting, which then increases the opportunity cost of investing.

2.3 Decommissioning option

We consider that a firm operates a nuclear power plant over few decades, and has the option of decommissioning. The value of the decommissioning project is:

$$F_d(x) \equiv \sup_{\tau_d \in \mathcal{V}_d} \mathbb{E}_x \left[\int_0^{\tau_d} e^{-\rho t} \pi_t dt - e^{-\rho \tau} U \right], \quad (16)$$

where τ_d is the decommissioning time, \mathcal{V}_d is the set of admissible stopping times, and U is the decommissioning cost. Given the decommissioning threshold, X_d , the optimal decommissioning time, τ_d^* , has the following form:

$$\tau_d^* = \inf \{ t \geq 0 \mid X_t \leq X_d^* \}. \quad (17)$$

The following differential equation, which is satisfied by the project value of the decommissioning, is derived from the Bellman equation,

$$\frac{1}{2}\sigma x^2 F_d''(x) + (\mu - \delta)x F_d'(x) - \rho F_d(x) + \alpha_0 x - C = 0. \quad (18)$$

The general solutions of this equation are given as follows:

$$F_d(x) = B_1 x^{\beta_1} + B_2 x^{\beta_2} + \frac{\alpha_0 x}{\rho - \mu + \delta} - \frac{C}{\rho}, \quad (19)$$

where B_1 and B_2 are unknown constants, and β_2 is the negative root of the characteristic equation $\frac{1}{2}\sigma^2\beta(\beta - 1) + (\mu - \delta)\beta - \rho = 0$, that is,

$$\beta_2 = \frac{1}{2} - \frac{\mu - \delta}{\sigma^2} - \sqrt{\left(\frac{\mu - \delta}{\sigma^2} - \frac{1}{2}\right)^2 + \frac{2\rho}{\sigma^2}} < 0. \quad (20)$$

The decommissioning project value must satisfy the following boundary conditions:

$$\lim_{x \rightarrow \infty} (B_1 x^{\beta_1} + B_2 x^{\beta_2}) = 0, \quad (21)$$

$$F_d(X_d) = -U, \quad (22)$$

$$F_d'(X_d) = 0. \quad (23)$$

Condition (21) requires that the decommissioning option becomes zero if the cash flow is very large. Therefore, from this condition, we have $B_1 = 0$. Conditions (22) and (23) are the value-matching and smooth-pasting conditions, respectively. From these conditions, we can obtain the decommissioning project value as follows,

$$F_d(x) = \frac{\alpha_0 x}{\rho - \mu + \delta} - \frac{C}{\rho} - \left(\frac{\alpha_0 X_d}{\rho - \mu + \delta} - \frac{C}{\rho} + U \right) \left(\frac{x}{X_d} \right)^{\beta_2}. \quad (24)$$

The decommissioning threshold is given by,

$$X_d = \frac{\beta_2}{\beta_2 - 1} \frac{\rho - \mu + \delta}{\alpha_0} \left(\frac{C}{\rho} - U \right). \quad (25)$$

Likewise, the now-or-never decommissioning threshold is $X_{d,npv} = \frac{\rho - \mu + \delta}{\alpha_0} \left(\frac{C}{\rho} - U \right) > X_d$, i.e., having the deferral option provides a value to waiting, which then increases the opportunity cost of decommissioning.

2.4 Replacement option

In this section, following Naito et al. (2010), we consider the valuation of a replacement project of nuclear power plants. The replacement project consists of two components: the decision to decommission an existing plant and the decision to construct a new plant.

The variable cost and the capacity factor of the existing plant are C^0 and α_0^0 , respectively, and the variable cost and the capacity factor of the new plant are C^1 and α_0^1 , respectively. We assume that the replacement leads to a decrease in the variable cost and an increase in the capacity factor, i.e., $C^0 \geq C^1$ and $\alpha_0^0 \leq \alpha_0^1$.

The value of the replacement project is:

$$\begin{aligned} F_r(x) &\equiv \sup_{\tau_r, \tau_i \in \mathcal{V}_r} \mathbb{E}_x \left[\int_0^{\tau_r} e^{-\rho t} \pi_t^0 dt - e^{-\rho \tau_r} U + \int_{\tau_i}^{\tau_i + L + T} e^{-\rho t} \pi_t^1 dt - e^{-\rho \tau_i} I \right], \\ &= \sup_{\tau_r, \tau_i} \mathbb{E} \left[\int_0^{\tau_r} e^{-\rho t} \pi_t^0 dt + e^{-\rho \tau_r} (F_i(X_{\tau_r}) - U) \right], \end{aligned} \quad (26)$$

where $\pi_t^0 = \alpha_0^0 X_t - C^0$, $\pi_t^1 = \alpha_0^1 X_t - C^1$, and the value of the construction project for the new plant is:

$$F_i(x) = \sup_{\tau_i} \mathbb{E} \left[\int_{s+\tau_i+T}^{s+\tau_i+T+L} e^{-\rho(t-s)} \pi_t dt - e^{-\rho(\tau_i-s)} I \right]. \quad (27)$$

In addition, τ_r is the decommissioning time of the existing plant, τ_i is the construction time of the new plant, and \mathcal{V}_r is the set of the pair of admissible decommissioning and construction times. Given the decommissioning threshold for the existing plant, X_r , the optimal decommissioning time, τ_r^* , has the following form:

$$\tau_r^* = \inf \{ t \geq 0 \mid X_t \leq X_r \}. \quad (28)$$

Likewise, given the construction threshold for the new plant, X_i , the optimal decommissioning time, τ_i^* , has the following form:

$$\tau_i^* = \inf \{ t \geq 0 \mid X_t \geq X_i \}. \quad (29)$$

The replacement option is the sequential one of decommissioning and construction. Therefore, we can solve the investment problem by working backward, i.e., by first finding the value of the construction project and then finding the value of the decommissioning project. Likewise equation (6), the value of the construction project for the new plant is:

$$F_i(x) = \left(A_1 \frac{\alpha_1 X_i}{\rho - \mu + \delta} - A_2 \frac{C_1}{\rho} - I \right) \left(\frac{x}{X_i} \right)^{\beta_1}, \quad (30)$$

where

$$X_i^* = \frac{\beta_1}{\beta_1 - 1} \frac{\rho - \mu + \delta}{A_1 \alpha_1} \left(\frac{A_2 C_1}{\rho} + I \right). \quad (31)$$

By using the value of the construction project, we can obtain the decommissioning threshold for the existing plant and the value of the replacement project. The following differential equation, which is satisfied by the project value of the replacement project, is derived from the Bellman equation,

$$\frac{1}{2} \sigma x^2 F_r''(x) + (\mu - \delta) x F_r'(x) - \rho F_r(x) + \alpha_0 x - C_0 = 0. \quad (32)$$

The general solutions of this equation are given as follows:

$$F_r(x) = B_3 x^{\beta_1} + B_4 x^{\beta_2} + \frac{\alpha_0 x}{\rho - \mu + \delta} - \frac{C_0}{\rho}, \quad (33)$$

where B_3 and B_4 are unknown constants. The replacement project value must satisfy the following boundary conditions:

$$\lim_{x \rightarrow \infty} (B_3 x^{\beta_1} + B_4 x^{\beta_2}) = 0, \quad (34)$$

$$F_r(X_r) = F_i(X_r) - U, \quad (35)$$

$$F_r'(X_r) = F_i'(X_r^*). \quad (36)$$

Condition (34) requires that the decommissioning option becomes zero if the cash flow is very large. Therefore, from this condition, we have $B_3 = 0$. Conditions (35) and (36) are the value-matching and smooth-pasting conditions, respectively. From these conditions, we can obtain the replacement project value as follows,

$$F_r(x) = \frac{\alpha_0 x}{\rho - \mu + \delta} - \frac{C_0}{\rho} - \left(\frac{\alpha_0 X_r}{\rho - \mu + \delta} - \frac{C_0}{\rho} + U - F_i(X_r) \right) \left(\frac{x}{X_r} \right)^{\beta_2}. \quad (37)$$

We can be solved for X_r by means of a numerical calculation method.

3. Results and Discussion

As shown in tables 1 and 2, we use the following parameter values of regarding the economics conditions and nuclear power plant for our numerical examples. Although we assume a base value of $\sigma = 0.2$, allow it to vary in order to perform sensitivity analyses.

Expected growth rate of P_t	μ	0.01
Volatility of P_t	σ	0–0.5
Discount rate	ρ	0.05
Initial electricity price (yen/kWh)	x	8.0

Table 1. Parameters with respect to economics conditions

Capacity factor for the existing plant	a_0^0	0.6
Capacity factor for the new plant	a_0^1	1.0
Decreasing rate of capacity factor	δ	0.02
Variable cost for the existing plant (yen/kWh)	C^0	5.0
Variable cost for the new plant (yen/kWh)	C^1	3.0
Construction cost (yen/kW)	I	400,000
Decommissioning cost (yen/kW)	U	30,000
Decommissioning cost (yen/kW) (Replacement)	U	40,000

Table 2. Parameters with respect to nuclear power plant

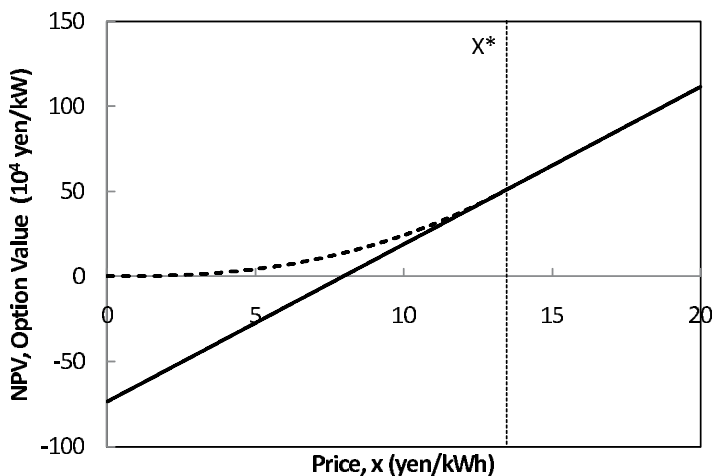


Fig. 1. Expected NPV and investment options ($\sigma = 0.2$). The threshold prices for construction is 13.256 yen/kWh. For Expected NPV, the construction threshold is 7.954 yen/kWh.

3.1 Construction option

In this section we show numerical examples of the model for construction option that is described in section 2.2.

At the initial electricity price, x , the expected NPV is 0.428×10^4 yen/kW. On the other hand, since the option value is 13.895×10^4 yen/kW, it is optimal to wait to invest in construction (see Figure 1). As shown in Figure 1, at more than the initial electricity price of 13.256 yen/kWh, it is better to construct rather than to wait now.

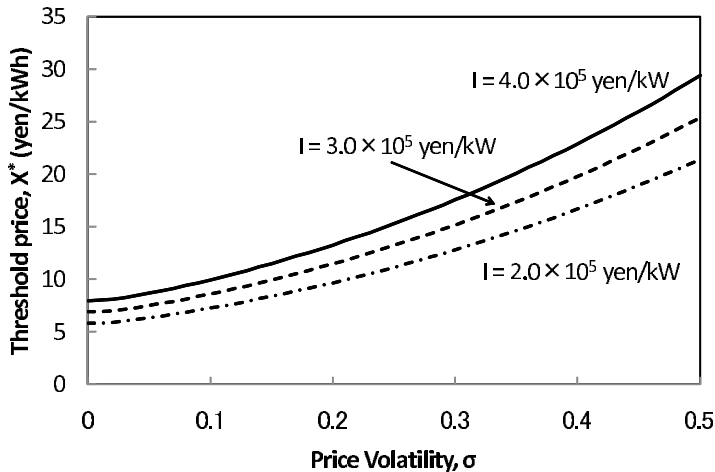


Fig. 2. Effect of uncertainty on the investment threshold

In general real options framework, as uncertainty increases, the value of waiting also goes up. Indeed, a more volatile electricity price increases the opportunity cost of immediate action. Consequently, although the option value of the entire investment opportunity increases, the cost of killing the deferral option also increases, thereby making it optimal to delay investment. For example, if the degree of uncertainty, that is, volatility increases from 0.2 to 0.3, then the investment threshold increases from 13.256 yen/kWh to 17.542 yen/kWh (see Figure 2).

In order to increase the competitiveness of nuclear power, it is effective to decrease the construction cost (OECD, 2000). Consequently, we analyze the effect of construction cost on the investment threshold. It can be seen from Figure 2 that as the construction decreases from 4.0×10^5 yen/kW to 3.0×10^5 yen/kW and 2.0×10^5 yen/kW, the investment threshold decreases, and consequently, the opportunity of investment increases. As volatility increases, the degree of the increase in the investment opportunity increases further. Therefore, it is found that when uncertainty is large, the effect of the decrease in construction cost on the investment decision.

Furthermore, likewise the investment threshold, the investment project value have a large influence on uncertainty. Figure 3 shows the effect of volatility on the investment project value at the initial electricity price. It is found that as volatility increases, the investment project value becomes large. This is because when volatility is large, the postponement of the investment is selected, and consequently, the probability of the investment at larger level of electricity price increases.

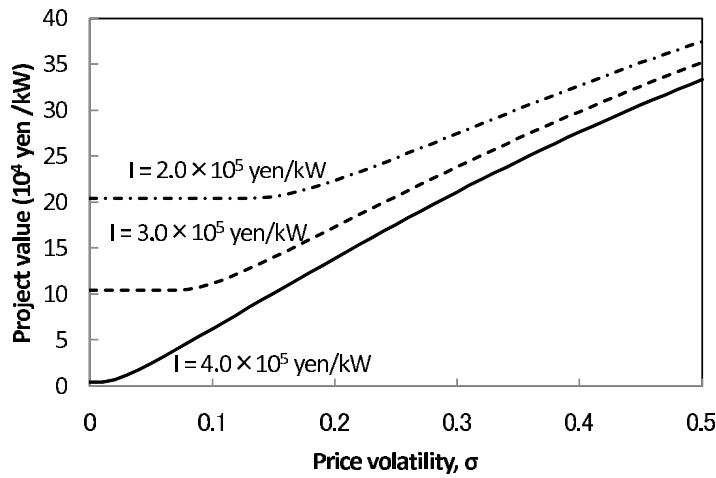


Fig. 3. Effect of uncertainty on the investment value

As the construction decreases from 4.0×10^5 yen/kW to 3.0×10^5 yen/kW and 2.0×10^5 yen/kW, the investment project value increases. Unlike the threshold, as volatility is large, the effect of decrease in construction cost becomes small.

3.2 Decommissioning option

In this section we show numerical examples of the model for decommissioning option that is described in section 2.3.

At the initial electricity price, x , the expected NPV is -1.752×10^5 yen/kW. On the other hand, since the value of decommissioning option is 8.012×10^4 yen/kW, it is optimal to wait to invest in construction (see Figure 4). It can be seen from Figure 4 that at less than the initial electricity price of 4.772 yen/kWh, it is better to decommission rather than to wait now.

$U(10^4$ yen/kW)	Price volatility, σ					
	0	0.1	0.2	0.3	0.4	0.5
1.0	9.886	6.591	4.943	3.735	2.863	2.232
2.0	9.772	6.514	4.886	3.692	2.830	2.206
4.0	9.543	6.362	4.772	3.606	2.764	2.155

Table 3. Effect of uncertainty on the decommissioning threshold

As shown in Table 3, as volatility is large, the threshold of decommissioning decreases. Thus, likewise the construction option, as uncertainty becomes large, the probability for the postponement of decommissioning increases. In Table 3 the effect of decrease in decommissioning cost on the threshold is shown. For example, for $\sigma = 0.2$, if the decommissioning cost decreases from 4.0×10^4 yen/kW to 1.0×10^4 yen/kW, then the decommissioning threshold increases from 4.772 yen/kWh to 4.943 yen/kWh, and consequently, the probability of decommissioning increases. We also show the effect of uncertainty on the increase in the decom-

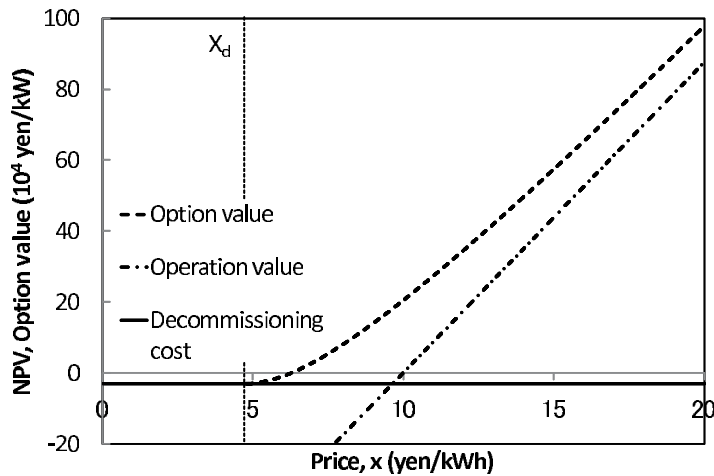


Fig. 4. Expected NPV and decommissioning options ($\sigma = 0.2$). The threshold prices for decommissioning is 4.772 yen/kWh. For Expected NPV, the decommissioning threshold is 9.543 yen/kWh.

missioning opportunity due to decreasing the decommissioning cost. Unlike the construction option as uncertainty is large, the degree of the increase in the probability of decommissioning becomes small.

Figure 5 shows the effect of uncertainty on the value of decommissioning project. Likewise the construction option, the project value increases with volatility. This is because when volatility becomes large, the postponement of decommissioning is selected, and consequently, the probability of decommissioning at smaller level of electricity price increases. Additionally, we also analyze the effect of the decrease in decommissioning cost on the project value. It is clear from Figure 5 that as decommissioning cost decreases, the project value increases.

3.3 Replacement option

In previous section, the decommissioning for existing plant is analyzed. However if the replacement project is evaluated, it is necessary to consider not only the decommissioning for existing plant but also the construction for new plant. Therefore, in this section, we show numerical examples of the model for replacement option that is described in section 2.4.

As described above, at the initial electricity price, x , the expected NPV for decommissioning project is -1.752×10^5 yen/kW. On the other hand, since the option value taking into account replacement is 9.895×10^4 yen/kW, it is optimal to wait to invest in construction (see Figure 6). The value of replacement option is larger than that of decommissioning option, 8.012×10^4 yen/kW, and consequently, it is found that the construction investment for new plant influences the value of decommissioning project. As shown in Figure 6, at less than the initial electricity price of $X_r = 6.298$ yen/kWh, it is appropriate to decommission, and after decommissioning, when the level of electricity price is more than $X_i = 13.256$ yen/kWh, it is appropriate to construct the new plant.

The effect of uncertainty on the thresholds are presented in Figure 7. The solid line denotes threshold in replacement option model, and the dotted and the dashed lines represent the

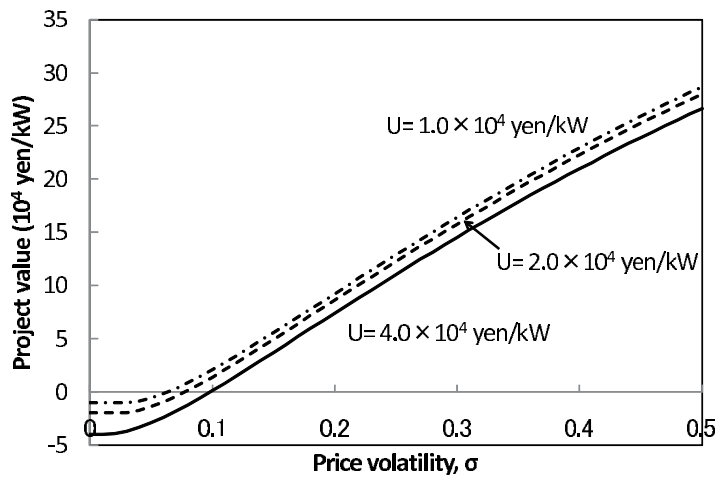


Fig. 5. Effect of uncertainty on the value of decommissioning project

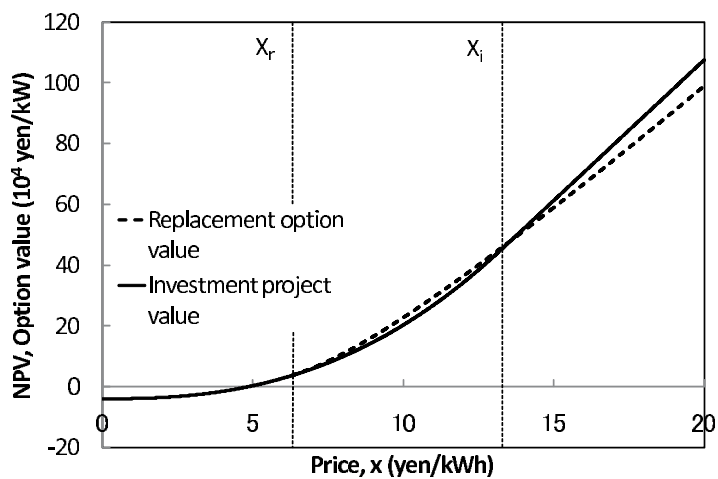


Fig. 6. Value of the replacement project ($\sigma = 0.2$). The threshold prices for replacement, X_r , is 6.298 yen/kWh. The construction threshold is 13.256 yen/kWh.

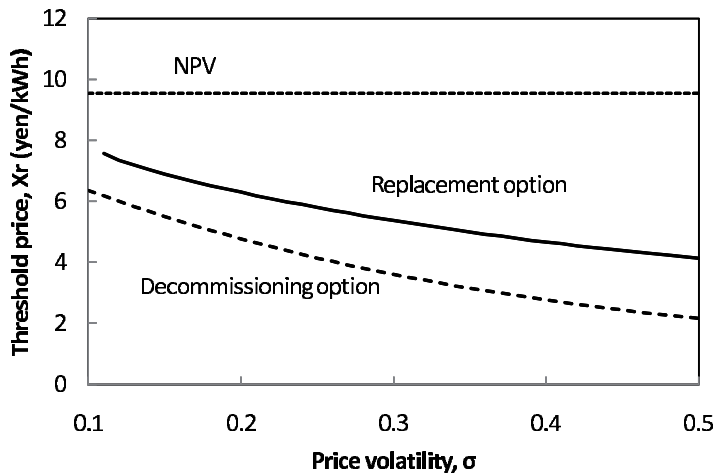


Fig. 7. Comparison of thresholds for expected NPV, decommissioning option, and replacement option ($U = 40,000$ yen/kW)

thresholds for the expected NPV and the decommissioning option model, respectively. The threshold for expected NPV is larger than those for the replacement option and the decommissioning option, and furthermore, the threshold for the replacement option is larger than that for the decommissioning option. This means that the decommissioning decision of the existing plant should stochastically be made earlier if the firm takes into account the replacement of the new plant.

Table 4. Effect of uncertainty on the replacement threshold

$U(10^4$ yen/kW)	Price volatility, σ			
	0.2	0.3	0.4	0.5
1.0	6.775	5.702	4.937	4.368
2.0	6.605	5.587	4.845	4.290
4.0	6.298	5.366	4.666	4.138

Table 4 shows the effect of decommissioning cost on the threshold of replacement. It can be seen from this table that as the decommissioning cost decrease, the threshold of decommissioning increases. Thus, likewise the decommissioning option, the probability of decommissioning increases due to the decrease in decommissioning cost. Additionally, when volatility is large, the effect of the decrease in decommissioning cost on the threshold becomes small. However, for replacement option the effect of the decrease in decommissioning cost, that is, the increase in threshold due to the decrease in decommissioning cost is large compared to decommissioning option. In replacement option the incentive to decommissioning is large due to taking into account the construction of the new plant, and consequently, the effect of the decrease in decommissioning cost on the probability of decommissioning becomes large.

$U(10^4 \text{ yen/kW})$	Price volatility, σ			
	0.2	0.3	0.4	0.5
1.0	13.325	21.569	28.910	35.176
2.0	12.489	20.760	28.092	34.340
4.0	10.876	19.172	26.474	32.681

Table 5. Effect of uncertainty on the value of replacement project

Likewise, we show the effect of decommissioning cost of the project value in Table 5. As the decommissioning cost decrease, the project value increase. The degree of the increase is larger than that of decommissioning option. For example, for $\sigma = 0.2$, when the decommissioning cost decreases from 4.0×10^4 yen/kW to 1.0×10^4 yen/kW, then whereas the value of decommissioning option increases by 1.821×10^4 yen/kW from 7.412×10^4 yen/kW to 9.234×10^4 yen/kW, the value of replacement option increases by 2.448×10^4 yen/kW from 10.876×10^4 yen/kW to 13.325×10^4 yen/kW. Consequently, likewise the threshold, for replacement option the effect of the decrease in decommissioning cost is large.

4. Summary

For CO₂ emissions reduction, it is necessary to maintain adequately the nuclear generating capacity, and moreover, to discern investment decisions such as decommissioning and refurbishment for aging nuclear power plants. In the future, the increase in uncertainty is expected, and consequently, economic evaluations under uncertainty are required.

In this chapter we have developed real options models to evaluate construction, decommissioning, replacement. For each problem, we show the effect of uncertainty and cost on optimal decision rules.

The models of construction, decommissioning, and replacement, which are represented in this chapter, are evaluation models for each single project. However, realistically, decommissioning and refurbishment for aging nuclear power plants must be considered as a problem that concerns the entire investment decision. Therefore, extension of this chapter's model towards choice model of investment decisions such as decommissioning, refurbishment, and replacement would be warranted.

5. References

- AEC (Japan Atomic Energy Commission) (2006). *Framework for Nuclear Energy Policy*, Tokyo.
- Dixit, A.K. & Pindyck, R.S. (1994). *Investment under Uncertainty*, Princeton University Press, Princeton, NJ.
- Gollier, C., Proult, D., Thais, F. & Walgenwitz, G. (2005). Choice of nuclear power investments under price uncertainty: Valuing modularity, *Energy Economics*, Vol. 27: 667–685.
- McDonald, R. & Siegel, D. (1986). The value of waiting to invest, *Quarterly Journal of Economics*, Vol. 101: 707–727.
- Naito, Y., Takashima, R., Kimura, H. & Madarame, H. (2010). Evaluating replacement project of nuclear power plants under uncertainty, *Energy Policy*, Vol. 38: 1321–1329.
- OECD NEA (Nuclear Energy Agency) (2000). *Nuclear Power in Competitive Electricity Markets*, Paris.
- Pindyck, R.S. (1993). Investment of uncertain cost, *Journal of Financial Economics*, Vol. 34: 53–76.

- Rothwell, R. (2006). A real options approach to evaluating new nuclear power plants, *Energy Journal*, Vol. 27: 37–53.
- Takashima, R., Naito, Y., Kimura, H. & Madarame, H. (2007). Decommissioning and equipment replacement of nuclear power plants under uncertainty, *Journal of Nuclear Science and Technology*, Vol. 44: 1347–1355.
- Takizawa, S., Omori, R., Suzuki, A. & Ono, K. (2001). Analysis of critical electricity price for the investment for constructing a nuclear power plant using real options approach, *Journal of Nuclear Science and Technology*, Vol. 38: 907–909.
- Trigeorgis, L. (1996). *Real Options: Management Flexibility and Strategy in Resource Allocation*, MIT Press, Cambridge, MA.

Artificial Intelligence Methods Applied to the In-Core Fuel Management Optimization

Anderson Alvarenga de Moura Meneses,
Alan Miranda Monteiro de Lima and Roberto Schirru
*Nuclear Engineering Program/COPPE - Federal University of Rio de Janeiro
Brazil*

1. Introduction

The In-Core Fuel Management Optimization (ICFMO), also known as Loading Pattern (LP) design optimization problem or nuclear reactor reload problem, is a classical problem in Nuclear Engineering. During the nuclear reactor fuel reloading operation periodically executed in Nuclear Power Plants (NPPs), part of the nuclear fuel is substituted. It is a real-world problem studied for more than four decades and several techniques have been used for its solution, such as optimization techniques and human expert knowledge. For example, early applications of Mathematical Programming methods for the solution of the ICFMO were made with Dynamic Programming (Wall & Fenech, 1965), and with Linear and Quadratic Programming (Tabak, 1968).

The ICFMO presents characteristics such as high-dimensionality, the large number of feasible solutions, disconnected feasible regions in the search space (Stevens et al., 1995) as well as the high computational cost of the evaluation function and lack of derivative information, which contribute to the challenge of the optimization of the ICFMO. Notwithstanding, algorithms known as generic heuristic methods, or *metaheuristics* (Taillard et al., 2001), have demonstrated an outstanding capability of dealing with complex search spaces, specially in the case of the ICFMO. Such Artificial Intelligence (AI) algorithms, besides the low coupling to the specificities of the problems, have some characteristics such as the memorization of solutions (or characteristics of solutions), which allows the algorithm to retain intrinsic patterns of optimal or near-optimal solutions or, in other words, "inner" heuristics as described by Gendreau & Potvin (2005). As search methodologies, metaheuristics may have in common: diversification, in order to explore different areas; mechanisms of intensification, in order to exploit specific areas of the search space; memory, in order to retain the best solutions; and tuning of parameters (Siarry & Zbigniew, 2008).

Metaheuristics such as Simulated Annealing (SA; Kirkpatrick et al., 1983), Genetic Algorithm (GA; Goldberg, 1989), Population-Based Incremental Learning (PBIL; Baluja, 1994), Ant Colony System (ACS; Dorigo & Gambardella, 1997) and Particle Swarm Optimization (PSO; Kennedy & Eberhart, 2001) have been applied to several problems in different areas with considerable success. In the case of the ICFMO, metaheuristics have provided outstanding results since the earliest applications of the SA to this problem (Parks,

1990; Kropaczek & Turinsky, 1991). In the last years, algorithms inspired in biological phenomena, either on the evolution of species or on the behavior of swarms, that is, paradigms such as Evolutionary Computation, specifically GA and PBIL, and Swarm Intelligence, specifically ACS and PSO, have represented the state-of-art group of AI algorithms for the solution of the ICFMO.

The main goal of this chapter is to present the ICFMO and the principal Artificial Intelligence methods applied to this problem (GA, PBIL, ACS, and PSO) and some of the results obtained in experiments which demonstrate their efficiency as metaheuristics in different situations. The remainder of this chapter is organized as follows. The ICFMO is discussed in section 2. An overview of the Evolutionary Computing algorithms GA and PBIL is presented in section 3. Section 4 presents the Swarm Intelligence techniques ACS and PSO. An overview of Computational Experimental Results are in section 5. Finally, conclusions are in section 6. The references are in section 7.

2. The In-Core Fuel Management Optimization

2.1 Theoretical aspects of the In-Core Fuel Management Optimization Problem

The In-Core Fuel Management Optimization (ICFMO), also known as LP design optimization or nuclear reactor reload problem, is a prominent problem in Nuclear Engineering, studied for more than 40 years. According to Levine (1987), the goal of the ICFMO is to determine the LPs for producing full power within adequate safety margins. It is a problem related to the refueling operation of a NPP, in which part of the fuel is substituted. Since a number n of Fuel Assemblies (FAs) are permuted in n positions of the core, it is a combinatorial problem. It is a multi-objective problem, with large number of feasible solutions, large number of local optima solutions, disconnected feasible regions, high-dimensionality and approximation hazards (Stevens et al., 1995).

The ICFMO may be stated in different ways. For example, it might be stated for a single plant or a community of plants (Naft & Sesonske, 1972). The problem might also be stated as single cycle, when it is considered only one time interval between two successive shut-downs, or multi-cycle, when more than one time interval is considered. For example, the system SIMAN/X-IMAGE (Stevens et al., 1995) was designed to support single or multi-cycle optimization.

Another approach is to consider the FAs' position as well as their orientation and presence of Burnable Poison (BP; Poon & Parks, 1992) or an ICFMO related approach as to optimize only the BP to be used (Haibach & Feltus, 1997), or to search for the best FAs' positions and BP (Galperin & Kimhy, 1991). It is also possible to search for the best LP, without regarding BP and orientation (Chapot et al., 1999; Machado & Schirru, 2002; Caldas & Schirru, 2008; De Lima et al., 2008; Meneses et al., 2009).

The ICFMO have multiple objectives, concerning economics, safety operational procedures and regulatory constraints, as stated in Maldonado (2005). Thus, it is possible to search solutions to the ICFMO within a multiobjective framework, with several (and possibly conflicting) objectives, in which the best solutions will belong to a trade-off surface (Pareto front). Notwithstanding, it is also possible to aggregate the objectives in only one objective function, as the *worth function* described by Galperin (1995), or the fitness function described by Caldas & Schirru (2008).

The group of techniques used in the ICMFO over the years encompasses manual optimization, Mathematical Programming, Optimization Metaheuristics and Knowledge-Based Systems. As a matter of fact, these approaches lead to three categories of computerized tools for decision support for the ICFMO: manual design packages, expert systems and optimization packages (Parks & Lewins, 1992). Knowledge-Based Systems have also been applied to the ICFMO and one early use of logical rules for generating LPs may be seen in Naft & Sesonske (1972).

Besides the important contributions of Mathematical Programming and Knowledge-Based Systems, Optimization Metaheuristics have been successfully applied to the ICFMO, with outstanding results in the solution of the ICFMO, despite the high complexity and lack of derivative information in the solution of the problem. Metaheuristics have low coupling to specificities of problems, and characteristics such as memorization of solutions (or characteristics of the solutions) generated during the search process (Taillard et al., 2001).

The ICFMO is a real-world problem with a complex evaluation function, consisting on codes based on the numerical solution of Reactor Physics methods. Several attempts to contour the high computational cost of the evaluations of solutions have been made, for example the usage of the characteristics of Artificial Neural Networks (ANNs) as universal approximators to perform the evaluation of the LPs substituting the reactor physics code, with less computational cost in the optimization phase. In this sense, ANNs have been used with Genetic Algorithms (GAs) for the ICFMO of PWRs (Erdoğan & Geçkinly, 2003) and advanced gas-cooled reactors (Ziver et al., 2004). The design of a searching method for the ICFMO must take into account that the time required to evaluate a single candidate LP is prohibitive, driving efforts in the sense of a lower number of evaluations in the optimization process.

The principal characteristics of the ICFMO are nonlinearity, multimodality, discrete solutions with nonconvex functions with disconnected feasible regions and high dimensionality (Stevens et al., 1995). Galperin (1995) analyzed the search space of the ICFMO in order to understand its structure and 300,000 patterns have been generated, with the evaluation of *performance parameters* corresponding to the candidate solutions. In this way, it has been demonstrated that there exists a large number of local optima in the region studied, about one peak per hundred configurations. Following this rationale one might roughly estimate 10^{11} local optima in the case of an octant symmetry model, which has approximately 10^{13} possible LPs. Therefore, gradient-based algorithms are not adequate to the ICFMO. Conversely, metaheuristics such as SA, PBIL, ACS, GA and TS have been applied to the ICFMO with considerable success.

After a time period, called operation cycle, it is not possible to maintain the NPP operating at the nominal power. At that time, the shutdown of the NPP is necessary for the reloading operation, when the most burned FAs (approximately 1/3) are exchanged by fresh nuclear FAs. The ICFMO consists in searching for the best reloading pattern of FAs, with an objective function evaluated according to specific criteria and methods of Nuclear Reactor Physics. Fig. 1 depicts the simplified schematic representation of 121 nuclear FAs (view from top) of a PWR NPP such as Angra 1, in the Southeast of Brazil. In practice, flat power distributions (that is, without power peaks that could compromise safety) within the reactor core are desirable therefore the octant symmetry may be used, which reduces the complexity of the problem. Fig. 2 depicts the octant symmetry for Angra 1 NPP. Except for the central FA, in gray, 20 FAs are permuted (frequently, and as a physical and production

restriction, FAs along the symmetry lines are not permuted with FAs that are not along the symmetry lines and vice versa). This model has been used by Chapot et al. (1999), Machado & Schirru (2002), Caldas & Schirru (2008), De Lima et al. (2008) and Meneses et al. (2009).

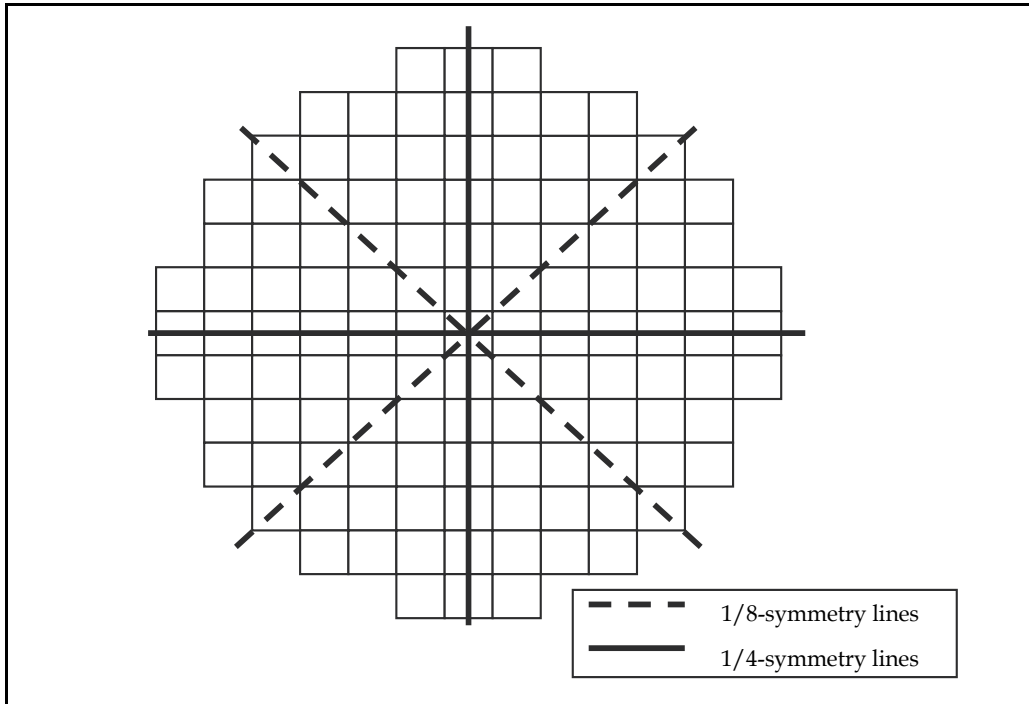


Fig. 1. Nuclear reactor core (view from top): 121 Fuel Assemblies and symmetry lines.

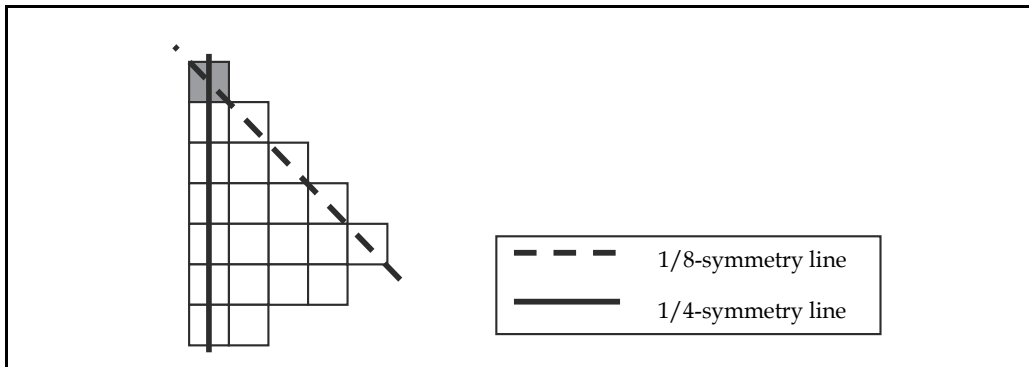


Fig. 2. Representation of the octant symmetry model: except for the central FA in gray, all of the 20 elements are permuted.

Meneses et al. (2010) discuss the mathematical formulation of the ICFMO for a single plant and single-cycle time period optimization, without considering orientation or BP positioning, subject to safety constraints. The ICFMO may be stated as variation of the Assignment Problem (AP; Vanderbei, 1992), with similarities on the constraints of position.

Machado & Schirru (2002) have applied ACS to the ICFMO, modeling the problem based on the Traveling Salesman Problem (TSP; Lawler et al., 1985; Papadimitriou and Steiglitz, 1982). The TSP is a well-known combinatorial optimization problem, in which the traveling salesman has to visit a given set of cities, starting from an initial city, visit each city only once and return to the starting city finding the shortest distance for the tour.

The formulations for the ICFMO based on the AP and TSP are equivalent in the following sense. According to Lawler (1963), the TSP is a special case of the Koopsman-Beckmann formulation and therefore “the n -city TSP is exactly equivalent to an $n \times n$ linear assignment problem” with the constraint that the permutations in the TSP must be cyclic. The advantage of making this point clear is that any technique applied to the TSP or to the AP may be equivalently adapted to the ICFMO, as it has been done for example with Optimization Metaheuristics such as GA, ACS and PSO.

In this way, the study of new techniques for solution of the ICFMO may also involve the solution of computer science benchmarks before applying them directly to the ICFMO. The primary reason is that there exist real-world problems that may not be benchmarked, which is the case for the ICFMO.

Thus, the validation of the code and a preliminary study of the behavior of an optimization metaheuristic for application to the ICFMO may be performed with problems such as the TSP, so that it is possible to investigate previously new techniques, as in the works of Chapot et al. (1999) and Meneses et al. (2009).

In sum, the ICFMO is a complex problem in Nuclear Engineering whose objectives are related to economics, safety and regulatory aspects. Its complexity is due not only to its combinatorial and non-polynomial characteristics, but also to the complexity of the evaluation function.

2.2 Simulation of Angra 1 Nuclear Power Plant with the Reactor Physics code RECNOd

Angra 1 NPP is a 2-loop PWR located at Rio de Janeiro State at the Southeast of Brazil, whose core is composed by 121 FAs. The Reactor Physics code RECNOd is a simulator for Angra 1 NPP. The development and tests related to the the 7th cycle of Angra 1 are detailed by Chapot (2000). With an octant-symmetry for the RECNOd simulation, FAs must be permuted except for the central FAs. In our experiments, FAs of the symmetry lines (quartets) are not supposed to be exchanged with elements out of the symmetry lines (octets). Chapot (2000) reports other situations in which this kind of symmetry is broken.

RECNOd is a nodal code based on the works described by Langenbuch et al. (1977), Liu et al. (1985) and Montagnini et al. (1994) and applied to optimization surveys in several works (Chapot et al., 1999; Machado & Schirru, 2002; Caldas & Schirru, 2008; De Lima et al., 2008, Meneses et al. 2009 and Meneses et al., 2010).

The nuclear parameters yielded by the code are, among others, the Maximum Assembly Relative Power (P_{rm}) and the Boron Concentration (C_B). The value of P_{rm} is used as a constraint related to safety. The computational cost of the RECNOd code is reduced since it does not perform the Pin Power Reconstruction. However, the usage of P_{rm} as a safety constraint does not violate the technical specifications of Angra 1 NPP (Chapot, 2000). For a maximum required radial power peak factor $F_{XYmax} = 1.435$ for Angra 1 NPP, the calculations yield a correspondent $P_{rm} = 1.395$. Any LP with $P_{rm} > 1.395$ is infeasible in the sense of the safety requirements.

C_B yielded by the RECNOd code is given at the equilibrium of Xenon, another aspect that reduces the computational cost of the processing, without impairing its validity for optimization purposes. Chapot (2000) demonstrated that it is possible to extrapolate and predict the cycle-length based on the C_B at the equilibrium of Xenon, in such a way that 4ppm are approximately equivalent to 1 Effective Full Power Day (EFPD). Moreover, 1 more EFPD is equivalent to a profit of approximately hundreds of thousand dollars. Thus, for the 7th cycle of Angra 1 NPP, the ICFMO might be stated as

$$\text{minimize } \frac{1}{C_B} \quad (1)$$

$$\text{subject to } P_{rm} \leq 1.395 \quad (2)$$

3. Evolutionary Computing Applied to the In-Core Fuel Management Optimization

3.1 Genetic Algorithm

The Theory of Evolution, as proposed by Darwin in 1859, had to be adapted because of the scientific development occurred in the 20th century. The Synthetic Theory of Evolution combines the findings of Genetics and other areas of modern Biology with Darwin's basic ideas. According to the Synthetic Theory, the main evolutionary factors are mutation, genetic recombination and natural selection, or the survival of the fittest. The Synthetic Theory paradigms can be outlined as follows.

(i) Nature (most often) or some external agent can change the genetic code, creating mutant individuals.

(ii) Through the sexual reproduction the genetic code of two individuals can be combined generating individuals with new characteristics.

(iii) Individuals more adapted to the environment are more likely to survive and reproduce, passing their characteristics to the offspring.

Based on these "Neo-Darwinian" principles, Holland (1975) developed the GAs. GAs play an important role in synthetic-intelligence research and have been quite successful when applied to function optimization. The basic condition to use GAs in function optimization is that any possible solution of a certain problem can be represented as a string of symbols (binary strings are generally the most adequate ones). In the biological metaphor, such strings can be seen as chromosomes and the symbols as genes.

The optimization process starts by random generation of an initial population of chromosomes (possible solutions). The next step is the evaluation of each chromosome according to its fitness, or response to the problem objective function. The evaluation will indicate how well the chromosome adaptation to the environment performs. Then, the three fundamental genetic operators are applied: reproduction, crossover and mutation.

According to Goldberg (1989), reproduction means the copy of a chromosome according to its fitness. The higher the fitness, the greater the probability that such chromosome contributes with more individuals to the next generation. Crossover and mutation can be explained as shown below.

Let X_1 and Y_1 be two chromosomes randomly chosen in the "mating pool" after the reproduction process:

$$\begin{aligned} X_1 &= 001|11 , \\ Y_1 &= 110|00 . \end{aligned}$$

Suppose we cut X_1 and Y_1 at the point indicated by the symbol “|”. Then we exchange the characters to the right of the crossover point creating two children-chromosomes that will be added to the population:

$$\begin{aligned} X_2 &= 00100 , \\ Y_2 &= 11011 . \end{aligned}$$

Both X_2 and Y_2 retain some characteristics of their parent-chromosomes but they will explore regions of the solution space not searched by X_1 and Y_1 . The mutation operator modifies locally a chromosome by changing a gene (bit). For instance, the chromosome

$$Z_1 = 11111$$

may suffer mutation in its fourth gene, becoming

$$Z_2 = 11101 .$$

The mutation avoids stagnation of the searching process and allows unexplored points of the space to be examined. As in the real world, in the GAs' universe mutation is an important source of species diversity.

Applying reproduction, crossover and, eventually, mutation to the initial population the second generation will be created. Generation after generation the evolution will proceed in cyclic manner until a stop criterion is reached.

Poon & Parks (1992) applied the GA to the ICFMO optimizing the positions of the FA, as well as their orientation and BP within the core. Chapot et al. (1999) presented results for genotype-phenotype decodings for the ICFMO. The genotype-phenotype decoding with Random Keys (also used with other metaheuristics) will be discussed in the next subsection.

3.1.1 Genotype-phenotype decoding model with Random Keys

Before one applies GAs to solve the TSP, a problem caused by the use of the classical crossover operator must be overcome. For instance, if one performs crossover on the two tours (A B C D E) and (E A C B D) at crossover point C, two offspring tours are yielded: (A B C B D) and (E A C D E). Both are non-valid tours, because in each case one city was not visited, while another city was crossed twice by the salesman. Recognizing this problem, several researchers presented solutions to the TSP, based on GAs, modifying the crossover operator. They created heuristic crossovers, as the Partially Mapped Crossover (PMX), Order Crossover (OX), Cycle Crossover (CX) and other methods described in Holland (1975) and in Oliver et al. (1987). Bean (1994) proposed the decoding of the genotype, instead of the modification of the crossover operator, a method called Random Keys (RK).

RKs are useful to map a solution with real numbers, which will work as *keys*, onto a combinatorial solution, that is, a candidate solution for a given combinatorial problem. There are several models for RK described by Bean (1994), and for the ICFMO the same

model as in the Single Machine Scheduling Problem (SMSM) is used, with no repetitions allowed.

Let's consider a representation of two chromosomes C_1 and C_2 in the GA, both corresponding to vectors of a five-dimensional real space. With the RK approach, for a chromosome $C_1 = [0.39 \ 0.12 \ 0.54 \ 0.98 \ 0.41]$, the decoded corresponding individual (a candidate solution for a five-dimensional combinatorial problem where no repetitions are allowed) would be $I_1 = (2, 1, 5, 3, 4)$, since 0.12 is the lesser number and corresponds to the second allele; 0.39 corresponds to the first allele and so forth. For a chromosome $C_2 = [0.08 \ 0.36 \ 0.15 \ 0.99 \ 0.76]$, the decoded individual would be $I_2 = (1, 3, 2, 5, 4)$.

If a crossover operation would be performed between the feasible individuals I_1 and I_2 for the SMSM, TSP or ICFMO, with a crossing site between the second and third alleles, the resultant offspring composed of the descending individuals $I_3 = (2, 1, 2, 5, 4)$ and $I_4 = (1, 3, 5, 3, 4)$ would be unfeasible for the TSP and the ICFMO, since I_3 and I_4 are not possible solutions for these problems since there is repetition of elements.

The RK guarantees that the offspring will be a representation of feasible individuals for these combinatorial problems where no repetition is allowed, since the crossover operation is performed upon the chromosomes, instead of directly upon the individuals. Given the two parent-chromosomes C_1 and C_2 , with a cross site between the second and third alleles, the descending chromosomes $C_3 = [0.39 \ 0.12 \ 0.15 \ 0.99 \ 0.76]$ and $C_4 = [0.08 \ 0.36 \ 0.54 \ 0.98 \ 0.41]$ would be decoded into feasible individuals $I_3 = (2, 3, 1, 5, 4)$ and $I_4 = (1, 2, 5, 3, 4)$.

The RKs model, used with considerable success not only with the GAs applied to the ICFMO, but with other metaheuristics such as the PBIL and PSO, which will be discussed in the next sections.

3.2 Population-Based Incremental Learning

The algorithm PBIL (Baluja, 1994) is a method that combines the mechanism of the GA with the simple competitive learning, becoming an important metaheuristic for the optimization of numerical functions and combinatorial problems.

The PBIL is an extension of the Equilibrium Genetic Algorithm (EGA) (Baluja, 1994). The EGA is an algorithm that describes the limit population of the GA for a breakeven point, supposing that this population is always being combined to achieve convergence. This process may be seen as a way of eliminating the explicit form of the recombination operator of the GA.

The aim of the PBIL algorithm is to create a probability vector with real numbers in each position, which generates individuals that present the best candidate solutions for the optimization of a function. For example, if the binary encoding is used as a representation of a solution for a problem, the probability vector will specify the probability for the vector contain the values 0 or 1 in each position. Thus, an example of a probability vector encoded by a six-bits representation is $P = [0.01 \ 0.03 \ 0.99 \ 0.98 \ 0.02]$, whose decoding will generate, with high probability the candidate solution vector $S = [0 \ 0 \ 1 \ 1 \ 0]$.

In order to achieve diversity of the population in the beginning of the search process, each position of the probability vector is defined with the value 0.5, that is, the probability of the generation of the values 0 or 1 in each position of the bit string is the same. This equiprobability in the generation of values makes random initial populations in the PBIL algorithm.

Since in the PBIL the entire population of individuals is defined from the probability vector, the operators used for the evolution of this population are not used directly on the population, as in the case of the Gas' operators, but on the probability vector. The operators of the PBIL are derived from the ones used in the GA (mutation operator) and the competitive learning networks (updating of the probability vector). As in the GA, the algorithm PBIL keeps a parallelism in the search process through the representation of several distinct points of the search space represented by means of the population.

During the search, the values of the probability vector are gradually changed from the initial values 0.5 to values close to 0.0 or 1.0, in order to represent the best individuals found in the population, at each generation.

The learning process is similar to the Learning Vector Quantization (LVQ; Kohonen, 1990), in which the ANN is trained with examples known *a priori*. In a similar fashion, the algorithm PBIL updates the probability vector using two vectors (the *best* V_B and the *worst* V_W) of the possible solutions. The best vector (with the highest fitness) changes the probability vector related to an individual so that the representation of the latter becomes closer to the representation of the former; the worst vector (with the lowest fitness) changes the probability related to an individual so that the representation of the latter becomes farther from the representation of the former.

During the search process, at a generation t , for a vector the values P_i of the probability vectors P are updated according to the equation

$$P_i^{t+1} = P_i^t \times (1,0 - L_r) + V_{Bi} \times L_r \quad (3)$$

in the case of the best vector V_B , where L_r is the learning rate.

For the worst value V_W , the vectors P are updated according to the equation

$$P_i^{t+1} = P_i^t \times (1,0 - L_{r_neg}) + V_{Wi} \times L_{r_neg} \quad (4)$$

where L_{r_neg} is the negative learning rate.

In sum, the aim of the equations is to update the probability vectors approximating them to the configuration of the best vector and departing them from the configuration of the worst vector of the population.

Machado (1999) applied the PBIL to the ICFMO. The application of Multi-Objective PBIL to the ICFMO is also described by Machado (2005). Caldas & Schirru (2008) developed the Parameter Free PBIL (FPBIL), with parameters replaced by self-adaptable mechanisms.

4. Swarm Intelligence Applied to the In-Core Fuel Management Optimization

4.1 Ant Colony System

The ACS was developed for solving combinatorial optimization problems that are NP-Hard, such as the Traveling Salesman Problem (TSP). To solve the TSP with the ACS, an ant k constructs a solution moving in a tour over the cities returning to the starting city. For each ant k there is associated a list $J_k(r)$ of cities to be visited, where r is the actual city of ant k . At each stage of the tour, the ant k selects the next city to be visited by means of a state transition rule (Gambardella & Dorigo, 1997) described by the equation.

$$s = \begin{cases} \max \{ [\text{FE}(r, s)]^\delta \times [\text{HE}(r, s)]^\beta \} & \text{if } q \leq q_0 \\ \text{Roulette} & \text{if } q > q_0 \end{cases} \quad (5)$$

where $\text{FE}(r, s)$ is a real positive value that represents the amount of pheromone associated to the arc (r, s) , $\text{HE}(r, s)$ is the value of the heuristic function relative to the move (r, s) from city r to the city s , parameters δ and β weigh the relative importance of the ants learning $\text{FE}(r, s)$ and the heuristic knowledge given by the heuristic function $\text{HE}(r, s)$, q is a random value with uniform probability in the range $[0, 1]$ and q_0 ($0 \leq q_0 \leq 1$) is a parameter of the algorithm and Roulette is a random variable selected according to

$$\text{Roulette} = \begin{cases} \frac{[\text{FE}(r, s)]^\delta \times [\text{HE}(r, s)]^\beta}{\sum_{z \in J_k(r)} [\text{FE}(r, z)]^\delta \times [\text{HE}(r, z)]^\beta} & \text{if } s \in J_k(r) \\ 0 & \text{if } s \notin J_k(r) \end{cases} \quad (6)$$

The transition rule represented by Eq. (5) defines the strategy for the probabilistic move of the next states taking in account the information yielded by $\text{FE}(r, s)$ and $\text{HE}(r, s)$. The pheromone values $\text{FE}(r, s)$ influence the way ants change their search space to benefit from the discovery of better tours; in other words, $\text{FE}(r, s)$ represents the artificial pheromone associated to the reinforcement learning technique. On the other hand, $\text{HE}(r, s)$ is related to problem-specific information, that is, specific heuristic about the optimization problem.

The use of a representative heuristic for the optimization problem is extremely important, since the first step of the algorithm will be done based on that information and not at random as, for example, in GAs.

That distribution expresses the probability that the ant, being in city r , will select the city s as his next move. The roulette is similar to the roulette used in Genetic Algorithms (Holland, 1975) to select individuals for the next generation.

As a means of cooperation among ants, the pheromone values $\text{FE}(r, s)$ are modified to favor the discovery of good solutions. Updating of pheromone values are made by means of a local updating rule and a global updating rule. The local updating rule is given by the equation

$$\text{FE}(r, s) = (1 - \rho)\text{FE}(r, s) + \rho\text{FE}_{\text{ZERO}} \quad (7)$$

where ρ is the pheromone evaporation parameter and FE_{ZERO} is the initial amount of pheromone.

The local updating rule is used after the application of the state transition rule and after the selection of the next city to be visited. In this way, the updating is applied while the solution is being constructed. The objective of the local updating rule is to stimulate the search over new regions of the search space avoiding premature convergence. The amount of pheromone on the arcs is reduced slowly in order to permit the artificial ants to diversify their search. This process is called pheromone evaporation.

The global updating rule is done according to the equation

$$\text{FE}(r, s) = (1 - \alpha)\text{FE}(r, s) + \alpha(W/\text{bfit}) \quad (8)$$

where α is the pheromone evaporation parameter, W is the user defined parameter that, together with the α parameter, expresses the learning rate of the algorithm and bf_{it} is the best fitness of the current configuration.

The global updating rule is applied after all the ants have constructed a complete tour and the tour has been evaluated by an objective function. This rule is considered the reinforcement learning of the algorithm.

Machado & Schirru (2002) applied the algorithm Ant-Q to the ICFMO. De Lima et al. (2008) introduced the Ant Colony Connective Networks (ACCN), a parallel implementation of ACS, for the ICFMO.

4.2 Particle Swarm Optimization

The PSO (Kennedy & Eberhart, 2001) was presented in 1995 and its algorithm models a collaborative search, taking into account the social aspects of intelligence. PSO was initially proposed to optimize non-linear continuous functions. The PSO is a bio-inspired collaborative system whose computational optimization implementation model has achieved considerable results in various knowledge areas.

A swarm with P particles performs the optimization in an n -dimensional search space. Each particle i has a position $x_i^t = [x_{i1} \ x_{i2} \ \dots \ x_{in}]$ and a velocity $v_i^t = [v_{i1} \ v_{i2} \ \dots \ v_{in}]$ at a iteration t , through the dimension $j = 1, 2, \dots, n$ updated according to the equations

$$v_i^{t+1} = w^t v_i^t + c_1 r_1^t (pbest_i - x_i^t) + c_2 r_2^t (gbest - x_i^t) \quad (9)$$

and

$$x_i^{t+1} = x_i^t + v_i^{t+1} \quad (10)$$

The inertia weight w^t may decrease linearly according to the equation

$$w^t = w - \frac{w - w_{min}}{t_{max}} t \quad (11)$$

where w is the maximum inertia constant, w_{min} is the minimum inertia constant, t_{max} is the maximum number of iterations and t is the current iteration. High values of w^t lead to global search making the particles explore large areas of the search space, while low values of w^t lead to the exploitation of specific areas.

At the right side of eq. (9), the first term represents the influence of the own particle motion, acting as a memory of the particle's previous behavior; the second term represents the individual cognition, where the particle compares its position with its previous best position $pbest_i$; and the third term represents the social aspect of intelligence, based on a comparison between the particle's position and the best result obtained by the swarm $gbest$ (global best position). Both c_1 and c_2 are acceleration constants: c_1 is related to the individual cognition whereas c_2 is related to social learning; r_1 and r_2 are uniformly distributed random numbers. The positions and velocities are initialized randomly at implementation. Eq. (10) describes how the positions are updated.

The positions x_i^t are then evaluated by an objective function or *fitness* of the problem $f(x_i)$. The positions vectors $gbest = [gbest_1 \ gbest_2 \ \dots \ gbest_n]$ and $pbest_i = [pbest_{i1} \ pbest_{i2} \ \dots \ pbest_{in}]$ are updated depending on the information acquired by the swarm, constructing its knowledge on the search space over the iterations.

As stated earlier, the PSO was initially developed for optimization of continuous functions. Its outstanding performance in such domain led the researchers to investigate the optimization of combinatorial problems with discrete versions of the PSO.

The first PSO model for discrete optimization was developed by Kennedy & Eberhart (1997). A discrete version of the PSO was presented with the representation of the particle's positions as bitstrings. The velocities were represented as probabilities of changing the bits of the positions.

Another important PSO model for combinatorial optimization was proposed by Salman et al. (2002), who applied the PSO to the optimization of the Task Assignment Problem (TAP). The main idea is that the particles fly in an n-dimensional space, but their position is mapped onto combinatorial solutions for the TAP, a problem in which the repetitions are allowed. In this case, the mapping onto combinatorial solution is simply obtained by truncating the components of the positions. Although it was proven to be a good solution for the TAP, this approach might not be used for other problems in which the repetition of elements is not allowed in the representation of solutions, such as the TSP or the ICFMO. Wang et al. (2003) presented a PSO model for the TSP whose equations were based on Swap Operators and Swap Sequences.

For the combinatorial problem of the ICFMO, Meneses et al. (2009) presented the implementation of the PSO using the RK (Bean, 1994), described in the subsection 3.1, without the use of local search procedures, since their usage in the ICFMO might not be interesting or appropriated. In fact, it is not possible to ensure that local search procedures, used, for example, for the optimization of the TSP, will be successful for the real-world ICFMO because of the following. When the order of two cities in a tour (candidate solution) for a TSP is changed locally, the resulting tour may be a shorter path or not, nevertheless it is always a feasible solution. In the case of the ICFMO, the core configuration obtained by exchanging two FAs may be unfeasible.

5. Computational Experimental Results

The investigation of Optimization Metaheuristics have provided important results over the years. The algorithms discussed have distinct characteristics that might be interesting in different situations. Table 1 exhibits results for the algorithms, based on data provided in several works. For example, when it is possible to perform a great number of evaluations, ACCN and FPBIL yield good results. For a lower number of generations, PSO is the algorithm with better results.

Reference	C_B	P_{m1}	Technique	Heuristics	Eval.
Chapot et al. (1999)	955	1.345	Manual	-	-
Chapot et al. (1999)	1026	1.390	GA	No	4000
Machado & Schirru (2002)	1297	1.384	Ant-Q	Yes	200
Machado (2005)	1242	1.361	PBIL	No	6000
Machado (2005)	1305	1.349	PBIL-MO ²	Yes	10000
De Lima (2008)	1424	1.386	ACCN	Yes	329000
Caldas & Schirru (2008)	1554	1.381	FPBIL	No	430364
Meneses et al. (2009)	1394	1.384	PSO	No	4000

¹ F_{XY} for Manual Optimization

² Multi-objective PBIL

Table 1. Results for several Optimization Metaheuristics.

6. Conclusion

The ICFMO is a prominent problem in Nuclear Engineering studied for more than 40 years. Characteristics such as a large number of feasible solutions, large number of local optima solutions, disconnected feasible regions, high-dimensionality and approximation hazards (Stevens et al., 1995). Its combinatorial characteristics, the lack of derivative information and the complexity of the problem motivate the investigation of AI generic optimization heuristic methods, or optimization metaheuristics. This chapter provided an overview of state-of-art algorithms of the Evolutionary Computing (GA and PBIL) and Swarm Intelligence (ACS and PSO). Such optimization metaheuristics have yielded outstanding results in the ICFMO. Results confirm that characteristics such as exploration, intensification, memory, retention of intrinsic patterns (“inner” heuristics) and low coupling to the specificities of the problem provide effectiveness in the search of near-optimal solutions for the ICFMO.

Acknowledgement

Portions of this text were published in the journals *Progress in Nuclear Energy* and *Annals of Nuclear Energy*.

7. References

- Baluja, S. (1994). Population-Based Incremental Learning: a method for integrating genetic search based function optimizations and competitive learning, Technical Report CMU-CS-94-163.
- Bean, J. C. (1994). Genetic Algorithms and Random Keys for Sequencing and Optimization. *ORSA Journal of Computing*, 6, 2
- Caldas, G. H. F. & Schirru, R. (2008). Parameterless evolutionary algorithm applied to the nuclear reload problem. *Annals of Nuclear Energy*, 35, 583-590
- Chapot, J. L. C.; Da Silva, F. C. & Schirru, R. (1999). A new approach to the use of genetic algorithms to solve the pressurized water reactor's fuel management optimization problem. *Annals of Nuclear Energy*, 26, 641-655
- Chapot, J. L. C. (2000). Otimização Automática de Recargas de Reatores a Água Pressurizada Utilizando Algoritmos Genéticos. D. Sc. Thesis, COPPE/UFRJ, Brazil (in portuguese).
- De Lima, A. M. M.; Schirru, R., Da Silva, F. C. & Medeiros, J. A. C. C. (2008). A nuclear reactor core fuel reload optimization using ant colony connective networks. *Annals of Nuclear Energy*, 35, 1606-1612
- Domingos, R. P.; Schirru, R. & Pereira, C. M. N. A. (2006). Particle swarm optimization in reactor core design. *Nuclear Science and Engineering*, 152, 197-203
- Dorigo, M. & Gambardella, L. M. (1997). Ant colony system: a cooperative learning approach to the traveling salesman problem. *IEEE Transactions on Evolutionary Computation*, 1, 53-66
- Eberhart, R. & Kennedy, J. (1995). A New Optimizer Using Particle Swarm Theory. *Proceedings of Sixth International Symposium on Micro Machine and Human Science*, 39-43
- Erdoğan, A. & Geçkinly, M. (2003). A PWR Reload Optimization Code (XCore) Using Artificial Neural Networks and Genetic Algorithms. *Annals of Nuclear Energy*, 30, 35-53
- Galperin, A. & Kimhy, Y. (1991). Application of Knowledge-Based Methods to In-Core Fuel Management. *Nuclear Science and Engineering*, 109, 103-110

- Galperin, A. (1995). Exploration of the Search Space of the In-Core Fuel Management Problem by Knowledge-Based Techniques. *Nuclear Science and Engineering*, 119, 144-152.
- Gendreau, M. & Potvin, J.-Y. (2005). Tabu Search. In: *Search Methodologies – Introductory Tutorials in Optimization and Decision Support Techniques*. Burke, E. K., Kendall, G. (Eds.), Springer.
- Goldberg, D. E. (1989). *Genetic Algorithms in Search Optimization and Machine Learning*. Addison-Wesley Publishing Company, Massachusetts
- Holland, J.H. (1975). *Adaptation in Natural and Artificial Systems*. University of Michigan Press, Ann Arbor, MI
- Kennedy, J. & Eberhart, R. C. (1997). A discrete binary version of the particle swarm algorithm, Conference on Systems, Man and Cybernetics, 4104-4109.
- Kennedy, J. & Eberhart, R. C. (2001). *Swarm Intelligence*. Morgan Kaufmann Publishers, San Francisco, CA.
- Kirkpatrick, S.; Gelatt, C. D. & Vecchi, M. P. (1983). Optimization by Simulated Annealing. *Science*, 220, 4598, 671-680
- Kohonen, T. (1990). The self-organizing map. *Proceedings of the IEEE* 78, 2, 1464-1480
- Kropaczek, D.J., Turinsky, P.J., 1991. In-Core Nuclear Fuel Management Optimization for pressurized reactors utilizing Simulated Annealing. *Nuclear Technology* 95, 9–31.
- Langenbuch, S.; Maurer, W. & Werner, W. (1977). Coarse mesh flux expansion method for analysis of space-time effects in large water reactor cores. *Nuclear Science and Engineering*, 63, 437-456
- Lawler, E. L. (1963). The Quadratic Assignment Problem. *Management Science*, 9, 586-599
- Lawler, E. L.; Lenstra, J. K.; Kan, A. H. G. R. & Shmoys, D. B. (Org.) (1985). *The Traveling Salesman Problem: a guided tour of combinatorial optimization*, John Wiley & Sons.
- Levine, S. (1987). In-Core Fuel Management of Four Reactor Types. *Handbook of Nuclear Reactor Calculation*, Vol. II, CRC Press
- Liu, Y. S. et al. (1985). ANC: A Westinghouse Advanced Nodal Computer Code. Technical Report WCAP-10965, Westinghouse.
- Machado, L. & Schirru, R. (2002). The Ant-Q algorithm applied to the nuclear reload problem. *Annals of Nuclear Energy*, 29, 1455-1470
- Machado, M.D. (2005). Algoritmo Evolucionário PBIL Multiobjetivo Aplicado ao Problema da Recarga de Reatores Nucleares. D. Sc. Thesis, COPPE/UFRJ, Brazil (in portuguese).
- Maldonado, G.I., 2005. Optimizing LWR cost of margin one fuel pin at a time. *IEEE Transactions on Nuclear Science*, 52, 996–1003
- Medeiros, J. A. C. C. & Schirru, R. (2008). Identification of nuclear power plant transients using the Particle Swarm Optimization algorithm. *Annals of Nuclear Energy*, 35, 576-582
- Meneses, A. A. M.; Machado, M. D. & Schirru, R. (2009). Particle Swarm Optimization applied to the nuclear reload problem of a Pressurized Water Reactor. *Progress in Nuclear Energy*, 51, 319-326
- Meneses, A. A. M.; Gambardella, L. M. & Schirru, R. (2010). A new approach for heuristic-guided search in the In-Core Fuel Management Optimization. *Progress in Nuclear Energy*, 52, 339-351
- Montagnini, B.; Soraperra, P.; Trentavizi, C.; Sumini, M. & Zardini, D. M. (1994). A well balanced coarse mesh flux expansion method. *Annals of Nuclear Energy*, 21, 45-53
- Naft, B. N. & Sesonske, A. (1972). Pressurized Water Reactor Optimal Fuel Management. *Nuclear Technology*, 14, 123-132

- Oliver, I. M.; Smith, D. J. & Holland, J. R. C. (1987). A study of permutation crossover operators on the traveling salesman problem. Proceedings of the Second International Conference on Genetic Algorithms and their Applications, 224-230
- Papadimitriou, C. H. & Steiglitz, K. (1982). *Combinatorial Optimization*, Prentice-Hall.
- Parks, G. T. (1990). An Intelligent Stochastic Optimization Routine for Nuclear Fuel Cycle Design. *Nuclear Technology*, 89, 233-246
- Parks, G. T. (1996). Multi-objective Pressurized Water Reactor Reload Core Design by Non-Dominated Genetic Algorithm Search. *Nuclear Science and Engineering*, 124, 178-187
- Poon, P.W. & Parks, G.T. (1992). Optimizing PWR reload core designs. Parallel Problem Solving from Nature II, 373-382
- Salman, A.; Ahmad, I. & Al-Madani, S. (2002). Particle Swarm Optimization for Task Assignment Problem. *Microprocessors and Microsystems*, 26, 363-371.
- Siarry, P. & Zbigniew, M. (Eds.) (2008) *Advances in Metaheuristics for Hard Optimization*, Springer.
- Stevens, J. G.; Smith, K. S.; Rempe, K. R. & Downar, T. J. (1995). Optimization of Pressurized Water Reactor Shuffling by Simulated Annealing with Heuristics. *Nuclear Science and Engineering*, 121, 67-88
- Tabak, D. (1968). Optimization of nuclear reactor fuel recycle via linear and quadratic programming. *IEEE Transactions on Nuclear Science*, 15, 1, 60-64
- Taillard, E.D.; Gambardella, L.M.; Gendreau, M. & Potvin, J.-Y. (2001). Adaptive memory programming: a unified view of metaheuristics. *European Journal of Operational Research*, 135, 1-6
- Vanderbei, R. J. (1992). *Linear Programming - Foundations and Extensions*. Kluwer Academic Publishers.
- Wall, I. & Fenech, H. (1965). Application of dynamic programming to fuel management optimization. *Nuclear Science and Engineering*, 22, 285-297
- Wang, K. P.; Huang, L.; Zhou, C. G. & Pang, W. (2003). Particle Swarm Optimization for Traveling Salesman Problem. *International Conference on Machine Learning and Cybernetics*, 3, 1583-1585
- Ziver, A. K.; Pain, C. C.; Carter, J. N.; de Oliveira, C. R. E.; Goddard, A. J. H. & Overton, R. S. (2004). Genetic algorithms and artificial neural networks for loading pattern optimisation of advanced gas-cooled reactors. *Annals of Nuclear Energy*, 31, 4, 431-457.

Certification of software in safety-critical I&C systems of nuclear power plants

Lic. Tech. Risto Nevalainen
Tampere University of Technology
Pori, Finland

M.Sc. (Eng) Juha Halminen
Teollisuuden Voima Oy
Olkiluoto, Finland

Lic. Tech. Hannu Harju
VTT Technical Research Centre of Finland
Espoo, Finland

M.Sc. (Eng) Mika Johansson
FiSMA ry
Espoo, Finland

Nuclear power plants have well-defined processes to acquire and qualify safety-critical systems. Ultimate goal is to maximise safety, without compromises in quality and reliability. Each new device and system in nuclear power plant shall be classified and qualified according to its safety requirements. Using modern technology means in practice that more and more components have programmable features. The reliability of such components has proven to be difficult to demonstrate due to the nature of flaws in software.

Standards and guides used by national authorities set licensing criteria for software used in the safety-critical systems of nuclear power plants. Nuclear power companies use commonly same standards and guides as authorities to avoid interpretation problems in qualification and licensing. Standards can be either generic, safety specific or nuclear domain specific. Also system manufacturers and software development units have adopted either nuclear domain specific or generic safety standards. Prerequisites for high-quality software and systems are in place.

Conformance with standards is not any absolute guarantee for safety. It can be achieved only by use of several different approaches, which all provide their own evidences and support for qualification and licensing. Certification is one way to package different methods together and build trust in achievement of maximal safety. In fact, certification is already de-facto "must" in highest safety category of software intensive safety-critical systems.

Certification should be aligned with system acquisition, development and commissioning processes to improve total effectiveness of qualification. Then it is also cost-effective and proactive rather than additional and isolated activity.

As a part of Finnish nuclear research program SAFIR2010, a project called CERFAS has defined necessary software certification services for nuclear industry needs. Main areas of the service are process assessment and product evaluation. Certification employs also several other method families, like inspections and reviews, independent V&V, model checking, conformance with selected reference standard(s) and use of selected measurements and analyses. Safety case is the main framework to integrate all methods together.

Keywords

Safety-Critical Software, Certification, Safety Case, Process Assessment, Product Evaluation, Conformance with Standards, Safety Systems

1. Introduction

When the first versions of nuclear specific system and software standards were written some 20 – 25 years ago, no generic software and quality standards like ISO/IEC 15504 (Process Assessment) or IEC/EN ISO 61508 (Functional Safety) existed or were not commonly known. So, each party developed their own criteria and terminology for their own needs.

Quite typically, nuclear power instrumentation and control (I&C) systems are industrial products and are not designed and manufactured uniquely for each application. Their platform is based on standard solutions and may be developed for many different purposes. Some subsystems may be old and not easy to qualify during the system delivery. The main evidence may be their historical development process and current operational history. They have many versions and variants and new changes to come. Only some minor part of the whole delivered system may consist of customer-specific application. When the system will be delivered into the nuclear power unit, it may require separate qualification of platform and application. As a whole, complete qualification can be very time-consuming and expensive.

As a result of the described development, there is clear need for an integrated and effective method to qualify software intensive systems in nuclear power units. Integration has three major areas: 1) Definition and harmonisation of requirements for software intensive systems in their different safety levels, 2) Integration of several approaches like SPICE and Failure mode effects and criticality analysis method, FMECA, to improve confidence of qualification and 3) Integration of the system acquisition and qualification processes to improve total effectiveness of the acquisition, delivery and commissioning processes.

Certification of software intensive systems can help in qualification. Because certification is very rigor and expensive process, it is needed mainly for most safety-critical systems and components. Certification of software is often limited to platform components. Certificate is normally valid for any further use of same software version, and can reduce certification cost per delivery.

The objective of SPICE method is to evaluate the process capability. SPICE is a brand name for ISO/IEC 15504 Process Assessment standard. The capability measurement system is based on ordinal 5-point capability level scale. Basically any process can be evaluated using the measurement system. In most cases, some predefined process reference model is used. Most known models are defined by ISO itself. ISO/IEC 12207 is the standard for software life-cycle processes. ISO/IEC 15288 is similar model for systems engineering. In most cases I&C systems for nuclear power plants are developed using a combination of software and systems engineering processes.

A modified FMECA method Tiira [9] has been used to bring evidence to the qualification process of safety-critical system. FMECA is effective to focus in most critical parts of the system, which have highest potential to cause failures. In hardware components, many well-defined methods can be used to show evidence about reliability and potential to failures. Redundancy can be used to reach required reliability and failure prevention level. For software-intensive components standard FMECA is less applicable, because software failure statistics is typically incomplete. Instead of statistics, target values for software reliability are used in Tiira. Software reliability and probability of failures to occur may be difficult to predict, even to calculate.

2. Overview of the requirements for qualification

2.1 Classification of systems according to safety

STUK (Säteilyturvakeskus, The Finnish Radiation and Nuclear Safety Authority) has defined four safety class levels for nuclear power unit (SC1 ... SC4, SC1 being the highest). IEC 61508 defines four safety integrity levels (SIL1 ... SIL 4, SIL4 being the highest). Some other standards have defined for example safety classes 1, 2 and 3 for systems, and safety categories A, B and C for functions. There is no clear mutual compatibility between various nuclear specific standards and their safety classifications. Also criteria and requirements to validate achievement of the defined safety class can be different. National regulators as STUK want to define their own requirements for the qualification process, to be able to carry out their monitoring and regulatory role.

Qualification of software intensive systems for nuclear power plant is needed in two different kind of contexts:

- Qualification of safety-critical systems. The main software reference standard is IEC 60880. Certification is often part of qualification (see section 7), especially for platform components. Safety category is mostly „A“, as defined in IEC 60880. SIL classification is normally not used directly, so SIL can be anything between 1- 4. Main focus is in product certification rather than process assessment, because of IEC 60880 and licensing requirements.
- Qualification of safety-related systems. The main software reference standard is IEC 62138. Systems are normally industrial products, which can be used also in nuclear power plants after their qualification. Certification is normally not required in Finland for these systems, classified either in category B or C. Focus is mainly in process assessment, because of easier IEC 62138 and licensing requirements.

Generic functional safety standard IEC 61508 uses term "safety-related" for any system. It can be used as additional reference and guidance for all kind of systems for nuclear power plants, belonging in safety category A, B or C. The term "safety system" should be used in category A systems.

One method for qualification of safety-related systems for nuclear power plants is called TVO SWEP (Software evaluation procedure). It has been developed originally during 2004 - 2006 as a joint effort of TVO, VTT Technical Research Centre of Finland and Finnish Software Measurement Association FiSMA. Main focus is systems in safety categories B and C. This article is mainly based on experiences from TVO SWEP in several deliveries for TVO.

During years 2007 – 2010 TVO SWEP was extended to safety-critical systems in safety category A. Many additional methods and techniques are needed to get required evidence. Quantitative understanding of product and safety is achieved by applying formal methods, like safety case.

2.2 Pre-qualification and qualification

The main phases of the qualification are **pre-qualification** and **application qualification**. SPICE is used mainly in the pre-qualification phase, together with relevant nuclear specific standards. Often pre-qualification covers the term certification. If needed, also application qualification is done, partly with the same methods. As a starting point, preliminary hazard analysis (PHA) is done as part of the user requirements definition step. A modified FMECA [9] method is used after PHA, and is maintained and completed during all qualification steps. Figure 1 shows the main steps of qualification and how it is integrated to main steps of system acquisition and development.

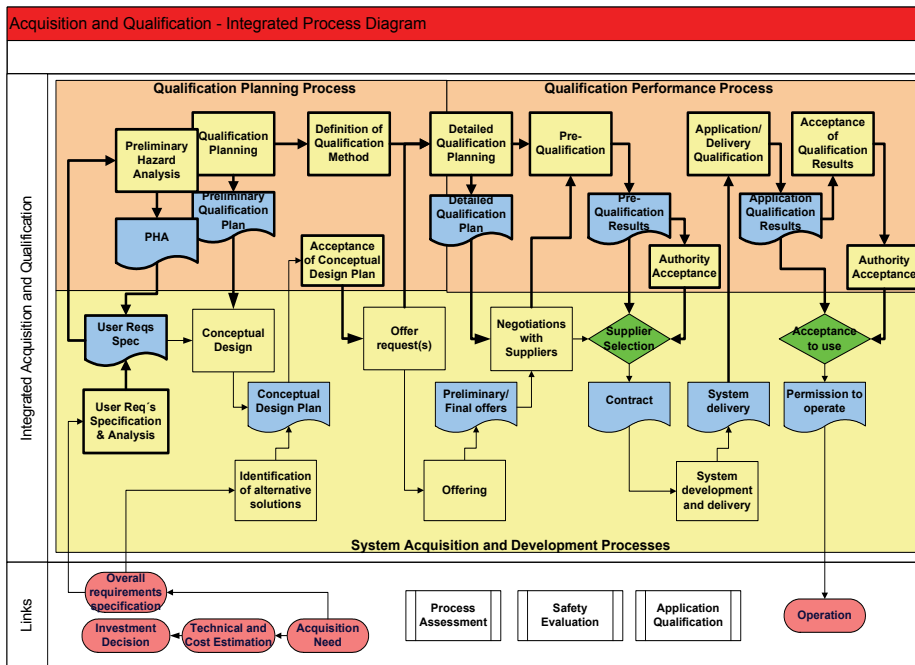


Fig. 1. The qualification process, integrated with I&C system acquisition

As Figure 1 illustrates, qualification is based on a detailed qualification plan. A typical input is PHA based on user requirements. It is very important to define safety requirements early in the acquisition process for each safety or safety-related function. When that is defined, the detailed qualification plan and tailoring of questionnaires can be done according to requirements.

Typically, the qualification needs a lot of technical data from system suppliers. Therefore the pre-qualification phase and necessary negotiations with system suppliers is in parallel with qualification planning. The suppliers are informed about the qualification, and are prepared to participate if needed.

Pre-qualification is meaningful to perform in full scale, if the system platform and the application are quite large systems and have typically several safety or safety-related functions. For small systems some less effort-intensive methods are used if possible. The pre-qualification is mainly a combination of detailed and evolved PHA, process assessment and conformance checks against necessary nuclear specific standards. Necessary documents are reviewed as part of assessment. Also verification and validation of technical documents and their safety functions are an essential part of the pre-qualification.

Qualification during application and system development is done when needed. As a process, it is quite similar as the pre-qualification. In most cases it includes further checks of system and application details. Also some additional requirements may evolve from selected normative standards. They may be identified during pre-qualification, but need more attention and evidence. Some typical topics are control of tests and their coverage during application development, and handling of system changes for each application.

3. ISO-based process assessment

ISO 15504 Part 5 (known as the SPICE model) is used in as the main source of process assessment in TVO SWEP method. The latest published ISO standard version ISO 15504 Part 5 is used as the baseline. Part 5 has all ISO 12207 processes and not all of them are relevant for qualification purposes. Many nuclear specific standards include quite similar concepts of processes as ISO 15504 Part 5, and they are also used as normative sources.

The workflow for process assessment shall satisfy ISO/IEC 15504 Part 2 requirements to be acceptable for qualification purpose. Workflow can be seen as combination of stakeholder responsibilities and main assessment phases. Figure 2 illustrates a typical workflow.

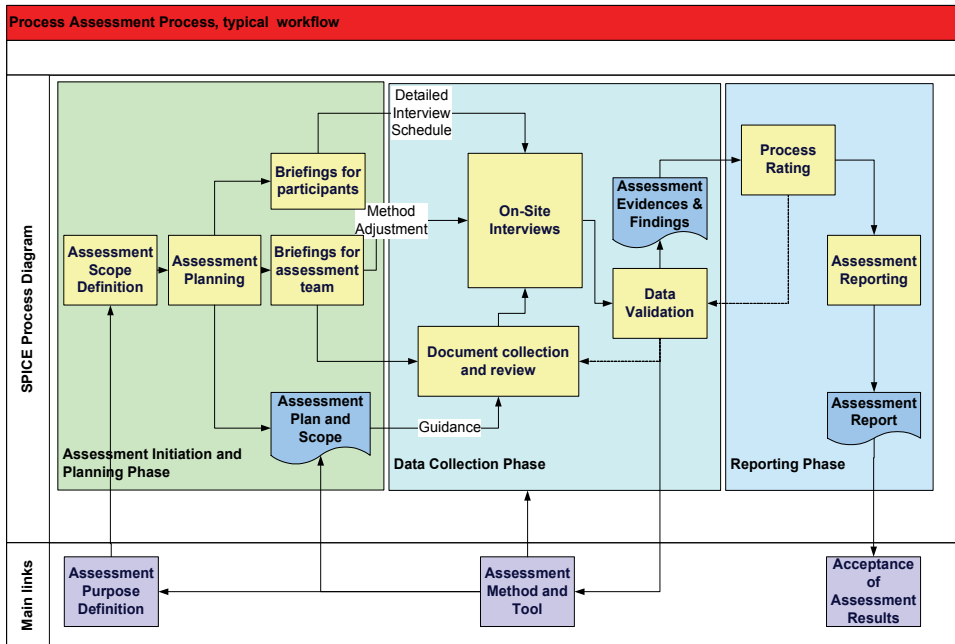


Fig. 2. A typical work flow of process assessment according to ISO/IEC 15504

The list of most relevant SPICE processes for qualification needs is presented in table 1. Not all SPICE processes are as relevant as others, and also the cost-effectiveness of process assessment indicates rather a short than complete list. The criterion for process selection has been alignment and integration of ISO 12207 processes and related nuclear specific standards in Table 1.

Process	Name	Main areas of integration with nuclear specific standards
ENG.1	Requirements elicitation	Detailed specification of safety functions and their SIL type according to PHA analysis results. Requirements for system testing.
ENG.2	System requirements analysis	Validation of each requirement, separate handling of safety requirements. Traceability.
ENG.3	System Architecture design	Allocation of each safety function. Overall architecture of the system. System validation planning.
ENG.4	Software requirements analysis	Specification and independent validation of each software function related to safety
ENG.5	Software design	Similarly as ENG.4. Planning of software verification tests.
ENG.6	Software construction	Module testing and documentation. Avoidance of unnecessary code.
ENG.7	Software integration	Test records. Validation of integration test results.
ENG.8	Software testing	Test records. Validation of software testing results.
ENG.9	System integration	Test records. Validation of system integration test results.
ENG.10	System testing	Test records. Validation of system test results.
ENG.11	Software installation	Installation test. Correct technical environment.
SUP.1	Quality assurance	Quality planning. Reviews and inspections at project level.
SUP.2	Verification	Independent tests and technical reviews.
SUP.3	Validation	Independent FAT and SAT tests.
SUP.7	Documentation	Done according to supplier's process and safety requirements.
SUP.8	Configuration management	Full traceability. Change control.
SUP.9	Problem resolution management	Full audit trail. Analysis of each defect and it's impacts. Common causes of failures.
SUP.10	Change request management	Full change records. Analysis of each change.
MAN.3	Project management	Quality planning. Verification and validation planning.
MAN.4	Quality management	Quality management activities according to supplier's process.
MAN.5	Risk management	Avoidance of product related risks.
MAN.6	Measurement	Measurement-based testing and validation, if possible.

Table 1. List of typical SPICE processes used in process assessment and qualification

Each process is assessed up to capability level 3 or higher, if possible. Level 3 is considered as the required capability level, because only standard processes and an organisation-wide quality system is required for product oriented assessment in safety critical and -related systems. Some processes need a lot of refinements and elaborations to comply with safety-critical system context, and that is done as part of integration of SPICE and nuclear specific standards. In most cases, an interpretation of each SPICE element is not enough, also extension of the processes with additional practices or alternative checklists are needed.

The result of SPICE assessment is a capability level for each process and a number of evidences. They can be used as “mass evidence” for more detailed safety analysis. SPICE capability level is not always the best way to express the real capability of each process. Therefore also an “capability index” is calculated as a ratio of evaluated practices and their sum compared to target level of the process.

Conformance against nuclear specific standards and their safety requirements is done mainly in parallel with SPICE assessment. Most requirements are used as interpretation rules of base and generic practices of each SPICE process. Also complementary methods and evaluations are needed, especially in software and system validation.

4. Additional requirements for process assessment of safety-critical systems

4.1 Basic types of assessment

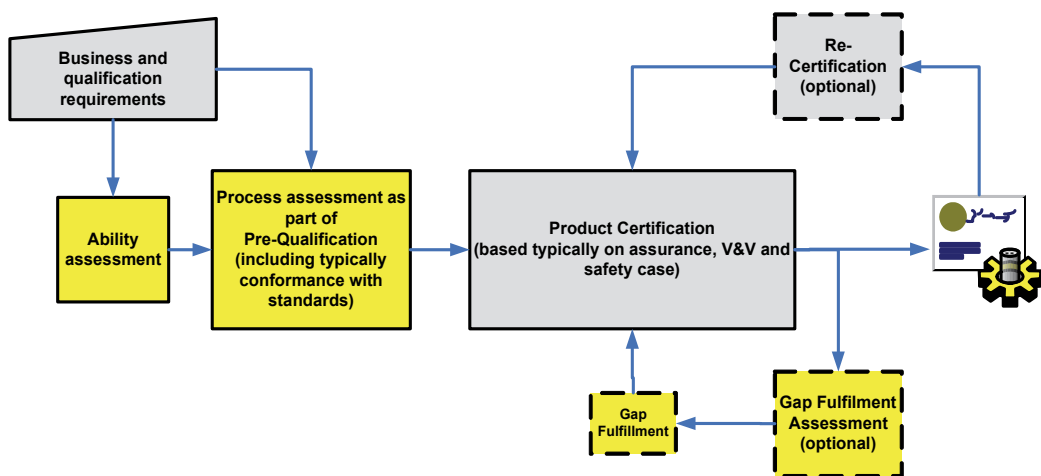


Fig. 3. Typical sequence of different process assessments (yellow boxes) during qualification and certification of safety-critical software

In CERFAS, we have specified three different basic types and “use cases” of process assessment (see figure 3). They are needed typically as a sequence:

- Short “ability assessment” to check overall readiness to develop and deliver safety-critical software. If overall ability of software organisation is low, then it leads to cancellation of the certification process or additional time to restart it. Document review is an essential part of this kind of light assessment.
- Full-scale “certification assessment” to support preliminary software qualification and provide evidence for software assurance and safety case during software certification process.
- “Gap fulfilment assessment” to prevent and fix potential causes of non-conformances of products and processes and their related risks when identified during certification process.

4.2 Ability assessment

Ability assessment is typically quite short, even only some days of effort. It can vary a lot, depending on the current level of software organisation and its products. Typical examples are:

- Assessment of software development processes (mainly ENG category in ISO/IEC 15504 Part 5).
- Review of core documentation or documents from a chosen specific topic, as evidences of process capability and conformance with selected reference standard(s).
- Conformance with selected reference standard(s), for example IEC 61508 Part 3, IEC 62138 or IEC 60880.

Quite often ability assessment is also a combination of several topics. To avoid heaviness and complexity of ability assessment, typical combination is only with two topics. An example could be conformance check + current implementation of bi-directional traceability.

4.3 Full-scale process assessment

Process assessment in CERFAS context is quite normal, SPICE – type process. Of course, it is more formal than most improvement oriented assessments. Evidences are collected and recorded systematically, and they are a solid basis for data collection, validation and ratings. Rigour of assessment is near to Scampi-A method in strictness and formalism [ARC1.2]. Results are reported as gaps to target level. Each gap can be classified by magnitude and risk, as defined in [ISO/IEC 15504-4].

One additional stakeholder in process assessment is the certification body. Typical responsibility is that customer organisation orders certification from a certification body. They decide together which references and methods are used in certification. One basic requirement is independent team for process assessment. Each team member has to fulfil competence requirements. Stakeholders and their relationships in qualification/certification driven process assessment are presented in figure 4.

One other additional requirement is satisfaction of accreditation rules. They are defined in ISO17020 family of standards. Most requirements for process assessment are same as for management system standards (for example ISO 9001). Assessment process must be documented and include competence requirements. Assessment must contain audit trail between assessment phases and intermediate results. Finally, if assessment leads to process certificate, it must be publicly available for intended audience.

Most of accreditation requirements are built in process assessment standards and models. Both SPICE and CMMI model families have such guidance. A specific variant of full-scale process assessment is use of CMMI safety extension as a reference model [+SAFE]. It has two process areas focused on safety, namely Safety Management and Safety Engineering.

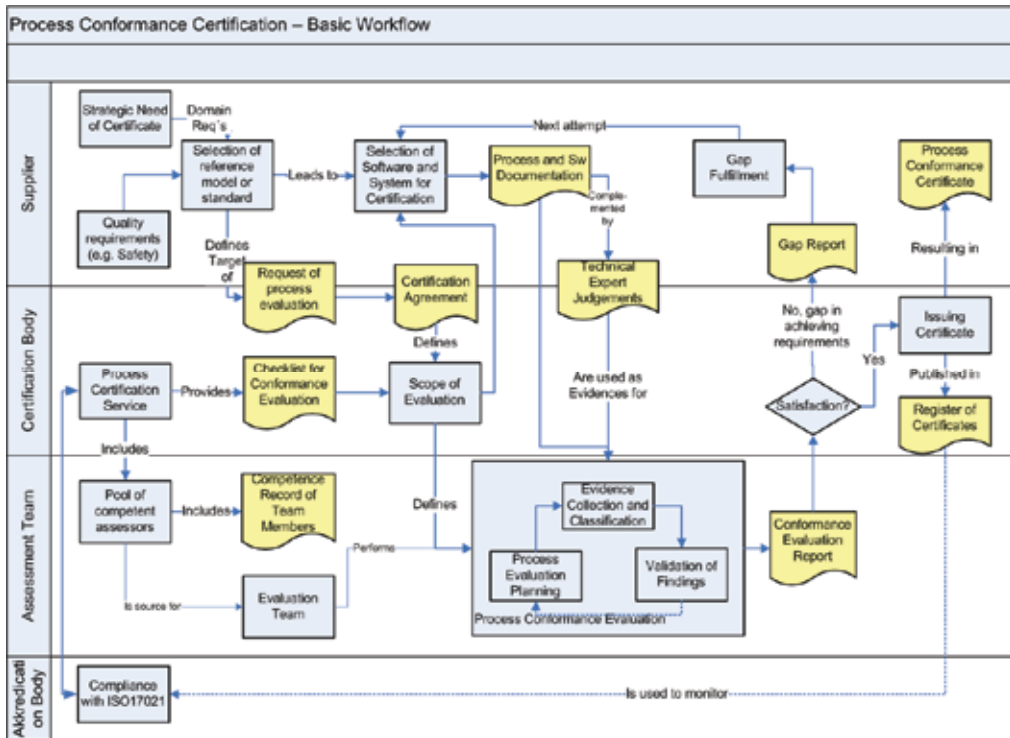


Fig. 4. Stakeholders, their main activities and typical workflow in qualification/certification oriented process assessment and conformance evaluation

ISO working group for process assessment [ISO/IEC JTC1 SC7/WG10] is developing a new reference and assessment model for safety related software domain, called ISO/IEC 15504 Part 10: Safety extension [ISO/IEC 15504-10]. The assessment model includes three new processes to be assessed. Two processes, Safety Management and Safety Engineering, follow the contents of CMMI safety extension. The third process, Tool Qualification, explicitly stresses the importance of the tools used to build safety related software. The assessment model is aligned with some selected safety standards. At the time of writing those are ISO/IEC 26262, IEC 61508, IEC 60880 and UK MoD Def Stan 00-56. In addition to the new processes, there will be also guidance on how to interpret software engineering processes of ISO/IEC 15504-5 and -6 in an assessment in safety related domain.

4.4 Gap fulfilment assessment

Third basic type of process assessment in CERFAS context is check of process improvements needed to get product certificate. This is needed in such cases that software is incomplete or erroneous during any phase of certification. Typical example could be design errors found during independent tests. Then the software organisation needs to change specification and/or design process so that errors can be prevented in advance or detected during design phase. Typical process improvement would be better inspection or quality assurance during early phases of software lifecycle. Sometimes also more formal process would be needed, maybe with model checking type quality assurance. These changes in development process

must be verified, and one easy and straightforward way is focused process assessment. There is nothing specific compared to normal SPICE - type process assessment in this phase.

4.5 Consolidation of process assessment in safety case analysis

In many industry areas, including nuclear industry, the safety of the system is documented in one or more safety cases. Bishop et al. define safety case as "A documented body of evidence that provides a convincing and valid argument that a system is adequately safe for a given application in a given environment" [Bishop1998]. One of the key characteristics common to safety case and process assessment is that they both rely on objective evidences. Typically these evidences are more or less the same ones, but assessment and safety case might look after different aspects from the evidence. For example for code review report, process assessment view might see that the review is done according to process, software measurement view calculates the total coverage of code review and module testing, and competence view checks if the reviewers have had appropriate skills for the task, as shown in Figure 5.

Assessment result as such (full or partial result sets, or risk analysis based on the gaps) can also be used as evidence in safety case, claiming that system is (or is not) programmed properly, and thus increase the confidence that the overall system is (or is not) safe. For example, one might be more confident on the quality of the end product, if engineering processes are at capability level 3 rather than 1.

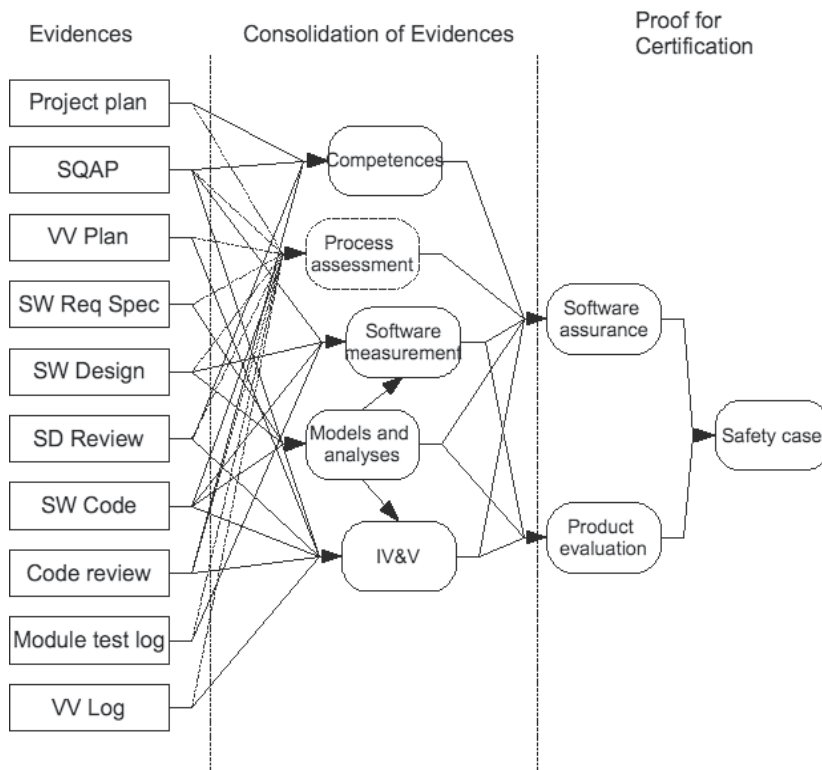


Fig. 5. Same evidences are consolidated into different modules for certification. The final claim that system is (or is not) safe consists of one or more safety cases.

How the actual consolidation is done is still in a conceptual phase. Any of the standards does not give detailed requirements. For example, they can require a certain metric to be collected, but the target values of the metrics are not defined. Also, the modules in Figure 5 could be arranged and linked in many ways, for example so that the “final result” would be Software Assurance Case.

5. Product safety evaluation with Tiira method

5.1 General

The starting point for safety analysis in TVO SWEP method is PHA (Preliminary Hazard Analysis). It defines the need for evidences to achieve required detection level for potential failures.

Tiira starts during or after the requirements specification phase. FMECA is used in requirements specification phase because it is important to

- evaluate as early as possible the failure modes of the I&C system/software in design and development project. The later the phase, the more difficult it is to find consequences of the failure mode and so estimate risk.
- follow the detection of potential software defects in sequential phases of design and implementation. Note. See later slides for the concept of detection.
- identify highest contributor to failures and follow how they are eliminated. This also means on early concentration of important factors of safety related failure modes.
- identify for reducing probability of failure occurring.

In TVO SWEP there are two important specialties of occurrence of causes of failure modes. The first, occurrence is related only to the hardware faults. Hardware faults are not analyzed by Tiira, meanwhile, it is presupposed that occurrence of the I&C system will be calculated and the target value (SIL) is replaced as occurrence number. The second, systematic errors are analyzed by Tiira with the concept of detection.

5.2 Basic principles to perform Tiira

Tiira is a risk-driven analysis tool with which we can identify failure modes of I&C systems caused by potential software faults. In addition to failure modes, Tiira identifies potential effects and causes, and means to mitigate risk.

In Tiira, so called APN (Action Priority Number) is used [ref. FMECA IEC 60812]. APN is composed of three numbers: Severity (SEV), Occurrence (OCC) and Detection (DET). Numbers SEV and OCC are determined from plant or equipment under control. The number DET is determined in knowledge how well we can observe occurrence of the potential failure mode due to software fault. Many factors affect to the number DET, e.g. capability of development process, test processes, and test results (coverage), designs (fault tolerance, fault avoidance, etc.). The number DET is the most important APN factor controlled by Tiira.

5.3 FMECA sheet used in Tiira

The set of hypothetical failure modes is reduced to a set of meaningful failure modes by discarding those for which the APN is enough low.

Based on original safety requirements, each potential failure is classified according to its severity, using for example 1 – 5 scale. Similarly, also the probability of occurrence and required detection rate are classified 1 – 5. SIL levels from IEC/EN 61508 are used as a reference to map each safety function and its required detection rate. As a result, these factors are multiplied into APN number. The calculated APN for each potential failure indicates, how much evidence is needed to achieve acceptable level of failure detection and so the APN as a whole. Figures 6 and 7 explain in more details most important method features.

Figure 6 presents a Tiira sheet with one example. Explanations of existing conditions per column are:

- 8. Severity number SEV: "How bad are the consequences of the failure mode?"
- 9. Occurrence number OCC: "What are the chances of the failure mode or the cause actually happening?" In Tiira-table, OCC-number is provided mainly for electronic, mechanics, etc.
- 10. Detection number DET: "What is the chance of catching the failure mode before it reaches the next operation or the customer?" For occurrence of software faults, DET-number is most important because control actions have impact on it more than SEV and OCC. In fact, SEV number remains the same during analysis.
- 11. Action Priority Number = SEV x OCC x DET

1 Ref.	2 Entry code	3 Potential failure mode (FM)	4 Effect on	5 Potential effect (E)	6 Potential cause (C)	7 Risk controls (RC)	8 Sev	9 Occ	10 Det	11 APN	12 Recommended action	13 Action taken	14 Sev	15 Occ	16 Det	17 APN
General	0	The irradiated fuel is too near the water surface of the pool	Safety	Danger of radiation for people at the pool	1. Operator drives the wagon too near the surface 2. Risk Controls are failed	1. Failure detection by operator at the pool, DET-1 2. Manual emergency stop, OCC-½ 3. Hardwired emergency stop, OCC-1 4. Mechanical stop, OCC-1 5. Position alarm of the mechanical stop, DET-½ 6. Brake system 7. Radiation alarm, DET-½ 8. Lock keys	5	2,5	3	37,5	1. Position detection of the mechanical stop 2. Radiation protection 3. Programmable safety stop 1-3: OCC-1	For further SW error detection evaluation, DET-1	5	1,5	2	15

Fig. 6. Use of severity, occurrence and detection variables to calculate APN. An example of one potential failure mode is presented just for illustration.

Figure 6 has one example potential failure mode. Analysis of it gives result APN value 37,5. Highest acceptable value is 25 using 1 – 5 scale, because result of maximum values in SEV x OCC x DET equation is 5 x 5 x 1 = 25. So, some additional controls are needed. They are specified in columns 12 and 13, leading to new APN value 15, which is acceptable. As seen from columns 15 and 16, both OCC and DET values have been changed to reach accepted value.

5.3 Evidence collection and analysis in Detection Table

Figure 7 is a sample from a so called Detection Table of the TVO SWEP method. Figure 7 shows only app. 40 lines from total of 200 items to improve failure detection. The full Detection Table covers software life cycle and related QA and V&V activities. It covers also all SPICE processes in table 1.

		Total reduction detection number: 1	
		APPLICATION	
Total average		0,72	0,71
Factors for verification rate		0,93	0,93
r	Size of the project	1	1
r	Degree of complexity of the design	1	1
r	Degree of novelty of the design	1	1
r	Degree of novelty of the technology	0,66	0,66
r	SIL	1	1
Verification of deriving the I&C requirements		0,92	0,66
SPICE	Pre-Q of the process, ENG.1 Req.s elicitation	0,66	0,66
r	Walkthrough of functional, performance and independence re	1	0,66
r	Walkthrough of the categorisation requirements, interfaces, t	1	0,66
r	Walkthrough of plant constraints	1	0,66
Verification of I&C specification		0,83	0,77
SPICE	Pre-Q of the process, ENG.2 System requirements analysis	0,91	0,91
SPICE	Pre-Q of the process, ENG.3 System architecture design	0,92	0,92
r	Walktrough of the I&C architecture	1	1
r	Walktrough of functions assignment	1	1
r	Walktrough of required analysis	0,33	NA
o	Formalised descriptions of system specification		
o	Review of traceability and consistence (TA)		
Verification of system detailed design and implementation		0,00	0,00
r	Walktrough of system design	NA	NA
r	Walktrough of system implementation	NA	NA
o	Review of traceability (TA)		
Verification of SW Requirements Specification, SRS		0,96	0,96
SPICE	Pre-Q of the process, ENG.4 Software requirements analysis	0,88	0,88
r	Walktrough of SRS	1	1
r	Walktrough of interfaces with HW, users, etc.	1	1
o	Analysis of SRS (Formalised descriptions)		
o	Prototyping of SRS requirements		
o	Review of traceability (TA)		
Verification of system test plans		1,00	1,00
r	Inspection of test plan	1	1
o	Review of traceability (TA)		
Verification of SW Design Specification, SDS		0,76	0,54
SPICE	Pre-Q of the process, ENG.5 Software design	0,91	0,91
r	Review of SDS (Walkthrough or Inspection)	0,66	0,66
r	Assessment of performance parameters (Proto)	0,66	0
r	Traceability of allocated functions (TA)	0,66	0
r	Assessment of data required (Inspection)	0,66	1
r	Analysis of fault tolerance (Inspection)	1	0,66

Fig. 7. A sample from an Excel based checklist to calculate detection index DET. An example is presented just for illustration.

Detection Table summarizes qualification findings in a composite index called "Total detection number DET". The idea is to use DET index as load or backing evidence in FMECA sheet (Column 10 - Column 16 in Figure 6). The table is separate for Pre-Qualification and Qualification phases. In most cases it is also separate for Platform and Application. Evidence in each phase is gathered by process evaluation (SPICE) and product safety evaluation (FMECA). Also compliance with nuclear specific standards is taken into account here.

SPICE capability level is converted to capability index, which summarizes detailed practice ratings at levels 1 - 3 for each process. It is normalized to get values between 0 - 1 for each capability level. Other evidences are detailed requirements from V&V processes, as defined in IAEA report no. 384 [6].

In the example of Figure 7, we present two columns for DET and its inputs. The right column is for the pre-qualification phase and the left column for the additional nuclear specific verification of the application. The pre-qualified system was in this case a radiation monitoring equipment. As seen in the example, also NA (Not Applicable) rating is allowed and used, if relevant input data or rating result is not available. Similar table is often needed also for the software platform.

In most cases the Severity and Occurrence parameters remain the same and only failure detection rate can be improved. As a result, Action Priority Number APN may reach an acceptable level. In our example (see columns 11 and 17 in figure 6) the goal was that each potential failure has APN value 25 or less. In our example that is the case, and the qualification has been successful. DET value has changed from 3 to 2, and Detection Table in figure 7 shows that we have achieved this one level reduction by a large amount of evidences and actions.

Finally, the aim is to determine the Reduction Detection Number RDN. RDN is typically a difference between DET number at FMECA table (see columns 10 and 16 in Figure 6 as an example). RDN can get a value 0 - 4. The Detection Table calculates the value of RDN automatically, based on the SPICE and V&V evidences. Calculated RND value is then used in Tiira FMECA table to reduce Detection rate. The index limits for for RDN value 0 - 4 are: <0.60, 0.60 - 0.74, 0.75 - 0.89, 0.90 - 0.98, 0.99 - 1.0.

6. Certification to support qualification

In Finland, a type acceptance certificate is required mainly in highest safety class of I&C equipments and systems in Nuclear Power Plants, and recommended in lowest safety classes. In the research project "Certification facilities for software (CERFAS)", the objective is to develop a Software Certification Service, SCS, able to certificate safety critical software for the demands in Finnish nuclear area. The framework of SCS is described in Figure 8.

Certification can be defined as "the process of assessing whether an asset conforms to predetermined certification criteria appropriate for that class of asset" [10]. This idea of conformance with criteria is the fundamental principle of certification. Certification is documenting compliance of a product and product development process to a standard such as IEC 60880 and IEC 61508 within a defined but possibly broad set of potential applications. In general, certification is seen in CERFAS as a service to support qualification and further licensing (Figure 8). Qualification includes a system qualification and an application qualification. The system qualification is documenting a justifiable argument to attain an

operating license for the complete realized system. On the other hand, the application qualification is documenting functional safety suitability for a specific system product in a specific target application.

Various areas of methods, standards and justification means are needed to support certification. Some examples are process assessment, product evaluation and use of different analyses and tests. For certification, an accredited Certification Body is needed. Type testing or other kind of Independent Verification and Validation (IV&V) is typically a fundamental part of the certification. Any CB needs a variety of services to run a certification service and to integrate different approaches as a coherent system.

Each certification type has its own assessment elements. The framework in CERFAS assumes that certification is based on some reference model, norm or set of criteria. Certificate itself is then a conformance statement against those requirements. Typically, such statement is justified by some methods, which include external audits, IV&V's, reviews and inspections, code analysis and type tests. Safety cases provide a formal argument to justify that a system is safe [11].

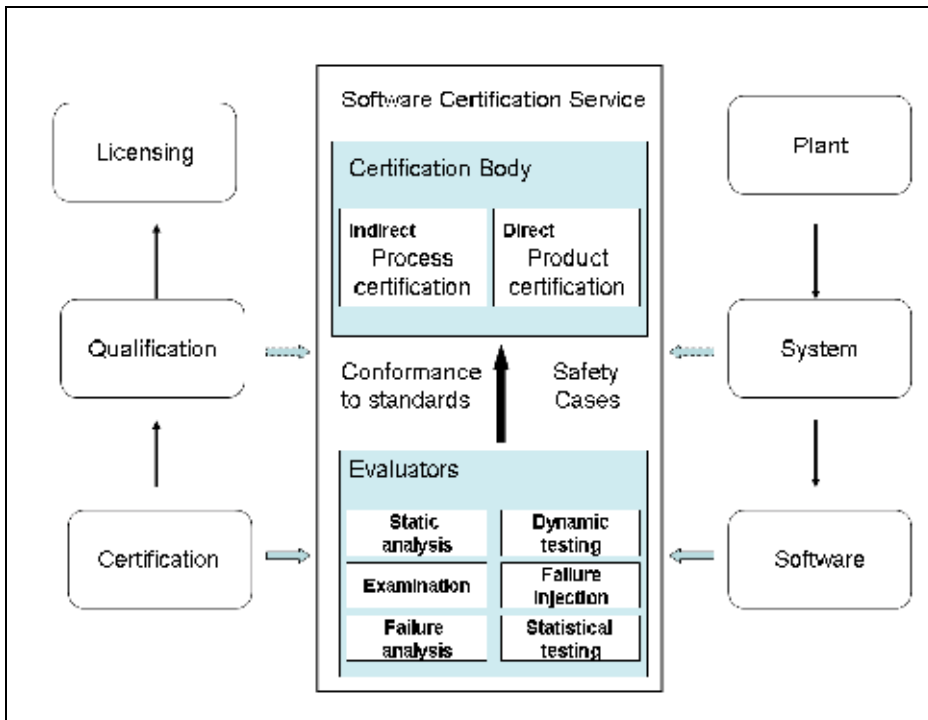


Fig. 8. CERFAS gives facilities for SCS including Certification Bodies and evaluators. Conformance to standards or other predetermined criteria is fundamental principle of certification.

7. Conclusions and future developments

Several real-life qualifications are already done by using TVO SWEP method. The goals of the method are achieved well, and the pre-qualification is effective. It is evident that TVO

SWEP needs still refinements and additional validation. Main difficulty is to collect evidences so systematically, that the necessary calculations and reports could be done as automatically as possible. Then the main focus can be in professional topics and may lead to useful win-win findings between TVO and the supplier.

Additional methods for software certification are also validated with real life cases. Certification is needed mainly in safety-critical systems. Attention is more in product evaluation than process assessment. Evaluation process is quite rigor and formal. Main form of results has been safety case, which quantifies all kind of evidences.

Other industries may have quite similar needs for qualification as nuclear power plants. For example control of railway and metro networks and traffic, electro medical devices like patient control systems and many military systems could be users of our method. Many standards are also under development, and can be seen as "second generation" of safety-critical systems. Some examples are ISO 26262 for vehicle industry and European standards for space industry (ECSS).

8. References

- YVL 5.5, Instrumentation systems and components at nuclear facilities. STUK 2002. IEC 61513, Nuclear power plants – Instrumentation and control for systems important to safety – General Requirements for Systems. 2001. IEC 62138, Nuclear Power Plants Instrumentation and Control Computer-based systems important for safety Software for I&C systems of safety classes 2 and 3. 2001.
- ISO/IEC 15504 Part 5. An Exemplar Process Assessment Model. 2006.
- Safety Guide, Software for Computer Based Systems Important to Safety in Nuclear Power Plants. 2000.
- IAEA 384, Verification and Validation of Software Related to Nuclear Power Plant Instrumentation and Control. 1999.
- IEC/EN 61508, Functional safety of electrical/electronic/ programmable electronic safety-related systems. 1998.
- Common Position of European Nuclear regulators for the licensing of safety critical software for nuclear reactors, EUR 19265, 2000.
- Harju, H. Ohjelmiston luotettavuuden kvalitatiivinen arviointi (The qualitative assessment of software dependability, Tiira method). VTT Technical Research Centre of Finland. VTT Research Notes 2066. 2000.
- ISO/IEC 24765, Systems and software engineering vocabulary. 2009.
- P. G. Bishop and R. E. Bloomfield. A methodology for safety case development, in Safety-Critical Systems Symposium, Birmingham, UK, Feb. 1998.

Author CVs

Risto Nevalainen

Director of Finnish Software Measurement Association FiSMA and Spinnet Oy.

Mr. Risto Nevalainen (Lic. Tech.) has long experience in software measurement and quality topics. His working experience includes position as managing director of Finnish Information Technology Development Center during 1989-1995. Before that he had different research and management positions for example in Technical Research Centre (VTT),

Technical University of Helsinki (HUT) and Finnish Prime Minister's Office. Mr. Nevalainen has participated in ISO15504 (SPICE) standard development since beginning. He is Competent SPICE Assessor and ISO9001 Lead Assessor. Risto Nevalainen is co-editor of ISO/IEC 15504 Part 5 upgrade.

Juha Halminen

Qualification and Commissioning Engineer in TVO.

Mr. Juha Halminen has ten years experience in nuclear equipment quality topics. His working experience includes qualification of new equipment with or without software to nuclear power plant safety systems. He has been the key person in developing software qualification procedures for TVO. He also works as a commission inspector of nuclear power plant safety systems. Mr. Halminen has performed assessments and audits using SPICE, ISO 9001, IEC 62138, IEC 60880 and KTA 3507. He has participated in MAGIC project from 2006 to 2008. Before that he was participated in business development work in Russia. During 1994-1995 he was researching influence of contamination and humidity to building stones, concrete and mortar in IBW Germany.

Hannu Harju

Senior Research Scientist in VTT

Lic.Tech. Hannu Harju has long experience of critical control systems and software. He has been as an assistant professor of system theory at Technical University of Lappeenranta and as a chief evaluator of control systems and software at Certification Department of Inspecta.

Mika Johansson

Inspector, Radiation and Nuclear Safety Authority Finland, on two year term from 2010 to 2012. Partner and co-founder, Spinet Oy.

Mr. Mika Johansson (M.Sc (Eng)) has been working as a trainer and consultant in quality and project management areas for more than ten years. He has been Executive Director in Finnish Software Measurement Association FiSMA from 2006 to 2010. In Spinet Oy, Mr. Johansson has performed assessments and audits using SPICE, CMMI, ISO9001, ISO/IEC 20000 and safety specific models since 2003. He has been part-time researcher in Tampere University of Technology in CERFAS project from 2007 to 2010. Mika Johansson is co-editor of ISO/IEC TR 15504-10 Safety Extensions.

Pressure sensing line diagnostics in nuclear power plants

Kang Lin and Keith E. Holbert
Arizona State University
U.S.A.

1. Introduction

Nuclear power plants (NPPs) have been designed to attain safe and reliable functioning through the monitoring and analysis of various critical operational parameters. Data obtained from monitoring systems provide for the control of feedwater flows, recirculation flows, reactor water levels, etc. and can be used to initiate emergency procedures, such as water injection into the reactor coolant system. Therefore, it is crucial for sensing equipment to precisely convey neutron flux, temperature, pressure, level, and flow of plant processes to assure the continued safe and reliable operation of a NPP.

A differential pressure transmitter is used to measure fluid flow and level while a non-differential transducer is utilized to measure absolute and gauge pressure. A NPP generally uses about 200 to 800 pressure and differential pressure sensors to measure the process pressure, level, and flow in its primary and secondary systems (Hashemian, 2006). Pressure transmitters are usually located away from the process to protect them from the adverse effects of ambient temperature, radiation, and vibration on the operability and qualified life of the sensor (Hashemian, 2006). For example, high ambient temperatures will have effects on the mechanical components of the transmitter and shorten the life of its electronics.

Pressure sensing lines, also referred to as impulse or instrument lines, are employed to couple a pressure transmitter to the process piping, reactor vessel, or primary flow elements to convey a pneumatic or hydraulic signal from the process to the sensors. In some industrial plants, the pressure sensors are generally installed near the ground using long sensing lines so that personnel can easily access the transmitter for replacement or maintenance purposes. However, process connections using sensing lines may be blocked by accumulations of impurities from the fluid. It is important for the sensing lines to be periodically purged, or blown down, in order to remove any foreign fluid and impurities that can degrade the accuracy of pressure transmitters.

Instrument lines can encounter a number of problems that can influence the accuracy and response time of a pressure sensing system. Sensing line problems that have been noticed in NPPs include

- blockages due to sludge, boron, or deposits,
- air or gas entrapped in low-pressure sensing lines,
- frozen sensing lines, and

- leakage from sensing lines.

Any one of these issues can increase the pressure sensing system response time or cause other problems. For instance, blockages, voids, or freezing in sensing lines can cause errors in pressure measurements and also affect the dynamic response of the pressure sensing system. Despite provisions usually made against these problems in the design of sensing lines, experience has shown that they do occur in many NPPs.

In this chapter, signal processing methods for online diagnostics of sensing lines are presented. The development and interpretation of these techniques requires mathematical modelling of the impulse lines, which is accomplished herein using the hydraulic-electric analogy. Results from applying the modelling and diagnostics to instrument lines in operational electric power plants are presented.

2. Background

As mentioned previously, pressure transmitters are sheltered from harsh environmental effects by siting them away from the process. Depending on the application, one or two sensing lines are used to couple a pressure sensor to the process piping, reactor vessel, or primary flow elements. Sensing lines are typically made of small diameter (on the order of 6 mm to 13 mm) stainless steel, carbon steel, or copper tubing in thicknesses of about 2 mm. Tubing is preferred over piping because it can be installed in one piece, reducing the possibility of leaks. Both *liquid-filled* and *gas-filled* impulse lines can be found in NPPs. Liquid impulse lines are typically filled with either the process liquid or oil depending on the sensing line design and application. Gas instrument lines are filled with steam, air, nitrogen, or other gases, and there is sometimes a transition in these lines to another medium, such as oil or water.

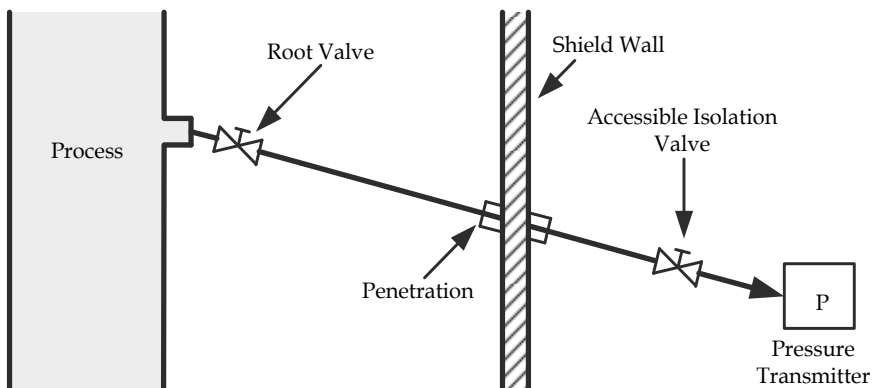


Fig. 1. Typical pressure sensing line inside a nuclear reactor containment.

Sensing lines vary in length, ranging from a few meters to 200 or 300 meters depending on the transmitter location and service in NPPs (Hashemian et al., 1993). Because the overall response time of the pressure sensing system is affected by the instrument line length, impulse lines are made as short as practically possible. Therefore, the average length of sensing lines for safety-related pressure transmitters is usually 10 to 50 meters (Hashemian et al., 1993). Fig. 1 shows a typical pressure sensing line inside a nuclear reactor containment

where the root and isolation valves are employed to connect the sensing line to the process and to a pressure transducer, respectively.

Sensing line installations are designed to allow for thermal expansion and vibration without deformation, to ensure drainage by gravity, and to provide for self-venting. For liquid-filled impulse lines, self-venting is accomplished by slanting the impulse line downward to allow any gas or air in the line to vent to the process. If the instrument line cannot be sloped as required, a high-point vent and low-point drain will be needed for liquid and gas sensing lines, respectively. The mechanical design, engineering, fabrication, installation, testing, and protection of power plant instrumentation sensing and control lines are addressed within industrial standards (ISA, 1999; ISA, 2005; ASME, 2007). These standards establish the applicable installation requirements and limits of instrumentation sensing and control lines and their instruments in both fossil and nuclear power plants.

Blockage, voids, or leaks in sensing lines can cause errors in pressure measurements and can also affect the dynamic response of the pressure sensing system. Although sensing lines are usually designed to avoid these problems, they still occur in industrial processes.

- *Blockage.* Blockages occur in sensing lines when solidification of boron, sludge, and other containments accumulate in the reactor water. Blockages also take place from obstructions because of improper line up or seating of isolation and equalizing valves and crimping of sensing lines. Partial blockages are detrimental only to the dynamic response time of the system and do not normally affect the static output of the system. However, the pressure information is totally lost when the blockage has built up to the level of completely obstructing the line. In addition, sensing line clogs can significantly increase the dynamic response time of pressure systems (Hashemian et al., 1993). Remedies that are practiced in several NPPs to remove deposits from sensing lines are to blow down, back fill, or drain the lines periodically. Condition monitoring based approaches also can be applied to deal with impulse line blockages by detecting their presence.
- *Voids.* Air or gas entrapped in liquid sensing lines can result in false pressure readings, sluggish response, and extraneous noise due to acoustic resonances. For instance, an air pocket in absolute pressure transmitters can cause the pressure indication to be lower than normal in addition to adding a delay in transmission of the pressure information. Voids are difficult to purge from the system, and the problem exists even though high pressures are involved.
- *Leakage.* A sensing line may have a root valve, one or more isolation valves, an equalizing valve, and other connections that can provide opportunities for leakage to happen, especially under high operating pressures. Any significant leakage or loss of fluid from an instrument line can induce a false pressure reading.

Examples of sensing line problems experienced by the U.S. nuclear power industry can be found within the Nuclear Regulatory Commission licensee event report (LER) database. Hashemian et al. (1993) uncovered 551 reports of impulse line problems from approximately 40,000 LERs spanning 1980–1992. Table 1 shows some examples of sensing line problems experienced by the nuclear power industry along with the particular pressure-related variable being sensed. An interesting case of blockage is that of a frozen sensing line. Freezing can take place in fluid sensing lines under cold weather conditions if the heat tracing of the sensing line is aged or damaged, or in the event of power loss. Although the

transmission of pressure ceases when the instrument line is completely frozen, the problem can be overlooked if the static working pressure remains registered by the transducer.

Failure Mode	Specific Problems	Locations of Problems
Blockage	Partial blockage due to sludge build-up Sensing lines plugged with boric acid Obstruction in low pressure line Magnetite in sensing line Frozen sensing line	Steam generator level Boric acid tank level Steam generator flow Steam generator level Steam generator pressure
Voids	Air pocket in low pressure line side Air pocket trapped in sensing line Entrapped air in sensing line	Steam generator level Pressurizer level Reactor water cleanup system flow transmitter
Leakage	Leak in instrument line Leak in upper-seal pressure sensing line due to weld crack from vibration	Safety-related nitrogen level Reactor coolant pump upper-seal cavity pressure

Table 1. Examples of sensing line problems (Hashemian et al., 1993)

The possibility of such pressure sensing line failure modes is an impetus to establish predictive maintenance (PM) programs. Equipment health monitoring is known by a variety of related endeavours including condition-based and reliability-centred maintenance (RCM). Figure 2 illustrates three basic approaches to equipment maintenance. Corrective (or reactive) maintenance is taken only after the component has failed. To avert breakdown, preventive approaches involve anticipatory actions based on a schedule or prediction. Scheduled maintenance, which may involve inspections and/or pre-emptive replacements, can be performed on either calendar or equipment use bases. PM is initiated on the basis of a detected onset of equipment malfunction or failure. RCM incorporates all three approaches while considering the importance of the equipment to the facility mission, and is generally based upon a failure modes and effects analysis.

To accomplish PM without interrupting equipment operation necessitates the use of online monitoring tools for signature analysis. Those signatures, in turn, must be scrutinized to ascertain whether the system or component is trending toward a failure condition. The originating signals are often the result of stochastic (random) processes. The nuclear power industry has traditionally referred to this technique as *noise analysis*. Noise analysis has been used for a variety of nuclear power plant applications including boiling water reactor stability, core barrel motion and moderator temperature coefficient of reactivity determination (Thie, 1981).

The capability to detect faults and to replace the components just prior to failure is desired by industry. By doing so, the consequences of unexpected equipment failures can be avoided. Online component monitoring can yield higher availability, extended life, and reduced costs. Incipient failure detection not only serves to avoid catastrophic failure, but also to assist in planning corrective actions (i.e., preventive maintenance). Incipient failure detection also has the ability to assist in achieving condition-based maintenance objectives. This chapter focuses on developing innovative techniques for detecting blockages, voids, and leakages in the pressure instrument lines.

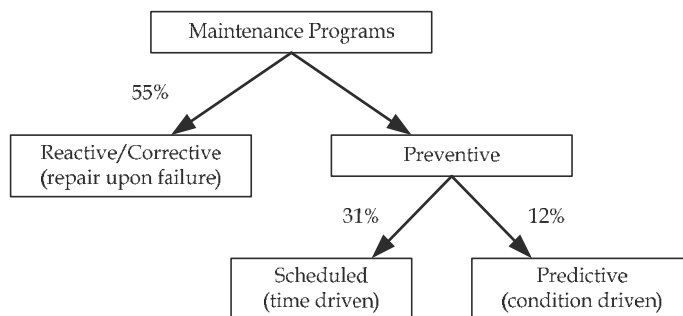


Fig. 2. Equipment maintenance approaches. The percentages represent the categorization of maintenance program in the U.S. from Sullivan et al. (2004) based on a survey in 2000.

3. Sensing Line Modelling

Instrument lines and pressure transmitters are the two major components forming a pressure sensing system. Therefore, to simulate a pressure measuring system, both the sensing line and the pressure transmitter should be modelled. A number of representations have been developed to study pressure transmitters and sensing lines dynamics (Barbero et al., 2000; Bergh & Tijdeman, 1965; Hashemian et al., 1993; Iberall, 1950; Müllens & Thie, 1989). The models presented in this chapter aim at deriving the pressure sensing system transfer function to facilitate the investigation of the pressure signal power spectral densities (PSDs) obtained for noise analysis. These models demonstrate how the system parameters—such as length and cross-sectional area of the sensing line, and the sensing line medium density and sound speed—affect the system transfer function and PSD resonances.

3.1 Hydraulic–Electric Analogy

The hydraulic–electric analogy that relates pressure and flow to voltage and current, respectively, has been well established and applied to a variety of disciplines, including pumping (Gogolyuk et al., 2004), pressure transducers (Clark, 1985), woody plant hydraulics (Tyree & Ewers, 1991), and the human arterial system (Westerhof et al., 1969). The hydraulic (or acoustic) and electrical analogues are summarized in Table 2. Schönfeld (1954) distinguishes between hydraulic and acoustic systems based on the fluid. Specifically, he places incompressible fluids, such as water, into the category of hydraulic systems, whereas acoustical system behaviour is affected by the fluid (*e.g.*, air) elasticity.

General	Electrical	Hydraulic-Acoustic
Flow variable	Current, I	Fluid flow, Q
Potential variable	Voltage, V	Pressure, p
Integrating element	Inductance, L	Inertance, $p = L (dQ/dt)$
Proportional element	Resistance, R	Fluid resistance, $R = p / Q$
Differentiating element	Capacitance, C	Fluid capacitance, $Q = C (dp/dt)$

Table 2. Analogies between electrical and hydraulic systems

The hydraulic–electric analogy also can be employed to the field of pipeline modelling. Consider laminar flow in a tube filled with an incompressible fluid where Q is the fluid

volumetric flow rate. Friction on the tube wall causes a loss of pressure potential, p . The friction-caused potential loss can be expressed as

$$\Delta p = R Q \quad (1)$$

For a round tube in both hydraulic and acoustic systems, the *hydraulic-acoustic resistance* may be represented by (Schönfeld, 1954; Olson, 1957)

$$R = 8 \mu \ell / (\pi r^4) \quad (2)$$

where μ is the dynamic viscosity, ℓ and r are the tube length and radius, respectively. Note that the tube diameter is assumed to be small compared to the tube length so that the end correction may be neglected. Expressions for R must be developed based upon the unique flow characteristics of a given system.

Consider a variable flow rate through a tube for both hydraulic and acoustic systems. Ignoring friction for the moment, a potential difference is required to accelerate or to decelerate the flow, amounting to

$$\Delta p = L dQ/dt \quad (3)$$

The factor L is called the *hydraulic-acoustic inertance* of the system and can be written as (Schönfeld, 1954)

$$L = \rho \ell / A \quad (4)$$

where A is the tube cross-sectional area and ρ is the fluid density. Similar to R , system-specific L expressions must be derived for diverse hydraulic-acoustic systems.

Hydraulic-acoustic potential energy is associated with the compression of a fluid or gas. Hydraulic-acoustic energy increases (decreases) as the fluid is compressed (expanded). *Hydraulic-acoustic capacitance* is the element that opposes a change in the applied pressure. The pressure in terms of the volume displacement, ΔV , can be expressed as (Olson, 1957)

$$p = c^2 \rho \Delta V / V \quad (5)$$

where V is the initial volume and c is the acoustic velocity of fluid in the sensing line. The hydraulic-acoustic capacitance, C , is defined via

$$p = \Delta V / C \quad (6)$$

From Eqs. (5) and (6), the acoustic capacitance of volume V is

$$C = V / (\rho c^2) \quad (7)$$

Physically speaking, the hydraulic-acoustic capacitance is used to represent a cavity or small volume with rigid boundaries.

For example, Hashemian et al. (1993) represented a pressure sensing system by a spring mass system as shown in Fig. 3. As the process pressure changes, the pressure surge is transmitted through the sensing line resulting in a volume change (ΔV_t) in the transmitter cavity. To describe the relationship between the volume change in the transmitter and the pressure required to induce the volume change, a term called *transmitter compliance* is employed. For a pressure change of Δp_s , the transmitter compliance (C_t) can be expressed using Eq. (6) as

$$C_t = \Delta V_t / \Delta p_s \tag{8}$$

Typical units for the compliance are cm^3/bar .

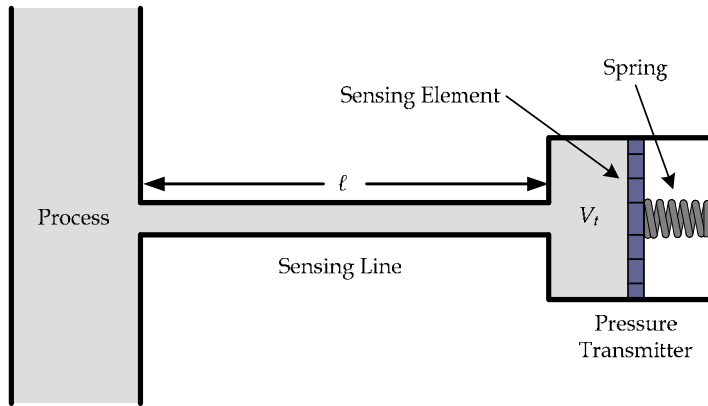


Fig. 3. Spring mass model of a pressure sensing system; after Hashemian et al. (1993).

3.2 Lumped Parameter Model Using Hydraulic-Electric Analogy

By applying the hydraulic–electric analogy, pressurized lines can be represented using electrical circuits, that is, a hydraulic tube is realized as an electric power transmission line. Therefore, similar to transmission line modelling, there are multiple circuit topologies (see Fig. 4) that can be used to accomplish sensing line lumped parameter modelling. The circuit parameters in Fig. 4 can be expressed as

$$R = \frac{8\mu\ell}{\pi r^4}; \quad L = \frac{\rho\ell}{\pi r^2}; \quad C = \frac{\pi r^2\ell}{\rho c^2} \tag{9}$$

Using the simple electrical circuit model of a hydraulic tube, as shown in Fig. 4(a), the transfer function between the input p_i and output p_o pressures can be derived as

$$\frac{p_o}{p_i} = \mathbf{H}_s(j\omega) = \frac{1/(j\omega C)}{R + j\omega L + 1/(j\omega C)} \tag{10}$$

This L-shaped model is a classic underdamped second-order system with a resonant frequency of

$$\omega_{s0} = \frac{1}{\sqrt{LC}} = \frac{1}{\ell/c} \quad (11)$$

The *pi*- and *tee*-shaped representations shown in Figs. 4(b) and 4(c), respectively, are referred to here as the general cases which share an identical transfer function of

$$\mathbf{H}_G(j\omega) = \frac{1}{(1 - \omega^2 LC/2) + j\omega RC/2} \quad (12)$$

which has a resonant frequency of

$$\omega_{G0} = \sqrt{\frac{2}{LC}} = \frac{\sqrt{2}}{\ell/c} \quad (13)$$

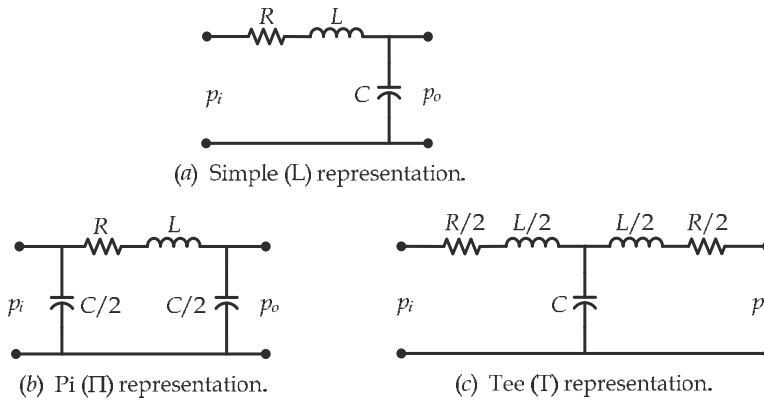


Fig. 4. Sensing line lumped parameter circuit models.

3.3 Sensing Line Model with Linear Distributed Parameters

The analytical solution for unsteady flow problems is obtained by using equations for continuity, momentum, and energy. These equations correspond to the physical principles of mass conservation and energy conservation. Applying these equations leads to a coupled nonlinear set of partial differential equations. After linearization, two linearized partial differential equations describing flow continuity and momentum can be derived as (Matko et al., 2000; Matko & Geiger, 2002; Izquierdo & Iglesias, 2002; Izquierdo et al., 2004):

$$L \frac{\partial Q}{\partial t} + R' Q = -\ell \frac{\partial p}{\partial x} \quad (14)$$

$$C \frac{\partial p}{\partial t} = -\ell \frac{\partial Q}{\partial x} \quad (15)$$

where x is distance along a pipe, t is time, and $R' = (\ell \rho f \bar{Q}) / (A^2 2r) = 2R$ with f being the dimensionless Darcy-Weisbach friction factor ($f = 64/\text{Re}$ for laminar flow), and \bar{Q} being the

average fluid volumetric flow rate. Solving Eqs. (14) and (15) by using initial fluid conditions, the linearized pressurized line model can be written as:

$$Q_i = \frac{1}{Z_c} \sinh(\sqrt{(R' + sL)sC}) p_o + \cosh(\sqrt{(R' + sL)sC}) Q_o \quad (16)$$

$$p_i = \cosh(\sqrt{(R' + sL)sC}) p_o + Z_c \sinh(\sqrt{(R' + sL)sC}) Q_o \quad (17)$$

where $Z_c = \sqrt{(R' + sL)/(sC)}$ is called the *characteristic impedance*, and Q_i and Q_o are the input and output flow rates, respectively. Therefore from Eq. (17), the “exact” transfer function for pipe pressure can be expressed as (Matko et al., 2000):

$$H_E(s) = \frac{p_o}{p_i} = \frac{1}{\cosh(\sqrt{(R' + sL)sC})} \quad (18)$$

The approximate resonant frequencies of the exact model can be derived as (Lin & Holbert, 2009a):

$$\omega_{En} = \frac{n\pi}{2\sqrt{LC}}, \quad n = 1, 3, 5... \quad (19)$$

The exact formula of Eq. (18) can be approximated by a second-order system (Matko et al., 2000):

$$H_A(s) = \frac{1}{[LC/2 + (R'C)^2/24]s^2 + R'Cs/2 + 1} \quad (20)$$

which has a resonant frequency at $\omega_0 \approx \sqrt{2/(LC)}$ – the same as the pi and tee models given in Eq. (13).

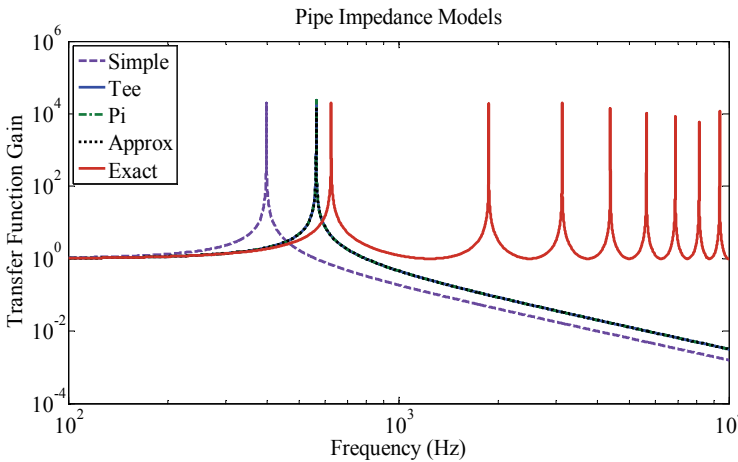


Fig. 5. Transfer functions for the exact (H_E), pi and tee (H_C), simple L (H_S), and approximate (H_A) pipeline models. The pi, tee and approximate models overlay one another. The pipe system parameters are $\ell = 60$ cm; $r = 0.8$ cm; $\mu = 0.01$ g/cm s; $\rho = 1$ g/cm³; $c = 150,000$ cm/s; $Re = 1000$; and $\bar{Q} = 6.25$ cm/s.

Lin and Holbert (2009a) compared the hydraulic-electric models described previously as shown in Fig. 5. The pi and tee models are nearly identical to the approximation of the exact model. Therefore, the pi and tee models are considered more accurate than the simple (L) expression. However, it can be recognized in Fig. 5 that the resonant frequencies of the pi, tee and approximate models do not match the fundamental resonant frequency of the exact model. Besides, the pi, tee and approximate models only reveal the first resonant peak and its location in the frequency domain while the exact model exhibits multiple resonant peaks. Furthermore, a high frequency roll-off appears in non-exact cases.

3.4 Equivalent Pi Circuit

In order to facilitate the implementation of the pipeline exact model for complex pressure system modelling, an equivalent circuit is introduced. The circuit shown in Fig. 6 is called an *equivalent pi circuit* that has been used in power transmission line modelling (Glover & Sarma, 2000). From Fig. 6, p_i and Q_i can be expressed in terms of p_o and Q_o as

$$p_i = \left(1 + \frac{Z}{Y}\right)p_o + ZQ_o \quad (21)$$

$$Q_i = \frac{1}{Y}\left(2 + \frac{Z}{Y}\right)p_o + \left(1 + \frac{Z}{Y}\right)Q_o \quad (22)$$

By comparing the coefficients of Eqs. (17) and (21), Z and Y are recognized as:

$$Z = Z_c \sinh\left(\sqrt{(R' + sL)sC}\right) \quad (23)$$

$$Y = \frac{Z_c \sinh\left(\sqrt{(R' + sL)sC}\right)}{\cosh\left(\sqrt{(R' + sL)sC}\right) - 1} \quad (24)$$

Overlays (not shown) of the transfer functions from the exact model and the equivalent pi representation are identical, as expected since the theory in Glover and Sarma (2000) shows them to be equal. In other words, the equivalent pi circuit representation yields the same frequency response as the exact model, *i.e.*, $\mathbf{H}_Z = \mathbf{Y}/(\mathbf{Y} + \mathbf{Z}) = \mathbf{H}_E$; there is no approximation involved.

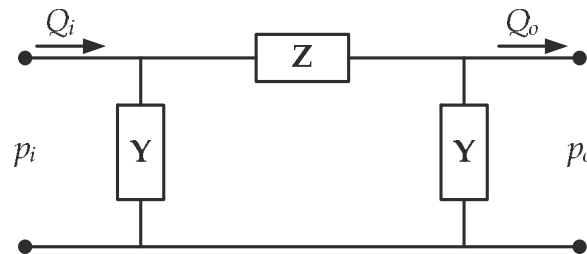
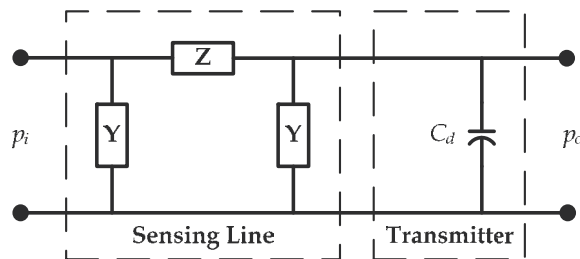


Fig. 6. Equivalent pi circuit for pressure sensing line exact model.

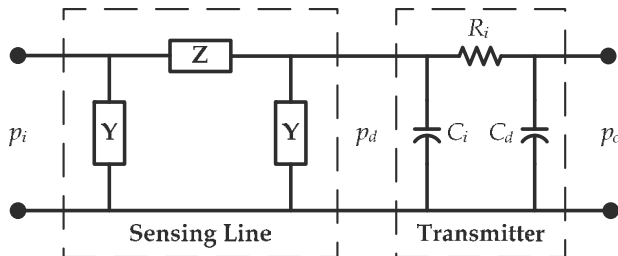
4. Sensing Line Diagnostics

In the previous section, various sensing line models have been presented, and the sensing line equivalent pi circuit representation is considered more accurate and easier to implement for impulse line diagnostics. To cooperate with the equivalent pi model of sensing lines, pressure sensor lumped parameter models are introduced here.

Typically, two types of pressure transmitters – motion-balance and force-balance – are used for safety-related pressure measurement in nuclear power plants. The major difference between them is how the movement of the sensing element is converted into an electrical signal. The transmitter modelling focuses on the component before the pressure-to-electrical signal conversion step. Therefore, the sensor representation presented here is valid for both types of pressure transducers.



(a) Pressure sensing system model with single diaphragm sensor representation



(b) Pressure sensing system model with inner structure sensor representation

Fig. 7. Two pressure sensing system models.

The simplest expression for a pressure transmitter is a single diaphragm. The diaphragm capacitance can be defined as

$$C_d = \Delta V_d / p_o \tag{25}$$

where ΔV_d is the displaced diaphragm volume and p_o is the pressure at the diaphragm at instant t . Hence, the pressure system model can be represented as shown in Fig. 7(a). However, this simple model may not be adequate in some cases. For example, the simple representation has been proved insufficient for understanding the laboratory measurements performed with a Rosemount capacitive transmitter (Blázquez & Ballestín, 1995). The reason is that the Rosemount sensors have an inner structure for pressure reduction. A low frequency real pole resulting from the inner structure dominates the frequency response of

the sensor. Therefore, the model should be modified as shown in Fig. 7(b). The inner structure of the Rosemount transmitter can be modelled with (Barbero et al., 2000):

- an isolating diaphragm (membrane) with capacity C_i ,
- a filling fluid of silicone oil instead of water,
- a smaller channel cross-section than that of the sensing line,
- a large resistance R_i for pressure reduction compared to sensing line ($R_i \gg R$), and
- a sensing diaphragm C_d .

4.1 Sensing Line Blockage

Extending the pressure sensing system model to a situation of blockage, one comes to the realization that all three parameters (R , L , and C) change (see Eq. (9)) as the original tube inner radius (r_i) decreases. The flow area reduction, as shown in Fig. 8, is denoted as $b = (r_B/r_i)^2$ where r_B is the pipe radius due to blockage.

The transfer function of a pressure sensing system consisting of a 50-meter long water-filled impulse line and an inner structure pressure transmitter was numerically computed for several cases: normal conditions and varying degrees of blockage. The effect of blockage on the transfer function is initially studied as shown in Fig. 9. From Fig. 9, it can be observed that the first resonant peak moves toward a lower frequency and the rest of the resonant peaks shift slightly toward lower frequencies as the blockage amount increases. In addition, all the resonant peak magnitudes are reduced as the blockage becomes larger. The effects on the transfer function under high blockage circumstances are demonstrated in Fig. 10. The impacts of severe blockages are consistent with what occurs in the earlier blockage cases (Fig. 9).

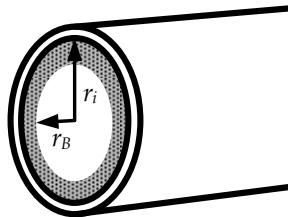


Fig. 8. A pipe with a uniform blockage amount along its length.

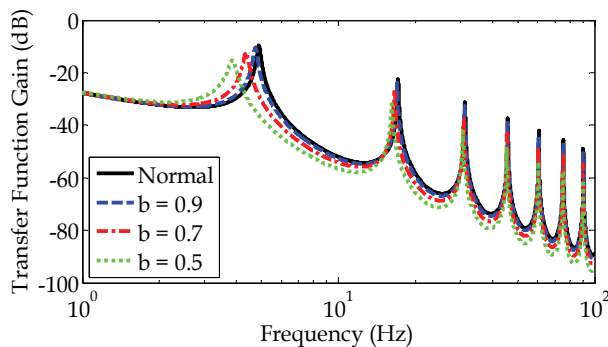


Fig. 9. Transfer functions of a pressure sensing system under normal condition and with sensing line blockages.

However, the first resonant peak disappears when the blockage reaches a certain level and the adjacent resonant peaks vanish one by one as the blockage level keeps increasing. Note the first four peaks of the transfer function with 0.01 cross section ratio (b) have disappeared in Fig. 10 while the remaining peaks are obscure but still exist. Moreover, the transfer function gain is considerably reduced with severe blockage occurring.

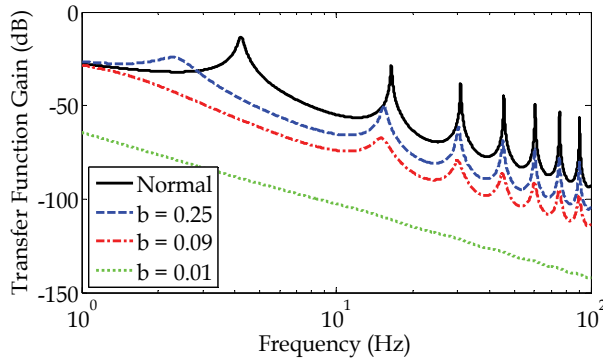


Fig. 10. Transfer functions of a pressure sensing system under normal condition and with severe blockages.

4.2 Sensing Line Voids

When voids (bubbles) appear inside a liquid-filled sensing line, the sensing line now contains a two-phase fluid. Bubbles can blend into the instrument line medium either homogeneously or heterogeneously. These two different mixing situations influence the transmitted signal differently. In this subsection, the sensing line fluid and the void media used for the studies are water and air, respectively. Another possible two-phase fluid is simply a water liquid-vapour mixture.

A homogeneous air-water mixture exists only when the air volume fraction is less than one percent (Sherstyuk, 2000). In the presence of air bubbles, the total volume inside the sensing line is the sum of the air volume, V_a , and water liquid volume, V_w , and the density of the air-water mixture can be expressed as (Barbero et al., 2000)

$$\rho_m = \beta \rho_a + (1 - \beta) \rho_w \quad (26)$$

where ρ_a and ρ_w are the air and water densities, respectively, at normal system pressure, and β is the void fraction by volume, $\beta = V_a / (V_a + V_w)$. The dynamic viscosity of a two-phase fluid can be estimated using the Grunberg equation (Grunberg & Nissan, 1949):

$$\ln \mu_m = X \ln \mu_a + (1 - X) \ln \mu_w + X(1 - X)d \quad (27)$$

where μ_a and μ_w are the air and water dynamic viscosities, respectively, at normal pressure, X is the void mole fraction, and d is the interaction parameter. The interaction parameter can be set to zero for the mixture of similar non-polar components so that the last term of Eq. (27) can be neglected. Consequently, Eq. (27) can be reduced as:

$$\ln \mu_m = X \ln \mu_a + (1 - X) \ln \mu_w. \quad (28)$$

By replacing the mole fraction with other parameters, Eq. (28) can be modified as:

$$\ln \mu_m = \frac{\beta \rho_a A_w}{(1 - \beta) \rho_w A_a + \beta \rho_a A_w} \ln \mu_a + \frac{(1 - \beta) \rho_w A_a}{(1 - \beta) \rho_w A_a + \beta \rho_a A_w} \ln \mu_w \quad (29)$$

where A_w and A_a are molar masses for water and air, respectively.

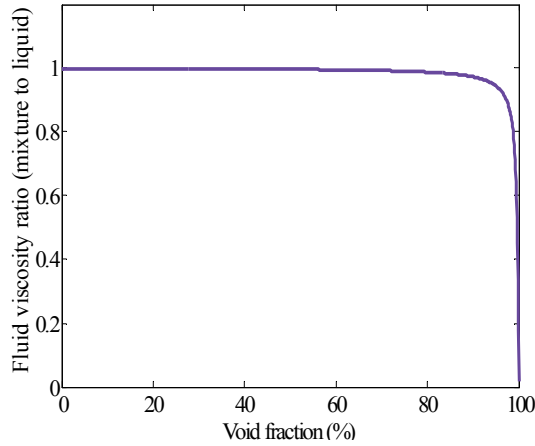


Fig. 11. The variation of the viscosity within a water-air mixture.

The variation of the viscosity within a water-air mixture is shown in Fig. 11. The density and dynamic viscosity changes affect the impulse line inductance (L) and resistance (R), respectively. However, the sensing line capacitance (C) varies much more than R and L not only through ρ but also via the sound velocity. Therefore, the sound velocity variation within a two-phase fluid is discussed below. Note that the voids are most likely air or water vapour; and the sensing line void model developed herein is valid for both cases.

A two-phase fluid has the elasticity of a gas and the density of a liquid (Barbero et al., 2000) so that the sound velocity decreases significantly, and consequently C increases. For a homogeneous mixture, the sound velocity can be calculated as (Landau & Lifshitz, 1959)

$$\frac{1}{c^2} \equiv \frac{\partial \rho}{\partial p} \quad (30)$$

Substituting with Eq. (26), Eq. (30) can be written as (Barbero et al., 2000)

$$\frac{1}{c^2} \equiv \frac{\partial \rho_w}{\partial p} (1 - \beta) + \frac{\partial \rho_a}{\partial p} \beta + (\rho_a - \rho_w) \frac{\partial \beta}{\partial p} \quad (31)$$

Mass conservation in the impulse line is applied to calculate the change in void fraction with pressure. With m_a and m_w corresponding to the air and liquid water masses, respectively,

$$\frac{m_a}{m_w} = \frac{\rho_a \beta}{\rho_w (1 - \beta)} \quad (32)$$

Taking the partial derivative with respect to pressure at both sides of Eq. (32) and noting that m_a/m_w is a constant, the partial derivative of the void fraction with respect to pressure can be derived as

$$\frac{\partial \beta}{\partial p} = \beta(1 - \beta) \left(\frac{1}{\rho_w c_w^2} - \frac{1}{\rho_a c_a^2} \right) \quad (33)$$

Substituting Eqs. (30) and (32) into Eq. (31), the sound velocity within a homogeneously mixed fluid, after some algebraic manipulations, is found to be

$$\frac{1}{c_{hom}^2} = \frac{1 - \beta}{c_w^2} + \frac{\beta}{c_a^2} + \beta(1 - \beta)(\rho_a - \rho_w) \left(\frac{1}{\rho_w c_w^2} - \frac{1}{\rho_a c_a^2} \right) \quad (34)$$

where c_a and c_w are the sound velocities in the air and water phases, respectively.

Fig. 12 shows the theoretical sound velocity variation within a homogeneous water-air mixture that has been experimentally proved (Gibson, 1970; Kafesaki et al., 2000); however, a homogeneous mixture has only been considered applicable when the air fraction (β) is less than 1% (Sherstyuk, 2000).

The transfer function of a pressure system with voids in the sensing line under the homogeneous mixture condition is shown in Fig. 13. The simulation is based on a pressure sensing system consisting of a 10-meter long water-filled impulse line and a single diaphragm pressure transmitter. As mentioned before, the homogeneous case is valid under the condition that the gas fraction is less than 1% (Sherstyuk, 2000). Hence, Fig. 13 shows the transfer functions for small amounts (< 1%) of air occurring within the impulse line. For the homogeneous mixture case, the appearance of bubbles makes significant feature changes to the original system transfer function curve as shown in Fig. 13. It can be seen that all resonant peaks shift dramatically toward lower frequencies. However, in a sensing line absent of flow, gas and liquid components eventually separate into a heterogeneous arrangement, which is now addressed.

Similar to the homogeneous air-water mixture case, a method that replaces the original R , L , and C parameters with new values calculated using the modified fluid density and sound velocity can be applied to the heterogeneous air-water mixture case (Barbero et al., 2000) as depicted in Fig. 14(a). By using this method, the network topology of the pressure sensing line model remains unchanged based on the void location, although the model parameters are affected. However, based on test results from the Kingston steam plant (Schohl, 1987a; Schohl, 1987b; Schohl et al., 1987; Schohl & Vigander, 1989), different air locations cause distinct effects on the pressure noise spectrum. Specifically, air present near the midpoint of the sensing line affects resonant frequencies much more than does air close to the beginning of the line.

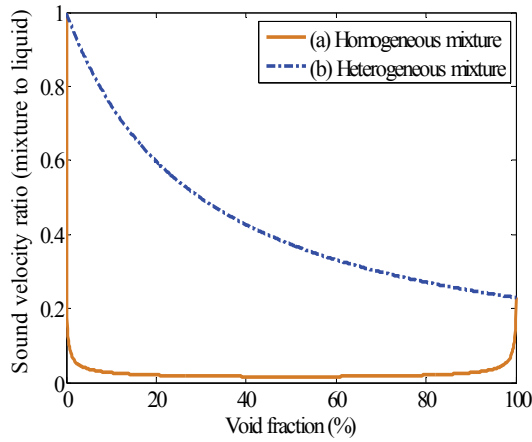


Fig. 12. Sound velocity variation within water–air mixtures.

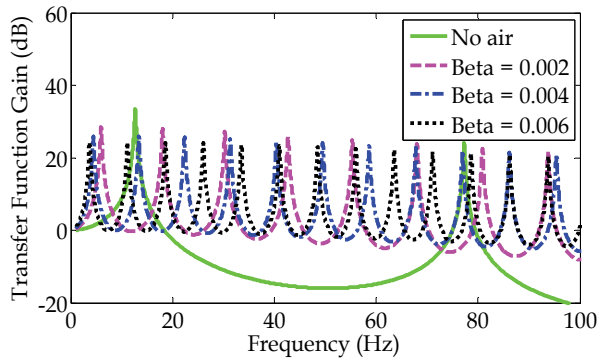
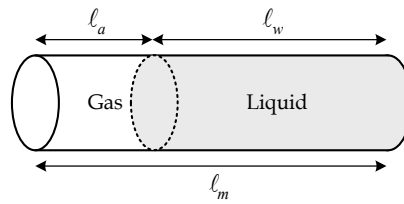
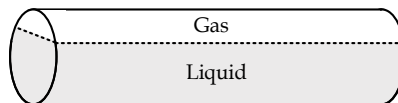


Fig. 13. Transfer functions of a pressure sensing system with air voids homogeneously mixed with the water fluid in the impulse line. Beta is the volumetric void fraction (β). The pipe system parameters are $l = 10$ m; $r = 6$ mm, $\mu = 0.004$ kg/m s; $c = 1500$ m/s; $\rho = 1000$ kg/m³; $Re = 1000$; and $\bar{Q} = 37.7$ cm³/s.



(a) Air and water are in series along the pipe



(b) Air and water are in parallel along the pipe

Fig. 14. Heterogeneous gas–liquid mixture geometries.

Another way to simulate the heterogeneous air-water mixture is to model an air section of length ℓ_a within a tube by an acoustic capacitor that is calculated using a lumped parameter representation (Müllens and Thie, 1985)

$$C_a = (\pi r^2 \ell_a) / (\rho_a c_a^2). \tag{35}$$

By using this depiction, sensing lines with voids occurring at different locations can be represented by the sensing line models as exemplified in Fig. 15. Note that the lumped parameter representation of voids is not applicable for the heterogeneous air-water mixture shown in Fig. 14(b), where the arrangement of air and water layers is in parallel along the pipe.

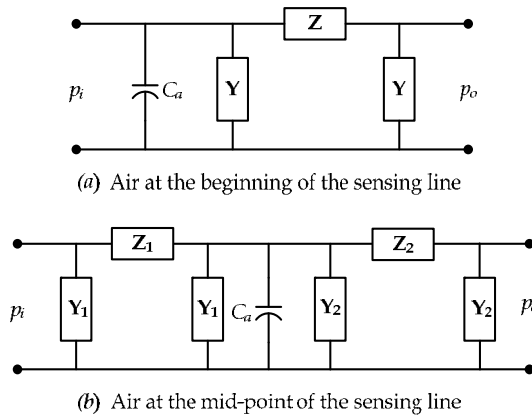


Fig. 15. Circuit models of tubes with voids occurring at different locations.

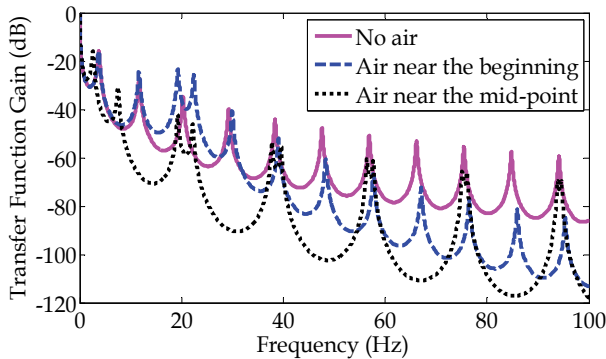


Fig. 16. Transfer functions of a water pressure system with air voids at the beginning and mid-point of the sensing line. The volumetric void fraction (β) is 0.0001.

Fig. 16 shows the transfer functions based on the lumped parameter void model for identical air pockets placed at two different locations along the sensing line. In the first case, an air pocket is positioned close to the beginning of the tube, and in the second instance, the air is located near the mid-point of the impulse line. It can be observed from Fig. 16 that even though the air volumes for both pockets are equal, the system transfer functions vary

significantly depending on where the void is located. These differences in transfer functions are physically attributable to the nonlinear system behaviour that results from site-dependent sound speed differences due to the air position (Barbero et al., 2000) as well as the concomitant changes in the standing wave frequencies (Schohl & Vigander, 1989).

4.3 Sensing Line Leakage

Leakage from a sensing line may be represented using the orifice equation of

$$Q = C_f A \sqrt{2\Delta p / \rho} \quad (43)$$

where C_f is a flow coefficient, and A is the flow area of the leak. The linearized orifice equation is

$$\delta p = \frac{\rho Q_0}{(C_f A)^2} \delta Q \quad (44)$$

where Q_0 is the steady-state leakage flow rate. The leak therefore becomes a parallel resistive term in the sensing line model. The equivalent resistance obtained from the linearized version of the orifice equation relating steady-state flow, Q_0 , and pressure, p_0 , provides two functional forms, specifically, $R = \rho Q_0 / (C_f A)^2 = \sqrt{2\rho p_0} / (C_f A)$. Generally, the flow coefficient, C_f , ranges from 0.6 for sharp edges to 1.0 for rounded edges. The former expression for R is more useful for determining the leakage amount (Q_0) from a PSD, whereas the latter expression is appropriate for selecting R values to perform initial scoping analyses based on the primary coolant system pressure (p_0). Using the equivalent pi representation, the leak may be placed at an arbitrary position along the sensing line, as depicted in Fig. 17.

Using the model of Fig. 17, a 50-m long, 2-cm diameter sensing line was simulated with a 1-mm diameter leak. The leak position was varied, specifically, at 25%, 50% and 80% of the tube length. The transfer function results shown in Fig. 18 demonstrate that although the resonant peak frequencies do not change, the peak amplitude does. In particular, the magnitude of the peak at the fundamental frequency decreases as the leak position moves from the inlet to the outlet, but other harmonics do not necessarily exhibit the same pattern. Such results are consistent with the theoretical and experimental observations by Lee et al. (2005; 2006) who found that the pattern of peak magnitude change can be utilized to determine the position of a leak in a pipeline. For large leaks, the fundamental resonant peak location also shifts to higher frequencies, as shown in Fig. 19.

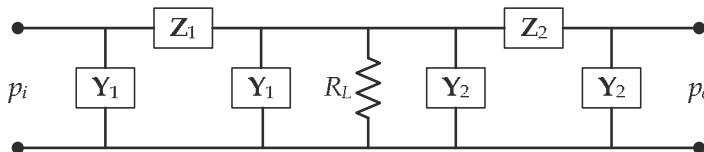


Fig. 17. Sensing line with leak somewhere between the sensing line inlet and outlet.

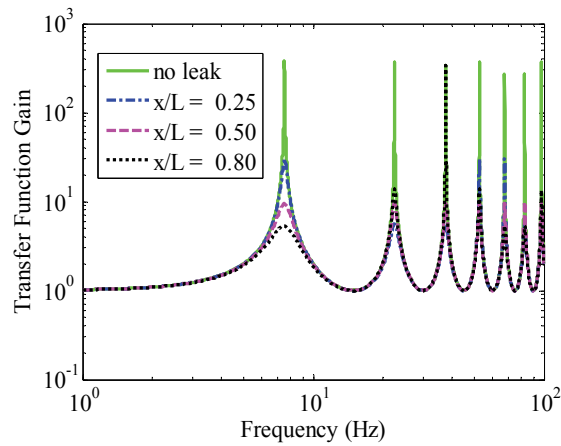


Fig. 18. Effect on sensing line transfer function by the position (x) of a 1-mm diam. leak within a 50-m long (L), 2-cm diam. sensing line with water at 15 MPa and 300°C.

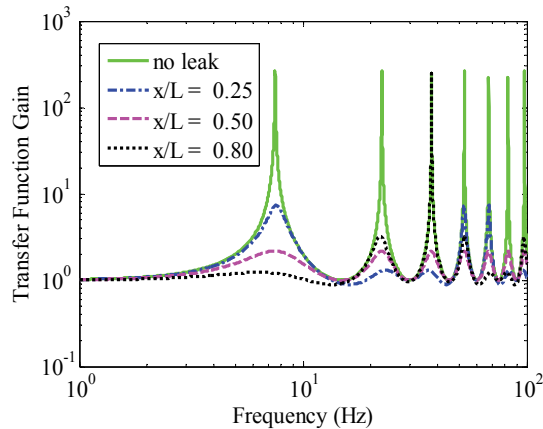


Fig. 19. Effect on sensing line transfer function by the position (x) of a 2.5-mm diam. leak within a 50-m long (L), 2-cm diam. sensing line with water at 15 MPa and 300°C.

5. Operational Data Analysis

In the previous section, the modelling of sensing line anomalies using the equivalent pi circuit representation has been presented. Operational data from a pressurized water reactor (PWR) and a coal-fired power plant are analyzed in this section to compare to the sensing line fault modelling.

5.1 Sensing Line Blockage in a PWR

Steam pressure measurements were taken from four steam generators. The four steam generators are identical so that the four pressure sensing systems are deemed similar to one another. Twenty minutes of pressure noise data were acquired using a 200 Hz sampling frequency with a low-pass filter cut-off of 67 Hz. Two different data sets were obtained

approximately three years apart under (1) normal (unblocked) conditions and (2) when the pressure sensing line of one transducer was blocked.

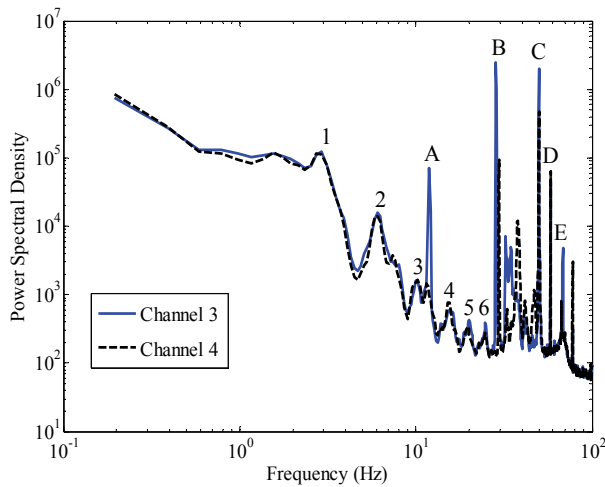


Fig. 20. PSDs of normal steam pressure noise data acquired at 200 Hz sampling frequency from Channels 3 and 4 (Lin & Holbert, 2009b).

Fig. 20 shows the PSDs of the noise signals obtained from Channels 3 and 4 before blockage occurs. There are a number of peaks in Fig. 20 for each PSD; however, some of the peaks originate from the other noise sources. Therefore, it is essential to identify the resonant peaks associated with the pressure sensing system. From Eq. (19) and simulation results for complete pressure sensing systems, it is known that the peak intervals are roughly equivalent. Based on this pattern, the resonant peaks caused by the pressure sensing system are enumerated as indicated in Fig. 20. To verify the peak recognition, the PSD from Channel 3 is compared to that from Channel 4. It can be seen in Fig. 20 that the two PSDs are almost identical up to the sixth peak while the higher frequency portion of the PSDs is not as similar as it is in the lower frequency region. The higher frequency data are corrupted by other noise sources. For example, peak C in Fig. 20 is the 50 Hz electrical noise. Because the data from both channels were measured through two similar pressure sensing systems, the shared resonant peaks are considered related to the pressure sensing system which agrees with the peak recognition result based on the uniform peak interval.

Fig. 21 shows the PSDs of the noise signals acquired from the blocked (Channel 3) and the normal (Channel 4) pressure sensing systems, respectively. It can be seen in Fig. 21 that the first three resonant peaks of Channel 3 have vanished due to the blockage and the magnitudes of the fourth and the sixth peaks are reduced significantly which is consistent with the severe blockage simulation result shown in Fig. 10. However, the PSD curve near the fifth peak location rises abnormally which is not found from the simulation result. This could be the result of plant equipment or operational variation since the normal data and abnormal data were taken three years apart. It is possible that the 1% upgrade in power for the NPP in the interim affected the later data.

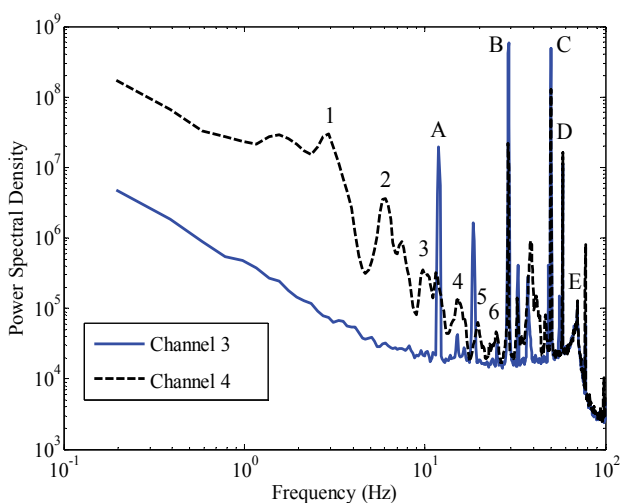


Fig. 21. PSDs of blocked and normal steam pressure noise data acquired at 200 Hz sampling frequency from Channels 3 and 4, respectively (Lin & Holbert, 2009b).

Based on Parseval's Theorem, the integral of the PSD is directly proportional to the signal variance (σ^2). From Figs. 9 and 10, it can be observed that the area under the transfer function curve of the pressure sensing system decreases as blockage increases. Therefore, in general, a reduced root mean square (rms), σ , noise level is anticipated for a blocked sensing line. However, this is not the case for the operational data presented here because, as mentioned above, the data are corrupted by other noise sources that manifest themselves in the higher frequency range of the PSDs shown in Figs. 20 and 21. In particular, there are several high frequency components appearing in the Channel 3 (blocked) PSD and with greater peak magnitudes as compared to the Channel 4 (normal) PSD. For this particular case, an alternative analysis method could be based on integrating the PSD up to and slightly past the sixth peak (i.e., before peak B).

5.2 Sensing Line Voids in a Fossil Unit

Field tests for void detection were conducted at the Kingston steam plant (Schohl, 1987a; Schohl, 1987b; Schohl et al., 1987; Schohl and Vigander, 1989) where nine coal-fired generating units are operating. A depiction of the sensing line for pressure measurement at the discharge of the Unit 1 raw water service pump is shown in Fig. 22. The 1.02-cm diam. copper line has a total length of approximately 80.5 m including an elevation gain of about 13.7 m from the pump, located in the power plant basement, to the control room pressure gauge. There are three tees along the line. Two of them were installed near the pump and the condenser respectively to provide locations for air injection. The third tee was placed under the control room (807) for attachment of a hydrophone.

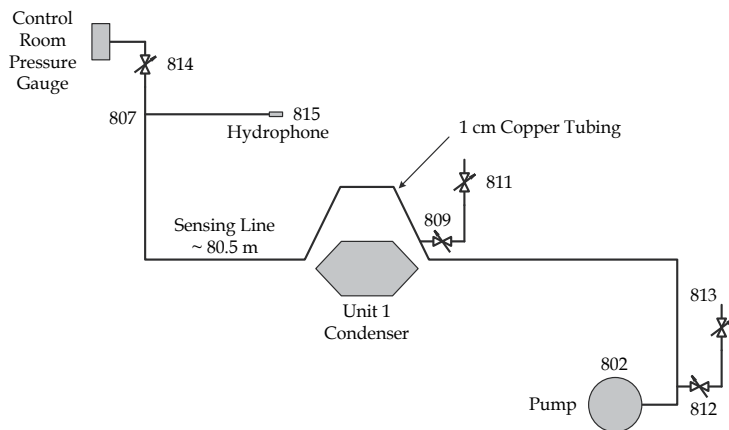


Fig. 22. Schematic of Kingston Unit 1 raw water service pump pressure impulse line, adapted from (Schohl, 1987a).

For the tests, the effects of the control room pressure gauge were removed by closing the in-line isolation valve (814) below the gauge. Then, measurements (termed “pseudo no-air” for reasons which will be explained later) taken after attempting to purge the line of air were compared with measurements recorded after air was inserted either close to the pump or near the condenser. The background flow noise was measured using the hydrophone at 815. To remove the random signal content, leaving the periodic components, spectra obtained from 40 consecutive time records, each 8 seconds long, were averaged together (Schohl, 1987a). Fig. 23 shows the effects of air added into the sensing line on power spectra of the flow noise with respect to air near the pump. According to Schohl (1987a), electrical noise appears in the PSD at 60 Hz, and pump first and second order harmonics occur at 29 Hz and 58 Hz, respectively. From Fig. 23, it can be recognized that added air manifests itself as an additional peak at 24.2 Hz, as noted by Schohl (1987a). This peak corresponds to surge oscillation of the column between the process line and the inserted air. Besides, except for the peak near 44 Hz, the resonant frequencies greater than 24 Hz are all moved slightly toward higher frequencies because of the added air.

In order to verify the developed pressure sensing system model, the raw water sensing line system (see Fig. 22) is represented using a five-segment impulse line equivalent pi circuit, as shown in Fig. 24, with the hydrophone and air realized by a single diaphragm capacitor, $C_d = \Delta V_d / p_o$, and acoustic capacitors, via Eq. (35), respectively. According to the Kingston test report (Schohl, 1987a), this sensing line was not equipped with air bleed lines so that there was no way to confidently purge all air from the line. Furthermore, the trapped air in the sensing line was distributed among several locations, with each location holding a small air pocket, rather than centralized at one location as a single large void. Therefore, in the network of Fig. 24, two small air pockets realized by two acoustic capacitors are inserted, respectively, at locations 809 and 814 which are two higher positions (see Fig. 22) considered more likely to trap air. Hence, we refer to these results as the “pseudo no-air” cases because of the two trapped air pockets which are included in the model.

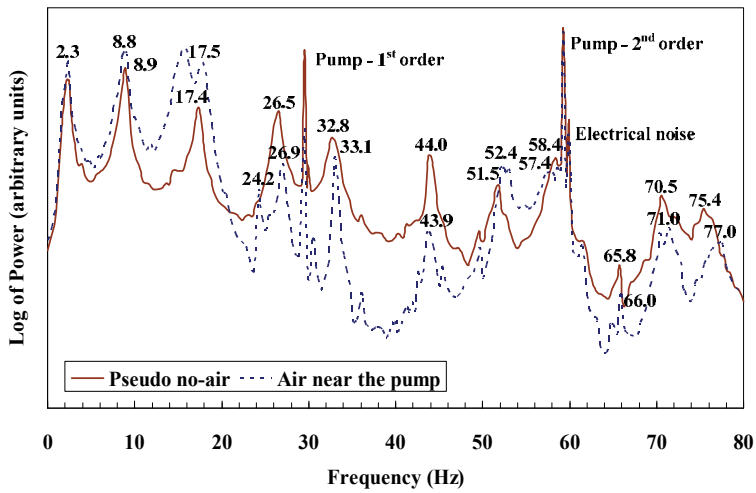


Fig. 23. The power spectra of the flow noise; data are from (Schohl, 1987a).

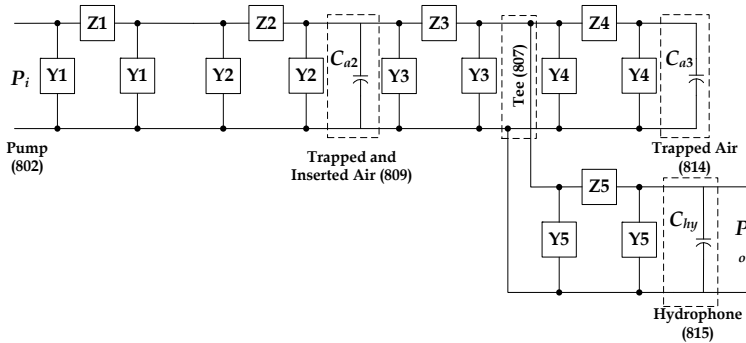


Fig. 24. Five-segment equivalent pi circuit model for the Kingston plant raw water pressure sensing line under the pseudo no-air condition.

Peak	Resonant Frequency (Hz)		
	Measured	Simulated	Difference
1	2.3	2.3	0 %
2	8.9	8.6	-3.4 %
3	17.4	17.1	-1.7 %
4	26.5	26.6	+0.4 %
5	32.8	32.0	-2.4 %
6	44.0	43.4	-1.4 %
7	51.5	51.5	0 %
8	58.4	57.8	-1.0 %
9	65.8	65.6	-0.3 %
10	70.5	70.7	+0.3 %
11	75.4	75.9	+0.7 %

Table 3. Comparison of pseudo no-air measured and simulated resonant frequencies

Table 3 shows an average absolute difference of 1.1% between the resonant frequencies of the measured data and the model with trapped air under the pseudo no-air situation, thereby verifying the model. To realize the air near the pump, another air capacitor equivalent to a 14.2 cm³ air pocket is inserted at location 812 as shown in Fig. 25. The simulation results based on the developed models are presented in Fig. 26. Comparing Figs. 23 and 26, it can be observed that the simulation results and the measured data still have good agreement after the air is inserted into the sensing line.

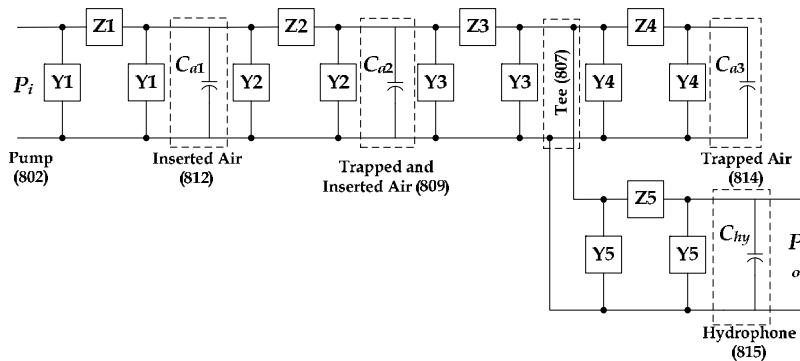


Fig. 25. Five-segment equivalent pi circuit model for the Kingston plant raw water pressure sensing line with an air pocket inserted near the pump (Lin & Holbert, 2010).

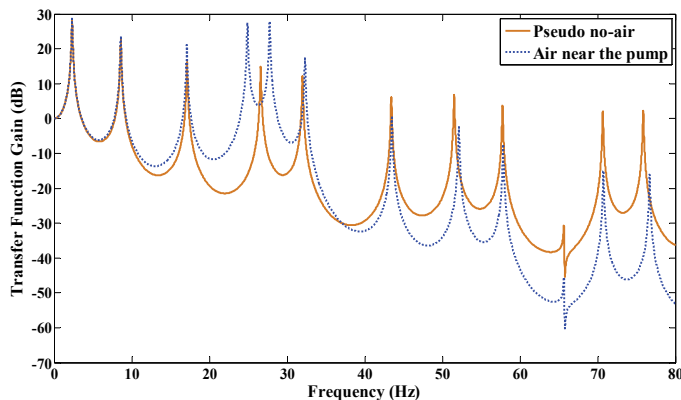


Fig. 26. Transfer functions of the Kingston steam plant raw water pressure sensing system based on the developed pressure system model.

6. Conclusions and Future Work

This chapter has detailed the establishment of online condition monitoring methods for pressure sensing systems. Each anomaly is uniquely represented by electrical equivalents, in particular:

- blockage – modified resistance, inductance, and capacitance,
- voids – additional parallel capacitance, and
- leakage – additional parallel resistance.

Models of blockage, voids, and leakage associated with instrument lines based on their electrical representations in conjunction with analyses of the operational data from a NPP

and field test measurements from an operating fossil power plant are presented. The operational data and field test measurement analysis results demonstrate behaviour consistent with the simulation results, and thereby validate the developed models.

Future research for extending the work presented in this chapter could include:

- studying the situation when multiple anomaly types occur in the sensing system,
- developing effective diagnostic indicators based on the spectral feature variations due to the presence of sensing line anomalies, and
- investigating the applicability of using the developed anomaly models for fault isolation and location.

7. References

- American Society of Mechanical Engineers (ASME) (2007). Power piping. *ASME Standard*, ASME B31.1.
- Barbero, J.; Blázquez, J. & Vela, O. (2000). Bubbles in the sensing line of nuclear power plant pressure transmitters: the shift of spectrum resonances. *Nuclear Engr. and Design*, Vol. 199, No. 3, 327-334.
- Bergh, H. & Tijdeman, H. (1965). Theoretical and experimental results for the dynamic response of pressure measuring systems. *National Aero and Astronautical Research Institute*, Amsterdam, NLR-TR F.238.
- Blázquez, J. & Ballestrín, J. (1995). Pressure transmitter surveillance: The dominant real pole case. *Prog. in Nucl. Energy*, Vol. 29, No. 3/4, 139-145.
- Clark, C. (1985). A differential pressure transducer for the measurement of high-frequency fluctuations in liquids. *Journal of Physics: Scientific Instruments*, Vol. 18, 297-302.
- Gibson, F. W. (1970). Measurement of the effect of the air bubbles on the speed of sound in water. *Acoustical Society of America*, Vol. 48, No. 5, 1195-1197.
- Glover, J. D. & Sarma, M. S. (2000). *Power System Analysis and Design*. Brooks/Cole, CA USA.
- Gogolyuk, P.; Lysiak, V. & Grinberg, I. (2004). Mathematical modeling of a synchronous motor and centrifugal pump combination in steady state. *Proc. of the IEEE PES Power System Conference and Exposition*, 1444-1448.
- Grunberg, L. & Nissan, A. H. (1949). Mixture law for viscosity. *Nature*, Vol. 164, No. 4175, 799-800.
- Hashemian, H. M.; Mitchell, D. W.; Fain, R. E. & Petersen, K. M. (1993). Long term performance and aging characteristics of nuclear plant pressure transmitters. Report prepared for the U.S. Nuclear Regulatory Commission, NUREG/CR-5851.
- Hashemian, H. M. (2006). *Maintenance of Process Instrumentation in Nuclear Power Plants*. Springer, ISBN 978-3-540-33703-4, Berlin, Germany.
- Iberall, A. S. (1950). Attenuation of oscillatory pressures in instrument lines. *Research of the National Bureau of Standards*, Vol. 45, No. 1, 85-108.
- International Society of Automation (ISA) (1999). Nuclear safety-related instrument-sensing line piping and tubing standard for use in nuclear power plants. *ISA Standard*, ISA 67.02.01-1999.
- International Society of Automation (ISA) (2005). Fossil fuel power plant instrument piping installation. *ISA Standard*, ISA 77.70-1994 (R2005).
- Izquierdo, J.; Pérez, R. & Iglesias, P. L. (2004). Mathematical models and methods in the water industry. *Mathematical and Computer Modelling*, Vol. 39, No. 11/12, 1353-1374.

- Izquierdo, J. & Iglesias, P. L. (2002). Mathematical modeling of hydraulic transients in simple systems. *Mathematical and Computer Modelling*, Vol. 35, No. 7/8, 801-812.
- Kafesaki, M.; Penciu, R. S. & Economou, E. N. (2000). Air bubbles in water: A strongly multiple scattering medium for acoustic wave. *The American Physical Society*, Vol. 84, No. 26, 6050-6053.
- Landua, L. D. & Lifshitz, E. M. (1959). *Fluid Mechanics*, Addison-Wesley, London.
- Lee, P. J.; Vítkovský, J. P.; Lambert, M. F.; Simpson, A. R. & Liggett, J. A. (2005). Leak location using the pattern of the frequency response diagram in pipelines: a numerical study. *Journal of Sound and Vibration*, Vol. 284, No. 3-5, 1051-1073.
- Lee, P.J.; Lambert, M. F.; Simpson, A. R.; Vítkovský, J. P. & Liggett, J. (2006). Experimental verification of the frequency response method for pipeline leak detection. *Journal of Hydraulic Research*, Vol. 44, No. 5, 693-707.
- Lin, K. & Holbert, K. E. (2009a). Applying the equivalent pi circuit to the modeling of hydraulic pressurized lines. *Mathematics and Computers in Simulation*, Vol. 79, No. 7, 2064-2075.
- Lin, K. & Holbert, K. E. (2009b). Blockage diagnostics for nuclear power plant pressure transmitter sensing lines. *Nuclear Engineering and Design*, Vol. 239, No. 2, 365-372.
- Lin, K. & Holbert, K. E. (2010). Void diagnostics in liquid-filled pressure sensing lines. *Progress in Nuclear Energy*, Vol. 52, No. 5, 503-511.
- Matko, D.; Geiger, G. & Gregoritz, W. (2000). Pipeline simulation techniques. *Mathematics and Computers in Simulation*, Vol. 52, No. 3, 211-230.
- Matko, D. & Geiger, G. (2002). Models of pipelines in transient mode. *Mathematical and Computer Modelling of Dynamical Systems*, Vol. 8, No. 1, 117-136.
- Müllens, J. A. & Thie, J. A. (1989). Pressure noise in pressurized water reactors. *U.S. Nuclear Regulatory Commission*, NUREG/CR-5383.
- Olson, H. F. (1957). *Acoustical Engineering*, D. Van Nostrand Co., ISBN 0193007045, Princeton.
- Schohl, G. A. (1987a). Tests at Kingston Plant of Techniques for Void Detection in Sensing Lines, Tennessee Valley Authority Report WR28-1-670-100.
- Schohl, G. A. (1987b). Additional Test and Analysis of Techniques for Air Detection in Sensing Lines, Tennessee Valley Authority Report WR28-1-670-102.
- Schohl, G. A.; Vigander, S. & Kuzniak, W. C. (1987). Detection of air in sensing lines from standing wave frequencies, *Transactions of the American Nuclear Society*, Vol. 55, 720-721.
- Schohl, G. A. & Vigander, S. (1989). Air detector for liquid-filled sensing lines. U.S. Patent, no. 4,858,460.
- Schönfeld, J. C. (1954). Analogy of hydraulic, mechanical, acoustic and electric systems. *Applied Scientific Research B*, Vol. 3, No. 1, 417-450.
- Sherstyuk, A. N. (2000). Speed of sound in a homogeneous liquid-air mixture. *Chemical and Petroleum Engineering*, Vol. 36, Nos. 5-6, 363-366.
- Sullivan, G. P.; Pugh, R.; Melendez, A. P. & Hunt, W. D. (2004). Operations & Maintenance Best Practices, A guide to achieving operational efficiency, Release 2.0, U.S. Department of Energy, Federal Energy Management Program.
- Thie, J.A. (1981). *Power Reactor Noise*. American Nuclear Society, ISBN 0-89448-025-1, La Grange Park, Illinois.
- Tyree, M. T. & Ewers, F. W. (1991). The hydraulic architecture of trees and other woody plants. *New Phytologist*, Vol. 119, No. 3, 345-360.
- Westerhof, N. et al. (1969). Analog studies of the human systemic arterial tree. *Journal of Biomechanics*, Vol. 2, No. 2, 121-143.

Probabilistic Safety Assessment and Risk-Informed Decision-Making

Marko Čepin
University of Ljubljana
Slovenia

1. Introduction

Probabilistic Safety Assessment is a standardized tool for assessing and improving nuclear power plant safety (ASME RA-S-2002, 2002; S-294, 2005; RA-S-2008, 2008). It is also used for assessment and improvement of the reliability of various systems in other industries, e.g. air and space industry and chemical industry. For the case of new nuclear power plants it may be required as a part of the safety analysis report, which is the main document needed for licensing of the plant operation.

2. History and State of the Art

Probabilistic risk analysis or probabilistic safety assessment has developed significantly in the last five decades from its first steps (Keller & Modarres, 2005), when the report known as WASH-740 was written in the year 1957 (WASH-740, 1957).

The term probabilistic risk analysis was more used in United States of America, while term probabilistic safety assessment was more used in Europe. Sometimes, the term probabilistic safety assessment was even used to specify only the systems reliability and accident sequences up to the core damage frequency, which may only refer to level 1, while the term probabilistic risk analysis was used to specify also the containment systems, which may refer to level 2, and consequence analysis, which may refer to level 3, in addition (NUREG/CR-2300, NUREG/CR-2815, 1985).

The WASH-740 study focused on the undesired consequences of large loss of coolant accident as the leading source of the worst radiation release into the environment.

A decade later, the risk curves were developed, which showed the small risk of nuclear power plants compared to other risks including risk caused by human activities and risk caused by nature itself (Farmer, 1967).

A report WASH-1400 was written in the year 1975 and a large debate followed about the applicability of the methods and results (WASH-1400, 1975). When the accident at Three Mile Island happened, it was soon concluded, that suggestions of WASH-1400 were very useful and wider applicability of the methods and results followed in the United States of America in order to prevent similar and other accidents (NUREG/CR-2300, 1982; NUREG/CR-2728, 1983; NUREG/CR-2815, 1985). Similarly, more efforts were put to

probabilistic safety assessment in other countries such as Germany (GRS, 1980) and France (Brisbois et al., 1990).

After the Chernobyl accident in Ukraine, the probabilistic safety assessment has become an obligation for all plants worldwide e.g. the Generic Letter 88-20 in United States of America (GL 88-20, 1988), e.g. the decree for probabilistic safety assessment in Slovenia.

A number of documents were prepared nationally (NUREG/CR-1150, 1989; NUREG/CR-4550, 1990; HSE, 1992) and internationally (50-P-4, 1992; 50-P-8, 1995; 50-P-12, 1996) including guidelines and examples of applications (NUREG/CR-6141, 1995). Wider performance of probabilistic safety assessment followed in the industry and in the regulatory bodies (YVL-2.8, 2003; S-294, 2005). The activities include the developed standards for probabilistic safety assessment (ASME RA-S-2002, 2002; S-294, 2005; IEC 61025, 2006; RA-S-2008, 2008). Standard ASME RA-S-2002 evolved from year 2002 to 2005 and 2008.

The further step of assessing risks was achieved by development of risk-informed decision-making, which has brought forward the risk analyses into the acceptance of decisions considering the risk analyses results. The background for risk-informed decision-making in United States of America is policy document from 1995 (60 FR 42622, 1995). The application procedures are described in regulatory guides, which evolved in years of their use (RG 1.174, 2002; RG 1.177, 1998; RG 1.200, 2007; RG 1.201, 2006). The practical applications are conducted (Vaurio, 1995; Harunuzzaman & Aldemir, 1996; Čepin & Mavko, 1997; Martorell et al., 2006).

National Aeronautics and Space Administration began to use probabilistic risk assessment methods in 1967, following the disastrous fire on Apollo 1 (PRA NASA Guide, 2002). Engineers completed a fault tree analysis for the entire Apollo system. They relied on highly conservative measures and data. They estimated so high failure probabilities for Apollo missions that the results led to a distrust of probabilistic risk assessment results. However, following the Challenger explosion in 1986, probabilistic risk assessment at national aeronautics and space administration was revived, and the Columbia break-up in 2003 reiterated the need for risk analyses.

National aeronautics and space administration used risk assessment and a combination of fault and event trees methods to model possible accident scenarios for the shuttle and International Space Station (ISS) programs (Maggio, 1996).

2.1 Lessons from the past

Unfortunately, the probabilistic safety assessment has always achieved more attention after some major accident. That was the case with Three Mile Island and Chernobyl in the nuclear industry and in the case of Apollo and Challenger in the case of space industry.

Nowadays, the probabilistic safety assessment is performed and it is used for decision-making in the most of the nuclear power plants and in the space programs (Apostolakis, 2004). The emphasis of probabilistic safety assessment to nuclear power plants as a standardised way to assess and improve safety is placed forward in this book.

3. Methods of Probabilistic Safety Assessment

The primary methods, which are integrated into probabilistic safety assessment, include fault tree analysis and event tree analysis (Kumamoto & Henley, 1996; NUREG/CR-2300,

1982; NUREG/CR-2815, 1985). The fault tree analysis is oriented to analyses of systems (NUREG-0492, 1981; Vesely et al., 2002; IEC 61025, 2006). The event tree analysis is oriented to connections between the systems (Papazoglou, 1998; Swaminathan & Smidts, 1999).

3.1 Fault Tree Analysis

The fault tree is a tool to identify and assess all combinations of undesired events in the context of system operation and its environment that can lead to the undesired state of a system (NUREG-0492, 1981; Vesely et al., 2002; Čepin & Mavko, 2002). It is not a process to identify all undesired events, but it is oriented only to those which can lead to the undesired state of the system.

Undesired state of the system is represented by a top event. The top event is an undesired event, which represents undesired state of the system of interest. The top event of the fault tree example on Fig. 1 is defined as "SS1 fails to deliver water from point A to point B" and it means that the safety system 1 fails to accomplish its mission.

The bottom part of Fig. 1 represents the example system, for which the fault tree is developed. SS1 system has to deliver specified amount of water from point A to B. Example system includes two redundant lines of the system. One line of the system is of enough capacity to accomplish success criteria of the system: line 1 or line 2 can realise the system mission.

Box B3 represents the pump B3, which has to run and box B4 represents the valve B4, which has to be open in order that the water is delivered to point B. Box B1 represents operator action, which insures water, if automatic pump operation and valve opening on line 1 are not successful. Box B5 represents the pump B5, which has to run and box B6 represents the valve B6, which has to be open in order that the water is delivered to point B. Box B2 represents operator action, which insures water, if automatic pump operation and valve opening on line 2 are not successful. The initial states of components include stopped pumps and closed valves.

The fault tree is developed in sense of faults. So, the top event usually means that the system under investigation fails or at least one of its functions fails. If the system success criteria require at least one out of two system portions to operate, the failure to meet this success criteria is represented in the top event as a failure of two out of two system portions. The duality between success criteria and failure occurrences has to be considered properly.

Logical gates connect the basic events to the top event. Logical gates on Fig. 1 are represented with abbreviations G_i (e.g. G_1 , G_2 , G_3 and G_4). They represent the logic connections between the components of the system. They include the logic connection between operation of the system and operator actions. They are identified by the name code and they include description. They are defined from point of view of possible faults, which can cause the top event. Each logical gate can be either the AND gate, where both input event occurrences are required for the output event, or the OR gate, where at least one of input event occurrences is required for the output event, or the K/N gate, where at least K input event occurrences are required for the output event. In theory, other logical gates can be used, such as NOR or NAND, but they are usually excluded from practical use. Negated gates are not desired because of assumptions used at evaluation of the fault trees.

Gate G_1 represents the failure of line 1 to deliver water to point B.

Gate G_2 represents the failure of line 2 to deliver water to point B.

The AND gate of the top event shows that both lines has to fail (line 1 has to fail and line 2 has to fail) in order that the system fails.

Gate G3 represents failures of automatic actions of pump B3 and valve B4 in order to provide water to point B.

Gate G4 represents failures of automatic actions of pump B5 and valve B6 in order to provide water to point B.

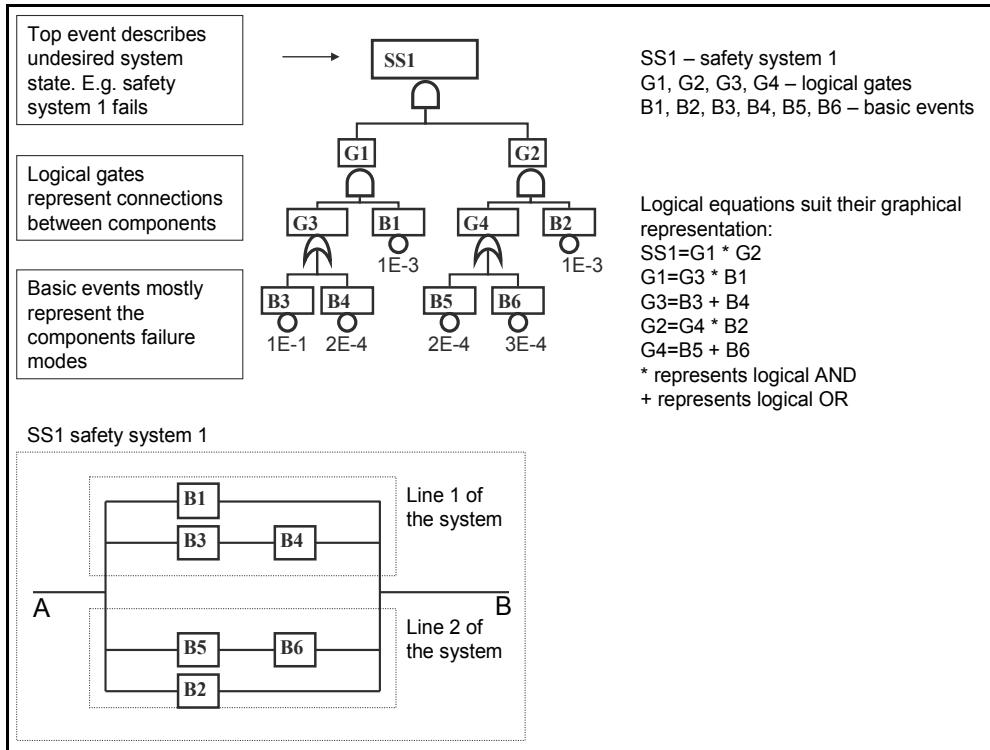


Fig. 1. Fault tree example

Basic events are the ultimate parts of the fault tree, which represent undesired events, such as component failure modes, missed actuation signals, human errors (NUREG/CR-1278, 1983), contributions of testing and maintenance activities and common cause contributions. Basic events on Fig. 1 are represented with abbreviations B_i (e.g. B1, B2, B3, B4, B5 and B6). They are identified by name code and they include description of the failure mode and identification of the component under investigation.

Basic event B3 represents failure of pump B3 to start and run for specified period of time at specified capacity. Basic event B4 represents failure of valve B4 to open and stay open for the specified period of time. Basic event B1 represents failure of operator to establish water flow if automatic action was not successful. Similarly is with basic events B2, B5 and B6 on the other line.

The fault tree is mathematically represented by a set of Boolean equations or by the fault tree figure itself. The Boolean equations and the fault tree for the example system are presented on Fig. 1.

Numbers below the basic events represent their failure probabilities, which are either obtained from data bases or they are calculated with the probabilistic models based on data about the previous experience with those or similar components and their failure modes that are defined in the respective basic events.

The qualitative fault tree analysis is the process of Boolean reduction of a set of Boolean equations. The rules of Boolean algebra are presented on Table 1. The sign for product suits the AND logic and the sign for sum suits the OR logic.

Boolean Law	Expressions		
Commutative Law	$X+Y=Y+X$	$XY=YX$	
Associate Law	$(X+Y)+Z=X+(Y+Z)$	$(XY)Z=X(YZ)$	
Distributive Law	$X(Y+Z)=XY+XZ$	$(X+Y)Z=XZ+YZ$	
Identity Law	$XX=X$	$X+X=X$	
Redundancy Law	$X(X+Y)=X$	$X+XY=X$	$(X')'=X$
Complementary Law	$X+X'=1$	$XX'=0$	
De Morgan's Theorem	$(XY)'=X'+Y'$	$(X+Y)'=X'Y'$	

Table 1. Rules of Boolean algebra

For the fault tree example from Fig. 1 it is needed that all five logical equations are inserted one to another in order to have one logical equation starting from top event and consisting of basic events as its parameters.

$$SS1 = ((B3+B4)*B1) * ((B5+B6)*B2) \tag{1}$$

Qualitative fault tree analysis identifies the minimal cut sets, which are the combinations of the smallest number of component faults that may cause the system fault. In other words, the minimal cut sets are combinations of the smallest number of basic events, which, if occur simultaneously, may lead to the top event.

The logical equation representing the fault tree has to be written as the sum of products. The rules of the Boolean algebra are used for rewriting of the equation. For example fault tree from Fig. 1 , eq. 2 represents such required reformulation of eq. 1.

$$SS1 = B3*B1* B5*B2+B4*B1*B5*B2+ B3*B1*B6*B2+ B4*B1* B6*B2 \tag{2}$$

The general expression for the minimal cut sets is the following.

$$SS = \sum_{i=1}^n MCS_i \tag{3}$$

SS - top event,

MCS_i - minimal cut set i,

n - number of minimal cut sets.

$$MCS_i = \prod_{j=1}^m B_j \quad (4)$$

m - number of basic events in minimal cut set i .

For the example fault tree from Fig. 1, the qualitative results indicate four minimal cut sets. Each includes four basic events. This means that the safety system 1 fails if basic events B3 and B1 and B5 and B2 occur or if basic events B4 and B1 and B5 and B2 occur or if basic events B3 and B1 and B6 and B2 occur or if basic events B4 and B1 and B6 and B2 occur.

Minimal cut set can be a single minimal cut set, if one basic event occurrence causes the top event, or in other words: one component failure causes the system failure. Minimal cut set can be a double minimal cut set, if two basic events occurrences cause the top event, or in other words: two component failures cause the system to fail. Minimal cut set can be a triple minimal cut set, if three basic events occurrences cause the top event. The example fault tree evaluation shows that four quadruple minimal cut sets are qualitative result of fault tree evaluation of the example fault tree.

Quantitative fault tree analysis includes the following results.

- Calculation of the system unavailability, which is one of the main risk measures at the system and component level, which is based on probability of failure of safety system components and which is obtained through calculation of the top event probability.

- Calculation of Risk Increase Factor (RIF, sometimes interpreted also as Risk Achievement Worth, RAW), which identifies components, which in case of their failure (failure probability assumed as 1), impact significantly the system (or plant) risk increase. For those components it is worth to maintain them well in order that the reliability of the system is not reduced (i.e. in order that the risk is not increased).

- Calculation of Risk Decrease Factor (RDF, sometimes interpreted also as Risk Reduction Worth, RRW), which identifies components, which in case of their complete success (failure probability is assumed as 0) impact significantly the system (or plant) risk decrease. For those components it is worth to improve their reliability in order that the reliability of the system is increased (i.e. in order that the risk is decreased).

The fault tree top event probability is calculated according to eq. 5.

$$Q_S = \sum_{i=1}^n Q_{MCS_i} - \sum_{i < j} Q_{MCS_i \cap MCS_j} + \sum_{i < j < k} Q_{MCS_i \cap MCS_j \cap MCS_k} - \dots + (-1)^{n-1} Q_{\bigcap_{i=1}^n MCS_i} \quad (5)$$

Q_{SS} - top event probability

Or, it can be approximated with the following equation - for Q_{mcsi} less than 0.1, the approximate results stay in 10% of accuracy in the conservative side (Čepin, 2005). If the negated events are considered in the fault tree analysis, the care should be taken about the use of approximations.

$$Q_{SS} = \sum_{i=1}^n Q_{MCS_i} \quad (6)$$

For the assumption that the basic events are mutually exclusive, the following can be used.

$$Q_{MCSi} = \prod_{j=1}^m Q_{Bj} \tag{7}$$

Q_{Bj} - probability of occurrence of basic event B_j

$$Q_{Bj} = Q_{Bj}(\lambda_j, \lambda_{oj}, q_j, T_{ij}, T_{tj}, T_{rj}, T_{pj}, \dots) \tag{8}$$

Q_{Bj} - probability of occurrence of basic event B_j

λ_j - operating failure rate of the equipment modeled in the basic event B_j ,

λ_{oj} - standby failure rate of the equipment modeled in the basic event B_j ,

q_j - probability of failure per demand of equipment modeled in basic event B_j ,

T_m - mission time,

T_{ij} - test interval of standby equipment modeled in basic event B_j ,

T_{tj} - test duration time of standby equipment modeled in basic event B_j ,

T_{rj} - repair time (i.e. mean time to repair or mean time to restore) of standby equipment modeled in basic event B_j ,

T_{pj} - test placement time of standby equipment modeled in basic event B_j (it specifies the timing of test).

Probability of occurrence of basic event is calculated according to selected equation. Simple example of probabilistic model for a component, which should actuate on a demand is shown on the following equation.

$$q = n_s / n \tag{9}$$

q - probability of failure per demand,

n_s - number of failed operations,

n - number of all operations.

Other probabilistic models are in more details presented in references (NUREG-0492, 1981; Vesely et al., 2002).

Risk Increase Factor is calculated according to the following equation (NUREG/CR-3385, 1983; NEI 00-04, 2005).

$$RIF_j = \frac{Q_{SS}(Q_{Bj} = 1)}{Q_{SS}(Q_{Bj})} \tag{10}$$

RIF_j ... Risk Increase Factor for equipment modeled in basic event B_j ,

$Q_{SS}(Q_{Bj})$ - top event probability,

$Q_{SS}(Q_{Bj}=1)$ - top event probability considering $Q_{Bj}=1$ (component B_j certainly fails).

Risk Decrease Factor is calculated according to the following equation.

$$RDF_j = \frac{Q_{SS}(Q_{Bj})}{Q_{SS}(Q_{Bj} = 0)} \tag{11}$$

$Q_{SS}(Q_{B_j}=0)$ - top event probability considering $Q_{B_j}=0$ (component B_j cannot fail).

3.2 Event Tree Analysis

The event tree analysis is a method used to represent potential accident sequences or scenarios associated with a particular undesired initiating event (Papazoglou, 1998; Swaminathan & Smidts, 1999; PRA NASA Guide, 2002).

The initiating event is an event, which may lead to the accident consequences. The event tree model describes the logical interrelationships between potential safety system function successes and failures in a timely manner after the initiating event.

Safety system functions are the means to prevent the accident or to mitigate its consequences. Human actions can also be considered similarly as the safety system functions. Each separate safety system function can be further analysed with the fault tree analysis.

The end states of the accident scenarios are plant damage states.

Fig. 2 shows a generalised example of the event tree. Initiating event can be event such loss of offsite power or important pipe break of specified size for example if nuclear power plant is the object of investigation.

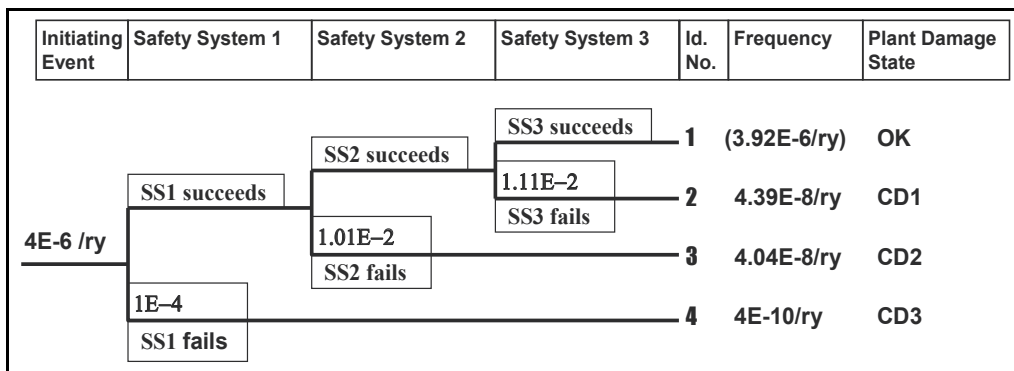


Fig. 2. Event tree – generalised example

After the initiating event, the safety system 1 should operate in sense that undesired plant damage states are reached. If the system succeeds the scenario goes upwards the event tree, if it fails, downwards at the node of safety system 1.

For all safety systems consecutively one after another as their operation follows the time and listing sequence, their success is shown in the event tree upwards from the previous node and failure is shown downwards from the node. The branches of the event tree which refer to safety system failure can be linked to a fault tree model of that safety system.

At the end, the plant damage states are identified. Code OK on the Fig. 2 means that the state of the plant is without the damage. The codes CD1, CD2 and CD3 are the codes for plant damage states. Universal plant damage state can be defined as core damage in the case of nuclear power plants.

The qualitative results of the event tree analysis include minimal cut sets for accident sequences. Accident sequence is a set of events, which result in a particular plant damage state. Example for the event tree on Fig. 2 is plant damage state 2, which ends with the CD1 plant damage state and includes initiating event, success of safety system 1, success of safety

system 2 and failure of safety system 3. If the fault trees for safety systems failures are linked to the event tree, the qualitative results of the event tree are similar as to results of the joined fault trees with the difference of presence of initiating event.

The quantitative results include accident sequences frequencies. Each accident sequence frequency is simplified as a product of initiating event frequency and safety system failure or success probabilities. If the event tree is linked with the fault trees for safety systems the initiating event frequency is multiplied with the results of the respected fault trees.

3.3 Fault Tree and Event Tree Integration

For the analysis of a nuclear power plant, several event trees are developed and each is linked with many fault trees. The results are then combined together through all respective scenarios and through all the event trees developed for the plant level analysis.

Fig. 3 shows the fault tree and event tree integration.

Probabilistic safety assessment includes tenths of event trees and hundredths of fault trees linking together thousands of gates and thousands of basic events.

If the plant damage state is core damage, the core damage frequency is the respective risk measure for the analysis at the plant level. Analyses up to the state of the reactor core are the subject of level 1 of the probabilistic safety assessment.

If the containment and its safety systems are considered in addition, the damage state can be radioactive releases to the environment. Analyses up to the state of the radioactive releases are the subject of level 2 of the probabilistic safety assessment. The large early release frequency is the respective risk measure for level 2.

Both risk measures: core damage frequency and large early release frequency are the indicators of the plant safety although the qualitative aspects of the results, which are the most important sets of component failures, which can lead to accident sequences, should not be forgotten. They have been the primary objective of the first probabilistic safety assessments.

The described procedures help to confront with risk analyses, which objectives are written in answers to three questions.

1. What can go wrong? Accident scenarios of the event trees give the answer. They can be at the level of the event tree or they can be at the level of linking with the fault trees, where each accident sequence is further represented by minimal cut sets.

How likely is it? The probabilities of failures of safety systems and the frequencies of initiating events together give the quantitative results and rank more likely and less likely accident sequences.

What are the consequences? Consequences are defined at the end states of the event trees and can be at the level of the state of the core for the level 1 of the probabilistic safety assessment, or they can be at the level of the state of the radioactive releases for the level 2 of the probabilistic safety assessment or they can be at the level 3 of the probabilistic safety assessment, which is oriented to the assessment to the dispersion of radioactive substances in the environment, where the weather conditions play the most important role.

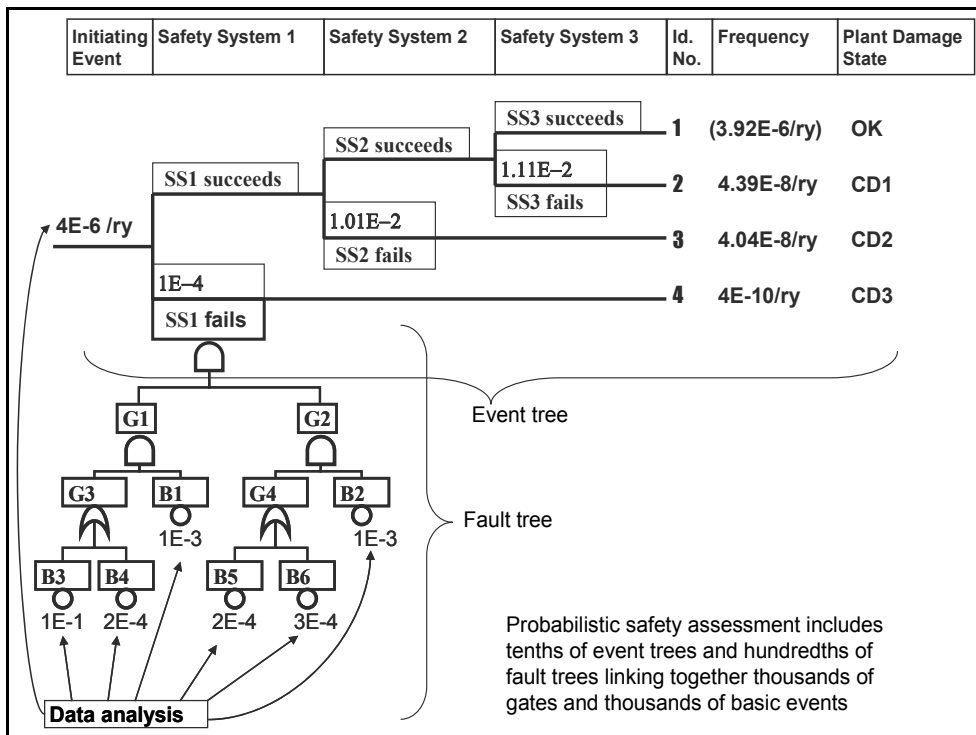


Fig. 3. Fault tree and event tree integration

The analyses show in general, that the risk of nuclear power plants is small compared to other risks to which we are exposed.

Probabilistic safety assessments provide a technique for assessing the safety of a particular facility and also an information base that is applicable to a wide variety of issues and decisions. Probabilistic safety assessment is far wider than only the presented fault tree and event tree integration. The probabilistic safety assessment includes the following main topics.

Information collection include collection of large amount of information including systems design descriptions with drawings, operating procedures, technical specifications, manufacturer requirements and recommendations for the testing and maintenance, other studies about the plant and standards about the equipment.

Analysis of human reliability and analysis of plant procedures includes the behaviour of operators during testing and maintenance and during routine operations and the diagnosis and actions of the operator teams after the occurrence of undesired initiating events.

Data-base development includes collection, classification and evaluation of generic reliability data when the specific data is not yet available and collection, classification and evaluation of plant specific data as a support for quantitative risk analyses.

Accident sequence quantification and systems quantification includes application of powerful computer codes for probabilistic safety assessment. Consideration of truncation or cut off is an important issue. Namely, the models are so large that it is not possible analytically solve the models. Approximations are made and negligible contributions are neglected (Čepin, 2005).

External event analysis includes consideration of earthquakes, fires, floods and other applicable external events for which it is necessary evaluate the plant response.

Uncertainty analysis is important as many of probabilistic models include parameters, for which is difficult to get accurate data. Approximations are done and uncertain models are used, which propagate to the results. The risk-informed decision-making has to consider the uncertainties of the evaluations.

Analysis of physical processes in materials exposed to high temperatures and pressures in normal and accident conditions is a difficult issue, which has to be performed. Many of those analyses are highly uncertain due to very demanding mathematical models of unknown processes.

Analysis of radionuclide release and transport in the environment is largely connected with weather conditions, which may impact the spread of the radionuclide materials in the environment.

Special section of the probabilistic safety assessment is its application for other modes than the full plant power operation, e.g. plant shutdown (Kiper, 2002; NUREG/CR-6144, 1995; NUREG-1449, 1992; IAEA-TECDOC-1144, 2000). Conduction of the analysis is focused to several time windows. One after another, each time window and each configuration is considered and in each time window the risks are assessed. The configuration with reactor head open for the refuelling is the most important configuration in terms of shutdown risk in nuclear power plants with pressurized water reactors.

3.4 Risk Criteria

The risk criterion is a term, which distinguishes between what is considered as an acceptable level of safety and what it is not (Čepin, 2007b).

The national approaches about risk criteria differ notably from country to country, so no commonly accepted international agreement exists (NKS-44, 2001; GS-1.14, 2002; Berg et al., 2003).

Quantitative risk objectives in United States of America consider individual and societal risk:

- The mean risk of an individual near a nuclear power plant (living within 1 mile radius) to receive an acutely lethal dose through a reactor accident is not to exceed $5E-7$ /year (this corresponds roughly to 0,1% of the risk from all fatal accidents).

- The risk for the general population within ten-mile-radius around a nuclear power plant to die of cancer as a result of the reactor operation should not exceed $2E-6$ /year (this corresponds to about 0,1% of the total cancer risk conditional on industrial activities).

In spite of the fact that no common criteria exist internationally, one can conclude that the production of electrical energy from nuclear power should not contribute notably to the overall risk is common to the national approaches.

The ALARA (As Low As Reasonably Achievable) principle is mostly acceptable, which states that the risk should be as low as it is reasonably achievable.

In addition, a common position exists that the future power plants should be better and safer than the current ones, which is the position of International Atomic Energy Agency.

Namely, the existing and future plants are distinguished in sense that the criteria are stricter in case of future plants for an order of magnitude.

The objective for core damage frequency for existing plants is $1E-4$ /reactor-year and for future plants it is $1E-5$ / reactor-year.

The objective for large early release frequency for existing plants is $1E-5$ / reactor-year and for future plants it is $1E-6$ / reactor-year.

3.5 Risk-Informed Decision-Making

In addition to the risk criteria for the nuclear power plant operation, the risk criteria in some countries are developed in two aspects considering the acceptability of changes.

- The first aspect includes permanent changes; e.g. assessment of acceptability of plant modifications.

- The second aspect includes temporary changes; e.g. consideration about the on-line maintenance.

Plant modification is a permanent change in the plant, which may be a physical change (e.g. an upgrade of a system, an addition of redundant equipment, a replacement of some components) or a non-physical change (e.g. improved plant operating procedure or improved testing and maintenance procedure, a change connected with certain requirement). An assessment of acceptability of plant modifications requires the risk criteria for permanent changes in the plant, because modification is a permanent change and it represents a potential for permanent change in risk.

On-line maintenance is a wide process of planning, analysing, preparation and implementation of the testing and maintenance of the plant equipment (mostly equipment, which is in stand-by), when the plant is operating, instead of performing those activities in the outage period, when the plant is shut down for refuelling. Consideration about on-line maintenance requires the risk criteria for temporary changes in the plant, because each activity of the on-line maintenance represents a temporary change and it represents a potential for temporary change in risk. In addition, consideration about on-line maintenance may require the risk criteria for permanent changes in the plant, because the approval of the overall concept of the on-line maintenance represents a potential for permanent change in risk.

The risk-informed decision-making is a term describing the process of assessing risks connected with technical decisions and considering of the risk results together with other means or with safety analyses to reach the most appropriate decisions.

The main and the most general rule is that the activities, which results in decrease of risk, are appreciated and mostly approved. Further, the activities, for which a small increase of risk is evaluated, can be considered acceptable, if the risk increase is small and if there are benefits of the change, which overrule the increase of risk, or if there are no methods and tools to evaluate completely the proposed change in terms of positive and negative aspects in terms of risk. Namely, sometimes it is difficult to evaluate quantitatively all the positive and negative aspects of proposed change in such extent that risk models qualitatively and quantitatively include all the positive and negative aspects of the proposed change.

Finally, if a large increase of risk is connected with proposed change, such change is not acceptable.

The risk of testing and maintenance of standby safety equipment with consideration of single configuration change can be represented by the core damage frequency or by the large early release frequency. Fig. 4 shows the increased risk as a result of outage of standby equipment i where the core damage frequency is the selected risk measure.

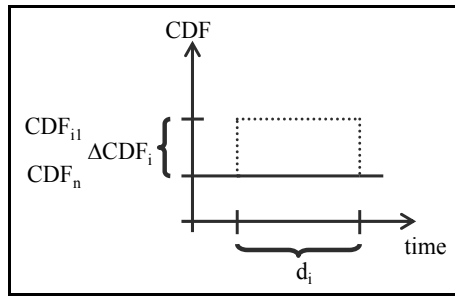


Fig. 4. The risk of testing and maintenance

The nominal risk is increased in an amount due to inoperable standby safety equipment at the time duration of testing and maintenance of equipment i . The increased risk ($Risk_i$) should be lower than the acceptance criteria, e.g. $Risk_{criteria}=1E-6$ (PSA Applications Guide, 1995; Čepin, 2007b), as it is in equation 15 below.

$$Risk_i = \Delta CDF_i \cdot d_i \quad (12)$$

where:

$$\Delta CDF_i = CDF_{i1} - CDF_n \quad (13)$$

ΔCDF_n - increase of core damage frequency due to outage of equipment i ,

CDF_n - core damage frequency for the nominal conditions of the plant,

CDF_{i1} - core damage frequency with equipment i unavailable due to testing or maintenance,

d_i ... time duration of testing or maintenance of equipment i .

If testing and maintenance is performed more frequently than yearly, the frequency of tests is considered in addition.

$$Risk_i = \Delta CDF_i \cdot d_i \cdot f_i \cdot T \quad (14)$$

f_i - frequency of testing and maintenance activities,

T - time interval considered (e.g. 1 year).

$$Risk_i < Risk_{criteria} \quad (15)$$

$Risk_{criteria}$ - limit of risk criteria.

The criteria may be different for one temporary change and for a cumulative impact of more temporary changes over certain time interval (Čepin, 2007b).

Examples of testing of standby safety equipment are diesel generators in a nuclear power plant. Diesel generators in a nuclear power plant are standby equipment, which should operate in the case if other sources of power system are lost. In such case, they provide power to the safety systems in order to cool the reactor, even if the reactor is in shutdown.

Table 2 shows the results of the risk evaluation, if the diesel generator 1 would be the candidate for the on-line maintenance in a nuclear plant.

The results include the core damage frequency of specific plant, its sensitivity to a specific change and the calculated increase of risk considering the risk increase due to inoperable equipment and the time duration of this inoperability.

The first column from the left identifies the status and the equipment, which may be subjected to the on-line-maintenance, which is diesel generator 1. The second column gives the core damage frequency for nominal conditions of the plant, which is the same for all on-line-maintenance activities of the same plant. The third column gives the allowed outage time, which is determined in technical specifications of the plant for the respective equipment and it is the longest possible time duration of testing and maintenance without shutting the plant down. The fourth column gives the core damage frequency with diesel generator 1 unavailable due to testing or maintenance. The fifth column gives the difference between the fourth and the second column, which represents the increase of core damage frequency with diesel generator 1 unavailable due to testing or maintenance. The sixth column gives the risk of on-line-maintenance for diesel generator 1, which is unavailable due to testing or maintenance. The risk is obtained by multiplying the increased core damage frequency with its duration, which is considered as the largest possible time duration, i.e. as the complete allowed outage time. The real risk is normally lower because the testing or maintenance is performed quicker than the complete allowed outage time. The seventh column gives the identification of the analyzed plant.

The risk results in table 2 show that on-line-maintenance of standby diesel generator 1 of plant NPP_S does not exceed the criteria (e.g. $Risk_i = Risk_{DG1} < 1E-6$) even if it is performed for the complete allowed outage time.

Equipment status	CDF_n (/ry)	AOT _i (h)	CDF_{i1} (/ry)	ΔCDF_i (/ry)	Risk _i	NPP ID
DG1 inoperable	3,48E-05	72	5,11E-05	1,63E-05	1,34E-07	NPP_S

Table 2. Results of risk evaluation

4. Analyses, Results and Applications

Applications of probabilistic safety assessment differ at the utility and at the regulatory body. Regulatory applications of probabilistic safety assessment include monitoring and assessing the effectiveness of rules and requirements, training of the regulatory body staff, risk follow-up, risk-based safety indicators, analysis of operational events, assessment of deviations, response to emergency conditions, ranking of safety issues, ranking of importance of plant equipment, risk-informed inspection, safety guidance and prioritisation of regulatory research. Utility applications of probabilistic safety assessment include:

- optimizations of technical specifications, including surveillance requirements optimization, changes and exemptions to technical specifications (Yang et al., 2000; Čepin & Martorell, 2002),
- support for modification of licensing basis and assessment of plant changes,
- management of in-service inspection and testing, optimization of maintenance, which includes preventive and corrective maintenance (Martorell et al., 2000; Čepin, 2002),
- configuration control and planning of maintenance at outages, prioritization of activities and scheduling of the activities (Harunuzzaman & Aldemir, 1996),
- improving training for operators and operational support stuff (Čepin, 2007a; Čepin, 2008),
- improving of plant procedures (Prošek & Čepin, 2008),

- improving plant vulnerability and security questions (Čepin et al., 2006; Čepin, 2009).

In addition, probabilistic safety assessment is used for the design of new plants and it represents a chapter of the final safety report.

5. Conclusion

Probabilistic safety assessment is a standardized tool for assessing and improving nuclear power plant safety. Its primary methods are the fault tree analysis and event tree analysis. The fault tree analysis is oriented to analyses of systems, while the event tree analysis is oriented to connections between the systems.

Qualitative fault tree analysis identifies the combinations of component faults that may cause the system fault. Quantitative fault tree analysis includes calculation of the system unavailability, calculation of risk increase factor, which identifies components, for which it is worth to maintain them well in order that the risk is not increased, calculation of risk decrease factor, which identifies components, for which it is worth to increase the redundancy or to improve their reliability in order that the risk is decreased.

The results of the event tree analysis include accident sequences and their frequencies. The core damage frequency and the large early release frequency are among the most common risk measures in probabilistic safety assessment of nuclear power plants.

Quantitative risk objectives vary from country to country. The common principle says that the production of electrical energy from nuclear power should not contribute notably to the overall risk. The risk criteria are stricter in case of future plants compared to existing plants.

The risk-informed decision-making evaluates risks connected with technical decisions and helps to reach the most appropriate decisions. The applications of the risk-informed decision-making include evaluations of temporary changes such as on-line maintenance and permanent changes such as procedural changes or plant modifications in a nuclear power plant.

6. References

- 50-P-12 (1996). Procedures for Conduction Probabilistic Safety Assessments of Nuclear Power Plants (Level 3), Safety Series No. 50-P-12, IAEA
- 50-P-4 (1992). Procedures for Conduction Probabilistic Safety Assessments of Nuclear Power Plants (Level 1), Safety Series No. 50-P-4, IAEA
- 50-P-8 (1995). Procedures for Conduction Probabilistic Safety Assessments of Nuclear Power Plants (Level 2), Safety Series No. 50-P-8, IAEA
- 60 FR 42622 (1995). Use of Probabilistic Risk Assessment Methods in Nuclear Activities: Final Policy Statement, Federal Register, Vol. 60, p. 42622, USNRC
- Apostolakis G. E. (2004). How Useful Is Quantitative Risk Assessment?, Risk Analysis, Vol. 24, pp. 515-520
- ASME RA-S-2002 (2002). Standard for Probabilistic Risk Assessment for Nuclear Power Plant Applications. The American Society of Mechanical Engineers. ASME, 2002; Addendum, 2005
- Berg H.P., R. Gortz, E. Schimetschka (2003). Quantitative Probabilistic Safety Criteria for Licensing and Operation of Nuclear Plants, BFS-SK-03/03

- Brisbois J., J.M. Lanore, A. Villemeur, J.P. Berger, J.M. De Guio (1990). Les études probabilistes de sûreté des centrales nucléaires françaises de 900 et 1300 MWe (Probabilistic Safety Assessments of French 900 and 1300 MWe Nuclear Power Plants).
- Čepin M. (2002). Optimization of Safety Equipment Outages Improves Safety, Reliability Engineering and System Safety, Vol. 77, pp.71-80
- Čepin M. (2005). Analysis of Truncation Limit in Probabilistic Safety Assessment. Reliability Engineering and System Safety, Vol. 87 (3), pp. 395-403
- Čepin M. (2007a). Importance of Human Contribution within the Human Reliability Analysis (IJS-HRA). Journal of Loss Prevention in the Process Industries, vol. 21, no. 3, pp. 268-276
- Čepin M. (2007b). The risk criteria for assessment of temporary changes in a nuclear power plant, Risk analysis, Vol. 27, no. 4, pp. 991-998
- Čepin M. (2008). DEPEND-HRA-A method for consideration of dependency in human reliability analysis, Reliability Engineering and System Safety, Vol. 93, no. 10, pp. 1452-1460
- Čepin M. (2009). Applications of the Fault Tree Analysis for Vulnerability Studies, Chapter 8 of: Nuclear Fuels: Manufacturing Processes, Forms and Safety, Nova Science Publishers
- Čepin M., B. Mavko (1997). Probabilistic Safety Assessment Improves Surveillance Requirements in Technical Specifications, Reliability Engineering and Systems Safety, Vol. 56, pp. 69-77
- Čepin M., B. Mavko (2002). A Dynamic Fault Tree, Reliability Engineering and System Safety, Vol. 75, No. 1, pp. 83-91
- Čepin M., Cizelj L., Leskovar M., Mavko B. (2006). Vulnerability Analysis of a Nuclear Power Plant Considering Detonations of Explosive Devices, Journal of Nuclear Science and Technology, Vol. 43, No. 10, pp. 1258-1269
- Čepin M., Martorell S. (2002). Evaluation of Allowed Outage Time Considering a Set of Plant Configurations, Reliability Engineering and System Safety, Vol. 78, pp. 259-266
- Farmer F. (1967). Reactor safety and siting: a proposed risk criterion, Nuclear Safety, pp. 539-548
- GL 88-20 (1988). Individual Plant Examination for Severe Accident Vulnerabilities--10CFR 50.54(f), Generic Letter, US NRC
- GRS (1980). Deutsche Risikostudie Kernkraftwerke, GRS
- GS-1.14 (2002). Criteria for the Performance of Probabilistic Safety Assessment Applications, CSN
- Harunuzzaman M., T. Aldemir (1996). Optimization of Standby Safety System Maintenance Schedules in Nuclear Power Plants, Nuclear Technology, Vol. 113, pp. 354-367
- HSE (1992). Safety Assessment Principles for Nuclear Plants, Health & Safety Executive, UK, London
- IAEA-TECDOC-1144 (2000). Probabilistic Safety Assessment of Nuclear Power Plants for Low Power and Shutdown Modes, IAEA
- IEC 61025 (2006). Fault Tree Analysis (FTA), IEC
- Keller W., M. Modarres (2005). A Historical Overview of Probabilistic Risk Assessment Development and its Use in the Nuclear Power Industry: A Tribute to the Late Professor Norman Carl Rasmussen, Reliability Engineering & System Safety, Vol. 89 (3), pp. 271-285
- Kiper K. L. (2002). Insights from an All-Modes PSA at Seabrook Station, International Topical Meeting on Probabilistic Safety Assessment, Detroit, Proceedings, pp. 429-434, ANS
- Kumamoto H., E. J. Henley (1996). Probabilistic Risk Assessment and Management for Engineers and Scientists, IEEE Press, New York

- Maggio G. (1996). Space Shuttle Probabilistic Risk Assessment: Methodology & Application, Proceedings Annual Reliability and Maintainability Symposium, IEEE, pp. 121-132
- Martorell S., S. Carlos, A. Sanchez, V. Serradell (2000). Constrained Optimization of Test Intervals Using a Steady-State Genetic Algorithm, Reliability Engineering and System safety, Vol. 67, pp. 215-232
- Martorell, S., Carlos, S., Villanueva, J. F., Sánchez, A. I., Galvan, B., Salazar, D., Čepin, M. (2006). Use of Multiple Objective Evolutionary Algorithms in Optimizing Surveillance Requirements, Reliability Engineering and System Safety, Vol. 91 (9), pp. 1027-1038
- NEI 00-04 (2005). 10 CFR 50.69 SSC Categorization Guideline, NEI
- NKS-44 (2001). J. Holmberg, U. Puikkinen, T. Rosquist, K. Simola, Decision Criteria in PSA Applications
- NUREG/CR-1150 (1989). Severe Accident Risks: An Assessment for Five US Nuclear Power Plants, US NRC
- NUREG/CR-1278 (1983). Handbook for Human Reliability Analysis with Emphasis on Nuclear Power Plants Application, US NRC
- NUREG/CR-2300 (1982). Probabilistic Risk Assessment Procedures Guide, US NRC
- NUREG/CR-2728 (1983). Interim Reliability Evaluation Program Procedures Guide, US NRC
- NUREG/CR-2815 (1985). Probabilistic Safety Analysis Procedures Guide, US NRC
- NUREG/CR-3385 (1983). Measures of Risk Importance and their Applications, US NRC
- NUREG/CR-4550 (1990). Analysis of Core Damage Frequency, USNRC
- NUREG/CR-6141 (1995). Handbook of Methods for Risk-Based Analyses of Technical Specifications, US NRC
- NUREG/CR-6144 (1995). Evaluation of Potential Severe Accident During Low Power and Shutdown Operations at Surry, Unit 1, NRC
- NUREG-0492 (1981). Fault Tree Handbook, US NRC
- NUREG-1449 (1992). Shutdown and Low Power Operation at Commercial Nuclear Power Plants in the United States, NRC
- Papazoglou I. A. (1998). Mathematical Foundations of Event Trees, Reliability Engineering and System Safety, Vol. 61, pp. 169-183
- PRA NASA Guide (2002). Probabilistic Risk Assessment Procedures Guide for NASA Managers and Practitioners, NASA
- Prošek A., M. Čepin (2008). Success criteria time windows of operator actions using RELAP5/MOD3.3 within human reliability analysis, Journal of Loss Prevention in the Process Industries, Vol. 21, no. 3, 260-267
- PSA Applications Guide (1995). Electric Power Research Institute, EPRI, TR-105396
- RA-S-2008 (2008). Standard for Level 1 / Large Early Release Frequency Probabilistic Risk Assessment for Nuclear Power Plant Applications, ASME
- RG 1.174 (2002). An approach for Using Probabilistic Risk Assessment in Risk-Informed Decisions on Plant-Specific Changes to the Licensing Basis, US NRC
- RG 1.177 (1998). An approach for Plant-Specific, Risk-Informed Decisionmaking: Technical Specifications, US NRC
- RG 1.200 (2007). An Approach for Determining the Technical Adequacy of Probabilistic Risk Assessment Results for Risk-Informed Activities, Rev. 1, US NRC
- RG 1.201 (2006). Guidelines for Categorizing Structures, Systems, and Components in Nuclear Power Plants According to their Safety Significance, Rev. 1, US NRC

- S-294 (2005). Probabilistic Safety Assessment (PSA) for Nuclear Power Plants, Regulatory Standard, Canadian Nuclear Safety Commission
- Swaminathan S, C. Smidts (1999). The Mathematical Formulation for the Event Sequence Diagram Framework, Reliability Engineering and System Safety, Vol. 65, pp. 103-118
- Vaurio J. K. (1995). Optimization of Test and Maintenance Intervals Based on Risk and Cost, Reliability Engineering and System Safety, Vol. 49, pp. 23-36
- Vesely W., J. Dugan, J. Fragola, J. Minarick, J. Railsback (2002). Fault Tree Handbook with Aerospace Applications, National Aeronautics and Space Administration, NASA
- WASH-1400 (1975). Reactor Safety Study: An Assessment of Accident Risks in US Commercial Nuclear Power Plants, NRC
- WASH-740 (1957). Theoretical possibilities and consequences of major accidents in large nuclear power plants (The Brookhaven Report), US AEC
- Yang J. E., T. Y. Sung, Y. Yin (2000). Optimization of the Surveillance Test Interval of the Safety Systems at the Plant Level, Nuclear Technology, Vol. 132, pp. 352-365
- YVL-2.8 (2003). Probabilistic safety analysis in safety management of nuclear power plants, STUK

Current status of fire risk assessment for nuclear power plants

Heinz Peter Berg¹, Marina Röwekamp²

¹*Bundesamt für Strahlenschutz,
Germany*

²*Gesellschaft für Anlagen- und Reaktorsicherheit (GRS) mbH,
Germany*

1. Introduction

Depending on design and operational characteristics of a nuclear power plant (NPP), operating experience worldwide has shown that fire can be a safety significant hazard. Thus, the regulators expect the licensees to justify their arrangements for identifying how fires can occur and spread, assessing the vulnerability of plant equipment and structures, determining how the safe operation of a plant is affected, and introducing measures to prevent a fire hazard from developing and propagating as well as to mitigate its effects.

Methods to analyze existing plants systematically regarding the adequacy of the implemented fire protection features can be deterministic as well as probabilistic ones. Fire risk assessment has become an integral part of probabilistic safety assessment (PSA) and, on an international level, fires have been recognized as one major contributor to the risk of NPP depending on the plant specific fire protection concept.

Operating NPP in Germany have been designed and constructed in different plant generations resulting in differences in the design and layout of fire protection features.

However, as a result of permanent supervision and specific fire safety reviews, comprehensive backfitting and upgrading measures have been realized including passive, mainly structural means (e.g. fire barriers) as well as active fire detection and extinguishing features and operational fire protection means (for manual fire fighting) resulting in significant improvements in fire safety, in particular of nuclear power plants built to earlier standards.

In the past, most of the engineering work in designing NPP fire protection features has been performed on a deterministic basis. Moreover, the use of deterministic fire analysis is current practice in Germany to review the fire protection status of operating NPP.

As an observation from other areas, the probabilistic approach provides different insights into design and availability of systems and components supplementing the results from deterministic analyses and enhances the understanding of fire risk compared to the consideration of deterministic analysis. Thus, probabilistic aspects have been taken into account for decision making on a case-by-case basis for fire protection aspects, too. A more

comprehensive fire risk assessment is recommended in the frame of periodic safety reviews (PSR) which are now a common tool in nearly all countries.

2. Deterministic Safety Status Analysis

Fire safety is already addressed in the safety criterion 2.7 “Fire and Explosion Protection” of the Safety Criteria for Nuclear Power Plants (BMI, 1977) and in the Incident Guidelines (BMI, 1994) requiring that protective measures against fires shall be taken by means of plant engineering. The specifications of these precautions are outlined in three nuclear safety standards defining and prescribing the basic requirements, fire safety measures regarding structural plant components, fire safety measures for mechanical and electrical plant components (KTA, 2000). The basic requirements describe the design principles, structural and equipment-related fire protection measures against building internal and external fires, operational fire protection measures as well as tests and inspections.

Part 2 covers location and accessibility of buildings, fire compartments, structural elements enclosing fire compartments, structural elements for rescue routes, ventilation systems as well as heat and smoke removal systems, cable ducts, cable support structures including mounting elements in the vicinity of cable fire shields. Moreover, a simplified validation procedure for determining the required fire resistance rating of structure-related fire protection measures. The German nuclear safety standards on fire protection are currently under revision.

The plant internal hazard fire has to be considered in the deterministic safety status analysis as part of the PSR in order to review if the protection goal oriented requirements outlined in the regulatory framework are met, but also more recent, corroborated findings are resolved, i.e. if the nuclear protection goals such as reactivity control and fuel element cooling are achieved by the fire protection features implemented.

3. Probabilistic Safety Assessment

For performing the PSR, a PSA Guide which has been issued in Germany by the regulatory body containing reference listings of initiating events for NPP with PWR and BWR respectively, which must be checked plant specifically with respect to applicability and completeness. Plant internal fires are included in these listings. Detailed instructions for the analysis of plant internal fires, fire frequencies and unavailability of fire detection and alarm features as well as data, e.g. on the reliability of active and passive fire protection means, are provided in the technical documents on PSA methods (FAK PSA, 2005a) and PSA data (FAK PSA, 2005b). These technical documents have been developed by a working group of technical experts from nuclear industry, research centres, universities, authorities and technical support organizations chaired by the BfS (Bundesamt für Strahlenschutz, Federal Office for Radiation Protection).

At present, it is international practice to perform a Fire PSA as part and supplement of the internal events PSA (EPRI, 2005; ANS, 2007). However, up to the time being probabilistic fire risk analysis (Fire PSA) is a methodology needing further development.

A Fire PSA is required in the German PSA Guide as explained earlier. In this context, a state-of-the-art approach for performing Fire PSA has been developed in Germany, which

has been exemplarily and completely applied to a German NPP with boiling water reactor (BWR) of the type BWR-69 for full power (FP) operation (von Linden et al., 2005).

It is the task of a Fire PSA to determine the annual frequency of fire induced core damage states (FCDF) of a NPP within the in advance defined global analysis boundary. The set of all compartments is the starting point of the fire analysis. The spatial plant partitioning should be performed in a way that all compartments characterize the global analysis boundary and that the compartments do not overlap. In this case, the annual frequency of fire induced core damage states of the plant results from the sum of all compartment related annual frequencies of fire induced core damage states.

It is assumed that compartments with a low fire load density do not impact the Fire PSA result. Such compartments are screened out before starting the detailed compartment and scenario specific analysis. The fire induced core damage frequencies of all the remaining compartments are determined in a first step using simplified and conservative assumptions. In the following, only such compartments must be analyzed in detail, for which in case of fire a relevant contribution to the FCDF of the whole plant is to be expected.

3.1. General approach for fire PSA

A comprehensive Level 1 Fire PSA has to be performed for power operation as well as shutdown plant modes. For the analysis, it is assumed that the plant contains *n* disjoint spatial units (so-called compartments) for the plant operational states mentioned in Table 1. The Level 1 Fire PSA aims on estimating the frequencies of fire induced damage states (in the most cases hazard states or core damage states) per reactor year (ry). The total FCDF is the result of adding up the FCDF for the entire compartments and plant modes including full power (FP) as well as low power (LP) and shutdown (SD) states.

$$FCDF = \sum_{i=1}^n \sum_{j=1}^m f_{ij} .$$

Compartment i	Plant operational state j					\sum_j
	1	...	j	...	m	
1	f_{11}	...	f_{1j}	...	f_{1m}	f_{1j}
...
i	f_{i1}	...	f_{ij}	...	f_{im}	f_{ij}
...
n	f_{n1}	...	f_{nj}	...	f_{nm}	f_{nj}
\sum_i	f_{i1}		f_{ij}		f_{im}	FCDF
	f_{FP}	$f_{LP/SD} = \sum_{j=2}^m f_{ij}$				

Table 1. Denominations of the fire induced core damage state frequencies per compartment and plant operational state (Röwekamp et al., 2010)

For estimating the overall plant FCDF (for the entire plant) the individual frequencies for each compartment *i* (*i* = 1, ..., *n*) and each plant mode *j* (*j* = 1, ..., *m*) have to be calculated. For minimizing this effort, a stepwise approach is chosen. If a screening approach provides

the result of f_{ij} exceeding a specific threshold a detailed analysis is carried out for estimating f_{ij} considering all the available information and data. A threshold value of $1.0 \cdot 10^{-7}/\text{ry}$ has been used for the Fire PSA for full power modes.

First, each compartment is analyzed with respect to fire specific aspects. If this analysis gives the result that no fire impairing nuclear safety can occur under the boundary conditions of plant mode being analyzed the compartment can be excluded from further analysis for this mode. This corresponds i.e. to the German fire load criterion of screening out compartments with a fire load density of less than $90 \text{ MJ}/\text{m}^2$ provided in (FAK PSA, 2005a).

For estimating the fire-induced core damage frequency f_{ij} for a specific compartment i and a plant mode j the compartment inventory as well as that of adjacent ones must be analyzed with respect to fire specific aspects and to the safety significance of the inventory. The potential fire event sequence can be analyzed by several fire scenarios with {source a , target z }, where the fire source a is located inside the fire compartment i to be analyzed, while the critical target z can be located in the same compartment i or in the adjacent ones. The fire-induced CDF f_{ij} is calculated corresponding to Figure 1 (Röwekamp et al, 2010). f_{ij} is the sum of all the critical fire scenarios with {source a , target z } identified for the compartment i and plant state j . In this context, a scenario is called a critical one if the target is an item, for which its failure causes an initiating event or which itself is a safety related component.

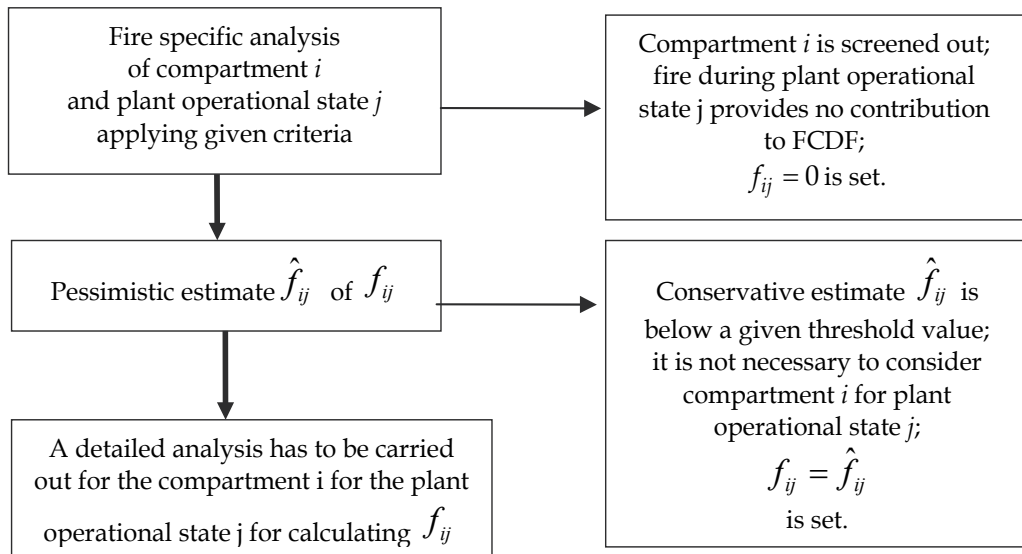


Fig. 1. Scheme for estimation of f_{ij} for compartment i and plant mode j

Some simplifications are particularly applied for a conservative estimate \hat{f}_{ij} of f_{ij} (cf. Figure 1). One assumption is that a fire inside a compartment i impairs the entire equipment in this compartment. Another one is that no fire source a is specified in the compartment i .

As a result, the fire occurrence frequency of the compartment i is used for calculating \hat{f}_{ij} .

Table 2 provides the characteristic parameters needed for determining for a given fire sequence { a, z } the fire induced CDF as well as the steps of the analysis for which they are

needed. This information is typically used in the frame determining f_{ij} for those scenarios not screened out before (cf. Figure 1, detailed analysis).

Characteristic Parameters		Analysis
a	fire source	Selection of a fire scenario with {source a , target z } in a compartment to be analyzed
z	fire target: A fire at the source a endangers equipment z .	
f_a	Fire occurrence frequency of fire source a	Calculation of f_a
$p_{z/a}$	Conditional failure probability for target z due to fire at source a	Estimation of $p_{z/a}$ by deriving and quantifying a fire specific event tree considering all aspects of fire suppression
$f_{z/a}$	Failure frequency of target z due to fire at source a	$f_{z/a} = f_a \cdot p_{z/a}$
IE	Initiating event (IE) due to failure or damage of target z	Estimation of IE depends on plant operational state to be analyzed; if the failure of target z does not result in an IE (z is safety related component), experts make a conservative assumption corresponding to approach given in the plant operating manual.
$p_{IE/z}$	Conditional occurrence probability of initiating event (IE) due to failure of target z	In many cases, estimation of $p_{IE/z}$ by expert judgment (simplified assumption: only one initiating event (IE) possible in case of target z failure)
$f_{IE/z}$	Occurrence frequency of an initiating event IE due to a fire at fire source a	$f_{IE/z} = f_{z/a} \cdot p_{IE/z} = f_a \cdot p_{z/a} \cdot p_{IE/z}$
$p_{SYS/IE}$	Conditional failure probability of safety functions required for control of the initiating event IE	Estimation of $p_{SYS/IE}$ by deriving and quantifying the systems specific event tree for control of the initiating event (IE); depending on the plant operational state to be analyzed the analyst can fall back to event sequences of the Level 1 PSA for full power as well as for low power and shutdown states; if target z is a safety related component, its failure has to be considered in the PSA plant model.
$f_{\{a,z\}}$	CDF for a fire at source a with target z	$f_{\{a,z\}} = f_a \cdot p_{z/a} \cdot p_{IE/z} \cdot p_{SYS/IE}$

Table 2. Scheme and parameters for estimating fire induced damage frequency $f_{\{a,z\}}$ for a given plant state

3.2. Screening analysis as described in the full power operation PSA documents for PSR

The screening process to identify critical fire compartments is an important first step within fire risk assessment. Such a screening analysis should not be too conservative so that an unmanageable number of fire scenarios remains for the detailed quantitative analysis. However, it must be ensured that all areas relevant for nuclear safety are investigated within the quantitative analysis.

The recent German documents on PSA methods (FAK PSA, 2005a) and PSA data (FAK PSA, 2005b) do only cover approaches for a Level 1 Fire PSA for full power operation. According to (FAK PSA, 2005a and 2005b), the systematic check of the entire plant compartments and/or compartment pairs can be performed in two different ways: Critical fire compartments can be identified within the frame of a qualitative (qualitative screening) or a quantitative process (screening by frequency). The qualitative screening allows - due to the introduction of appropriate selection criteria - the determination of critical fire compartments with a limited effort. Applying the screening by frequency, critical fire compartments are identified by means of a simplified event tree analysis.

The systematic analysis of all plant compartments and/or compartment pairs requires detailed knowledge of the plant specific situation.

3.3 Plant partitioning analysis

3.3.1 General approach

It is the task of a Fire PSA to determine and to assess fire induced plant hazard states or plant core damage states for the NPP. A plant hazard state (HS) occurs if the required safety functions fail. A core damage state (CDS) occurs, if also intended accident management measures fail.

In the following, the recent German Fire PSA methodology (Türschmann et al., 2005) is explained for deriving fire induced core damage frequencies. An analogous approach is applied for obtaining fire induced plant hazard state frequencies.

For determining fire induced CDF it is in principle necessary to identify all those permanently as well as temporarily present combustibles (fire loads) in the plant, for which by any potential ignition a fire impairing nuclear safety is possible. For quantification of the consequences the annual combustible specific f_a has to be determined for each fire load a being present. The fire induced CDF of the entire NPP is derived from the sum of f_a related to the entity of combustibles present. In practice, it is impossible to determine the f_a for each combustible being present in a plant. Therefore, several combustibles are grouped in an appropriate manner, i.e. locally interconnected plant areas, so-called compartments, are generated inside the buildings. In case of a partitioning of the entire plant into disjoint compartments not overlapping each other the annual FCDF is derived from the sum of all compartment related f_{i1} .

Practical considerations suggest analyzing compartments according to the plant specific identification system. Depending on the compartment specific characteristics a different partitioning of compartments may be necessary in exceptional cases, e.g.:

- Compartments with internally implemented fire barriers (e.g. long cable channels, cable ducts, etc.);
- Compartments with cable routes/raceways protected by wraps, coatings, etc. (such a cable duct or channel should be understood as compartment itself);

- Extremely large fire compartments (reactor annulus, big halls (e.g. turbine hall), staircases, etc.).

Performing Fire PSA starts by determining the building structures to be analyzed (Türschmann et al., 2006). This task requires some sensitivity, insofar as the effort of the analytical work can be drastically reduced selecting compartments by engineering judgement for the detailed analyses based on the knowledge of the plant in general, of the plant's fire protection in particular and, in addition, of the calculation methods used in the Fire PSA.

A compromise has to be made for the optimum partitioning between the greatest level of detail (analysis of each individual fire load) and too little details in the plant partitioning. The only requirement to be met is that each fire load considered has to be correlated only to one compartment.

3.3.2 Exemplary analysis for a BWR-69 type nuclear power plant in Germany

Five buildings of the entire NPP have been found to be representative for being analyzed within the Level 1 Fire PSA for full power plant states (Röwekamp et al., 2006) exemplarily performed for a German BWR-69 type NPP (see Table 3).

Building	Number of Compartments	
	Using identification system	To be analyzed
Reactor Building	306	351
Switchgear Building	165	203
Turbine Building	82	106
Diesel Building	25	26
IES Building*	36	42
total	614	728
* bunkered independent emergency systems building (IES building)		

Table 3. Spatial partitioning of the buildings relevant for Fire PSA in a BWR type reference plant analyzed

The spatial plant partitioning for the plant analyzed is principally based on the given plant specific identification system. In a few exceptional cases deviations from this procedure have to be mentioned, e.g. the subdivision of the very large reactor annulus into quadrants, or that of extremely long cable rooms and stairways. Some fire protected (sealed) cable ducts (raceways) without compartment numbers have been reassigned.

The analytical step of the spatial partitioning into compartments and the complexity of the following analyses can be simplified if the tasks are carried out building by building. It is possible to exclude those buildings from the Fire PSA, for which it can be demonstrated that there are no components present, whose fire induced functional failure might impair nuclear safety (so-called safety related components). It should be simultaneously checked, if a fire in a compartment of such a building has the potential of spreading to any other building with safety related components.

The partitioning of the NPP into compartments is an important step in performing a Fire PSA. In the frame of this step of the analysis it is the major task to make available all the data and information necessary to calculate the compartment related f_{ij} .

3.4 Fire PSA database

For performing a quantitative fire risk assessment, a comprehensive database must be established which should, e.g., include initiating frequencies, reliability data for all active fire protection means, details on fire barriers and their elements, etc. Detailed information is needed on potential ignition sources, fire detection and extinguishing systems, and manual fire fighting capabilities including the operational fire protection (fire brigade, etc.). Further information on secondary fire effects, safety consequences, analysis of the root cause of the event and corrective measures, etc. would be helpful. It should be pointed out that plant specific data are to be applied as far as feasible. However, generic reliability data have been provided as an additional input (Berg & Röwekamp, 2000).

The database for performing a Fire PSA is developed based on a partitioning of all the buildings to be analyzed. Basis for the building selection is the entire nuclear power plant.

In particular, the following four questions have to be answered by means of the collected data:

- (1) Can an initial incipient fire ("pilot fire") develop to a fully developed fire spreading all over the compartment?
- (2) Which damage can be caused by a fire inside the compartment?
- (3) Is fire spreading/propagation to adjacent compartments possible?
- (4) How can damage of components by the fire and its effects be prevented?

Question (1) mainly concerns the type and amount of combustibles present inside the compartment and their protection (e.g. protective coatings and wraps for cables, enclosures of combustible lubricants, fuels, charcoal, etc.). Based on these data, the compartment specific fire load density (fire load per compartment floor size) can be estimated. Only in case of ignition a fire occurs. Therefore, the entity of the potentially permanently or temporarily available ignition sources (e.g. staff attendance frequency, availability of hot surfaces, amount of mechanical and electrical equipment present) in the compartment have to be compiled for answering question (1).

The answer to question (2) mainly depends on the inventory of the compartment. That means there must be an allocation of the entire compartment inventory (components and equipment including cables) to the corresponding compartments. The required equipment functions as well as the potential consequences of their failure or malfunction have to be known. The inventory has to be classified. Distinguishing between important safety related equipment (so-called PSA components) and equipment, for which their failure results in a transient or an initiating event (so-called IE components) is necessary.

For answering question (3) the entire building structures of the NPP must be included in the database. For each compartment, the fire compartment boundaries (fire barriers such as walls, ceilings, floors including all the fire barrier elements, e.g. doors and dampers) as well as the connections between compartments (e.g. doors, hatches, ventilation ducts, cable raceways and their attributes) have to be known and documented. In this context, it has to be ensured that the questions (1) and (2) cannot only be answered for the compartment being analyzed but also for the entity of compartments adjacent to it.

Question (4) - to what extent damage by fire can be prevented - can only be answered based on information about the fire protection features being implemented in the initial fire

compartment itself and its adjacent compartments. This concerns all the potential means for fire detection and alarm as well as for fire suppression.

The Fire PSA database must meet the following requirements:

- Provision and compilation of compartment related primary data for all compartments in the entire NPP necessary to answer the questions (1) to (4);
- Compilation of data and information such as list of inventory or generation of sets of compartments applying different criteria (e.g. accumulation of compartments being openly connected to each other);
- Derivation of compartment specific characteristics such as fire load density, fire occurrence frequency or fire spreading probability from one compartment to another based on the primary data for calculating f_{ij} (see 3.6 below).

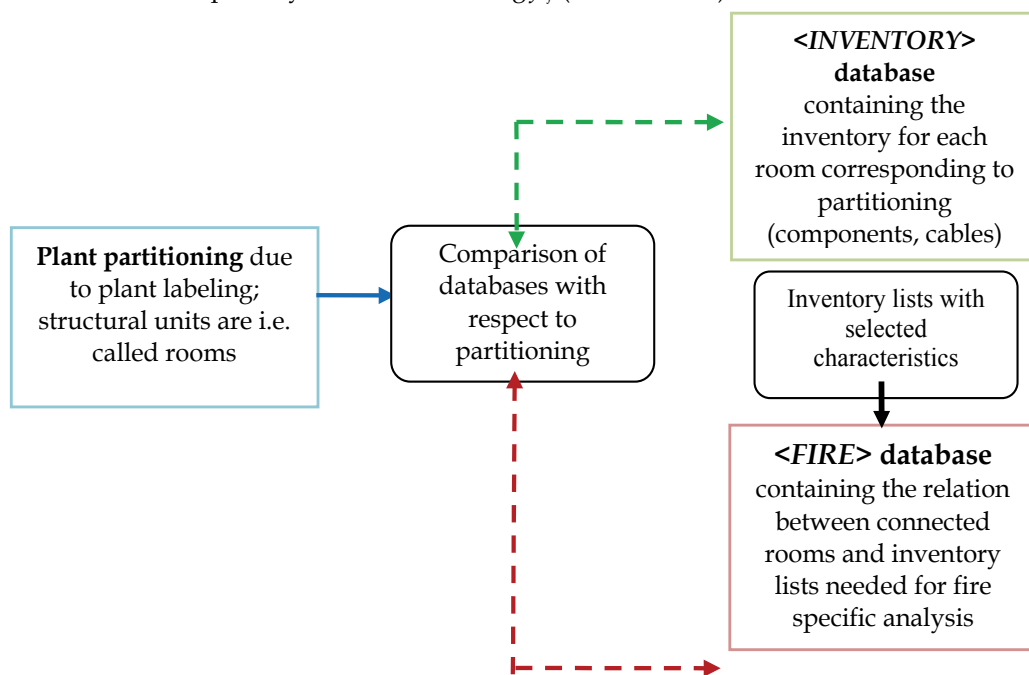


Fig. 2. Fire PSA Database from (Röwekamp et al., 2010)

Such a database enables a flexible overview and examination of the primary data available and guarantees the traceability of the Fire PSA analyses.

The basic structure of the Fire PSA database as well as some important input and output parameters are depicted in Figure 2.

The database is composed of two databases, the database <INVENTORY> containing the data on the compartment specific inventory, and a database <FIRE> containing for each compartment all the needed compartment related fire specific information.

3.5 Simplified fire effects analysis within the screening by standardized fire simulations

The actual Fire PSA enhancements also aim on developing an approach for applying standardized fire simulations by means of relatively simple, publicly available zone models such as CFAST.

In this approach, which still has to be validated for a complete application, generalized basic scenarios, so-called cases and sub-cases, have been defined in a first step for representative compartments and their characteristics with the corresponding dependencies of those parameters affecting the fire event sequence and the fire consequences significantly. As a second analytical step, each fire event sequence has been characterized by means of so-called design fires carrying different input parameter including standardized time sequences and heat release rates taking into account the combustibles typically available.

In this context, the significant parameters for binning of standard compartments to groups are floor size, room height, fire load and/or fire load density, natural and forced ventilation conditions, as well as the type of fire. An example of different standard cases is given in (Frey et al., 2008; Röwekamp et al., 2008).

For a set of characteristic fire compartments standardized fire simulations with CFAST have been successfully carried out. For automating these simulations, specific program modules and interfaces for handling the input and output data as well as information retrievals are needed. The main components for the automation are presented in Table 4 and Figure 3.

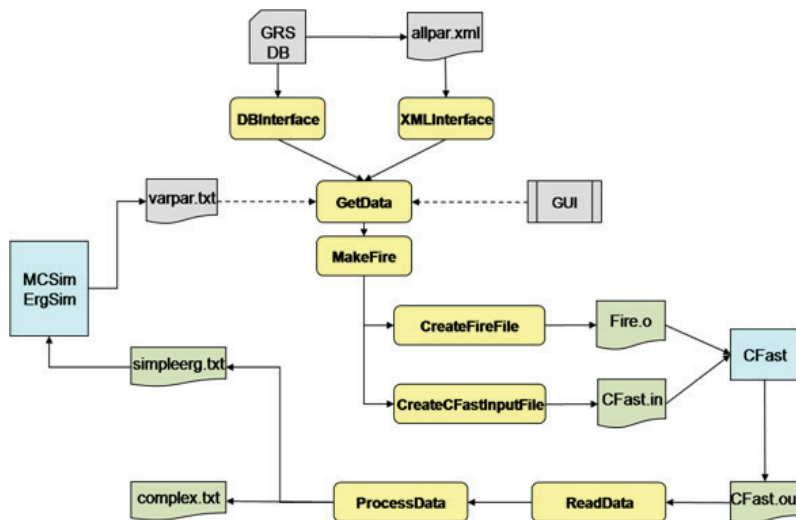


Fig. 3. Approach for automated standard fire simulations with CFAST from (Frey et al., 2008)

Module	Meaning/Task
GRS DB	Containing the geometric and fire related information on compartments in a MS ACCESS® database
allpar.xml	Alternative to the database containing all input data (XML format) needed für CFAST simulations
DBInterface	Interface for using data from alternative data sources
XMLInterface	Converting XML structure and the data included in the allpar.xml file to a C++-class; alternative to the direct data transfer by the DBInterface
GetData	Method oriented interface for sampling data stored in ReadXML and mapping them in a class structure

Module	Meaning / Task
<i>MakeFire</i>	Estimating the parameters of a standardized HRR course using information from <i>allpar.xml</i> and storing them in a class / object
<i>CreateFireFile</i>	Creating the CFAST for the fire target <i>Fire.o</i>
<i>CreateCFastInputFile</i>	Writing the CFAST input file <i>CFast.in</i> by means of the <i>GetData</i> data structure
<i>Fire.o</i>	Fire object imported by the CFAST application
<i>CFast.in</i>	Containing all data on fire compartment, fire barriers, ventilations and systems engineering
<i>CFast</i>	Program logic starting the CFAST simulation
<i>ReadData</i>	Reading out time dependent output (e.g. hot gas temperatures) from the CFAST-output file <i>cfast.n.csv</i> storing them in an adequate class
<i>ProcessData</i>	Assessing the output data imported by <i>ReadData</i> depending on the program logic by means of criteria (e.g. effects on safety significant targets)
<i>Simple.erg</i>	Output text file E for process control in case of performing a Monte Carlo simulation; solving problem oriented equations for limiting states for being able to assess the effects of different parameters on safety significant targets
<i>Complex.txt</i>	Output text file for all simulation results for further processing and use of time dependent sequences of the individual simulations
<i>MCSim (iBMB)</i>	Generating user defined discrete random variables for Monte Carlo simulations and evaluating the distribution function of the output values providing mean values and standard deviations and the resulting safety margin β
<i>Varpar.txt</i>	Data file created by <i>MCSim</i> containing random values for those parameters, defined as 'stochastic' ones in the input file <i>allpar.xml</i>
<i>GUI</i>	Grafic User Interface for calculations' control

Table 4. Modules for automated standardized CFAST fire simulations from (Frey et al., 2008)

In this context, it has to be mentioned that a probabilistic calculation for individual compartments is possible, if distributions for single parameters can be provided.

3.6 Stepwise compartment fire analysis

Based on the data and information contained in the database (see 3.4), the fire induced core damage frequency f_{ij} has to be determined for each compartment i and each plant mode j (see Figure 1).

In the frame of an exemplary Fire PSA performed for a BWR-69 type NPP, in total 351 compartments are analyzed within the reactor building. For 287 compartments the fire load density is less than 90 MJ/m². For all of the remaining compartments the frequencies of fire induced plant hazard states are pessimistically estimated. The sum of the estimated frequencies for 64 compartments equals 2.3 E-03/a. For 28 compartments, this frequency exceeds 1.0 E-07/a. The sum of the frequencies for the entire compartments with a very small frequency value is equal 2.5 E-07/a so that the frequency value for the 28 compartments covers more than 99 % of the sum of all pessimistically estimated frequency

values. Finally, the frequency of fire induced plant hazard states of the reactor building is estimated to be $3.8 \text{ E-}06/\text{a}$. This is the result of summarizing the plant hazard state by fire for all the 28 compartments. Considering accident management measures the reactor building fire induced core damage frequency is estimated to $7.8 \text{ E-}07/\text{a}$ for the reference plant.

3.7 Frequency calculation for fire induced core damage states

The in 3.4 mentioned necessary classification of the entity components of the NPP is extremely time-consuming in the run-up of estimating the fire induced CDF. As mentioned before, in particular, two classes of components have to be distinguished being significant:

- A component is called IE-component, if its failure alone or together with additional failures of other components has got the potential to be an initiating event (IE).
- A component is called a PSA-component, if its failure is regarded as a basic event in the fault trees of the corresponding Level 1 internal events PSA.

Depending on the fire growth a fire event may cause damage. The extent of the damage is characterised by the set of components affected/impaired. By means of assessing the extent of damage, in particular affecting IE components, it can be found, in how far the fire induced core damage may induce an initiating event (IE) modelled in the Level 1 internal events PSA.

The compartment related fire induced frequency of core damage states f_{ij} results from the product of

- the fire induced IE frequency and
- the unavailability of system functions required to control the adverse effects of the corresponding IE.

The unavailability of the required system functions is calculated by means of the Level 1 internal events PSA plant model taking into consideration the failures of the components from the set of components affected by fire.

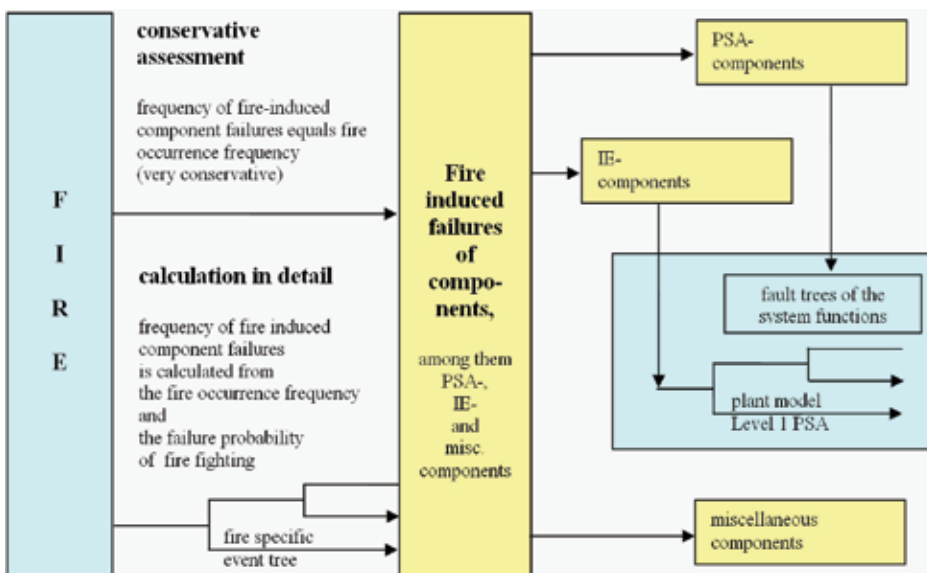


Fig. 4. Estimation und calculation of f_{ij}

The GRS code CRAVEX is applied for determining those components failed by the fire and its effects and their failure probabilities, in order to perform these analyses in an as far as practicable automatic manner. CRAVEX combines the fire specific and compartment specific data for determining the fire induced component failures and the PSA models for estimating core damage frequencies. It supplements the screening process as well as the detailed analyses, because the event and fault trees contained in these models describe in detail the interconnection between component failures and the occurrence of damage states. The following input data are generated by means of the database (see Figure 1): compartment specific fire occurrence frequencies, all probabilities of fire propagation to adjacent compartments, and the inventory list of all compartments affected by fire.

Furthermore, compartment related f_{ij} can be estimated by CRAVEX (see Figure 4). The Level 1 internal events PSA plant model and the fire induced component failure probabilities are used as input data for the calculations. The approach of these calculations by CRAVEX is in principle depicted in Figure 5 for an individual fire scenario. The fire occurrence is assumed inside a compartment C_i with $i = 1, \dots, N$.

The Level 1 internal events PSA plant model and the fire induced component failure probabilities are used as input data for the calculations.

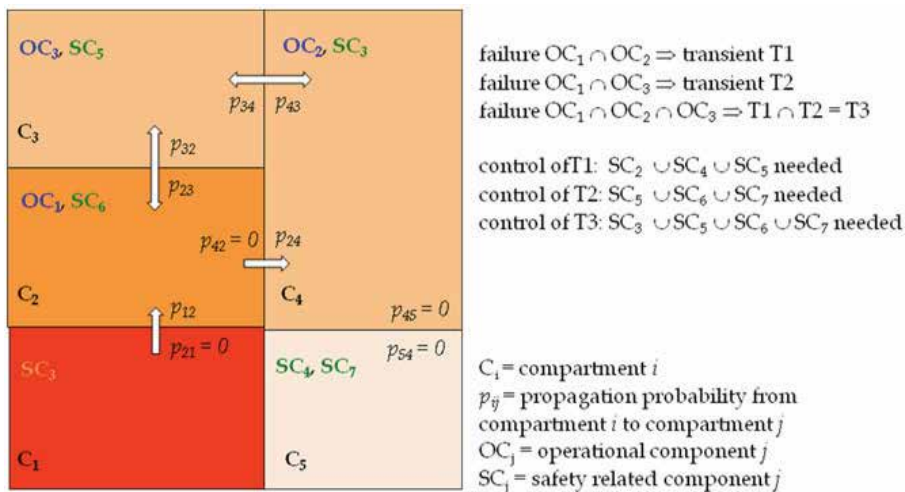


Fig. 5. Compartment configuration with fire source, components, and propagation paths

3.7.1 Frequency estimation (pessimistic estimate)

The following assumptions are made for pessimistic estimations:

- All active functions of the components in the compartments affected by fire are failed. This is considered for the initial fire compartment as well as for all the compartments, to where the fire may propagate.
- The fire occurrence frequencies are known for each compartment. The compartment specific fire occurrence frequencies are determined by means of the Berry method (Berry, 1979). The building fire frequencies needed as input for calculating compartments specific frequencies are estimated plant specifically.
- The so-called fire propagation probability is a pessimistic estimate of the probability of a fire propagating from a given compartment to an adjacent one. The fire propagation

probabilities are automatically calculated for each pair of adjacent compartments applying pessimistic assumptions for the unavailability of fire detection and suppression as well as for the fire barriers separating compartments.

For estimating the compartment specific fire induced CDF it is additionally assumed that the active component functions fail corresponding to the fire occurrence frequency of the initial fire compartment, where the fire started, that means that the possibilities of fire detection and suppression are neglected.

3.7.2 Frequency calculation in detail

For a detailed quantification, the pessimistic assumptions used by the estimation have to be verified and possibly corrected taking into consideration detailed plant specific information as explained earlier.

The realistic assessment of the fire induced damage frequencies is very important. For this assessment, fire specific event trees are developed and quantified. The development of fire specific event trees for compartments requires knowledge on the plant specific fire protection such as:

- Equipment including fire protection features (e.g. fire detection and alarm features, fire extinguishing means, fire barriers and their elements), arrangement of combustibles, presence and type of potential ignition sources inside the initial fire compartment and adjacent compartments;
- Verification of possible fire sources in the compartments;
- Examination of the fire occurrence frequency roughly estimated by means of the method of Berry based on the information concerning compartment inventory and the compartment characteristics (replacing the application of the more generic top-down-method within the screening by a bottom-up approach for estimating as far as possible realistic compartment specific frequencies);
- Plant specific unavailability of fire protection equipment in the compartments;
- Analysis of human behaviour and performance in case of fire;
- Using results of existing fire simulations or – in difficult cases - performing additional calculations for the compartment under consideration.

The reactor building of the reference plant having been analyzed consists of 351 compartments, among them 47 compartments on the building level 01. In 15 of the above mentioned 47 compartments the fire load density exceeds the threshold value of 90 MJ/m² during full power operational plant states. The analysis of possible compartment related fire damages gives the result that important PSA related components are present in 12 of the 15 compartments so that a fire in these compartments will cause an IE. The identified transients are exclusively transients induced by cable failures (e.g. by erroneous signals or failures of the power supply of solenoid valves of the main steam isolation valves). The fire related PSA component failures are taken into account when calculating compartment specific fire induced CDF. The fire induced core damage frequency is revealed from a possibly modified fire occurrence frequency taking into consideration fire extinguishing means.

4. Potential Improvements

The fire occurrence frequencies directly affecting the finally resulting core damage frequencies have been determined based on realistic and as far as practicable plant specific

data. In principle, the results of the approach of Berry (Berry, 1979) have been used for estimating the fire occurrence frequencies. This methodology compares compartments within a building to each other with respect to the potential for ignition. Based on the fire frequency for the total building compartment specific frequencies are estimated. Depending on the amount of data used for calculating the building specific fire frequency the approach is more or less conservative.

Taking also the plant specific operating experience on all incipient fires into account as far as possible realistic fire frequencies can be estimated. For the reactor building of the reference plant this resulted in a relatively high fire occurrence frequency of $1.6 \text{ E-}01/\text{a}$ in comparison to that of a Fire PSA for another NPP applying only generic data ($6.9 \text{ E-}03/\text{a}$). Furthermore, all possibilities of fire propagation from the initial compartment to adjacent ones and to further compartments have been considered. By this systematic approach it could be demonstrated that fire propagation is less important for the probability of fire induced initiating events and the unavailability of system functions.

The Level 1 FP Fire PSA having been performed for the reference plant resulted in a fire induced CDF of $1.9 \text{ E-}06/\text{a}$. This value is higher than the CDF value of $1.4 \text{ E-}06/\text{a}$ for internal events in case of full power operational states. Approx. 69 % of the CDF result from fires inside the reactor building, while fires in the auxiliary building provide a contribution of approx. 17 %.

The compartment based Fire PSA uses the assumption that in case of fire non-suppression all equipment including cables inside the fire compartment will fail. In case of applying this methodology to cable channels the approach may be too conservative. Depending on the protection of the channels these have to be treated as separate sub-compartments. The results of the Fire PSA may be optimized by systematically checking if protected cable channels have been treated correctly.

For the plant under consideration, the Fire PSA provided some recommendations for improving the fire protection: In a few cable channels in the auxiliary building and the independent emergency systems building no fire detectors are installed. An early fire detection and suppression cannot be ensured. The frequency of an incipient fire for these channels is the same as the fire induced damage frequency. On the other hand, the fire occurrence frequencies estimated are too pessimistic. In conclusion, the installation of automatic fire detectors in these compartments will reduce the compartment specific fire induced damage frequency.

Similar improvements can be performed in specific compartments inside the reactor building. The installation of fire detector chains with 2 - 4 fire detectors in compartments for the pre-heaters, an installation stairwell, a room with a control board for the safety valves, and other process rooms will significantly reduce the compartment specific CDF.

The fire load density of the compartment for the additional water supply vessel inside the reactor building has been treated quite pessimistically. The plant documentation provided a fire load of 560 MJ resulting in a fire load density significantly lower than the threshold value of 90 MJ/m^2 for the compartment floor size of approx. 50 m^2 . However, the compartment has been included in the analysis due to the permanently as well as temporarily available fire loads. Here again, the core damage frequency may be reduced by installation of more suitable fire detection features or by reducing the fire loads.

5. Specific Consideration for Low Power and Shutdown States

5.1 Differences in the approach for power operation and shutdown states

As explained earlier, the recent German approach for Fire PSA contains the following steps of the analysis:

- A systematic plant partitioning of the entire plant, and
- An as far as necessary detailed estimation of FCDF for each of the compartments.

Working step	Differences between power operation and shutdown states
1. Plant partitioning	
1.1. Selection of buildings	Building selection by classified inventory lists (PSA and IE components); different amount of PSA and IE components can lead to different buildings to be analyzed
1.2. Building partitioning	Partitioning mainly due to given building structures with fire specific aspects being considered; plant state does not make significant difference
2, Estimation of fire induced damage state frequencies per compartment and plant operational state	
2.1. Fire occurrence frequency	Estimation of the fire occurrence frequency by Berry methodology is the same for differing plant operational states, but the input data are different
2.2. Fire damage frequency	Same methodology for fire damage frequency calculation, but differing database for different plant operational states
2.3. Core damage frequency	The corresponding PSA plant models for Level 1 PSA for power operation and shutdown states are applied; for low power and shutdown states it is important if and in which detail human actions can be performed.

Table 5. Analytical steps of a Fire PSA for power operation and shutdown states (Röwekamp et al., 2010)

When further sub-dividing these analytical steps some differences in the approach for power operation and shutdown states become visible (see Table 5).

The analyses for German NPP have demonstrated that it has to be considered in the estimation of compartment specific fire occurrence frequencies for LP/SD that there temporarily fire loads being present and that maintenance and repair work is particularly performed in those plant areas and compartments being isolated. This may result in a change of the compartment specific fire occurrence frequencies. However, the probability of relevant fire induced damage in an isolated compartment is low, as - with only very few exceptions - initiating events do not occur in such compartments and safety functions remain available.

5.2 Specific considerations for screening

The first working step is a fire specific compartment analysis corresponding to given criteria for the given plant operational mode (FP or LP/SD). Up to the time being, a fire load density criterion of screening out compartment with fire load densities lower than 90 MJ/m² is applied due to (FAK PSA, 2005a). This criterion resulted from safety demonstrations for non-nuclear industrial buildings. For mechanically ventilated compartments in nuclear installations it has been demonstrated that a fire in a compartment with a fire load density of only 10 MJ/m² may result in temperatures exceeding 200 C and thus may impair the function of sensitive electrical equipment and cables. Ongoing research activities suggest replacing this screening criterion in the future by a fire specific qualitative screening criterion considering the really in the compartment present ventilation conditions and fire propagation velocities applying the fire load density values only for a fire specific ranking of compartments.

During LP/SD so-called transient fire loads and/or additional ignition sources are temporarily present in those rooms where these are needed for maintenance and repair activities including hot work. This could be demonstrated for the reference NPP by the logs from the Fire PSA plant walk-through. For this type of activities specific work permits for isolation of systems/components and clearance procedures for the work including hot work permits for fire relevant activities corresponding to the plant operating manual including specific requirements for the unit control room and shift personnel are needed. All the provisions for preparing and performing maintenance and backfitting activities including procedures for electrical as well as process engineering isolations of components and systems correspond to these work permits. In case of temporary presence of additional potential ignition sources and fire loads specific preventive measures are foreseen corresponding to the plant fire protection manual, e.g.:

- Protecting the affected area against sparks from welding,
- Covering and isolating openings, gaps, slots, grates, etc.,
- Providing additional portable fire extinguishers,
- Installation of fire watches in case of fire detectors not being active,
- Ensuring highly effective mechanical ventilation,
- Limiting gas reservoirs for activities with gas to a daily amount;
- Eliminating combustibles in the hot work area,
- Protective covering of combustibles which cannot be eliminated,

There is no difference between FP and LP/SD plant modes within the compartment screening due to the 90 MJ/m² fire load density criterion. This criterion is only applied for deciding if there can be a fire with potentially significant damage in the compartment. By inserting transient fire loads during LP/SD states the fire load density may be increased exceeding the threshold value of 90 MJ/m² so that the compartment can no longer be screened out. The practical application has demonstrated that this happens only under the above mentioned boundary conditions with the corresponding protection measures and mainly in those compartments where the most components are isolated during LP/SD. However, it is necessary to roughly estimate the change in the compartment fire load density. This has to be considered, e.g. in the simulations of the fire sequence.

Changes in the ignition conditions due to hot work and isolation of electrical systems and components play an important role for estimating fire occurrence frequencies. However, it has to be discussed (particularly for fire occurrence frequency estimation in the frame of

screening) if the Berry parameters (Berry, 1979) applied for FP states can also be applied for LP/SD states. It has to be considered that the prerequisites for the occurrence of an initial incipient fire do not change in those compartments not being isolated during LP/SD, while for the isolated compartments the consequences have to be balanced. Isolation of electrical components reduces the fire risk, hot work increases it.

In addition, hot work activities correspond to the presence of personnel in the affected compartment resulting in an early manual fire detection and suppression. Recent German research activities have demonstrated that an evaluation of the hot work permits is particularly needed for observing and considering potential peculiarities during these activities typically performed during LP/SD from the beginning of the analysis and being able to consider those time periods explicitly for the fire occurrence frequency estimation.

5.3 Particular requirements for low power and shutdown states

The fire protection regulations and standards do not only have to be applied for FP modes but also for LP/SD modes, in particular:

- Control room and shift regulations (part of the plant operating manual),
- Maintenance rules (part of the plant operating manual),
- Alarm regulation (part of the plant operating manual),
- Fire protection regulation (part of the plant operating manual),
- Fire protection concept,
- Service instruction concerning tasks, organization, skills, and training, and of the on-site fire brigade.

In the following, some aspects significant in particular for LP/SD modes are pointed out. During the operation and tripping time period compliance with the following rules for minimizing transient fire loads and potential ignition sources is required:

- Transient fire loads have to be avoided as far as practically possible.
- All people working on-site are obliged to keep their work places as far as practically possible free from combustible materials and/or to eliminate them from these materials in the shortest possible time period.
- Combustible solids, liquids, and gases are only permitted to be present at the work place in an amount needed per one shift.
- Drained vessels no longer in use, formerly filled with combustible liquids have to be stored in a special storage room for scrap and lubricants.
- Handling and treatment of liquid or gaseous combustibles is only permitted under given prerequisites and standards specified in the corresponding work order.
- Hot work (work with open flames, welding, cutting, etc.) requires specific written hot work permits before starting the activities. The required necessary protective provisions including fire watches and control walk-troughs are explicitly specified in the hot work permit.

5.4 Exemplary results for a BWR-69 type nuclear power plant in Germany

For the BWR-69 type reference plant being analyzed it could be demonstrated that for LP/SD plant modes the same six buildings as for FP modes have to be analyzed. The spatial partitioning is principally based on the plant specific identification system of the entire NPP. In a few exceptional cases there were deviations from this procedure, e.g. the sub-division of

the large reactor annulus into quadrants, or very long cable rooms and stairways. Some fire protected (sealed) cable raceways without compartment numbers were reassigned.

The screening has been performed in the same manner for FP and LP/SD plant modes. In this context, it has to be stated that particular differences in the screening of compartments result from maintenance and repair activities including hot work. Significant findings have not been observed for the plant being analyzed. As an important finding it has to be mentioned that many connections between compartments have pessimistically to be assumed open during LP/SD, as the activities being performed during these periods often create conditions where barriers elements (e.g. doors, cable penetration seals, etc.) are being left open or blocked due to practical reasons for the ongoing activities.

Building	Plant Operational State			
	FP		LP/SD	
	No. of fires	Fire occurrence frequency	No. of fires	Fire occurrence frequency
Reactor Building (without Containment)	4	1.6 E-01	6	2.4 E-01
Switchgear Building	8	2.9 E-01	3	1.2 E-01
Turbine Building	4	1.6 E-01	11	4.0 E-01
Diesel Building	0	1.7 E-02	0	1.7 E-02
Independent Emergency Systems (IES) Building	0	1.7 E-02	0	1.7 E-02
Other buildings and plant areas	16		15	
Total	32		35	

Table 6. Fire events and occurrence frequencies (expected values) in the reference plant for full power and low power / shutdown states

On the other hand, the higher presence of humans during these operational modes in the buildings results in early detection of situations which could create a fire and/or a manual fire detection and suppression during the incipient fire phase. This may explain the first rough results when comparing fire occurrences during FP and LP/SD. In total 67 fire events occurred in the reference plant from 1980 (start of commercial operation) to the end of 2008, 32 of these during FP modes, and 35 during LP/SD modes. Only one of these was reportable due to the German reporting criteria, 66 were incipient fire events below the reporting thresholds. Table 6 provides the corresponding building specific event distribution and fire frequencies (Röwekamp et al., 2010).

Determining fire occurrence frequencies for LP/SD plant modes the durations of the different phases of the operational modes and the frequencies estimated for each phase have to be considered. For selected buildings, e.g. the diesel building, there are nearly no differences between FP and LP/SD states. In this case, the approach is the same for both

operational modes. For all the other buildings the approach has to be adjusted to the boundary conditions and data stored in the Fire PSA database for this mode.

6. Conclusions and Outlook

A state-of-the-art methodology for Fire PSA has been developed and successfully applied for a German NPP. This methodology is based on a combined multi-step qualitative and quantitative screening approach applying a comprehensive database specifically developed for the application within the frame of Fire PSA. The approach being applied enables to automatically perform several analytical steps of the Fire PSA. Some of the automatisms, e.g. the calculation of compartment specific fire occurrence frequencies or the probabilities of fire propagation to adjacent and further compartments, have been successfully implemented in the database. Standardized input data files have been provided for other applications of the Fire PSA database, e.g. for determining fire induced core damage frequencies by means of the simulation code CRAVEX.

Up to now, the Fire PSA database has not yet been completely adapted from full power plant modes to low power and shutdown modes. Investigations, which data have to be changed or added for these states, are still ongoing.

Another recent development focuses on fire induced cable failures and circuit faults, which are broadly discussed on an international level (EPRI, 2005). In this context, a cable failure mode and effect analysis (FMEA) for all the PSA related cables has been developed (Herb & Piljugin, 2008) and tested for a fire compartment, which had been identified as significant in the frame of the Fire PSA. This leads to the requirement to enlarge the Fire PSA database considering additional data needed for a cable FMEA and/or combining the compartment inventory matrix with the cable database of the FMEA. The activities for implementation of the cable FMEA approach in the Fire PSA methodology are ongoing.

A further development will cover the characteristics of compartments and components for supplementing the automatic data supply, such as data on the room heights for fire simulations with the zone model CFAST or the description of the ventilation systems for assessing smoke propagation.

In addition, an uncertainty and sensitivity analysis has been performed for the reference plant Fire PSA providing not only mean values for fire induced CDF but also for quantifying major uncertainties. This will increase the level of confidence of the Fire PSA results.

It has to be pointed out with respect to the statistical data applied in the frame of an as far as possible realistic Fire PSA that the existing national database, in particular data on compartment specific as well as component specific fire occurrence frequencies and on the reliability of fire protection features, has to be further improved and expanded. Moreover, the human influence has to be considered carefully.

The use of internationally available generic data (e.g. for fire occurrence frequencies), mainly from the U.S. and France, is not always appropriate for application within Fire PSA for German plants due to differences in design, inspection and maintenance. However, the German data being presently available do not always allow providing a verified database because only a very small amount of approx. 30 fire events had to be obligatory reported to the national supervisory authorities. Therefore, the OECD FIRE Database Project which was started by OECD/NEA in 2003 to collect fire event data and meanwhile comprises more

than 340 fire events from twelve NEA member countries (OECD, 2009) may supplement performing Fire PSA for German NPP by further input data.. First test applications of this database with up to the end of 2008 in total 343 fire events have been successfully performed (Berg et al., 2009; Berg et al., 2010).

7. References

- American Nuclear Society (ANS) (2007). *Fire PRA Methodology*, ANSI/ANS-58.23-2007
- Berg, H. P.; Forell, B.; Fritze, N. & Röwekamp, M. (2009). First National Applications of the OECD FIRE Database. *Proceedings of SMiRT 20, 11th International Seminar on Fire Safety in Nuclear Power Plants and Installations, August 17-19, 2009, Helsinki, Finland*
- Berg, H. P.; Frey, W.; Röwekamp, M. & Türschmann, M. (2009). Fire PSA for a German BWR-Enhanced Results and Potential Plant Specific Improvements, *Proceedings of the ESREL Conference 2009, Prague, Taylor & Francis Group, London, pp. 2123–2130, GRS-A-3496*
- Berg, H. P.; Fritze, N.; Forell, B. & Röwekamp, M. (2010). Risk oriented insights in transformer fires at nuclear installations. *Proceedings of the ESREL Conference 2010, Rhodes, September 5 – 9, 2010, in press*
- Berg, H. P. & Röwekamp, M. (2000). Reliability Data Collection for Fire Protection Features, *Kerntechnik 65, No 2-3 (May 2000) 102-107, ISSN 0932-3902*
- Berry, D. L.; Minor, E.E. (1979). *Nuclear Power Plant Fire Protection, Fire Hazard Analysis, NUREG/CR-0654, SAND 79-0324, September 1979*
- Bundesminister des Innern (BMI) (1977). *Sicherheitskriterien für Kernkraftwerke vom 21.10.1977, Bekanntmachung des Bundesministers des Innern, Bundesanzeiger Nr. 206 vom 3.11.1977*
- Bundesminister des Innern (BMI) (1994). *Leitlinien zur Beurteilung der Auslegung von Kernkraftwerken mit Druckwasserreaktoren gegen Störfälle im Sinne des § 28 Abs. 3 der Strahlenschutzverordnung – Störfall-Leitlinien, Bekanntmachung vom 18. Oktober 1983 mit Neufassung des Kap. 4 vom 21./22. April 1994*
- EPRI/NRC-RES (2005). *Fire PRA: Methodology for Nuclear Power Facilities - Final Report, NUREG/CR-6850, September 2005*
- Facharbeitskreis (FAK PSA) (2005a). *Probabilistische Sicherheitsanalyse für Kernkraftwerke: Methoden zur probabilistischen Sicherheitsanalyse für Kernkraftwerke, Stand: August 2005, BfS-SCHR-37/05, Salzgitter, October 2005*
- Facharbeitskreis (FAK PSA) (2005b). *Probabilistische Sicherheitsanalyse für Kernkraftwerke: Daten zur probabilistischen Sicherheitsanalyse für Kernkraftwerke, Stand: August 2005, BfS-SCHR-38/05, Salzgitter, October 2005*
- Frey, W.; Herb, J.; von Linden, J.; Piljugin, E.; Röwekamp, M.; Türschmann, M.; Hosser, D. & Riese, O. (2008). *Methoden zur Abschätzung des Risikobeitrags redundanzübergreifender Brandschäden, Gesellschaft für Anlagen und Reaktorsicherheit (GRS) mbH, GRS-A-3425, Köln*
- Herb, J. & Piljugin, E. (2008). FMEA of Cable Failures within Fire PSA, *Proceedings of the 9th International Probabilistic Safety Assessment and Management Conference (PSAM 9), May 2008, Hong Kong, China, on CD*
- Nuclear Safety Standards Commission (Kerntechnischer Ausschuss, KTA) (2000). *Fire Safety in Nuclear Power Plants.*

- Part 1: *Basic Requirements*, KTA 2101.1 (12/2000),
- Part 2: *Fire Protection of Structural Plant Components*, KTA 2101.2 (12/2000)
- Part 3: *Fire Protection of Mechanical and Electrical Plant Components*, KTA 2101.3 (12/2000)
- Organization for Economic Cooperation and Development (OECD) OECD/NEA/CSNI (2009). FIRE Project Report: "Collection and Analysis of Fire Events (2002-2008) – First Applications and Expected Further Developments". NEA/CSNI/R(2009)6, Paris
- Röwekamp, M.; Türschmann, M.; von Linden, J.; Kirchner, J. W. & Berg, H. P. (2006). Fire PSA for a German BWR (BWR-69 type) – methodology applied and results, *Proceedings of the 8th International Probabilistic Safety Assessment and Management Conference (PSAM 8)*, New Orleans, May 2006, paper 0052, on CD
- Röwekamp, M.; Türschmann, M.; Piljugin, E.; Riese, O. & Hosser, D. (2008). Actual Developments in the Advanced German Fire PSA Methodology, *Proceedings of ANS PSA 2008*, Knoxville, TN, USA, September 7 – 11, on CD
- Röwekamp, M.; Riese, O. & Berg, H. P. (2009). Improvements in the German Fire PSA Methodology Demonstrated at a German BWR Built to Earlier Standards, *Proceedings 17th International Conference on Nuclear Engineering (ICONE-17)*, paper 75595, Brussels, July 2009, on CD
- Röwekamp, M.; Türschmann, M.; Schwarz, M. & Berg, H. P. (2010). Database for A Comprehensive Fire PSA. *Proceedings of the 10th International Probabilistic Safety Assessment and Management Conference (PSAM 10)*, June 7 – 11, paper 113, Seattle, USA, on CD
- Türschmann, M.; von Linden, J. & Röwekamp, M. (2005). Systematisches Auswahlverfahren für probabilistische Brandanalysen, *Schriftenreihe Reaktorsicherheit und Strahlenschutz*, BMU-2005-667, ISSN 0724-3316
- Türschmann, M.; Röwekamp, M & Berg, H. P. (2006). Durchführung einer Brand-PSA mit aktuellen Methoden, *Tagungsbericht Jahrestagung Kerntechnik 2006*, Aachen, May 2006, pp 208 – 212, INFORUM-Verlag (Ed.), Deutsches Atomforum, Bonn, ISSN 0720-9207
- von Linden, J., Klein-Heßling, W.; Piljugin, E.; Röwekamp, M. & Türschmann, M. (2005). Ausgewählte probabilistische Brandanalysen für den Leistungs- und Nichtleistungsbetrieb einer Referenzanlage mit Siedewasserreaktor älterer Bauart, *Schriftenreihe Reaktorsicherheit und Strahlenschutz*, BMU-2005-666, ISSN 0724-3316
- von Linden, J.; Röwekamp, M.; Türschmann, M. & Berg, H. P. (2009). Methods for a Fire PSA Exemplary Applied to a German BWR-69 Type Nuclear Power Plant, *Kerntechnik*, Vol. 74, No. 3 (May 2009) 106–110, ISSN 0932-3902

Application of Probabilistic Methods to the Structural Integrity Analysis of RBMK Reactor Critical Structures

G. Dundulis, R. Kulak*, R. Alzbutas and E. Uspuras
Lithuanian Energy Institute, 3 Breslaujos, LT-44403 Kaunas, Lithuania
**RFK Engineering Mechanics Consultants, USA*

1. Introduction

One of the main requirements for building structures and components of nuclear power plants is that during extreme internal and/or external loading the structural integrity of the buildings and components installed in the building should be retained. Analytical solutions and sophisticated numerical models are used to evaluate the structural integrity of these structures. In case of dynamic loading, impact energy is transformed into the energy of plastic deformation of the structures. The transient behaviour of the structures during transient loading is a complex phenomenon due to various factors such as inertia effects, large deformations, and inelastic behaviour. It is, thus, not possible to obtain analytical solutions for general cases; so sophisticated numerical models are necessary for analysis. The finite element method (FEM) has been used extensively to simulate many applications in structural dynamics (Nagel, 2005; Aljawi, 2002; M. Yamashita, 2005, Olabi, 2008, Lee, 2004). Finite element codes are able to accurately model the plastic deformation via bending, compression or full collapse of the structures. After the terrorist attacks in New York and Washington D. C. using commercial airliners, the structural integrity assessment of civil airplane crashes into civil structures has become very important. Since these attacks, researchers from many countries have simulated aircraft crash into building structures. The FEM methodology mainly was used for the aircraft crash analysis (Bossak, 2003, Brinkmann, 2006, Dundulis, 2007a, Muragishi, 2001, Ramalingam, 2002).

Due to the tendency for increased nuclear safety, the analysis of dynamic loading shall demand multidisciplinary optimization of the methods used. However, simulation-based multidisciplinary optimization generates deterministic optimum design, which are frequently pushed to the limits of design constraint boundaries, leaving little or no room for tolerances (uncertainty) in modelling, simulation uncertainties, and manufacturing imperfections. Consequently, deterministic optimum designs that are obtained without consideration of uncertainty may result in unreliable designs, indicating the need for Reliability-Based Design Optimization (Youn, 2004).

The selection of the numerical simulation methods, preparation of models for analysis, evaluation of the material properties and loads are very important for structural integrity analysis of critical nuclear power plant structures subjected to either internal or external

extreme loading events. It is known that every material parameter is uncertain. The uncertainty of strength parameters is especially characteristic for concrete material. In order to ensure that buildings are reliable and safe in case of accidental transient loading, it is very important to evaluate uncertainty associated with loads, material properties, geometrical parameters, boundaries and other parameters. Therefore, it is necessary to account for the uncertainty in these quantities when performing a structural integrity evaluation (Podula, 2006). This can be accomplished through probabilistic analyses to see if a combination of values of relevant parameters could lead to failure and to determine the probability of failure (Alzbutas, 2003, Lyle, 2007). Therefore, a probability-based structural integrity analysis was performed as the integration of deterministic and probabilistic methods using existing state-of-the-art software for both the whipping pipe event and the aircraft crash event. The methodology of the probability-based structural integrity analysis that integrates deterministic and probabilistic methods is explained in this chapter. The application of this methodology to two Ignalina Nuclear power plants (NPP) postulated accidents is presented. Ignalina NPP that have a RBMK type reactor are quite different in comparison to power plants with PWR or BWR types reactors. Several events have been identified for these plants that can compromise the integrity of critical structural components. The Chernobyl RBMK reactor accident is the most serious accident in the history of the nuclear industry. Typically, RBMK reactors do not possess the conventional containment structure. Only the Ignalina NPP contains two RBMK 1500 reactors, which is the most advanced version of the RBMK reactor, and has a pressure suppression type confinement, which is referred to as the Accident Localization System (ALS) (Almenas, 1998). However the ALS encloses only about 65% of the entire cooling circuit. It does not enclose the sections of piping most vulnerable to rupture in case of the dangerous loss-of-coolant accident. Ruptured piping can lead to a whipping pipe impacting onto the inside of a critical exterior wall.

The finite element method is used for deterministic strength analysis of building and piping. The deterministic finite element software NEPTUNE (Kulak, 1988) was used here for structural integrity analysis. This software can analyze the transient structural response of the concrete and steel structures, which undergo large displacements and nonlinear material response during transient loading, including object impact onto the structures.

The Monte Carlo Simulation, First Order Reliability Method, and the combined Monte Carlo Simulation and Response Surface method were used for the probabilistic analyses of failure of the structures in case of the transient loading. The ProFES (Cesare, 1999) software was used for the probabilistic analysis of structural failure. ProFES is a probabilistic analysis system that allows performing probabilistic finite element analysis in a 3D environment that is similar to modern deterministic finite element analysis.

The developed probability-based approach (Kulak et al., 2003, Alzbutas et al., 2004) was used to analyze failures of RBMK reactor critical structures of the Ignalina NPP. This methodology was applied to the analysis of a group-distribution-header pipe whip, which results from a guillotine break, and subsequent impact to the adjacent walls (Alzbutas et al., 2003, Dundulis et al., 2005). This is a postulated accident for the Ignalina NPP RBMK-1500 reactors. Also, the probabilistic analysis of building failure was performed for an external event induced accident, that is, impact by a commercial aircraft (Dundulis et al., 2007c).

2. Probabilistic Analysis Methods

Probabilistic methods provide a means to assess the affect of design uncertainties and manufacturing/construction tolerances on the reliability and performance of structures. The proposed probability-based approach for integrated analysis of structure failure includes the use of several methods, which are combined to study the problem. In this chapter, the Monte Carlo Simulation, First Order Reliability Method, and the combined Monte Carlo Simulation and Response Surface method were introduced for the probabilistic analyses of failure of the structures subjected to severe transient loading.

2.1 Monte Carlo Simulation Method

The Monte Carlo Simulation (MCS) is a method, which is suitable for simulations that execute relatively quickly (e.g. simple linear finite element models or closed form expressions), because it typically requires a large number of response variables and limit state function evaluations. The precision of the evaluations depends on the number of evaluations and the chosen value of the failure probability. MCS method is mainly used to study the initial estimates and sensitivity of the response variables as well as the effect of uncertainties of system properties and uncertain model parameters to the probability of limit states (e.g. some failure states). Uncertainties in numerical values are modelled as random variables with specified characteristics. Confidence ranges and subjective probability distribution describe the state of knowledge about all uncertain parameters. Initially using the MCS method, sets of random variables (i.e., different combinations of these random variables) are generated, and then each set is used as input for separate deterministic runs. The values of the random variables are based on their individual probability density functions. Estimates of probabilities are determined by a simple statistical analysis of the simulation results. Therefore, the most important random variables and limit states for further analysis may be selected according to the results of MCS. The aim of such initial analysis is to identify and at least roughly quantify the response of all potentially important uncertain parameters. Least important parameters are then discarded in subsequent analysis and this provides a substantial computational cost savings.

2.2 First Order Reliability Method

The First Order Reliability Method (FORM) is an approximation method that estimates the probability of an event under consideration—typically named a “failure”. This method redefines the limit state in terms of the input variables and searches the point for the combination of values that is most likely to cause failure. This point is often referred to as the design point or the most probable point. The method then fits a linear surface at the most probable point and uses this surface (along with transformations for any non-normal random variables) to compute probabilities.

FORM is characterized by the iterative, linear (hence the term ‘first-order’) approximation to the performance function. It uses analytical schemes to approximate the failure probability and is reported to be computationally very efficient compared to MCS, especially for scenarios corresponding to low probabilities of failure (Bjerager 1990). Also, FORM is the preferred method for evaluating small probabilities because for the same precision as MCS it often requires the least number of deterministic (finite element) model runs, which is very important when large FE models are used. With FORM, the computational effort is

proportional to the number of random variables and limit states. FORM is more efficient than MCS in terms of computing time and accurate results can be obtained even when the failure probability is low. All the random parameters must, however, be continuous and large errors can also result if there are local minima in the limit state or high non-linearity. Despite these limitations, FORM is the most popular reliability analysis method; it can be easily extended to non-linear limit states; and it has a reasonable balance between ease of use and accuracy.

2.3 Response Surface/Monte Carlo Simulation Method

The hybrid Response Surface/Monte Carlo Simulation (RS/MCS) method is used to determine a polynomial function, which expresses the failure probability. The Response Surface (RS) method is similar to the FORM described above. However, while the FORM deals directly with the performance function, the RS method involves approximating the original, complicated system performance function with a simpler, more computationally tractable model. This approximation typically takes the form of a first or second order polynomial:

$$Y(x) = Y(x_1, \dots, x_n) \sim a_0 + a_1x_1 + \dots + a_nx_n + a_{n+1}x_1^2 + \dots + a_{2n}x_n^2 + a_{2n+1}x_1x_2 + \dots \quad (1)$$

Determination of the constants is accomplished through a linear regression about some nominal value, typically the mean. Using this performance function the probability of failure can be estimated using MCS. Thus, this fitted response-surface is used as a replacement or proxy for the deterministic model with initial parameters, and all inferences related to probabilistic analysis for the original model are derived from this fitted model (Khuri, 1987). The hybrid RS/MCS method is proposed to be used in order to study the relation between failure probability and parameters of initial model.

3. Finite Element Modelling of the Building Structures and Components

Sophisticated analysis of complex structures is possible using powerful numerical techniques on modern computer workstations. This may aid in a better understanding of the behaviour of the structures under transient loads. The most general approach for numerical analysis is the finite element method. The finite element method is a numerical analysis technique used by engineers, scientists, and mathematicians to obtain solutions to the differential equations that describe, or approximately describe a wide variety of physical (and non-physical) problems. Physical problems range in diversity from solid, fluid and soil mechanics, to electromagnetism or dynamics.

The underlying premise of the method states that a complicated domain can be sub-divided into a series of smaller regions in which the differential equations are approximately solved. By assembling the set of equations for each region, the behaviour over the entire problem domain is determined. Each region is referred to as an element and the process of subdividing a domain into a finite number of elements is referred to as discretization. Elements are connected at specific points, called nodes, and the assembly process requires that the solution be continuous along common boundaries of adjacent elements.

The finite element method is used for deterministic strength analysis of building structures and components. In this work, the deterministic finite element software NEPTUNE (Kulak, 1988) was used for structural integrity analysis.

The NEPTUNE code is based upon the central difference explicit integrator. Thus, the code does not employ stiffness or flexibility matrices but is based upon a nonlinear internal nodal force vector. This approach is ideal for transient, nonlinear analyses in which metals are deforming in an elastoplastic mode, concrete is cracking/crushing and contact impact is taking place. When individual elements reach a failed state, their contributions to the internal nodal force vector is reduced to zero and there is no change required to the solution algorithm.

The central difference integrator is used to solve the equations of motions. This integrator is well suited for the treatment of transient (short duration) problems in which the variation of element eigenvalues over the mesh is not large. The acceleration, velocity, and displacement are obtained from central difference formulas:

$$\ddot{u}_{ii}(n) = (f_{ii}^{ext}(n) - f_{ii}^{int}(n)) / m_{ii}(n), \text{ no sum} \quad (2)$$

$$\dot{u}_{ii}(n+1/2) = \dot{u}_{ii}(n-1/2) + \Delta t \ddot{u}_{ii}(n) \quad (3)$$

$$u_{ii}(n+1) = u_{ii}(n) + \Delta t \dot{u}_{ii}(n+1/2) \quad (4)$$

where "i" refers to the coordinate direction (x, y, z), "I" refers to the node number, and "n" is the time step number.

The analyses examples of the building structures and piping systems are presented in this section. The following section describes the nonlinear finite elements used to model building and piping components.

3.1 Finite elements for modeling reinforced concrete

The walls of the building structures are composed of several structural components: concrete, reinforcing bars and embedded steel-frame columns. Several types of elements are needed to properly model this complex wall structure. The wall of the building was modelled using an enhanced version of the four-node quadrilateral plate element developed by Belytschko, et al. (1984) for metallic structures. The formulation of this element is based upon the Mindlin theory of plates and uses a velocity strain formulation. The element was further developed by Kulak and Fiala (1989) and Kulak et al. (1997) by incorporating the features to represent concrete and reinforcing steel (Fig. 1). Subsequently, additional failure criteria were added, and this enabled the modified element to model concrete cracking, reinforcing bar failure and gross transverse failure.

The concrete failure model used is the Hsieh-Ting-Chen four-parameter model. The model uses the following four-parameter criterion involving the stress invariants I_1 , J_2 and the maximum principal stress σ_1 (Kulak, 1997):

$$f(I_1, J_2, \sigma_1) = a \frac{J_2}{f_c^2} + b \frac{\sqrt{J_2}}{f_c} + c \frac{\sigma_1}{f_c} + d \frac{I_1}{f_c} - 1 = 0 \quad (5)$$

The four failure parameters (a , b , c , d) are determined so that they represent the following four failure states:

1. Uniaxial tensile strength, $f_t = 0.1 f_c$
2. Uniaxial compressive strength, f_c

3. Equal biaxial compressive strength, $f_{bc}=1.15 f_c$;
4. Combined triaxial compression, $f_{pc}=0.8 f_c, f_{cc}=4.2 f_c$.

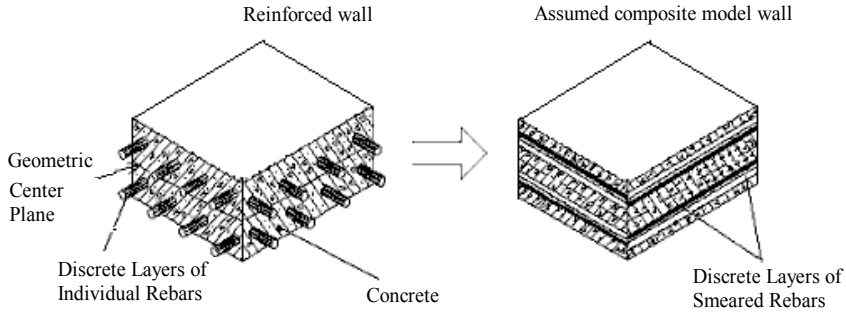


Fig. 1. Section through wall/slab and equivalent finite element model with distinct layers of smeared reinforcing bars

With Eq. (5) the strength capacity of the concrete in a multiaxial stress space can be characterized by the Hsieh-Ting-Chen four-parameter model failure surface (Kulak, 1997). A von Mises type loading function is used to determine elastic-plastic response. If the von Mises function is used alone, the same behaviour is implied in both tensile and compressive region, which is not true for concrete. Therefore, the von Mises function is used with Hsieh-Ting-Chen failure criterion that would produce different tensile and compressive responses. The failure surface of concrete in 2D space is schematically presented in Fig. 2.

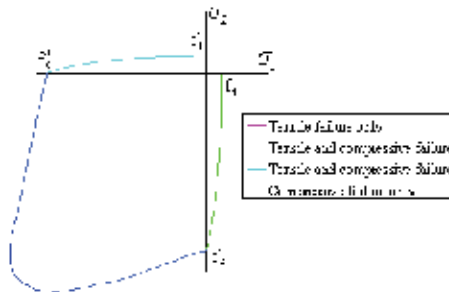


Fig. 2. Schematic representation of the failure surface

The transverse shear failure of a reinforced concrete slab is considered by an empirical formula (Kulak, 1997):

$$\tau_u = (0.05(pf_y - \sigma_y) + 0.5)\sqrt{f_c}; \dots \text{where} \dots 0.5\sqrt{f_c} \leq \tau_u \leq 4.5\sqrt{f_c} \tag{6}$$

Terms of equation (6) are the following: σ_y is the normal stress, f_y is the yield strength of reinforcement, p is the reinforcement ratio, f_c is the compressive strength of concrete.

A typical uniaxial compression - tension behaviour of concrete is shown in Fig. 3. It is known that the cracked concrete of a reinforced concrete element can still carry some tensile

and compressive stress in the direction normal to the crack. The stress reduces to zero in tension for a strain e_t and stress reduces to zero in compression for a strain e_c .

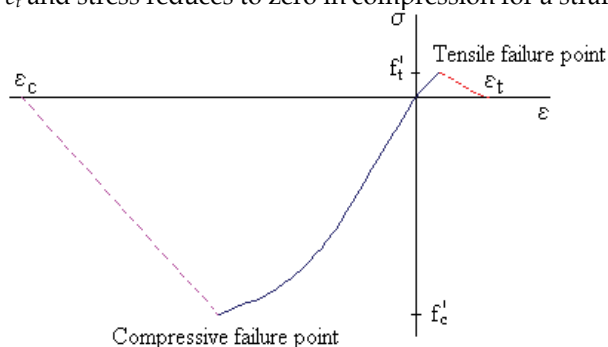


Fig. 3. Compression – tension behavior of concrete

The strain e_t at which the stress reduces to zero in tension and the strain e_c at which the stress reduces to zero in compression are used in this analysis. The value e_t is 0.000768 (4 times the tensile failure strain) and the value e_c is 0.0141 (3 times the compressive failure strain).

NEPTUNE calculates stresses at the centre of the concrete plate element at five integration points through the thickness and in each rebar layer. In the concrete plate element, layers of individual reinforcing bars within the concrete walls are represented by smeared uniformly distributed layers of steel. The thickness of these layers is determined by assuming that the cross-sectional areas of the reinforcing bars are spread uniformly along the respective pitch of the layers. The direction of reinforcement is specified in the concrete plate element. Transverse wall reinforcement and liner are neglected in the analytical model.

The steel-frame columns embedded in the ALS walls were modelled using a three-dimensional beam element (Belytschko et al., 1977). This beam element transmits moments, torque and axial forces and is a general six (6) degree of freedom element (i.e., three global translation and rotational components at each end of the beam). This element has a uniform cross-section and is capable of undergoing large deformations and can model elasto-plastic material response. The cross-section change of shape is not accounted for in any analysis.

3.2 Finite elements for modelling pipes

Pipelines were modelled using three-dimensional pipe elements. For the global solution of a pipe whip event, the use of a pipe element capable of undergoing large displacements in three-dimensional space was required. The pipe element in the NEPTUNE code was an enhanced version of a beam/pipe element developed by Belytschko and Schwer (Belytschko, 1977). The material model used can handle elasto-plastic behaviour. Validation of the use of the NEPTUNE code for pipe whip and impact problems was reported by Kulak and Narvydas (Kulak, 2001).

3.3 Finite elements for modelling contacts

For the two impact scenarios, the node-to-line contact element (Kulak, 1985 and Kulak, 1989) was employed. The node-to-line contact element, which is a three-node element, was

deployed in the following way. One node is attached to an appropriate finite element on the mesh representing the ruptured pipe or other structural component and the two other nodes are attached to an appropriate finite element on the mesh for the neighbouring structural component (pipe or wall) in which the contact occurs. This contact element is used for problems with simple geometry and when the contact-impact location is approximately known *a priori*. Since the connectivity is known *a priori*, no contact search algorithm needs to be used. Because of the simplicity of this approach, it is computationally very fast.

4. Coupling of Probabilistic and Deterministic Software

Because of the complexity needed to treat the physics that occurs during failure of NPP structures and consequence phenomena, analysts must rely on using sophisticated computer codes to model the accidents and their effects. The majority of these codes are deterministic codes in the sense that all the physical parameters used to define geometry, material properties, loadings, etc. as well as the computational parameters used in the analyses have fixed values. These values usually are chosen by the analysts/engineer as best estimate values. Thus, the results from these analyses do not take into account the range of variation of these parameters or the effect that different combinations of the parameters uncertainty have on the conclusions drawn from the analyses. With this approach, the probabilistic aspect of the parameters is neglected.

On the other hand, in this work the probabilistic nature of the important parameters are taken into account to provide a more realistic assessment of safety issues. With this approach, a probabilistic analysis engine is coupled to a deterministic finite element engine to provide for integrated deterministic and probabilistic analysis of failure probabilities. Thus, two stand alone software packages are combined to provide probabilistic analysis capability for critical NPP structures.

In general, deterministic software (DS) is used for the deterministic analysis of system failure, accidents and/or consequences. In order to perform a probabilistic simulation, many deterministic analyses are performed using different values of the random variables defined by the probabilistic software (PS). The PS collects the results from the DS and performs a statistical analysis. Once all the deterministic computations are performed and transferred to the PS, the probabilistic software can determine probability estimate of system failure and/or consequences.

The initial part of the work is to develop the coupling translator, which consists of pre-processor and postprocessor used for data flow between deterministic and probabilistic software. The translator can be developed, using almost any advanced programming language (e.g. C++, Visual Basic or Perl). The language used should be suited to extract information from one text file and generate another as the main work is usually related to the input file preparation and output file data extraction. If the PS and/or DS are interactive software tools, the analyst works from a graphical user interface (GUI) and the translator also should be adapted to it.

There are five main steps to perform integrated probabilistic analysis:

1. Import a deterministic model (finite element model);
2. Define the random variables (initial set can be screened using sensitivity analysis);
3. Describe the failure criterion (based on deterministic criteria);

4. Run deterministic analysis to obtain the response for each set of random variables;
5. Analyse and review the results (probabilistic estimates).

The integration process starts when the DS input file, which represents the deterministic model, is processed (imported) by the translator. A pre-processor is used to provide the PS with information as to which parameters are to be used in the current deterministic model as random variables. This is necessary especially if the user can browse and select properties via the GUI provided by PS.

Most of the time when the translator is running, it is modifying the values of the random variables in the DS input file according to the values determined by the PS, and retrieving the values of the response variables from the DS output file for the probabilistic analysis by PS. At the end of computations, PS prepares an analysis report giving the results of the probabilistic analysis. Fig. 4 graphically shows the interactions among the user, PS, DS and the translator, which consist of pre-processor and post-processor.

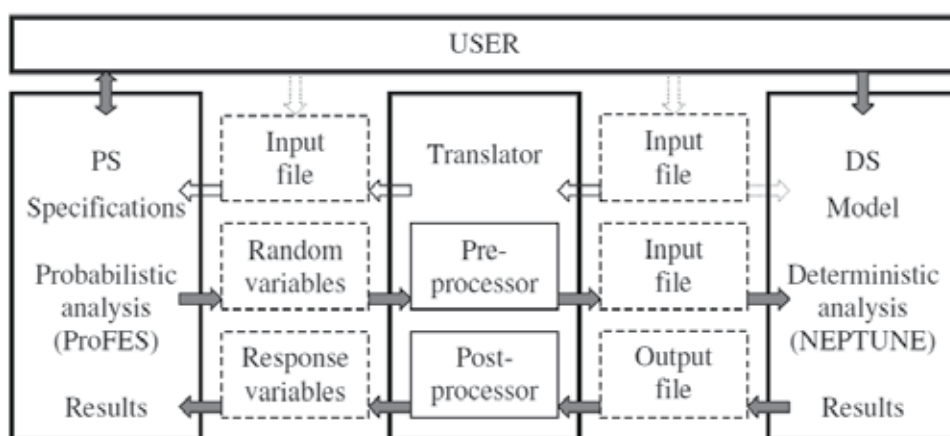


Fig. 4. The integration of models and different probabilistic methods

The first step in using PS with an integration of DS is to start PS. Then, the analyst imports the DS model into PS using the import interface. Next, the probabilistic model must be setup. This is done by selecting random variables, specifying distributions, setting correlations, designating dependent variables, defining limit states, etc. This part depends on the type of probabilistic analysis. In general, random variables and specific distributions with their parameters are specified. The list of considered variables depends on quantities from DS, which are available in input files and are proposed to be treated as changeable or random variables. The distribution functions and distribution parameters for each random variable are specified. Then, prior to each model call (i.e., DS calculation) corresponding values from the DS input file are modified by translator according to the values selected by PS. The list of response variable is also identified in initial stage. The response variables correspond to the requested output quantities (e.g. displacements, stresses, strain, etc.) according to which the failure parameters (e.g. failure rate, probability of failure) are calculated in the final stage.

Practically, probabilistic methods provide a means to assess the effects of uncertainties associated with material properties, component geometry data and loads in predicting structure reliability and performance. In order to perform a probabilistic analysis of an

building or component failure due to transient loading, the NEPTUNE and ProFES software were coupled. The probabilistic software ProFES was developed by the Computational Mechanics Group of ARA's Southeast Division, located in Raleigh NC (Cesare, 1999). ProFES allows quick development of probabilistic models from model executables, analytical formulations, or finite element models. It is possible to use ProFES independently to perform probabilistic simulations using functions internal to ProFES or functions that can be manually typed in. ProFES can be used as an add-on to the modelled executables, so it is possible to perform probabilistic studies using the deterministic models.

Here the NEPTUNE (Kulak and Fiala, 1998) software was used to perform deterministic transient analysis of an building and component during the dynamic loading on the values for the random variables selected by ProFES. By default, NEPTUNE input/output cannot be imported directly into ProFES. Thus, for this purpose, a special ProFES/NEPTUNE coupling code, *pnglue*, was developed at Argonne National Laboratory (Kulak, 2003). The code was programmed in Perl because it is well suited to extracting information from one text file and generating another. Since it is an interactive software tool, the analyst works from a graphical user interface. Initially a NEPTUNE input file is processed (imported) by *pnglue* to provide ProFES with information as to which values are available in the current model. This is necessary so that the user can browse and select properties via the graphical user interface provided by ProFES. Most of the time when *pnglue* is running, it is modifying the identified random variables in the NEPTUNE input file according to the values determined by ProFES and to retrieve the response variables from the NEPTUNE output file for probabilistic analysis by ProFES. At the end of computations, ProFES prepares an analysis report giving the results of the probabilistic analysis.

5. Structural Integrity Analysis Using Probabilistic Methods Applications to Ignalina NPP

The above methodology of the probability-based structural integrity analysis that integrates deterministic and probabilistic methods was applied to safety analysis of the Ignalina NPP. The application of this methodology to two postulated accidents, i.e. the pipe whip impact and aircraft impact, is presented in this chapter.

The preparation of models for analysis, evaluation of the material properties and loads are very important for structural integrity analysis of nuclear power plant building and components. The material parameter is uncertain. In order to ensure structural integrity analysis results of the buildings and component are reliable it is very important to evaluate uncertainty associated with loads, material properties, geometrical parameters, boundaries and other parameters. Therefore, it is necessary to account for the uncertainty in these quantities when performing a probabilistic structural integrity evaluation.

5.1 Probabilistic Analysis of Pipe Whip Impact

5.1.1 Model for the Analysis of Damage to the Adjacent Wall

The subject of this investigation is the collision between the group distribution header (GDH) and the adjacent wall that would result from a guillotine break at the blind end of a group distribution header. Structural integrity of the group distribution header support-wall is also important. Therefore, the group distribution header, the impacted wall and the

support wall (items 3, 1, 2, respectively, in Fig. 5 (a)) are included in the model of a whipping group distribution header analysis.

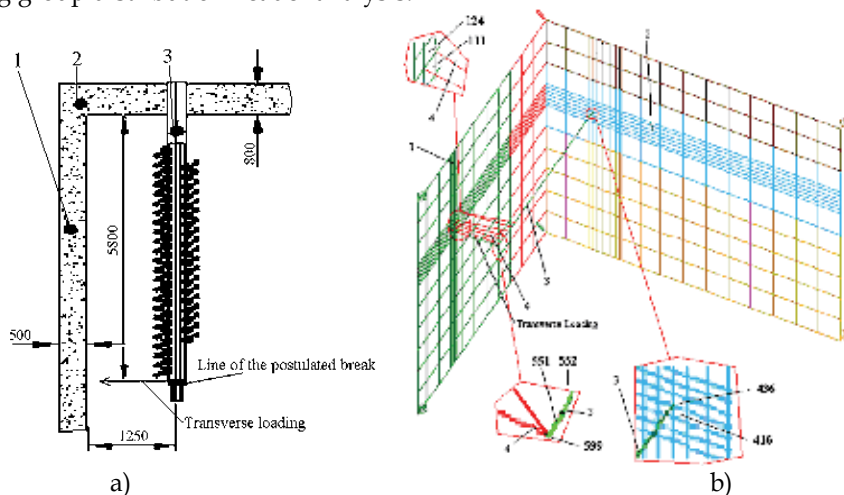


Fig. 5. Top view of the group distribution header's in the compartment (a) and combined schematic models of the GDH pipes and concrete walls (b) for investigation of impact to reinforced concrete wall: 1 - adjacent impacted-wall, 2 - GDH's support-wall, 3- broken GDH, 4 - contact element between GDH pipe and wall, 111 - number of rebar element adjacent to nodes of GDH and wall contact, 124 - number of concrete element adjacent to nodes of GDH and wall contact, 416 - number of rebar element adjacent to node of the whipping GDH pipe fixity, 436 - number of concrete element adjacent to node of the whipping GDH pipe fixity, 599 number of end node of the whipping GDH, 551, 552 - number of the whipping GDH pipe elements.

GDH is a horizontal cylinder (pipe) with outside diameter of 0.325 m, wall thickness of 0.015 m, and is about 6 m long. The distance from the centreline of the outboard group distribution header to the inside surface of the adjacent wall is 1.25 m (Fig. 5). The thickness of the impacted wall is 0.5 m and has the following reinforcement: 28 mm diameter reinforcement bars with a pitch of 200 mm and 16 mm diameter reinforcement bars with a pitch of 200 mm. The thickness of the supporting wall is 0.8 m with the following reinforcement: 28 mm diameter reinforcement bars with a pitch of 200 mm and 16 mm diameter reinforcement bars with a pitch of 200 mm.

The compartment walls were modelled using the four-node quadrilateral plate element (see section 3.1). The group distribution header's were modelled using three-dimensional pipe elements (see section 3.2). The FE model prepared for the investigation of a whipping GDH impact onto reinforced concrete wall is presented in Fig. 5 (b). After a guillotine break, the GDH can impact the nearest wall of the compartment.

Regarding material properties, the model analysed has two basic parts: the group distribution header that is made from 08X18H10T steel and the compartment walls that are made from M300 reinforced heavy concrete. More detailed descriptions of the geometry of the group distribution header, adjacent piping and surrounding walls and material properties are presented in (Dundulis et al., 2007a).

The transient analysis of a guillotine pipe break was reported in (Dundulis et al., 2007a). It was conservatively assumed that the transverse load applied to the end of the group distribution header was equal to the axial load. This load was also applied here in the probabilistic analysis. This essentially is an upper bound load. The load was not treated as a random variable in the analyses based on Monte Carlo Simulation and First Order Reliability method. However, the load of the guillotine break is uncertain. The Response Surface /Monte Carlo Simulation method was used to express failure probability as function of the loading and to investigate the dependence between impact load and failure probability.

5.1.2 Probabilistic Analysis Results

The aim of the uncertainty analysis is to identify and quantify all important uncertainty parameters. Ranges and subjective probability distribution describe the state of knowledge about all uncertain parameters. In probabilistic analysis, uncertainties in numerical values are modelled as random variables. The following mechanical properties and geometrical parameters important to strength of structures were simulated as random variables:

- Uncertain mechanical properties:
 - Concrete - Poisson ratio, Young's modulus, uniaxial tensile strength of pipe support-wall (walls No. 1 and 2 in Fig. 5);
 - Rebar - Yield stress (wall No. 1 and 2 in Fig. 5);
 - Pipe - Poisson ratio, Young modulus, Yield stress (pipes No. 3, Fig. 5);
 - Contact modulus (contact element between group distribution header and impacted-wall).
- Uncertain geometry data:
 - Reinforced concrete - Rebar area (wall No. 1 and 2 in Fig. 5);
 - Pipe - thickness and mid-surface radius of the pipe (pipe No. 3 in Fig. 5).

Values for the coefficient of variation were adopted from the following two paper: Hsin, 2001 and Braverman, 2001. In this analysis, the logarithmic normal distribution was used for mechanical properties and geometry parameters. The selected random variables, distributions and coefficients of variation are presented in Table 1 and Table 2.

Material	Distribution	Parameter	Mean	Coeff. of Variation	Comment
Reinforced Concrete					
Concrete (1, 2 walls - Fig. 1)	Log. Normal	Poisson's ratio	0.2	0.1	
	Log. Normal	Young's modulus	2.7e+10	0.1	Unit: Pa
	Log. Normal	Tensile strength	1.5 e+6	0.1	Unit: Pa
Reinforcement bars (1, 2 walls)	Log. Normal	Yield stress	3.916e+8	0.03	Unit: Pa
Group Distribution Header Pipe					
Austenitic Steel	Log. Normal	Young's modulus	1.8e+11	0.03	Unit: Pa
	Log. Normal	Poisson's ratio	0.3	0.03	
	Log. Normal	Yield stress	1.77e+08	0.03	Unit: Pa
Contact of Pipe	Normal	Contact modulus	1.8e+11	0.1	Unit: Pa

Table 1. The material properties and parameters expressed as random variables

Material	Distribution	Parameter	Mean	Coeff. of Variation	Comment
Reinforced Concrete					
Reinforcement bars	Log. Normal	Reinforcement layer thickness (data for 1 rebar as example).	0.00491	0.05	Unit: m
Group Distribution Header Pipe					
Austenitic Steel	Log. Normal	Wall thickness	0.015	0.05	Unit: m
	Log. Normal	Mid-surf. radius of pipe	0.155	0.05	Unit: m

Table 2. The geometry parameters of random variable

The aim of the transient analysis was to evaluate:

- Structural integrity of adjacent wall after impact;
- Structural integrity of the group distribution header support-wall.

The following limit states were assumed for the case of the group distribution header impact on the adjacent wall:

1. Limit State 1 - Contact between the broken group distribution header and the adjacent wall occurs.
2. Limit States 2, 3, 4, 5 and 6 - The concrete element adjacent to node of the group distribution header and wall contact reaches the ultimate strength in tension and the crack in concrete starts to open. NEPTUNE calculates stresses of the concrete element at five integration points. Therefore, the same limit states at all five integration points through wall thickness were checked.
3. Limit States 7, 8, 9, 10 and 11 - The concrete adjacent to the group distribution header fixity in the support-wall reaches the ultimate strength in compression and loses resistance to further loading. The same limit states at all five integration points through wall thickness were checked.
4. Limit State 12, 13, 14, 15 - The strength limit of the first layer of rebars in the concrete wall at the location of impact is reached and the rebars can fail. The same limit states at all four layers were checked in analysis using Monte Carlo Simulation method. In case of First Order Reliability method, the computational effort is proportional to the number of random variables and limit states. The probabilities of the failure of all rebars layers were received very small and similar in Monte Carlo Simulation analysis. Because of this, the Limit State 12 (the strength limit of the first layer of rebars) was used in analysis using First Order Reliability method.
5. Limit State 16, 17, 18, 19 - The strength limit of the first layer of rebars in the concrete support wall at the location of the group distribution header fixity is reached and the rebars can fail. The same limit states at all four layers were checked in analysis using Monte Carlo Simulation method. In case of First Order Reliability Method, the computational effort is proportional to the number of random variables and limit states. The probabilities of the failure of all rebars layers were received very small and similar in Monte Carlo Simulation analysis. According this the Limit State 16 (the strength limit of the first layer of rebars) was used in analysis using First Order Reliability method.

It is important to calculate the probability of concrete failure in the same run at all five integration points. Therefore, the following two system events were used in the probability analysis:

- System event 1 – Limit state 2, limit state 3, limit state 4, limit state 5 and limit state 6. This system event is evaluated as true if all the limit states are true. This system event evaluates the probability of crack opening in concrete at all integration points of the impacted wall, i.e., a complete crack through the wall.
- System event 2 – Limit state 7, limit state 8, limit state 9, limit state 10 and limit state 11. This system event is evaluated as true if all the limit states are true. This system event evaluates the probability of concrete failure (in compression) at all integration points at the location of the group distribution header fixity in support wall.

5.1.2.1 Probabilistic Analysis Results Using Monte Carlo Simulation Method

The Monte Carlo Simulation method was used to study the sensitivity of the response variables and the effect of uncertainties of material properties and geometry parameters to the probability of limit states. Twenty-nine random variables were screened; however, only the significant ones are discussed here. The screening of insignificant random variables from the large number of input random variables was performed using 95% confidence limits for sensitivity measures (acceptance limits for correspondent random variables). In order to have the possibility to compare different values, the sensitivity measures and 95% confidence limits were normalized.

The absolute value of a sensitivity measure is proportional to the correspondent random variable significance. The input random variable is considered insignificant when the correspondent sensitivity measure is close to zero. The sensitivity measures are likely to be within the acceptance limits if the random variable is insignificant. The response sensitivity measure ($dY/d\mu$) is expressed as the derivative of the mean of the response variable with respect to the mean of the input random variable. The response sensitivity measures with acceptance limits are presented in Fig. 6. The “Input Random Variables” numbers are presented along the x - axis.

The following input random variables are the most significant random variables for the impacted wall at the location of concrete element number 124 (Fig. 5 (b)):

- Poisson’s ratio of the impacted-wall concrete (1 – Fig. 5) – input random variable 1;
- Young’s modulus of the impacted-wall concrete (1 – Fig. 5) – input random variable 2;
- Tensile Strength of the impacted-wall concrete (1 – Fig. 5) – input random variable 3;
- Yield Stress of the impacted-wall rebars (1 – Fig. 5) – input random variable 8;
- Young’s modulus of the whipping group distribution header (3 – Fig. 5) – input random variable 25;
- Wall thickness of the whipping group distribution header (3 – Fig. 5) – input random variable 28;
- Mid-surface radius of the whipping group distribution header (3 – Fig. 5) – input random variable 29.

These input random variables have the greatest positive (1, 2, 3, 25) or negative (8, 28, 29) influence on all integration variables points of concrete element 124.

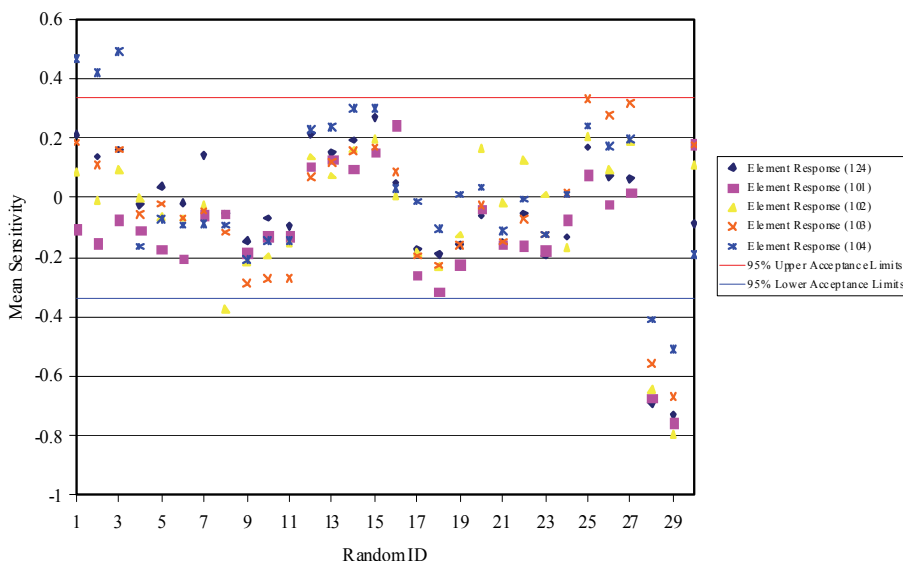


Fig. 6. Significant Random Variables for Element Response (124, 101, 102, 103, 104) Stress Equivalent.

According to the results of the sensitivity analysis related to response variables, materials properties, geometry data and limit states, the following additional items have the greatest influence on the probability of failure for the support-wall:

- Poisson’s ratio of the support-wall concrete (2 - Fig. 5) - input random variable 9;
- Young’s modulus of the support-wall concrete (2 - Fig. 5) - input random variable 10;
- Tensile Strength of the support-wall concrete (2 - Fig. 5) - input random variable 11.

All the previously listed random variables were used in the First Order Reliability method analysis as input random variables.

5.1.2.2 Probabilistic Analysis Results Using First Order Reliability Method

The FORM was used to study the probability of failure of the impacted-wall and the support-wall. The FORM is a preferred method for evaluating a small number of random variables and limit states (failure of concrete, reinforcement bars and group distribution header). The reason for this is that for the same precision as MCS, it often requires the least number of finite element model runs. With FORM, the computational effort is proportional to the number of random variables and limit states. Therefore the MCS sensitivity analysis was used to choose mechanical properties and geometrical parameters important to strength of structures for random variables in FORM. These random variables were presented in above subsection. The same limit states were used in the FORM analysis as the limit states used in MCS analysis. The number of simulations was 1419. The logarithmic normal

distribution of material properties and geometry data also was used for this analysis. The results of probabilistic analysis for limit states are presented in the Table 3 and Table 4.

Limit State	Definition	Probability	Beta
1	Nod. Response (599) Displ. Dir. 2 (Y) > 1.0875	0.981858	2.09373
2 - 6	El. Response (124) Stress Equivalent > 1.5e+6	~0.500~0.502	0.001~0.005
7 - 11	El. Response (436) Stress Equivalent < -1.7e+7	0.391 ~0.499	-0.002~-0.28
12 -13	El. Response (111) Stress Equivalent > 5.9e+8	0.326 ~ 0.11	-0.448~-1.22

Table 3. Results related to each Limit State

Name	Probability	Beta
Limit State 2 & Limit State 3 & Limit State 4 & Limit State 5 & Limit State 6	0.013	-2.22695
Limit State 7 & Limit State 8 & Limit State 9 & Limit State 10 & Limit State 11	0.0126	-2.23846

Table 4. Data of the System Event

The calculated probability of 'Limit State 1' is 0.982. This limit state probability indicates that contact between the whipping group distribution header and the adjacent wall will occur with probability of 0.982.

For the adjacent impacted-wall (element 124), the calculated probability of 'Limit States 2, 3, 4, 5 and 6' is from 0.500 to 0.502 (Table 3, 2-6). This indicates that the ultimate tensile strength of concrete will be reached at the five integration points and cracking in these layers may occur. The probability for a through crack in the concrete wall was calculated using System Event 1, which determines, for the same computer run, if cracking occurs in all the layers of the concrete element. The calculated probability of 'System Event 1' is 0.013 (Table 4). Thus, the probability for a through crack to develop is 0.013.

For the support-wall (concrete element number 436, which is the concrete element adjacent to the node at which the GDH is attached to the concrete wall), the calculated probability for 'Limit states 7, 8, 9, 10 and 11' is from 0.391 to 0.499 (Table 3, 7-11). These limit states indicate that the ultimate compressive strength of concrete will be reached at the five integration points and failure may occur. The system event was used for the analysis of probability of failure during the same computer run at all integration points of the concrete element. The calculated probability of 'System Event 2' is 0.0126 (Table 4). Thus, the ultimate compressive strength of concrete will be reached with a probability 0.0126, and the support-wall may fail at the location where the group distribution header is attached with a probability 0.0126.

For the impacted wall (element 111), the probability for 'Limit State 12' to be reached was 0.327. This limit state indicates that the ultimate stress of the rebars in the first rebar layer will be reached and the bars may fail. For the support-wall (element 416), the probability for 'Limit State 13' to be reached was 0.11. This limit state indicates that the ultimate stress of the rebars in first rebar layer will be reached with a probability 0.11 and this layer may fail.

5.1.2.3 Probabilistic Analysis Results Using Response Surface/Monte Carlo Simulation Method

The load of the guillotine break is uncertain, and it is widely accepted that to determine the loading from a guillotine break experiment is very difficult. Therefore, it is important to estimate the probability of failure of the impacted neighbouring wall due to the magnitude of the transverse load applied to the group distribution header. The RS/MCS method was used to express failure probability as a function of the loading and to investigate the dependence between impact load and failure probability.

In the first part of the RS/MCS analysis, the RS method was used to obtain dependence functions between the response variables and the input random variables. The number of RS simulations performed was 100. In the second part of the RS/MCS analysis, the MCS method was used to determine the probability of failure based upon these dependence functions. The number of MCS performed was 1,000,000.

The deterministic transient analysis of the whipping group distribution header was performed using the loading presented in paper Dundulis et al., 2007a. This load was also applied in the probabilistic analysis with the MCS and FORM. In fact this load is an upper bound load, and, in the MCS and FORM studies, it was not applied as a random variable but was considered to be deterministic. For the RS part of the RS/MCS analysis, a different loading was used than the one used in the First Order Reliability method analysis. The RS/MCS method in ProFES could not handle all the random variables related to the critical loading points (Dundulis et al., 2007a). So the mean value for the loading was defined to be a constant value of 338 kN in the range from 0.00 s up to 0.012 s and zero thereafter. The load value 338 kN is a half of the maximum load value (677 kN). The uniform distribution was used for loadings in RS part of the RS/MCS analysis. The distribution range of loading was from 0 N to the maximum loading of 677 kN.

In the RS/MCS analysis the same mechanical properties and geometrical parameters identified above as being important for the strength of structures were selected as random variables. The logarithmic normal distribution of material properties and geometry parameters were used for this analysis. The same limit states were also used in the RS/MCS analysis as those limit states used in the MCS and the FORM analysis.

Using the RS method, the dependence functions between response variables and input random variables were calculated. In the second part of the RS/MCS analysis, which is the MCS method, these functions were used to determine the failure probability.

The probability to reach the ultimate strength for compression of concrete in the support-wall as a function of the applied loads is presented here. As an example, the following equation was obtained from the RS analysis for the determination of the failure probability in relation to Limit State 7 (Table 3) - "Element Response (436 is the element number (first integration point)) Stress Equivalent > -1.7e+7":

$$y = -1.04735e+007 + -7.15074*L1 + -1.48883*L1 + 2.04335e+006*P1 + 0.00034832*Y1 + 9.06781e+007*u1 + -0.0222667*r1 + 1.85264e+006*P4 + 0.000158399*Y4 + - 7.98442e+006*u4 + -2.10484e-007*Y7 + 1.02299e+009*t7 - 1.53013e+007*m7 \quad (7)$$

where the response variable y is used in limit state: $y > -1.7e+7$; L1 - LoadUnit 1-1 and LoadUnit 1-3; P1 - Poisson's ratio of wall 1 (Fig. 5), Y1 - Young's modulus of wall 1, u1 - Uniaxial tensile strength of wall 1, r1 - Yield stress of reinforcement bar in wall 1, P4 -

Poisson's ratio of wall 4, $Y4$ - Young's modulus of wall 4, $u4$ - Uniaxial tensile strength of wall 1, $Y7$ - Young's modulus of pipe 7, $t7$ - thickness of pipe 7, $m7$ - mid-surface radius of pipe 7.

L1 - LoadUnit 1-1 and Load 1-3 are loading points at different times, i.e. LoadUnit 1-1 at 0 second, LoadUnit 1-3 - at the time when the whipping group distribution header moves outside of the diameter of the group distribution header end cap (0.012 second). The random variables included in this equation are explained in the section 5.1.2.1.

The dependence function, Eq. (7), which was obtained using the RS method, was applied as an internal response functions in the MCS analysis. The number of MCS simulations was 1,000,000. In Eq. (7) the loads L1 and L3 were assumed equal. They were changed step-by-step while the probability of the limit state has been changing from 0 to 1. The normal distribution with Coefficient of Variation equal 0.1 (10%) for loading and the logarithmic normal distribution of material properties and geometry parameters was used in this analysis. In Eq. (7), the nominal values of material properties and geometry parameters were the same as used in other analysis.

The analysis results are presented in Fig. 7. According to these result the relation between the probability of the 'Limit State 7' and the applied loads was determined. The compressive strength limit of concrete element 436 is first reached at a loading approximately equal to 550 kN, and the concrete failure probability reaches 1 at a load of approximately 950 kN. Note, the probability of failure at a load of 677 kN is about 0.4, which is good agreement with the results from the First Order Reliability method analysis.

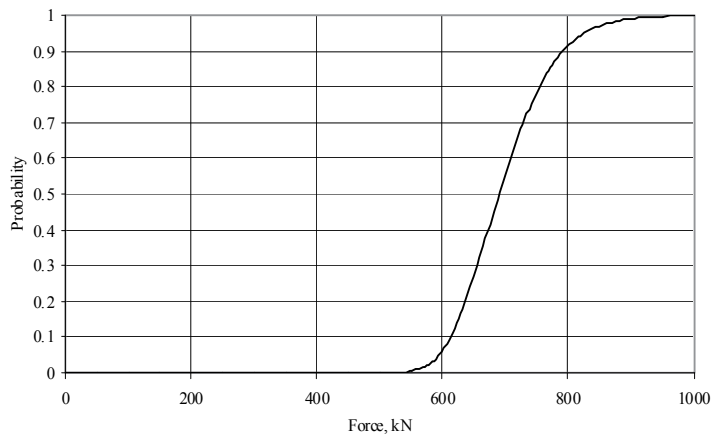


Fig. 7. The failure probabilities of concrete element adjacent to node of the group distribution header pipe fixity (node 436) to compression at dynamic loading due to guillotine rupture

5.2 Probabilistic Analysis of an Aircraft Crash

5.2.1 Model for the Analysis of Failure of the Building

The subject of this investigation is the integrated analysis of building failure due to impact by a commercial aircraft. The model of the Igalina NPP reactor building that was used for the deterministic analysis of aircraft impact was reported by Dundulis et al., 2007b. One run

of that Ignalina building model using the NEPTUNE code takes approximately one hour. This duration is extremely long for performing the large number of runs needed for a probabilistic analysis. Therefore, a modification of the original FE model used in the deterministic analysis of the Ignalina NPP building is used for the probabilistic analysis (Dundulis et al., 2007c). The impacted wall and the adjacent walls and ceilings are included in the modified FE model of the Ignalina NPP building. The modified finite element model is presented in Fig. 8. One crash/impact location was considered. Arrows depict the assumed impact area of the aircraft. The impact direction is assumed to be perpendicular to the selected wall of the building.

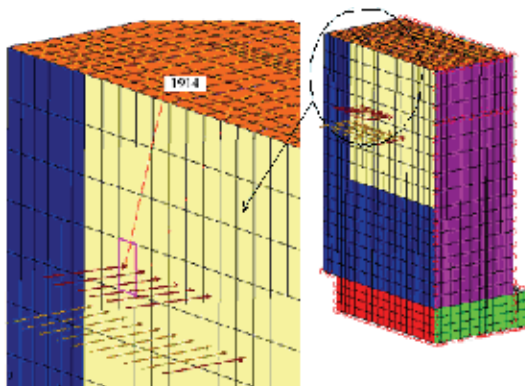


Fig. 8. Finite element model of the Ignalina NPP building for aircraft crash analysis

The wall of the building was modelled using the four-node quadrilateral plate element (see section 3.1). Some composite metal frames, made from different steel components, are imbedded in the walls. These structures were modelled using separate beam finite elements (see section 3.1) and were added to the walls and slabs at appropriate locations along the edges of quadrilateral elements.

5.2.2 Probabilistic Analysis Results

In probabilistic analysis of failure of the building due aircraft crash as in case of pipe whip impact analysis, uncertainties in numerical values are modelled as random variables. The following mechanical properties and geometrical parameters, which determine the strength of the structures, were used as random variables:

- Mechanical properties: Concrete – Young’s modulus, stress points of the compressive stress-strain curve of the impacted and support walls; Reinforcement bar – stress points of the stress-strain curve of the impacted wall and support walls.
- Geometry data: Concrete wall – thickness of the impacted wall and support walls; Reinforced concrete – rebar area of the impacted wall and support walls.

The selected random variables, distributions and coefficients of variation of the mechanical properties of concrete and reinforcement bars, and geometry data are used same methodology as for pipe whip impact (section 5.1, Table 1 and Table 2).

The points defining the load curve are considered to be random variables. These points represent the beginning/end points at which different components of the aircraft structure (e.g., fuselage, wings, engine, etc.) begin to contact or end contact on the building wall.

Thus, in a sense, this approach takes into account the variations in loading from the individual structural components. The normal distribution for the load points is used. The load data is presented in paper Dundulis et al., 2007c.

The objective of the transient analyses is to evaluate the effects of an aircraft crash on an Ignalina NPP building structure. The structural integrity analysis was performed for a portion of the Accident Localization System (ALS) using the dynamic loading of an aircraft crash impact model caused by civil aircraft travelling at a velocity of 94.5 m/s. The aim of the transient analysis was to evaluate:

- Structural integrity of the impacted wall of the building;
- Structural integrity of the building walls adjacent to the impacted wall.

Based on the objective of the transient analyses, the following limit states were selected:

- Limit States 1-5 - The concrete in element number 1914 (Fig. 8) in the impact area reaches the ultimate strength in tension and a crack starts to open. This impacted wall is the outside wall of the ALS and a through-the-thickness crack should not develop. Additional description see in section 5.1.2 "Limit states 2, 3 ..".
- Limit States 6-10 - The concrete element of the support wall of the building reaches the ultimate strength in compression and a compressive failure occurs. This neighbouring wall is an inside compartment wall of the ALS and the cracks in this wall may open. Therefore, the strength of wall was evaluated for compression. The same limit states at all five integration points through the thickness were checked.
- Limit State 11- 13 - The splice failure strain limit of 4% for the rebars in element number 1914 (Fig. 8) would be reached and the rebars would fail. All three layers (i.e., L1 through L3) of rebars were checked. Note, Layer L3 is on the impact side of the wall.
- Limit State 14- 17 - The splice failure strain limit of the first layer of rebars in the interior concrete wall is reached and the splice would break. The same limit states at all four layers of the reinforcement bars were checked.

It is important to calculate the probability of concrete failure at all five integration points in the same computer run. Also it is important to calculate probability of reinforcement bar failure in all layers in same run. Therefore, the following four system events were used in the probability analyses:

- System Event 1 - Limit state 1 - 5. This system event is evaluated as true if all the limit states are true within the same run. Additional description see in section 5.1.2 "System Event 1 ..".
- System Event 2 - Limit state 6 - 10. This system event is evaluated as true if all the limit states are true within the same run. Additional description see in section 5.1.2 "System Event 2 ..".
- System Event 3 - Limit state 11 - 13. This system event is evaluated as true if all the limit states are true within the same run. This system event evaluated the probability of rebar failure at all layers of the impacted wall.
- System Event 4 - Limit state 14 - 17. This system event is evaluated as true if all the limit states are true within the same run. This system event evaluated the probability of rebar failure at all layers of the neighbouring support wall.

5.2.2.1 Probabilistic Analysis Results Using Monte Carlo Simulation Method

Using the MCS probabilistic analysis method, the probabilities of limit states and the probability of failure for system events were calculated for both the impacted wall and the adjacent interior wall, which provides support to the impacted wall. The number of MC simulations was 3000. It should be pointed out that because of the small number of MC simulations performed, the probabilistic analysis using the MCS method was performed as a scoping study.

For the impacted wall, the calculated probability of 'Limit states 1 -3' is from 0.645 to 0.964. These probabilities indicate that the tensile failure surface of the concrete element within the impact area will be reached at three of the five integration points and a crack could develop in these three layers. The calculated probability of 'Limit states 4 -5' is very small, i.e., at the fourth integration point it is 0.007, and at the fifth integration point it is 0. These values indicate that the probability of a crack opening in the fourth and fifth layers of this concrete element is very small.

The probability of a crack opening at all five integration points in a concrete element within the impact area during the same run was calculated. The system event was used to analyze this probability of failure. The calculated probability of 'System event 1' is 0. This indicates that, within the same run, the tensile failure surface of the concrete at all the integration points of this element is not reached, and the probability of crack opening in the concrete element of impacted wall is very small.

The calculated probabilities for 'Limit states 11 - 13' and of 'System event 3' are also 0. This indicates that the splice failure strain of the rebars within the impact area will not be reached in any of the rebars, and the probability of rebar splice failure is very small. For layers 1, 2 and 3 of the impacted wall, the probabilities for concrete failure are near 1. In contrast, for concrete layers 4 and 5 and the rebars of the impacted wall, the probabilities are near 0.

Based on these results, only very small probabilities of failure exist in several layers of concrete and in all layers of rebars. Therefore in the next section, the FORM method was used for additional evaluation of failure probabilities of the impacted wall.

For the interior support wall, the calculated probabilities of 'Limit states 6 -10' and of 'System event 2' are 0. Thus, the compressive failure surface of the concrete of the support wall will be reached with a probability of 0 for all the integration points of this element, and the probability of compressive failure is very small. The calculated probability for 'Limit states 14 - 17' and of 'System event 3' are also 0. This indicates that the splice failure strain for the rebars in the support wall will not be reached for any of the rebar layers, and the probability of a rebar splice failure is very small.

For the interior wall, the probabilities of failure are 0 for all concrete layers and rebar layers. Since this wall is an inside wall of the building and is not very important for leak tightness of the ALS, no additional evaluation of the probability of failure of this wall was carried out.

5.2.2.2 Probabilistic Analysis Results Using First Order Reliability Method

FORM was used to study the probability of failure of the impacted wall of the Ignalina NPP building due to the effects of an aircraft crash onto the building..

The same mechanical properties and geometrical parameters used in the MCS analysis of the impacted wall were used as random variables in the FORM analysis. The 'Limit states 1-5' and 'Limit states 11-13,' (see section 5.2.2) were used here in this analysis. It is important to calculate the probability of concrete failure at all five integration points of the element

within the same run. Similarly, it is important to calculate the probability of reinforcement bar failure in all three layers within the same run. Therefore, the two system events were used in the probability analysis, i.e. the 'System event 1' and 'System event 3' (see section 5.2.2). The number of simulations performed was 1419. The probabilities of limit states and system events were calculated. The results of the probabilistic analysis are presented in Tables 5 and 6.

Limit State	Definition	Probability	Beta
1-5	CF ¹ at IP1-IP5: StE ² > 3.79e+06	0.498~0.51	-5.78e-3~4.12e-3
11	RBF ³ in L1: SE ⁴ > 0.04	0.2296	-7.4e-1
12-13	RBF in L2/L3: SE > 0.04	0.003/5.3236e-171	~-2.7616

Table 5. Failure probabilities for Limit States in Element 1914 (¹CF-Concrete Failure, ²StE-Stress Equivalent, ³RBF-Reinforcement bar failure, ⁴SE-Strain Equivalent)

Name	Probability	Beta
Through-the-thickness CF ¹ (i.e., Failure in LS 1 through 5)	0.0266	-1.93307
Failure of all RBL ² (i.e., failure in LS 11 through 13)	0	-4.01317

Table 6. Failure probabilities for System Events in Element 1914 (¹CF-Concrete Failure, ²RBL-Reinforcement Bar Layers)

The calculated probabilities for 'Limit states (LS, Table 5) 1 - 5' are from 0.498 to 0.510. This indicates that the tensile failure surface of the concrete in the impact area could be reached at each of the five integration points (IP1 through IP5) but not during the same computer run. Thus, a crack in each layers of this concrete element could open. The probability of a crack occurring at all five integration points in the concrete element during the same run was calculated (i.e., System Event 1, Table 6), and the value was 0.0266. This indicates that the probably of the ultimate strength for tension being exceeded through the thickness of the concrete element in the impact area is 0.0266. Recall that the MCS indicates that the probability for System Event 1 was 0.

The probability for 'Limit State 11,' which checks for failure of the first rebar layer (L1) in the concrete wall at the location of impact, was found to be 0.2296. The calculated probabilities for 'Limit States 12 and 13' are very small; the probabilities for the third and fourth rebar layers were 0.003 and ~0, respectively. These limit state values indicate that the probability for splice failure of the rebars in the third and fourth rebar layers is very small. The probability of exceeding the splice failure strain in all rebar layers of the impacted wall (i.e., System Event 2) was 0. Thus, the aircraft should not penetrate the reinforcement in the impacted wall.

5.2.2.3 Probabilistic Analysis Results Using Response Surface / Monte Carlo Simulation Method

During an aircraft crash, the dynamic impact loading is uncertain. Therefore, it is important to estimate the dependence of the failure probability of the building due to the uncertainty in loading. The RS/MCS method was used for the determination of such a relation

expressed by the probability-loading function. In this section only concrete failure (limit state 1) is presented.

First using the modified finite element model of the building, a limited number of MC simulations were performed to determine the response surfaces, i.e., the probability functions for failure of the walls of the Ignalina NPP building. Then the MCS method was used on the response surfaces to study the probability of failure of the building walls as indicated by concrete cracking and reinforcement bar rupture (Dundulis et al., 2007c). In this analysis the probability function was used as an internal function in ProfES to determine the failure probability, which greatly reduces computational effort.

The same mechanical properties and geometrical parameters used in the MCS and FORM analyses were also used as random variables in the RS/MCS method. Also, the same limit states used in the FORM analysis were used in the RS/MCS analyses.

As a basis, the loading function for a civil aircraft traveling at 94.5m/s (Dundulis et al., 2007b) was used. The nonlinear function consists of a series of straight line segments with the peak load of 58MN occurring at 0.185s. Because of limitations on the number of random variables imposed by ProfES, it was necessary to use a surrogate loading function that was a linear function starting at 0 MN at the instant of impact and reaching a peak value of 58MN at 0.185s. It is noted that this surrogate function provides a larger impulse than the original function. For this part of the analysis, which is to do a preliminary study of the effect that the loading has on the probabilistic analysis, the peak load was varied, arbitrarily, from 0MN to 700MN, and the time at which the peak load occurred was kept constant at 0.185s. The probability distribution function for the loading was chosen to be uniform distribution.

Using the modified FE model, two hundred (200) MC simulations were performed to determine the probability functions for Limit States 1 (see section 5.2.2). The distribution for the loading was assumed to be uniform. The range of loading was from 0.02 MPa to 2.2 MPa, and this loading range encompassed the probability of failure range from 0 to 1. The maximum point of loading used in the deterministic transient analysis of civil aircraft travelling at a velocity of 94.5 m/s crash is 1.557 MPa (correspond to 58 MN). Using the Response Surface Method, the dependence functions for the response variables based on the input random variables were calculated.

The probabilistic function for Limit State 1, which is the development of a crack on the initial tension side of the wall, is given by:

$$Y1=2.726e+6-2.816*L-2.743e+6*T+0.043*c1+0.012*c2+0.005*c3+2.991e+008*R1+1.320e+9*R3-1.775e+9*R4-0.004*s1-0.007*s2-0.004*s3+0.008*s4 \quad (8)$$

where Y1 - Limit State 1, i.e. $Y1 > 3.79e+6$; (the value $3.79e+6$ is the concrete experimental ultimate strength in tension); L - maximum force loading (pressure) point in impacted wall; T - wall thickness of the impacted wall; c1, c2 and c3 - stress points 1, 2 and 3 for concrete respectively; R1, R3 and R4 - thickness of reinforcement bars in the first, third and fourth layers, respectively; s1, s2, s3 and s4 - stress points 1, 2, 3 and 4 for the steel reinforcement bars, respectively.

The equations obtained using the RS method were used as internal response functions in the subsequent MCS analysis. The number of MCS simulations was 1,000,000. The probability

function (8) was used to determine the relationship between the probability of 'Limit state 1' being reached and the applied load, i.e. peak value of the impact force. The force loading was applied to the assumed aircraft impact area in the form of pressure in the transient analysis of Ignalina NPP building. The pressure value was recalculated to a force value and the probability results were presented as the relation between probability and force. The results of the probabilistic analysis are presented in Fig. 9. The probability of failure for Limit State 1 (concrete element reaches ultimate strength in tension) is zero (0) up to 10 MN, and the probability of failure is 1 at the resultant force approximately equal to 80 MN. Note, the maximum force used in the deterministic structural integrity analysis of the Ignalina NPP building for an aircraft impacting into the building at 94.5 m/s is approximately equal to 58 MN.

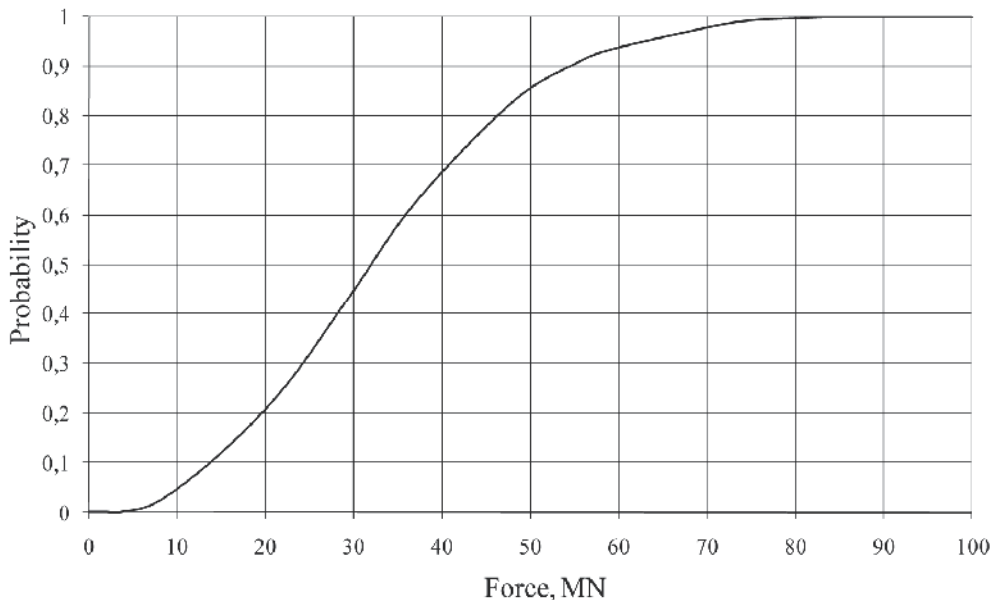


Fig. 9. Probability of a crack developing in the initial tension side of the impacted wall

6. Conclusions

The probability-based approach that integrates deterministic and probabilistic methods was developed to analyse failures of NPP buildings and components. This methodology was applied to safety analysis of the Ignalina NPP. The application of this methodology to two postulated accidents—pipe whip impact and aircraft crash—is presented in this chapter.

The NEPTUNE software system was used for the deterministic transient analysis of the pipe whip impact and aircraft crash accidents. Many deterministic analyses were performed using different values of the random variables that were specified by ProfES. All the deterministic results were transferred to the ProfES software system, which then performed probabilistic analyses of piping failure and wall damage.

A probabilistic analysis of a group distribution header guillotine break and the damage consequences resulting from the failed group distribution header impacting against a neighbouring wall was carried out.

The Monte Carlo Simulation method was used to study the sensitivity of the response variables and the effect of uncertainties of material properties and geometry parameters to the probability of limit states and also for probability of failure of building structures.

The First Order Reliability method was used to study the probability of failure of building structures. The results of the probabilistic analyses show that the MCS method— using a small number simulations—is more conservative than the FORM method when determining large values for failure probability. The MCS method, however, is not conservative for determining small values for failure probability.

The Response Surface / Monte Carlo Simulation method was used in order to express failure probability as function and to investigate the dependence between impact load and failure probability.

With the large uncertainty in values for material properties and loadings that exist in complex structures—such as nuclear power plants—it is not acceptable to only perform a deterministic analysis. Probabilistic analysis as outlined in this chapter and applied to two extreme loading events is a necessity when credible structural safety evaluations are performed.

7. References

- Almenas, K., Kaliatka, A., Uspuras, E. (1998). *Ignalina RBMK-1500. A Source Book, extended and updated version*, Ignalina Safety Analysis Group, Lithuanian Energy Institute.
- Aljawi, A. A. N. (2002). Numerical Simulation of Axial Crushing of Circular Tubes. *JKAU: Eng. Sci.*, Vol. 14, No. 2, 3-17.
- Alzbutas, R., Dundulis, G., Kulak, R. (2003). Finite element system modelling and probabilistic methods application for structural safety analysis. *Proceedings of the 3-rd safety and reliability international conference (KONBiN'03)*, p. 213-220, . ISBN 1642-9311, Gdynia, Poland, May 27-30, 2003.
- Alzbutas, R., Dundulis G. (2004). Probabilistic Simulation Considering Uncertainty of Ruptured Pipe Stroke to the Wall at the Ignalina Nuclear Power Plant. *Energetika*, No. 4, p. 63-67, ISSN 0235-7208.
- Bjerager, P. (1990). On computation methods for structural reliability analysis. *Structural Safety*, Vol. 9(2), pp. 79 -96.
- Belytschko, T., Lin, J.I. and Tsay, C.S. (1984). Explicit algorithms for nonlinear dynamics of shells. *Computer Methods in Applied Mechanics and Engineering*, Vol. 42, pp. 225-251
- Belytschko, T. Schwer, L. and Klein, M.J. (1977). Large displacement, transient analysis of space frames. *Int. J. Num. Meth. Engrg.*, Vol. 11, pp. 64-84.
- Bossak, M., Kaczowski, J. (2003). Global/local analysis of composite light aircraft crash landing. *Computers & Structures*, Vol. 81, Iss. 8-11, pp. 503-514.
- Braverman, J. I., Miller, C.A., Ellingwood, B. R., Naus D. J., Hofmayer, C. H., Bezler, P. and Chang, T. Y. (2001). Structural Performance of Degraded Reinforced Concrete Members. *Transaction 17th International Conference on Structural Mechanics in Reactor Technology*, 8 pp, Washington, USA, August 12-17, 2001, (CD-ROM version).

- Brinkmann, G. (2006). Modular HTR confinement/containment and the protection against aircraft crash. *Nuclear Engineering and Design*, Vol. 236, pp. 1612-1616.
- Cesare, M.A. and Sues, R.H. (1999). PROFES, Probabilistic Finite Element System - Bringing Probabilistic Mechanics to the Desktop. *American Institute of Aeronautics and Astronautics*, AIAA 99-1607, 1-11 p.
- Dundulis, G., Alzbutas, R., Kulak, R., Marchertas, P. (2005). Reliability analysis of pipe whip impacts. *Nuclear engineering and design*. Vol. 235, p. 1897-1908, ISSN 0029-5493.
- Dundulis, G., Uspuras, E., Kulak, R., Marchertas, A. (2007a). Evaluation of pipe whip impacts on neighboring piping and walls of the Ignalina Nuclear Power Plant, *Nuclear Engineering and Design*. Vol. 237, Iss. 8, p.848-857, ISSN 0029-5493.
- Dundulis, G., Kulak, R. F., Marchertas, A. and Uspuras, E. (2007b). Structural integrity analysis of an Ignalina nuclear power plant building subjected to an airplane crash. *Nuclear Engineering and Design*, Vol. 237, p. 1503-1512, ISSN 0029-5493.
- Dundulis, G., Kulak, R.F., Alzbutas, R., Uspuras, E. (2007c). Reliability analysis of an Ignalina NPP building impacted by an airliner. *Proc. of the 19th international conference Structural mechanics in reactor technology (SMiRT 19)*, p. 1-8, Toronto, Canada, August 12-17, 2007.
- Hsin, Y. L., Hong, H. (2001). Reliability analysis of reinforced concrete slabs under explosive loading, *Structural Safety*, vol. 23, pp. 157-178.
- Khuri, A.I. and Cornell, J.A. (1987). *Response Surfaces: Design and Analyses*, Marcel Dekker, New York.
- Kulak, R.F. and Fiala, C. (1988). Neptune a System of Finite Element Programs for Three Dimensional Nonlinear Analysis. *Nuclear Engineering and Design*, vol. 106, pp. 47-68.
- Kulak, R. F., and Fiala, C. (1989). A Method for Three-Dimensional Structural Analysis of Reinforced Concrete Containments. In: *Shin, Y. S., Wang, C. Y., Colton, J. D. and Kulak, R. F. (Eds.), Shock and Wave Propagation, Fluid Structure-Interaction and Structural Response*, Vol. 159, pp. 115-123, ASME PVP Conf., Honolulu, Hawaii.
- Kulak, R.F., Pfeiffer, P.F. and Plaskacz, E.J. (1997). Modelling of containment structures on high performance computers. *Nuclear Engineering and Design*, vol. 174, pp. 143-156.
- Kulak, R. F. and Narvydas, E. (2001). Validation of the NEPTUNE Computer Code for Pipe Whip Analysis. *Transactions 16th International Conference on Structural Mechanics in Reactor Technology(SMiRT 16)*, Washington DC, USA, 2001.
- Kulak, R.F. and Marchertas, P. (2003). Development of a Finite Element Based Probabilistic Analysis Tool. *Transaction 17th International Conference on Structural Mechanics in Reactor Technology*, pp. 8, Paper B215, Prague, Czech Republic, 2003.
- Lee, Y. S., Kim, H. S., Kang, Y. H., Chung, S. H., Choi, Y. J. (2004). Effect of irradiation on the impact and seismic response of a spent fuel storage and transport cask. *Nuclear Engineering and Design*. Vol. 232, pp. 123-129.
- Lyle K. H., Stockwell A. E.; Hardy R. C. (2007). Application of probability methods to assess airframe crash modeling uncertainty. *Journal of aircraft*, vol. 44, No 5, pp. 1568-1573
- Muragishi, O., Kawasaki, T., Yoshikawa, T., Kada, K., Fijita, T., Kohsaka, A. (2001). Damage Analysis of Super Large Floating Structure in Airplane Collision, *Transaction of the ISOPE International Journal of Offshore and Polar Engineering*, Vol. 11, No. 2, pp. 117-124.
- Nagel, G.M. and Thambiratnam, D.P. (2005). Computer simulation and energy absorption of tapered thin-walled rectangular tubes. *Thin-Walled Structures*, vol. 43, pp. 1225-1242.

- Olabi, A.G., Morris, E., Hashmi, M.S.J. and Gilchrist, M.D. (2008). Optimised design of nested oblong tube energy absorbers under lateral impact loading. *Int. J. Automotive Technology*, vol. 35, pp. 10–26.
- Padula, S., Gumbert C., and Li W. (2006). Aerospace Applications of Optimization under Uncertainty. *Optimization and Engineering*, Vol. 7, No 3, pp. 317-328
- Ramalingam, V.K., Lankarani, H. M. (2002). Analysis of impact on soft soil and its application to aircraft crashworthiness. *International Journal of Crashworthiness*, Vol. 7, Iss. 1, pp. 57 - 66.
- Yamashita, M. and Gotoh, M. (2005). Impact behavior of honeycomb structures with various cell specifications - numerical simulation and experiment. *Int. J. Impact Eng.* Vol. 32, 618–630.
- Youn, B.D., Choi, R.-J., and Gu, L. (2004). Reliability-Based Design Optimization for Crashworthiness of Vehicle Side Impact. *Structural Multidisciplinary Optimization* vol. 26, pp. 272-283.

Biofouling and its control in seawater cooled power plant cooling water system - a review

K.K. Satpathy^{1*}, A.K. Mohanty¹, Gouri Sahu¹,
S. Biswas², M.V.R. Prasad¹ and M. Sivanayagam²

¹*Environmental and Industrial Safety Section, Indira Gandhi Centre for Atomic Research, Kalpakkam, Tamil Nadu, India, 603102*

²*Loyola Institute of Frontier Energy, Loyola College, Chennai, India*

1. Introduction

Biofouling may be defined as the attachment and subsequent growth of a community of usually visible plants and animals on manmade structures exposed to seawater environment. Man has long been aware of this problem. In the fourth century B.C., Aristotle is reported to have stated that small "fish" (barnacles) were able to slow down ships. Fouling of ship hulls, navigational buoys, underwater equipment, seawater piping systems, industrial or municipal intakes, beach well structures, oil rigs and allied structures has often been reported. In the past few decades, the list of affected structures has expanded. Now, reports are common regarding the biofouling that affects Ocean Thermal Energy Conversion (OTEC) plants, offshore platforms, moored oceanographic instruments and nuclear and other submarines. The impact of biofouling on sea front structures is staggering. Ships show a 10% higher fuel consumption caused by increased drag and frictional resistance resulting from hull and propeller fouling. Water lines lose their carrying capacity and speed of flow owing to biofouling growth along pipe systems. The heat exchanger performance declines due to attachment of biofoulants. Many marine organisms themselves face the constant problem of being colonized and overgrown by fouling organisms. Immobile plants and animals are generally exposed to biofouling and consequent loss of species and community assemblages. Biofouling also promotes corrosion of materials. The money and material needed for fouling protection measures are indeed exorbitant. It is estimated that the marine industry incurs an expenditure of 10 billion sterling pounds a year to combat the situations arising from biofouling worldwide (Satpathy, 1990). A lot of research effort has been devoted to understand the fundamental ecology and biology of fouling environments, organisms and communities in diverse settings.

The huge requirement of cooling water as well as accrescent demand on the freshwater has led to the natural choice for locating power plants in the coastal sites where water is available in copious amount at relatively cheap rate. For example, a 500 MW (e) nuclear power plant uses about 30 m³sec⁻¹ of cooling water for extracting heat from the condenser

and other auxiliary heat exchanger systems for efficient operation of the plant. However, use of seawater, brings associated problems such as colonization of biota which stands in the way of smooth operation of the plant. Unfortunately, every cooling system with its concrete walls forms a suitable substrate for marine growth. Some of the conditions which favour the development of a fouling community in power plants are (a) continuous flow of seawater rich in oxygen & food, (b) reduction in silt deposition, (c) lack of competition from other communities and (d) reduction in the density of predators. Broadly speaking the effects of marine growth on the power plant are (a) losses in plant efficiency, (b) mechanical damage and (c) problem for the integrity of the cooling circuits needed for safety of nuclear plants (Nair, 1987). Hence biofouling control aims to achieve efficient operation of the power station at all times. It is therefore necessary for power plant designers to make a rational choice regarding the most suitable control method to combat biofouling problem in a practical, yet economically feasible & environmentally acceptable manner.

1.1 Economic impacts of biofouling

Economics involved in the biofouling problem of power plant as quoted by various authors are cited here to emphasize the importance of biofouling control.

A 5mm Hg condenser back pressure improvement can equal to 0.5% improvement in the turbine heat rate which approximately equal to 3 additional megawatts of generating capacity (Drake, 1977). Similar increase in condenser back pressure due to fouling in a 250 MW (e) plant can cost the utility about \$ 2.5 lakhs annually (Chow et al., 1987). One report estimates that fouling by Asiatic clam alone costs the nation over a billion \$ annually (Strauss, 1989). Costs for one day unplanned outage can run into 0.3% of their earning per year, taking 300 days operation. Hence eliminating one unplanned outage can more than pay for measures taken to maintain cooling water tube cleanliness. Waterside resistance accounts for 72% of the total resistance to heat transfer of the tube. Of this, the film which forms in a condenser tube accounts for a significant 39% and the rest 33% is due to scaling (Drake, 1977).

The experience of Marchwood (Southampton) showed that between 1957 and 1964, 4000 condenser tubes failed due to mussel fouling leading to leakage. Apart from the loss of generation, these leaks contaminated the feed water system and accelerated the boiler water side corrosion, resulting in boiler tube failures (Coughlan and Whitehouse, 1977). The inlet culverts had to be drained for manual cleaning at least once in a year. Average quantity of mussel removed was 40 tons but could be as high as 130 tons. Similar stations at Pools (Dorset) had a maximum 300 tons (Coughlan and Whitehouse, 1977). About 300 tons of mussel shells were removed each time by shock chlorination from MAPS intake tunnel on two occasions. Cost (at 1975 prices) of dropping a 500 MW (e) oil-fired station at Fawley (Southampton) was 15000 pounds per day due to fouling, excluding repairs. The cost of chlorine for this unit for the whole year of 1975 was 7500 pound. The consequence of inadequate chlorination at Inland station eventually led to the unit being taken off load for manual cleaning of condenser (Coughlan and Whitehouse, 1977). It has been observed by the CEGB investigating team on biofouling control practices that stress corrosion cracking of admiralty brass condenser tubes was attributed to ammonia produced by bacteria (Rippon, 1979).

The cleaning out of biofouling from the cooling water intake tunnels and culverts is generally very expensive; for instance 4000 man hours were used to clean the culverts and to remove 360 m³ of mussels at Dunkerque in 1971 (Whitehouse et al., 1985). Within a very short time at Carmarthen Bay Power Station, which was commissioned in July 1953, seed

mussels and various species of marine life were noticed around the main intake to the cooling water system. By April 1954 the fouling was so severe that plant was shutdown daily, increasing to 3 times per shift by mid July when operation of the station became almost impossible (James, 1967). At the Tanagwa Power Station in Japan the concrete underground conduit was covered with layers of attached organisms sometimes measuring to about 70 cm thickness. A large quantity of jelly fish (150 tons/day) was also removed from this station in one instance (Kawabe et al., 1986).

An analysis of all tube failures at Kansai Electric Power Corporation (Japan) in 1982 and 1983 showed that 94% of all tube failures were related to macrofouling lodged in the tubes (Kawabe et al., 1986). Microfouling seems to be a major obstacle to the successful development of the ocean thermal conversion concept into a useful solution to the world's energy supply (Corpe, 1984 and Darby, 1984). It has been reported that up to 3.8% loss in unit availability in large power plants could be attributed to poor condenser tube and auxiliary system reliability (Syrett and Coit, 1983). A 250 micron thick layer of slime may result in up to a 50% reduction in heat transfer by heat exchangers (Goodman, 1987).

1.2 Bio-growth in different sections of a cooling water system

A typical cooling water system of a power plant involves a pre-condenser system and the heat exchangers which includes main condenser and process water heat exchangers. The pre-condenser system involves the intake structures and the cooling water system from intake to the pump house. The intake system is either an open canal or pipeline or a tunnel. It has been observed that macrofouling generally takes place in the pre-condenser system whereas, microfouling is observed in the condenser and process water heat exchangers. This could be due to difference in the various features like flow, temperature, space etc at different parts of the cooling water system. In spite of various physical measures such as trash rack, intake screen, travelling water screen, to control biofouling, the tiny larval forms of various organisms enter the system, settle and colonize inside it and finally affect the smooth operation of the cooling water system. These organisms clog cooling water flow endangering the safety-related systems at some power plants. During the construction, when the tunnel is ready and the biocide treatment plant is yet to be operational, the intake structure gets severely fouled by macrofoulers. Despite efforts to provide an effective design of heat exchanger and careful attention to the maintenance of the design operating conditions, it is likely that fouling on the water side of the heat exchangers will occur unless suitable precautions are taken. The common practice of taking water from natural sources such as rivers and lakes for cooling purposes means that it contains micro- and macro-organisms, which will colonize the heat transfer surfaces, to the detriment of cooling efficiency. The problem will be aggravated by the fact that the temperature of the waterside surface in the heat exchanger is usually close to the optimum temperature for maximum microbial growth. In addition, water from natural sources contains nutrients from the breakdown of naturally occurring organic material. Unless this bioactivity is controlled the efficiency of the heat exchanger will be seriously reduced.

1.3 Biofouling and safety consequences of nuclear power plants

Many nuclear power plants have experienced fouling in their cooling water systems (Satpathy, 1996). These fouling incidents have caused flow degradation and blockage in a

variety of heat exchangers and coolers served directly by raw water. In addition, loose shells from dead organisms are carried by the flow until they are trapped or impinged in small piping, heat exchangers, or valves. Often the results of fouling that have accumulated behind inlet valves and in heat exchanger water boxes degrade or compromise the safety function of safety-related components. Events of this nature have occurred at several nuclear plants, which prompted the Nuclear Regulatory Commission of USA to issue warning requiring plants to determine the extent of biofouling and to outline their strategy for controlling it (Henager et al., 1985). A few typical incidents reported in the literature are outlined here. Brunswick power plant I and II reported blockages of their Residual Heat Removal (RHR) heat exchangers in 1981 (Imbro and Gianelli, 1982) by American oyster (*Crassostrea virginica*) shells. This produced high differential pressures across the divider plate and caused the plate to buckle. The result was a total loss of the RHR system. The plant was forced to provide alternate cooling. American oysters had accumulated in the inlet piping to the RHR heat exchangers, because the chlorination had been suspended for an extended period. RHR heat exchangers at Unit II were also fouled and severely plugged. The Salem II (S.M. Stoller Corp. 1983) and the Arkansas Nuclear I power plant have reported flow blockages to containment fan cooling units (plugging a backpressure control valve, which restricted flow in the containment fan cooling units) and fouling of containment cooling units respectively (Nuclear Regulatory Commission, 1984, Haried, 1982). Blue mussel shells deposits in the water jacket cooler of a diesel generator at Salem I & Millstone II plant caused the generator to overheat and subsequently trip off (S. M. Stoller Corp. 1977). An industrial processing plant experienced severe Asiatic clam (*Corbicula fluminea*) fouling in its fire protection lines because of frequent flow testing at reduced flow rates. When full flow testing was initiated after several years of operation, the sudden flow surge caused severe blockage in the main and branch piping (Neitzel et al., 1984). Fouling in fire protection systems by Asiatic clam has also been reported at Browns Ferry (Tennessee Valley Authority, 1981) and McGuire power plant (Duke Power Co., 1981). The main condenser at Browns Ferry 1 was severely fouled with Asiatic clams only a few months after the plant began operation in 1974 and the problem increased subsequently (Rains et al., 1984). At Pilgrim I power plant, blue mussels blocked cooling water flow and caused an increase in differential pressure across the divider plates, forcing the plates out of position leading to loss of Reactor Building Closed Cooling Water (RBCCW) heat exchanger capacity (Imbro, 1982). At Trojan power plant, Asiatic clams plugged one of the heat exchangers that cool the lubricating oil to the main turbine bearings (Portland General Electric Co., 1981). Temporary stoppage of normal preventive maintenance during an extended plant shutdown at San Onofre I power plant allowed barnacles (*Pollicipes plymerus*) to incapacitate a component cooling water heat exchanger (Henager et al., 1985). In the same plant a butterfly valve malfunctioned on the seawater discharge side of the cooling water heat exchanger because massive growth of barnacles had reduced the effective diameter of the pipe and impeded valve movement (Henager et al., 1985). In September 1984, St. Lucie power plant reported plugging of its intake screens by Jellyfish (Henager et al., 1985). In August 1983, Calvert Cliffs I power plant tripped manually to avoid an automatic turbine/reactor trip due to low condenser vacuum, which was the result of shutting down two of six circulating cooling water pumps because their inlet screens had become plugged with fish (Nuclear Regulatory Commission, 1984).

1.3.1 Events that could exacerbate fouling

Some of the non-fouling events could cause a normal biofouling situation to become serious. Generally they are three types; 1) environmental events that affect fouling populations within the plant and in the vicinity of the plant, 2) plant operating events or procedures that may dislodge or kill fouling organisms, and 3) biofouling surveillance and control procedures that may exacerbate fouling.

a. Environmental Events

The following environmental events could occur at nuclear power plants site and affect safe plant operation. Dynamic shocks due to seismic activity, explosions (intentional and accidental), or similar events could loosen fouling organism from their substrate and these can subsequently clog heat exchangers downstream. Heavy rain storms and flooding could wash bivalves from their substrate and carry them into the intake pumps. It can also create a thermal shock which could kill fouling organisms and fish leading to blockage of cooling water systems. Heavy rains also have the potential of creating an osmotic shock due to a rapid decrease in the salinity of the cooling water source resulting in massive killing of fouling organisms. Toxic chemical spills (pesticides, herbicides, industrial chemicals, oil, etc.) due to tanker spills and leakage of pipe line upstream of the plant could kill fouling organisms in the cooling water source and within the plant.

b. In-plants

Some transients and operating procedures that occur during the operation of nuclear power plants can affect biofouling. Although, most of these procedures are necessary, however, several improvements could be made to eliminate or reduce biofouling events associated with these procedures. The following in-plant events have occurred at nuclear power plants leading to dislodge or movement of fouling organism. Sudden changes in flow velocity (increases in velocity) have washed accumulations of bivalves into heat exchangers. Changes in flow direction may also cause bivalves to move into areas with higher velocity from where they can be swept downstream. Sudden gush of cooling water (Water hammer) has been implicated as a cause of heat exchanger clogging at Arkansas Nuclear I plant (due to dislodging of Asiatic clams) and at the Brunswick plant (American oysters) allowing them to be swept into their Residual Heat Removal heat exchangers (Harried, 1982). Thermal shock from either a rapid cooling or heating of the raw water can kill bivalves. At pilgrim power plant, the inadvertent routing of heated water into the service-water intake structure from a condenser backwashing operation caused a massive kill of blue mussels in the intake structure and in the service-water headers (Satpathy et al., 2003). The plant was forced to reduce power to 30% while blue mussels continued to break loose and plug the Reactor Building Closed Cooling Water (RBCCW) heat exchangers. This continued for approximately 3 months. Allowing bivalve shells to accumulate in the intake structure and in areas of the raw-water system encourages clogging and lead to reduced suction head and vortexing problems in the circulating water and service-water. It was reported that accumulations of Asiatic clam shells and silt up to 90 cm (3 ft) deep are not uncommon in the intake structure (Satpathy et al., 2003). Blue mussels have also been described as forming 1.2-m-thick (4-ft-thick) mats on the walls of intake structures (Henager et al., 1985). Starting up of inactive systems has led to clogging when precautions were not taken to prevent bivalves from entering and growing in those systems. The initial flow surge through the system can carry loose bivalves and shells into constricted areas downstream. Chronic fouling has been reported in raw-water cooling loops that are used infrequently (Henager et al., 1985).

Chemical such as diesel oil, lubricating oil, and other toxic chemicals used at nuclear plants could spill in the intake structure and kill fouling organisms. Pump cavitation from plugged suction lines to the pumps would result in increased wear and decreased performance of service-water booster pumps and the main pumps in the fire protection system. The vibration of lines associated with cavitating pumps may also dislodge bivalves and cause fouling downstream. Flushing fouling organisms into drains and sumps could cause plugging and subsequent flooding of equipment rooms. This could damage electrical equipment such as pump motors, electronic instrumentation, and motor-controller valves. Leaking valves have allowed the continuous flow of water to carry food and oxygen to bivalves. Several utilities indicate this as a major cause of fouling in plants (Henager et al., 1985). The same effect may occur in lines where valves are inadvertently left in the semi-opened position. Near stagnant conditions in water systems provide ideal conditions for bivalve growth. This is especially true for Asiatic clams. Most plants typically operate with nearly 80% of the cooling loops in this condition (Neitzel et al., 1984) in order to maintain redundant cooling loops in standby condition. Damaged or missing intake screens and strainers have allowed adult organisms to be sucked into the cooling water system. Also, severe plugging from weeds, grass, and ice have caused the automatic strainer wash systems to malfunction at Salem 1 plant (S.M.Stoller Corp. 1978) and at Indian Point 3 plant (S.M. Stoller Corp. 1983).

c. Surveillance and control procedures

Biofouling control techniques can be divided into two major categories, detection / surveillance and control / prevention programs. Surveillance refers to detecting the biofouling and the subsequent flow degradation. The goal of control techniques, however, is to limit biofouling to a safe and acceptable level. Surveillance and control procedures could cause organisms to flourish or to become dislodged (Daling and Johnson, 1985). Thermal backwashing, although an effective method of killing bivalves, can result in enhanced clogging of heat exchangers when measures are not taken to remove the bivalves that are killed. It is also important to account for the time lag between the thermal treatment and the detachment of the bivalves. This is especially true for blue mussel and American oyster fouling. Thermal backwashing should be scheduled to prevent bivalves from growing large enough to block condenser tubes. Similarly, when shock chlorination is used to kill the established community and subsequently care is not taken to remove them, they accumulate and clog downstream (Fig. 1).



Fig. 1. Removed fouling organisms from the tunnel of a seawater cooled nuclear power plant (Madras Atomic Power Station) by shock chlorination

Increased flow rates during testing can wash bivalves into heat exchangers. This is especially true of Asiatic clam fouling because adults lose the ability to attach to substrates and will be flushed into downstream heat exchangers at increased flow rates. The initial flow testing or flushing of a stagnant, infested line has led to an unexpectedly large number of bivalves which occurred at Browns Ferry 1 power plant, when the condenser circulating water system was started up after construction was completed. An intermittent chlorination system that malfunctioned and released a massive dose of chlorine to the intake killed large numbers of bivalves. These bivalves later detached and clogged heat exchangers. The intermittent chlorine application would not control bivalves in the system, but a large chlorine spill may be concentrated enough and last long enough to kill bivalves.

The following enhanced growth events have occurred at nuclear power plants due to procedures or strategies. Infrequent or inadequate chlorination caused by faulty or wrongly calibrated chlorinating metering systems or by intentional, intermittent applications of chlorine have allowed bivalves to survive in raw-water systems. Personnel from several plants remarked that bivalve fouling became worse when the chlorination system was out of service for an extended period. Intermittent chlorination to control slime and other microfouling has been ineffective in controlling bivalves because, they are able to close their shells tightly during periods of chlorination. Failure to chlorinate normally stagnant cooling loops, which already have a high potential for fouling, can substantially increase the fouling potential of the system. Frequent flow testing, particularly if done at low flow velocity, may improve the growth potential of the system by providing a more frequent supply of food and oxygen to bivalves. This effect is intensified if flow testing is not concomitant with chlorination. The intermittent, "non-design" use of the fire protection system to water lawns and wash equipment has also provided enhanced conditions for Asiatic clam growth.

1.4 Biofouling at Madras Atomic Power Station

The best approach to understand biofouling problem in a seawater cooled power plant is by taking a typical example which has been studied well. The Madras Atomic Power Station (MAPS) located at Kalpakkam (12° 33" N; 80° 11" E) consists of two units of Pressurized Heavy Water Reactor (PHWR), each of 235 MW (e) capacity. Seawater is used at the rate of 35 m³sec⁻¹ as the coolant for the condenser and process cooling water systems. A sub-seabed tunnel located 53 m below the bottom terrain draws seawater (**Fig. 2**). The tunnel is 468 m long and 3.8 m in diameter. It is connected at the landward end to the pump house through a vertical shaft of 53 m deep and 6 m diameter called forebay. Similarly, the seaward end of the tunnel is connected to a vertical shaft of 48 m and 4.25 m diameter called intake. Seawater enters the intake through 16 windows located radially at the intake structure, 1 m below the lowest low water spring tide. The tunnel, intake and forebay shafts support a heavy growth of benthic organisms such as mussels, barnacles, oysters, ascidians etc. The high density of these fouling organisms inside the tunnel/cooling systems could be attributed to continuous supply of oxygen & food and removal of excretory products by the passing seawater providing a conducive environment for their settlement and growth. In addition, absence of any potential predator inside the cooling system supports a luxuriant growth of these communities. The physical shape of the tunnel is such that it is an isolated system open at both ends; seawater samples can be collected at intake as the control location, whereas, samples collected at forebay after flowing past the fouling communities can be investigated for change in its physicochemical properties.

Biofouling in the cooling system of seawater-cooled power plants is a universal problem (Brankevich et al., 1988; Chadwick et al., 1950; Collins, 1964; Holems, 1967; James, 1967; Relini, 1980; Satpathy, 1990). It is of considerable interest as it imposes penalty on power production, impairs the integrity of cooling system components and in some cases even precipitates safety problems associated with cooling system of nuclear power plants (Henager et al., 1985; Rains et al., 1984), which has been already discussed. Different aspects of biofouling in the cooling conduits of coastal power plant from tropical as well as temperate regions have been studied by several researchers (Brankevich et al., 1988; Chadwick et al., 1950; Collins, 1964; Holems, 1967; James, 1967; Relini, 1984; Satpathy, 1990; Sashikumar, 1991). The problem of biofouling in a tropical seawater cooled power plant can be understood by explaining a typical case study. Studies carried out in this regard from Indian coast have not been exhaustive however, from Kalpakkam coast, south east coast of India, it has been immense due to its importance to the existing MAPS. Biofouling has been a serious problem in the cooling water system of MAPS. It had affected adversely the cooling system and performance of the plant (Sashikumar, 1991; Rajagopal, et al., 1991; Satpathy et al., 1994). Investigation on the fouling problems of MAPS cooling system indicated extensive settlement of macro-fouling organisms inside the tunnel, which was calculated to be around 580 tonnes (Nair, 1985) that caused severe pressure drops in the cooling circuits.

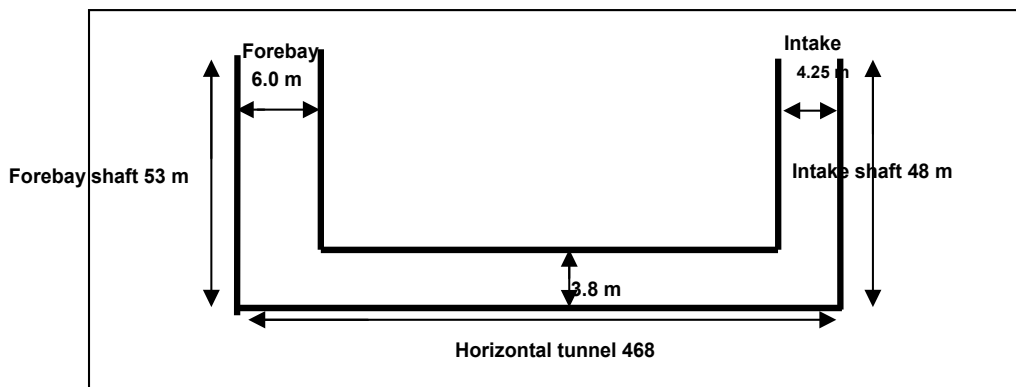


Fig. 2. Schematic diagram of the cooling water structure of MAPS

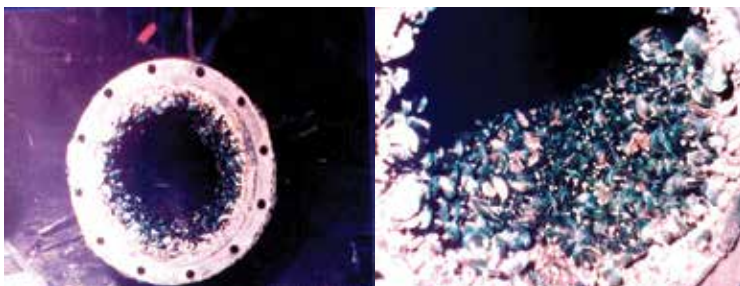


Fig. 3. A view of bio-growth inside seawater pipe lines from MAPS

The intake submarine tunnel was observed to have a maximum of 25 cm thick layer of fouling organism with an average of 18 cm (Satpathy et al., 1994). A typical blockage of a

cooling water pipe is shown in **Fig. 3**. In addition stupendous growth of fouling organisms on the intake screen (**Fig. 4a**) of MAPS impedes its smooth operation (Satpathy, 1996). The condenser tubes of MAPS were severely affected by the clogging of dead green mussel (**Fig. 4b**) (Satpathy, 1996). Similarly, jelly fish ingress and clogging of intake and traveling water screen forcing the plant authorities to shut down the reactor (Masilamani et al., 2000), has been another problem. Albeit, it is a seasonal issue, it also plays havoc with the operation of the cooling water system and ultimately power plant operation.

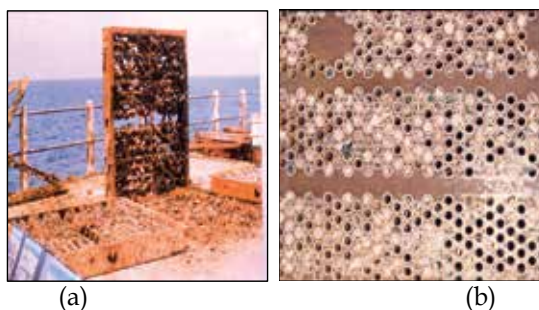


Fig. 4. Blockage of intake screen by fouling organisms (a) and blockage of condenser tubes by green mussels & barnacles (b)

2. Description of the locality

Kalpakkam coast (12° 33' N Lat. and 80° 11' E Long.) is situated about 80 km south of Chennai (**Fig. 5**). At present a nuclear power plant (MAPS) and a desalination plant are located near the coast. MAPS uses seawater at a rate of 35 m³sec⁻¹ for condenser cooling purpose. The seawater is drawn through an intake structure located inside the sea at about 500 m away from the shore. After extracting heat, the heated seawater is released into the sea. Two backwaters namely the Edaiyur and the Sadras backwater system are important features of this coast. These backwaters are connected to the Buckingham canal, which runs parallel to the coast. Based on the pattern of rainfall and associated changes in hydrographic characteristics at Kalpakkam coast, the whole year has been divided into three seasons viz: 1) Summer (February-June), 2) South West (SW) monsoon (July-September) and 3) North East (NE) monsoon (October-January) (Nair and Ganapathy, 1983). Seasonal monsoon reversal of wind is a unique feature of Indian Ocean that results in consequent change in the circulation pattern (La Fond, 1957; Wyrтки, 1973), which is felt at this location too. The wind reversal occurs during the transition period between the SW monsoon and NE monsoon. In general, the SW to NE monsoon transition occurs during September/ October and the NE to SW transition occurs during February/ March. The pole-ward current during SW monsoon changes to equator-ward during the SW to NE monsoon transition, whereas, a reverse current pattern is observed during the transition period between NE to SW monsoon (Varkey et al., 1996; Vinaychandran et al., 1999; Haugen et al., 2003). Subsequent to the change in the current pattern, the alterations of coastal water quality have been reported (Somayajulu et al., 1987; Ramaraju et al., 1992; Babu, 1992; Saravanane, 2000). The phenomenon of upwelling has also been reported to occur during the pre-NE monsoon period in the southeast coast of India in low temperature and high saline water mass (De Souza et al., 1981; La Fond, 1957; Ramaraju et al., 1992, Suryanarayan and Rao, 1992). During

the period of NE monsoon and seldom during SW monsoon monsoon, the two backwaters get opened to the coast discharging considerable amount of freshwater to the coastal milieu for a period of 2 to 3 months. This part of the peninsular India receives bulk of its rainfall (~70%) from NE monsoon. The average rainfall at Kalpakkam is about 1200 mm. However, with the stoppage of monsoon, a sand bar is formed between the backwaters and sea due to the littoral drift, which is a prominent phenomenon in the east coast of India, resulting in a situation wherein the inflow of low saline water from the backwaters to sea is stopped. This location had been badly affected by 2004 mega Tsunami, which devastated the entire east coast of India and had maximum impact at this part of the coast.



Fig. 5. A map of the study area, Kalpakkam coast, Bay of Bengal

The mean tidal range varied from 0.3 - 1.5 m. The coastal currents at Kalpakkam has seasonal character and during SW monsoon the current is northerly (February to October) with a magnitude of 0.2 - 1.8 km/h and during NE monsoon the current is southerly (October to February) with a magnitude of 0.1 - 1.3 km/h. The wind speed varied from 10-40 km/h. These monsoonal winds cause a) southerly (~ 0.5 million m³/y) & northerly (~ 1 million m³/y) littoral drift (Satpathy et al., 1999). The seawater temperature has two maxima (Apr/May & Aug/Sept) and two minima (Dec/Jan & June/July) (Satpathy and Nair, 1990; Satpathy et al., 1999; Satpathy et al., 1997).

3. Hydrobiological features of coastal waters

3.1. Methodology

Seawater samples were collected weekly near the MAPS cooling water intake for estimation of water quality parameters such as pH, salinity, dissolved oxygen (DO), turbidity,

chlorophyll-*a* and nutrients such as, nitrite, nitrate, ammonia, total nitrogen, silicate, phosphate and total phosphorous. Water temperature was measured at the site using a mercury thermometer of ± 0.1 °C accuracy. Salinity was measured using Knudsen's method (Grasshoff et al., 1983). Estimation of DO was carried out following the Winkler's method (Parsons et al., 1982). pH was measured using a pH probe (Cyberscan PCD 5500) with accuracy of ± 0.01 . Turbidity was measured using Turbidity meter (Cyberscan IR TB100) with accuracy of ± 0.01 NTU. Chlorophyll-*a* and nutrients were analyzed following the standard methods of Parsons et al. (1982) using a double beam UV visible spectrophotometer (Chemito).

3.2 Results

Hydrographical parameters at this coast bear pronounced seasonal variations (Satpathy et al., 2008, 2010). Temperature varies from 26.0 (August) to 31.8 °C (May) indicating that the annual gradient remained ~ 5.8 °C. Seawater temperature is characterized by two maxima, one during April/ May and another during September/ October coinciding with the trend in atmospheric temperature. pH values ranged between 8.00 and 8.30 with maximum value during NE monsoon period. Salinity ranged from 24.91 (November) – 35.90 psu (May), which showed a unimodal oscillation. Dissolved oxygen (DO) values fluctuated between 4.2 and 6.1 mg l⁻¹. Values of turbidity varied between 9.21 and 21.42 NTU. Chlorophyll-*a* concentration varies between 1.42 and 7.51 mg m⁻³ during the month of November and August respectively.

The maximum value of pH observed, coincides with NE monsoon period during which not only the precipitation, but also the discharges from the nearby backwaters affect the magnitude of pH as well as salinity significantly. As expected, the lowest salinity value coincides with the local maximum precipitation period (NE monsoon period) and also with the maximum influx of fresh water from the two nearby backwaters. The highest salinity value coincides with the peak summer. DO shows an irregular pattern of distribution except for the fact that during NE monsoon period, relatively high values are observed as expected due to input of oxygen rich freshwater. Turbidity exhibits a bimodal oscillation with one peak during July (pre-monsoon) and another during December (NE monsoon). This is attributed to the relatively high phytoplankton density observed during pre-monsoon and heavy silt-laden freshwater influx during NE monsoon seasons. A significant positive correlation ($p \geq 0.01$) between turbidity and chlorophyll has been observed and is testimony to the above observation during pre-monsoon period (Satpathy et al., 2010). Chlorophyll-*a* values are found to be the lowest during November/ December (NE monsoon) and highest during August/ September (Southwest-Northeast monsoon transition). Relatively high concentration of chlorophyll-*a* coincides with summer and pre-monsoon period, when relatively stable as well as optimal conditions of salinity, temperature, light, nutrient levels (conducive for production of copious amount of phytoplankton) prevails. Depletion of chlorophyll concentration during monsoon period is mainly associated with low saline, low temperature, low irradiance and high turbidity condition.

Nutrient concentrations in general show well pronounced seasonal variation mostly influenced by monsoonal rain. The two back waters, which are part of the ecosystem at this location, receive various wastes (domestic, agricultural etc.) from the nearby township and villages and thereby get enriched with nutrients. These backwaters get open to the coastal water during the NE monsoon period resulting in influx of the nutrient rich fresh water into the coastal milieu, which

enhances the nutrient levels in the coastal water. Relatively low values are observed during pre-monsoon and post-monsoon period (April-August) which is attributed to their utilization by phytoplankton, as evident from the matching chlorophyll values during the same period. Increased levels of phosphate is also observed during September which has been associated with the phenomenon of upwelling, an event that generally occurs during pre-monsoon (August – September) period along the Indian east coast (La Fond, 1957; De Souza et al., 1981; Ramaraju et al., 1992; Suryanarayan and Rao, 1992).

4. Biofouling potential of Kalpakkam coastal waters

A close perusal of literature on biofouling studies point that they have been triggered mainly based on two sound logics, such as scientific interest or technological need associated with maritime activities. The methodology such as, size of panel, duration of exposure, panel material, location of exposure etc used for biofouling studies largely remain similar by many workers. Researchers with academic interest look for ecological succession, species diversity, breeding pattern, seasonal variations, larval availability, climax community, that is more towards qualitative assessment and linking them with environmental factors. However, investigations with technological need look for quantitative assessment such as, biomass, % of area coverage, density and occurrence interval. Notwithstanding the interest driven by either, the three important parameters for practical use undoubtedly are a) type of foulants, b) their growth rate and c) their seasonal variations, which decides the use of an economic and environment-friendly fouling control strategy. Biofouling problem is not only site specific, but also have been reported to be different for two different power plants drawing same source of cooling water (Karande et al., 1986), which has been attributed to different design and different material of use. An evaluation of composition and abundance of the fouling communities available in coastal waters provides an array of information particularly for the effective antifouling measures to be adopted in the cooling water systems.

In order to devise an effective biofouling control measure for Prototype Fast Breeder Reactor (under construction) cooling water system, it is essential to evaluate the present biofouling potential at Kalpakkam coastal waters. Considering a big hiatus lapsed between the last study (almost 20 years old) and the present need, a study was carried out with the following objectives; to find out a) the present seasonal settlement pattern of biofoulers, dominant species and breeding pattern, b) any change, as compared to that of earlier reported data and c) the role of physico-chemical characteristics of coastal water on biofouling. Moreover, this coast was severely affected by 2004 tsunami. Thus, the present study also brings out any change in settlement pattern, diversity, biomass and population density between pre- and post-Tsunami period.

4.1 Material and Methods

The present study was carried out between May 2006 to April 2007, in the coastal waters of Kalpakkam in the vicinity of MAPS. The study area is located at the intake of MAPS Jetty. Water depth at the study site is ~8 m. Teak wood panels (each 12 x 9 x 0.3 cm) were suspended on epoxy coated mild steel frames from MAPS jetty. The panels were suspended at 1 m below the lowest low water mark, approximately 400m away from the shoreline. Three series of observations (weekly, monthly and cumulative at 30 d intervals) were made.

Weekly & monthly observations were considered under short-term observations and cumulative was considered under long-term observation. Two unique features of this study are, for the first time a) fouling data at an interval of 7d is available and b) photographs of each series are digitally available for future comparison. Different evaluating parameters viz. composition of organisms, number of organisms, growth rate, both % of number and % of area coverage, biomass (g. per 100 sq. cm) were used to study the fouling pattern. Fouling concentration was assessed by counting the foulants available on the panels. Total biomass was calculated using a correction factor due to the absorption of water by the panels for specified time periods. The growth rate was recorded by measuring the size of macrofoulers. Apart from the above-mentioned parameters, diversity indices such as species diversity (D), species richness (R) and evenness (J) were also calculated following Shannon-Weaver (1963), Gleason (1922) and Pielou (1966).

4.2. Results

4.2.1. Fouling Community

A list of organisms collected from test panels are given in **Table 1**. The total number of taxa involved in the fouling process at Kalpakkam coastal waters are found to be 30 during the present investigation.

4.2.2. Biomass

Biomass values of weekly panels ranged from 1-11 g. per 100 sq. cm (**Fig. 6a**). The lowest and highest biomass values for weekly panels were obtained in the months of November and December respectively. In the monthly observation, the lowest (17 g. per 100 sq. cm) and the highest (46 g. per 100 sq. cm) were observed in April and November respectively (**Fig. 6b**). In case of cumulative panel, a steep increase in biomass was observed from 28 d (77 g. per 100 sq. cm), 56 d (97 g. per 100 sq. cm), 112 d (185 g. per 100 sq. cm) to 150d (648 g. per 100 sq. cm) (**Table 2**) onwards.

4.2.3. Settlement pattern in short-term (weekly and monthly) panels

A wide variation was observed in the number of settled organisms on weekly panels. Major fouling organisms observed were barnacles, hydroids, ascidians, oysters, sea anemones and green mussels. In addition to these sedentary organisms, some epizoic animals like errant polychaetes, flat worms, amphipods, crabs were also observed. Number of fouling organisms, number of species and % of area coverage are given in **Table 2**.

Coelenterata

Campanulariidae	<i>Obelia bidontata</i> Clarke <i>Obelia dichotoma</i> Linnaeus <i>Clytia gracilis</i> M.Sars
Aiptasiidae	<i>Aiptasia</i> sp

Annelida

Nereidae	<i>Pseudonereis anomala</i> Gravier <i>Platynereis</i> sp
----------	---

Serpulidae	<i>Serpula vermicularis</i> Linnaeus <i>Hydroides norvegica</i> Gunnerus
Sabelidae	<i>Daychone</i> sp <i>Sabellistarte</i> sp
Arthropoda	
Pycnogonidae	<i>Pycnogonium indicum</i> Sunder Raj
Balanidae	<i>Balanus amphitrite</i> Darwin <i>Balanus reticulatus</i> Utonomi <i>Balanus tintinnabulum</i> Linnaeus <i>Balanus variegatus</i> Darwin
Corophidae	<i>Corophium madrasensis</i> Nayar <i>Corophium triaenonyx</i> Stebbing
Amphithoidae	<i>Paragrubia vorax</i> Chevreaux
Ectoprocta	
Membraniporidae	<i>Membranipora</i> sp
Electridae	<i>Electra</i> sp <i>Acanthodesia</i> sp
Mollusca	
Mytilidae	<i>Perna viridis</i> Linnaeus <i>Perna indica</i> Kuriaose <i>Modiolus undulatus</i> Dunker
Olividae	<i>Olivancillaria gibbosa</i> Born
Ostreidae	<i>Crassostrea madrasensis</i> Preston <i>Ostrea edulis</i> <i>Saccostrea cucullata</i> Born
Urochordata	
Didemnidae	<i>Didemnum psammathodes</i> Sluiter <i>Lissoclinium fragile</i> Van Name

Table 1. List of fouling organisms observed on the test panels suspended in the Kalpakkam coastal waters

The lowest and the highest numbers of foulants for weekly panels were 1 (November) and 136 per sq. cm (October) respectively (**Fig. 6c**). Fouling intensity was relatively high during summer and SW monsoon period, whereas during NE monsoon period, negligible intensity was observed. In monthly observation, the maximum (69 per sq. cm) and the minimum (12 per sq. cm) population density were obtained in September and January respectively (**Fig. 6b**). From July to September (SW monsoon) an increasing trend was observed, whereas from October onwards (NE monsoon) the fouling intensity started declining. Once again after January the fouling density was found to increase. This almost followed the salinity variation pattern observed for this coastal water. The percentage (%) of area coverage on weekly panels showed a well marked variation ranging between 0.08 and 100% (**Fig. 6d**), whereas, in case of monthly observation, it was found to be 89 - 100%. In monthly observation, maximum area coverage (100%) was found during July -August, November - January and March (**Fig. 6b**). However, during weekly survey, maxima (80 - 100%) were attained in August - September and November.

4.2.4. Variation in seasonal settlement of fouling organisms

Barnacle: Among the different groups, barnacles were found to be the most dominant fouling community and its accumulation on the test panels was observed throughout the year. During the present study period, barnacles were represented by four species such as, *Balanus amphitrite*, *B. tintinabulum*, *B. reticulatus* and *B. variegatus*, which were found to be the most dominant on weekly (12.4 - 99%) as well as monthly (5.9 - 85.2 %) panels. On weekly panels, barnacle settlement was continuous with peaks observed during June-July and November -March. In case of monthly panels, large numbers were observed during July, November-December and March-April. During weekly and monthly observation maximum growth (size) obtained were 0.5-1 mm and 2-3 mm respectively.

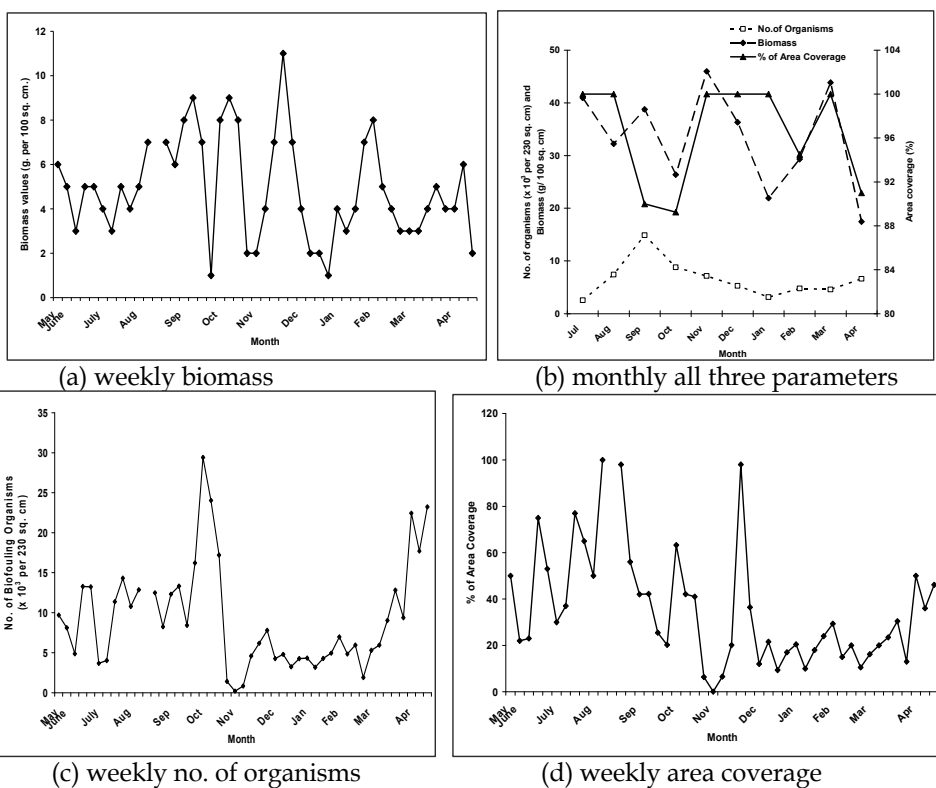


Fig. 6. Variations in no. of organisms, biomass and % of area coverage on weekly and monthly panels

Hydroids: Hydroids were only second to barnacles in abundance as well as seasonal occurrence and were dominated by *Obelia* sp. They started appearing on the panels after 5d immersion. The growth of hydroids was recorded by measuring the length from base to tip. A maximum length of 5 mm on weekly panel and 17 mm on monthly panel was observed. Its % composition varied between 0.64 & 81.62 % and 1.66 & 37.28 % during weekly and monthly investigation respectively.

Ascidians: *Didemnum psammathodes* and *Lissoclinum fragile* were the ascidian species encountered during the present observation. In the weekly observation, the occurrence of

ascidians was generally restricted to March-April and June - August, with peak settlement during March-April. Monthly observation also depicted the dominance of ascidians during March-April and June-July, but with maximum density during June.

Sea anemones: Sea anemones, also a prominent group among the fouling assemblages, were represented by *Sertularia* sp., *Aiptasia* sp. in both weekly as well as monthly observations. They were found settling from September/ October onwards and formed a group particularly abundant during NE monsoon period. Their rate of growth was 1.5 mm diameter in 7 d and 8 mm diameter in 30 d observation and the settlement was relatively less during SW monsoon period.

Green Mussels: Green mussels (*Perna viridis*) were the most important constituent of the fouling community. They were mostly found attached to the mild steel frames during short-term investigation and their absence was encountered during the entire weekly observation. However, during monthly survey, their % composition varied from 0.08 - 11.02 % and their colonization was generally observed during May-September with vigorous settlement during May-June and August - September.

4.2.5. Seasonal settlement on long-term (cumulative) panels

During the present observation, long-term panels were studied up to 150 days after which panels were lost due to entanglement of the frames and could not be retrieved. In the Kalpakkam coastal waters considerable settlement of barnacles, green mussels and ascidians were observed on the long-term panels. Apart from that, colonization of hydroids, oysters and sea anemones was also observed on the long-term panels. In addition to these sedentary organisms, epizoic animals like errant polychaetes, flat worms, amphipods, crabs were also observed. Peak settlement period of foulants, succession and climax community are represented in **Table 2**. Fouling succession was very prominent during the long-term observation as compared to weekly and monthly observation. Barnacles were the first to settle on the long-term panels and by the time they were of 14 mm in size, they were followed by hydroids and polychaete worms during the month of May. During this period, barnacle population remained largely unaffected by the secondary settlers. Ascidians began to colonize on the panels from June. Fully developed ascidian colonies completely covered the barnacles and other organisms by July and they remained till the end of August. Disappearance of ascidians was noticed from the month of September. Green mussels started appearing from August, whereas the peak colonization of mussels was observed from September onwards and it was maintained till mid-November.

Percentage composition of barnacles initially increased upto 56 d and subsequently reduced significantly on the long-term panels as follows (15%, 28%, 13% and 5% on 28 d, 56 d, 112 d and 150 d old panel respectively). Green mussel, which was absent upto 28 days, started appearing subsequently and occupied 41% by 56d and reached 90% by 150d. Accumulation of juvenile green mussels occurred after 28 days along with the pre-existing community consisting of barnacles, hydroids, oysters, polychaete worms, flat worms & sea anemones. The mussels attained 0.5-1 cm in size by 56 d and from 112 d onwards, the panels were fully covered with adult green mussels of size 3 - 5 cm. (**Fig. 7**). The relative abundance of fouling community observed for 28 d, 56 d, 112 d and 150d are given in **Fig. 8**.

	Nair et al., 1988	Sashikumar et al., 1989	Sashikumar et al., 1990	Rajagopal et al., 1997	Present study		
					Weekly	Monthly	Cumulative
No. of organisms (x 10 ³ per 230 sq. cm)	----	----	----	----	(0.185-29) x 10 ³	(2 - 15) x 10 ³	(0.166- 63) x 10 ³
No. of species	----	21	----	105	30		
% of Area coverage	----	62 (Dec.)-100% (Jul.-Aug) - Monthly	53 (Nov.)-100% (Apr., Jul.- & Aug) - Monthly	34 (Feb.)-72% (Oct.)-Monthly	0.08 (Nov.)-100% (Aug.)	89 (Oct.)-100% (Jul./ Aug.)	100%
Biomass (g/ 100 sq. cm)	43 d -33; 128d - 52; 150 d- 135	56d -90; 120d -105; 150d -1000	45d - 32; 60d - 52; 130d- 50; 160d - 138	56d -750; 125d -1870; 150d - 1750	1 - 11	17 - 46	28d - 77; 56d -97; 112d -185; 150- 648
Peak settlement	Barnacles (Mar.-Jul.) Hydroids (Feb. - Aug.) Ascidians-May Sea anemone (Sep. - Oct.) green mussels-September onwards	Barnacles (throughout the year) Hydroids (Feb. - Nov.) Ascidians (Mar. -Aug.) Sea anemone - NE monsoon	Barnacles (Throughout the year) Hydroids (Mar. -Apr. & Sep.) Ascidians (Apr. - Aug.) Sea anemone (Feb. - Oct.)	Barnacles throughout the year Green mussels (Apr. - Aug.)	----	----	Barnacles (Mar. - Jul.) Green Mussel (<i>Perna viridis</i>) - (Sep.-Nov.)
Diversity indices							
SD			1.21(125d)-1.69(75d)		SD (0.05-0.96)	SD(0.5-1.55)	0.43(150d) -1.60(56d)
SR			0.04(150d) - 0.11(65d)		SR(0.11-0.69)	SR(0.45-1.0)	0.36(150d) -0.80(56d)
E					E (0.08 - 0.99)	E (0.26-0.74)	0.31(150d) -0.73(56d)
Succession	Barnacles, hydroids, sea anemone, ascidians, green mussels	Barnacles, hydroids, ascidians, sea anemone, green mussels	Barnacles, hydroids, ascidians, sea anemones, green mussels	Barnacles, ascidians, green mussels	----	----	Barnacles, hydroids, sea anemone, Ascidians, green mussels
Climax community	Barnacles	Green Mussel (<i>Perna viridis</i>)	Ascidians	Green Mussel (<i>Perna viridis</i>)	----	----	Green mussels

Table 2. Comparison of present fouling data with earlier reported values

4.3. Discussions

4.3.1. Fouling Community

During the present investigation, the total number of fouling organism taxa observed at Kalpakkam coastal waters was 30, which is comparable with that of the observation of Sashikumar et al. (1989). However, Sashikumar et al. (1989) have observed presence of a few species of fishes, which were not encountered during the present study. Change in coastal water quality particularly the chlorophyll content may be one of the possible causes for such minor difference in fouling community. In contrast to the above, Rajagopal et al. (1997) have reported almost 3.5 times higher number of fouling species (105) than that of ours as well as that of Sashikumar et al. (1989) from the same location. In this regard, it is imperative to mention here that values with wide variations have been reported from both east and west coast of India. For example, 121 taxa from Visakhapatnam harbour, 37 taxa from Kakinada (Rao and Balaji, 1988), 42 taxa from Goa (Anil and Wagh, 1988) and 65 taxa from Cochin harbour (Nair and Nair, 1987) have been reported respectively. It is interesting to mention here that although Sashikumar et al. (1989) and Rajagopal et al. (1997) have studied from same location and during the same period, the no. of taxa observed by them differ substantially. Conveniently, Rajagopal et al. (1997) have neither discussed this aspect nor provided any plausible explanation for observation of such high no. of taxa as compared to that of Sashikumar et al. (1989).

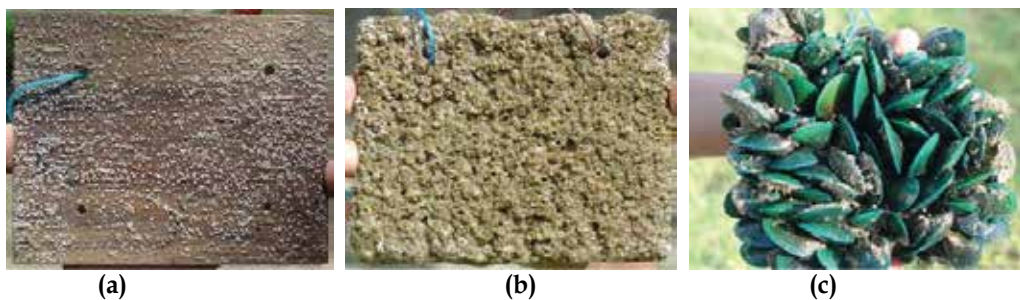
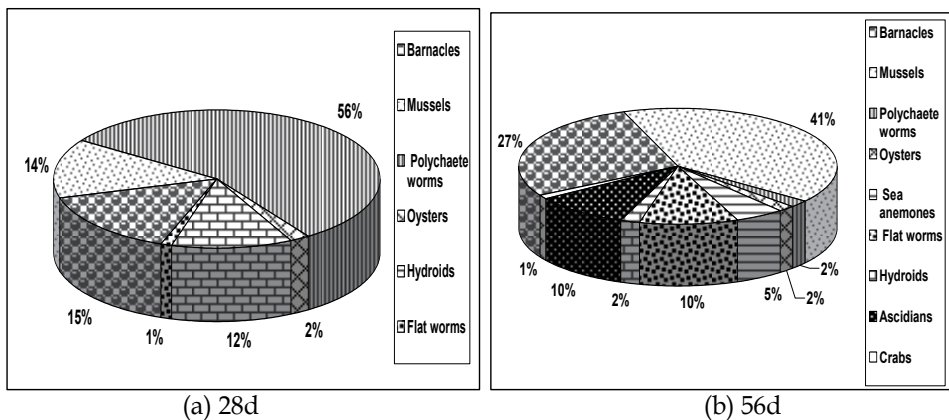


Fig. 7. A view of a weekly panel (a) A view of a monthly panel (b) A view of 112 d old panel, covered with green mussels (c)



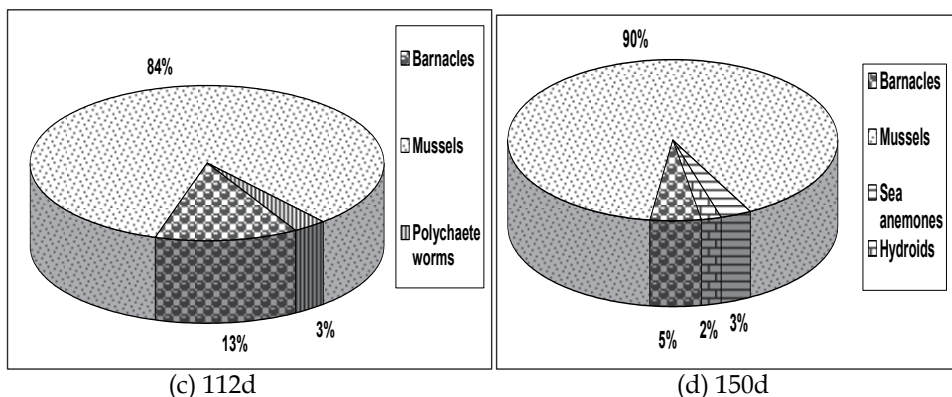


Fig. 8. Relative abundance of fouling organisms for (a) 28 d, (b) 56 d, (c) 112 and (d) 150d old panels exposed to Kalpakkam coastal waters

Although, direct comparison of the present observation with that of the earlier data is not justified on account of reasons, such as, differences in the exposure methodology, substratum and level of systematic identification, however, such wide variations as above observed by the three investigators (Present study, Rajagopal et al., 1997 and Sashikumar et al., 1989) from the same location under comparable conditions calls for further detailed investigations.

4.3.2. Seasonal settlement pattern on short-term (weekly and monthly) observation

The seasonal settlement of foulants in case of short-term panels was found to be quite different from that of the long-term panels, as described in the following discussion. The weekly panels showed well marked variation in population density of organisms. The lowest density was found during NE monsoon period, which could be due to the lowering of salinity level in the surface water during the above period. It is important to mention here that about 1000 mm of rainfall is received at Kalpakkam from NE monsoon. Moreover, with the onset of NE monsoon, the sea water current reverses from north to south as a result of which low saline riverine water from northern Bay of Bengal (BOB) (Varkey et al., 1996) coupled with the monsoonal precipitation deepens the salinity to the lowest during this period. It is known that salinity plays a crucial role in the growth, development and diversity of macro-foulants in the marine environment. Additionally, a relatively low temperature, which is not favorable for biogrowth was also prevailed during this period. It looks quite reasonable to speculate that substantial reduction in salinity and temperature along with enhanced suspended matter prevailed during NE monsoon period could have contributed for the low fouling density as well as low species diversity observed during this period. A relatively high fouling intensity on weekly panel was observed during summer and SW monsoon period. During this period, a comparatively high stable salinity, temperature and low turbidity prevailed, which is in general conducive for promoting large settlement of macrofoulants. This period also harvested highest number of phytoplankton count in this locality. The above observation was also substantiated by the positive correlation matrix value obtained between salinity & fouling density ($p \geq 0.01$) and chlorophyll/ phytoplankton density & organism density ($p \geq 0.001$) (Table 3). This showed that abundance of fouling organism at this locality was regulated mainly by two important factors namely, salinity and phytoplankton. Previous studies (Nair et al., 1988) showed peak settlement

rates during May and June, whereas during the present study, an extension of this period up to September – October was observed. The present variation as compared to earlier could be due to the temporal variability in reproductive cycles, which was related either directly or indirectly to seasonal changes in the physical environment including temperature, salinity, phytoplankton productivity and light characteristics (Sashikumar et al., 1989). A close look at the present physico-chemical and biological characteristics of the Kalpakkam coastal water reveals substantial reduction in phytoplankton density, chlorophyll concentration and enhancement in suspended matter including that of nutrient in the recent past particularly after Tsunami (Satpathy et al., 2008). A detailed impact of Tsunami on the coastal milieu is reported elsewhere (Satpathy et al., 2008). Possibly these changes are also typified in the change in macrofouling settlement pattern as observed during the present study. A significant difference was observed between successive weeks (**Fig. 9**), with respect to number of foulers, % of area coverage, growth rate etc. The selection pressure exerted by the ambiance itself on the recruitment of fouling organisms could be responsible for the above observation. In this context Sutherland (1981) states that, in natural habitats development of a fouling community is influenced by seasonal variations in larval recruitment, competition by dominant species and frequency of disturbance like predation. The variation in fouling density pattern in monthly panel almost followed the variability in salinity trend, which strengthened the fact that salinity is one of the major dominating factors responsible for fouling composition or settlement in the tropical coastal regions.

Variables	No of organisms	Biomass	% Area coverage	Temp	pH	Salinity	DO	Turbidity	Chl- a	Phyto density
No of organisms	1									
Biomass	0.359	1								
% Area coverage	0.504^b	0.518^b	1							
Temp	0.197	-0.271	-0.292	1						
pH	-0.023	-0.475^b	-0.432^b	0.116	1					
Salinity	0.515^b	0.047	0.452^b	0.195	-0.325	1				
DO	-0.160	-0.004	-0.128	-0.381^c	0.119	-0.430^b	1			
Turbidity	-0.090	-0.065	0.445^b	-0.307	-0.150	0.073	-0.276	1		
Chl- a	0.458^b	-0.098	0.502^b	-0.016	-0.259	0.685^a	-0.332	0.423^b	1	
Phyto density	0.442^b	0.139	0.465^b	-0.196	-0.264	0.547^a	-0.145	0.355	0.839^a	1

a- $p \geq 0.001$; b- $p \geq 0.01$; c- $p \geq 0.05$

Table 3. Correlation between biofouling and hydrographical parameters

November (NE monsoon period) coincided with low intensity of biofouling for monthly and cumulative; however, % of area coverage was found to be the highest during one of the weeks in November. Although, the highest % coverage was observed during NE monsoon, a period of low salinity, however, both these parameters are positively correlated. Similarly, turbidity and % of area coverage showed a positive correlation, in spite of the fact that high turbidity generally does not support abundant settlement. This contradiction can be argued out that, the period of low salinity and high turbidity was not favorable for settlement of most of the organisms. That is, the competition was almost nil and only organisms (barnacle and mussel), which can thrive well

under the above environmental conditions grew fast and covered the entire area indicating a significant relationship between salinity and turbidity with % of area coverage (Iwaki & Hattori, 1987). Considering the fact that no weekly data was available from this location, this forms the benchmark for future reference as well as impact studies.

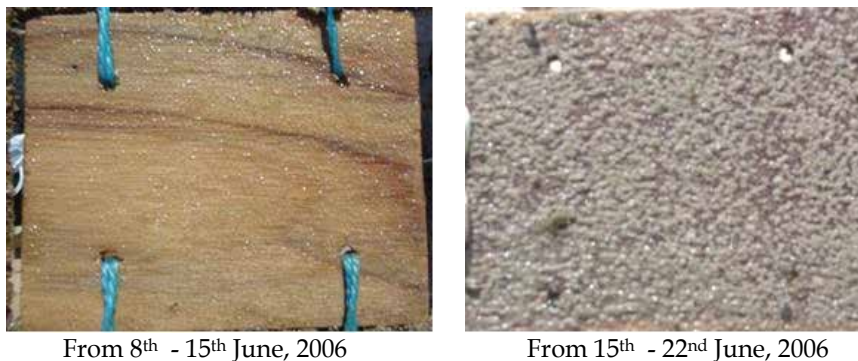


Fig. 9. Variations in fouling pattern observed on the test panels between two successive weeks

4.3.3. Variations in seasonal settlement of fouling organisms

Barnacles: Among the different groups of fouling organisms, barnacles are reported to be the most important group and all time breeders (Godwin, 1980; Nair et al., 1988). In the present study also, barnacles were found to be the most dominant fouler and its presence found throughout the year. Nair et al. (1988) and Sashikumar et al. (1990) have also reported the settlement of barnacles throughout the year at this location during the period 1986-87. On weekly panels, settlement was continuous with peaks during June-July and from November -March. Settlement of barnacle is known to be favored in illuminated area (Brankevich et al., 1988; Sashikumar et al., 1989; Rajagopal et al., 1997), notwithstanding the contradictory observation of Dahlem et al. (1984) and Venugopalan (1987). Considering the fact that southeast coast of India receives good illumination throughout the year, it is appropriate to assume from the present as well as earlier data that this would have supported the settlement of barnacle throughout the year on the test panel. In case of monthly panels, large numbers were observed during July, November-December and March-April. Although fouling density was high during September/ October, barnacle population was found to be the lowest in September. Settled green mussels (*Perna viridis*) prior to September established their dominance on the panel surface by September/October, thereby not facilitating further settlement by barnacles. This could be the possible reason for relatively low settlement of barnacles during September. Dominance of other foulants over barnacles resulting in their population reduction has also been reported by Nelson (1981) on natural substrates. Territorial behavior of barnacles could also be another important cause of its population reduction during a particular period of the present investigation. It is reported that newly settled barnacles maintain a distance of ~2 mm from the earlier settled barnacles or other settling organisms, which is known as 'Territorial behaviour' of barnacles (Crisp, 1961). As fouling density rises, the territorial separation gets weakened and as a consequence barnacle mass gets reduced (Crisp, 1961). The settlement pattern of barnacles during the present study showed similarity with the previous studies

reported from coastal waters of southeast coast of India (Nair et al., 1988; Rajagopal et al., 1997). In contrast to the present study as well as that of Nair et al. (1988) and Rajagopal et al. (1997), relatively low barnacle population during June-July has been reported by Sashikumar et al. (1989). This disparity among different studies as far as peak settlement period of organisms is concerned, could be attributed to the variation in the influence of environmental parameters on breeding cycle of the organisms. The above agreement is strengthened by the fact that effect of array of environmental variables on reproduction cycle of different organisms greatly differs (Sutherland, 1981). Rajagopal et al. (1997) have reported six species of barnacle as against four observed by us. Possibly a long-term study would throw more light on this.

Maximum growth rate on weekly and monthly panel was observed during June and July respectively. This period was once again a period of stable salinity, temperature and nutrient, which was conducive for high growth. The present observation matches with those of Iwaki et al. (1977) in Matoya Bay and Sashikumar et al. (1989) from this locality. Although, Nair et al. (1988) have reported a relatively high growth rate as compared to the above report, however, the period of maximum growth rate matches with the present study.

Hydroids: The peak settlement of this group was during July-August (SW monsoon) and January-March. The accumulation of this group was prominent on the edges of the panels. Selection of edges by the hydroids for their settlement could be due to the very location, which was found to be favorable for their filtration. On the other hand, had they settled on the panel surface, their growth would not have been faster due to crowding by other foulers. The present observation is found to be parallel with that of the findings of Nair et al. (1988) and Sashikumar et al. (1989). Interestingly, Rajagopal et al. (1997) reported peak settlement of hydroids during NE monsoon, an observation contrary to the present as well as those of Nair et al. (1988) and Sashikumar et al. (1989). NE monsoon period, a period of the lowest salinity, temperature and highest turbidity concomitant with low penetration of light, leads to lowest phytoplankton production. Under these conditions, settlement in general has been reported to be low to very low, and thus long-term studies again would provide a plausible answer to the above ambiguity.

Ascidians: Ascidians are a very important group of fouling organisms having a world-wide geographical distribution (Swami and Chhapgar, 2002). It has been reported that in temperate waters only a single generation is established each year, in contrast to two to four generations per year are established in tropical waters (Miller, 1974). During the weekly observation of the present study, the occurrence of ascidians was generally restricted to March-April and June - August, with peak settlement during March-April. Monthly observation also showed the dominance of ascidians in March-April and June-July, but with maximum density during June. This revealed that almost seven months in a year ascidians did not settle on the panel. In the south west coast of India (New Mangalore port), their appearance on the panel was also restricted only to 4 to 5 months in an year. Results of this study coupled with that of Khandeparker et al. (1995) clearly demonstrate that ascidians are a dominant group of macrofouling community in the Indian coastal water during pre-monsoon and late post-monsoon months. Such dominance of ascidians during a certain period of weekly and monthly observation could be attributed to the increased larval density & their ability to undergo dedifferentiation and redifferentiation during that period (Sebastian & Kurian, 1981). The ascidians dedifferentiate and form a heap of cells within a small ectodermal bag and when favourable conditions set in, the cells rebuild the tissues

and redifferentiate into an adult ascidian (Khandeparker et al., 1995). Such interaction of the breeding period of foulants in the development of fouling communities has been reported by Chalmer (1982). Total absence of ascidians was encountered from September to December. This showed that early pre-monsoon to early post-monsoon period is not conducive for ascidian settlement at this coast. Even before the onset of NE monsoon, reversing of current (September/ October) from north to south takes place. This brings the low saline water from the north to the south and subsequently during NE monsoon period (October-January) salinity and temperature drop to the minimum till the end of January, the late-NE monsoon period. This clearly demonstrates that settlement of ascidians, highly dependent on salinity level. Similar observations have also been made by Swami and Chhapgar (2002). Although, they have reported the settlement of about 10 ascidian species, however, most of the ascidian species were absent during monsoon months. Ascidians have short larval life cycle lasting for a few hours and are very sensitive to minor variation in salinity content. Khandeparker et al. (1995) while studying the co-relation between ascidian larval availability and their settlement have clearly demonstrated that ascidian larvae were not available during monsoon and early post-monsoon in coastal water. Salinity, during monsoon period in Mangalore coastal water, decreased marginally (~33 psu), whereas at this location it drops significantly (~25 psu). As a pure marine form, ascidians are not able to survive at low salinity (Renganathan, 1990). Thus, it was not surprising to observe total absence of ascidian on the panel during September-December period. Increased suspended load (during monsoon) and dominance of green mussels on panels (from September onwards) could be other important causes of disappearance of ascidian population (Khandeparker et al., 1995). The present trend in the settlement pattern of ascidians agrees with the studies by Sashikumar et al. (1989) and Nair et al. (1988). However, observations of ours as well as those of Nair et al. (1988) and Sashikumar et al. (1989) are not in tandem with that of Rajagopal et al. (1997), who have reported the presence of ascidians throughout the year including the unfavorable NE monsoon period.

Sea anemones: sea anemones are soft bodied conspicuous members of the marine fouling community. The observation of heavy colonization of sea anemone during September /October to NE monsoon period agrees with the earlier reports (Nair et al., 1988; Sashikumar et al., 1989; Rajagopal et al., 1997).

Green mussels: Green mussels (*Perna viridis*) are one of the most important constituents of the fouling community. The first peak of green mussel settlement coincided with the seasonal temperature and salinity maxima of the present study. Rajagopal et al. (1997) also reported the maximum *P. viridis* settlement during relatively high temperature and salinity condition. However, the second peak was observed corresponding to the maximum phytoplankton density and relatively high salinity during August-September, indicating the significant influence of the availability of food resources and salinity on the larval abundance and settlement of mussels (Pieters et al., 1980; Newell et al., 1982). Paul (1942) also recorded the settlement of this species in Madras harbor during March to November with a distinct peak during August - September. The trend observed on settlement of mussels corroborates the finding of Seed (1969) and Myint and Tyler (1982), who have explained in their classical papers on the role of temperature, salinity and food availability on mussel breeding periodicity.

Other fouling organisms: Other fouling organisms observed include bryozoans (Ectoprocta), oysters, polychaete worms & flat worms etc and some other crustaceans such

as, crabs (both larvae and juveniles), amphipods & juvenile lobsters. Settlement pattern of bryozoans (Ectoprocta) did not show any definite trend in their temporal variation on short-term panels. However, Rajagopal et al. (1997) have noticed bryozoan settlement during January - May, with peak colonization during February - March, when other fouling recruitment was less. Khandeparker et al. (1995) have reported heavy settlement of bryozoan during December-March from New Mangalore Port. The information available on the life history of bryozoan larvae in Kalpakkam coastal waters is at low key. Hence, to understand their indefinite trend, it requires more knowledge on their developmental biology. Appearance of juvenile oysters (*Crassostrea madrasensis*, *Ostrea edulis*) was observed in almost all the months, with peak settlement during August. However, during weekly survey they did not appear at all. The present study recorded considerable contribution (maximum, ~7%) by oysters to the fouling community during August on monthly panels, which has not been observed by other workers from this locality (Nair et al., 1988; Sasikuamr et al., 1989; Rajagopal et al., 1997). Price et al. (1975) have stated that the growth of oysters was the highest in August i.e. after their spawning, when glycogen reserves are restored. Growth ceases during winter, except in Florida, where growth was continuous throughout the year (Sellers and Stanley, 1984). It is interesting to note that stable environments inhibit better growth for oysters (Sellers and Stanley, 1984). We are unable to explain the cause of non-availability of oysters during earlier studies (Rajagopal et al., 1997; Sasikuamr et al., 1989; Nair et al., 1988). Though the peak settlement of polychaete worms (*Serpula vermicularis*, *Hydroides norvegica*) (0.05-2.1% - Monthly and 2 - 56% - cumulative) was observed in January during monthly observation, its availability as temporary settler was noticed during most part of the study period. Khandeparker et al. (1995) have also reported the year-round breeding activity of this organism from west coast of India. During the initial period of cumulative observation (28d), polychaete density was found to be dominant, which gradually disappeared during the subsequent days. Tube-dwelling polychaetes were found to have higher covering capacity than barnacles (Anil et al., 1990; Kajihara et al., 1976). Flat worms were found to be settled in relatively less numbers as compared to the other foulants during the entire short-term observation. Settlement of sponges, clams and snails were also occasionally noticed on the panels. Other crustaceans (amphipods, lobster juveniles, crab juveniles) started appearing from August onwards with high abundance during September. Despite, being a very significant component of the fouling assemblage in marine environment, macroalgae, showed its total absence at Kalpakkam coastal waters during the present investigation, which might have been due to competition for space, predation and grazing (Carpenter, 1990). Earlier workers too have not reported the settlement of macroalgae on the exposed panels from this locality.

4.3.4. Seasonal settlement on long -term (cumulative) panels

Long-term observation showed distinct fouling succession. To follow changes or succession occurring within the fouling community, cumulative/ long-term panels are more suitable than the short-term period (Rajagopal et al., 1997). Barnacles were found to be the first community settled on the long-term panels (maximum size 14 mm). Hydroids and polychaete worms were the next to settle during the month of May. Barnacle population remained unaltered by the secondary settlers during this period. By June, ascidians started appearing on the panels and by July they fully covered the barnacles and other organisms. Sashikumar et al. (1990) have also reported the similar pattern of ascidian colonization on

long-term panel. Thus, ascidians can be considered as a temporary 'stable point' in the fouling community development. According to Sutherland (1981), the term 'stable point' is to describe the succession of foulers. Disappearance of this group was noticed from the month of September, which could be due to the dominance of other fast growing foulers such as green mussels (*Perna viridis*). Sashikumar et al. (1989) also observed similar pattern of colonization on long-term panels.

During the present study, green mussel was found to be the climax community. This could be due to the fast growing and competitively superior green mussels establishing dominance on panel surfaces such that other fouling organisms are left with little space to settle. Richmond and Seed (1991) have also reported that competitively dominant species like green mussels are often successful due to their large body size, fast growth rate, extended longevity and prolonged larval life. According to the previous study by Rajagopal et al. (1997), the peak settlement of green mussels (*P. viridis*) occurred in April-June as well as one or two months immediately preceding it. However, the present study showed that only from mid-July onwards mussels started appearing on the test panels and the peak was observed in September. It is apparent to assume that a shift in the peak settlement period of mussels has taken place, possibly due to the change in coastal water characteristics and the same could be confirmed over a long period of study. Surprisingly and interestingly both Nair et al. (1988) and Sashikumar et al. (1989) have not reported settlement of green mussel on their test panel, which is not in tandem with the observation of ours as well as that of Rajagopal et al. (1997).

4.3.5. Biomass

The lowest and highest biomass values for weekly panels were obtained in the months of November and December respectively, which could be attributed to the difference in peak settlement period of macrofoulants contributing more to the fouling biomass. In spite of the influence of NE monsoon, the highest value was observed during November (Monthly biomass) and December (Weekly biomass), which could be attributed to the elimination of most of the organisms due to unfavourable condition of the ambience (such as low salinity, high turbidity, low phytoplankton density leading to food scarcity etc) and survival of the most tolerant foulers (such as barnacles and green mussels). This exclusion of organisms leads to reduction in intra- and inter-specific competition, which ultimately facilitates the growth of better adapted foulants (Iwaki & Hattori, 1987). Thus, barnacles and green mussels were found to contribute maximum to the total fouling biomass during the above period.

The abrupt increase in biomass in 150d old panel could be ascribed to the dominance of green mussels, *P. viridis* during the month of October. It is worth comparing the present data with those of Nair et al. (1988), Sashikumar et al. (1989) and Rajagopal et al. (1997) with respect to both short-term and long-term panels. Biomass observed on short-term panels (15-30d) exposed by Sashikumar et al. (1989) ranged from 1 to 7 g. per 100 sq. cm and Nair et al. (1988) under similar condition observed a biomass ranged from 9 to 51 g. per 100 sq. cm. Karande et al. (1983) have reported 45 g. per 100 sq. cm biomass on 30 days exposed wooden panel from Kalpakkam coast. In contrast, Rajagopal et al. (1997) observed a biomass ranged from 130 to 640 g. per 100 sq. cm, a phenomenal increase. Such abnormal increase as above has not been explained by him as well as he has not compared his values with those of others. The present values ranged from 17 to 46 g. per 100 sq. cm (30d) and 1 to 11 g. per 100

sq. cm (7d) compares well with Karande et al. (1983), Nair et al. (1988) and Sashikumar et al. (1989). A comparison of biomass values observed on long-term panels during the present study with that of the earlier studies (**Table 2**) are almost comparable with the values of Sashikumar et al. (1989). However, they marginally differ from that of Nair et al. (1988). On the contrary to all the above observation, Rajagopal et al. (1997) have reported significantly high biomass values. Reports of still higher values than that of Rajagopal et al. (1997) have been observed even from temperate waters (Trondheim, Norway - 760 g/ 100 sq.cm). It is worthwhile to mention here that such wide variations in biomass values could be due to an array of factors such as differences in exposure mechanism, substratum, time of exposure and dynamism of environmental variables, however, it needs further investigation to explain as to how such variations could be accounted scientifically.

4.3.6. Diversity Indices

The diversity indices showed wide variations between weekly and monthly surveys. During weekly observations, species diversity has shown its maxima (0.84) in the month of September and minima (0.32) in February. The highest value (0.41) and lowest value (0.11) of species richness was observed in the months of October and May respectively. The maximum and minimum values for evenness were 0.85 (May) and 0.32 (December) respectively. However, during cumulative observations the highest species diversity occurred on 56 d (1.60) panel and a steep reduction was noticed on 150 d (0.43) panel during which green mussels almost dominated the fouling community. Although, it is fairly logical to attribute the dominance of green mussels to the above observed low diversity value, the role of the competition among dominant species for space, predation & grazing and survival of a superior & better-adapted community by eliminating other species can not be ignored (Sashikumar et al., 1990). Such dominance of superior species appears to be a periodic phenomenon. Every species has a particular period of dominance, thus, no species can dominate the fouling assemblage for a very long duration. The significant reason behind this is the frequent variations in larval settlement and abundance in the open coastal waters (Raymont, 1983). Similar trend was also observed in species richness and evenness.

4.4. Biofouling studies on metal panels

Similar to that of the biofouling studies on the wooden panels, fouling studies on metal panels (SS 304, SS 316, mild steel, titanium, copper, aluminium brass, admiralty brass, cupronickel and monel) has also been initiated in order to find out the biofouling potential of these metals. Initial results showed maximum abundance of biofoulers on the Titanium panel (7.9×10^3 organisms per 222 sq. cm.) followed by Stainless steel (SS 316L) (6.5×10^3 organisms per 222 sq. cm.). Settlement of organisms was found to be minimum in case of aluminium brass and admiralty brass. Barnacles (Juveniles) were found very scarcely on Cu and Cu-Ni panels. Biomass values were the highest for the Titanium (28.7 g. 100 sq. cm.) and the lowest was observed in Cu (0.6 g. 100 sq. cm.). In case of SS 316L, SS 304 L, Titanium, Monel and MS (Mildsteel) the % of area coverage was found to be 100% and due to negligible settlement of organisms, area coverage was not considered for Admiralty brass and Aluminum brass panels.

5. Impact of biofouling on control strategy

Selection of a suitable biofouling control strategy, particularly the chemical control methods, for a cooling water system mainly depends upon the physicochemical properties of the cooling water itself. Often, it has been found that the applied fouling control method becomes inefficient due to ability of the fouling organisms to alter the chemistry of the cooling water. The present study, carried out at MAPS is such a typical example which showed that a continuous monitoring of the cooling water at the outfall discharge is equally important as that of the intake water to find out the efficiency of the chemical control method (chlorination in this case). Studies with references to impacts of the activities of fouling organisms residing inside a cooling system on the cooling water quality are a few (Venugopalan and Nair, 1990; Satpathy et al., 1992; Satpathy, 1999, Satpathy et al., 2006; Masilamani et al., 1997). The intake tunnel works as a model to study the cooling water quality characteristics such as pH, DO, suspended matter, chlorophyll, nutrient etc as fresh seawater enters at one end (intake) and comes out at the other end (forebay) after passing through the tunnel with fouling organisms growing inside. A study was carried out to assess the impact of the activities of fouling community on the physicochemical properties of the cooling water in order to assess any possible interference in the operation and maintenance of the cooling water system.

5.1. Methods

All parameters were measured following standard methods as mentioned in section 3.1 of this chapter.

5.2. Results and discussion

The pre-condenser cooling water system of MAPS, comprising of the vertical shafts of intake & forebay and the sub-seabed tunnel nurtures well-established fouling communities comprising of 49 species (Venugopalan et al., 1991) dominated by the green mussel *Perna viridis* and barnacles (Sashikumar, 1991). The green mussel alone accounted for more than 410 tonnes (Rajagopal et al., 1991) out of the total estimated biomass of about 580 tonnes (Nair, 1985) present inside the tunnel. This huge accumulation of biofouling organisms inside the tunnel affected the quality of water that passed through it by various activities such as consumption of oxygen & detritus matter, release of faeces & pseudo-faeces and excretion of ammonia etc. Although the tunnel was cleaned to the extent of 60-70 % in 1987, the present status is unknown.

An increase in pH & turbidity and decrease in DO content was noticed in the forebay samples as compared to that of the intake. The pH values ranged from 7.68-8.30 and 7.76-8.30 in the intake and forebay respectively. The monthly average values showed marginally higher pH at forebay on most of the observations (**Fig. 10a**). The salinity values in the forebay compared to the intake samples was comparable. A significant increase in the turbidity was noticed in the forebay as compared to the intake. Values of turbidity ranged from 4.28-24.56 NTU and 6.12-27.53 NTU in the intake and forebay samples respectively. The monthly average values of turbidity varied between 9.73 ± 2.15 - 17.38 ± 2.26 NTU in intake and 11.10 ± 3.00 - 22.59 ± 2.83 NTU in the forebay (**Fig. 10b**). The increase in turbidity could be due to the excretion of the faecal matters by the biofouling community. However, the role of water velocity inside the tunnel, as high as 2 m sec^{-1} could be a factor that causes the resuspension of the deposited sedimentary

particles causing an increase in the turbidity. Similar increase in turbidity and suspended matter has been reported by Venugopalan & Nair (1990) and Satpathy (1999) in the forebay samples. The role of suspended matter in the process of biofouling is crucial as it provides a large area to the bacteria and fungi for their growth (Bhosle et al., 1989) thereby enhancing the possibility of biocorrosion in the cooling system. The high siltation rate in the pump chambers in the forebay causing problems in smooth operation of the pumps is another effect of the suspended matter generated in the tunnel. Though, suspended matter contents in the coastal water in a long run could increase marginally, however it could reach equilibrium after a cycle is established. However, situation may change if a series of power plants are located at the same location within a short distance.

Decrease in the DO contents in the forebay due to its consumption by the residing biofouling community was one of the noteworthy features observed during the study, which corroborates the earlier studies made by Venugopalan & Nair (1990) and Satpathy (1999). DO contents ranged from 4.37-6.34 mg l⁻¹ and 3.85-5.89 mg l⁻¹ at the intake and forebay respectively (**Fig. 10c**). Its monthly average values varied between 4.72±0.29- 6.06±0.50 for intake samples and 4.51±0.17- 5.39±0.19 for the forebay samples. The magnitude of difference of DO contents between the intake and forebay ranged from 0.1-1.1 mg l⁻¹. The wide variations of difference in DO concentration between intake and forebay could be due to the different flow rates of the seawater transported through the tunnel as has been reported earlier (Venugopalan & Nair, 1990) and they have shown that the consumption of DO by the fouling organisms increased with increasing flow rate. Though the oxygen depletion has very little impact on power plant operation, this can be utilized as an advantage to kill the biofouling organisms residing the cooling water system. It has been reported that, during shut down conditions or at very low flow rate, the oxygen levels could come down to almost negligible amount (Satpathy, 1999; Satpathy and Nair, 1990). This process could be utilized to kill the settled organisms and clean the cooling water system.

Almost all the nutrients showed an increasing trend from intake to forebay during the present study however, they do not bear much significance towards biofouling control process. The ammonia, total nitrogen (TN), phosphate and total phosphorous (TP) concentrations were always higher in the forebay than that of intake whereas nitrate and silicate did not show any clear trend although most of the time forebay values were relatively high as compared to intake. Ammonia values increased from intake to forebay (**Fig. 10d**) and ranged from below detection limit (BDL)- 12.90 µ mol l⁻¹ and 0.06- 10.42 µ mol l⁻¹ in the intake and forebay samples respectively. The increased level of all the nitrogenous nutrients in the forebay could be due to the fact that all the organisms produce reduced nitrogen compounds as byproducts of the metabolic activities and released to the environment by excretion (Chen *et al.*, 1994). Further, the increase in ammonia contents in the forebay could be attributed to its generation as the chief excretory product of marine invertebrates (Clarke *et al.*, 1994). Experiments by Masilamani *et al.* (2001) has shown that at normal temperature and salinity conditions, the quantity of ammonia excreted is about 5 µ mol l⁻¹h⁻¹ individual⁻¹ for a size group of 8-9 cm of *Perna viridis*, the chief macrofoulant in the MAPS tunnel. Ammonia is well known to accelerate the corrosion rate in copper based alloys used as condenser tube material in power plants (Rippon, 1979). The presence of ammonia in substantial quantity and on continuous basis in the cooling water system could be detrimental for the durability of aluminum brass condenser tube of MAPS. Also, the efficiency of chlorine, used as the biocide to control the biofouling in a cooling water system, gets reduced in presence of ammonia due to its reaction with chlorine to

form chloramines. These chloramines are about 200 times less effective than free chlorine (Venkateswarlu, 1990) as antifouling control measure. Moreover, chloramines are relatively stable compound and are toxic to fishes at concentrations > 0.1 ppm (Brungs, 1973). Thus, presence of fouling organisms inside a cooling water system not only affects directly the performance of cooling water system but also has deleterious impact indirectly in variety of ways. Therefore, biofouling control is essential even when it does not affect the cooling water system directly.

A significant decrease in the chlorophyll-*a* concentration was observed in the forebay samples (Fig. 11). The decrease in the chlorophyll-*a* content could be due to the consumption of the phytoplankton by the biofoulers, which are filter feeders. Moreover, chlorination also accounts for this decrease in chlorophyll-*a* contents in the forebay water as this biocide is used for the control of biofouling. Earlier studies (Satpathy, 1999) at the same locations also depicted similar trend by this photosynthetic pigment. This is further supported by the studies of Saravanane et al., 1998; Venugopalan and Nair (1990) and Sahu et al. (2006), which showed an expected decrease in phytoplankton density at the forebay compared to the intake point.

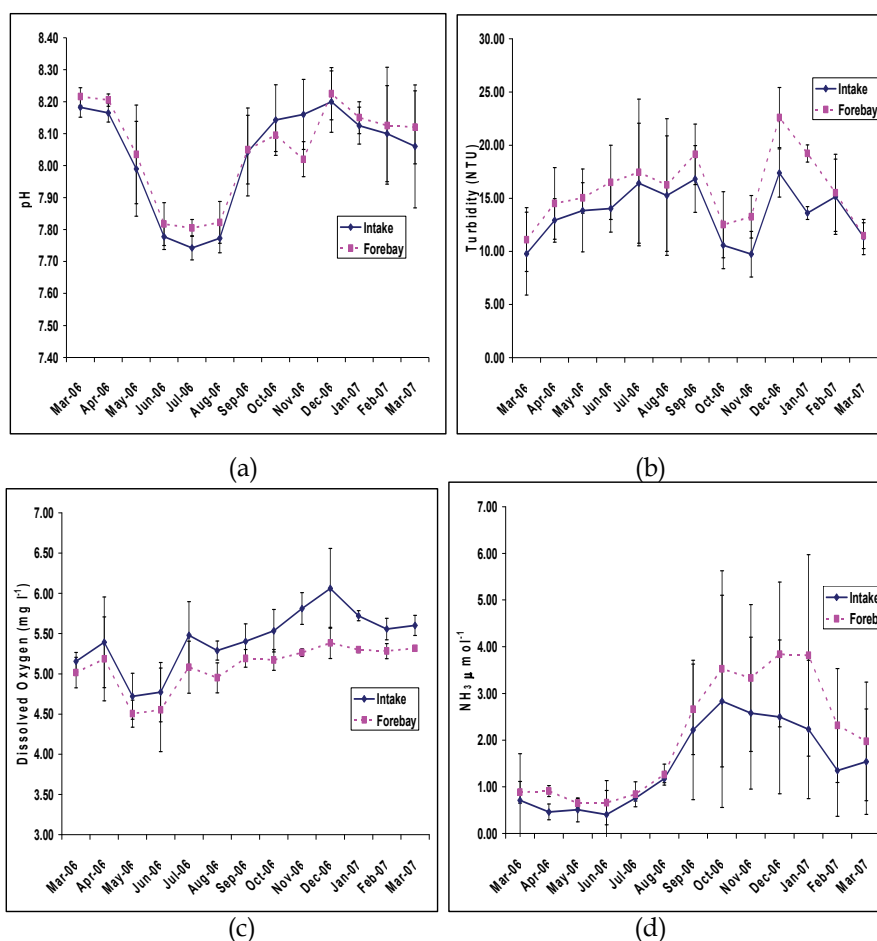


Fig. 10. Monthly variations in pH (a), turbidity (b), dissolved oxygen (c) and ammonia (d) at intake and forebay of MAPS

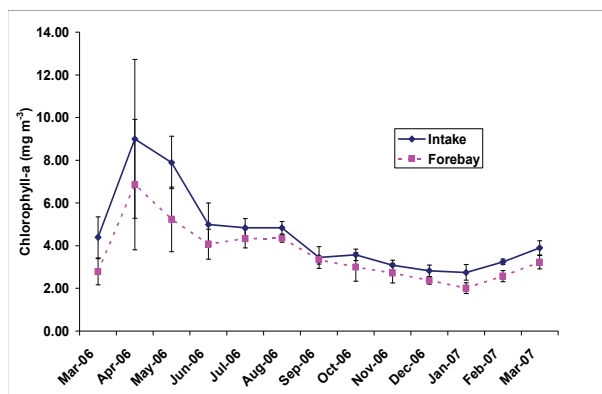


Fig. 11. Monthly variation in chlorophyll-a at intake and forebay of MAPS

6. Biofouling control

The principal objective of biofouling control technique is to prevent the aquatic organisms from growing to sizes large enough to cause flow degradation. Most control strategies are designed to treat the larval and juvenile stages of fouling organisms, although some of these strategies are effective against adults as well. Owing to the complexity of the nature of aquatic life, which colonizes a submerged surface, a general solution to biofouling problem is not feasible. Selection of control measures is governed by many factors; viz: efficiency, cost & environmental acceptability. Biofouling control by manual cleaning of power plant cooling circuits is difficult as well as uneconomical. Although methods like Amertap, spongeball, screens of various sizes, heat treatment and different biocides are in use for prevention and control of biofouling, chlorination stands out as the most widely used and efficient method owing to its proven effectiveness, easy availability and relatively low cost. Chlorination of cooling water was first tried in the United States in 1924 at the Commonwealth Edison Company's Northwest Station on an experimental basis to combat biofouling. These formal experiments showed that chlorination would prevent biofouling. Over the years chlorination has been accepted as the most widely used biocide for biofouling control. However, recently implemented Environmental Protection Agency (EPA) and state limitations on allowable chlorine discharges in plant effluents have become a stumbling block in chlorination practices (Satpathy, 1990). This restriction has caused the utilities to seek alternative treatment methods and methods to minimize chlorine discharges. Although this chapter deals with, in detail chlorination aspects in biofouling control in power plant cooling water system, however, some of the alternatives to chlorination are also discussed below.

6.1. Physical methods

Physical methods are adopted essentially to prevent the entry of macroorganisms of certain size into the cooling conduits (Whitehouse et al., 1985). Screens of various mesh size (10 mm - UK and Japan, 4mm - France and Italy, 4 to 10 mm - Netherlands and 10 to 25 mm - India) are used at different locations like intake point and pump house to act as a first line of defence against large debris, seaweed, fishes jelly-fishes mussel clumps, barnacles, fishes, & other macro organisms (Satpathy, 1990). The use of screen themselves cause sometimes

problem as they become blocked by seaweed or Jellyfishes etc. Although, it prevents the entry of macro organisms, it cannot prevent entry of tiny larvae and thus the growth inside the cooling system.

6.2. Flow

The relative motion between cooling water and the substratum also determines the type and extent of fouling settlement. At high flow-rates the shear stress of the water often exceeds the shear strength of many organisms and this mechanism is used to control biofouling (Satpathy, 1990). For example in Italy at Vado Ligure, the cooling water intake of a power plant (1320 MW (e), four 2.2 m dia culverts of 1400-1500 m long) was kept fouling-free for 14 years by maintaining a velocity of 11 ft/sec (Whitehouse et al., 1985). Flow rates of 2.5-3.0 m/s will be necessary to prevent settlement of mussels, but already settled mussels are not detached at these flow rates. Moreover, it is operationally difficult to maintain such constant flow as above without any hiatus. Thus, during low flow or shutdown period, the settled organisms could not be detached even at higher flow than the above.

6.3. Heat treatment

It is well known that response of biological systems to temperature is very pronounced. Though metabolic activity increases with temperature up to a certain temperature, once the optimum temperature is surpassed metabolic activity of nearly all organisms gets affected adversely (Masilamani et al., 2002). Taking advantage of this temperature and metabolic activity relationship, biofouling control methods based on temperature changes have been used in power plant cooling systems (Whitehouse et al., 1985). This method is routinely used in a few plants in USA, England, Italy, Netherland and Russia. Heat treatment for macrofouling control has been used for biofouling control (Fisher et al., 1984). Here the heated effluent from the condenser is diverted through the intake tunnel which when passed through the condenser picks up more heat. By manipulation of this heated water through different parts of the cooling system for a specified period, killing of the biofoulants is achieved. It appears that 40° C for one hour is enough to eliminate mussel and other fouling organisms. The duration and temperature is given by the equation below.

$$T = 50 - 2.46 \ln t$$

(T= temperature (°C) required to kill the foulants during heat treatment period of 't' minutes)

The disadvantage of this treatment are (a) power station has to operate at reduced power level during the period of treatment (b) this cannot be tried in existing power station where the system is not designed & (c) it cannot control slime in the condensers. Since it has been proved economical in temperate countries, it should be more economical in tropical countries wherein the organisms are already living close to their lethal temperature limit. However, it has not been popular ever since its inception possibly. In this method the organisms are killed rather than controlled, thus ecologically not benign.

6.4. Mechanical methods

Both manual and mechanical methods such as Taprogge, Amertap system and MAN system (Satpathy, 1990) have been used to keep microfouling under control. In all these system scouring action of sponge rubber ball or MAN brushes clean the condenser tubes when passed through it intermittently or continuously. These methods have not been popular as they are only useful for microfouling control in condenser section and moreover, its cost is prohibitive.

6.5. Osmotic control method

Most marine organism cannot tolerate salinity below 3 ppt (Satpathy et al., 1999) and below this salinity they are killed. Therefore settlement of marine organisms on cooling conduit surfaces can be controlled by varying the salinity.

6.6. Bromine based compounds

Chemistry of bromine has proved beyond doubt that bromine in different forms could be a simple, cost effective alternative to chlorination for biofouling control (Satpathy, 1990). Although bromine is delivered in different practical forms, it is the hypobromous acid (HOBr) which is formed during hydrolysis that is responsible for the biocidal action. Bromine chloride is more attractive as a biocide because of the following advantages: (i) rapid residual decay benefits the environment and also causes lower condenser corrosion rates, (ii) high solubility, (iii) high density that permits large amounts of liquid BrCl to be supplied in small container, (iv) viability in a broad temperature and pH range, (v) it is more economical if the cost of maintaining EPA regulation of discharge limit is taken into account.

6.7. Ozone

Ozone is well known for its value as a bactericidal agent (Nair et al., 1997). It is an extremely strong oxidant compared to chlorine. It is very effective due to its high oxidation potential. It is also less toxic and less persistent than chlorine. Unlike chlorine it does not contribute to the chloride content of the cooling water nor does it generate undesirable byproducts and therefore, is environmentally more acceptable. The potential of ozone for biofouling control has been tried at Public Service Electric & Gas plant, New Jersey sites. Disadvantages like (i) difficulty to achieve uniform distribution, (ii) high ozone demand in presence of bromide as well as in polluted water, (iii) ozoniser occupying large space (lack of compressibility) & necessity for on-site generation and (iv) high cost have restricted the use of ozone largely for treatment of potable water and sewage in Europe. Moreover, there is very little information available on the possible corrosion of condenser tubes. Like chlorine ozone also is affected by pH, temperature, and organics.

6.8. Bioactive compounds

There may be no greater way to fight nature than with nature itself; it is important to study fouling organisms biology in order to help prevent them from becoming a nuisance. Nemertine pyridyl alkaloids (chemical compounds from worms) may be used for the inhibition of *Balanus amphitrite* (barnacle) larvae. Studies in Caribbean sponges have shown that purified, extracted compounds from them deter bacterial attachment. Since bacterial

attachment is often the initial step of the biofouling process, these sponges and their chemistry may help to prevent the succession to larger organisms. A member of the ascidian group, *Distaplia nathensis*, is also showing promise - used in an extract, it inhibits byssal production in the mussel *Perna indica* (Murugan and Ramasamy, 2003). A byssus is a mass of filaments which the mussel uses to attach itself to a surface. Dark brown bacteria provide the best attachment for oyster larvae, but there are other bacteria which produce polysaccharides that are toxic to oysters; in other words, they may be used to prevent biofouling by oysters. Immunoglobulins provide a natural biocide for planktonic and sessile bacteria. Some species of bacteria can be used against other biofouling organisms. *Pseudoalteromonas* spp., marine bacteria, produces bioactive compounds with an inhibitory effect and can be used to prevent biofouling by algae like *Ulva lactuca* and by barnacles like *Hydroides elegans* and *Balanus amphitrite*. Extensive research is still needed to determine the exact method of applying this knowledge.

6.9. Other control agents

Iodine, hydrogen peroxide, potassium permanganate and iron (VI), chlorine dioxide etc have been tried however, due to one or the other reason (no information on toxicity to aquatic life, corrosion aspect, and economical aspect); they have not been popular in power plant cooling system. Antifouling coatings made up of organometallic compounds and copper oxide and other types of paints have also been tried in power plant cooling systems for biofouling control. Commercial cuprous oxide formulation must provide a leach rate of $10 \mu\text{g Cu cm}^{-2} \text{ day}^{-1}$ (Little and De Palma, 1988). However, the highly toxic nature of paints like Tributyl tin oxide with leach rate of $1\text{-}5 \mu\text{g Sn cm}^{-2} \text{ day}^{-1}$, which leads to reversal of sex, "imposex" in some aquatic organisms, has led to ban of metal based paints giving rise to the demand of low surface energy silicon based paints. Copper has not been popular due to high cost, operational difficulty and short life span. Acrolein, an effective antifouling agent but is expensive, highly toxic and also highly flammable (Satpathy, 1990).

Settlement of fouling organisms in the seawater intake tunnel is generally controlled by chlorination (~ 0.5 ppm residual). However, when the tunnel is ready and waiting for the chlorination plant to become operational, which generally extends from a few months to a year or two, there is a need to keep the tunnel free from fouling during this period. Thus, antifouling coating could be the only plausible method to combat fouling inside the tunnel/pipe, conveying cooling water from intake to pump house, during this gestation period. In view of this, a study was carried out to screen three different antifouling paints (Nukote, Paint-2 and Sigma Glide), for their biofouling control potential with the objective of assessing temporal variations in settlement pattern, growth rate, biomass and area coverage by fouling organisms. The results of three different proprietary antifouling paints which were assessed for their biofouling control potential in PFBR tunnel are given below. Panels were exposed to coastal waters by suspending them from MAPS jetty and were retrieved after a specified time. During each retrieval total biomass, type of organisms settled and area coverage were assessed (Table 4).

Important observations

- The Nukote paint was found more prone to biofouling and the attachment of organisms was found to be with strong adhesiveness as compared to other two paints. The area coverage attained 100% just after a period of 17 days of exposure and the panel remained fully covered throughout the 5 months study period (Fig. 12).

- Bio-growth on Paint-2 was found to be relatively less as compared to that of the Nukote paint and 100% area coverage was observed only after 66 days of exposure. Biomass was found to be relatively low in almost all the observations as compared to that of the Nukote paint. The area coverage reduced significantly from about 95% on 37th day to about 40% on 45th day (Fig. 12). This was due to the easy peeling off of the organisms from the panel surface. One of the most important observations was that barnacles grew on the base metal of the panel by penetrating the paint coating (Fig. 13) and thus adversely affected the panel integrity.
- Rate of bio-growth on Sigma Glide was the highest as compared to the other two paints. However, it showed a unique behaviour of detachment of organisms very easily as compared to the other two paints (Fig. 13). The area coverage did not attain 100% during the 35 days of study. This indicated that, the adhesiveness of organisms attached to the panels coated with paint-2 and Sigma Glide was relatively weak. Thus it would get peeled off in a dynamic cooling water system (during flow) and as well as in presence of chlorine.

From the above observations it was concluded that Sigma Glide showed promising positive results for its use against biofouling in a typical cooling water system (tunnel) for a limited time period.

Day	Biomass (g/100 cm ²)			Area coverage (%)		
	Nukote	Paint-2	Sigma Glide	Nukote	Paint-2	Sigma Glide
7				25	15	25
15	11.1	8.0	8.8	90	60	50
31	18.7	18.4	45.4	100	80	90
37	19.7	16.7	54.6	100	95	90
45	19.0	15.8		100	40	
52	18.7	9.8		100	60	
66	41.0	41.0		100	100	
80	26.3	34.3		100	70	
108	27.3	36.0		100	90	
122	33.2	45.0		100	40	
150	68.2	76.6		100	70	

Table 4. Temporal variations in biomass and area coverage of biofouling organisms on panels coated with different antifouling paints

The adverse effects of ionising radiation on biological systems were evident since its discovery (Satpathy et al., 1999). Therefore, attempts were made to dope radioactive materials into antifouling coating. Studies carried out using Thallium-204 radioisotopes demonstrated significant antifouling capability of this material. However, the dosage required (20 rads/h) was considered to be too high for comfortable handling by untrained operators (Satpathy, 1990). Nuclear power plants, which have highly trained operators in handling radioactive materials, could consider this as a viable technique for control of biofouling.

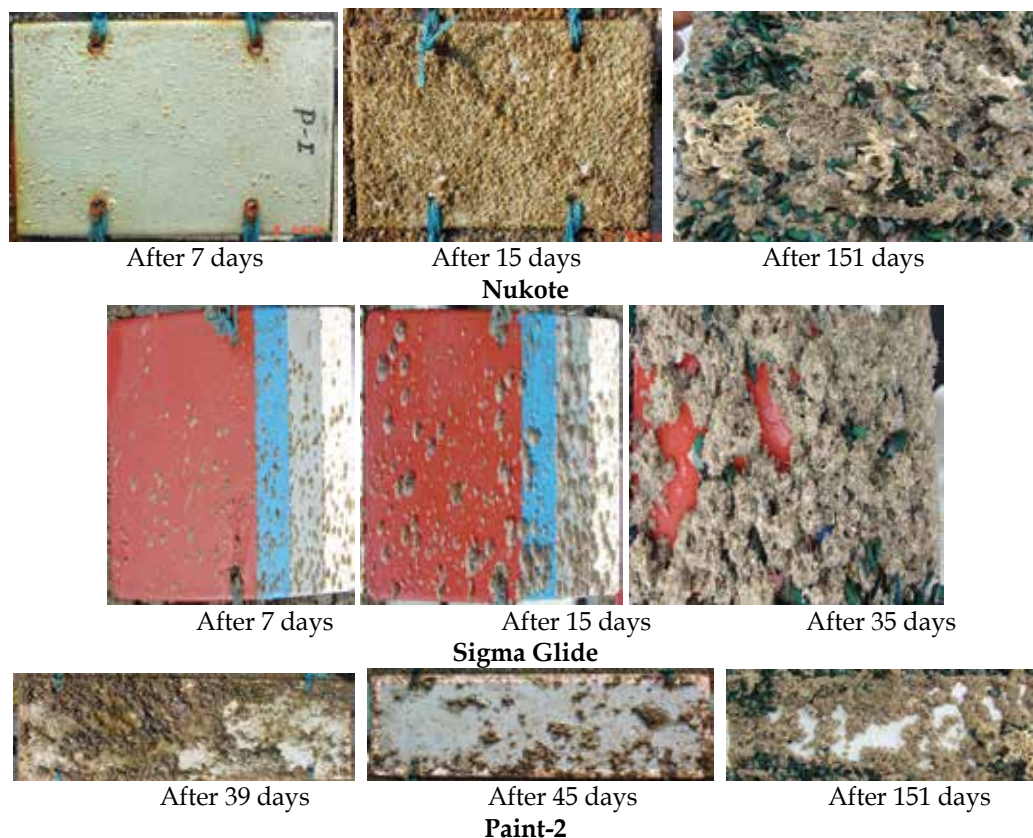


Fig. 12. Growth of fouling organisms on panels coated with antifouling paints with different exposure periods

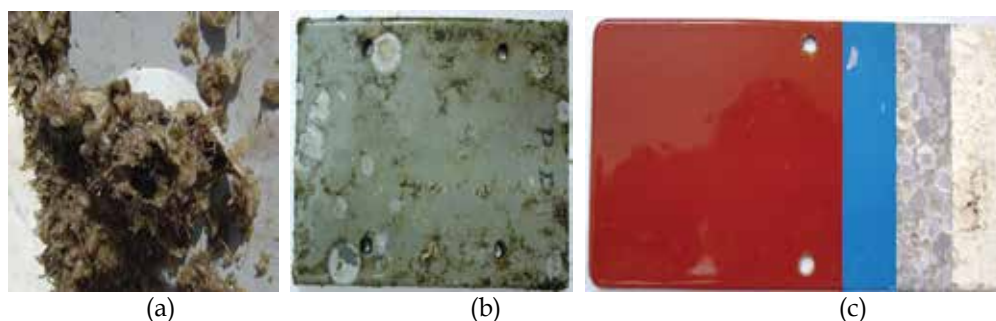


Fig. 13. (a) Penetration of barnacle through the paint coating (Paint-2), (b) after removal of bio-growth (Nukote-151 days old) and (c) After removal of bio-growth (Sigma Glide-35 days old)

6.10. Chlorine

Although alternative biocides are available, chlorine still remains the most common method for biofouling control in cooling water systems and is often preferred to others because of its

proven effectiveness, easy availability and relatively low cost. An approximate comparison of cost difference of biocides has been made and given in **Table 5**. It is used to overcome both slime in the condenser and macrofouling in the pre-condenser sections. However, the exact mechanism of biocidal action of chlorine or any other oxidizing biocide still remains an academic puzzle. Theories proposed by various workers have been described in detail by White (1972) and Rippon (1979). The basic principle is when an oxidizing agent diffuses through the cell wall of an organism, it oxidizes the enzyme groups preventing further metabolic activity and thereby bringing about death to the organism. In case of macroorganisms the death is brought about by the reduction in growth by means of decrease in filtration rate and consequent decrease in food availability combined with pathological effects (Masilamani et al., 2002).

Both microfouling and macrofouling can successfully be controlled by intermittent and low dose continuous chlorination respectively. Although, environmental stipulations due to the toxic effects of the by-products formed during chlorination are some of the recent barriers for its continuance, it has also safety problems currently encountered particularly with respect to its operations. Chlorination has not been fully successful as safety associated with transport; storage & handling of chlorination plant have come in its way. To overcome this, in-situ generation of chlorine by electro-chlorination has come very handy to power plant authorities. In this process according to the need chlorine is generated at the cooling water intake site and added then and there. A few plants in India (Tata Thermal, Mumbai, & NTPC, Viskhapatanam) have adopted this state-of-the-art mode and are successful in smooth operation of chlorination plant. In addition, uniform distribution has been another problem and needs an R & D effort to design such system. Although, it is easier said than done, a good amount of R&D work is essential before a precise chlorination regime is put into pragmatic use. This section discusses in details the chemistry of chlorination such as chlorine demand, chlorine decay, break point chlorination, speciation of chlorine residual and role of temperature and ammonia on chlorination in biofouling control. Moreover, targeted chlorination is also discussed briefly.

Chlorine (gas)	1
Chlorine (electrochlorination)	2.5
Sodium hypochlorite	5.0
TBTO	0.8
Tin	0.2
Ozone	high
Bromine chloride	2.5
Chlorine dioxide	5.0
Chlorinated Bromide salt	10.0
Organic biocides	very high
Iodine	40.0

Table 5. Cost comparison of different biocides (arbitrary units)

6.10.1. Chemistry of Chlorination

Chlorine when added to water almost instantaneously forms hypochlorous acid (HOCl).



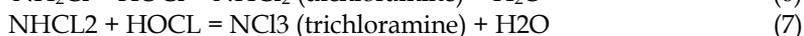
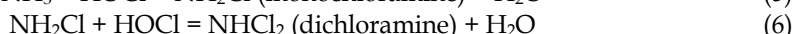
This HOCl is largely responsible for the biocidal action of chlorine. The possible mechanisms of biocidal action of chlorine is based on the basic principle that HOCl easily penetrates through the cell wall of the organism, and being an oxidizing agent, oxidizes the enzyme groups responsible for the growth of the organisms and bring about death in the case of micro organisms. However, in the case of macro-organisms in addition to cellular damages, the process of death is also accelerated by the reduction in growth, decrease in filtration rate, decrease in food availability, as well as pathological effects. HOCl being a weak acid it undergoes partial dissociation to give H⁺ and OCl⁻.



This equilibrium is pH dependent and so also the fraction of total chlorine present. It is known that HOCl is a better biocide than OCl⁻ due to its (a) electrical neutrality, (b) structural similarity with that of water facilitating easy penetration through cell wall and (c) the process of penetration being more of a physical process than a chemical one requiring less amount of energy. Thus, from the point of view of efficiency of treatment it is beneficial to have more amount of undissociated HOCl in the cooling water in order to exploit the total potential of chlorine as a biocide. If cooling water happens to be seawater, the pH of which is about 8, when chlorine is added to seawater a little more than 80 % of the total chlorine will be present as OCl⁻ (**Fig. 14a**). However, the presence of about 65 mg of bromide per kg of seawater compensates this disadvantage. HOCl gets converted to HOBr as follows (Venkateswarlu, 1990):



A major portion (75 %) of HOBr remains undissociated at seawater pH (**Fig.14b**). Thus, in seawater it is the bromine species which plays a significant role as a biocide after the addition of chlorine. Moreover, the conversion of HOCl to HOBr in seawater is pH dependent as evident below (**Table 6**). It is important to have knowledge on HOBr conversion kinetics (Goodman, 1987), which would facilitate the location of chlorine injection point in order to achieve 100% HOBr conversion. Molecular chlorine, hypochlorous acid, hypobromous acid, hypobromite and hypochlorite ions are called free chlorine (oxidant) (White, 1972). In stead of free or combined chlorine or bromine it is appropriate to use the term free residual oxidant, combined residual oxidant and total residual oxidant due to the existence of one or more species at a given time. However, for convenience sake the former is used in this chapter. Almost all natural waters contain ammonia or amines which combine with chlorine to give chloramines and bromamines and they are called combined chlorine (equation 5-7). Although, they have biocidal action however, the magnitude is significantly lower than that of free chlorine (White, 1972).



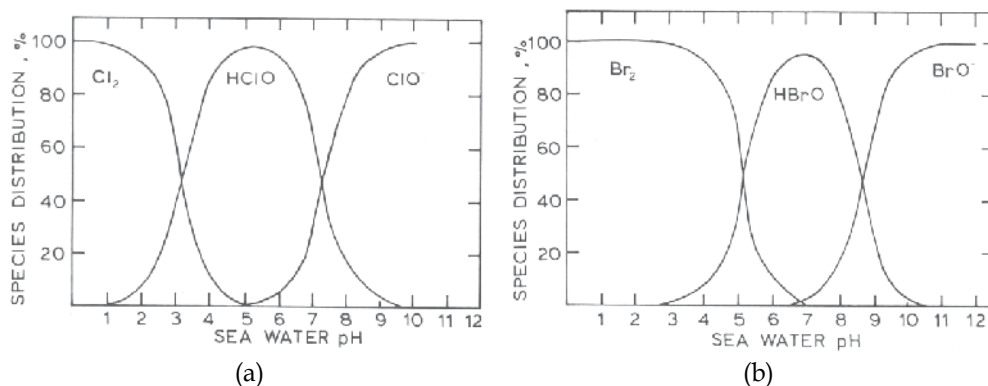


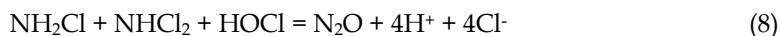
Fig. 14. Distribution of chlorine (a) and bromine (b) species with pH

The combination of both free chlorine and combined chlorine is called total residual chlorine or total residual oxidants. In this regard, it is worthwhile to maintain here that biofouling organisms settled inside a cooling system could affect the efficiency of chlorination as they produce ammonia as their excretal product. A variation of ammonia production with different size of mussel at two different temperatures is given in Fig. 15a. The amount of mono, di- and tri- chloramine present in the water during chlorination depends on pH and NH_3 content of cooling waters. The effectiveness of various chlorine species with regard to their biocidal action to organisms follows the following order, free chlorine > hypochlorite ion > chloramines

pH	Time, s
6	2
7	3
8	10
9	80

Table 6. Kinetics of HOBr conversion with pH (Goodman, 1978)

In water containing ammonia nitrogen, a typical reaction occurs called break-point reaction. The formation of mono, di- and trichloramine depends on chlorine to NH_3 ratio. If Cl_2 to NH_3 ratio (molar) < 1, formation of mono- chloramine takes place, when this ratio exceeds 1, dichloramine is formed and finally when it exceeds 1.5 trichloramine is formed. However, mono-, di- and trichloramine using a reaction give rise to disappearance of chlorine by the following equation.



The striking feature of this reaction is that even when initial chlorine concentration is increased, the total residual chlorine concentration is decreased due to the above reaction. The point where total residual chlorine reaches a minimum in the curve is called break-point. A typical break point curve is given in Fig. 15b. After this point most of the residuals are free residuals and it increased with increased chlorine dose. This phenomenon is very important in the context of disinfection of drinking water and also in the case of shock chlorination. That is a chlorine dose, beyond break point chlorination is advisable to achieve a very high disinfection factor.

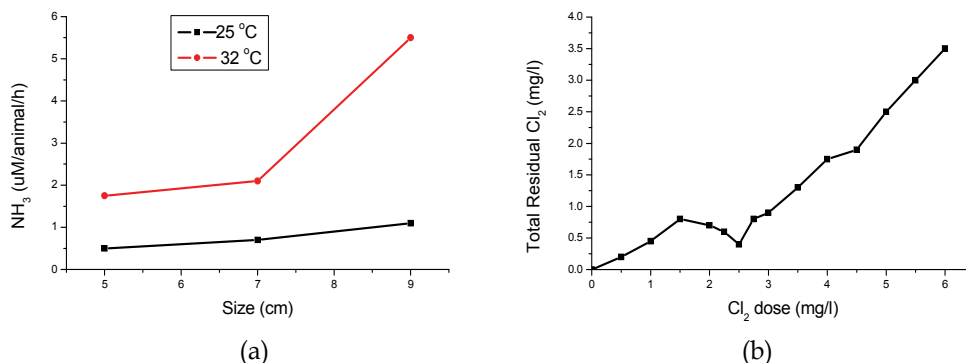


Fig. 15. Variations of ammonia production with different sizes of mussels at two different temperatures (a) and a typical break point curve (b)

To eliminate already established fouling community, shock chlorination is used. Moreover, sometimes during very low flow or no flow situation, the cooling water is soaked with chlorine for a specified time to kill the settled fouling community and the process is called soak chlorination.

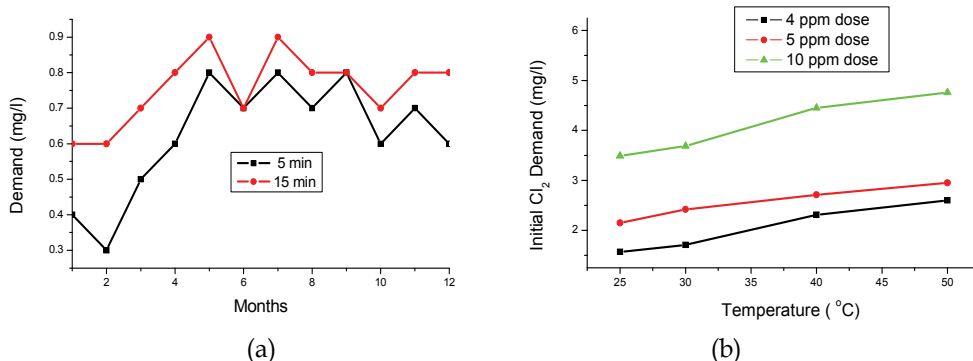


Fig. 16. Monthly variations of chlorine demand in the coastal water of Kalpakkam (a) and interrelation between temperature and chlorine demand

Chlorine can also disappear through reactions with reducing inorganic compounds such as S⁻, Fe⁺⁺ and NO₂⁻ and gets itself reduced to chloride. It also can react with organic materials by substitution forming chloro-organic compounds and also can oxidize them, converting them to another higher oxidation level compound or decomposed into CO₂ and H₂O. These reactions are called chlorine demand reactions and this amount of chlorine is not available for biocidal action (White, 1972). This chlorine demand among others mainly depends on time of contact, temperature, chlorine dose, and more importantly the quality of the cooling water which varies from month to month and even day-to-day depending on the location. It is essential to have a

full knowledge of the chlorine demand of cooling water for a period of at least two years, so as to avoid under chlorination as well as over chlorination (Venkateswarlu, 1990).

Seawater samples from PFBR site were collected and were dosed with 1 mg l⁻¹ and 10 mg l⁻¹ standard chlorine solution (prepared from bleaching powder). The iodometric method as described by White (1972) was employed for the determination of residual chlorine after different contact times (5, 30, minutes). Similarly, for 10 ppm chlorine dose residual chlorine was measured after 5 & 15 minutes. A typical example of monthly variations of chlorine demand in cooling water is given in Fig. 16a. It clearly depicts that to maintain a particular residual at the outlet of the cooling water throughout the year; a variable dose is essential rather than a constant one which is generally adopted. Moreover, the dependence of temperature on chlorine demand is explained in Fig. 16b.

Chlorine demand at low doses: Chlorine demand results showed that the demand varied widely from a minimum 0.3 to a maximum 0.9 mg l⁻¹. The variation clearly pointed out that different amount of chlorine has to be added to the cooling water during different months to maintain a particular residual for effective biofouling control and minimal damage to the environment. The results also showed that the demand increased with increasing time (Fig. 16a) indicating that during relatively longer residence time (shut down period) appropriate quantity of Cl₂ has to be added to maintain the residual taking long duration and low flow rate into account. The duration of demand study is decided based on the residence time, the cooling water spends inside the cooling water system.

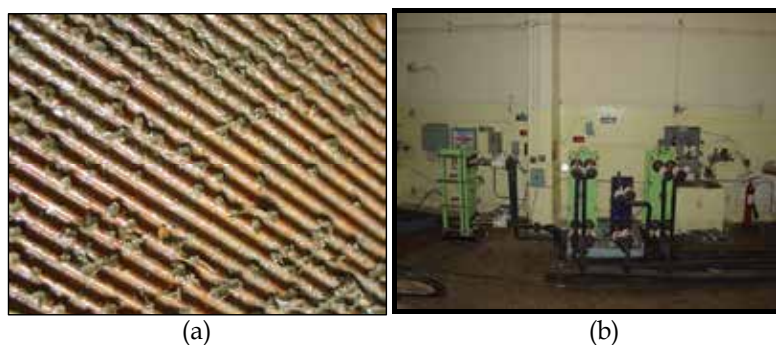


Fig. 17. A view of a plate heat exchanger (a) & the plate heat exchanger facility at MAPS (b)

Chlorine Demand at 10 ppm doses: The Process Seawater Heat Exchanger (PSWHX) of PFBR is going to be plate type instead of tube type, which is being used at MAPS. Unlike tube type, which has got a gap of about 25 mm diameter, the gap between any two plates in plate type of heat exchanger is very small (3 to 4 mm). A pictorial view of Titanium plate heat exchanger & biogrowth on it is shown in Fig. 17. Considering the bio-growth potential of seawater at Kalpakkam, there is every likelihood that PSWHX would get into severe biofouling unless proper remedial measures are taken. In view of this, a new regime called targeted chlorination (Chow et al., 1987) with relatively high dose (10-20 ppm) and short duration (10-20 min) has been suggested to overcome this problem. In this context, the chlorine consumption in the side reaction at 10 ppm dose and short duration (5 and 15 minutes) has been carried out. The result (Fig. 18) showed that 10 to 25 % chlorine is consumed during this short period leaving the remaining for bio-fouling control in the plate HX. To precisely and accurately decide the dose

and duration, a dynamic loop has been set up with facility to carry out experiments at different flow rates for biofouling control in PSWHX.

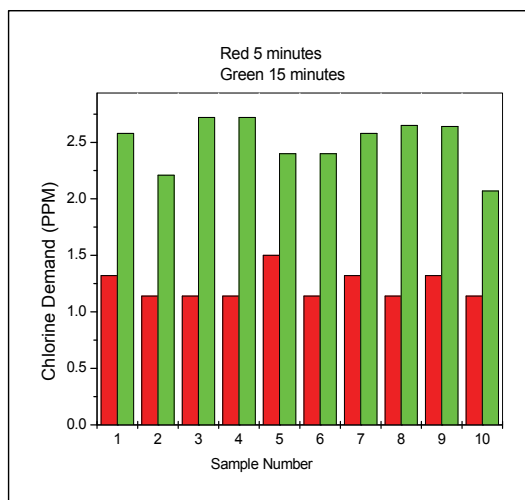


Fig. 18. Chlorine demand for 10 ppm dose for 5 and 15 minutes contact time

6.10.2. Macrofouling control

To overcome the problem of macro fouling, long term low level continuous chlorination is usually used and such a practice is also effective in the control of condenser slime. This was originally started at Carmarthen power station U.K. The dose employed is insufficient to kill mussels but sufficient to create an environment to deter them from settling in the cooling water system and to cause them to move out (and hence the term exomotive chlorination) (Beauchamp, 1966; Garey, 1980; and Kasper and Taft, 1984). Exomotive chlorination is found to be economical and relatively harmless to important nontarget commercial organisms. Some of the chlorination schedules being practiced in operating power stations are given in **Table 7**. Owing to the safety problem associated with the transport and storage of liquid chlorine, there have been attempts to look for alternative sources of chlorine. Other sources such as liquid hypochlorite solution and chlorine from electrolysis of brine of seawater have been tried in UK, USA, France and Italy (Whitehouse et al., 1985). Transport and storage of hypochlorite solution as well as some safety risks have become stumbling blocks for its use. Though safety problems are eliminated in electrochlorination, other drawbacks such as considerable financial investment, (capital cost 50 % and production cost 20 % higher than liquid chlorine), as well as difficulties in maintenance of particular residual levels (due to varying seasonal chlorine demand) remain. There are also safety problems associated with the production of large volumes of hydrogen gas and poor efficiency of the electrolysis process at lower temperature which made electrochlorination not very attractive. A recent successful use of a combination of copper and chlorine has been reported by both CEGB and EPRI. Results of both showed that the chlorine and copper system was at least 6 times as effective as chlorine alone against macrofouling and three times as effective against microfouling (Strauss, 1989). Three major common problems associated with the use of chlorine irrespective of its source are: (i) safety associated with transport and storage (ii) long term potential threat to marine life and (iii) carcinogenicity of chloroorganics which are produced

during chlorination (Brungs, 1977; Fiessinger et al., 1985; Saravanane et al., 1998, Satpathy et al., 2008). Whitehouse (1975) gives a detailed account of the effect of chlorine on aquatic life.

Location	Chlorination Schedules	Sources
Kansai Electric Power Company, Japan	0.0-0.2 ppm residual continuous.	Kawable et al.,1987
Tanagawa Power Station, Japan	0.5 ppm residual 4 times per day for 1 hr.	Kawable et al.,1987
Carmarthen Bay Power Station, UK.	0.02-0.05 ppm residual continuous.	James,1967
France	1 ppm dose	Whitehouse et al.,1985
Maps, India	0.5 ppm residual continuous	Namboodiri, 1987
Le Havre, Italy	0.5 ppm dose continuous.	Whitehouse, et al., 1995
Coastal Station in the UK	continuous low level chlorination	Whitehouse, 1978
Netherlands.	0.2 ppm free available halogen just before condenser, once in 4hrs. for 4 hrs	Jenner, 1983

Table 7. Chlorination practice being followed at different operating power plants.

In 1982 EPA guideline stipulated that chlorine discharge from power plants should not be more than 0.2 ppm for 2 hours as total residual chlorine or total residual oxidant (Rittenhouse, 1987). Recent EPA recommendation sets acceptable total chlorine limits at 0.05 mg/1 for a period of 30 minutes in any 24 hour period. The environmental pollution prevention agreement in Japan stipulates that residual chlorine levels at the water outlets must not be detectable (Kawabe et al., 1986). Sometimes an abundance of ammonia and a high pH (>8) make biofouling control with chlorine very difficult (Chiesa and Geary, 1985). At slightly higher doses chlorine also accelerates corrosion of Cu and mild steel particularly at higher velocity (Stone et al., 1987, Reiber et al., 1987 and Pisigan and Singley, 1987).



Fig. 19. Mussel valve monitoring experimental setup and a mussel with sensors attached

Although low level continuous chlorination appears to be a panacea for controlling bivalves, pulsed biocide dosing, a new concept has been proposed as a more effective tool than the former. Bivalves, as soon as it senses biocide, closes its shells and so also filtration, a process solely responsible for feeding and respiration of these organisms. They tend to open their shells after a certain period of time and immediately close if the biocide presence in water continues. Thus, instead of chlorinating continuously, chlorine can be injected at intervals coinciding with the closing and opening intervals of the mussel shell to take advantage of this behaviour. Knowledge on this closing and reopening of mussels will be useful for deciding the optimum frequency of pulsed biocide dosing so that operational cost and environmental damage due to biocide is minimised. However, this interval is not generic and information on the same is not

available in literature. A micro-sensor based magnetic reed relay (**Fig. 19**) has been designed and developed to sense the opening and closing of the mussels. Once standardised, it could be implemented to reduce operational cost and save the environment.

6.10.3. Microfouling/ Slime control

Microbiological fouling in cooling water is caused by biofilms. The biofilms are loose configurations of many different kinds of bacteria; a slimy substance they produce called exopolysaccharide (EPS) holds it all together. Biofilms, which cause dental cavities and diseases such as cystic fibrosis, are ubiquitous in virtually all kinds of water piping. In industrial processes, biofilms can cause corrosion and seriously affect flow, pressure drop, and the efficiency of heat transfer from metal surfaces. In the case of slime control, chlorine is used on the basis of two principles, (i) let the slime accumulate for a predetermined length of time, then start chlorination for a period during which the adhesive slime forming organisms will be killed and then washed away by the velocity of water, (ii) the interval between successive treatment should not be long enough for the accumulated slime to attain a thickness, which will interfere with heat transfer. A variation in biofilm thickness with time in the coastal water of Kalpakkam is shown in **Fig. 20a**. Such a practice involving operation of chlorination at pre-determined intervals for a specified duration (usually 30 minutes) is known as intermittent chlorination. Frequency is determined by the above two factors. Duration is decided by the turnover time for the cooling system. Magnitude and type of residual chlorine (free or total) is decided by the type of slime. The point of chlorine application should be located as close as possible to the inlet of the heat exchanger to take care of the free chlorine component of the residual. It is important that the kinetics of speciation of residual chlorine is studied for cooling water so as to decide the location of injection. **Fig. 20b** shows the variation in residual chlorine speciation with time.

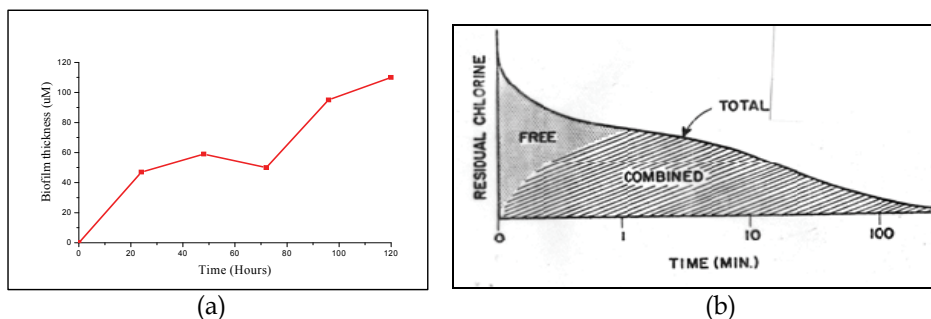


Fig. 20. Rate of biofilm formation in the coastal waters of Kalpakkam and speciation of residual chlorine with time

7. Conclusion

Chlorination for biofouling control in cooling water system was initiated way back in 1924. Even after eight and half decades, chlorine remains the most widely used biocide for biofouling control barring a few cases wherein other propriety chemicals have crept in. It appears that under the present known knowledge and economical viability it will still continue to rule the roost. Thus, its chemistry for cooling water is studied well before it is applied to cooling water. In the present study, seasonal variation in chlorine demand was observed. Therefore, it is essential that the

chlorine demand values are quantified precisely and accurately so that under and over chlorination is avoided. Moreover, the operational cost of chlorination is optimized so that with minimum Cl_2 , maximum biocidal efficiency is achieved. Although, other methods have been proved to control biofouling in laboratory scale, they have not been able to replace chlorine in plant scale.

Life supporting activities such as respiration, feeding, metabolism and excretion of the biofoulers settled inside the cooling water system could considerably alter the cooling water quality both chemically and biologically affecting the control regime adversely. Results of settlement pattern of biofouling organisms reveal that, before attempting to finalize the control regime (mode, frequency, duration etc), a thorough knowledge on the type of organisms, their breeding pattern, climax species etc is essential.

8. References

- Anil, A. C. & Wagh, A. B. (1988). Aspects of biofouling community development in the Zuary estuary, Goa, India. In: *Marine biodeterioration: advanced technique applicable to the Indian Ocean*, M. P. Thompson, R. Sarojini, & R. Nagabhushanam, (Eds.), 529-537, Oxford & IBH publishing (P) Ltd., New Delhi, India
- Anil, A. C.; Chiba, K. & Okamoto, K. (1990). Macrofouling community structure and ecology of barnacles in Hamana Bay (Japan), *Biofouling*, 2, 137-150
- Babu, M. T. (1992). Equator-ward western boundary current in the Bay of Bengal during November-December 1983, *Physical Processes in the Indian Seas (Proceedings of First Convention, IASPSO)*, pp. 57-62
- Beauchamp, R. S. A. (1966). Low level chlorination for the control of marine fouling. C.E.G.B. Report no. RD/L/M 147, 1-7
- Bhosle, N. B.; Nandkumar, K. & Wagh, A. B. (1989). Influence of particulate matter on microfouling biomass in the Arabian Sea, *Biofouling*, 2, 65-74
- Brankevich, G.; Bastida, R. & Lemmi, C. (1988). A comparative study of biofouling settlements in different sections of Necochea power plant (Quequen port, Argentina), *Biofouling*, 1, 113-135
- Brungs, W. A. (1977). General consideration concerning to the toxicity to aquatic life of chlorinated condenser effluent, In: *Biofouling control procedures; technology and ecological effects*, L.D. Jensen, (Ed.), 109-113, Marcel Dekker, New York
- Brungs, W. H. (1973). Literature review of the effects of residual chlorine on aquatic life, *Journal of Water Pollution*, 45, 2180-2193
- Carpenter, R. C. (1990). Competition among marine macroalgae: a physiological perspective, *Journal of Phycology*, 26, 6-12
- Chadwick, W. L.; Clark, F. S. & Fox, D. L. (1950). Thermal control of marine fouling at the Redondo stem station of southern California Edison Company, *Transactions American Society of Mechanical Engineering*, 72, 127-131
- Chalmer, P. N. (1982). Settlement patterns of species in a marine fouling community and some mechanisms of succession, *Journal of Experimental Marine Biology and Ecology*, 58, 73-86

- Chen, J. C.; Chen, C. T. & Cheng, S. Y. (1994). Nitrogen excretion and changes of haemocynine, protein and free amino acid levels in the haemolymph of *Penaeus monodon* exposed to different concentrations of ambient ammonia- N at different salinity levels, *Marine Ecology Progress Series*, 110, 85-94
- Chiesa, R. & Geary, D. (1985). Evaluation of alternative chemicals for power plant condenser biofouling control, *Proceedings of 46th Annual meeting, International Water Conference*, ICW 85-42, pp. 1-10, Pittsburgh
- Chow, W. (1987). Targeted chlorination schedules and corrosion evaluations, American Power Conference, Chicago
- Clarke, A.; Thomas, E. P. & Whitehouse, M. J. (1994). Nitrogen excretion in the Antarctic limpet *Nacella concinna* (Strebel, 1908), *Journal of Molluscan Studies*, 60, 141-147
- Collins, T. M. (1964). A method for designing seawater culverts using fluid shear for the prevention of marine fouling. CERL Report no. RD/1/N93/64, 1-5
- Corpe, W. A. (1984). The microfouling problem and the future of the ocean thermal conversion program, *MTS Journal*, 13, 21-25
- Coughlan, J. and Whitehouse, J. (1977). Aspects of chlorine utilization in the UK, *Chesapeake Science*, 18, 102-111
- Crisp, D. J. (1961). Territorial behavior in barnacle settlement, *Journal of Experimental Biology*, 38, 429-446
- Dahlem, C.; Moran, P. J. & Grant, T. R. (1984). Larval settlement of marine sessile invertebrates on surfaces of different colour and position, *Ocean Science and Engineering*, 9, 225-236
- Daling, P. M. & Johnson, K. I. (1985). Current status of biofouling surveillance and control Techniques, *Bivalve fouling of nuclear power plant service water systems*, NUREG/CR-4070, PNL-5300 U.S. NRC, Washington, D.C.
- Darby, J. B. Jr. (1984). Ocean thermal conversion material issues, *Journal of Materials for Energy Systems*, 6, 130-137
- De Souza, S. N.; Naqvi, S. W. A. & Reddy, C. V. G. (1981). Distribution of nutrients in the western Bay of Bengal, *Indian Journal of Marine Sciences*, 10, 327-331
- Drake, R. C. (1977). Increasing heat exchanger efficiency through continuous mechanical tube maintenance, In: *Biofouling control procedures; technology and ecological effects*, L.D. Jensen, (Ed.), 43-53, Marcel Dekker, New York
- Duke Power Co. 1981, Letter from W.O. Parker to J.P. O'Reilly transmitting Duke Power company's response to the NRC IE Bulletin 81-03 for the McGuire Nuclear Plants
- Fiessinger, F.; Rook J. J. and Duguet, J. P. (1985). Alternative methods for chlorination, *The Science of Total Environment*, 47, 299-315
- Fisher, E. C. (1984). Technology for control of marine biofouling - a review. In: *Marine biodeterioration- an interdisciplinary study*, J. D. Costlow, (Ed.), 261-290, Naval Institute press, Annapolis Maryland
- Garey, J. F. (1980). Selective alternatives to conventional chlorination, EPRI Report no EA-1588, 1-94
- Gleason, H. A. (1922). On the relation between species and area, *Ecology*, 3, 156-162
- Godwin, W. (1980). Ecology of the coastal fauna around Madras Atomic Power Plant, Ph. D. Thesis, University of Madras, Madras, India

- Goodman, P. D. (1987). Effect of chlorination on materials for sea water cooling system: A review of chemical reactions, *British Corrosion Journal*, 22, 65-62
- Haried, J. A. (1982). Evaluation of events involving service water systems in nuclear power plants, NUREG/CR-2797, ORNL/NSIC-207, U.S. NRC, Washington, D.C.
- Haugen, V. E.; Vinayachandran, P. N. and Yamagata, T. (2003). Comment on Indian Ocean: Validation of the Miami Isopycnic coordinate ocean model and ENSO events during 1958-1998, *Journal of Geophysical Research*, 108, 3179, doi: 10.1029/2002JC001624
- Henager, C. H.; Daling, P. M. & Jhonson, K. I. (1985). Factors that may intensify the safety consequences of biofouling, *Bivalve fouling of nuclear power plant service water system*, NUREG/CR 4070, U.S. NRC, Washington, Washington, D.C.
- Holems, N. (1967). Mussel settlement in the cooling water intake screens at the Poole power station, CERL Report No. RD/1/N/137/67, Leatherhead, Surrey
- Imbro, E. V. (1982). Engineering evaluation of the salt service water system flow blockage at the Pilgrim nuclear power station by Blue Mussels (*Mytilus edulis*), Office for analysis and evaluation of operational data, U.S. NRC, Washington, D.C.
- Imbro, E.V. & Gianelli, J.M. (1982). Report on service water system flow Blockages by Bivalvine Mollusks at Arkansas Nuclear one and Brunswick, Office for analysis and evaluation of operational data, U.S. NRC, Washington, D.C.
- Iwaki, T. & Hattori, H. (1987). First maturity and initial growth of some common species of barnacles in Japan, *Bull. Fac. Fish. Mie. Univ.*, 14, 11-19
- Iwaki, T.; Hibino, K. & Kawahara, T. (1977). Seasonal changes in the initial development of fouling communities in Matoya Bay, *This. Bull.*, 4, 11-29
- James, W. G. (1967). Mussel fouling and use of exomotive chlorination, *Chemical Industries*, 994-996
- Kajihara, T.; Hirano, R. & Chiba, K. (1976). Marine fouling animals in the bay of Hamana - kobe, Japan, *The Veliger*, 18, 361-366
- Karande, A. A.; Gaonkar, S. N. & Swami, B. S. (1986). Marine biofouling and its assessment in Indian waters, *Proceedings of 3rd Indian Conference on Ocean Engineering*, 2, pp. 21-35, IIT, Powai, Bombay, India
- Karande, A.; Srinivasan, A. K. & Viswanathan, R. (1983). Marine biofouling in sea water tunnel. NCML/ BARC Report, Bombay, India
- Kasper, J. R. & Taft, E. P. (1984). Macrofouling control at steam electric generating station- A case for continuous low level chlorination, *Proceedings of American Power Conference*, pp. 960-964, Chicago
- Kawabe, A. (1986). Effect of flow dynamics on attachment of marine organisms for copper and copper alloys seawater pipes, *Communication*, 53, 422-423
- Khandeparker, D. C.; Anil, A. C. & Venkat, K. (1995). Larvae of fouling organisms and macrofouling at New Mangalore port, west coast of India, *Indian Journal of Marine Sciences*, 24, 37- 40
- La Fond, E. C. (1957). Oceanographic studies in the Bay of Bengal, *Proceedings of Indian Academy of Sciences*, 46, 1-46
- Little, B. J. & De Palma, J. R. (1988). Marine Biofouling, In: *Materials for marine systems and structures*, D.F. Hanson, (Ed.), 90-121, Trans Tech Publications, Switzerland

- Masilamani, J. G.; Azariah, J.; Nandakumar, K.; Jesudoss, K.; Satpathy, K. K. & Nair, K. V. K. (2001). Excretory products of green muscle *Perna viridis* and their implication on power plant operation, *Turkish journal of Zoology*, 25, 117-125
- Masilamani, J. G.; Jesudoss, K. S.; Nandakumar, K.; Satpathy, K. K.; Nair, K. V. K. & Azariah, J. (2000). Jelly fish ingress: A threat to smooth operation of coastal power plants, *Current Science*, 79(5), 567-569
- Masilamani, J.G., Jesudoss, K.S., Nandakumar, K., Satpathy, K.K., Nair, K.V.K. & Azariah, J. (1997). Physiological response of the green mussel *Perna viridis* in relation to size and salinity. Proceedings of Indian Academy of Sciences, B63 (4), p305-314.
- Masilamani, J.G., Nandakumar, K., Satpathy, K.K., Jesudoss, K.S., Nair K.V.K. & Azariah, J. (2002). Lethal and sublethal responses of chlorination on green mussel *Perna viridis* in the context of biofouling control in power plant cooling system. Marine Environmental Research, 53(1), p65-76.
- Masilamani, J.G., Satpathy, K.K., Jesudoss, K.S., Nandakumar, K., Nair K.V.K. & Azariah, J. (2002). Influence of temperature on the physiological responses of the bivalve; *Brachidontes striatulus*. Marine Environmental Research. 53(1), p51-64.
- Miller, R. H. (1974). A note on the breeding season of three ascidians on coral reefs at Galeta in the Caribbean Sea, *Marine Biology*, 28, 127-129.
- Murugan, A. & Ramasamy, M. S. (2003). Biofouling deterrent activity of the natural product from ascidian, *Distaplia nathensis*, *Indian journal of marine sciences*, 32(2), 162-164
- Myint, U. M. & Tyler, P. A. (1982). Effects of temperature, nutritive and metal stressors on the reproductive biology of *Mytilus edulis*, *Marine Biology*, 67, 209-223
- Nair, K. V. K. (1985). Impact of nuclear power station on the hydrographical characteristics of Kalpakkam coastal waters, *Proceedings of Symposium on sea water quality demand*, pp. 13.1-13.10, NCML, Bombay
- Nair, K. V. K. (1987). Biofouling problems in cooling conduits of power stations. In: *Advances in aquatic biology & fisheries: Symposium to facilitate Dr. N.B. Nair*, 257-262, Kerala University, Trivandrum
- Nair, K. V. K.; Murugan, P. & Eswaran, M. S. (1988). Macrofoulants in Kalpakkam coastal waters, east coast of India, *Indian Journal of Marine Sciences*, 17, 341-343
- Nair, K. V. K.; Satpathy, K. K. & Venugopalan, V. P. (1997). Bio-fouling control: Current methods & new approaches with emphasis on power plant cooling water system. In: *Fouling organism of the Indian oceans, biology and control technology*, R. Nagbhusanam, (Ed.), 158-188, Oxford & IBH Publishing Company, New Delhi, India
- Nair, K.V.K.; Ganapathy, S. (1983). Baseline ecology of Edayur-Sadras estuarine system at Kalpakkam. I: General hydrographic and chemical feature, *Mahasagar*, 16, 143-151
- Nair, N. U. & Nair, N. B. (1987). Marine biofouling dynamics in and around the Cochin harbour. *Proceedings of National seminar on estuarine management*, Trivandrum, India

- Neitzel, D.A.; Johnson, K.I.; Page, T.L.; Young, J.S. & Daling, P.M. (1984). Correlation of bivalve biological characteristics and service water system design, In: *Bivalve Fouling of Nuclear Power Plant Service Water Systems*, Vol. 1, 1-119 U.S. Nuclear Regulatory Commission, Washington
- Nelson, W.G. (1981.) Inhibition of barnacle settlement by Ekofisk crude oil, *Marine Ecology Progress Series*, 5, 41-43
- Newell, R. I. E.; Hilbish, T. J.; Koehn, R. K. & Newell, C. J. (1982). Temporal variation in the reproductive cycle of *Mytilus edulis* L. (Bivalvia, Mytilidae) from localities in the east coast of the United States, *Biology Bulletin*, 162, 299-310
- Nuclear Regulatory commission. (1984). Power reactor events, NUREG/BR-0051, Vol.5, No.4. U.S. NRC, Washington, D.C.
- Paul, M. D. (1942). Studies on the growth and breeding of certain sedentary organisms in the madras harbour, *Proceedings of Indian Academy of Sciences*, 150, 1-42
- Pielou, P. P. (1966). The measurement of diversity in different types of biological collections, *Journal of Theoretical Biology*, 13, 131-144
- Pieters, H.; Kluytmans, J. H.; Zandee, D. I. & Cadee, G. C. (1980). Tissue composition and reproduction of *Mytilu edulis* in relation to food availability, *Netherlands Journal of Sea Research*, 14, 349-361
- Pisigan, R. A. Jr. and Singley, J. E. (1987). Influence of buffer capacity, chlorine residual and flow rate on corrosion of mild steel and copper, *Journal of American Water Works Association*, February, 62-70
- Portland General Electric Co. (1981). Letter from B.D. Witners to R.H. Engelken transmitting Trojan Nuclear Plant's Response to IE Bulletin 81-03
- Price, A. H.; Hess, C. T. & Smith, C. W. (1975). Observations of *Crassostria virginica* cultured in the heated effluent and discharged radionuclides of a power reactor, *Proceedings of National shellfish Association*, 66, 54-68
- Rains, J. H., Foley, W. J., & Hennik, A. (1984). Flow blockage of cooling water to safety system components by *Corbicula* sp. (Asiatic clam) and *Mytilus* sp. (mussel), USNRC, Report No. NUREG/CR 3054, Washington, D.C.
- Rajagopal, S.; Nair, K. V. K.; Velde, G. V. D. & Jenner, H. A. (1997). Seasonal settlement and succession of fouling communities in Kalpakkam, east coast of India, *Netherlands Journal of Aquatic Ecology*, 30, 1-17
- Rajagopal, S.; Sashikumar, N.; Azsariah, J. & Nair, K. V. K. (1991). Some observations on biofouling in the cooling water conduits of a coastal power plant, *Biofouling*, 3, 311-324
- Ramaraju, V. S.; Sarma, V. V.; Rao, P. B. & Rao, V. S. (1992). Water masses of Visakhapatnam shelf, In: *Physical processes in Indian seas (Proceedings of First Convention, ISPSO, 1992)*, pp. 75-78
- Rao, S. K. & Balaji, M. (1988). Biological fouling at Kakinada, Godavary estuary, Oxford IBH publisher, New Delhi, India
- Raymont, J. E. G. (1983). Plankton and productivity in the Oceans: Vol. II - Zooplankton, Pergamon press
- Reiber, S. H.; Ferguson, J. F. & Benjamin, M. M. (1987). Corrosion monitoring and control in the Pacific northwest, *Journal of American Water Works Association*, 79, 71-74

- Relini, G.; Bianchi, C. N. & Pisano, E. (1980). Macrofouling in the conduits of a middle Tyrrhenian power station, *Proceedings of 5th International Congress on Marine Corrosion and Fouling*, pp. 279-292, Madrid
- Renganathan, T. K. (1990). Systematics and ecology of Indian ascidians, In: *Marine Biofouling and power plants*, K. V. K. Nair & V. P. Venugopalan, (Eds.), 263-271, BARC, Bombay, India
- Richmond, M. D. & Seed, R. (1991). A review of marine macrofouling communities with special reference to animal fouling, *Biofouling*, 3, 151-168
- Rippon, J. E. (1979). UK Biofouling Control Practices, *EPRI symposium on biofouling in condensers*, 1-36, Atlanta, USA
- Rittenhouse, R. C. (1987). Biofouling/oil/additives: work ahead, *Power Engineering*, February, 8
- S. M. Stoller Corp. (1977). DG heat exchangers clogged with mussels- inadequate chlorination schedule, In: *Nuclear power experience*, Vol. PWR-2, Section VIII, subsection B, 40
- S. M. Stoller Corp. (1978). Service pump strainers damaged by Ice- excessive silt build up, In: *Nuclear power experience*, Vol PWR-2, section VIII, Subsection B, 50
- S. M. Stoller Corp. (1983). SW filter drive motor shaft key sheared, pump seized - Excessive debris, In: *Nuclear power experience*, Vol PWR-2, section VIII, Subsection B, 130
- Sahu, G.; Satpathy, K. K.; Laxmi, S.; Prasad, M. V. R.; Murthy, P. S. & Venkatesan, R. (2006). Spatial and temporal variation in phytoplankton community in the coastal waters of Kalpakkam and their impact on fouling, *Proceedings of Recent Advances in Marine Antifouling Technology*, pp. 538-552, Chennai, India
- Saravanane, N., Satpathy, K.K., Nair, K.V.K. & Durairaj, G. (1998). Preliminary observations on the recovery of tropical phytoplankton after entrainment. *Thermal Biology*, 23(2), p91-97.
- Saravanane, N.; Nandakumar, K.; Durairaj, G. & Nair, K. V. K. (2000). Plankton as indicators of coastal water bodies during southwest to northeast monsoon transition at Kalpakkam, *Current Science*, 78, 173-176
- Saravanane, N.; Satpathy, K.K.; Nair, K.V.K. & Durairaj, G. (1998). Studies on the recovery of entrained phytoplankton after passage through an atomic power station cooling circuits, *Journal of Thermal Biology*, 23, 91-97
- Sashikumar, N. (1991). Ecology and control of biofouling in a coastal power station with special reference to *Megabalanus tintinabulum* (L), Ph. D. Thesis, University of Madras Madras, India
- Sashikumar, N.; Nair, K. V. K. & Azariah, J. (1990). Colonization of marine foulants at a power plant site, *Proceedings of Indian Academy of Sciences*, 99, 525-531
- Sashikumar, N.; Rajagopal, S. & Nair, K. V. K. (1989). Seasonal and vertical distribution of macrofoulants in Kalpakkam coastal waters, *Indian Journal of Marine Sciences*, 18, 270-275
- Satpathy, K. K. & Nair, K. V. K. (1990). Impact of power plant discharge on the physico-chemical characteristics of Kalpakkam coastal waters, *Mahasagar - Bulletin of National Institute of Oceanography*, 23, 117-125

- Satpathy, K. K. (1990). Biofouling control measures in power plants- a brief over view. *Proceedings of specialists meeting on marine biodeterioration with special reference to power plant cooling systems*, pp. 153-166, WSCL, Kalpakkam, Tamil Nadu, India
- Satpathy, K. K. (1996). Seasonal distribution of nutrients in the coastal waters of Kalpakkam, East Coast of India, *Indian Journal of Marine Sciences*, 25, 221-224
- Satpathy, K. K. (1996). Studies on the chemical feature of cooling water systems in the context of scaling, biofouling and corrosion control, Ph.D. Thesis, University of Madras, Madras, India
- Satpathy, K. K. (1999). Effect of biofouling on the cooling water quality of a nuclear power plant, *Bulletin of Electrochemistry*, 15, 143-147
- Satpathy, K. K.; Jebakumar, K. E. & Bhaskar, S. (2008). A novel technique for the measurement of temperature in outflow water from a coastal power plant with notes on chlorination and phytoplankton determinations, *Journal of Thermal Biology*, 33, 209-212
- Satpathy, K. K.; Mohanty, A. K.; Prasad, M. V. R.; Bhaskar, S.; Jebakumar, K. E. & Natesan, U. (2006). Impact of biofouling community on the cooling water quality with special emphasis on its nutrient content, *Proceedings of the International Conference on Recent Advances in Marine Antifouling Technology*, pp. 326-337, NIOT, Chennai, India
- Satpathy, K. K.; Mohanty, A. K.; Prasad, M. V. R.; Natesan, U. & Sarkar, S. K. (2010). Seasonal variation in physicochemical properties of coastal waters of kalpakkam, east coast of India with special emphasis on nutrients, *Environmental Monitoring and Assessment*, 164, 153-171
- Satpathy, K. K.; Mohanty, A. K.; Prasad, M. V. R.; Natesan, U.; Sarkar, S. K. & Rajan, M. (2008). Post-Tsunami changes in water quality of Kalpakkam coastal waters, east coast of India with special references to nutrients, *Asian Journal of Water Environment and Pollution*, 5, 15-30
- Satpathy, K. K.; Nair, K. V. K. & Mathur, P. K. (1992). Some observations on the water quality characteristics of coastal seawater and sub-seabed tunnel, *Mahasagar – Bulletin of National Institute of Oceanography*, 25, 73-82
- Satpathy, K. K.; Nair, K. V. K. & Mathur, P. K. (1994). Chlorine demand & chemical control of biofouling in power plant cooling system, In: *Recent developments in biofouling control*, M. P. Thompson & R. Nagbhusanam, (Eds.), 397-407, Oxford & IBH Publishing Company, New Delhi
- Satpathy, K. K.; Venugopalan, V. P. & Nair, K.V.K. (1999). Barnacle fouling control technology in power plant cooling system, In: *Barnacle fouling ecophysiology & control technology*, M. P. Thompson & R. Nagbhusanam, (Eds.), 359-379, American Institute of Biological Sciences, Washington D.C.
- Satpathy, K.K., Jebakumar, K.E. & Kannan, S.E. (2003). Experience of Bio-fouling Problem and its control in the seawater cooled power plants in India. Seminar on condenser cooling water system of PFBR, Kalpakkam. p1-20.
- Satpathy, K.K., Nair, K.V.K. & Mathur, P.K. (1997). Distribution of nutrients in Kalpakkam coastal waters. In: *Advances in Environmental Sciences* (Ed. C.S.P. Iyer, Educational book publishers New Delhi), p181-186.
- Sebastian, V. O. & Kurian, C. V. (1981). *Indian Ascidians*, Oxford & IBH Publishing Company, New Delhi, India

- Seed, R. (1969). The ecology of *Mytilus edulis* (Lamellibranchiata) on exposed rocky shores. 1. Breeding and settlement, *Oecologia*, 3, 227-316
- Sellers, M. A. & Stanley, J. G. (1984). Species Profiles: Life histories and environmental requirements of coastal fishes and invertebrates (North Atlantic) American Oyster, TR EL-82-4, 15, U. S. Fish and Wildlife Service, U.S. Army Corps of Engineers
- Shannon, C. E. & Weaver, W. (1963). *The mathematical theory of communication*, University of Illinois Press, Urbana
- Somayajulu, Y. K.; Ramana Murthy, T. V.; Prasanna Kumar, S. & Sastry, J. S. (1987). Hydrographic characteristics of central Bay of Bengal waters during southwest monsoon of 1983, *Indian Journal of Marine Sciences*, 16, 207-217
- Stone, A.B., Spyridakis, D.E., Benjamin, M.M., Ferguson, J.F., Reiber, S. and Osterhus, S. (1987). The effect of short term changes in water quality, on copper and zinc corrosion rates, *Journal of American Water Works Association*, February, 75-82
- Strauss, S. D. (1989). New methods, chemicals improve control of biofouling, *Power*, January, 51-52
- Suryanarayan, A. & Rao, D. P. (1992). Coastal circulation and upwelling index along the east coast of India, *Physical Processes in the Indian Seas (Proceedings of First Convention, ISPSO)*, pp. 125-129
- Sutherland, J. P. (1981). The fouling community at Beaufort, North Carolina: a study in stability, *Nature*, 118, 499-519
- Swami, B. S. & Chhapgar, B. F. (2002). Settlement pattern of ascidians in harbour waters of Mumbai, west coast of India, *Indian Journal of Marine Sciences*, 31, 207-212
- Syrett, B. C. and Coit, R. L. (1983). Causes and prevention of power plant condenser tube failure, *Material Performance*, February, 44-50
- Tennessee Valley Authority. (1981). Letter from L.M. Mills to J.P. O'reilly transmitting TVA'S response to the NRC IE Bulletin 81-03 for the Brown's Ferry Nuclear Plants
- Varkey, M. J.; Murthy, V. S. N. & Suryanarayan, A. (1996). Physical oceanography of the Bay of Bengal and Andaman Sea, In: *Oceanography and Marine Biology, An Annual Review*, A. D. Ansell; R. N. Gibson and M. Barnes, (Eds.), UCL Press, 34, 1-70
- Venkateswarlu, K. S. (1990). Marine biofouling and its chemical control in power industry, *Chemical Business*, 20, 39-41
- Venugopalan, V. P. & Nair, K. V. K. (1990). Effect of biofouling community on cooling water characteristics of a coastal power plant, *Indian Journal of Marine Sciences*, 19, 294-296
- Venugopalan, V. P. (1987). Studies on biofouling in the offshore waters of Arabian Sea. Ph. D. Thesis, University of Bombay, Bombay, India
- Venugopalan, V. P.; Rajagopal, S.; Sashikumar, N. & Nair, K. V. K. (1991). Marine biology of a seawater tunnel on the east coast of India, In: *Oceanography of the Indian Ocean*, B. N. Desai, (Ed.), 253-259
- Vinaychandran, P. N.; Masumoto, Y.; Mikawa, T. & Yamagata, T. (1999). Intrusion of the southwest monsoon current into the Bay of Bengal, *Journal of Geophysical Research*, 104, 11077-11085
- White, G. C. (1972). *Handbook of chlorination*, Van Nostrand Reinhold Company, New York

- Whitehouse, J. W. (1975). Chlorination of cooling water: a review of literature on the effects of chlorine on aquatic organisms, CEGB Report no. SD/L/M/M 496, 1-22
- Whitehouse, J. W.; Khalanski, M; Sargolia, M. G. & Jenner, H. A. (1985). The control of biofouling in marine & estuarine power stations. A collaborative report by CEGB, EDF, ENEL & KEMA. NW/R 19
- Wyrcki, K. (1973). Physical oceanography of the Indian Ocean, In: *Biology of the Indian Ocean*, B. Zeitzshel, (Ed.), Springer Verlag Berlin, New York

Atmospheric corrosion studies in a decommissioned nuclear power plant

Manuel Morcillo, Eduardo Otero, Belén Chico and Daniel de la Fuente
Centro Nacional de Investigaciones Metalúrgicas (CENIM-CSIC)
 Spain

1. Introduction

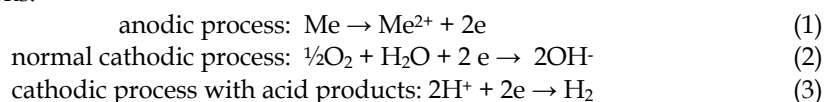
1.1. Fundamentals of the atmospheric corrosion of metals

Metallic corrosion progresses at a very low rate at room temperature in a perfectly dry atmosphere and for practical purposes may be ignored, but on humid surfaces is a very relevant phenomenon. The mechanism is electrochemical, with an electrolyte constituted by an extremely thin moisture film of just a few monolayers or an aqueous film of hundreds of microns in thickness due, for instance, to rain or dew (Rozenfeld, 1972; Barton, 1976; Feliu & Morcillo, 1982; Kucera & Mattson, 1986; Costa et al., 2006).

A considerable part of the damage that atmospheric corrosion causes to structures and equipment may be attributed to the condensation of humidity as a result of periodic cooling of the air. The formation of dew depends on the relative humidity (RH) of the air and the change in the metal surface temperature. The drier the atmosphere, the more the temperature must fall in order for humidity to condense; while at high RH a slight drop in temperature can lead to the saturation in humidity of the atmosphere. The fraction of time in which an atmosphere presents a high RH level has been shown to be a good indicator of its potential aggressivity.

Even in non-saturated atmospheres, where the formation of dew is theoretically not possible, water vapour may condense as a result of capillary and chemical condensation phenomena. Capillary condensation is favoured by rough surfaces, surfaces covered with porous corrosion products, and surfaces upon which dust has been deposited. Chemical condensation is due to the hygroscopic properties of certain polluting substances deposited on the metal surface, or the corrosion products themselves.

The corrosion reaction rate rises with the concentration of substances capable of ionising in the moisture film. Under this film the metal corrodes due to the cathodic process of reduction of oxygen from the air. Hydrogen ion discharging is only a relevant reaction when there is a high degree of pollution by acid products. Anodic corrosion of the metal (*Me*), when bivalent, and the aforementioned cathodic processes may be expressed in simplified terms by the reactions:



1.1.1. Time of wetness of the metallic surface

The atmospheric corrosion process is the sum of the partial (individual) corrosion processes that take place every time an electrolyte layer forms on the metal. Aqueous precipitation (rain, snow or fog) and the condensation of humidity due to temperature changes are, without doubt, the main promoters of atmospheric corrosion; if τ_i is the duration of each individual period of surface wetting and v_i is the mean corrosion rate in that period, the total corrosion after n periods will be:

$$c = \sum_{i=1}^n v_i \tau_i \quad (4)$$

τ_i includes both times of high RH and times of precipitation by rain, mist, fog, etc. v_i can vary greatly depending on the specific circumstances created by the different possible degrees of surface wetting and atmospheric pollution.

The sum of the partial times of surface wetting $\tau = \sum_{i=1}^n \tau_i$ constitutes what is known as the time of wetness (TOW), during which metallic corrosion is possible. Good correlation has been found between the TOW and the time during which RH exceeds a certain humidity level, generally above 70% (Rozenfeld, 1972; Barton, 1976).

1.1.2. Atmospheric pollution

As has been noted, corrosion is not likely below a certain RH level, due to the lack of an appreciable electrolyte film on the metal surface. The corrosion of iron and other metals is generally insignificant at a RH below 60-80%. Even when the RH exceeds this value, for the corrosion rate to be really considerable the atmosphere must also be polluted.

Of all atmospheric pollutants, NaCl and SO₂ are the commonest airborne corrosive agents. NaCl is incorporated in the atmosphere from the sea, and its strongest effects are seen close to the shoreline, where the air carries large amounts of salt and pulverised seawater. SO₂ of anthropic origin can reach considerable concentrations in atmospheres close to thermal power plants or otherwise polluted by smoke from industrial, domestic or transport-related sources. It is originated by burning fuels that contain sulphur.

These two chemical substances, NaCl and SO₂, greatly stimulate the corrosion of wetted metallic surfaces since they raise the activity of the aqueous film. For this reason, atmospheric corrosion in areas close to the sea usually considerably exceed what is expectable in unpolluted inland areas. The same goes for SO₂ emission sources, in whose surroundings corrosion processes are accelerated. Numerous experimental studies have been carried out to quantify the relationship between corrosion rates and atmospheric SO₂ levels, and abundant information is available in the literature.

Quantitative information on chlorides is somewhat scarcer. Nevertheless, it has been perfectly established that chloride pollution plays an important role when its concentration exceeds certain levels.

1.1.3. Indoor atmospheric corrosion

Indoor atmospheric corrosion is a particular case of atmospheric corrosion experienced by metals exposed to the atmosphere in an enclosed environment (Leygraf & Graedel, 2000).

The factors influencing metal corrosion in indoor environments are basically the same as in outdoor exposure, although the atmospheric parameters can be very different (Chawla & Payer, 1991).

In outdoor environments, water interacts with the surface of materials in the form of adsorbed moisture, condensed water and direct precipitation. Indoors, the only relevant components in the formation of wetted surfaces are water and pollutants adsorbed from the atmosphere. Condensation is possible indoors, but requires an unusual combination of external weather conditions and indoor environmental conditions. This can be the case in warm, humid climates, and even in air-conditioned buildings, where water sometimes condenses on surfaces that are cooled below the dew point. Condensation may be capillary (favoured by the deposition of dust or the presence of corrosion products) or chemical (due to the hygroscopicity of these products). The levels of suspended solids and gaseous atmospheric pollutants are usually considerably lower indoors than outdoors.

The absence of visible aqueous films in indoor atmospheres and the much lower levels of the agents that favour chemical and capillary condensation make it more difficult for the electrolyte layer necessary for the development of electrochemical corrosion processes to form. The lower concentration of gaseous pollutants is another reason why metallic corrosion is notably lower in indoor environments (Chawla & Payer, 1991).

1.2. Corrosion studies in the decommissioned Vandellós I nuclear power plant

Vandellós I is a graphite-moderated, gas-cooled nuclear power plant of 497 MW capacity located in the province of Tarragona, Spain. It is the first nuclear power plant in Spain to be decommissioned. The decommissioning and dismantling plan is being coordinated by the National Radioactive Waste Management Company (ENRESA, Madrid, Spain).

Level 2 of the process, according to the International Atomic Energy Agency (IAEA, Vienna, Austria) nomenclature, was completed in 2002. The present step is a 30-year waiting period known as latency, whose purpose is to allow radiation inside the reactor containment vessel to fall to levels that permit its complete dismantling with a minimal radiological impact, in order to return the site to its original state. Thus it is necessary to guarantee the containment's integrity during this time by assessing the possible risk of corrosion of the complex metallic structures located in its interior.

For this reason, besides determining the outdoor atmospheric corrosivity of the power plant site and constantly monitoring the temperature and relative humidity inside the reactor containment, ENRESA is monitoring the corrosivity of this indoor atmosphere to different types of structural steels.

This chapter describes the methodology followed to evaluate outdoor atmospheric corrosion at the power plant site and indoor atmospheric corrosion inside the concrete reactor containment during the latency period of decommissioning. Outdoor and indoor atmospheric corrosion rate results are also reported.

2. Outdoor atmospheric corrosion at the nuclear power plant site

Vandellós I nuclear power plant is located in an area where previous studies have indicated an atmosphere polluted only by sea salinity (pure marine atmosphere) and the practical absence of any other pollutants that can influence metallic corrosion processes (SO_2 , NO_x , etc.).

Atmospheric salinity is a parameter related with the amount of marine aerosol present in the atmosphere. Saline particles in marine atmospheres accelerate metallic corrosion processes because chlorides give rise to soluble corrosion products, in contrast to the scarcely soluble products that form in rural atmospheres. Dissolved marine chlorides also considerably raise the conductivity of the electrolyte layer on the metal surface and tend to destroy any existing passivating film.

Salinity in marine atmospheres varies within very broad limits (Bonnarens & Bragard, 1981; ISO 9223, 1992; Johnson & Stanners, 1981). While extremely high values have been recorded close to breaking waves, salinity at other points on the shoreline with calmer waters is more moderate.

The marine aerosol concentration decreases with altitude (Blanchard & Woodcock, 1980; Strekalov & Panchenko, 1994; Lovett, 1978). For this reason, raising a metal above ground level generally results in less corrosion as the number of saline particles reaching its surface decreases.

Despite the vast volume of information in the literature concerning the corrosion of metals in marine atmospheres, quantitative information on the effect of salinity on atmospheric corrosion is very scarce. Papers on this subject often make reference to a study carried out more than 50 years ago in Nigeria by Ambler and Bain (Ambler & Bain, 1955). The authors of this chapter have discussed the relationship between salinity and steel corrosion based on published data referring to research performed in different parts of the world (Morcillo et al., 1999) (Figure 1). Salinity values up to 100 mg Cl-/m².day promote only a slight increase in the steel atmospheric corrosion rate, which becomes faster as the salinity rises up to 400 mg Cl-/m².day. After this point the increase in corrosion with salinity is once again only slight, and subsequently seems to stabilise for higher atmospheric salinity values.

The wind, which stirs up and transports particles of sea water, is the force responsible for the salinity present in marine atmospheres. Oceanic air is rich in marine aerosols resulting from the evaporation of drops of sea water that are mechanically transported by the wind. The origin, concentration and vertical distribution of marine aerosol over the surface of the sea has been studied by Blanchard and Woodcock (Blanchard & Woodcock, 1980).

Marine aerosol is composed of fine solid or liquid particles suspended in the air (jet drops, film drops, brine drops and sea-salt particles) of sizes of between 0.1 and 400 μm (Blanchard & Woodcock, 1980; Zezza & Macri, 1995). In marine atmospheres the aerosol concentration varies according to the altitude and wind speed.

The larger marine aerosol particles (diameter $>10 \mu\text{m}$), known as falling particles, remain in the atmosphere for only a short time; the greater the particle size, the shorter the time. In contrast, particles of a diameter of $<10 \mu\text{m}$, known as buoyant particles, may travel hundreds of kilometres in the air without sedimenting. According to Ambler and Bain (Ambler & Bain, 1955), the corrosion of metallic surfaces is only caused by salt particles and saline drops of a size of more than 10 μm . Given that these particles remain for just a short

time in the atmosphere, corrosion completely loses its marine character just a few hundred metres inland.

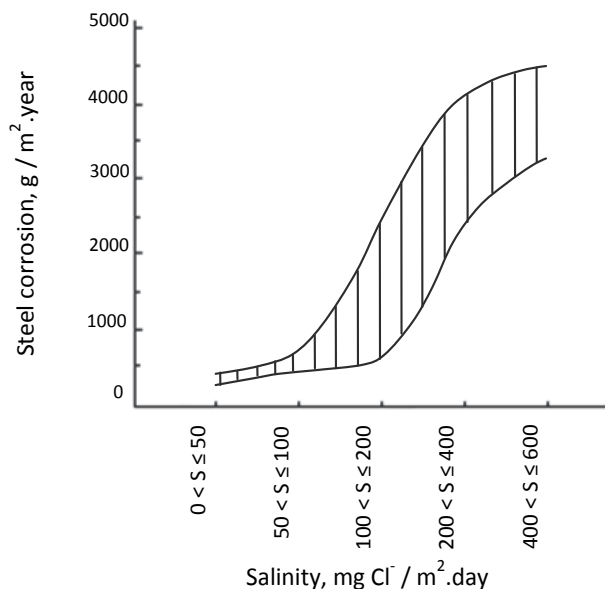


Fig. 1. Relation between salinity and steel corrosion (Morcillo et al., 1999)

However, the distance from the sea is not in itself always the only determining factor for the corrosion rate, which also depends on the topographic and orographic features of the land and on the intensity and direction of prevailing winds, etc.

Abnormally high salinity levels are sometimes recorded as a result of storms, which in just a few hours can deposit larger amounts of salt than the normal wind regime during an entire month.

However, a higher wind speed does not always mean an increase in salinity, which is ultimately dependent on the wind direction. In fact, an increase in the wind speed can even cut the amount of pollution by purifying the atmosphere. This naturally depends on the location of the site in relation to the sea and on the direction and type of the winds blowing at any given time.

Although in principle it would seem reasonable to assume that the presence of marine aerosol in coastal regions would be governed by the speed, direction and duration of marine winds (those proceeding from the sea), the topography and orography of the land and the general wind regime of the local area can also lead continental winds to influence salinity values. This has been shown in a study by the Russian Academy of Sciences (Strekalov & Panchenko, 1994; Strekalov, 1988), in which the authors report observations made over long time periods in Murmansk and Vladivostok, reaching the conclusion that in both areas the transportation of chlorides depended on the average speed of total winds (marine + continental) and on the product of the wind speed by its duration ("wind strength").

Thus, it was of practical interest to quantify atmospheric salinity at Vandellós I nuclear power plant site and its effect on the metallic corrosion process. Specific research work has been carried out in this coastal area of Tarragona (Spain) with the dual aim of determining:

a) the influence of atmospheric salinity on metallic corrosion at this location; and b) the influence of winds on the recorded salinity values.

2.1. Effect of atmospheric salinity on metallic corrosion

2.1.1. Experimental

The study has been carried out in three open-air corrosion testing stations located at different distances from the shoreline (Figure 2) (Chico et al., 1997). Use has preferentially been made of CLIMAT specimens. The CLIMAT test (Classification of Industrial and Marine Atmospheres), also known as the "wire on bolt" technique, is a method for determining the corrosivity of an atmosphere. This procedure was first used in the United States by Bell Telephone Laboratories (Compton et al., 1955) to assess the possible galvanic effects of bimetallic unions in the atmosphere. The technique was subsequently developed by the company Alcan (Doyle & Wright, 1969) to assess the suitability of steel core reinforced aluminium conducting cables for electricity transmission lines. Godard and Doyle (Doyle & Wright, 1969; Godard, 1963; Doyle & Godard, 1963; Doyle & Godard, 1969; Doyle & Wright, 1971) are the researchers who have most widely applied this technique.

The CLIMAT test is a simple and economical method that yields reliable results in a short time (three month periods). This technique assesses the mass loss experienced by a wire wound strongly round the thread of a bolt which behaves cathodically in relation to the wire.

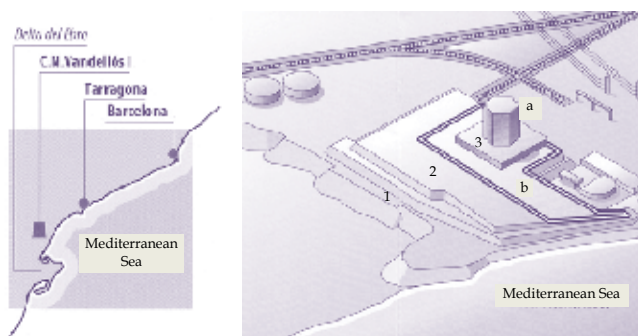


Fig. 2. Sketch with location (points 1 to 3) of corrosion stations

Figure 3 shows a set of the specimens used in the CLIMAT test. Four different types of specimens were tested: Al/Fe, Al/Cu, Al/PVC and Al (spiral). Standard dimensions and materials were used (Morcillo & Feliu, 1977) in order to allow comparison with the results obtained in previous studies and by other researchers.

Each series of specimens was exposed for three months, after which they were withdrawn and replaced by a fresh series. In total four consecutive testing periods were evaluated. At the end of the test the wire was unwound from the bolt and the corrosion products were removed from the wire using specific solutions (ISO 9226, 1992), calculating the mass loss (ISO 8407, 1991) expressed as a percentage of the initial mass.

Together with the CLIMAT specimens, flat carbon steel and galvanised steel specimens (Fig. 3) were also exposed in the testing stations for a one year period.



Fig. 3. View of a corrosion station (and corrosion samples) equipped with devices for recording meteorological (wind speed and direction (a), temperature and relative humidity (b) and pollution (salinity (c) and SO₂ (d)) parameters

In order to determine the aggressivity of the different atmospheres the following meteorological and pollution parameters were recorded: temperature, relative humidity, time of wetness, environmental salinity and SO₂ (Fig. 3). Salinity was determined monthly by the wet candle method (ISO 9225, 1992) and sulphur dioxide by the lead peroxide candle method (BS 1747, 1963). Automatic sensors were used to measure the temperature and relative humidity of the air. The time of wetness (TOW) was determined by calculating the number of hours in which RH ≥ 80% and T > 0°C (ISO 9223, 1992).

2.1.2. Results

Table 1 displays the environmental and corrosion data obtained at the three testing stations.

Corrosion station no.	Environmental data			Corrosion data					
	TOW (hours)	SO ₂ (mg / m ² .day)	Salinity (mg Cl ⁻ / m ² .day)	CLIMAT specimens (%)				Flat specimens	
				Al/spiral	Al/PVC	Al/Fe	Al/Cu	C steel	Galvanised steel
1	2325	7.08	95.56	0.32	0.44	5.94	6.57	29.46	4.72
2	1339	6.93	50.07	0.30	0.32	2.86	3.46	24.35	2.59
3	2462	8.22	26.39	0.22	0.19	1.56	1.86	22.64	1.53

Table 1. Mean anual values of environmental and corrosion data obtained in the three testing stations (Fig. 2)

2.1.3. Discussion

2.1.3.1. Damage functions

The environmental and corrosion data obtained with the CLIMAT specimens in the four exposure periods (spring, summer, autumn and winter) was studied in order to establish its significance in the corrosion process.

For this purpose, statistical analysis was performed with the assistance of a specific computer program (BMDP Statistics computer software).

The data was fitted according to the following linear equation:

$$C = a_1 + a_2 T + a_3 RH + a_4 TOW + a_5 Cl + a_6 S \quad (5)$$

where a_i ($i = 1$ to 6) are constants, C is aluminium corrosion (%), T is the average temperature ($^{\circ}C$), TOW is the time of wetness (hours), S is the average SO_2 pollution value ($mg/m^2 \cdot day$), and Cl is the average chloride pollution value ($mg/m^2 \cdot day$).

The resulting damage functions between corrosion and environmental parameters are shown below, along with their corresponding correlation coefficients (R).

Specimen type	Equation	R
Al (spiral)	$C = -0.147 + 0.015 T + 0.002 Cl$	0.80 (6)
Al/PVC	$C = 0.097 + 0.003 Cl$	0.82 (7)
Al/Fe	$C = 0.185 + 0.054 Cl$	0.93 (8)
Al/Cu	$C = 0.315 + 0.059 Cl$	0.91 (9)

Salinity is the variable of greatest significance for all types of CLIMAT specimens. Temperature also emerges as a significant variable only in the case of the Al (spiral) specimen.

Since the atmospheres in question are of a pure marine character with practically no SO_2 pollution, it is not surprising that the Al/Cu specimens, which are sensitive to both marine and industrial atmospheres, only reflect the influence of environmental salinity.

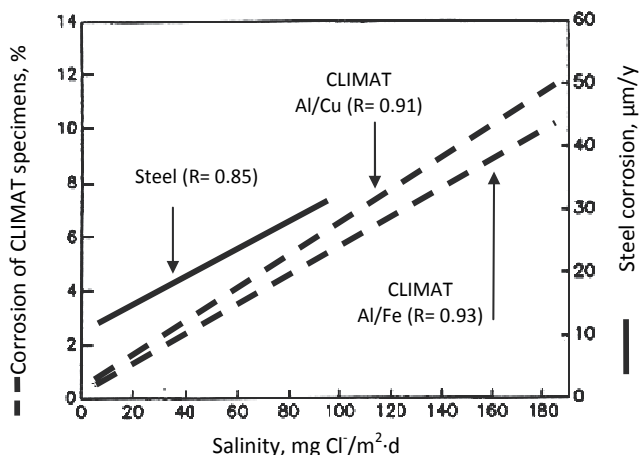


Fig. 4. Relation between the degree of corrosion on Al/Fe and Al/Cu CLIMAT specimens and flat steel specimens and the atmospheric salinity

Figure 4 shows the relationships encountered between salinity and corrosion of the Al/Fe and Al/Cu CLIMAT specimens and the carbon steel specimens. Since these are pure marine atmospheres, both Al/Fe and Al/Cu CLIMAT specimens are equally valid when it comes to determining the scope of metallic corrosion, thus confirming the observations made by other researchers (Doyle & Wright, 1982).

2.1.3.2. Effect of distance from the sea

In order to obtain a broader view of this aspect, in addition to the corrosion data obtained in the present study consideration has also been made of information reported in the literature, principally from Godard, Doyle and Wright (Doyle & Godard, 1969; Doyle & Wright, 1971; Doyle & Wright, 1982) and the Canadian company ALCAN (Doyle & Wright, 1969). These researchers found that corrosion decreases with the distance from the shoreline following a hyperbolic law:

$$X^{1/3} + Y^{1/3} = K \text{ (constant)} \quad (10)$$

where X is the distance from the shoreline and Y is the marine corrosivity index (MCI, Al/Fe). In other words, the variation in the MCI with the distance from the shore is not linear but decreases rapidly in the first few hundred metres and subsequently more gradually; by 1 km inland the value is greatly reduced, and by 2 km inland an asymptotic value is reached.

Furthermore, they note that the higher the MCI at the shoreline, the greater the reach of marine penetration inland.

This function seems to have a certain validity in marine atmospheres, since it is also fulfilled for flat specimens used by other researchers (Amblar & Bain, 1955).

Figure 5 shows the CLIMAT data obtained in this study along with data reported by other researchers (Doyle & Godard, 1969) using CLIMAT specimens on the south-east coast of South Africa (Durban), the north coast of Colombia (Galerazamba), and the east coast of the United States (Kure Beach).

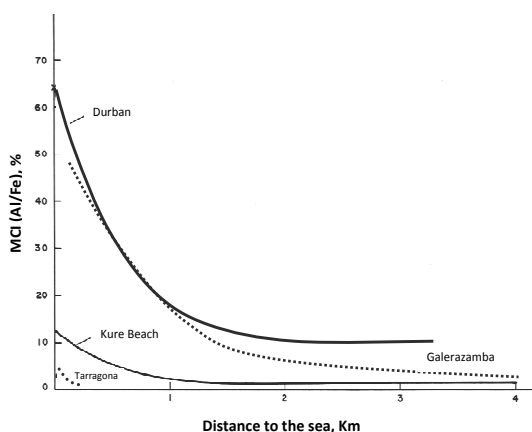


Fig. 5. Relation between the marine corrosivity index (MCI) and the distance from the shoreline

The results obtained in our study also reflect this behaviour, although the K constant values are notably lower (equation 10) due to the lower corrosivity of the atmosphere where the study was carried out.

The higher the K value, the greater the atmospheric corrosion at a given distance from the shoreline and the greater the reach of the marine atmosphere inland.

2.1.4. Conclusions

- Atmospheric salinity is the variable of greatest significance in the metallic corrosion process at Vandellós I nuclear power plant site. A clear linear relationship is established between atmospheric salinity and metallic corrosion, irrespective of the type of corrosivity sensor used (CLIMAT specimen or flat specimen).
- Being a pure marine atmosphere, both Al/Fe and Al/Cu couples can be used as atmospheric salinity and corrosion sensors.
- The decrease in atmospheric salinity inland from the shoreline is exponential, with a notable drop in salinity in the first few hundred metres followed by a more gradual decrease at greater distances inland.

2.2. Influence of the wind regime on atmospheric salinity

2.2.1. Experimental

Information on winds was obtained on the same corrosion station as the salinity data (Figure 3) (Morcillo et al., 2000). Wind speed and direction data was measured with an anemometer and a wind vane and gathered by a 1256 meteodata station (Geónica), recording data every 10 s and calculating averages every 10 min. Atmospheric salinity data was retrieved every 3 months.

2.2.2. Results

Salinity data are displayed in Table 2. Attention is drawn to the high value obtained in the eighth month of testing (March). The monthly distribution of wind frequencies, in hours, for marine winds, *M*, and total winds (marine + continental), *T*, for the different wind speed intervals is shown in Table 3.

2.2.3. Discussion

It seems reasonable to assume that atmospheric salinity will be determined mainly by marine winds, i.e. those blowing from the sea towards the land and thus liable to carry marine aerosol.

Month	August	September	October	November	December	January	February	March	April
Salinity (mg Cl/m ² .day)	27.90	26.37	29.10	10.77	7.31	12.34	8.33	114.47	20.37

Table 2. Chloride pollution of the atmosphere at the nuclear power plant site.

The testing site is situated on a section of shoreline on the Mediterranean coast, between 40° 57' and 40° 58' latitude, running in SW-NE direction. The range of marine wind directions, including those corresponding to the shoreline, comprises NE, ENE, E, ESE, SE, SSE, S, SSW and SW. The remaining wind directions may be considered continental.

It is interesting to know how each different wind direction contributes to the salinity values recorded in the testing stations.

			Velocity interval (m/s)											
			Cal-0.5	0.51-0.75	0.76-1.0	1.1-1.5	1.6-2.0	2.1-3.0	3.1-5.0	5.1-7.0	7.1-10.0	10.1-13.0	13.1-18.0	> 18.1
Frequency distribution of the wind (h)	Aug.	T	1	7	25	98	136	249	150	14	19	7	9	23
		M	1	1	13	46	79	195	112	5	4	3	9	6
	Sep.	T	2	10	24	82	114	171	184	53	42	32	5	1
		M	0	4	6	27	45	95	76	3	0	0	0	0
	Oct.	T	4	5	27	105	113	197	104	10	14	7	0	0
		M	0	1	9	33	39	100	33	3	0	1	0	0
	Nov.	T	5	14	44	170	110	158	113	30	40	27	6	0
		M	0	6	13	47	44	69	41	0	0	0	0	0
	Dec.	T	5	12	48	97	81	117	172	44	106	54	7	0
		M	0	1	9	39	45	55	56	1	0	0	0	0
	Jan.	T	0	3	24	48	62	138	155	65	83	78	63	2
		M	0	0	7	15	39	69	39	0	0	0	0	0
	Feb.	T	4	19	34	83	86	124	152	64	59	27	3	0
		M	1	5	8	32	54	63	44	6	0	0	0	0
	Mar.	T	2	7	36	78	76	136	176	63	55	26	11	0
		M	0	2	12	20	40	81	101	29	6	0	0	0
	Apr.	T	6	14	54	78	102	153	95	23	59	21	10	11
		M	2	3	17	24	62	126	61	3	0	0	7	6

Table 3. Frequency distribution of total winds (marine + continental), T, and marine winds, M, for the exposure period.

Salinity obviously depends not only on the wind speed (v) but also on the number of hours (n) that the wind is blowing in each direction, i.e. the product of $v \times n$, which in meteorology is known as the "wind strength".

Figure 6 illustrates the variation in atmospheric salinity and in marine and total wind strength over time. The variation in total winds (marine + continental) does not coincide with chloride transportation towards the land, since the maximum total wind strength is recorded in the month of January while the maximum salinity corresponds to the month of March. The variation in marine wind strength is that which most closely follows the variation in salinity.

However, not all the marine wind directions contribute in the same way to the transportation of salinity from the sea towards the land; otherwise, April and August, and not only the month of March, would also present high salinity values.

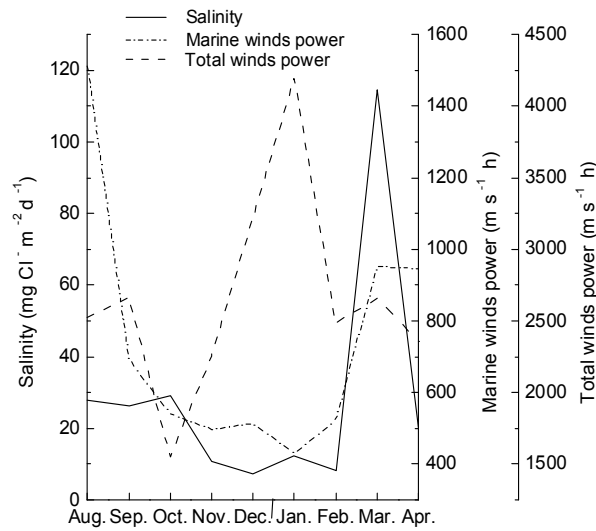


Fig. 6. Relation between atmospheric salinity and wind strength (total and marine)

Plotting the monthly variation in the strength of each marine wind direction shows that the ENE direction (Figure 7) is that which most closely mirrors the variation in salinity data. The marine wind directions that apparently contribute most to the transportation of marine aerosol towards the land may be referred to as 'saline winds'.

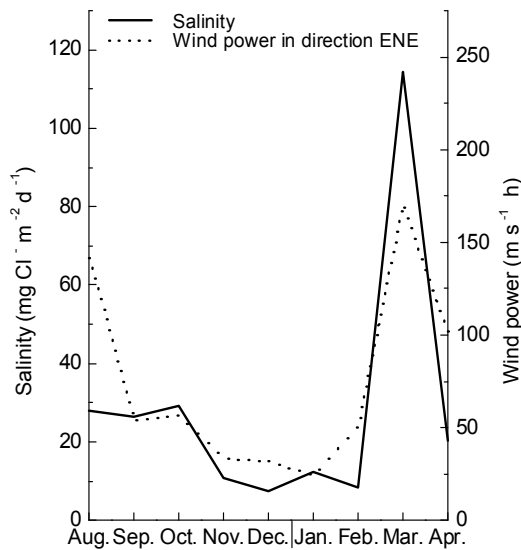


Fig. 7. Relation between atmospheric salinity and wind strength in ENE direction

With regard to a critical wind speed, above which the effect of marine aerosol transportation towards the land is greater, different functions have been tested to relate monthly salinity with the weighted average wind speed. The term weighted average wind speed (v_{mp}) is defined by the expression:

$$v_{mp} = \frac{\sum v_i n_i}{N} \quad (11)$$

where v_i is the mean value of the wind speed range (Table 3) in a given direction, n_i is the number of hours the wind blows in that direction and wind speed range, and N is the total number of hours the wind blows in that direction in all the wind speed ranges.

Of all the tested functions, the polynomial type function is that which provides the best fits, coinciding with the aforementioned studies in Russia (Strekalov & Panchenko, 1994). Figure 8 shows the variation in salinity with the weighted average monthly wind speed for marine winds in ENE direction. For reference purposes, the figure also includes the plot obtained in Vladivostok (Russia) for total winds (marine + continental) according to Strekalov (Strekalov & Panchenko, 1994). As can be seen, the patterns of the three plots are similar. The plot corresponding to winds in the ENE direction seems to indicate a critical speed, close to 3 m/s, above which the transportation of marine aerosol increases considerably.

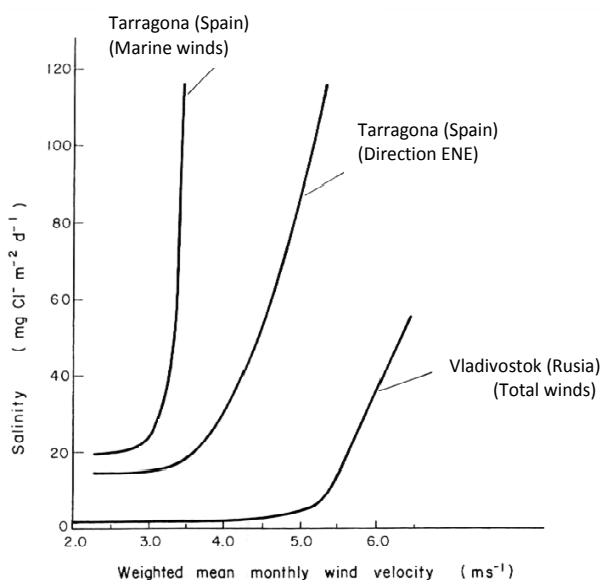


Fig. 8. Relation between atmospheric salinity and weighted mean monthly wind speed for marine winds, winds in ENE direction and total winds (marine + continental), the latter according to Strekalov (Strekalov & Panchenko, 1994)

Another means of establishing the critical speed is by analysing the salinity variation plots for the different months of exposure and the number of hours/month during which the wind speed exceeds a certain value, e.g. 1 m/s, 2 m/s, 3 m/s, etc. Figure 9 shows the plot for wind speeds above 3 m/s corresponding to the ENE direction. As can be seen, the variation in salinity and the number of hours/month during which the wind is blowing in that direction follow very similar patterns.

According to Figure 9, the wind only needs to blow for a relatively short time (27 h/month) at speeds above 3 m/s in a direction with a great influence on the transportation of marine aerosol (ENE direction in this case) for atmospheric salinity to acquire important values.

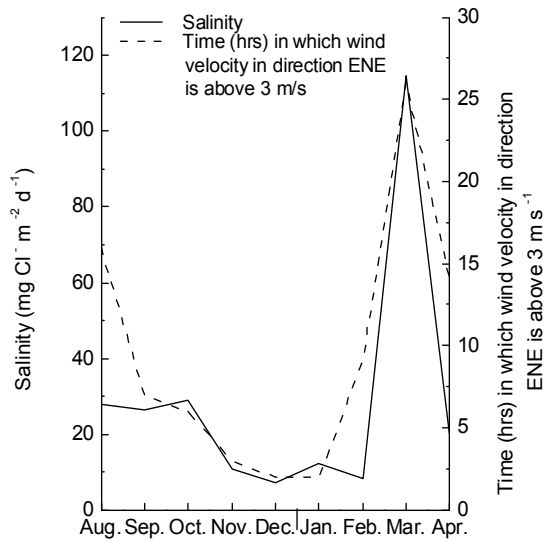


Fig. 9. Relation between atmospheric salinity and number of hours in which the wind speed in ENE direction is above 3 m/s

2.2.4. Conclusions

- This study shows that there are certain marine wind directions (which may be termed 'saline winds') that seem to contribute most to the transportation of marine aerosol from the sea towards the land. At Vandellós I nuclear power plant site, saline winds correspond mainly to the ENE direction.
- There seems to be a critical speed for saline winds above which coastal atmospheric salinity is notably higher. In the present study this critical speed is situated close to 3 m/s.
- The atmospheric salinity of this coastal area seems to depend on the persistence (number of hours) of saline winds above the critical speed.

3. Indoor atmospheric corrosion inside the reactor containment

There follows a description of the experimental technique designed to measure corrosivity inside the reactor containment of the decommissioned Vandellós I nuclear power plant (Otero et al., 2007).

3.1. Constant monitoring of air temperature and relative humidity

The air temperature and relative humidity (RH) are the indoor parameters of greatest influence on the conservation of the reactor containment's internal structures and are constantly monitored.

Temperature measurements are performed using thermocouples located at three levels inside the containment (18, 30 and 49 m) and with different orientations. Figure 10 shows the average temperature values obtained in the upper part of the containment over a two-year period. The temperature remained within the 15°C to 23°C range throughout this period.

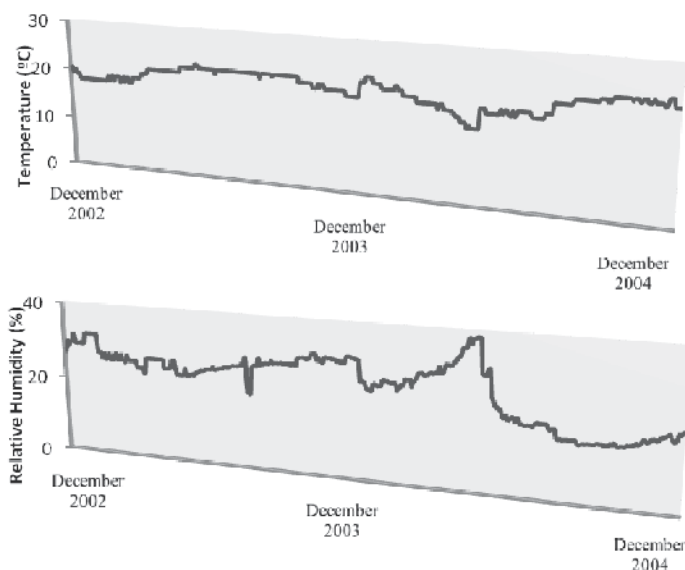


Fig. 10. Average temperature and RH values obtained in the upper part of the reactor containment during a two-year period. An apparent correlation between humidity and temperature (higher temperature = lower humidity) is observed.

RH is measured using a closed circuit system to sample the containment's atmosphere through three extraction tubes located at different heights (high, medium and low), close to the thermocouples, and one return tube. The system is comprised of an extraction pump, filters, connectors for sampling bottles, and an online hygrometer for RH measurements. Figure 10 shows the average RH measured during the same two-year period as the temperature data, with humidity values in the 15% to 38% RH range. The strength of the radiation field in the test environment is sufficiently low to ignore radiolysis effects.

3.2. Assessment of atmospheric corrosivity inside the reactor containment

The corrosivity of the atmosphere inside the reactor containment is monitored in accordance with ISO 11844-2 (ISO 11844-2, 2005). The techniques selected for this study are "Determination of Corrosion Rate by Mass Changes" (Annex A) and "Determination of Corrosion Rate by Resistance Measurements" (Annex C).

The gravimetric method in Annex A is based on determining the mass change experienced by small rectangular metallic specimens ($50 \times 10 \times 0.5$ mm) after different exposure times in the indoor atmosphere. All the tests are carried out in triplicate. Due to the low corrosion rates found in indoor environments, the gravimetric method requires a sensitivity of ± 10 mg/m², and in view of the size of the test specimens a microbalance is used to obtain the necessary sensitivity.

The electrical resistance method described in Annex C of the standard is based on the increase in ohmic resistance that a thin metal film experiences when its cross section decreases. The sensors used in this technique basically consist of two elements, one of which is exposed to the atmosphere (and whose ohmic resistance increases as it corrodes) and another that is isolated from the environment (and whose resistance remains constant). The

measurements involve determining the relationship between the two resistance values. Changes in the corrosion rate are shown by variations in the slope of the graph obtained by plotting the results as a function of time. As a result of advances in electronics and data processing, equipment is now available that allows this type of measurement to be carried out in a quick and simple way and which yields data that directly indicates the mean penetration (attack) experienced by the sensor's exposed element due to corrosion.

Determination of corrosion rate by mass changes. For practical purposes, the steels used for the metallic structures located inside the containment have been classified into three groups: a) cold-workable carbon steels; b) low-carbon engineering steels; and c) low-alloy Cr-Mo slow creep-resistant steels. The study tested three representative steels, taking one from each group. The gravimetric specimens (50 x 10 x 0.5 mm) were finished with 320-grade abrasive polishing.

As a result of restrictions on opening the containment and the exceptional safety measures that are adopted in such cases, the withdrawal of mass-change specimens is programmed to occur once every five years.

Determination of corrosion rate by resistance sensor measurements. Determining the corrosion rate by electrical resistance measurements has the advantage of yielding instantaneous data, and the fact that it is not necessary to open the reactor containment to obtain the data. In the present study, electrical resistance measurements are made every three months. Of all the commercially available resistance sensors, an 8-mils (203.2 μm) thick, flat atmospheric probe type in UNS K03005¹ pipe grade carbon steel was selected. The measuring equipment used was a CK-4 Corrosometer² by Rohrback Cosasco Systems Inc. (Santa Fe Springs, California). The typical sensitivity of this method is 0.1% of probe life (i.e. its "useful thickness") (ASTM G96-90, 2001). The probe life is normally limited to approximately 50% of the probe element thickness. For the present study, use has been made of steel sensors with a thickness of 8 mils (203.2 μm) and thus a sensitivity of 0.1 μm , in proportion to the sensor thickness.

3.2.1. Experimental setup

Figure 11 shows a general diagram of the experimental setup. The experimental device was installed in the upper part of the reactor containment via three apertures in the ceiling, suspended from a two-disc fixture anchored to the bottom of the seal plugs.

The mass-change specimens and the electrical resistance sensor were placed on a rack which was lowered into the reactor containment through the apertures in the ceiling with the assistance of a manual pulley. The rack suspension cable was fixed to the seal plug and the resistance sensor's connection cable passed through a gland in the centre of the plug. The experimental device was suspended half-way between the containment ceiling and the top of the metallic structures inside the containment. Figure 12 shows a rack being lowered into the containment.

¹ UNS numbers are listed in *Metals and Alloys in the Unified Numbering System*, published by the Society of Automotive Engineers (SAE International) and cosponsored by ASTM International.

² Trade name

3.2.2. Results

This section presents the corrosion data obtained during the first three years of the study.

3.2.2.1. Measurements obtained with gravimetric specimens

After being carefully withdrawn from the containment, the gravimetric specimens were stored in small boxes containing a desiccant for their transfer to the laboratory. Prior to removal of the corrosion products by pickling, in order to determine the mass losses experienced after three years of exposure inside the containment, the specimens were cleaned carefully with compressed air to remove any dust from their surface and photographs were taken.

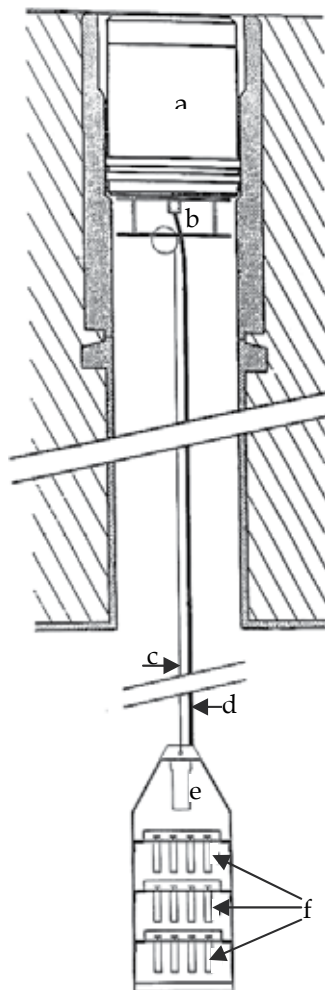


Fig. 11. General setup: (a) seal plug; (b) two-disc fixture anchored to seal plug; (c) braided cable from which rack is suspended; (d) cable connecting resistance sensor to corrosimeter; (e) electrical resistance sensor; (f) gravimetric specimens.

A 50 vol% hydrochloric acid (HCl) pickling solution was employed, using hexamethylenetetramine ($C_6H_{12}N_4$) as inhibitor in a proportion of 3.5 g/L (ISO 9226, 1992). The pickling time was 2 min in all cases, with gentle stirring at room temperature, followed by three quick rinses with stirring in distilled water and two quick immersions with stirring in 96% (v/v) ethanol (C_2H_5OH) and absolute ethanol, followed by immediate drying with compressed air. Observation with a binocular microscope, at x20 magnification, confirmed the removal of the corrosion products.

ISO 11844-1 (ISO 11844-1, 2006) expresses mass gain and loss rates in $mg/m^2.y$. In the case of steel, ISO classifies the corrosivity of indoor atmospheres as a function of mass gain and loss into five categories, as shown in Table 4.



Fig. 12. Insertion of rack with mass-change specimens and electrical resistance sensor into the reactor containment

Designation	Corrosivity	Mass loss rates ($mg/m^2.y$)	Mass gain rates ($mg/m^2.y$)
IC1	Very low	$V_{corr} \leq 70^{(A)}$	$V_{im} \leq 70^{(B)}$
IC2	Low	$70 < V_{corr} \leq 1,000$	$70 < V_{im} \leq 700$
IC3	Medium	$1,000 < V_{corr} \leq 10,000$	$700 < V_{im} \leq 7,000$
IC4	High	$10,000 < V_{corr} \leq 70,000$	$7,000 < V_{im} \leq 50,000$
IC5	Very high	$70,000 < V_{corr} \leq 200,000$	$50,000 < V_{im} \leq 150,000$

(A): V_{corr} = mass loss rate; (B) V_{im} = mass gain rate

Table 4. ISO classification of the corrosivity of indoor atmospheres as a function of mass loss and gain experienced by carbon steel (gravimetric tests) (ISO 11844-1, 2006)

A more direct description of the attack due to corrosion may be obtained by expressing corrosion behaviour in terms of a "mean penetration rate", in $\mu m/y$. This also has the advantage of using the same units as the electrical resistance sensors, thus allowing simple comparison between the results obtained with the two techniques. In order to calculate the corrosion rate in terms of "mean penetration", a value of $7.85 g/cm^3$ was taken as the density of the three types of steel.

The mean corrosion rates obtained by applying the gravimetric technique are set out in Table 5. As can be seen, the mean mass loss rates determined with this method are in the lower limit of the IC2 designation (low corrosivity).

3.2.2.2. Measurements obtained with the electrical resistance sensor

The theoretical sensitivity of this method is a one unit variation in the measurement, which in the case of the installed sensors corresponds to a 0.1 μm increase in the mean penetration. However, several factors (ASTM G96-90, 2001) may influence the measurements to an estimated degree of ± 4 units, and thus fluctuations up to this amount should not be interpreted as a reliable indication of corrosion unless a systematic trend is seen in successive measurements.

Table 6 displays the thickness loss values (μm) obtained with the electrical resistance sensors during the first three years of exposure. The fluctuations obtained with each sensor remain within a narrow interval of $\pm 0.2 \mu\text{m}$, which means that corrosion rate estimates cannot be made since the mean penetration experienced by the sensors during this time period is less than their sensitivity threshold.

Group	Type of steel	Containment aperture	Mass loss rates		Mass gain rates
			$\mu\text{m}/\text{y}$	$\text{mg}/\text{m}^2\cdot\text{y}$	$\text{mg}/\text{m}^2\cdot\text{y}$
Cold-workable carbon steels	ASTM C1035	A	0.010	79	26
		B	0.016	128	54
		C	0.004	34	9
		Mean	0.010	80	30
Low-carbon engineering steels	ASTM A516 Grade 60	A	0.015	121	33
		B	0.018	139	54
		C	0.005	41	12
		Mean	0.013	100	33
Low-alloy Cr-Mo slow creep-resistant steels	F-1252	A	0.021	163	49
		B	0.020	158	59
		C	0.003	24	18
		Mean	0.015	115	42

Table 5. Mass loss and gain rates obtained for the three steels below the three containment apertures.

Date	Containment aperture		
	A	B	C
Feb 2002	4.3	3.7	3.9
May 2002	4.3	3.9	3.8
Sept 2002	4.3	3.8	3.9
Jan 2003	4.2	3.8	3.9
Jun 2003	4.2	3.8	4.0
Dec 2003	4.5	3.8	4.1
Dec 2004	4.3	4.0	4.1
Mar 2005	4.3	3.8	3.9

Table 6. Thickness losses in μm obtained with electrical resistance sensors

3.2.3. Discussion

Inspection of the gravimetric specimens upon withdrawal after three years of exposure revealed the presence of corrosion products which in no case fully covered the surface of the specimens. Figure 13 displays an image obtained using scanning electron microscopy (SEM)

at x500 magnification of an area of an F-1252 (UNS G41400) steel specimen with corrosion products that can be seen to follow the direction of the surface finish.

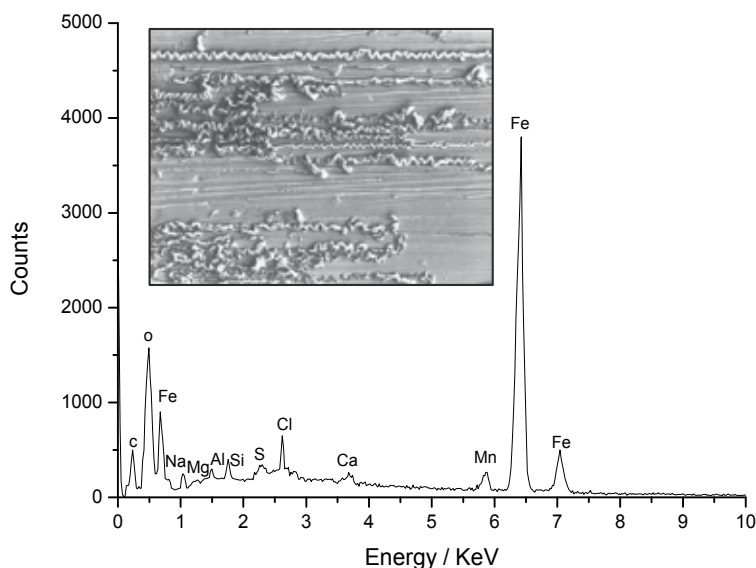


Fig. 13. Appearance of an F-1252 steel specimen in an area with corrosion products (x500) and corresponding EDS microanalysis.

Figure 13 also shows the energy-dispersive spectrum (EDS) obtained by microanalysis of the corrosion product patches formed. Attention is drawn to the presence of Cl in the corrosion products, which indicates the participation of chloride ions in the atmospheric corrosion process. This is not surprising considering the proximity of the power plant to the shoreline. The air is treated before it enters the reactor void by means of filtration of coarse particulates and dehumidification, so only fine to medium-sized salt aerosol particulates are able to enter the reactor containment.

The fact that extremely low corrosion rates are determined, despite the presence of chloride ions, may be attributed to the very low RH (Figure 10) inside the containment, which is below the RH necessary for the formation of moisture films on the metallic surface. Corrosion only takes place by capillary condensation in the grooves on the test specimens, and by the occurrence of differential aeration corrosion processes in these zones.

As can be seen in Table 5, the mean values of the mass loss rates obtained were in the interval from 0.010 $\mu\text{m}/\text{y}$ to 0.015 $\mu\text{m}/\text{y}$.

Mean annual carbon steel corrosion rates of 22.6 μm to 29.5 μm were obtained in the different outdoor testing stations (see Table 1), 1,500 to 3,000 times greater than the carbon steel corrosion rates recorded inside the reactor containment.

With reference to the results in Table 5, if the mass gain rate (V_{im}) is adopted as a criterion, the indoor atmospheric corrosivity below the three containment apertures (A, B and C) belongs to category IC1 "very low corrosivity" (Table 4). However, according to the mass loss rates (V_{corr}), the indoor atmospheric corrosivity belongs to category IC1 below containment aperture C for all the three studied steels, while the corrosivity below

containment apertures A and B lies within the range of category IC2 "low corrosivity", albeit closer to the lower limit of this category than the upper limit (Table 4).

With regard to the electrical resistance sensors, as has been noted above, the sensors used have a theoretical sensitivity of 0.1 μm average penetration. The small fluctuations in the successive electrical resistance measurements carried out over the three-year period do not allow reliable estimates of the corrosion rate (expressed as mean penetration) and simply indicate that the corrosion experienced by the sensors during this period was lower than or equal to their sensitivity. Since the mean penetration experienced by the sensors during the three years of exposure was less than or equal to 0.1 μm , the annual corrosion rate was less than or equal to 0.03 $\mu\text{m}/\text{y}$.

The gravimetric method confirms the above result, yielding maximum corrosion rates of 0.02 $\mu\text{m}/\text{y}$ (Table 5). This method also indicates a difference in corrosivity between the various sites of the experimental devices: the corrosivity below containment aperture C was considerably lower (one order of magnitude less) than below apertures A and B, where the corrosivity was similar. The reason for these differences may lie in small temperature and RH variations between each site.

3.2.4. Conclusions

- The design used to measure the atmospheric corrosion rate inside the reactor containment was shown to work acceptably well, allowing the evaluation of this parameter in accordance with international standards.
- The corrosivity of the atmosphere inside the reactor containment vessel was close to the lower limit of ISO 11844-1 (ISO 11844-1, 2006) corrosivity category IC2 "low corrosivity". As to whether this corrosivity poses a risk to the structures present inside the containment, the very low corrosion rates obtained with both electrical resistance measurements and the gravimetric method indicate that the generalised corrosion experienced by the structures during this period is negligible for practical purposes.

Acknowledgements

The authors wish to express their gratitude to Empresa Nacional de Residuos Radioactivos S.A. (ENRESA) for the funding and the facilities provided for the performance of these studies, and especially to Alejandro Rodríguez for his constant support and guidance.

4. References

- Ambler, H.R., Bain, A.A.J. (1955). Corrosion of metals in the tropics. *J. Appl. Chem.* **5**, 437-467.
- ASTM G96-90. (2001). "Standard guide for on-line monitoring of corrosion in plant equipment (electrical and electrochemical methods)", West Conshohocken, PA, ASTM International.
- Barton, K. (1976). *Protection against atmospheric corrosion*. Wiley and Sons, 0-471-01349-8, London.
- Blanchard, D.C., Woodcock, A.H. (1980). The production, concentration and vertical distribution of the sea-salt aerosol. *Ann. N. Y. Acad. Sci.* **338**, 330-347.
- BMDP Statistics computer software.

- Bonnarens, E., Bragard, A. (1981). *Recherche collective sur la corrosion atmospherique des aciers*. Report EUR 7400. Commission of the European Communities (Directorate General Information Market and Innovation), Luxembourg.
- BS 1747. (1963). "Methods for the measurement of air pollution. Part. 4. The lead dioxide method." British Standards Institution, London.
- Chawla S., Payer, J.H. (1991). Atmospheric corrosion. A comparison of outdoor vs. indoor, *La Metalurgia Italiana*, **84** (2), 135-138.
- Chico, B., Mariaca, L., Otero, E., Morcillo, M. (1997) Evaluación de la corrosión atmosférica en ambientes marinos mediante probetas alambre sobre tornillo. *Afinidad*. LIV, **469**, May-June, 241-245, 0001-9704.
- Compton, K.G., Mendizza, A., Bradley, W.W. (1955). Atmospheric galvanic couple corrosion. *Corrosion*. **11**, 383t-392t, 0010-9312.
- Costa, J.M., Morcillo, M., Feliu, S. (1989). Efecto de los parámetros ambientales en la corrosión. In: *Encyclopedia of environmental control technology*. Cheremisinoff, P.N. (Ed), 197, Gulf Publishing, 0-87201-245-X, Houston.
- Doyle, D.P., Godard, H.P. (1963). A rapid method for determining the corrosivity of the atmosphere at any location. *Nature*. **200** (4912) 1167-1168, 0028-0836.
- Doyle, D.P., Godard, H.P. (1969). Rapid determination of corrosivity of an atmosphere to aluminium. *Proceedings of the 3rd International Congress on Metallic Corrosion*. pp. 429-437. Moscow, MIR Publishers.
- Doyle, D.P., Wright, T.E. (1969). Climat test shows corrosivity. Alcan news. Marzo.
- Doyle, D.P., Wright, T.E. (1971). A rapid method for predicting adequate service lives for overhead conductors in marine atmospheres. The Institute of Electrical and Electronic Engineers (IEEE), Winter Power Meeting, New York, Paper 71. CP 172-PWR.
- Doyle, D.P., Wright, T.E. (1982). Rapid methods for determining atmospheric corrosivity and corrosion resistance. In: *Atmospheric Corrosion*. Ailor, W.H. (Ed), 227-243, Wiley and Sons, 0-471-86558-3, New York.
- Feliu, S., Morcillo, M. (1982). Corrosión y protección de los metales en la atmósfera. Bellaterra, S.A., 84-7290-031-2, Barcelona.
- Feliu, S., Morcillo, M., Feliu, S. Jr. (1993). The prediction of atmospheric corrosion from meteorological and pollution parameters - 1. Annual corrosion & - 2. Long-term forecasts. *Corrosion Science*. **34** (3), 403-422
- Godard, H.P. (1963). Galvanic corrosion behaviour of aluminium in the atmosphere. *Materials Protection*. **2** (6) 38-47
- ISO 8407 (1991). Corrosion of metals and alloys. Procedures for removal of corrosion products from corrosion test specimens. Geneve, Switzerland, International Organization for Standardization.
- ISO 9223 (1992). "Corrosion of metals and alloys. Corrosivity of atmospheres. Classification". Geneve, Switzerland, International Organization for Standardization.
- ISO 9225 (1992). "Corrosion of metals and alloys. Corrosivity of atmospheres. Measurement of pollution". Geneve, Switzerland, International Organization for Standardization.
- ISO 9226 (1992). "Corrosion of metals and alloys. Corrosivity of atmospheres. Determination of corrosion rate of standard specimens for the evaluation of corrosivity". Geneve, Switzerland, International Organization for Standardization.

- ISO 11844-2. (2006). "Corrosion of Metals and Alloys – Classification of low corrosivity of indoor atmospheres – Part. 1: Determination and estimation of indoor corrosivity", Geneve, Switzerland, International Organization for Standardization.
- ISO 11844-2. (2005). "Corrosion of Metals and Alloys – Classification of low corrosivity of indoor atmospheres – Part. 2: Determination of corrosion attack in indoor atmospheres", Geneve, Switzerland, International Organization for Standardization.
- Johnson, E., Stanners, J.F. (1981). *The characterisation of corrosion test sites in the community*. Report EUR 7433. Commission of the European Communities (Directorate General Information Market and Innovation), Luxembourg.
- Kucera, V., Mattson, E. (1986). Atmospheric corrosion. In: *Corrosion mechanisms*. Mansfeld, F. (Ed.), 211, Marcel Dekker, Inc., 0-8247-7627-5, New York.
- Leygraf, C. Graedel, T.E. (2000). *Atmospheric corrosion*, Wiley-Interscience, 0-471-37219-6, New York.
- Lovett, R.F. (1978). Quantitative measurement of airborne sea-salt in the North Atlantic. *Tellus*. **30**, 358-364.
- Morcillo, M., Feliu, S. (1977). Análisis de la corrosividad atmosférica en España mediante probetas "alambre sobre tornillo". *Rev. Metal Madrid*. **13** (4), 212-222, 0034-8570.
- Morcillo, M., Chico, B., Mariaca, L., Otero, E. (1999). Effect of marine aerosol on atmospheric corrosion. *Mat. Perform.* **38**, 72-77, 0094-1492.
- Morcillo, M., Chico, B., Mariaca, L., Otero, E. (2000). Salinity in marine atmospheric corrosion: its dependence on the wind regime existing in the site. *Corrosion Science*. **42**, 91-104, 0010-938X.
- Otero, E., de la Fuente, D., Chico, B., Madrid, F., Naranjo, V., Morcillo, M. Atmospheric corrosion monitoring inside the reactor vessel of a retired nuclear power plant. *Corrosion*. **63** (6), 591-597, 0010-9312
- Rozenfeld, I.L. (1972). *Atmospheric corrosion of metals*. NACE, Houston, TX.
- Strekalov, P.V. (1988). Wind regimes, chloride aerosol particle sedimentation and atmospheric corrosion of steel and copper. *Protection of metals*. **24** (5), 630-641, 0033-1732.
- Strekalov, P.V., Panchenko, Yu.M. (1994). The Role of marine aerosols in atmospheric corrosion of metals. *Protection of metals*. **30** (3), 254-263, 0033-1732.
- Zezza, F., Macri. (1995). Marine aerosol and stone decay. *The science and the total environment*. **167**, 123-143.

Stochastic wind profiles determination for radioactive substances released from nuclear power plants

Kelen Berra de Mello, Marco Túllio de Vilhena and Bardo E.J. Bodmann
*Universidade de Caxias do Sul, Centro de Ciências Exatas e Tecnologia Rua Francisco
Getúlio Vargas 1130, 95070-560 Caxias do Sul, RS
Universidade Federal do Rio Grande do Sul, PROMEC & PPGMAp Av. Osvaldo Aranha
99/4, 90046-900 Porto Alegre, RS
Brazil*

Abstract

In this review we discuss a stochastic turbulent wind profile based on the three-dimensional stochastic Langevin equation for Gram-Chalier probability density function and a known mean wind velocity. Its solution permits to simulate radioactive substances dispersion in a turbulent regime, which is of interest for nuclear reactor accident scenarios and their related emergency actions. We discuss the stochastic Langevin equation together with an analytical method for solving the three-dimensional and time dependent equation which is then applied to radioactive substance dispersion for a stochastic turbulence model. The solution is obtained using the Adomian Decomposition Method, which provides a direct scheme for solving the problem without the need for linearisation and any transformation. The results of the model are compared to case studies with measured data and further compared to procedures and predictions from other approaches.

1. Introduction

Increasing energy demand and the related climate problem has beside other options reawaken nuclear energy as one possible pathway out of the as problematic predicted future perspectives, such as electricity shortages, fossil fuel price increases, global warming and heavy metal emissions from fossil fuel use among others. Estimates indicate that within the next two decades electrical energy consumption will double, which implies an increase in nuclear power plants. Experience gathered along the nuclear history has sharpened the rules and regulations that lead to the commissioning of latest generation nuclear technology. One of the issues is the choice of the site considering meteorological aspects as well as possible accident scenarios and their related emergency actions. In this line the following contribution focuses on the question of radioactive material dispersion after discharge from a nuclear power plant. The atmosphere is considered the principal vehicle by which radioactive materials that are either released from a nuclear power plant in experimental or eventually in accidental events could be dispersed in the environment and result in radiation exposure of plants, animals and last not least humans. Thus, the evaluation of airborne radioactive material transport in the

atmosphere is one of the requirements for design and licensing of a nuclear power plant. In order to analyse the (possible) consequences of radioactive discharge atmospheric dispersion models are of need, which have to be tuned using specific meteorological parameters and conditions in the considered region. Moreover, they shall be subject to the local orography and supply with realistic information on radiological consequences of routine discharges and potential accidental releases of radioactive substances. Furthermore, case studies by model simulations may be used to establish limits for escape of radioactive material from the power plant into the atmosphere.

To this end in the present study, the wind profile with its turbulent properties for the different stability regimen in the planetary boundary layer are determined using the non-linear stochastic Langevin equation for a known average wind velocity field and probability density functions depending on the regimen in consideration. We show how the model is solved analytically using the decomposition method which then may provide short, intermediate and long term (normalized) concentrations and permit to assess the probability of occurrence of high contamination level case studies of accidental scenarios and additionally serve as a supplement for designing emergency response plans. The stochastic character of the process is implemented using the appropriate Gaussian, bi-Gaussian and Gram-Charlier probability distributions for the different stabilities. Exactness of the solution is manifest in stable convergence, which we control by a Lyapunov theory inspired criterion. The most adequate probability distribution is indicated by a novel statistical validation index, which from comparison to experimental data selects the most significant model. Comparison to the Copenhagen and to other deterministic approaches shows the advantage of the present analytical approach even for considerably rugged land relieves.

The stochastic character of turbulence is implemented using the Gram-Charlier probability distribution. Exactness of the solution is manifest in stable convergence, which we control by a Lyapunov theory inspired criterion. The most adequate probability distribution for the wind scenario of interest is indicated by a novel statistical validation index, which from comparison to experimental data selects the most significant approach. Comparison to the Copenhagen and to other deterministic approaches shows the advantage of the present analytical approach even for considerably rugged land relieves.

Our chapter is organised as follows. In section 2 we report on the state of the art of stochastic wind profile modelling, and show how a closed form solution may be obtained by Adomian's decomposition method. In 3, we present the numerical results for three probability density functions and in section 4 we come to our conclusions.

2. Stochastic Wind Profile Modelling

Dispersion of radioactive material in the planetary boundary layer is a stochastic process and thus obeys a stochastic law which may be expressed as a set of stochastic differential equations. For a time dependent regime considered in the present work, we assume that the associated Langevin equation adequately describes such a dispersion process, which we test by comparison to other methods in order to pin down computational errors and finally analyse for model adequacy. We are aware of the fact that up to date there do exist a variety of models and approaches to the problem, either based on numerical schemes, stochastic simulations or (semi-)analytical approaches and indicate in the further a selection of models. Numerical approaches may be found in the works of Tangerman Tangerman (1978), Brebbia Brebbia (1981), Chock et al. Chock et al. (1996), Sharan et al. Sharan et al. (1997) and Huebner et al. Huebner et al. (2001). There are various models that have been used effectively in the past

to describe tracer dispersion Zannetti (1990), Seinfeld and Pandis (1998), Arya (2003), Arya (1999), and many of them make use of analytical approaches Lin and Hildemann (1997); Seinfeld and Pandis (1998); Sharan et al. (2003). One also finds semi-analytical methods, where we mention the works of Parlange Parlange (1971), Dike Dike (1975), Henry et al. Henry et al. (1991), Grisogono and Oerlemans Grisogono and Oerlemans (2001), Metha and Yadav Metha and Yadav (2003), Carvalho et al. Carvalho et al. (2005a) and Carvalho and Vilhena Carvalho and Vilhena (2005).

Upon developing a model one typically faces various problems. First one has to identify a differential equation that shall represent a model or a physical law. Once the law/model is accepted as the fundamental equation one challenges the task of solving the equation in many cases approximately and analyse the error of approximation and numerical errors in order to validate its prediction against experimental data. Experimental data of a stochastic process typically spread around average values, i.e. are distributed according to probability distributions. Hence, the model shall within certain limits reproduce the experimental findings. Since the fundamental equation is already a simplification deviations may occur which in general have their origin in a model error superimposed by numerical or approximation based errors. In case of a genuine convergence criterion one may pin down the error analysis essentially to a model validation. Since in general convergence is handled by heuristic convergence criteria, a model validation is not that obvious. Thus we show with the present discussion, that our semi-analytical approach does not only yield an acceptable solution to the Langevin equation but predicts tracer concentrations closer to observed values which is also manifest in the statistical analysis.

Simulation of substance dispersion in the Planetary Boundary Layer (PBL) through a Lagrangian particle model by the use of the Langevin equation and its diffusion equation limit (random displacement equation) usually has been solved by the method of Itô calculus Gardiner (1985); Rodean (1996). More recently one of the authors developed the Iterative Langevin Solution (ILS) method, which solves the Langevin equation in a semi-analytical manner by the method of successive approximations, known as Picard's iterative method. The method is principally characterised by the following steps: Application of Picard's procedure on the Langevin equation, to be more specific, integration, linearisation of the stochastic non-linear term and iterative solution of the resultant equation, which permits to evaluate an analytical expression for the velocity. Details of this approach may be found elsewhere Carvalho and Vilhena (2005); Carvalho et al. (2005a;b; 2007a;b); Szinvelski et al. (2006).

An alternative analytical method for solving linear and non-linear differential equations was developed by Adomian Adomian (1988), known as the decomposition method. The decomposition procedure permits to cast the solution into a convergent series by using the necessary number of iterations for both linear and non-linear deterministic and stochastic equations. The advantage of this method is that it provides a direct scheme for solving the problem without the need for linearisation or transformations. There exists a vast literature about applications of this method to a broad class of physical problems and we cite the works we considered relevant for the further discussion Adomian (1988; 1994; 1996); Dehghan (2004); El-Wakil et al. (2006); Eugene (1993); Inc (2004); Laffer and Abbaoui (1996). Thus the present work extends the list of methods that solve the Langevin equation assuming a Gram-Chalier turbulence condition by Adomian's approach. The variety of methods, numerical solution of the Langevin equation (integrated according to the Itô calculus), analytical solution of the Langevin equation (derivation of Uhlenbeck and Ornstein Uhlenbeck and Ornstein (1930)), Iterative Langevin Solution (ILS) and solution by decomposition (ADM) is validated consid-

ering the measured data of ground-level concentration from a tracer experiment Gryning and Lyck (1984).

2.1 The decomposition method for a stochastic process

A time dependent stochastic process μ is typically characterized by its time evolution, which depends on stochastic contributions, such as expectation values (E_n) of mean field character (E_0) and higher moments (here E_2), respectively. In our case we consider the Langevin equation to describe turbulence.

$$\mu(t + \tau) - \mu(t) = \int_t^{t+\tau} E_0(\mu(t'), t') dt' + \int_t^{t+\tau} (E_2(\mu(t'), t'))^{\frac{1}{2}} d\Sigma(t') \quad (1)$$

Here $d\Sigma$ is a stochastic measure for random motion and E_0 represents a drift like term, whereas E_2 is a measure for diffusion intensity, which satisfy the usual Lipschitz continuity condition in order to ensure the existence of a unique strong solution. In case of a Wiener process $\mu(t)$ is Markovian, but in our case we presume that the process is an Itô process, i.e. it depends on the present and previous values, hence the integral form of mean field and fluctuation contributions. Note, that the integral form will be used further down in order to set-up the solution following Adomian's prescription, which we resume in the following.

One may rewrite the stochastic equation from above (1) as a differential equation, upon using the limit $\tau \rightarrow 0$ and separating all terms depending on the process μ including the differential operator (LHS of equation (2)) from the noise generating term $G(t)$ (the stochastic contribution, last term in eq. (1)).

$$\mathcal{L}[\mu(t)] = \mathcal{L}_L[\mu(t)] + \mathcal{L}_N[\mu(t)] = G(t) \quad (2)$$

According to Adomian, one splits the linear operator, that includes the derivatives \mathcal{L}_L with known inversion from the non-linear terms \mathcal{L}_N . Further we write $\mu(t)$ as a sum of a convergent sequence $\mu_i(t)$, still to be specified, and the non-linear term is cast into a sum of so called Adomian functional polynomials Adomian (1988).

$$\mu(t) = \sum_{i=0}^{\infty} \mu_i(t) \quad \mathcal{L}_N[\mu] = \sum_{i=0}^{\infty} A_i \quad (3)$$

For the non linear part we use a normal convergent operator expansion

$$\frac{\partial^m}{\partial \mu^m} (\mathcal{L}_N[\mu]) = \frac{\partial^m F}{\partial \mu^m} = F^{(m)} \quad (4)$$

and rewrite the non-linear term as

$$\begin{aligned}
 \mathcal{L}_N[\mu] &= \sum_{n=0}^{\infty} \frac{1}{n!} \underbrace{\frac{\partial^n F}{\partial \mu^n} \Big|_{\mu=\mu_0}}_{F_0^{(n)}} \left(\sum_{m=1}^{\infty} \mu_m \right)^n \\
 &= \lim_{r \rightarrow \infty} \sum_{n=0}^{\infty} \frac{1}{n!} F_0^{(n)} \sum_{\substack{k_1, \dots, k_r \\ \Sigma k_i = n}} \left(\binom{n}{\{k_i\}_1^r} \prod_{m=1}^r \mu_m^{k_m} \right) \\
 &= F_0^{(0)} + \sum_{n=1}^{\infty} \left(F_0^{(1)} \mu_n + \sum_{j=2}^n \frac{1}{j!} F_0^{(j)} \sum_{\substack{k_1, \dots, k_{n-1} \\ \Sigma k_i = j}} \left(\binom{j}{\{k_i\}_1^{n-1}} \prod_{m=1}^{n-1} \mu_m^{k_m} \right) \right)
 \end{aligned} \tag{5}$$

where we introduced the shorthand notations for the derivative terms $F_0^{(n)}$ and the polynomial coefficients $\binom{n}{\{k_i\}_1^r} = \binom{n}{k_1, \dots, k_r}$. Introducing these terms into the original differential equation permits to identify corresponding terms, that give rise to the iterative scheme in the spirit of Adomian as shown next.

$$\begin{aligned}
 \sum_{i=0}^{\infty} \mathcal{L}_L[\mu_i(t)] &= G(t) - \\
 &- F_0^{(0)} - \sum_{n=1}^{\infty} \left(F_0^{(1)} \mu_n + \sum_{j=2}^n \frac{1}{j!} F_0^{(j)} \sum_{\substack{k_1, \dots, k_{n-1} \\ \Sigma k_i = j}} \left(\binom{j}{\{k_i\}_1^{n-1}} \prod_{m=1}^{n-1} \mu_m^{k_m} \right) \right)
 \end{aligned} \tag{6}$$

There are many possibilities to set up an iterative scheme which upon truncation to n terms in A_n and $n + 1$ terms in μ_n yields an approximate solution in analytical form. Instead of solving the original Langevin equation we cast the problem into a set of simpler equations which may be solved because the integral operator \mathcal{L}_L^{-1} is known.

$$\begin{aligned}
 \mathcal{L}_L[\mu_0] &= G \\
 \mathcal{L}_L[\mu_1] &= -A_0 = -F_0^{(0)} \\
 \mathcal{L}_L[\mu_2] &= -A_1 = -F_0^{(1)} \mu_1 \\
 \mathcal{L}_L[\mu_3] &= -A_2 = -F_0^{(1)} \mu_2 - \frac{1}{2} F_0^{(2)} \mu_1^2 \\
 &\vdots \\
 \mathcal{L}_L[\mu_{n+1}] &= -A_n = -F_0^{(1)} \mu_n - \sum_{j=2}^n \frac{1}{j!} F_0^{(j)} \sum_{\substack{k_1, \dots, k_{n-1} \\ \Sigma k_i = j}} \left(\binom{j}{\{k_i\}_1^{n-1}} \prod_{m=1}^{n-1} \mu_m^{k_m} \right) \\
 &\vdots
 \end{aligned} \tag{7}$$

The way we have set up the iterative scheme defines the seed $\mu_0(t)$ of the functions iteration by the stochastic contribution as source term, whereas the remaining iterators are simply given by the Adomian functional polynomials as source terms of the equations to be solved. Note that in order to evaluate the i -th iteration step μ_i the μ_j with $j < i$ are known from the previous iteration steps. Moreover, the functional expansion of the non-linear term around the function μ_0 shows how the stochastic term effectively enters in the remaining terms μ_i with $i > 0$ from the non-linearity.

2.2 A convergent closed form solution

The iteration defines a convergent series towards μ for all t in a certain domain, thus the solution $\mu = \lim_{n \rightarrow \infty} \sum_{i=0}^n \mu_i$ is manifest exact. Since this scheme defines an explicit analytical expressions for the μ_i and A_i , respectively, one arrives at a procedure which permits to solve the differential equation without linearisation in closed form. The procedure has been applied to a variety of non-linear problems but an analytical procedure for testing convergence to the best of our knowledge has not been presented in literature, only numerical schemes may be found, see for instance refs. Inc (2004) and Aminataei and Hosseini (2007).

In general convergence is not guaranteed by the decomposition method, so that the solution shall be tested by a convenient criterion. Since standard convergence criteria do not apply for the present case due to the non-linearity and stochastic character, we present a method which is based on the reasoning of LyapunovBoichenko et al. (2005). While Lyapunov introduced this conception in order to test the influence of variations of the initial condition on the solution, we use a similar procedure to test the stability of convergence while starting from an approximate (initial) solution μ_0 (the seed of the iteration scheme).

Let us denote $|\delta Z_n| = \|\sum_{i=n+1}^{\infty} \mu_i\|$ the maximum deviation of the correct from the approximate solution $\Gamma_n = \sum_{i=0}^n \mu_i$, where $\|\cdot\|$ signifies the maximum norm. Then convergence occurs if there exists an n_0 such that the sign of λ is negative for all $n \geq n_0$.

$$\lambda = \frac{1}{\|\Gamma_n\|} \log \left(\frac{|\delta Z_n|}{|\delta Z_0|} \right) \quad (8)$$

In the further we apply the decomposition method as presented in general form above to the problem of tracer dispersion for three different turbulence probability density functions, i.e. Gaussian, bi-Gaussian and Gram-Chalier, respectively. The analysis of convergence is applied to all cases that shows that for $n_0 = 4$ the approach is convergent with an error less than 1%.

3. The Langevin Equation for Stochastic Turbulence

The stochastic equation (1) may be interpreted in terms of the Langevin equation, where μ represents the turbulent velocity vector with components u_i . In the Langevin equation Rodean (1996) the time evolution of the turbulent velocity is driven by a dissipative term and a second term which may be understood as the gradient of a potential that depends on the fluctuations of the turbulent velocity and represents a mean field interaction of the pollutant with the environment it is immersed. The last term represents the stochastic contribution due to a continuous series of particle collisions.

$$\frac{du_i}{dt} + \alpha_i u_i = \beta_i + \gamma_i u_i^2 + (C_0 \varepsilon)^{\frac{1}{2}} \xi_i(t). \quad (9)$$

Here u_i with $i = 1, 2, 3$ is a Cartesian component of the turbulent velocity, which is related to the infinitesimal displacement and the wind velocity U_i by $dx_i = (U_i + u_i)dt$. The coefficients

$\alpha_i, \beta_i, \gamma_i$ of eq. (9) depend on the employed probability density function. Here C_0 is the Kolmogorov constant, ε is the rate of turbulence kinetic energy dissipation, and ζ_i is a random increment according to a probability density function.

Upon application of the described decomposition method from above (see 2.1) on equation (9), the turbulent velocity is decomposed into a series and the non-linear contribution is taken care of by Adomian's procedure.

$$\frac{d}{dt} \left(\sum_{n=0}^{\infty} u_{i,n} \right) + \alpha_i \left(\sum_{n=0}^{\infty} u_{i,n} \right) = \beta_i + (C_0 \varepsilon)^{\frac{1}{2}} \zeta_i(t) + \gamma_i \left(\sum_{n=0}^{\infty} A_{i,n} \right), \quad (10)$$

where the non-linear term is $\sum_{n=0}^{\infty} A_{i,n} = u_i^2$.

In the iterative scheme the stochastic component is absorbed in the first term u_0 of the expansion and thus propagates through all subsequent terms, whereas the non-linear (mean field) term enters as a correction from the second term on. For any given truncation m the solution for the considered problem (9) is given in closed analytical form summing up the terms $\sum_{n=0}^m u_{i,n}$.

So far we have not defined the probability density function, that characterizes the type of turbulence which is correlated to the stability of the planetary boundary layer (PBL). In the studies of turbulent dispersion the stochastic behaviour may be classified according to stationarity or non-stationarity, according to spatial properties as homogeneity or non-homogeneity and according to the profile of the wind distribution, as Gaussian or non-Gaussian. When employing Lagrangian models one usually considers stationary and homogeneous turbulence in horizontal sheets and non-homogeneous and either Gaussian or non-Gaussian in the vertical direction depending on the stability condition. In stable or neutral conditions the velocity distribution may be considered Gaussian, whereas during convective conditions the velocity distribution is non-Gaussian because of the skewness of the turbulent velocity distribution, which has its origin in up- and down-drafts with different intensity. In the following we present the solutions for the Gram-Chalier probability density functions together with their model validation against the data from the Copenhagen experiment Gryning and Lyck (1984).

3.1 The Copenhagen experiment

The Copenhagen tracer experiment Gryning and Lyck (1984) was carried out in the northern part of Copenhagen. A tracer (SF_6) was released without buoyancy from a tower at a height of 115m and collected at the ground-level positions in up to three crosswind arcs of tracer sampling units. The sampling units were positioned 2km – 6km from the point of release. A total of nine tracer experiment runs were performed in stability conditions as shown in table 1. The site was mainly residential with a roughness length of 0.6m. Wind speeds at 10 and 115 meters were used to calculate the coefficient for the vertical exponential wind profile, which is used to model the wind speed.

$$\chi = \left[\frac{\log \left(\frac{U(115)}{U(10)} \right)}{\log \left(\frac{115}{10} \right)} \right]$$

$$U(z) = U(10) \left[\frac{z}{10} \right]^\chi \quad (11)$$

where $U(10)$ is the wind speed in 10m and $U(115)$ is the wind speed in 115m, respectively.

Run	L (m)	z_i (m/s)	u_* (m/s)	w_* (m/s)	$U(10)$ (m/s)	$U(115)$ m	h
1	-37	1980	0.36	1.8	2.1	3.4	1980
2	-292	1920	0.73	1.8	4.9	10.6	1920
3	-71	1120	0.38	1.3	2.4	5.0	1120
4	-133	390	0.38	0.7	2.5	4.6	390
5	-444	820	0.45	0.7	3.1	6.7	820
6	-432	1300	1.05	2.0	7.2	13.2	1300
7	-104	1850	0.64	2.2	4.1	7.6	1850
8	-56	810	0.69	2.2	4.2	9.4	810
9	-289	2090	0.75	1.9	5.1	10.5	2090

Table 1. Meteorological parameters measured during the Copenhagen experiment. L is the Monin-Obukhov length, z_i the convective boundary layer height, u_* is the local friction velocity, w_* is the convective velocity scale, $U(10)$ is the wind speed in 10m and $U(115)$ is the wind speed in 115m and h is the PBL height.

For the simulations, the turbulent flow is assumed inhomogeneous only in the vertical direction and the transport is realized by the longitudinal component of the mean wind velocity. The horizontal domain was determined according to sampler distances and the vertical domain was set equal to the observed PBL height. The time step was maintained constant and was obtained according to the value of the Lagrangian decorrelation time scale ($\Delta t = \tau_L/c$), where τ_L must be the smaller value among τ_{L_u} , τ_{L_v} , τ_{L_w} and C is an empirical coefficient set equal to 10. In Equation (10), the product $C_0\varepsilon$ is calculated in terms of the turbulent velocity variance σ_i^2 and the Lagrangian decorrelation time scale τ_{L_i} Hinze (1986); Tennekes (1982), which are parametrised according to a scheme developed by Degrazia et al. (Degrazia et al. (2000)). These parametrisations are based on Taylor's statistical diffusion theory and the observed spectral properties. The concentration field is determined by counting the particles in a cell or imaginary volume in the position x, y, z . The integration eq. (10) was computed by the Romberg method.

3.2 Solution for Gaussian turbulence

In the case where a Gaussian probability density function describes best the stochastic turbulence the coefficients of the Langevin equation (9) and (10) are

$$\alpha_i = \frac{C_0\varepsilon}{2\sigma_i^2}, \quad \beta_i = \frac{1}{2} \frac{\partial \sigma_i^2}{\partial x_j}, \quad \gamma_i = \frac{1}{2\sigma_i^2} \left(\frac{\partial \sigma_i^2}{\partial x_j} \right). \quad (12)$$

In Table (2) we compare the experimental findings with the model predictions by the proposed procedure (ADM - Adomian Decomposition Method), by the Itô method Rodean (1996), by the ILS method Carvalho and Vilhena (2005) and the early analytical derivation (ANA) by Uhlenbeck and Ornstein Uhlenbeck and Ornstein (1930). From the comparison one observes a reasonable agreement among the models and also with the experimental data. In the following table the numerical convergence of the ADM approach for a Gaussian probability density function (pdf) is indicated. The convergence analysis shows that already a few terms represent an analytical solution with spurious error only. The figures 1 show the Lyapunov exponent of

Exp.	Distance (m)	Observed ($\mu g m^{-2}$)	Predictions C_y ($\mu g m^{-2}$)			
			ADM	ILS	Itō	ANA
1	1900	2074	2092	2770	1486	2320
1	3700	739	1281	725	1001	2026
2	2100	1722	1496	1699	1344	1290
2	4200	944	850	1489	1117	1059
3	1900	2624	2601	2710	2415	2366
3	3700	1990	1605	2136	1649	2066
3	5400	1376	1273	1328	1073	2062
4	4000	2682	2379	2726	1947	1565
5	2100	2150	2586	2138	2042	2090
5	4200	1869	1818	2484	1967	1701
5	6100	1590	1568	2206	1690	1819
6	2000	1228	951	915	872	853
6	4200	688	619	775	718	651
6	5900	567	488	673	612	622
7	2000	1608	1172	1606	1015	1320
7	4100	780	680	1290	660	1145
7	5300	535	554	933	548	1170
8	1900	1248	1228	1252	1099	726
8	3600	606	723	522	887	667
8	5300	456	489	416	737	682
9	2100	1511	1433	1660	1330	1334
9	4200	1026	884	1135	1162	1068
9	6000	855	630	894	962	1115

Table 2. Concentrations of nine runs with various positions of the Copenhagen experiment and model prediction by the approaches ADM, ILS, Itō and ANA, using a Gaussian probability density function.

the Adomian approach depending on the number of terms for the 9 experimental runs. Note, that the more negative the exponent λ the more stable is convergence. Figure (2) shows the dispersion of the Copenhagen experimental data in comparison with their model predictions by ADM, Itō, ILS, ANA. Note, that the closer the data are grouped to the bisector the better is the agreement between experiment and prediction.

In figure 3 we show the linear regression of each model, where the closer their intersect is to the origin and the closer the slope is to unity the better is the approach. By comparison one observes that the present approach yields the best description of the data. Details of the regression may be found in table 4. In order to perform a model validation we introduce an index κ which if identical zero there is a perfect match between the model and the experimental findings.

$$\kappa = \sqrt{(a - 1)^2 + \left(\frac{b}{\bar{C}_o}\right)^2} \quad \text{with} \quad \bar{C}_o = \frac{1}{n} \sum_{i=1}^n C_{oi} \quad (13)$$

Here a is the slope, b the intersection, C_{oi} the experimental data and \bar{C}_o the arithmetic mean. Since both the experiment and the model are of stochastic character, fluctuations are present,

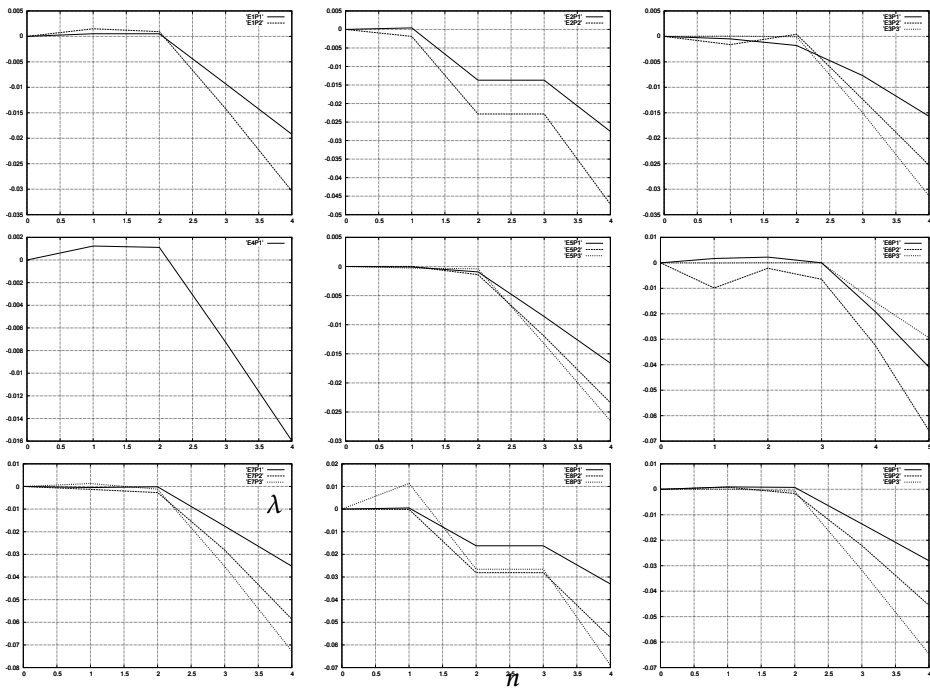


Fig. 1. Lyapunov exponent λ of the Adomian approach depending on the number n of terms for the 9 experimental runs.

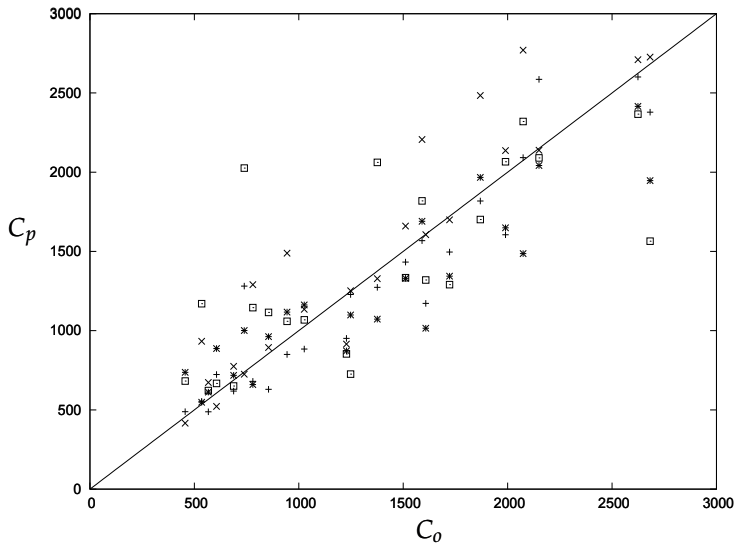


Fig. 2. Dispersion diagram of predicted (C_p) against measured values (C_p) by ADM (+), ILS (\times), Itō (*), ANA (\square).

Run	Terms	$C_v (\mu g m^{-2})$		
1	u_0	2063.595	1289.481	
	$u_0 + u_1$	2010.773	1340.828	
	$u_0 + u_1 + u_2$	2011.426	1308.431	
	$u_0 + u_1 + u_2 + u_3$	2092.073	1281.515	
	$u_0 + u_1 + u_2 + u_3 + u_4$	2092.073	1281.515	
2	u_0	1417.238	823.5428	
	$u_0 + u_1$	1356.679	855.5662	
	$u_0 + u_1 + u_2$	1495.957	850.2274	
	$u_0 + u_1 + u_2 + u_3$	1495.957	850.2274	
	$u_0 + u_1 + u_2 + u_3 + u_4$	1495.957	850.2274	
3	u_0	2549.781	1563.213	1292.831
	$u_0 + u_1$	2615.559	1607.727	1250.595
	$u_0 + u_1 + u_2$	2600.684	1526.362	1253.927
	$u_0 + u_1 + u_2 + u_3$	2601.178	1604.603	1272.520
	$u_0 + u_1 + u_2 + u_3 + u_4$	2601.178	1604.603	1272.520
4	u_0	2376.284		
	$u_0 + u_1$	2444.419		
	$u_0 + u_1 + u_2$	2427.065		
	$u_0 + u_1 + u_2 + u_3$	2379.459		
	$u_0 + u_1 + u_2 + u_3 + u_4$	2379.459		
5	u_0	2134.523	1525.608	1454.858
	$u_0 + u_1$	2215.876	1523.247	1491.563
	$u_0 + u_1 + u_2$	2544.441	1794.193	1626.543
	$u_0 + u_1 + u_2 + u_3$	2586.452	1817.632	1567.856
	$u_0 + u_1 + u_2 + u_3 + u_4$	2586.452	1817.632	1567.856
6	u_0	959.1522	567.4748	471.1268
	$u_0 + u_1$	912.4229	619.4894	518.6852
	$u_0 + u_1 + u_2$	890.4201	605.0680	454.2511
	$u_0 + u_1 + u_2 + u_3$	942.7131	620.3289	483.5103
	$u_0 + u_1 + u_2 + u_3 + u_4$	951.0098	619.3738	1488.264
7	$u_0 + u_1 + u_2 + u_3 + u_4 + u_5$	951.0098	619.3738	1488.264
	u_0	1087.322	699.6638	585.6924
	$u_0 + u_1$	1122.203	687.8445	624.9547
	$u_0 + u_1 + u_2$	1098.108	682.8063	537.3536
	$u_0 + u_1 + u_2 + u_3$	1171.588	679.6330	554.0372
8	$u_0 + u_1 + u_2 + u_3 + u_4$	1171.588	679.6330	554.0372
	u_0	1184.016	787.5058	489.2957
	$u_0 + u_1$	1150.614	780.2734	502.6539
	$u_0 + u_1 + u_2$	1228.163	722.6319	489.3400
	$u_0 + u_1 + u_2 + u_3$	1228.163	722.6319	489.3400
9	$u_0 + u_1 + u_2 + u_3 + u_4$	1228.163	722.6319	489.3400
	u_0	1404.454	853.9096	679.9700
	$u_0 + u_1$	1332.897	825.2356	681.6997
	$u_0 + u_1 + u_2$	1523.163	876.8478	661.7837
	$u_0 + u_1 + u_2 + u_3$	1433.129	884.0126	630.3093
	$u_0 + u_1 + u_2 + u_3 + u_4$	1433.129	884.0126	630.3093

Table 3. Numerical Convergence of ADM using a Gaussian pdf.

but in the average model and experiment shall coincide, thus the introduced index represents a genuine model validation.

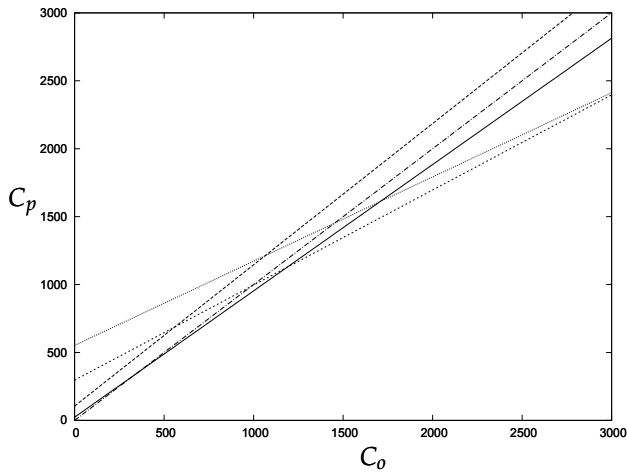


Fig. 3. Linear regression for the ADM (—), ILS (---), Itō (· · · · ·) and ANA (· · · · ·) with a Gaussian pdf. The bisector (· · · · ·) was added as an eye guide.

Modelo	Regression	R^2	κ
ADM	$y = 0,93x + 23,50$	0,89	0,07
ILS	$y = 1,04x + 105,51$	0,87	0,09
Itō	$y = 0,70x + 296,13$	0,83	0,37
ANA	$y = 0,62x + 552,32$	0,33	0,56

Table 4. Comparison of the linear regressions of ADM, ILS, Itō and ANA for a Gaussian pdf.

3.3 Solution for bi-Gaussian turbulence

In the convective boundary layer, the heating of the air layer close to the ground produces turbulent flux which gives origin to the so-called up- and down-drafts. This phenomenon is not symmetric but has a more intensive contribution from the up-drafts. Because of mass conservation the down-drafts occupy a larger area. As a consequence the stochastic term shall be asymmetric which excludes the Gaussian probability density as a convenient function. There is no indication for a unique probability density function so far, nevertheless the following characteristics shall be present.

- The probability density shall have an enhanced tail towards higher velocities, that indicate the more energetic up-drafts, but with a smaller integral proportion than down-drafts.
- The probability density shall have a pronounced maximum at negative velocities, i.e. the down-drafts.

One finds typically two types of asymmetric probability density functions in the literature, the bi-Gaussian and the Gram-Chalier distribution, where the latter is represented by a truncated series of Hermite polynomials.

In the further we discuss the bi-Gaussian probability density function, which contains a linear superposition of two Gaussian functions, one with maximum probability at a positive velocity, the other one at a negative value as for instance in ref. Baerentsen and Berkowicz

(1984). Baerentsen e Berkowicz (1984) used a pair of Langevin equations, one for up- and one for down-drafts, each with its specific Gaussian function. In this work we condense this phenomenon in one equation, introducing a sum of two Gaussian functions with different parameters and relative weight.

$$P(z, w) = A_1 P_1(z, w) + A_2 P_2(z, w) \quad (14)$$

where A_1 and A_2 define the relative proportions between up- (P_1) and down-drafts (P_2) for the vertical turbulent velocities (w).

$$P(z, w) = \frac{1}{\sqrt{2\pi}} \frac{A_1}{\sigma_1} \exp \left[-\frac{1}{2} \left(\frac{w - m_1}{\sigma_1} \right)^2 \right] + \frac{1}{\sqrt{2\pi}} \frac{A_2}{\sigma_2} \exp \left[-\frac{1}{2} \left(\frac{w - m_2}{\sigma_2} \right)^2 \right] \quad (15)$$

Here, m_1, m_2 are the average probabilities of P_1 and P_2 , respectively, and σ_1 and σ_2 represent the standard deviations of each distribution. The mean up- and down-draft velocities are

$$m_1 = \langle w_1 \rangle \quad \text{and} \quad m_2 = \langle w_2 \rangle, \quad (16)$$

and the respective standard deviations are

$$\sigma_1 = \left(\langle w_1^2 \rangle \right)^{\frac{1}{2}} \quad \text{and} \quad \sigma_2 = \left(\langle w_2^2 \rangle \right)^{\frac{1}{2}}. \quad (17)$$

A general prescription on how to determine the parameters $A_1, A_2, m_1, m_2, \sigma_1$ and σ_2 consists in the usage of generating functional of moments.

$$\langle w_n \rangle = \int_{-\infty}^{\infty} w^n P(z, w) dw \quad (18)$$

From the normalisation and the first four statistical momenta one obtains an equation system which eliminates the unknowns.

$$A_1 + A_2 = 1 \quad (19)$$

$$A_1 m_1 + A_2 m_2 = 0 \quad (20)$$

$$A_1 (m_1^2 + \sigma_1^2) + A_2 (m_2^2 + \sigma_2^2) = \sigma_w^2 \quad (21)$$

$$A_1 (m_1^3 + 3m_1\sigma_1^2) + A_2 (m_2^3 + 3m_2\sigma_2^2) = \langle w^3 \rangle \quad (22)$$

$$A_1 (m_1^4 + 6m_1^2\sigma_1^2 + 3\sigma_1^4) + A_2 (m_2^4 + 6m_2^2\sigma_2^2 + 3\sigma_2^4) = \langle w^4 \rangle \quad (23)$$

Upon application of the bi-Gaussian probability density function the expression for the deterministic coefficient of the vertical dimension in the Langevin equation is then,

$$a_w = -w \frac{A_1 P_1 \sigma_1^2 + A_2 P_2 \sigma_2^2}{\sigma_1^2 \sigma_2^2} \frac{C_0 \epsilon}{2P} + \left(\frac{A_1 w_1 P_1}{\sigma_1^2} + \frac{A_2 w_2 P_2}{\sigma_2^2} \right) \frac{C_0 \epsilon}{2P} + \frac{\phi}{P}. \quad (24)$$

Using the deterministic coefficient the Langevin equation reads

$$\frac{dw}{dt} + \frac{A_1 P_1 \sigma_1^2 + A_2 P_2 \sigma_2^2}{\sigma_1^2 \sigma_2^2} \frac{C_0 \epsilon}{2P} w = \left(\frac{A_1 w_1 P_1}{\sigma_1^2} + \frac{A_2 w_2 P_2}{\sigma_2^2} \right) \frac{C_0 \epsilon}{2P} + \frac{\phi}{P} + (C_0 \epsilon)^{\frac{1}{2}} \xi_w(t), \quad (25)$$

where ϕ is obtained upon application of the bi-Gaussian probability density function Luhar et al. (1996):

$$\begin{aligned} \phi = & -\frac{1}{2} \left(A_1 \frac{\partial w_1}{\partial z} + w_1 \frac{\partial A_1}{\partial z} \right) \operatorname{erf} \left(\frac{w - w_1}{\sqrt{2}\sigma_1} \right) \\ & + w_1 P_1 \left[A_1 \frac{\partial w_1}{\partial z} \left(\frac{w^2}{\sigma_1^2} + 1 \right) + w_1 \frac{\partial A_1}{\partial z} \right] + \frac{1}{2} \left(A_2 \frac{\partial w_2}{\partial z} + w_2 \frac{\partial A_2}{\partial z} \right) \operatorname{erf} \left(\frac{w - w_2}{\sqrt{2}\sigma_2} \right) \\ & + w_2 P_2 \left[A_2 \frac{\partial w_2}{\partial z} \left(\frac{w^2}{\sigma_2^2} + 1 \right) + w_2 \frac{\partial A_2}{\partial z} \right]. \end{aligned} \quad (26)$$

In a more compact form this yields for the Langevin equation with a bi-Gaussian probability density function (25)

$$\frac{dw}{dt} + \alpha_w w = \beta_w + \gamma_w + (C_0 \varepsilon)^{\frac{1}{2}} \xi_w(t), \quad (27)$$

where

$$a_w = \frac{A_1 P_1 \sigma_1^2 + A_2 P_2 \sigma_2^2}{\sigma_1^2 \sigma_2^2} \frac{C_0 \varepsilon}{2P}, \quad \beta_w = \left(\frac{A_1 w_1 P_1}{\sigma_1^2} + \frac{A_2 w_2 P_2}{\sigma_2^2} \right) \frac{C_0 \varepsilon}{2P} \gamma_w = \frac{\phi}{P}.$$

In Table (5) the concentrations of the measurements together with theoretical predictions of ADM, ILS and Itô are presented. Table (6) shows the numerical convergence of the ADM method. As already evident in the previous case also for the bi-Gaussian probability density function only a few terms are necessary in order to represent a solution.

Figure (5) shows the dispersion plot of the experimental values against the theoretical predicted values by ADM, ILS and the Itô calculus.

We also apply the model validation as introduced in the previous section to the model application with the bi-Gaussian probability density function. One observes that the all three approaches are more or less close to the bisector, however the comparison with the model validation from the previous case shows that the Gaussian probability density function seems more adequate for the stability condition of the experiment which is also manifest in the smallest κ for ADM.

From the comparison of the regressions in table 7 one recognizes that the three approaches behave similar with respect to R^2 but show larger values for κ in comparison to the case where the Gaussian probability density function defined the stochastic character of the turbulence.

3.4 Solution for Gram-Chalier turbulence

The use of the Gram-Chalier probability density function for stochastic Lagrangian models was proposed by Ferrero e Anfossi (1998) Ferrero et al. (2000), which makes use of an expansion in Hermite polynomials. In the present discussion we use the series until the fourth resulting in an asymmetric probability density function for the vertical turbulent velocities.

$$P(r, z) = \frac{e^{-\frac{r^2}{2}}}{\sqrt{2\pi}} (1 + c_3 H_3 + c_4 H_4), \quad (28)$$

where

$$c_3 = \frac{1}{6} \mu_3, \quad c_4 = \frac{1}{24} (\mu_4 - 6\mu_2 + 3), \quad (29)$$

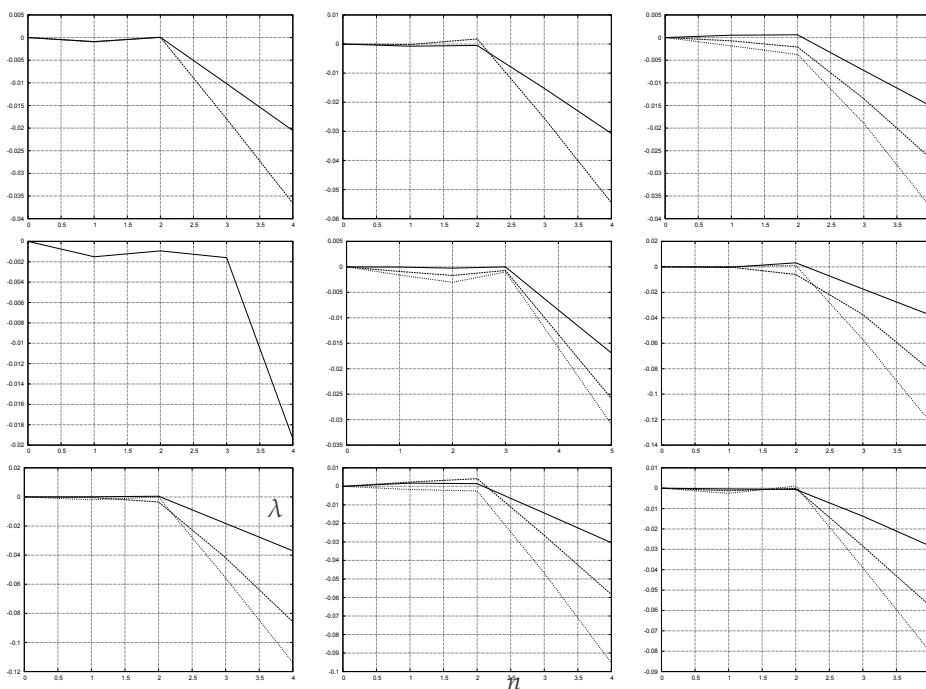


Fig. 4. Lyapunov exponent λ of the Adomian approach depending on the number n of terms for the 9 experimental runs using the bi-Gaussian pdf.

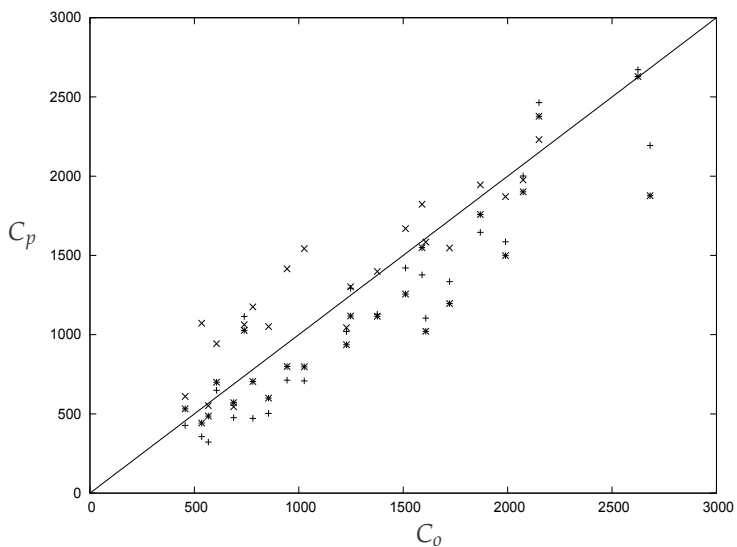


Fig. 5. Dispersion diagram of predicted (C_p) measured against measured (C_o) values by by ADM (+), ILS (x) and Itō (*) for a bi-Gaussian pdf.

Exp.	Distance (m)	Observation ($\mu\text{g m}^{-2}$)	Prediction C_y ($\mu\text{g m}^{-2}$)		
			Bi-Gaussian	ILS	It \bar{o}
1	1900	2074	2001	1976	1901
1	3700	739	1115	1063	1027
2	2100	1722	1335	1547	1196
2	4200	944	713	1415	799
3	1900	2624	2672	3020	2629
3	3700	1990	1586	1871	1499
3	5400	1376	1129	1399	1116
4	4000	2682	2194	3001	1877
5	2100	2150	2464	2231	2378
5	4200	1869	1646	1945	1758
5	6100	1590	1377	1823	1549
6	2000	1228	1020	1044	936
6	4200	688	476	545	571
6	5900	567	322	552	486
7	2000	1608	1104	1584	1021
7	4100	780	472	1175	704
7	5300	535	357	1072	442
8	1900	1248	1293	1302	1118
8	3600	606	649	943	700
8	5300	456	427	610	532
9	2100	1511	1421	1669	1256
9	4200	1026	708	1543	797
9	6000	855	503	1051	600

Table 5. Concentration from the Copenhagen experiment and predictions from ADM, ILS and It \bar{o} using a bi-Gaussian pdf.

$$H_3 = r^3 - 3r, \quad H_4 = r^4 - 6r^2 + 3, \quad (30)$$

and $r = u_i/\sigma_i$. In the case of Gaussian turbulence equation (28) recovers the normal distribution with c_3 and c_4 equal zero. The Gram-Charlier probability density function of the third order is obtained by the choice $c_4 = 0$. Upon application of equation (28) in the equation of the deterministic coefficients yields,

$$a(x_i, u_i) = \frac{f_i}{h_i} \frac{\sigma_i}{\tau_{L_i}} + \sigma_i \frac{\sigma_i}{x_j} \frac{g_i}{h_i}, \quad (31)$$

where $j = 1, 2, 3$ and $j \neq i$, τ_{L_i} is the Lagrangian correlation time scale and f_i , g_i and h_i are expressions as shown below.

$$f_i = -3C_3 - r_i(15C_4 + 1) + 6C_3r_i^2 + 10C_4r_i^3 - C_3r_i^4 - C_4r_i^5 \quad (32)$$

$$g_i = 1 - C_4 - r_i^2(1 + C_4) - 2C_3r_i^3 - 5C_4r_i^4 + C_3r_i^5 + C_4r_i^6 \quad (33)$$

$$h_i = 1 - 3C_4 - 3C_3r_i - 6C_4r_i^2 + C_3r_i^3 + C_4r_i^4 \quad (34)$$

Run	Terms	$C_v (\mu g m^{-2})$		
1	u_0	1930,605	1164,849	
	$u_0 + u_1$	1988,625	1097,584	
	$u_0 + u_1 + u_2$	1923,805	1169,695	
	$u_0 + u_1 + u_2 + u_3$	2000,73	1114,916	
	$u_0 + u_1 + u_2 + u_3 + u_4$	2000,73	1114,916	
2	u_0	1268,718	705,3707	
	$u_0 + u_1$	1310,076	706,2147	
	$u_0 + u_1 + u_2$	1299,548	687,1277	
	$u_0 + u_1 + u_2 + u_3$	1335,249	713,1350	
	$u_0 + u_1 + u_2 + u_3 + u_4$	1335,249	713,1350	
3	u_0	2645,291	1388,329	934,7424
	$u_0 + u_1$	2569,380	1520,158	1152,943
	$u_0 + u_1 + u_2$	2545,731	1592,848	1132,120
	$u_0 + u_1 + u_2 + u_3$	2671,856	1585,870	1129,320
	$u_0 + u_1 + u_2 + u_3 + u_4$	2671,856	1585,870	1129,320
4	u_0	1918,952		
	$u_0 + u_1$	2183,475		
	$u_0 + u_1 + u_2$	2156,671		
	$u_0 + u_1 + u_2 + u_3$	2201,707		
	$u_0 + u_1 + u_2 + u_3 + u_4$	2193,560		
5	u_0	2342,774	1341,859	1061,910
	$u_0 + u_1$	2573,369	1572,562	1340,005
	$u_0 + u_1 + u_2$	2527,639	1664,515	1371,924
	$u_0 + u_1 + u_2 + u_3$	2585,538	1545,632	1290,100
	$u_0 + u_1 + u_2 + u_3 + u_4$	2464,081	1646,118	1376.838
6	$u_0 + u_1 + u_2 + u_3 + u_4 + u_5$	2464,081	1646,118	1376.838
	u_0	1024,609	470,6826	312,2561
	$u_0 + u_1$	1016,280	481,9288	311,2449
	$u_0 + u_1 + u_2$	925,6591	476,7062	308,4274
	$u_0 + u_1 + u_2 + u_3$	1019,558	476,3795	321,7595
7	$u_0 + u_1 + u_2 + u_3 + u_4$	1019,558	476,3795	321,7595
	u_0	1048,864	510,2945	401,3791
	$u_0 + u_1$	1042,545	439,8970	378,0348
	$u_0 + u_1 + u_2$	1012,276	479,4384	400,1880
	$u_0 + u_1 + u_2 + u_3$	1104,080	472,1360	357,2161
8	$u_0 + u_1 + u_2 + u_3 + u_4$	1104,080	472,1360	357,2161
	u_0	1280,617	646,3909	378,3521
	$u_0 + u_1$	1193,205	662,8212	402,9780
	$u_0 + u_1 + u_2$	1219,809	702,0541	443,7521
	$u_0 + u_1 + u_2 + u_3$	1293,085	649,3011	427,3928
9	$u_0 + u_1 + u_2 + u_3 + u_4$	1293,085	649,3011	427,3928
	u_0	1452,223	652,5918	469,1815
	$u_0 + u_1$	1438,980	729,6335	493,3640
	$u_0 + u_1 + u_2$	1433,919	656,2526	448,3562
	$u_0 + u_1 + u_2 + u_3$	1420,842	707,7180	503,2054
	$u_0 + u_1 + u_2 + u_3 + u_4$	1420,842	707,7180	503,2054

Table 6. Numerical convergence of ADM for a bi-Gaussian pdf.

Inserting the deterministic coefficient (31) into the Langevin equation renders the latter

$$\frac{du_i}{dt} = \frac{f_i}{h_i} \frac{\sigma_i}{\tau_{L_i}} + \sigma_i \frac{\partial \sigma_i}{\partial x_j} \frac{g_i}{h_i} + (C_0 \varepsilon)^{\frac{1}{2}} \zeta_i(t). \quad (35)$$

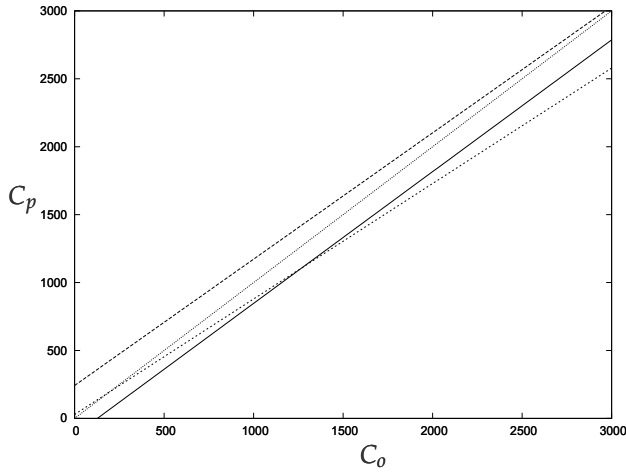


Fig. 6. Linear regression for the ADM (—), ILS (---) and Itō (- · - ·) with a Bi-Gaussian pdf. The bisector (- · - ·) was added as an eye guide.

Model	Regression	R^2	κ
ADM	$y = 0,97x - 123,47$	0,89	0,10
ILS	$y = 0,93x + 242,34$	0,89	0,19
Itō	$y = 0,85x + 29,07$	0,86	0,15

Table 7. Comparison of the linear regressions using the bi-Gaussian probability density function.

In short hand notation this reads

$$\frac{du_i}{dt} = \alpha_i + \beta_i + (C_0\epsilon)^{\frac{1}{2}} \xi_i(t), \tag{36}$$

where

$$\alpha_i = \frac{f_i}{h_i} \frac{\sigma_i}{\tau_{L_i}}, \tag{37}$$

$$\beta_i = \sigma_i \frac{\partial \sigma_i}{\partial x_j} \frac{g_i}{h_i}. \tag{38}$$

In table (8) we present the concentrations of the Copenhagen experiment together with the results from the ADM, ILS and Itō approaches.

Table 9 shows the numerical convergence of the ADM method. As in the two previous cases only a few terms reproduce with considerable fidelity the exact solution with a Gram-Chalier probability density function. Figure (8) shows the dispersion plot of observed against predicted data. In Figure (9) are shown the linear regression for the three approaches. All three methods, ADM, ILS and Itō reproduce reasonably well the expected bisector. Using the model validation index κ shows that for all three probability density functions the ADM approach yields results closest to the expected concentration profile.

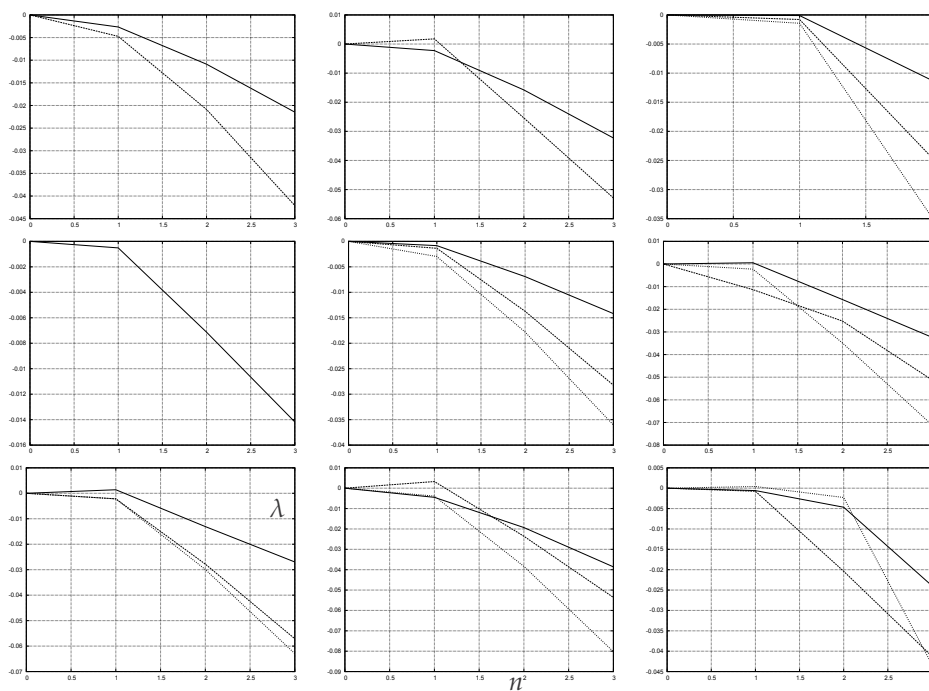


Fig. 7. Lyapunov exponent λ of the Adomian approach depending on the number of terms n for the 9 experimental runs using the Gram-Charlier pdf.

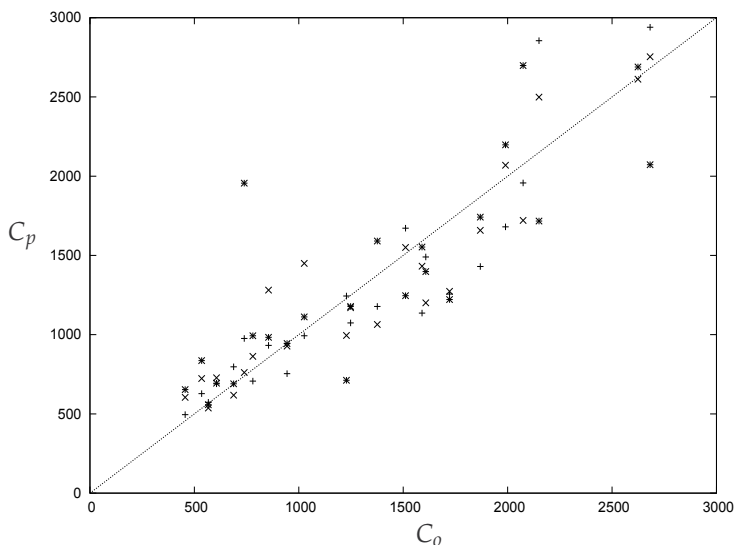


Fig. 8. Dispersion diagram of predicted (C_p) against observed values (C_o) with a Gram-Charlier probability density function.

Exp.	Distance (m)	Observation ($\mu\text{g m}^{-2}$)	Prediction C_y ($\mu\text{g m}^{-2}$)		
			ADM	ILS	Ito
1	1900	2074	1957	1721	2698
1	3700	739	976	761	1956
2	2100	1722	1256	1273	1222
2	4200	944	754	928	944
3	1900	2624	3426	2612	2689
3	3700	1990	1680	2069	2198
3	5400	1376	1178	1064	1591
4	4000	2682	2940	2754	2072
5	2100	2150	2855	2499	1717
5	4200	1869	1430	1658	1742
5	6100	1590	1136	1432	1553
6	2000	1228	1244	995	712
6	4200	688	797	618	690
6	5900	567	573	537	558
7	2000	1608	1490	1201	1398
7	4100	780	707	863	993
7	5300	535	628	723	836
8	1900	1248	1074	1170	1178
8	3600	606	690	728	694
8	5300	456	495	604	653
9	2100	1511	1672	1550	1246
9	4200	1026	993	1450	1112
9	6000	855	932	1281	983

Table 8. Concentration of the Copenhagen experiment in comparison to the predictions by ADM, ILS and Itō using a Gram-Chalier pdf.

As already mentioned before, the model validation indicates the Gaussian probability density function implemented together with the ADM approach as the most adequate description for the Copenhagen experiment by virtue of $\kappa = 0.07$ being significantly smaller than all other realizations. This was also to be expected from the stability conditions given in table 1, which characterize the turbulence regime as strong convective. It is worth mentioning that since convergence is genuinely controlled the present procedure permits to pin down model limitations which in other approaches are hidden in numerical imprecision or approximations.

4. Conclusions

In this paper we presented an analytical solution of the three-dimensional stochastic Langevin equation applied to radioactive substance dispersion for Gaussian, bi-Gaussian and Gram-Chalier turbulence, respectively. The solution was obtained using the Adomian Decomposition Method (ADM) whose principal advantage relies in the fact that the non-linearity can be taken care of without linearisation or simplifications. Further, the stochastic part is absorbed in the initial term of the iteration and thus propagates through all the subsequent iteration terms. For the Langevin equation the non-trivial questions of uniqueness and convergence

Run	Terms	$C_y (\mu g m^{-2})$		
1	u_0	2134,374	905,1679	
	$u_0 + u_1$	1958,222	975,6816	
	$u_0 + u_1 + u_2$	1957,265	976,3862	
	$u_0 + u_1 + u_2 + u_3$	1957,265	976,3862	
2	u_0	1215,582	733,3223	
	$u_0 + u_1$	1258,735	683,5825	
	$u_0 + u_1 + u_2$	1256,363	754,4139	
	$u_0 + u_1 + u_2 + u_3$	1256,363	754,4139	
3	u_0	3431,128	1602,438	1114,993
	$u_0 + u_1$	3422,063	1700,270	1165,802
	$u_0 + u_1 + u_2$	3425,766	1679,948	1177,613
	$u_0 + u_1 + u_2 + u_3$	3425,766	1679,948	1177,613
4	u_0	3066,27		
	$u_0 + u_1$	2911,51		
	$u_0 + u_1 + u_2$	2939,85		
	$u_0 + u_1 + u_2 + u_3$	2939,85		
5	u_0	2817,202	1396,448	1075,217
	$u_0 + u_1$	2858,730	1434,506	1134,203
	$u_0 + u_1 + u_2$	2855,275	1429,748	1136,310
	$u_0 + u_1 + u_2 + u_3$	2855,275	1429,748	1136,310
6	u_0	1273,45	851,0902	525,1321
	$u_0 + u_1$	1304,966	797,4598	559,2511
	$u_0 + u_1 + u_2$	1243,54	797,4534	572,6406
	$u_0 + u_1 + u_2 + u_3$	1243,54	797,4534	572,6406
7	u_0	1461,67	672,4225	613,2297
	$u_0 + u_1$	1868,749	699,8157	631,2928
	$u_0 + u_1 + u_2$	1489,976	707,4423	627,6641
	$u_0 + u_1 + u_2 + u_3$	1489,976	707,4423	627,6641
8	u_0	973,0740	691,4625	512,5447
	$u_0 + u_1$	1074,354	702,0862	497,4521
	$u_0 + u_1 + u_2$	1073,538	690,2837	494,8708
	$u_0 + u_1 + u_2 + u_3$	1073,538	690,2837	494,8708
9	u_0	1647,435	1054,789	898,2956
	$u_0 + u_1$	1662,513	963,0107	883,1010
	$u_0 + u_1 + u_2$	1671,778	992,9380	936,4106
	$u_0 + u_1 + u_2 + u_3 + u_4$	1671,788	992,9380	932,4106

Table 9. Numerical convergence of ADM using a Gram-Chalier pdf.

Model	Regression	R^2	κ
ADM	$y = 1,09x + 113,83$	0,85	0,12
ILS	$y = 0,90x + 112,17$	0,87	0,13
ITO	$y = 0,78x + 324,52$	0,62	0,33

Table 10. Comparison of the linear regressions for the ADM, ILS and Itō approach using the Gram-Chalier probability density function.

for the Adomian approach in stochastic problems is given since the drift and dispersion terms

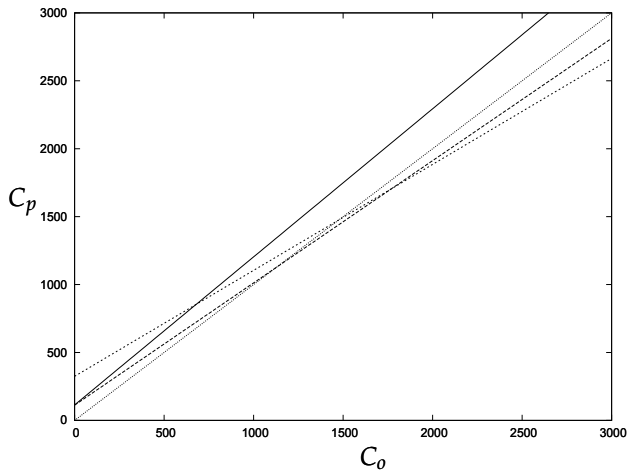


Fig. 9. Linear regression using the Gram-Charlier probability density function

satisfy a Lipschitz condition.

We showed in a general form how to construct a recursive scheme where convergence is understood. A genuine criterion was introduced based on Lyapunov's theory, that in our case tests stability of convergence. Application of that criterion showed that in all three cases only up to five terms are necessary so that the approximate solution differs from the real solution by less than one percent. On the one hand, the generality of the proposed solution with respect to the considered probability density functions on the other hand the controlled convergence permits to validate the model in question. In this line we introduced a novel index, that describes the deviation of the model prediction from the one represented by the experimental data, using the relation between predicted to observed tracer concentrations. Based on this index we verify that the model with the Gaussian density function yields within the phenomenon inherent fluctuations the best agreement between model and observation. Among the three probability distributions the Gaussian one is from the physics point of view considered the most adequate for the Copenhagen experiment.

Furthermore, the ADM solution was validated by comparison with experimental data against the prediction of other models, i.e. the numerical solution of the Langevin equation by integration according to the Itô calculus, the analytical solution of the Langevin equation (ANA) following the derivation of Uhlenbeck and Ornstein and the Iterative Langevin Solution (ILS). A statistical analysis showed good agreement between predicted and measured data and all values are within the range that are characteristic for other state-of-the-art approaches. The ranking from the analysis defines the sequence ADM, ILS, Itô, ANA, which is manifest in the fact that the ratio of predicted to observed concentrations in the ADM approach was reasonably close to the bisector. Thus, the present approach may be considered a valuable procedure to simulate tracer dispersion in the atmosphere until new improvements will alter the present picture.

We believe that we have done a step into a new direction with the present contribution, that may be useful to analyse meteorological aspects as well as simulate possible scenarios, for the purpose to analyse (possible) consequences of radioactive discharge and its relation to radiological consequences of routine discharges and potential accidental releases of radioactive

substances from nuclear power plants. Furthermore, these case studies by model simulations may be used to establish limits for escape of radioactive material from the power plant into the atmosphere. Since measurements are typically performed in a limited set of positions a calibrated model is able to reconstruct the three dimensional wind velocity field considering especially the contributions by turbulence. To the best of our knowledge up-to-date the tracer technique is not used for site evaluation, but could supply valuable information on the wind properties for a given region of interest and its time-behaviour.

5. References

- G. Adomian, A Review of the Decomposition Method in Applied Mathematics, *J. Math. Anal. Appl.* 135 (1988) 501-544.
- G. Adomian, *Solving Frontier Problems of Physics: The Decomposition Method*, Kluwer, Boston, 1994.
- G. Adomian, Solution of coupled non-linear partial differential equations by decomposition, *Comp. Math. Appl.* 31 (1996) 117-120.
- A. Aminataei, S.S. Hosseini, *Applied Mathematics and Computation* 186, 1, (2007) 665-669.
- S.P. Arya, *Air Pollution Meteorology and Dispersion*, Oxford University Press, New York, 1999.
- S.P. Arya, (2003), A review of the theoretical bases of short-range atmospheric dispersion and air quality models, *Proc. Indian Natn. Sci. Acad.* 69A (2003) 709-724.
- Baerentsen, J. H. and Berkowicz, R.: 1984, "Monte-Carlo Simulation of Plume Diffusion in the Convective Boundary Layer", *Atmos. Environ.* 18, 701-712.
- C.A. Brebbia, *Progress in Boundary Element Methods*, Pentech Press, London, 1981.
- V.A. Boichenko, G.A. Leonov, V. Reitmann, *Dimension theory for ordinary equations*, Teubner, Stuttgart (2005).
- Burden, Richard L.: *Numerical analysis*. 8th ed., Thomson-Brooks/Cole, Belmont, CA (2005).
- J.C. Carvalho and M.T. Vilhena, Pollutant dispersion simulation for low wind speed condition by the ILS method, *Atmos. Environm.* 39 (2005) 6282-6288.
- J.C. Carvalho, E.R. Nichimura, M.T. Vilhena, D.M. Moreira, G.A. Degrazia, An iterative langevin solution for contaminant dispersion simulation using the Gram-Charlier PDF, *Environm. Mod. And Soft.* 20 3 (2005a) 285-289.
- J.C. Carvalho, M.T. Vilhena, D.M. Moreira, An alternative numerical approach to solve the Langevin equation applied to air pollution dispersion, *Water Air and Soil Pollution* 163 1-4 (2005b) 103-118.
- J.C. Carvalho, M.T. Vilhena, M. Thomson, An iterative Langevin solution for turbulent dispersion in the atmosphere, *J. Comp. Appl. Math.* 206 (2007) 534-548.
- J.C. Carvalho, M. T. Vilhena, D. M. Moreira, Comparison between Eulerian and Lagrangian semi-analytical models to simulate the pollutant dispersion in the PBL. *Appl. Math. Model.* 31 (2007) 120-129.
- D.P. Chock, P. Sun, S.L. Winkler, Trajectory-grid: an accurate sign-preserving advection-diffusion approach for air quality modelling, *Atmos. Environ.* 30 6 (1996) 857-868.
- G.A. Degrazia, D. Anfossi, J.C. Carvalho, C. Mangia, T. Tirabassi, H.F. Campos Velho, Turbulence parameterization for PBL dispersion models in all stability conditions, *Atmos. Environ.* 34 (2000) 3575-3583.
- M. Dehghan, The use of Adomian decomposition method for solving the one dimensional parabolic equation with non-local boundary specification, *Int. J. Comput. Math.*, 81 (2004) 25-34.

- M.V. Dike, *Perturbation Methods in Fluid Mechanics*, Academic Press, New York, 1975.
- S.A. El-Wakil, A. Elhanbaly, M.A. Abdou, Adomian decomposition method for solving fractional non-linear differential equations, *Appl. Math. Comput.* 182 1 (2006) 313-324.
- Y. Eugene, Application of the decomposition to the solution of the reaction-convection-diffusion equation, *Appl. Math. Comput.* 56 (1993) 1-27.
- E. Ferrero, D. Anfossi, G. Tinarelli, M. Tamiazzo, Inter-comparison of Lagrangian stochastic models based on two different PDFs, *International Journal of Environment and Pollution*, Vol. 14 (2000) pp. 225 - 234.
- C.W. Gardiner, *Handbook of stochastic methods for physics, chemistry and the natural sciences*, Springer-Verlag, Berlin, 1985.
- B. Grisogono and J. Oerlemans (2001), Katabatic flow: analytic solution for gradually varying eddy diffusivities, *J. Atmos. Sci.*, 58, 3349-3354.
- S.E. Gryning and E. Lyck, Atmospheric dispersion from elevated source in an urban area: comparison between tracer experiments and model calculations, *J. Climate Appl. Meteor.* 23 (1984) 651-654.
- S.R. Hanna, Confidence limit for air quality models as estimated by bootstrap and jackknife re-sampling methods, *Atmos. Environm.* 23 (1989) 1385-1395.
- R.C. Henry, R.C., Y.J. Wand, K.A. Gebhart (1991), The relationship between empirical orthogonal functions and sources of air pollution, *Atmos. Environ.*, 25A, 503-509.
- Hinze, J.O.: *Turbulence*. Mc Graw Hill, vol. 1, CRC Press, Inc., Florida (1986).
- K.H.H., Huebner, D.L. Dewhurst, D.E. Smith, T.G. Byrom, *Finite Element Method for Engineers*, J. Wiley & Sons, New York, 2001.
- M. Inc, On numerical solutions of partial differential equations by the decomposition method, *Kragujevac J. Math.* 26 (2004) 153-164.
- P. Laffer and K. Abbaoui, Modelling of the thermic exchanges during a drilling: resolution with Adomian's decomposition method, *Math. and Comp. Model.* 23 10 (1996) 11-14.
- J.S. Lin and L.M. Hildemann, Analytical solutions of the atmospheric diffusion equation with multiple sources and height-dependent wind speed and eddy diffusivities, *Atmos. Environ.* 30 (1997) 239-254.
- Luhar, A. K., Hibberd, M. F., and Hurley, P. J.: 1996, "Comparison of Closure Schemes Used to Specify the Lagrangian Stochastic Dispersion Models for Convective Conditions", *Atmos. Environ.* 30, 1407-1418.
- K.N. Metha and A.K. Yadav, *Indian J. Pure and Appl. Math.*, 34, p.963, 2003.
- J.Y. Parlange, , Theory of water movement in soils: I. One-dimensional absorption, *Soil Sci.*, 111 2 (1971) 134-137.
- H.C. Rodean, *Stochastic Lagrangian models of turbulent diffusion*, American Meteorological Society, Boston, 1996.
- M. Sharan, E.J. Kansa, S. Gupta, Application of the multi-quadric method for numerical solution of elliptic partial differential equations, *Applied Mathematics and Computation* 84 (1997) 275-302.
- J.H. Seinfeld and S.N. Pandis, *Atmospheric Chemistry and Physics*, J. Wiley & Sons, New York, 1998.
- M. Sharan, M. Manish, K. Yadav, Atmospheric dispersion: an overview of mathematical modelling framework, *Proc. Indian Natn Sci. Acad.* 69A 6 (2003) 725-744.

- C.R.P. Szinvelski, M.T.M.B.Vilhena, J.C. Carvalho, G.A. Degrazia, Semi-analytical solution of the asymptotic langevin equation by the Picard iterative method, *Environm. Mod. And Soft.* 21 3 (2006) 406-410.
- G. Tangerman, Numerical simulations of air pollutant dispersion in a stratified planetary boundary layer, *Atmos. Environ.* 12 (1978) 1365-1369.
- H. Tennekes H., Similarity relation, scaling laws and spectral dynamics, in: F.T.M. Nieuwstadt and H. Van Dop (Eds.), *Atmospheric Turbulence and Air Pollution Modelling*, Reidel, Dordrecht, 1982, pp. 37-68.
- G.E. Uhlenbeck and L.S. Ornstein, On the theory of the Brownian motion, *Phys. Rev.* 36 (1930) 823-841.
- P. Zannetti, *Air Pollution Modelling*, Southampton, Comp. Mech. Publications, UK, 1990.

Carbon-14 in Terrestrial and Aquatic Environment of Ignalina Nuclear Power Plant: Sources of Production, Releases and Dose Estimates

Jonas Mazeika
*Nature Research Centre
Vilnius University
Lithuania*

1. Introduction

The development history of nuclear power in world already has over passed the limit of 50 years. This time span was sufficiently long for many nuclear reactors to complete their operation stage and to enter the decommissioning stage. The Ignalina NPP (INPP), Lithuania, is one of them. Its operation history only lasted for 26 years for different reasons but mainly the political ones. The INPP consists of two RBMK-1500 reactor units, Unit 1 and Unit 2 (Almenas et al., 1998). The "1500" refers to the designed electrical power in units of MW. Its designed thermal rating is 4800 MW. The nominal thermal power is 4250 MW, and the nominal electrical power is 1300 MW. The RBMK is a graphite-moderated boiling water channel-type reactor with the principle of electricity generation the same as for boiling water reactors (BWRs).

The Ignalina NPP is located in the north-eastern part of Lithuania near the borders of Belarus and Latvia (Fig. 1). The NPP uses the Lake Druksiai as a natural reservoir for cooling water. The surface area and volume of the lake are 4.9×10^7 m² and 3.7×10^8 m³, respectively. The maximum depth is 33 m, while the average depth is 7.6 m. The Lake Druksiai is a flow-through lake with six small creeks flowing in and one river, with a water regulation dam, flowing out.

The two reactor units, Unit 1 and Unit 2, were put into operation in December 1983 and August 1987, respectively. As a part of the obligations of the European Union Accession Treaty, Lithuania was required to shut down Units 1 and 2 of the INPP and to decommission them as soon as possible. Unit 1 was shut down on December 31, 2004 and Unit 2 on December 31, 2009. During the 26 years of operation, the INPP has produced 307.9 billion kWh of electricity: Unit 1 - 136.9 billion kWh and Unit 2 - 170.2 billion kWh. The total amount of electricity sold is 279.8 billion kWh (<http://www.iae.lt>). The INPP operational history and the routine radiation in environment monitoring data evidenced that INPP was operated safely and helpfully for the society.

The routine monitoring of radiation in environment of NPPs often does not include some important nuclides, namely carbon-14 (^{14}C), which have or may have significant contribution to effective dose of human exposure in the whole nuclear fuel cycle. ^{14}C (half-life 5730 years, maximum beta particles energy of 156 keV) occurs naturally in the environment due to the cosmic-ray (secondary neutrons) induced production in the lower stratosphere and upper troposphere on nitrogen atoms ($^{14}\text{N}(\text{n,p})^{14}\text{C}$) (Libby, 1946; Raaen et al., 1968). The naturally occurring cosmogenic ^{14}C is generated at a rate of 1.5×10^{15} Bq/year.



Fig. 1. Study area location

At the beginning of the 19th century, the concentration of ^{14}C , compared to the stable isotope ^{12}C , in the atmosphere began to decrease due to the increased burning of fossil fuel and consequent anthropogenic emissions via the Suess effect (Fairhall & Young, 1970). In the 1950s, when many atmospheric nuclear weapon tests took place, the ^{14}C concentration in the air rose sharply to a maximum (double the natural concentration), and gradually decreased in 1960s and later after cessation of atmospheric tests. The ^{14}C activity in the atmosphere has decreased steadily due to CO_2 uptake by the oceans and by the biosphere (Hertelendi & Csongor, 1982; Levin & Kromer, 2004). ^{14}C is also artificially produced in all types of nuclear reactors by the similar neutron-induced reactions on isotopes of carbon, nitrogen and oxygen present in the fuel, cladding, coolant, moderator and structural materials of the reactor (NCRP, 1985; IAEA, 2004). A fraction of the generated ^{14}C is released continuously during normal operation of NPPs, mainly in two chemical forms; oxidized, i.e. carbon dioxide (CO_2), and reduced, which mostly is in the form of CH_4 (Levin et al., 1988). For all types of reactors, except pressure water reactors (PWRs), most of the gaseous releases of ^{14}C are in the form of $^{14}\text{CO}_2$ (IAEA, 2004).

^{14}C is referred to as one of the difficult-to-measure nuclides (pure beta emitters) due to the presence of other radionuclides in a sample. ^{14}C is rarely measured in process media of nuclear reactors and even in gaseous releases from nuclear plants notwithstanding that equipment for monitoring ^{14}C in gaseous releases is today commercially available. However,

releases of gaseous ^{14}C from nuclear power reactors result in prevailing dose fraction compared to all radionuclides. This is a case for the INPP (Nedveckaitė et al., 2000).

In 2002, the Government of Lithuania approved the adoption of the “immediate dismantling” strategy for decommissioning of both INPP units. A key component of this decommissioning strategy is to dispose of operating and decommissioning waste in a near-surface repository (NSR). ^{14}C as a long-lived and mobile in the environment radionuclide and due to large inventory has been recognized as one of the most important nuclides in the assessments of doses for future generations arising from INPP NSR for low- and intermediate-level, short-lived radioactive waste (LILW) disposal. Based on the scaling factor method (Lukauskas et al., 2006; Plukis et al., 2008), a preliminary inventory of ^{14}C for NSR with capacity for disposal of approximately 100 000 m³ of waste was evaluated as 1.43×10^{13} Bq. Similar figures of ^{14}C inventory were evaluated for NSRs in other countries: Japan, Rokkasho-Mura disposal facility, first 40 000 m³, maximal inventory - 3.37×10^{12} , Spain, El Cabril disposal facility, maximum permissible activity - 2.00×10^{13} Bq (IAEA, 2004). From radioactive waste long-term management point of view, the importance of ^{14}C is also due to the large total mass of graphite per RBMK-1500 reactor (more than 1800 tons) and consequently there is a large ^{14}C inventory in graphite (IAEA, 2006). Based on calculations of graphite impurities activation, ^{14}C and tritium contribute mostly (respectively 3.91×10^{14} Bq and 2.19×10^{14} Bq) to the total activity of all the irradiated graphite constructions of the reactor (Ancius et al., 2004). It is the rough upper limit estimate, derived assuming that activation products are retained in the graphite. Activated graphite of INPP due to the high specific activity (up to 5×10^5 Bq/g) of the long-lived ^{14}C is classified as the long-lived radioactive waste.

The worldwide nuclear power operational experience gives evidence that ^{14}C is continuously released to environment from NPPs, is key radionuclide of NSRs for LILW disposal, forms significant fraction of irradiated graphite radionuclide inventory, retains in the spent nuclear fuel and consequently will be disposed of in geological repositories for long-lived high activity waste in the form of spent fuel or radioactive waste arising from spent fuel reprocessing. In this sense, we can consider ^{14}C as one of the most powerful environmental tracers of nuclear fuel cycle. Because of the biological importance of carbon (^{12}C , ^{13}C and ^{14}C) and, consequently, the biological incorporation of radioactive ^{14}C through photosynthesis, it is of great interest to run ^{14}C measurements in environment, especially if ^{14}C is not monitored in releases as was a case in the INPP operational history. Considering that ^{14}C specific activities of terrestrial and aquatic plants may vary according to the atmospheric $^{14}\text{C}/^{12}\text{C}$ ratio, many studies have investigated atmospheric and sometimes aquatic ^{14}C activities in the vicinities of nuclear power plants using vegetation as bioindicators (Obelic et al., 1986; Levin et al., 1988; Loosli & Oeschger, 1989; Buzinny et al., 1995; Milton et al., 1995; Milton & Kramer, 1998; Stenström et al., 1996; Mikhajlov et al., 1999; Magnusson et al., 2004; Mazeika et al., 2008).

The main aim of this study is to investigate how terrestrial and aquatic vegetation (organic carbon, Corg) and dissolved inorganic carbon (DIC) of aquatic environment recorded the ^{14}C activity excess compared to the contemporary ^{14}C background level during the whole period of the INPP operation (the end of 1983–the end of 2009). The ^{14}C activity excess data allow evaluating the order of magnitude of gaseous and liquid release rates due to operation of the NPP what can partially substitute direct ^{14}C release monitoring data and give basis for approximate dose estimates. The other goals are: to give closer look on ^{14}C activity aerial

dynamics in terrestrial environments (in 1996 and 2001); to present first experimental data on ^{14}C activities in different process water systems of the INPP reactor and in various water clean-up systems, namely, in evaporator concentrates and spent ion-exchange resins (taken in 2002). This chapter mostly presents the summarization of $^{14}\text{CO}_2$ specific activities in terrestrial and aquatic plants and $\text{H}^{14}\text{CO}_3^-$ specific activities in aquatic environment measured during various research projects performed in the INPP vicinity.

2. Methods

2.1 ^{14}C production in nuclear reactors

The normal operation of NPPs produces various radionuclides by fission within the fuel or by neutron activation in the structural materials and component systems of the reactor. The escape of these radionuclides from the reactor and its auxiliary process systems during operation time generates a variety of solid, liquid and gaseous radioactive waste. Despite that the design of the reactor ensures minimized escaping of radionuclides from technological systems, some radionuclides, namely ^{14}C , are continuously discharged in various effluents to environment.

The major ^{14}C producing neutron activation reactions in NPP reactors are (IAEA, 2004; Buchuev et al., 2002):

(a) The $^{14}\text{N}(n,p)^{14}\text{C}$ reaction with a very high thermal neutron capture cross-section (1.82 barn (1 barn = 10^{-24} cm²)); (b) The $^{17}\text{O}(n, \alpha)^{14}\text{C}$ reaction with a high thermal neutron capture cross-section (0.24 barn); (c) The $^{13}\text{C}(n, \gamma)^{14}\text{C}$ reaction with a low cross-section (0.9×10^{-3} barn); (d) The $^{15}\text{N}(n,d)^{14}\text{C}$ reaction with a very low cross-section (2.5×10^{-7} barn); (e) The $^{16}\text{O}(n, ^3\text{He})^{14}\text{C}$ reaction with a very low cross-section (5.0×10^{-8} barn).

Most of ^{14}C is produced in nuclear power reactors by $^{14}\text{N}(n,p)^{14}\text{C}$ reactions with nitrogen in fuels, moderators and coolants as a primary impurity, by $^{17}\text{O}(n, \alpha)^{14}\text{C}$ reactions in oxide fuels, moderators and coolants, and by $^{13}\text{C}(n,\gamma)^{14}\text{C}$ reactions in graphite moderators. Reactions (a) (b) and (c) are the most important contributors to ^{14}C production in thermal reactors. ^{14}C is also a ternary fission product, but the amount produced in this way is negligible.

The substrate atoms for the activation reactions (i.e. nitrogen, oxygen and carbon) occur widely in fuel, and in cladding, moderator, coolant or structural material, either as major constituents or as impurities. In consequence, ^{14}C produced in a reactor can be released directly to the environment from the coolant and/or moderator in a gaseous form or in much smaller quantities as liquid effluents. ^{14}C can remain in the reactor core until a reactor is decommissioned (e.g. in the graphite moderator of RBMK reactors). In INPP the spent fuel is stored in dry interim storage facility as long as 50 years before the final disposal.

^{14}C is produced in the fuel and coolant and is distributed wherever gas or fluid streams take place in NPP. Leakage of NPP systems allows an eventual release to the environment. As it is reported in (NCRP, 1985; Milton et al., 1995; IAEA, 2004), heavy water reactors (CANDU) and RBMK reactors have highest ^{14}C release rates compared to other types of reactors. The estimated ^{14}C release rate for 14 operating RBMK reactors in East Europe is 1.85×10^{12} Bq/year per reactor. The normalized emission level of ^{14}C from the RBMK type reactor in the Russian Federation has been estimated to be $1.0 \pm 0.3 \text{ TBq} \times \text{GW}(\text{e})^{-1} \times \text{year}^{-1}$ (Gaiko et al., 1985).

The following systems have been considered to be release pathways for gaseous ^{14}C from a BWR (IAEA, 2004):

(a) The condenser steam jet air ejector; (b) The turbine gland seal condenser exhaust; (c) The reactor building purge exhaust; (d) The turbine building ventilation system exhaust; (e) The radioactive waste building ventilation system exhaust.

The condenser steam jet air ejector is expected to be the most significant release point (>99% of total ^{14}C release).

A simplified scheme of main ^{14}C flows based on radioactive waste generation streams in INPP (Plukis et al., 2008) is presented in Fig. 2.

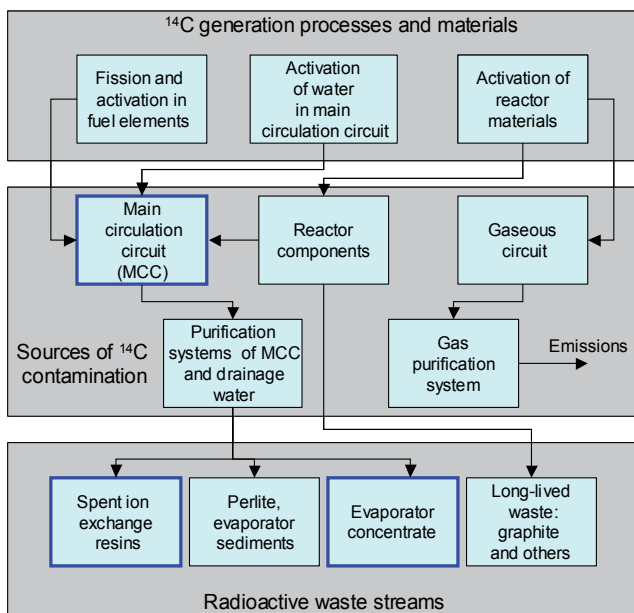


Fig. 2. A simplified scheme of main ^{14}C flows in INPP. Blue borders show studied reactor water and radioactive waste objects

^{14}C can enter the main circulation circuit (MCC) coolant (reactor water) of INPP due to fuel cladding defects, corrosion of metal structures of reactor core components and direct generation in the coolant. The ^{14}C from contaminated coolant of MCC can be further transferred to the final waste or to environment by three main routes: (i) the retention of ^{14}C in structural materials of NPP, (ii) the loss of a coolant through leakages to the drainage system, and (iii) the chemical purification of a coolant by ion exchange resins and perlite. The design of RBMK with only one circuit leads to a continuous release of ^{14}C through the ventilation stack.

2.2 Sampling and measurements

^{14}C in the INPP environment has been studied in terrestrial and aquatic plants, annual tree radial growth rings, and surface water and, at a smaller scale, in unconfined groundwater in various research projects during the whole operation period of INPP.

The main biota samples, including tree rings, as well as water samples from surface water bodies and groundwater monitoring wells (up to 20 m depth) were collected at a short distance (0.5-2 km) from the power plant (Figs. 3-4).

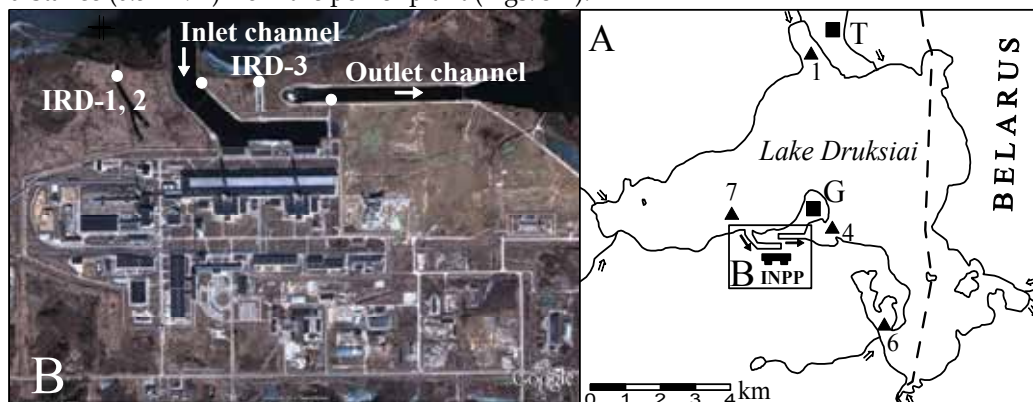


Fig. 3. Surface water and biota sampling points in Lake Druksiai and in terrestrial environment (A), and in the main channels related to INPP industrial site (B)

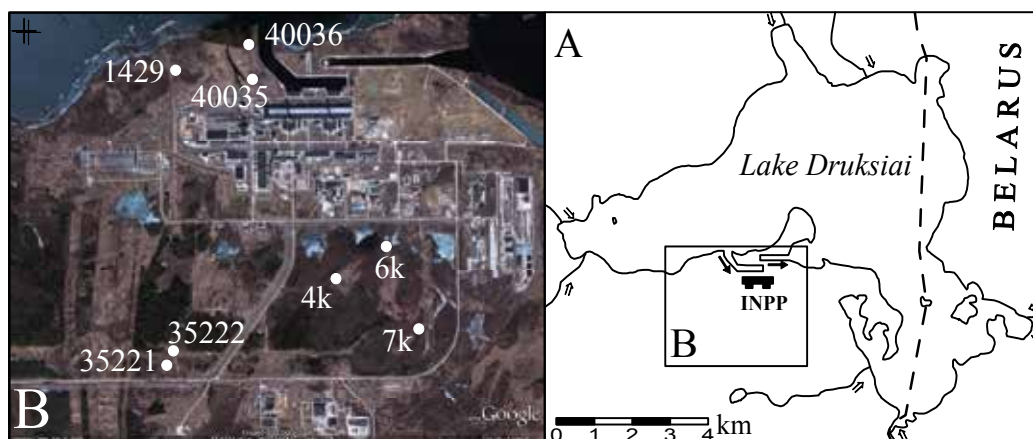


Fig. 4. Groundwater sampling points close to INPP industrial site (B)

Most often terrestrial plant samples were collected from two areas: Tilze (T monitoring site) and Grikiniskes (G monitoring site). T site is attributed to background area where impact of INPP is low and negligible. G site is located in the so called "impact zone" which basing on simple semi-empirical Gaussian plume model for estimating long-term average radionuclide concentrations in air (Gusev & Beliajev, 1986; Metodology..., 1995) was considered as mostly affected by airborne release from the INPP. Terrestrial plant samples from wider area were collected in 1996 (wormwood stems) and in 2001 (alder leaves) at a longer distance (up to 30 km) from the INPP. The terrestrial plant samples for recent years included the following species: European blueberry, Kuhn brake, Roth. rough smallreed, Hull common heather, Shimp stair-step moss and others. The aquatic samples were of macrophytes *Myriophyllum spicatum*, *Ceratophyllum demersum* and filamentous algae mainly.

Several cross-sections of the trunk of pine trees from the background regions of Lithuania and "impact zone" for separating the annual tree rings were taken in 1996, 2002 and 2003.

The water sampling by precipitating DIC from the water for ^{14}C activity concentration in the Lake Druksiai measurement have been already started before the INPP operation (Mazeika, 2002). After the start of INPP operation the new monitoring points on surface water bodies related to the INPP industrial site were established: cooling water inlet channel (IC), heated water outlet channel (OC), industrial discharge and rain water drainage (IRD) channels 1, 2, and 3 (Fig. 3).

The measurements of ^{14}C activity concentration in DIC of groundwater started during the INPP pre-operation period. In the course of time, the general view of groundwater monitoring network has changed. The network of recent years is shown in Fig. 4 (the groundwater monitoring network on site which is operated by the INPP is not included).

Groundwater sampling is mainly attributed to three monitoring well groups. The first group of wells with numbers 1429, 40035 and 40036 is installed in the "impact zone" on groundwater flow pathway down the INPP. Well No 1429 is very shallow with screening interval of 3-5 m. It has the longest period of sampling and is directly related to operational radioactive waste storage area. Wells No 40035 and 40036 with screening interval of 18-20 m are located close to groundwater flow draining boundaries (Lake Druksiai and channels IRD-1 and 2). These wells capture more diluted groundwater flow path lines compared to well 1429. The second group of wells with numbers 35221 and 35222 is not related directly to the INPP site. However these wells with screening interval of 10-20 m are installed in the quarry where the sludge from the Visaginas wastewater treatment plant was disposed of in the period preceding the quarry re-cultivation. An interest (from the point of view of radiation protection) to this area has occurred due to the fact that domestic wastewater from the INPP (from shower and laundry facilities, etc.) was treated at the same wastewater treatment plant. The third group of wells with numbers 4k, 6k and 7k are attributed to the "background area" as they are on the groundwater flow pathway upwards the INPP.

Vegetation and tree annual ring samples (up to 50 g) were dried, pyrolysed in no oxygen atmosphere. The charred material was left for further procedures. Dried carbonates (up to 150 g) precipitated in field from surface and ground water samples in alkaline media adding NaOH and CaCl_2 into water were converted to CO_2 by treatment with HCl. The collected CO_2 was stored for further procedures.

The specific activity of ^{14}C in environmental samples was measured by liquid scintillation counting (LSC) method (Gupta & Polach, 1985; Arslanov, 1985). A conventional procedure for benzene synthesis was applied (Kovaliukh & Skripkin, 1994). The several steps were followed: (1) reaction of carbon containing sample material (CO_2 for DIC of water and charred carbon for vegetation samples) with Li in the metallic reactor under vacuum at the temperature 600-700°C receiving Li_2C_2 , (2) hydrolysis of Li_2C_2 , receiving C_2H_2 , (3) synthesis of benzene by cyclotrimerization of C_2H_2 using a catalyst containing aluminous-silicate and activated with V_2O_5 , (4) purification of benzene from moisture remains by adding H_2SO_4 and by vacuum sublimation, and (5) adding the scintillation admixtures, PPO and POPOP, to benzene produced from sample material. The ^{14}C specific activity of benzene was determined by liquid scintillation counting. The main performance parameters of the spectrometric system for ^{14}C in benzene form with 3 mL Teflon vials were as follows: background count rate of 0.41 +/- 0.04 CPM; counting efficiency of 71.3±0.8%; and Figure of Merit (Efficiency²/Background) of 12 380±700.

The ^{14}C results were presented as specific activity in Bq/kg C or in percent of modern carbon, pMC (1 pMC - 2.26 Bq/kg C) (Stuiver & Polach, 1977). As bicarbonate ion is the main chemical form of ^{14}C in the water, the ^{14}C activity concentration in Bq/m³ is calculated from two experimentally measured values such as HCO_3^- concentration and ^{14}C specific activity relative to carbon. As concentration of bicarbonate ion in the surface water is relatively constant, the both units pMC and Bq/m³, express the same variation figure in time. However in the course of time, the concentration of bicarbonate ion in the groundwater ranges significantly in closely located wells or even in the same well. For groundwater it is useful to compare ^{14}C data expressed in both units, in pMC as is common for isotope geochemistry and dating issue, and in Bq/m³ what is essential for radiation protection issue.

One limited sampling campaign in 2002 was aimed to measure ^{14}C activity in different process water systems of the reactor and in various water clean-up systems, namely, in evaporator concentrates and spent ion-exchange resins. The obtained data together with other available data (Plukis et al., 2008) were used for statistical analysis of radionuclide specific activities in the INPP technological media and radioactive waste and for the calculation of the corresponding scaling factors. Correlations of difficult-to-measure radionuclides to the key radionuclide ^{60}Co showed that the scaling factor method could be applied to the RBMK-1500 reactor waste characterization.

The samples from the process water systems of the reactor and various water purification systems were provided by the INPP staff. The main processes of ^{14}C extraction from liquid samples were acid stripping and wet oxidation (Veres et al., 1995; Uchrin et al., 1998) transferring dissolved inorganic carbon (DIC) and dissolved organic carbon (DOC) into $^{14}\text{CO}_2$, while the latter one was precipitated in the form of BaCO_3 . For ion-exchange resins, an initial amount of material (2 g) was boiled in the 5-8% NaOH over 1-2 hours in order to transfer the groups of anions into solution which was separated from resins and treated with the sulphuric acid and hydrogen peroxide in the same way as for other liquid samples. Chemical yield of ^{14}C extraction was not less than 80%. Barium carbonate was mixed with selective carbon dioxide absorbent and scintillation cocktail. ^{14}C activity in the resulting solution was measured by the LSC method. ^{14}C counting efficiency was in range of 20-40% and was estimated on BaCO_3 sample with the known ^{14}C activity. This sample was prepared from the standard sodium carbonate (Na_2CO_3) solution.

The uncertainty of the ^{14}C estimations (statistical radiometric error) was reported at 2 and 1 sigma-level for the tree rings samples and for all other studied samples, respectively. The quality of ^{14}C determinations in our laboratory was sufficiently reliable what was periodically tested through participating in various inter-comparisons. The tests indicated that most of the low activity ^{14}C determinations are of high (1.5%) precision. Lower precision (up to 15%) of the ^{14}C determinations is evident for higher activity samples from the INPP process media.

3. Results and discussion

The main data on ^{14}C in terrestrial and aquatic plants, in DIC of surface water and groundwater for the whole period of observations are summarized in Figs 2-9. Some new ^{14}C data attributed to wider species diversity of terrestrial and aquatic plants for recent period of observations (2007-2009) are in detail presented in Tables 1 and 2.

3.1 ^{14}C in the terrestrial environment

The ^{14}C specific activity in the terrestrial annual vegetation from the “impact zone” of INPP was compared with the ^{14}C activity in the local background areas and in the air of the Northern Hemisphere for the period 1983-2008 (Fig. 5).

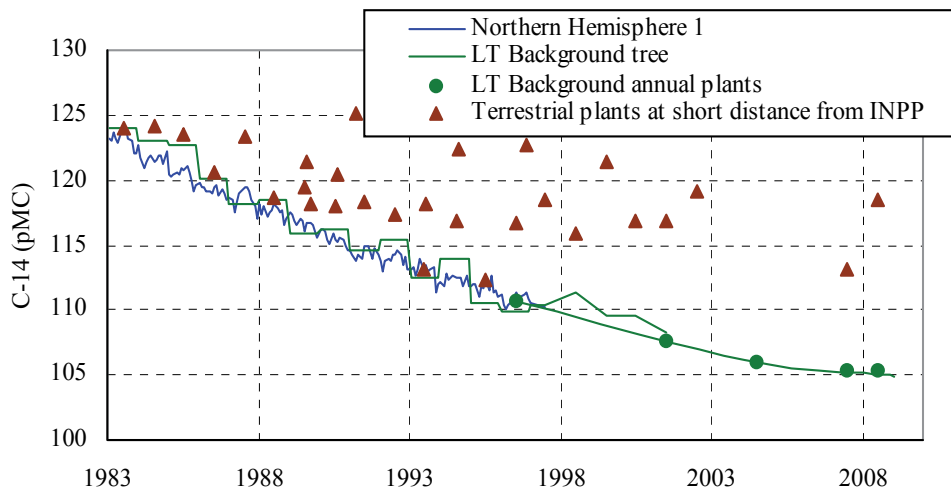


Fig. 5. The ^{14}C specific activity of terrestrial plants at short distance from INPP for the period of INPP operation 1983-2008, compared with ^{14}C activity in air of Northern Hemisphere according to Hua & Barbetti (2004) and with local background ^{14}C level

^{14}C background plots were built from several data sets: Northern Hemisphere data for the period 1983-1997 (Hua & Barbetti, 2004), local tree rings data (Mazeika et al., 2008) and data on annual vegetation from the Lithuanian national parks. All three data sets are in good correlation and show the continuous ^{14}C of thermonuclear weapon tests to decline from 124 pMC in 1983 to 106 pMC in 2008. Nowadays, the ^{14}C background is approaching the ^{14}C level of cosmogenic origin. Most of ^{14}C data for the “impact zone” of INPP are clearly above the background level with maximal excess of 10-15 pMC for 1988-2008. Evident variability of ^{14}C excess is related to aerial position of samples.

The aerial distribution of ^{14}C activity in the annual vegetation was analyzed twice – in 1996 and in 2001. Specific activity of ^{14}C in wormwood stems (12 samples) ranged from 96 to 123 pMC in 1996, and from 107 to 178 pMC in alder leaves (23 samples) in 2001. The lowest ^{14}C values were in line with the background ones, and the highest values gave the same ^{14}C excess of 10-15 pMC. However one sample of 2001 had ^{14}C excess up to 70 pMC. In both cases, the highest specific activity of ^{14}C was detected in the zone north-east of the INPP. This “impact zone” coincides with the dominant wind direction.

The analyzed data are in line with ^{14}C in tree rings analysis (Mazeika et al., 2008), which revealed a ^{14}C excess in tree rings near the INPP in the same area. At the beginning of the INPP operation, the ^{14}C excess was negligible whereas in 1996-2002, the ^{14}C excess value was up to 5-11 pMC. For the period of 2003-2006 the data are lacking however judging by

^{14}C data for 2007–2008 there is an evidence of ^{14}C excess in the same area - up to 10 pMC level (Table 1).

Sampling point location	Species	Sampling date	^{14}C (pMC $\pm 1\sigma$)
INPP region, Grikiniskes (G locality in Fig. 3), "impact zone" of INNP	European blueberry	28-06-2007	110.1 \pm 0.9
	Kuhn brake	28-06-2007	108.2 \pm 1.3
	Roth. rough smallreed	28-06-2007	108.7 \pm 1.1
	Roth. rough smallreed	28-08-2008	110.8 \pm 0.5
	Hull common heather	28-06-2007	113.2 \pm 1.3
	Hull common heather	28-08-2008	112.7 \pm 0.5
	Shimp stair-step moss	28-08-2008	118.5 \pm 0.5
Zarasai district, Tilze (T locality in Fig. 3), local background	Shimp stair-step moss	28-06-2007	104.7 \pm 1.1
	Kuhn brake	28-06-2007	104.5 \pm 1.3
	Shimp stair-step moss	29-08-2008	104.6 \pm 0.5
	Hull common heather	29-08-2008	104.9 \pm 0.5
	Roth. rough smallreed	29-08-2008	106.5 \pm 0.5
Lithuanian national parks (not shown)	European blueberry	28-06-2007	101.4 \pm 0.8
	Kuhn brake	01-08-2007	102.7 \pm 1.3
	Hull common heather	01-08-2007	105.4 \pm 1.2

Table 1. ^{14}C specific activity in terrestrial plants from INPP "impact zone" and background areas in 2007-2008

Following the approach presented in (Mazeika et al., 2008) we can again support the estimation that maximal ^{14}C release rate from the INPP is of order 10^{13} Bq/year. In the case of an atmospheric release, the nuclide-specific routine release conversion factors, representing the ratio of the annual effective dose for a critical group member (Sv/year) at the location of the highest predicted radionuclide concentration in air, to the activity released from the INPP (Bq/year), are set (Nedveckaitė et al., 2000; LAND, 42–2001). The effective dose resulting from the ^{14}C mentioned release rate is 2.0×10^{-3} mSv/year.

3.2 ^{14}C in the aquatic environment

In the aquatic environment, ^{14}C basically may be involved into two main components: into the water as part of dissolved bicarbonate ions, HCO_3^- , and into the plant tissue as Corg. Both chemical forms of ^{14}C are directly or indirectly related to atmospheric CO_2 . Therefore in the lakes with short water residence in the system time ^{14}C activity in both chemical forms is similar. As the significant area of Lake Druksiai belongs to airborne release from the INPP impact zone, the atmospheric $^{14}\text{CO}_2$ may slightly enhance the ^{14}C level. If ^{14}C is released to the lake with liquid effluents in inorganic and organic chemical forms it can be traced investigating both DIC of water and Corg of macrophytes as both carbon compartments are interacting in biogeochemical cycle of aquatic ecosystem.

^{14}C activity measurements in DIC of several surface water bodies with different frequency have been performed since 1975 (Fig. 6).

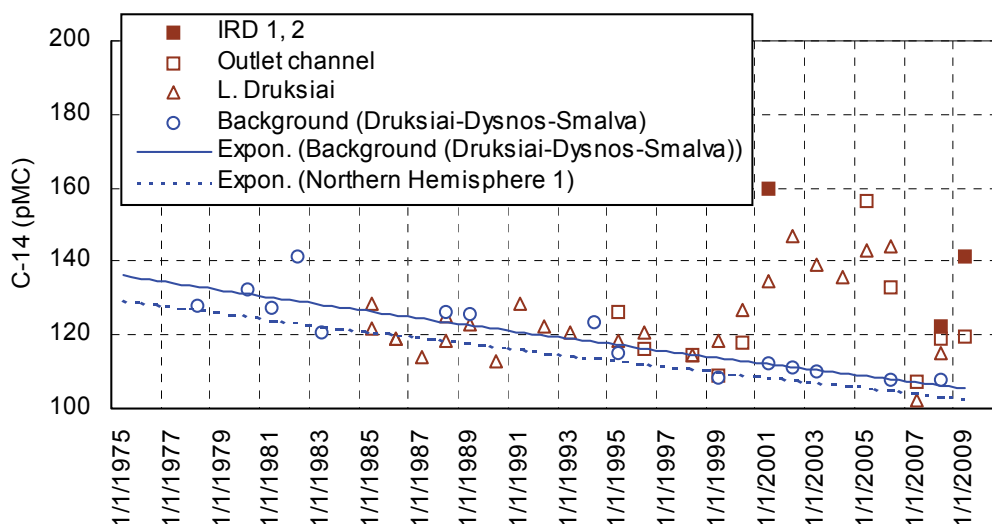


Fig. 6. The ^{14}C specific activity of DIC in water bodies related to INPP at short distance from INPP for the period 1975–2009, compared with ^{14}C activity in air of Northern Hemisphere according to Hua & Barbetti (2004) and with local background ^{14}C level

Several data sets were used as ^{14}C background: the Northern Hemisphere data for the period 1975–1997, the data on the Lake Druksiai before the INPP operation, and the data on the Lake Dysnos and rivulet Smalva during the INPP operation. ^{14}C activity trend lines generated from the Northern Hemisphere data and local lakes data are very comparable.

For a significant period (1983–1999) of ^{14}C monitoring in DIC of surface water, the influence of INPP has been hardly recognized. ^{14}C activity in DIC from the Lake Druksiai and cooling water inlet channel has increased in 2002–2006 with the ^{14}C excess of 30–35 pMC above the background level. The similar ^{14}C activity trend was observed in the technical water inlet channel, which represented ^{14}C activity diluted and averaged to almost all lake water volume. The IRD 1, 2 channel is a water body with the lowest diluted effluents and enhanced ^{14}C activity in DIC in 2001 (159 pMC) and 2009 (142 pMC). The traceable ^{14}C excess in DIC of the water from the Lake Druksiai allows evaluating the order of ^{14}C release rate from the INPP to the water of $\sim 10^8$ Bq/year using radionuclides activity dilution factors derived in (Mazeika & Motiejunas, 2003). The effective dose resulting from the ^{14}C mentioned release rate is $\sim 3.0 \times 10^{-4}$ mSv/year. ^{14}C in aquatic plants from the Lake Druksiai was measured occasionally and most systematically in recent years (Fig. 7, Table 2).

For ^{14}C excess evaluation, the same background data sets as for terrestrial plants were used. The evident ^{14}C excess in aquatic plants with significant variability for the period 1995–2008 is the main finding. The highest ^{14}C values (up to 172 pMC) were observed in the lake area close to monitoring station No 7 (Fig. 3) where the effluents discharged by IRD 1, 2 channel (maximum ^{14}C activity in biota in 2007 was 263 pMC) were interacting with plants in short distance before diluting and averaging in lake water masses. The macrophytes were recognized as good bioindicators to show a short-term ^{14}C variation during the vegetation

season. ^{14}C data on DIC of water and Corg of plants in the aquatic environment are in agreement and complements each other.

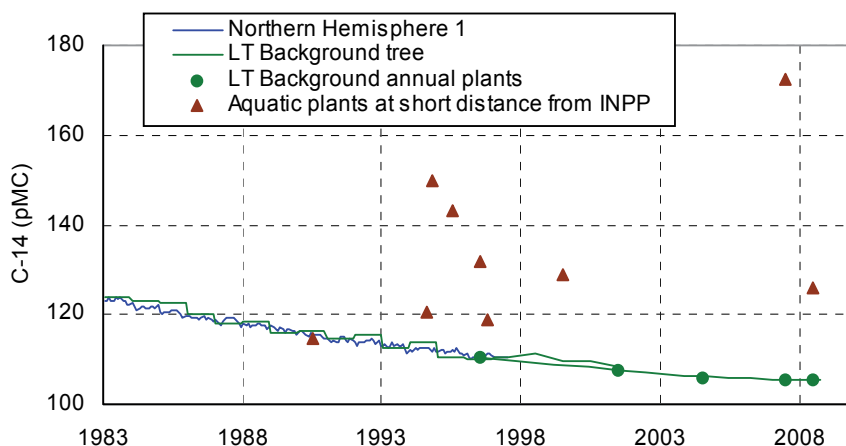


Fig. 7. The ^{14}C specific activity of aquatic plants at short distance from INPP, compared with ^{14}C activity in air of Northern Hemisphere according to Hua & Barbetti (2004) and with local background ^{14}C level

Sampling point location (See location on Fig. 3)		Species	Sampling date	^{14}C (pMC $\pm 1\sigma$)
Technical water from INPP outlet channel (OC)		<i>Myriophyllum spicatum</i>	27-06-2007	108.8 \pm 1.6
			28-08-2008	127.7 \pm 0.6
Drainage channel (IRD-1, 2)		<i>Ceratophyllum demersum</i>	27-06-2007	262.6 \pm 2.0
			28-08-2008	172.9 \pm 7.7
Lake Druksiai	1 station	Filamentous algae	27-06-2007	111.1 \pm 0.9
		<i>Myriophyllum spicatum</i>	27-06-2007	119.3 \pm 1.9
		<i>Ceratophyllum demersum</i>	24-09-2008	118.8 \pm 1.0
	4 station	<i>Ceratophyllum demersum</i>	27-06-2007	111.6 \pm 1.5
		<i>Myriophyllum spicatum</i>	27-08-2008	125.9 \pm 0.7
	6 station	<i>Ceratophyllum demersum</i>	27-06-2007	106.3 \pm 1.5
	7 station	<i>Ceratophyllum demersum</i>	27-06-2007	172.3 \pm 2.8
			27-08-2008	123.4 \pm 0.9

Table 2. ^{14}C specific activity in aquatic plants from Lake Druksiai and channels related to INPP industrial site in 2007-2008

3.3 ^{14}C in the groundwater

The main chemical form of ^{14}C in the groundwater is bicarbonate ions or more generally defining DIC. A small fraction may be in organic carbon. Both chemical forms of ^{14}C in the groundwater originate in the soil-unsaturated zone system through the carbon biogeochemical cycle. They are related to atmospheric CO_2 and have often the same or similar ^{14}C specific activity respect to carbon. Even if these specific activities are equal, the volumetric activity of ^{14}C in the water from DIC will be higher then that from organic carbon due to significant differences in chemical concentrations of those two components in common groundwater. ^{14}C specific activity in the groundwater with short residence time usually is close to that of the atmospheric CO_2 . There are often cases when aquifer matrix involves carbonate material, groundwater interacts with matrix long time and by presence of CO_2 surplus transfers HCO_3^- to the water from solid "old" carbonates not containing ^{14}C . These processes of ^{14}C geochemical dilution in the groundwater are well studied in the isotope hydrology (Clark & Fritz, 1997). In such cases, ^{14}C specific activity in DIC of groundwater may be significantly lower then in the atmospheric CO_2 .

If ^{14}C is released to the groundwater with liquid effluents in inorganic and organic chemical forms it can be traced investigating firstly DIC of groundwater. For 1987–2009, ^{14}C specific activity of DIC in the water (pMC) and ^{14}C volumetric activity concentration (in Bq/m^3) are presented in Figs. 8, 9.

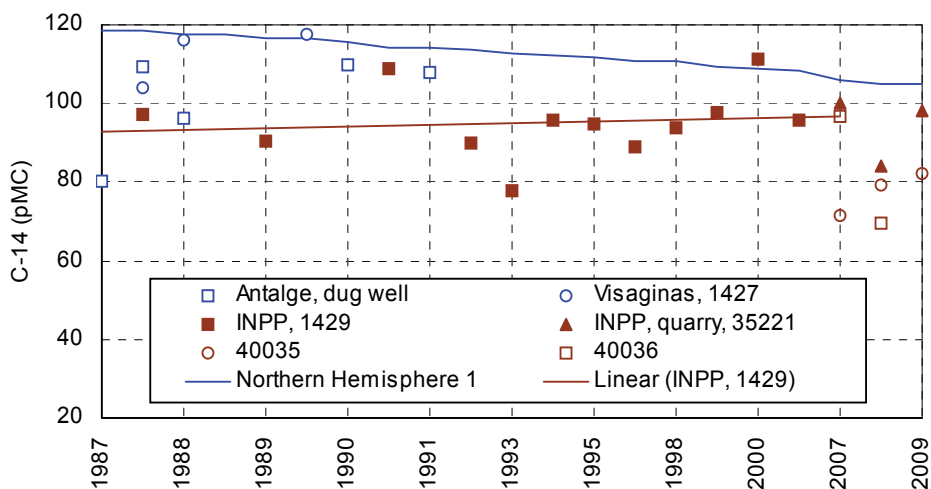


Fig. 8. The ^{14}C specific activity of DIC in groundwater at short distance from INPP for the period 1987–2009 (Antalge, shallow dug well, and Visaginas, well No 1427, are located at long distance from INPP)

As regards the ^{14}C data in pMC units, we found out that all ^{14}C values in the groundwater are close to or below the atmospheric air ^{14}C background line. ^{14}C in DIC of groundwater from some places is originally diluted by HCO_3^- with low isotope ratio $^{14}\text{C}/^{12}\text{C}$. However the ^{14}C trend line for well No 1429 has a slightly increasing tendency what is in opposite with the atmospheric background trend and traces weak INPP impact. As groundwater

carbonate system under different aquifer conditions may have different DIC sources and bicarbonate concentrations, we calculated ^{14}C activity concentration from two experimentally measured values such as HCO_3^- concentration and ^{14}C specific activity relative to carbon (Fig. 9).

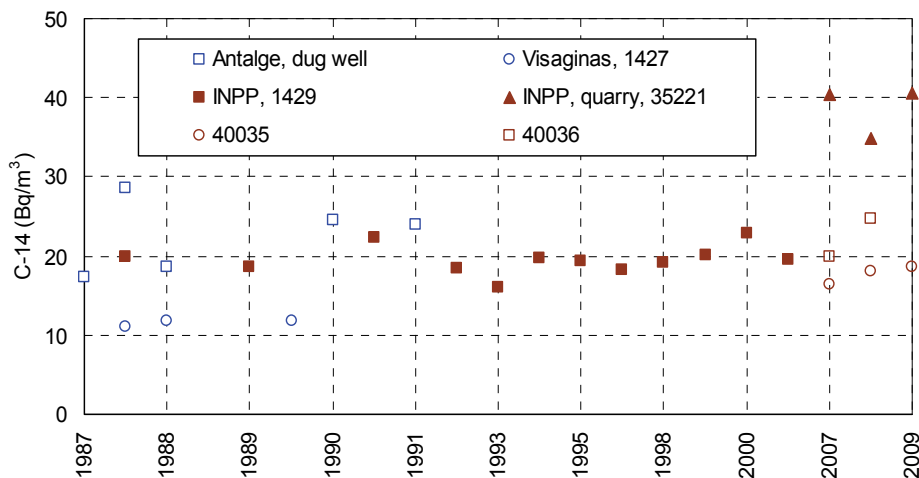


Fig. 9. The ^{14}C activity concentration in groundwater at short distance from INPP for the period 1987–2009 (Antalge, shallow dug well, and Visaginas, well No 1427, are located at long distance from INPP)

In this case, the influence of INPP on ^{14}C content in the groundwater was possible to notice for one quarry observation well. In 2007–2009, the ^{14}C activity concentration in the groundwater from observation well 35221 of the quarry was higher ($40.4 \pm 0.4 \text{ Bq/m}^3$) than the activity in other observed wells ($10\text{--}20 \text{ Bq/m}^3$) due to high HCO_3^- concentration (up to 930 mg/l). In the quarry, the sludge with high concentration of organics from the Visaginas wastewater treatment plant was disposed of and covered with an artificial soil layer. The sludge organics contained enhanced levels of ^{14}C and other radionuclides, firstly ^{60}Co . Due to microbial oxidation of organics under closed conditions, CO_2 generation with enhanced ^{14}C content might have taken place what formed high HCO_3^- concentration in the groundwater. Moreover, the activity concentration of ^{60}Co in the water from quarry observation well No 35221 was measurable – up to 11 Bq/m^3 while in water from other observation wells ^{60}Co was never detected. As it was evidenced from the long-term ^{14}C data series, the groundwater systems are closed from contamination by radionuclides and are rarely and insignificantly influenced by the INPP.

3.4 Some data on ^{14}C in reactor process media

As the main circulation circuit water (primary circuit water) and some other water streams of INPP are continuously purified, ionic species such as $\text{H}^{14}\text{CO}_3^-$ will be adsorbed onto the ion-exchange resins and concentrated. After use, the spent ion-exchange resins will be finally cemented and disposed of as LILW in NSR. The activity of resins comprises the main

fraction of radioactive inventory in the various waste forms disposed of in LILW facilities (Magnusson, 2007).

Different types of samples from the INPP process media were preliminary considered for determination of ^{14}C total specific activity (sum of organic and inorganic species): water from the spent nuclear fuel pools, water from the primary circuit, evaporator concentrates, and spent ion exchange resins (Table 3).

Sample No	Sample description and taking date	^{14}C activity concentration
1	Water from the primary circuit, 22 July 2002	<0.05 Bq/l
2		0.10 ± 0.04 Bq/l
3		<0.05 Bq/l
4		<0.05 Bq/l
5	Water from the spent nuclear fuel pools, 12 July 2002	0.64 ± 0.08 Bq/l
6		0.70 ± 0.09 Bq/l
7		0.25 ± 0.04 Bq/l
8	Evaporator concentrates, July 2002	0.55 ± 0.12 MBq/l
9	Spent ion exchange resins, November 2002	70 ± 9 kBq/kg

Table 3. ^{14}C in process water and operational radioactive waste of INPP

The averaged specific activity of ^{14}C in water samples was estimated as follows: from the primary circuit - less than detection limit (0.05 Bq/l); from the spent nuclear fuel pools - 0.5 Bq/l. Considerably higher specific activity of ^{14}C was determined in evaporator concentrates and spent ion exchange resins - 0.55 MBq/l and 70 kBq/kg, respectively.

Low ^{14}C activity in reactor water of BWRs was reported in (Magnusson, 2007) as well. As in case with BWRs, the low ^{14}C activity in RBMK reactor water illustrates effective purification of water from inorganic ^{14}C species by means of ion exchange resins. Other results on ^{14}C in the INPP process media are in line with ^{14}C data for BWRs presented in (Magnusson, 2007). The obtained data were used for the calculation $^{14}\text{C}/^{60}\text{Co}$ scaling factors applied to the RBMK-1500 reactor waste characterization.

4. Conclusion

The ^{14}C concentration near the INPP has been studied by analysing various samples from terrestrial and aquatic environments and groundwater using conventional liquid scintillation counting. A comparison between the specific activity of ^{14}C at short distances from the INPP and ^{14}C specific activity of the background level has revealed the ^{14}C excess over the whole operation period of the INPP (the end of 1983–the end of 2009).

By studying tree rings and annual terrestrial plants in the terrestrial environment mostly continuous ^{14}C excess was delineated recently approaching 10 pMC that can be formed by $^{14}\text{CO}_2$ annual release of magnitude 10^{13} Bq with the maximal value of normalized release rate $11 \text{ TBq} \times \text{GW}(\text{e})^{-1} \times \text{year}^{-1}$. In comparison with the other radionuclide releases from the INPP and respective doses (Motiejunas et al., 1999), the effective dose resulting from the ^{14}C is the highest reaching 2.0×10^{-3} mSv/year. Nevertheless, this dose estimate is much lower than the ^{14}C dose occurring from the ^{14}C of natural production in the atmosphere ($\sim 12 \times 10^{-3}$ mSv/year).

In the aquatic environment, the ^{14}C activity in DIC from the cooling basin increased only in 2002–2006 with the ^{14}C excess of 30–35 pMC above the background level what could be caused by the ^{14}C release rate from the INPP to water $\sim 10^8$ Bq/year. The highest ^{14}C excess in aquatic plants (up to 65 pMC) with significant variability was detected in the period 1995–2008. The groundwater system was rarely and insignificantly influenced by the INPP. Thus the effective dose resulting from the ^{14}C in the aquatic environment was very low.

It was confirmed that the majority of ^{14}C contained in the gaseous waste (e.g. reactor off-gases) was released from the INPP to the atmosphere during the operation time with the total ^{14}C activity roughly of $\sim 2.0 \times 10^{14}$ Bq. Only a small quantity of ^{14}C was released via liquid effluents from the INPP. A large quantity of ^{14}C is retained in the structural materials of the reactor (graphite moderator mainly with ^{14}C of 7.82×10^{14} Bq per two units) and in the radioactive waste (LILW with ^{14}C of 1.43×10^{13} Bq), which will be handled during the INPP decommissioning phase. For waste containing high levels of ^{14}C , such as graphite, that may exceed the waste acceptance requirements for the near surface disposal, no disposal facility is available at present. This waste only can be kept in an interim storage until a suitable disposal facility (e.g. deep geological disposal) or other disposal and treatment alternatives become available.

5. References

- Almenas, K.; Kaliatka, A. & Uspuras, E. (1998). *Ignalina RBMK-1500, a Source Book*, Lithuanian Energy Institute, ISBN 9986-492-35-1, Kaunas, Lithuania
- Ancius, D.; Ridikas, D.; Remeikis, V.; Plukis, A.; Plukiene, R. & Cometto, M. (2004) Evaluation of the activity of irradiated graphite in the Ignalina Nuclear Power Plant RBMK-1500 reactor. *Nukleonika*, Vol. 50, No. 3, 113-120, ISSN 0029-5922
- Arslanov, Kh.A. (1985). *Radiocarbon: Geochemistry and Geochronology*, Leningrad University Press, Leningrad (in Russian)
- Buchuev, A.V.; Zubarev, V.N. & Prochin, I.M. (2002). Composition and quantity of impurities in graphite of industrial reactors. *Atomnaya energija*, Vol. 92, No. 4. 298-302, ISSN 0004-7163 (in Russian)
- Buzinny, M.; Kovalyukh, N.; Likhtarjov, I.; Los, I.; Nesvetajlo, V.; Pazdur, M.F.; Skripkin, V.; Shkvorets, O. & Sobotovich, E. (1995). Ecological chronology of nuclear fuel cycle sites. *Radiocarbon*, Vol. 37, No. 2, 469-473
- Clark, I.D. & Fritz, P. (1997). *Environmental isotopes in hydrogeology*, Lewis, Boca Raton, FL
- Fairhall, A.W. & Young, J.A. (1970). *Radionuclides in the environment*, Advances in Chemistry Series Vol. 93., American Chemical Society, Washington, D.C.
- Gaiko, V.B.; Korablev, N.A.; Solovev, E.N.; Trosheva, T.I.; Shamov, V.P.; Umanets, M.P. & Shcherbina, V.G. (1985). Discharge of carbon-14 at nuclear power plants with RBMK-1000. *Atomnaya energija*, Vol. 59, No. 2, 144-145, ISSN 0004-7163 (in Russian)
- Gupta, S.H. & Polach, H.A. (1985). *Radiocarbon Practices at ANU – Handbook*, ANU, Canberra
- Gusev, N.G. & Beliajev, V.A. (1986). *Radioactive releases into biosphere, reference book*, Energoatomizdat, Moscow (in Russian)
- Hertelendi, E. & Csongor, E. (1982). Anthropogenic ^{14}C excess in the troposphere between 1951 and 1978 measured in tree rings. *Radiochemical and Radioanalytical Letters*, Vol. 56, No. 2, 103-110
- <http://www.iaea.lt>

- Hua, Q. & Barbetti, M. (2004). Review of tropospheric bomb ^{14}C data for carbon cycle modeling and age calibration purposes. *Radiocarbon*, Vol. 46, 1273-1298
- IAEA (2004). *Management of waste containing tritium and carbon-14*, Technical Report Series No. 421, International Atomic Energy Agency, Vienna, Austria
- IAEA (2006). *Characterization, treatment and conditioning of radioactive graphite from decommissioning of nuclear reactors*, IAEA-TECDOC-1521, International Atomic Energy Agency, Vienna, Austria
- Kovaliukh, N.N. & Skripkin, V.V. (1994). An universal technology for oxidation of carbon-containing materials for radiocarbon dating, *Abstract and Papers of Conference on Geochronology and Dendrochronology of Old Town's and Radiocarbon Dating of Archaeological Findings*, pp. 37-42, ISBN 9986-19-061-4, Vilnius, October - November 1994, Vilnius University Press, Vilnius, Lithuania
- LAND 42-2001. *Limits of discharge of radioactive substances from nuclear facilities and basic requirements for monitoring of radioactive effluents and monitoring of the environment*, Normative document of the Ministry of Environment of the Republic of Lithuania, State Journal, 2001, No. 13-415
- Levin, I.; Kromer, B.; Barabas, M. & Münnich, K.O. (1988). Environmental distribution and long-term dispersion of reactor ^{14}C around two German nuclear power plants. *Health Physics*, Vol. 54, No. 2, 149-156
- Libby, W.F. (1946). Atmospheric helium three and radiocarbon from cosmic radiation. *Physical Review*, Vol. 69, 671-672
- Loosli, E.H. & Oeschger, H. (1989). ^{14}C in the environment of Swiss nuclear installations. *Radiocarbon*, Vol. 31, No. 3, 747-753
- Lukauskas, D.; Plukiene, R.; Plukis, A.; Gudelis, A.; Duskesas, G.; Juodis, L.; Druteikiene, R.; Lujaniene, G.; Luksiene, B. & Remeikis, V. (2006). Method to determine the nuclide inventory of low-activity waste of the RBMK-1500 reactor. *Lithuanian Journal of Physics*, Vol. 46, No. 4, 497-503, ISSN 1392-1932
- Magnusson, Å. (2007). ^{14}C Produced by Nuclear Power Reactors - Generation and Characterization of Gaseous, Liquid and Solid Waste, Lund University, Sweden, *Doctoral Dissertation*, ISBN 978-91-628-7248-9
- Magnusson, A.; Stenström, K.; Skog, G., Adliene, D.; Adlys, G.; Hellborg, R.; Olariu, A.; Zakaria, M.; Rääf, C. & Mattsson, S. (2004). Levels of ^{14}C in the terrestrial environment in the vicinity of two European nuclear power plants. *Radiocarbon*, Vol. 46, No. 2, 863-868
- Mazeika, J. & Motiejunas, S. (2003). Evaluation of aquatic routine radioactive releases from the Ignalina Nuclear Power Plant. *Ekologija*, No. 4, 36-42, ISSN 0235-7224
- Mazeika, J. (2002). *Radionuclides in Geoenvironment of Lithuania*, Institute of Geology, ISBN 9986-615-32-1, Vilnius, Lithuania
- Mazeika, J.; Petrosius, R. & Pukiene, R. (2008). Carbon-14 in tree rings and other terrestrial samples in the vicinity of Ignalina Nuclear Power Plant, Lithuania. *Journal of Environmental Radioactivity*, Vol. 99, 238-247
- Methodology for assessing the radiological consequences of routine releases of radionuclides to the environment* (1995), Radiation Protection 72-Report-EUR 15760EN, Brussels-Luxembourg

- Mikhajlov, N.D.; Kolkovsky, V. & Pavlova, I.D. (1999). Radiocarbon distribution in northwest Belarus near the Ignalina nuclear power plant. *Radiocarbon*, Vol. 41, No. 1, 75-79
- Milton, G.M. & Kramer, S.J. (1998). Using ^{14}C as a tracer of carbon accumulation and turnover in soils. *Radiocarbon*, Vol. 40, No. 2, 999-1011
- Milton, G.M.; Kramer, S.J.; Brown, R.M.; Repta, C.J.W.; King, K.J. & Rao, R.R. (1995). Radiocarbon dispersion around Canadian nuclear facilities. *Radiocarbon*, Vol. 37, No. 2, 485-496
- Motiejunas, S.; Nedveckaite, T.; Filistovic, V.; Mazeika, J.; Morkeliunas, L. & Maceika, E. (1999). Assessment of environmental impact due to radioactive effluents from Ignalina NPP. *Environmental and Chemical Physics*, Vol. 21, No. 1, 8-18, ISSN 1392-740X
- NCRP (1985). *Carbon-14 in the environment*, National Council on Radiation Protection and Measurements, NCRP Report No. 81, USA
- Nedveckaite, T.; Motiejunas, S.; Kucinskas, V.; Mazeika, J.; Filistovic, V.; Jusciene, D.; Maceika, E.; Morkeliunas, L. & Hamby, D.M. (2000). Environmental releases of radioactivity and the incidence of thyroid disease at the Ignalina Nuclear Power Plant. *Health Physics*, Vol. 79, No. 6, 666-674
- Obelic, B.; Krajar-Bronic, I.; Srdoc, D. & Horvatinic, N. (1986). Environmental ^{14}C levels around the 632 MWe nuclear power plant KRSKO in Yugoslavia. *Radiocarbon*, Vol. 28, No. 2A, 644-648
- Plukis, A.; Remeikis, V.; Juodis, L.; Plukiene, R.; Lukauskas, D. & Gudelis, A. (2008). Analysis of nuclide content in Ignalina NPP. *Lithuanian Journal of Physics*, Vol. 48, No. 4, 375-379
- Raaen, F.F.; Ropp, G.A. & Raaen, H.P. (1968). *Carbon-14*, McGraw-Hill, New York
- Stenström, K.; Erlandson, B.; Hellborg, R.; Wiebert, A. & Skog, G. (1996). Determination of the $^{14}\text{CO}_2$ and the total airborne ^{14}C releases from two Swedish light-water reactors using accelerator mass spectrometry. *Radioactivity and Radiochemistry*, Vol. 7, No. 1, 32-36
- Stuiver, M. & Polach, H.A. (1977). Reporting of ^{14}C data. *Radiocarbon*, Vol. 19, 355-363
- Uchrin, G.; Hertelendi, E.; Volent, G.; Slavik, O.; Morávek, O.; Kobal, I. & Vokal, B. (1998). Carbon-14 measurements at PWR type nuclear power plants in three Middle European countries. *Radiocarbon*, Vol. 40, No. 1, 439-447
- Veres, M.; Hertelendi, E.; Uchrin, G.; Csaba, E.; Barnabás, I.; Ormai, P.; Volent, G. & Futó, I. (1995). Concentration of radiocarbon and its chemical forms in gaseous effluents, environmental air, nuclear waste and primary water of a pressurized water reactor power plant in Hungary. *Radiocarbon*, Vol. 37, No. 2, 473-497

Impact of radionuclide discharges from Temelín Nuclear Power Plant on the Vltava River (Czech Republic)

Eduard Hanslík and Diana Ivanovová
*T. G. Masaryk Water Research Institute
Czech Republic*

1. Introduction

Temelín Nuclear Power Plant (Temelín plant) is located on the upper Vltava River in south Bohemia. The Vltava is an important resource of drinking water for Prague. Its water affects also quality of the Elbe River on the territory of both the Czech Republic and the Federal Republic of Germany.

Since 1989, possible impacts of the Temelín plant have been studied in a number of research projects. The first two projects (Hanslík, 1995, Hanslík, 1998) were sponsored by the Czech Ministry of the Environment and its main objectives were to examine pre-operational environmental conditions (a reference level) in terms of concentrations of radioactive and non-radioactive polluting substances in components of the environment, particularly in the hydrosphere, and to predict possible impacts of future operation of the Temelín plant. Special attention paid to the hydrosphere was associated with requirements for protection of water quality in the Vltava River. The observation and research activities continued during the period 1999-2008 within the framework of a project sponsored by Czech Power Company (Hanslík, 1999a, 2000, 2001a, 2002, 2003, 2004a, 2005a, 2006a, 2007, 2008). These studies subsequently continued in a project on Research and protection of hydrosphere – research of relationships and processes in water component of the environment focused on impacts of human pressures, the sustainable use and protection of the hydrosphere and legislative tools (MZP 0002071101 and SP/2e7/229/07 sponsored by the Czech Ministry of the Environment).

The main objectives of these projects were to assess the impacts of waste water discharged from the Temelín plant on the activities of tritium, radio caesium and strontium in hydrosphere, to compare these impacts with the residual contamination from the atmospheric tests of nuclear weapons and the Chernobyl accident in the last century and to evaluate long-term spatial and temporal trends in the activities of these radionuclides that have been monitored at sampling sites not affected and affected by the outflow of waste water from the Temelín plant.

Specific results of these projects have been reported in technical journals and international conferences (Hanslík et al., 1999b, Hanslík et al., 2001b, Hanslík et al., 2005b, Hanslík et al., 2009a-c, Ivanovová & Hanslík, 2009a-b). This Chapter reviews and summarises the main results of the projects.

2. Description of the study area

Beginning of the construction of the Temelín plant dates back to 1986. The plant is located in the basin of the upper Vltava River in south Bohemia (Fig. 1). It consists of two PWR reactors, each with capacity of 1000 MW_{el}. Pilot operation of the first reactor was launched in June 2002 and of the second one in April 2003. Since May 2003, the Temelín plant has been in full operation. The development of the output of the Temelín plant is illustrated in Fig. 2.

For the operation of the two reactors, the plant needs 1 200 l/s (annual mean) of technological water. It discharges 300 l/s (annual mean) of waste water, including the returning cooling water and purified waste water.

Two of the reservoirs (Hněvkovice and Kořensko), which have been constructed on the Vltava River, serve for water management purposes of the plant. Water for the plant is abstracted from Hněvkovice Reservoir (put into operation in 1991) and pumped into storage tanks with capacity of $2 \times 15\,000\text{ m}^3$, from which it flows by gravity. The waste water is discharged into the Vltava River through turbines of hydroelectric power station located at Kořensko Dam.

Annual mean discharge (Q_a) at Kořensko Dam is 50 m³/s and ensured ecological discharge (Q_{355}) is 9.45 m³/s. This dam is located upstream from Orlík Reservoir, which is the first receiving water body of the waste waters from the Temelín plant. Its storage capacity is $720 \times 10^6\text{ m}^3$, which is fed by water from three main tributaries of the reservoir, the Vltava, Lužnice and Otava Rivers, whose annual mean discharges are 30.6 m³/s, 23.6 m³/s and 23.5 m³/s respectively.

The water from the Orlík Reservoir flows into the Elbe River through a cascade of other downstream reservoirs, Kamýk ($12.9 \times 10^6\text{ m}^3$), Slapy ($269.3 \times 10^6\text{ m}^3$), Štěchovice ($10.4 \times 10^6\text{ m}^3$) and Vrané ($11.1 \times 10^6\text{ m}^3$), built on the Vltava River.

The study area has been affected by contamination from the atmospheric tests of nuclear weapons and the Chernobyl accident in the last century.

3. Observation and data

The observations of changes in concentrations of radioactive and non-radioactive polluting substances were made for tributaries of the Orlík Reservoir, the Vltava, Lužnice and Otava Rivers, which are located upstream from the waste water outflow from the Temelín plant and represent therefore reference conditions ("reference sampling sites"), and in the Vltava River downstream from the outflow of waste water from the plant (Fig. 3) ("affected sampling sites").

The observation involved concentrations of the polluting substances in surface water, bottom sediments and fish species (Table 1).

Particular attention was paid to the time changes in the concentrations of anthropogenic radionuclides ³H, ⁹⁰Sr, ¹³⁴Cs and ¹³⁷Cs in hydrosphere because these radionuclides, possibly present in the effluent returns from the Temelín plant, are identical to those remaining in the environment after the Chernobyl accident and atmospheric tests of nuclear weapons.

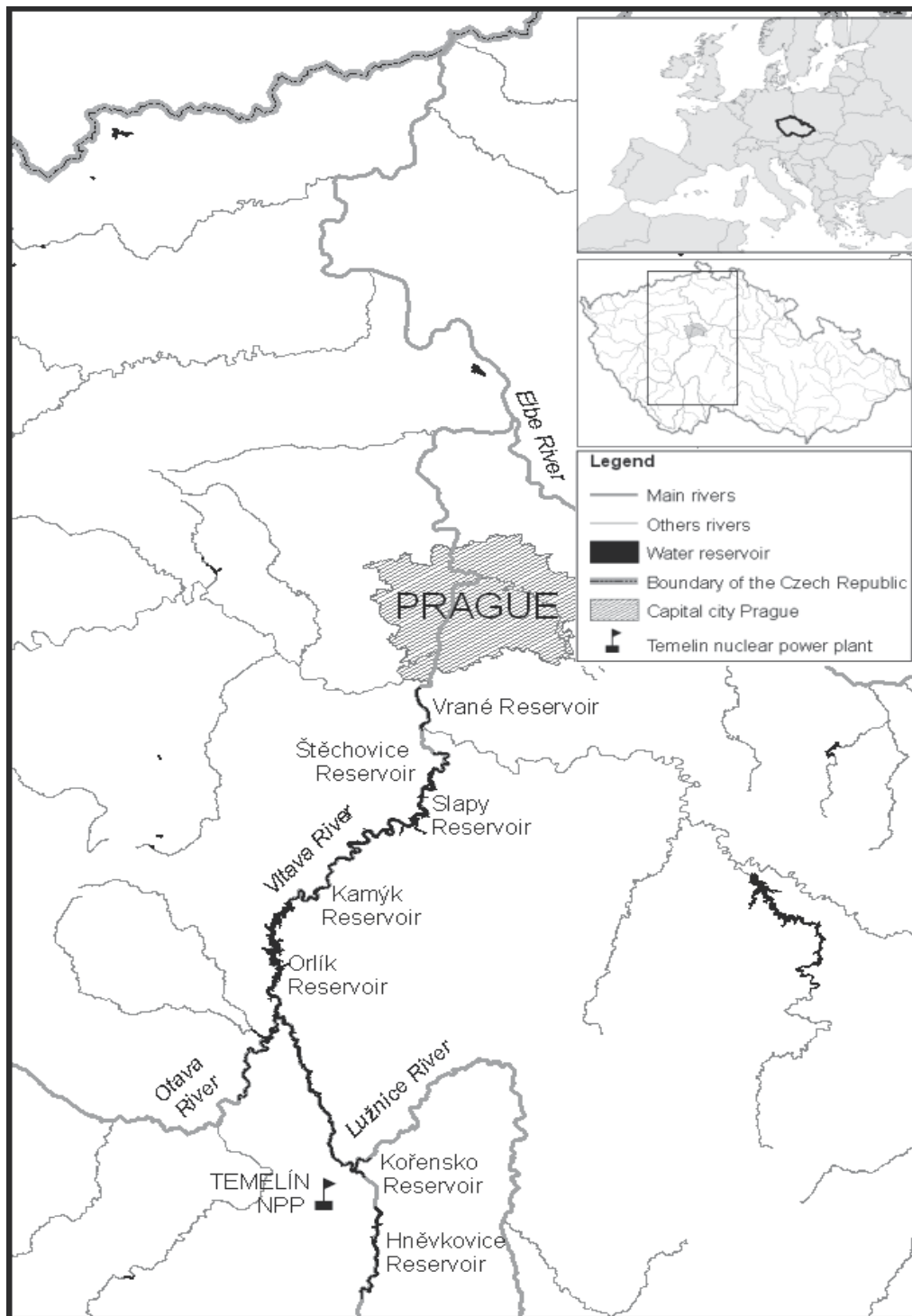


Fig. 1. The study area

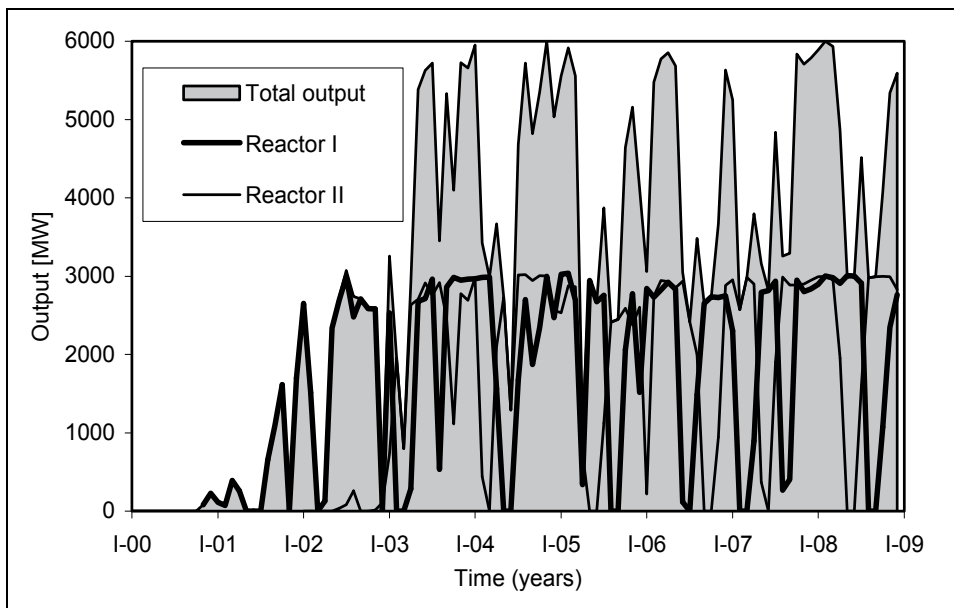


Fig. 2. Development of the output of Temelín plant in the period 2001 – 2008

Component of the environment		Year of the observation beginning from 1990																		
		0	1	2	3	4	5	6	7	8	9	0	1	2	3	4	5	6	7	8
Surface water	³ H	x	x	x	x	x	x	x	x	x	x	x	x	x	x	x	x	x	x	x
	¹³⁷ Cs				x	x	x	x	x	x	x	x	x	x	x	x	x	x	x	x
	⁹⁰ Sr					x	x	x	x	x	x	x	x	x	x	x	x	x	x	x
	TSS	x	x	x	x	x	x	x	x	x	x	x	x	x	x	x	x	x	x	x
Bottom sediment	¹³⁴ Cs	x	x	x	x	x	x	x	x											
	¹³⁷ Cs	x	x	x	x	x	x	x	x	x	x	x	x	x	x	x	x	x	x	x
Biomass (Fish)	¹³⁷ Cs					x	x	x	x	x	x	x	x	x	x	x	x	x	x	x

Table 1. Observation periods of the polluting substances in components of the environment

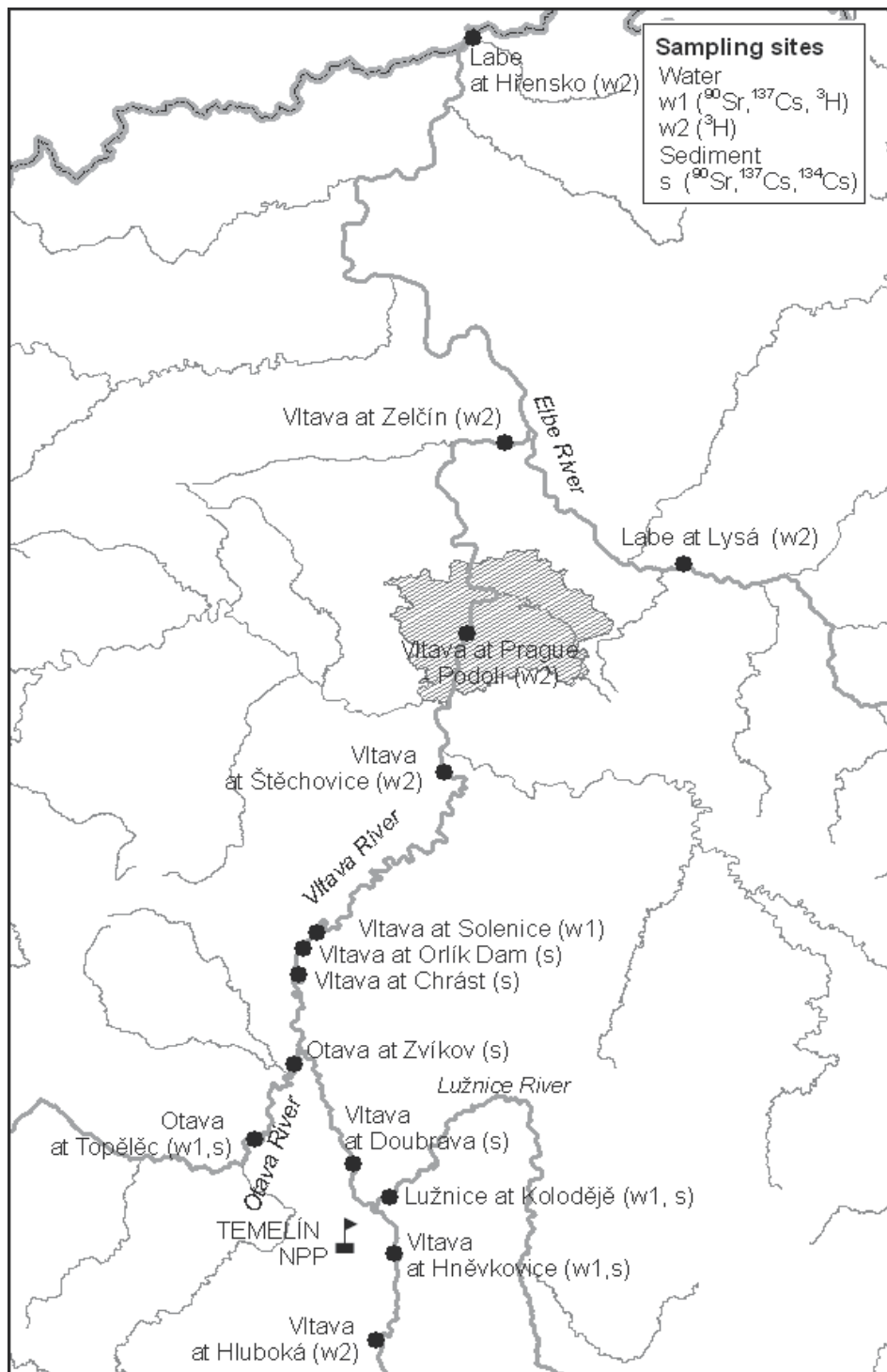


Fig. 3. Map showing sampling sites

4. Analytical methods

4.1. Radiological method

For sample collection and processing, the methods specified in ČSN EN 25667-1 (1994) and 2 (1994) Standards and ČSN EN ISO 5667-3 (1996), 4 (1994) and 6 (1994) were applied. Quality control practices of the T. G. Masaryk Water Research Institute (T.G.M. WRI) Radioecological Laboratory are performed according to the Standard ČSN EN ISO/IEC 17025 (2001). The laboratory takes part in national and international proficiency testing.

Large samples of water (50 l) were taken with frequency of four in a year. The samples were immediately stabilized with nitric acid to pH 1 and then, after transportation to the laboratory, condensed by vaporization. The vaporized samples were ignited (350 °C) and closed into Petri dishes. The radionuclides concentrations in water were determined in total solids (both in dissolved and suspended solids). Samples of water (1 l) for determination of ^3H and total suspended solids (TSS) were taken with frequency of four in a year.

Samples of bottom sediments were taken from the top layer (0 – 10 cm) by a diver at six sites involving the Vltava River tributaries and the Orlick Reservoir. The frequency of the sampling was one sample in a year. Granularity of the samples was generally less than 2 mm. For the analysis, the samples were dried at 105 °C and hermetically sealed in the measuring containers.

Samples of fish were also taken with annual frequency. These samples were dried.

The ^{134}Cs and ^{137}Cs concentrations were analysed according to Standard ČSN ISO 10 703 (1999) using gamma-spectrometry. A Canberra device was used. The measurement duration was set up in accordance with requested minimum detectable activity (MDA) of ^{137}Cs at the level of significance of $\alpha=\beta=0.05$. The MDA of ^{137}Cs in water for counting time of 2 days was 0,5 mBq/l. In the sediments, the MDA of ^{137}Cs for counting time 8 h was approximately 0.5 Bq/kg. The results of ^{137}Cs activity in fish (dried samples) were converted to activity in wet weight. The MDA of ^{137}Cs in fish (wet weight) for counting time of 2 days was 0.1 Bq/kg.

^{90}Sr was determined in water by using a standard method after radiochemical separation (Čapková, 1993). Its activity was detected from the residuum after igniting via detection of yttrium 90 after radiochemical separation. Value of MDA of strontium 90 was 3 mBq/l. These methods were verified and recommended by the International Atomic Energy Agency (IAEA, 1996) in Vienna within the framework of its technical assistance organised in co-operation with the Ministry of the Environment of the CR and the State Office for Nuclear Safety.

The tritium concentrations were determined by using Quantulus 1220 and TriCarb low-level liquid scintillation spectrometers. The determination was performed according to ISO 9698 Standard (1996). The relative efficiency of tritium measurement was 26%. The MDA was set according the expected activities. For mixture of 8 ml of sample and 12 ml of scintillation solution and alternatively counting time of 800 minutes (samples from reference sampling sites) and 300 minutes (samples from affected sampling sites), the detection limit was 1.2 Bq/l and 2.2 Bq/l respectively at the level of significance of 0.05. Calibration was performed by using ^3H standard provided by Czech Metrological Institute.

In general, values below the MDA were included into the assessment and were substituted by 0.5 values of these limits. The measured values were used for calculation of annual average activities. Values of annual mean river discharges were provided by the Czech Hydrometeorological Institute.

4.2. Mathematical methods

The analytical data on the concentrations of radionuclides in water, sediments and biomass were assessed by using several mathematical methods, which are briefly described below. The effective ecological half-lives were evaluated from the decrease in a radionuclide activity according to the equation (Smith & Beresford, 2005):

$$T_{\text{eff}} = \frac{\ln 2}{\lambda_{\text{eff}}} \quad (1)$$

where T_{eff} is effective ecological half-life (y),
 λ_{eff} effective ecological decay constant of the radionuclide activity concentration (1/y).

Ecological half-lives were calculated by using an equation in the form (Smith & Beresford, 2005):

$$\frac{1}{T_{\text{ecol}}} = \frac{1}{T_{\text{eff}}} - \frac{1}{T_{\text{p}}} \quad (2)$$

where T_{ecol} is ecological half- life (y),
 T_{eff} effective half- life (y),
 T_{p} physical half- life (y).

For a trend analyses, a kinetic equation of the first order was used in the form (an example for ^{137}Cs):

$$\ln c_{^{137}\text{Cs}} = -\lambda_{\text{eff}} t + q \quad (3)$$

where $c_{^{137}\text{Cs},j}$ is annual average ^{137}Cs concentration in surface water (mBq/l) in year j ,
 λ_{eff} effective rate of decline in ^{137}Cs concentration (1/y), involving the physical decay constant (λ_{p}) and the ecological rate of the decrease (λ_{ecol}), $\lambda_{\text{eff}} = \lambda_{\text{p}} + \lambda_{\text{ecol}}$ (1/y),
 t time of the monitoring in years,
 q natural logarithm of activity at the beginning of the observation

The annual depositions of suspended solids in a reservoir were calculated from an equation in the form:

$$D_{\text{S},j} = \left(\sum_{t=1}^n c_{\text{S},j,t} Q_{j,t} t + c_{\text{S},j,ia} Q_{j,ia} t - c_{\text{S},j,o} Q_{j,o} t \right) \times 10^{-3} \quad (4)$$

where $D_{\text{S},j}$ is deposition of suspended solids in a reservoir in individual years (j) (t/y),
 $c_{\text{S},j,t}$ annual mean concentration of suspended solids (j) in tributaries (t) (kg/m³),
 $c_{\text{S},j,ia}$ annual mean concentration of suspended solids (j) in the inflow from inter-basin area (ia) (kg/m³),
 $c_{\text{S},j,o}$ annual mean concentration of suspended solids (j) in the outflow from a reservoir (kg/m³),
 $Q_{j,t}$ annual mean inflow (j) from tributaries (t) (m³/s),
 $Q_{j,ia}$ annual mean inflow (j) from the inter-basin area (m³/s),
 $Q_{j,o}$ annual mean outflow (j) from a reservoir (m³/s),

The deposition of suspended solids can also be calculated for individual years by the following formula and expressed in percentages:

$$D_{S,j} = \frac{\sum_{t=1}^n c_{S,j,t} Q_{j,t} + c_{S,j,ia} Q_{j,ia} - c_{S,j,o} Q_{j,o}}{\sum_{t=1}^n c_{S,j,t} Q_{j,t} + c_{S,j,ia} Q_{j,ia}} \times 100 \quad (5)$$

where $D_{S,j}$ is deposition of suspended solids in a reservoir in individual years (j) (%).

Similarly, based on the results of the ^{137}Cs activity monitoring in all substances in water (dissolved as well as undissolved solids), the deposition of ^{137}Cs can be determined by the formula:

$$D_{A,137\text{Cs},j} = \left(\sum_{t=1}^n c_{137\text{Cs},j,t} Q_{j,t} + c_{137\text{Cs},j,ia} Q_{j,ia} - c_{137\text{Cs},j,o} Q_{j,o} \right) \times 10^{-9} \quad (6)$$

where $D_{A,137\text{Cs},j}$ is deposition of ^{137}Cs in individual years (j) (GBq/y),

$c_{137\text{Cs},j,t}$ annual mean activity of ^{137}Cs (j) in tributaries (t) of a reservoir (Bq/m^3),

$c_{137\text{Cs},j,ia}$ annual mean activity of ^{137}Cs (j) the inflow from inter-basin area (ia) (Bq/m^3),

$c_{137\text{Cs},j,o}$ annual mean activity of ^{137}Cs (j) in the outflow from a reservoir in Bq/m^3 .

Concentration factors (CF in l/kg) for fish samples were calculated according Smith & Beresford, (2005) (an example for ^{137}Cs and Orlik Reservoir):

$$\text{CF} = \frac{\bar{a}_{137\text{Cs}}}{\bar{c}_{137\text{Cs}}} \quad (7)$$

where $\bar{a}_{137\text{Cs}}$ is annual average ^{137}Cs concentration in fish (wet weight) (Bq/kg),

$\bar{c}_{137\text{Cs}}$ annual average ^{137}Cs concentration in water in tributaries of Orlik Reservoir (Bq/l).

Committed effective dose from tritium ingestion with drinking water (by adult) was calculated using the equation (IAEA, 2003):

$$E = h(a17)_{3\text{H},\text{ing}} I_{3\text{H},\text{ing}} \quad (8)$$

where E is committed effective dose from intake of tritium by ingestion of drinking water (Sv/y),

$h(a17)_{3\text{H},\text{ing}}$ committed effective dose per ingested unit for tritium intake by the group of adults (age >17) (Sv/Bq),

$I_{3\text{H},\text{ing}}$ intake via ingestion of tritium during 1 year (Bq/y), calculated as: $I_{3\text{H},\text{ing}} = c_j V$

where c_j is annual average tritium concentration in year j (Bq/l),

V consumption of drinking water by a member of the public (700 l/y).

5. Non-radioactive pollution from the Temelín plant

The results of the water quality monitoring show that non-radioactive substances discharged with waste water from the Temelín plant are highly influenced by the quality of the technological water extracted from the Vltava River at Hněvkovice. The Temelín contribution to dissolved solids includes mainly sulphate anions, added to the water as aluminium sulphate for the technological water treatment, and salts from the ion exchange filters. As an example of organic pollution, the biological oxygen demand (BOD₅) showed a significant decrease as compared to its values in supplied water, which is attributable to self-purification capacity of the cooling circuit, sedimentation of solid substances and other factors. A contribution of the biological waste water treatment plant to BOD₅ values is small. The Temelín plant reliably meets the limit values for discharged substances specified in the water management permit (Fechtnerová, 2002 - 2006).

6. Tritium

6.1. Tritium concentration

In conjunction with operation of nuclear power plants, high attention is paid to problems associated with the environment contamination by tritium. Tritium is emitted with waste waters from nuclear power plants into the environment and the discussions concerning tritium emissions are evoked by the fact that concentrations of tritium emitted into surface waters and other components of the environment exceed those of other radionuclides by several orders of magnitude.

The aims of the studies were to quantify tritium quantities discharged from Temelín plant into surface waters in the Vltava River basin and main tritium components stemming from natural processes and those originating from man activities (residual pollution from atmospheric tests on nuclear weapons in the last century and the atmospheric transfer from nuclear facilities worldwide). The intention was also to quantify tritium outflows into the Vltava River and to compare the results with data provided by Czech Power Works, joint stock company, which operates the Temelín plant.

6.2. Natural and artificial components of tritium background in the Vltava River basin

Tritium is permanently produced in upper layers of the atmosphere by nuclear reactions caused by cosmic radiation. The tritium reaction $^{14}\text{N} (n, ^3\text{H}) ^{12}\text{C}$ is evoked by fast neutrons generated by cosmic rays. The natural processes of tritium generation were studied by Libby (1946) and subsequently e.g. by Nir et al. (1966). According to results published in the literature, the world mean rate of tritium production consequently to cosmic radiation is 0.16 to 0.20 tritium nucleuses on one square centimetre of the land surface in one second. Value of 0.19 tritium nucleuses on one square centimetre in one second is relevant to the world tritium activity of 960 PBq (960×10^{15} Bq). Knowledge from satellite observation was used by Flamm et al. (1962), who derived that additional 0.4 tritium nucleuses on one square centimetre in one second, which exceeds that produced by cosmic radiation by a factor of two, originates from intensive solar activity. Tritium production by natural processes is estimated in the range from 150 to 200 PBq/y (NCRP, 1979). The tritium quantity of natural origin is constantly at a level of 2.6 EBq.

It is reported that mean tritium activity in the hydrosphere originating from natural processes is between 0.12 and 0.59 Bq/l. Results of the application of a seven-component model showed that tritium concentration in the air humidity is 0.61 Bq/l, in surface waters it is 0.38 Bq/l and in surface layers of oceans it is 0.06 Bq/l. It is reported that tritium concentration in human body is 0.46 Bq/l, which is relevant to annual dose of $1,2 \times 10^{-5}$ mSv/y. The dose of natural origin is therefore very small as compared to that originating from ionizing radiation, which is about 3 mSv/y (UNSCEAR, 1993).

For complete information on tritium sources and its occurrence in the environment, it is necessary to consider the fact that its concentrations are still affected by its main source in the past, the tests of nuclear weapons in the atmosphere. It has been estimated that till 1963, when the treaty on restriction of the tests of nuclear weapons was concluded (the Partial Test Ban Treaty), 114.7 EBq ($114,7 \times 10^{18}$ Bq) of tritium was emitted into the environment. The tritium activity remaining after the tests of the nuclear weapons was 43.3 EBq in 1980, 24.6 EBq in 1990 and 14.1 EBq in 2000 (NCRP, 1979). It can be derived from this data the remaining tritium activity in 2012 will still be 7.1 EBq. In 2030, the remaining tritium activity will be identical to that originating from natural processes, that is 2.6 EBq but this component presently still dominates.

For the studies of tritium activities in the Czech Republic, data from the period 1977 – 2008 were available from literature sources (Hanslík & Mansfeld, 1983) and from results of measurements made by staff of T.G.M. WRI (Hanslík et al., 1999b, Hanslík et al., 2006b, Ivanovova & Hanslík, 2009b).

The data from the whole period were used for calculation of effective ecological decay constant (λ_{eff}) and effective ecological tritium half-life. The data from “reference sampling sites” from the period 1990 – 2008, were used for more detailed analysis of the components of the water pollution by tritium.

The results showed that in the river reaches, which are not affected by waste water discharges from the Temelín plant, the mean tritium activity was 3.1 Bq/l at the beginning of the analysed period (1990) and 1.05 Bq/l at its end (2007). These results are in harmony with those of the observations performed by Palomo et al. (2007), who reported that tritium concentrations in samples taken in October 2005 and January 2006 in the vicinity of Asco Nuclear Power Plant (Spain) are in the range between less than 0.6 and 0.93 Bq/l.

For the analysis of the trends in tritium concentrations, the Equation 3 has a form as follows:

$$\ln c_{3\text{HB},j} = -\lambda_{\text{eff}} + q \quad (9)$$

where $c_{3\text{HB},j}$ is annual average tritium concentration in surface water, representing the contamination from atmosphere tests of nuclear weapons, its generation by natural processes and the atmospheric transfer from nuclear facilities worldwide (background), based on the results of field measurements (Bq/l),

λ_{eff} effective ecological decay constant describing a decrease in concentrations of tritium (1/y),

q natural logarithm of tritium activity at the beginning of the observation.

Using the Equation 9, effective ecological tritium half-life $T_{\text{eff}} = 8.1$ years for the whole period (1977-2008) was calculated.

More detailed analysis of the period 1990 – 2008, showed that decreasing trend in the tritium activities was gradually lessening. For this period, the effective ecological half-life

was 12.3 years. This can be attributed to the facts that relatively small tritium activities originate also from a constant component, which is stemming from the cosmic radiation and from the atmospheric transfer from nuclear facilities worldwide. This component was considered also to be constant in the analysed period.

These factors were therefore eliminated in subsequent analysis by subtracting these components. For the modified approach (elimination of the components originating from cosmic radiation and the atmospheric transfer from nuclear facilities worldwide), the effective ecological half-life (T_{eff}) derived from the period 1990 – 2008 was 8.4 years, which is shorter than that derived by using the unmodified approach.

These results were compared with data published in the period after termination of atmospheric tests of nuclear weapons in 1963. According to Bennet (1973), mean tritium concentration in this year in 20 rivers in United States was 100 Bq/l. The decrease in tritium concentration observed in this period was faster as compared to the effective half-life $T_{\text{ef}} = 8.1$ years calculated in our study from the period 1977 – 2008. Bogen et al. (1979) reported that effective ecological half-life increased from 3 years in the period closely after termination of the tests of nuclear weapons to 5 years in about 1978. This can be explained by tritium migration into lower water levels in oceans, which is reflected in its decreasing concentration.

6.3. Impacts of the Temelín plant

Decision of Regional Authority (Permit on Water management, 2007) specifies a limit of 66 TBq/y tritium activity that can be discharged with waste waters from Temelín Nuclear Power Plant if 2 reactors of the plant are in operation. In harmony with the development of the operation, the tritium activity discharged from the plant has been increasing since 2001 (Fig. 4).

The mean annual tritium concentrations in the Vltava River consequently exhibited an increasing trend, which is attributable to gradual increase in the output of the plant associated with increasing discharged quantity of tritium. In 2001, the tritium concentrations in the Vltava River did not exceed maximum from the period before the operation of Temelín plant. In 2002, the tritium concentrations were affected by discharges from pilot operation of the plant but diluted by high river flows in this year. Low precipitation and therefore low flows in 2003 were reflected in the observed maximum concentration of 39 Bq/l (November 2003). The highest mean annual concentrations of tritium were subsequently observed in 2008.

The results of the monitoring of the tritium concentrations in the Vltava River below the outflow of waste waters from the Temelín plant show that the mean tritium concentrations are at a level below 3% of the pollution standard ($c_{\text{average}} = 700$ Bq/l) specified in Guidance document to Resolution of the Czech Government No. 229/2007 Coll. The mean concentrations and also maximum concentrations did not exceed an indicative limit of 100 Bq/l specified in a Decree of the State Institute for Nuclear Safety No. 307/2002 and EC Council Directive on the quality of water intended for human consumption (98/83/EC).

The results of tritium monitoring in the Vltava River at Solenice, in reference locality on the Vltava River at Hluboká, and river flows were used for calculation of tritium outflows and there comparison with the data provided by the operator of the plant, Czech Power Works – Temelín NPP (Fechtnerová, 2002–2006, Lysáček, 2007–2009).

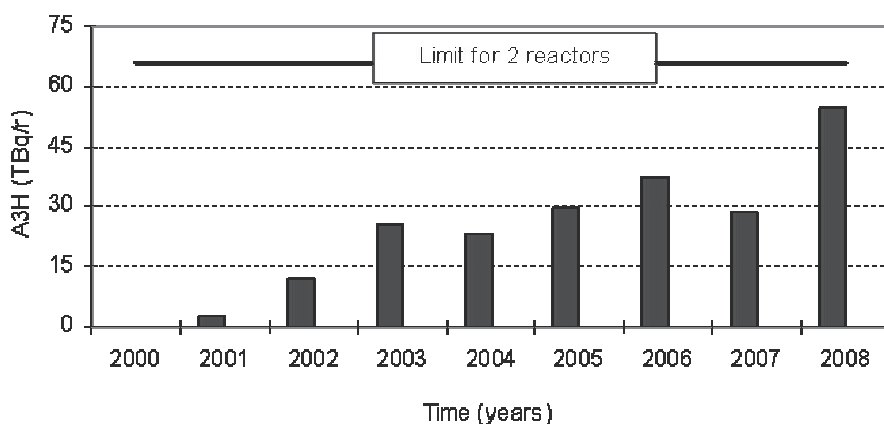


Fig. 4. Annual outflows of tritium discharged with waste water from Temelín Nuclear Power Plant in the period 2000 – 2008

The annual outflows of tritium activity ($A_{3Hcor.,j}$ in Bq/y or TBq/y) in the Vltava River at Solenice (corrected by subtracting the background activity) were calculated as follows:

$$A_{3Hcor.,j} = c_{3Hj}Q_jt - c_{3HBj}Q_jt \quad (10)$$

where c_{3Hj} is mean annual tritium concentration in year j (Bq/m³),
 c_{3HBj} see Equation (9),
 Q_j mean annual river flow in year j (m³/s),
 t duration of a year in seconds.

The results of the calculation are summarized in Table 2, which shows that the tritium outflows (in the Vltava River at Solenice) calculated from the independent monitoring are until 2003 below the values derived from the data provided by the operator of the Temelín plant. The tritium outflows in 2002 were affected by extremely high river flows in this year. During 2003, which was dry, the tritium was accumulated in Orlick Reservoir consequently to low flows and therefore long delay time. For water storage in Orlick Reservoir of $720 \cdot 10^6$ m³ and tritium concentration of 1000 Bq/m³ (average background), the accumulated tritium quantity is 0.7 TBq. In 2004, a part of the accumulated tritium was discharged from the reservoir (Hanslík & Ivanovová, 2004b). In 2006 and 2007, the tritium outflows calculated from the monitoring exceeded those derived from Temelín data. The differences between the results are probably attributable to uneven tritium outflows from Temelín plant during a year and consequent shift of the tritium outflow from the reservoir between the years. If we take into account the fact that tritium outflow is calculated from 12 samples in a year and other uncertainties (accuracy of river flow data), we can conclude that the results are in good harmony.

Year	Results of monitoring in the Vltava at Solenice			Temelín NPP data
	Total outflow	Background	Total outflow - background	
(TBq)				
2001	4.2	3.5	0.7	2.8
2002	15.6	6.0	9.6	11.9
2003	21.0	3.0	18.0	25.1
2004	33.9	3.5	30.4	23.0
2005	29.0	4.4	24.6	29.6
2006	55.4	4.9	50.5	37.3
2007	39.5	3.0	36.5	28.4
2008	46.8	2.5	44.3	54.3
Sum	245.5	30.8	214.7	216.4

Table 2. Annual tritium outflows calculated from the results of tritium monitoring in the Vltava River at Solenice and from data provided by the operator of Temelín Nuclear Power Plant

Continuous attention has been paid to the monitoring of tritium activities in the Vltava at Prague (Podolí), where water is abstracted for drinking water supply purposes. The tritium concentrations in the period 2002 - 2008 are together with the Vltava River flows in sampling days shown in Fig. 5. The results show that the tritium concentrations in the Vltava River at Podolí are affected by the operation of the reservoirs on the Vltava River, in addition to the effect of tritium dilution in the Vltava River reach (whose main tributaries are the Otava, Sázava and Berounka Rivers) downstream from the outflow of the waste water from the Temelín plant. This is substantiated by the relatively high tritium concentrations in January 2004, which were coupled with high outflows of the water from the Orlick Reservoir. The high tritium concentrations were caused by the fact that the tritium was accumulated in the reservoir during low flows in extremely dry period in the third and fourth quarters of 2003. A similar situation occurred again in the winter season at the end of 2004 and at the beginning of 2005 but the increase in the tritium concentration was lower than that in 2003.

7. Concentrations of ⁹⁰Sr, ¹³⁴Cs and ¹³⁷Cs

Decision of Regional Authority (Permit on Water management, 2007) specifies a limit 1 GBq/y for other activation and fission products (expressed as gross beta excluding tritium).

7.1. Concentrations of ¹³⁷Cs in water

Temporal changes of the ¹³⁷Cs concentrations in water samples taken from Orlick Reservoir and its tributaries were studied for two periods, 1990-1994 and 1995-2008.

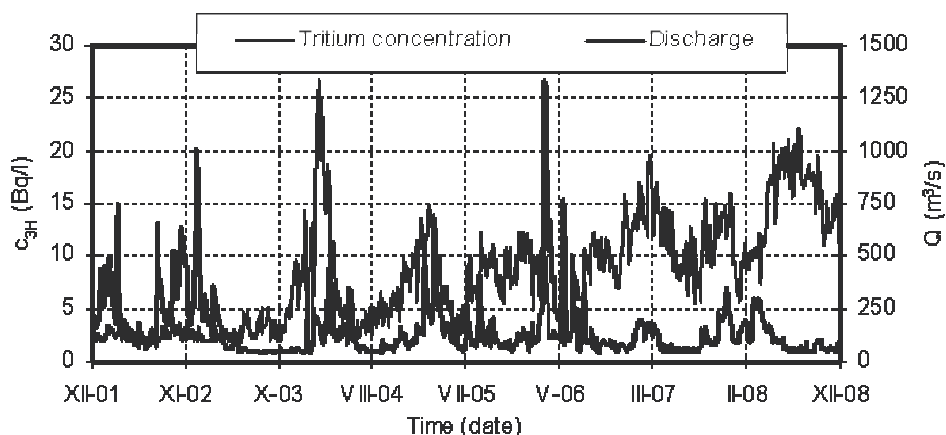


Fig. 5. Tritium concentrations (c_{3H}) and river flows (Q) in the Vltava River at Prague - Podolí in the period 2002 - 2008

The effective ecological half-lives (T_{eff}) in water in individual tributaries and outflow from Orlick Reservoir (Table 3) were evaluated in the range 1.1 - 2.2 y for the period 1990 - 1994 and 5.9 - 10.4 y for the period 1995 - 2008. The ecological half-lives (T_{ecol}) are in the range 1.2 - 2.4 y for the period 1990 - 1994 and 7.4 - 15.8 y for the period 1995 - 2008.

The results of studies showed that a decrease in the concentrations ^{137}Cs , which was observed before the plant operation, continued also during the subsequent period.

An example is shown in Fig. 6 for Vltava River at Hněvkovice (source of technological water) and the Vltava River at Solenice (downstream from the Temelín waste water outflow). In 2008, the average activity of ^{137}Cs in Hněvkovice was 0.8 mBq/l and 0.4 mBq/l in Solenice.

Period	1990 - 1994		1995 - 2008	
	T_{eff} (y)	T_{ecol} (y)	T_{eff} (y)	T_{ecol} (y)
Tributaries of Orlick Reservoir				
The Vltava River at Hněvkovice	1.5	1.6	7.5	10.1
The Lužnice River at Koloděje	2.2	2.4	10.4	15.8
The Otava River at Topělec	1.1	1.2	6.5	8.3
The outflow from Orlick Reservoir (the Vltava River at Solenice)	1.5	1.5	5.9	7.4

Table 3. The evaluated effective ecological half-lives and ecological half-lives of ^{137}Cs in water in the tributaries and outflow of the Orlick Reservoir in the periods 1990 - 1994 and 1995 - 2008

The results of the studies focused on the vicinity of the Temelín plant are in agreement with similar studies on changes in the water contamination after the Chernobyl accident. For example, Zibold et al. (2001) observed a faster decrease of ^{137}Cs concentration in the period 1986-1988, and the second slower phase in 1989-2000. Similarly, Smith & Beresford (2005) reported that the rate of decline of the ^{137}Cs concentration in the Pripjat River was decreasing in recent years. The effective half-lives of 1.2 years (dissolved phase) and 1.7 y

(particulate phase) in the period 1987 – 1991 increased to 3.4 y (dissolved phase) and 11.2 y (particulate phase) in the period 1995 –1998. This increase in T_{eff} has also been observed in Belarus, Ukraine and Finland (Smith & Beresford, 2005).

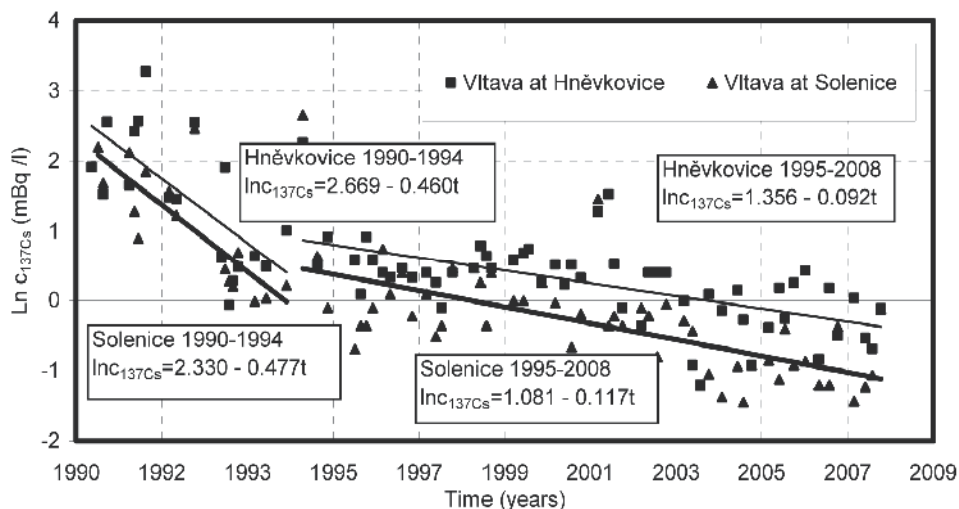


Fig. 6. Time changes of ^{137}Cs concentration ($C_{137\text{Cs}}$) in the Vltava River at Hněvkovice (source of technological water) and the Vltava River at Solenice (downstream from the Temelín waste water outflow) in the periods 1990-1994 and 1995-2008

7.2. Concentrations of ^{90}Sr in water

Temporal changes of the ^{90}Sr concentrations in water samples taken from Orlick Reservoir and its tributaries were studied for period 1993 – 2008.

The effective ecological half-lives (T_{eff}) in water in individual tributaries and outflow from Orlick Reservoir (Table 4) were evaluated in the range 6.8 – 12.4 y and the ecological half-lives (T_{ecol}) were in the range 9 – 21.8 y.

Period	1995 - 2008	
	T_{eff} (y)	T_{ecol} (y)
Tributaries of Orlick Reservoir		
The Vltava River at Hněvkovice	12.4	21.8
The Lužnice River at Koloděje	6.8	9.0
The Otava River at Topělec	8.3	11.6
The outflow from Orlick Reservoir (the Vltava River at Solenice)	8.5	12.0

Table 4. The evaluated effective ecological half-lives and ecological half-lives of ^{90}Sr in water in the tributaries and outflow of the Orlick Reservoir in the period 1993 – 2008

An example is shown in Fig. 7 for Vltava River at Hněvkovice and the Vltava River at Solenice. In 2008, the average activity of ^{90}Sr in Hněvkovice was 3.5 mBq/l and 2.5 mBq/l in Solenice.

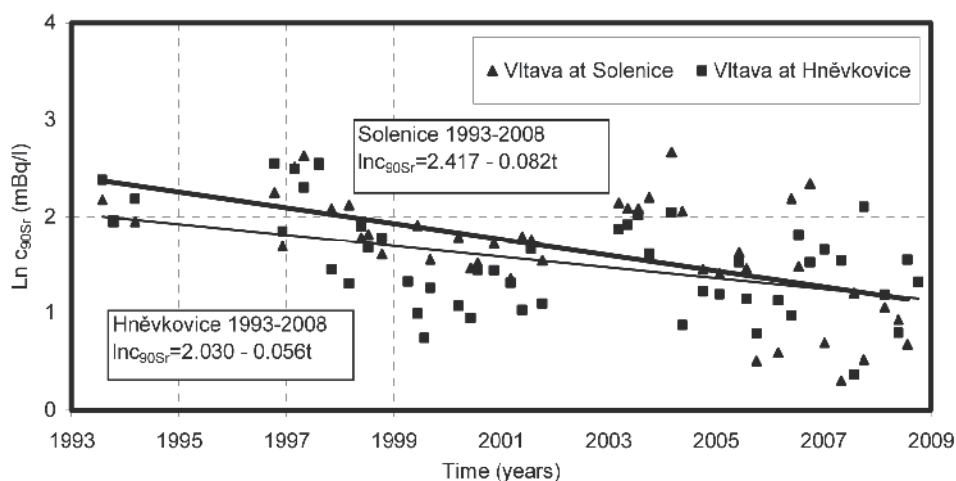


Fig. 7. Time changes of ^{90}Sr concentration ($c_{90\text{Sr}}$) in the Vltava River at Hněvkovice and the Vltava River at Solenice in the period 1993-2008

The concentrations of anthropogenic radionuclides ^{137}Cs and ^{90}Sr in the hydrosphere downstream from waste water discharge from the Temelín plant originate therefore mainly from the residual contamination from atmospheric tests of nuclear weapons and the Chernobyl accident. These activities show a decreasing trend in time. At present, the detected activities concentrations in surface water are near the detection limits.

7.3. Concentrations of radionuclides in sediments

The results of the analysis of sediments showed that the residual contamination from the atmospheric tests of nuclear weapons and the Chernobyl accident in the last century is dominant as compared to possible impacts of waste waters from the Temelín plant on sediment contamination. Apart from ^{134}Cs , ^{90}Sr and ^{137}Cs , the results of the monitoring did not substantiate sediment contamination by any other activation and fission products.

The concentrations of radiocesium in the individual river sites were different, which is attributable to inhomogeneous caesium deposition after the Chernobyl accident, different grain sizes of the sediments at the individual river sites, and different sediment transportation processes.

The activities of these radionuclides are decreasing in time. The rates of decline are similar for reference sampling sites and affected sampling sites river sites therefore the trends of decline were evaluated for average annual activities from all observed sites. The assessment of ^{134}Cs was stopped in 1998 because from this year all observed values were below the MDA. The effective half-life was 1.6 y for ^{134}Cs (for the period 1990-1998) and estimated ecological half-life was 7.8 y. For ^{137}Cs the effective half-life was 6.2 y for the period 1990-2008. The estimated ecological half-life was also 7.8 y.

Fig. 8 shows the decreasing trends in the ^{137}Cs and ^{134}Cs concentrations in sediments.

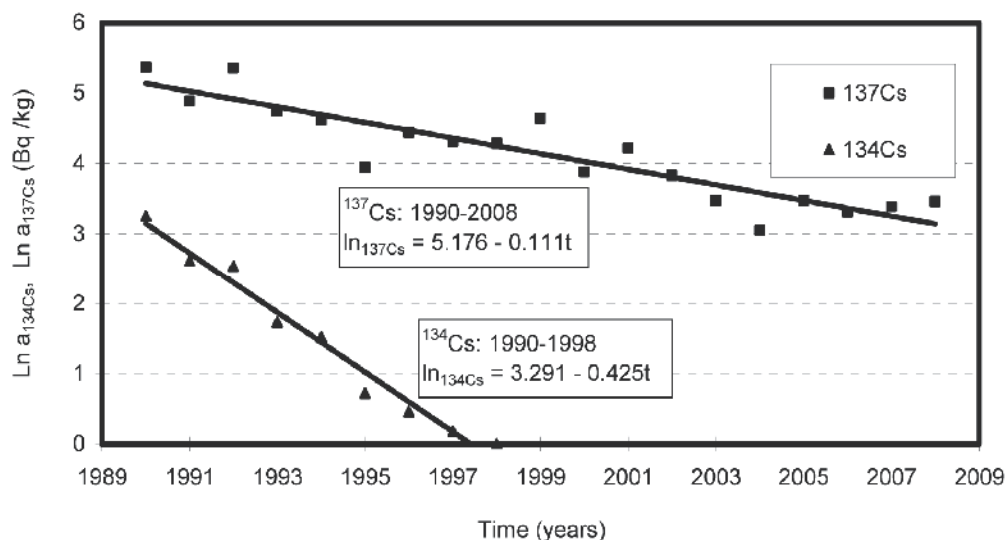


Fig. 8. Time changes of annual average concentrations of ^{134}Cs ($a_{134\text{Cs}}$) and ^{137}Cs ($a_{137\text{Cs}}$) in bottom sediments (dry matter) in Orlík Reservoir and its main tributaries in the periods 1990 – 1998 (^{134}Cs) and 1990 – 2008 (^{137}Cs)

8. Depositions in Orlík Reservoir

Data on river flows and concentrations of suspended solids, ^{90}Sr and ^{137}Cs were used to assess possible impacts of the reservoir on monitored matters.

Annual mean concentrations of suspended solids in samples from Orlík Reservoir and its tributaries were used together with annual mean flows for derivation of a relationship between suspended solids deposition in Orlík Reservoir and annual mean flow (Fig. 9). Subsequently, it was derived that the annual deposition of suspended solids ranged between 71% – 95% (with the average value of 86%) of the inflow of the suspended solids.

In mass unit, the annual mean deposition is 29 700 tons. The deposition of suspended matter in Orlík reservoir expressed in percentages did not show any time dependence.

The annual deposition of ^{137}Cs was derived between 36% and 76% (1.0 – 19.2 GBq) with the average value of 61%. The annual deposition was decreasing in time (Fig. 10) consequently to half life of 7.1 years (in the period 1990 – 2008). The temporal trend of the decrease is in harmony with observed trends in ^{137}Cs activity in water and bottom sediments in the study area (Hanslík et al., 2009c). The deposition of ^{137}Cs was greater in 2002 consequently to higher precipitation in this year as compared to that in the other years of the period 1996 – 2008. The mean percentage ^{137}Cs deposition was lower than that of the suspended solids. This result indicates that a part of ^{137}Cs concentration is dissolved in water and its deposited component is fixed on solid particles. This assumption is in harmony with the high level of distribution coefficient K_d for ^{137}Cs reported for the Constance lake and the Rhine River in the range 4.6×10^4 – 2.7×10^6 l/kg (Smith & Beresford, 2005). The decrease in the deposition of ^{137}Cs in Orlík reservoir with the effective ecological

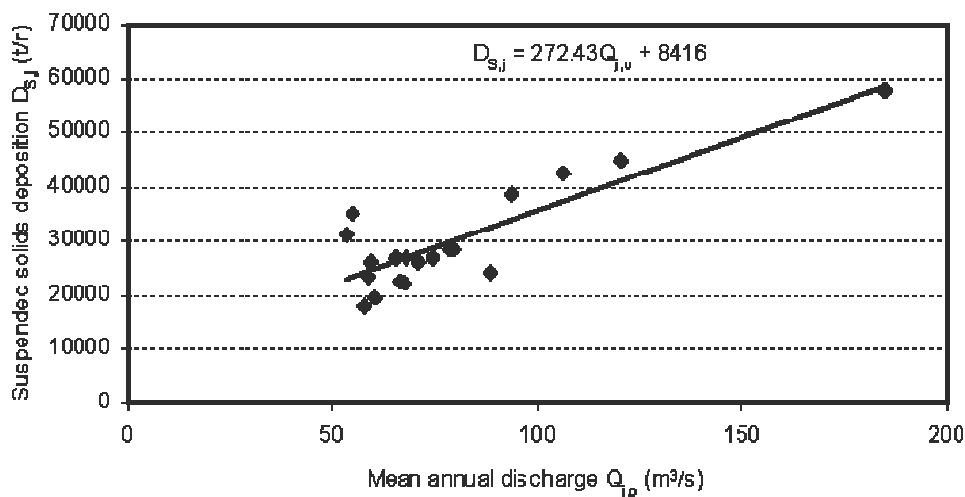


Fig. 9. Dependence of the suspended solids deposition in Orlík reservoir on the annual mean flow

half life of 7.1 years is in agreement with the half life of 6.2 years of the decrease in annual mean activity of ^{137}Cs in bottom sediments sampled during the period 1990 – 2008 from the reservoir and its tributaries.

The analysis of ^{90}Sr concentrations showed that the outflow from the reservoir exceeds that of the inflow from the tributaries and the inter-basin area. The percentage outflow of ^{90}Sr was detected in the range from -37% to 72% with the average value of 20%.

The outflow of ^{90}Sr from the reservoir corresponds with its higher mobility and lower values of K_d (750 – 1800 l/kg) published for the area surrounding Chernobyl Nuclear Power Plant (Smith & Beresford, 2005). The increased activity of ^{90}Sr at sampling sites that was detected from the monitoring after the extreme flood event in 2002 corresponds with the results obtained for the Dněpr Reservoirs, where significantly increased activity of ^{90}Sr was detected in water after the winter flood consequently to blockage of the river by ice floes (Vakulovsky et al., 1994).

It was also derived for ^{90}Sr that its residual pollution exceeds its contribution originating from wastewater discharges from Temelín Nuclear Power Plant. Annual discharges of ^{90}Sr in the period 2002 – 2008 were in the range < 0.0002 – < 0.003 GBq/y (Fechtnerová, 2003–2006, Lysáček, 2007–2009).

Annual activities of ^{90}Sr and ^{137}Cs discharged from the Temelín plant were significantly lower than the activities in the inflow and outflow from Orlík Reservoir. The concentrations of ^{90}Sr and ^{137}Cs originate from the atmospheric fall-out consequently to the atmospheric tests of nuclear weapons and Chernobyl accident in the last century.

The data on the outflows and depositions of ^{137}Cs and ^{90}Sr were compared with published results focused on the ratio of the mean activities of dissolved radioactive substances and suspended solids between the inflows and outflows from open European lakes and reservoirs in the period 1987 – 1994, that is after the Chernobyl accident (Smith & Beresford, 2005, Smith et al., 1997). In case of ^{137}Cs the detected ratio in the individual lakes ranged

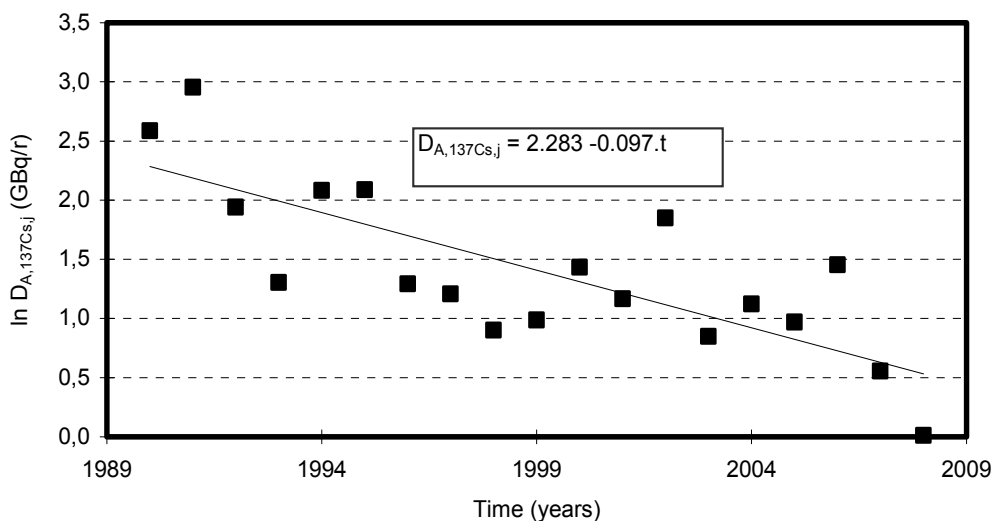


Fig. 10. Decrease in ^{137}Cs deposition in Orlik reservoir during 1990 – 2008

from 0.08 – 2.22, in case of ^{90}Sr the detected range was 0.66 – 1.44. For ^{90}Sr , the values of the ratio of its mean annual activity in the inflow and outflow from Orlik reservoir was 0.58 – 3.91 with the average value of 0.89 in the period 1996 – 2008, which was in accordance with the published results. The observed ratio of the annual mean activities of ^{137}Cs in the inflow and outflow from Orlik reservoir ranged from 1.56 to 4.11 with the average value of 2.76 in the period 1990 – 2008 and therefore this result exceeds significantly the published values (Smith & Beresford, 2005, Smith et al., 1997). The increased deposition of ^{137}Cs corresponds with the increased deposition of suspended solids in the range from 3.49 to 21.5 with the mean value of 9.00 derived for the identical period.

9. Bioaccumulation

A specific analysis was aimed at assessing ^{137}Cs concentrations in fish samples taken from Orlik Reservoir and its tributaries. Temporal changes of the ^{137}Cs concentrations were studied for two periods, 1986 – 1990 and 1994 – 2008. The results of the study were used for evaluation of ^{137}Cs temporal trends and evaluation of concentration factor and committed effective dose.

Temporal changes in ^{137}Cs concentrations in fish in Orlik Reservoir in the periods 1986 – 1990 and 1994 – 2008 are shown in Fig. 11.

Evaluated effective ecological half-lives (T_{eff}) for fish were 1.0 y for the period 1986 – 1990 and 6.1 y for the period 1994 – 2008 and ecological half-lives (T_{ecol}) were 1.1 y and 7.7 y respectively. Observed rates of decrease in ^{137}Cs concentrations in fish were approximately identical as in water. The evaluated rates of decrease in ^{137}Cs concentrations in fish are shorter than those published in literature. Brittain et al. (1991) reported that T_{eff} of ^{137}Cs in fish was 3.0 y for the period 1986 – 1989. The results from the period 1994 - 2008 confirm

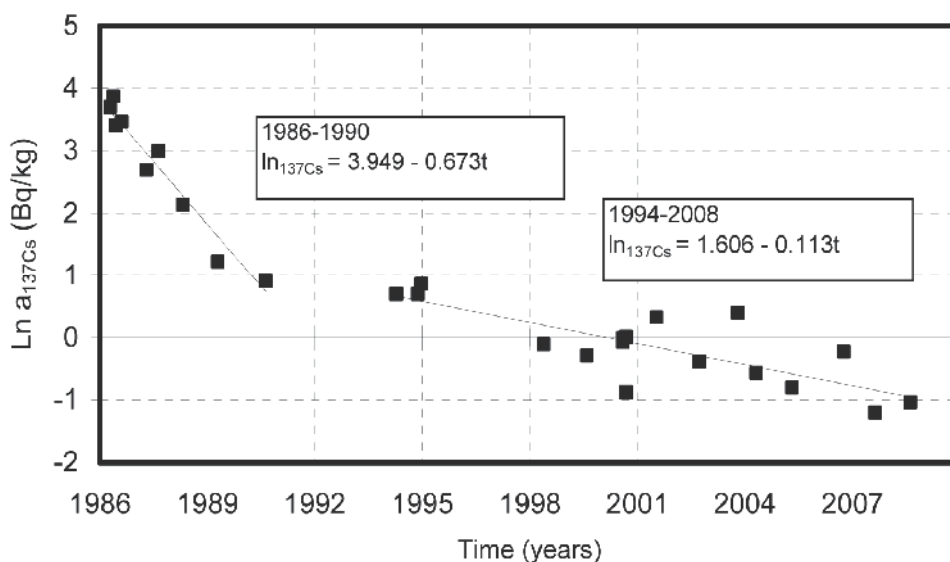


Fig. 11. Temporal changes of ^{137}Cs concentration ($a_{137\text{Cs}}$) in fish (wet weight) in Orlík Reservoir in the periods 1986 – 1990 a 1994 – 2008

that the rates of the decline in ^{137}Cs activity may decrease to values close to those determined by the physical decay half-life (Smith et al., 2000).

The results of the observation and analysis of ^{137}Cs concentration in fish were used for calculation of ^{137}Cs concentration factors in fish and radiation doses that could originate from fish ingestion (see Chapter on Radiation doses).

Fig. 12 shows results of the calculation of ^{137}Cs concentration factors in fish. The values of the concentration factors range from 92 to 671 l/kg, with the average value of 338 l/kg during the period 1990 – 2008.

These values are lower than those published by Smith et al. (2000) who reported the range between 82 – 14 424 l/kg with the average value 1912 l/kg. This could be attributed to the fact that the Czech study used ^{137}Cs activity in total solids in water (both in dissolved and non-dissolved solids), while Smith et al. (2000) used ^{137}Cs concentration in filtered water.

10. Radiation doses

The results from the above analyses were used for calculation of radiation doses that could originate from ingestion of fish (^{137}Cs) or water from the Vltava and Elbe Rivers (tritium). The committed effective dose from ^{137}Cs was derived from results of ^{137}Cs in fish via ingestion with 10 kg fish (by adult). Within the first few months after the Chernobyl accident it would be 4.9 μSv and since 2004 it is smaller than 0.1 $\mu\text{Sv}/\text{y}$. Possible impact of radioactive waste waters from the Temelín plant was not substantiated.

Tritium concentrations were used for calculation of radiation doses from possible use of the water from the Vltava River at Solenice and the Elbe River at Hřensko for drinking water supply purposes. The calculated doses are given in Table 5. The average dose in the period

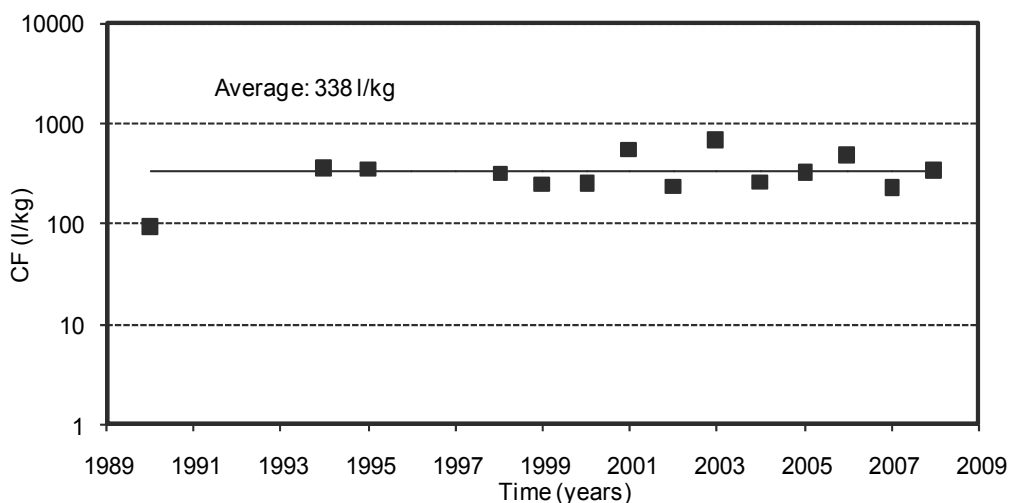


Fig. 12. ¹³⁷Cs concentrations factors in fish during the period 1990 – 2008

River site	Year	2001	2002	2003	2004	2005	2006	2007	2008
Vltava at Solenice	C _{3H} (Bq/l)	1.42	2.67	10.2	13.5	9.68	15.5	17.6	22.0
	E _{3H} (μSv/y)	0.018	0.034	0.128	0.170	0.122	0.195	0.222	0.277
Elbe at Hřensko	C _{3H} (Bq/l)	1.68	1.87	2.25	4.61	4.32	4.61	4.40	6.35
	E _{3H} (μSv/y)	0.021	0.024	0.028	0.058	0.054	0.058	0.055	0.080

Table 5. Annual average tritium concentrations (C_{3H}) in the Vltava at Solenice and the Elbe at Hřensko and committed effective doses (E_{3H}) due to tritium ingestion from water drinking by adults

2003 – 2008 was 0.186 μSv/y for the Vltava at Solenice and 0.056 μSv/y for the Elbe at Hřensko (the international boundary with the Federal Republic of Germany).

The calculated doses are below the limit specified in the permit issued by the State Agency for Nuclear Safety, which is 3 μSv/y for tritium and other activation and fission products. For a comparison, the calculated dose from the average ¹³⁷Cs concentration in the Vltava at Solenice calculated from the period 2001 – 2002 is 0.011 μSv/y. This dose has been mainly due to global fallout and the Chernobyl accident. The estimated radiation doses due to the operation of the Temelín plant are negligibly small.

11. Summary

The results of systematic monitoring of possible impacts of the Temelín plant on the hydrosphere show that the waste water discharges meet the limits specified in the permit on water management (Decision of Regional Authority - Permit on Water management, 2007) and in the Government Decree No. 61/2003 Coll. Concentrations of anthropogenic radionuclides in the hydrosphere downstream from the waste water outflow from the

Temelín plant are mainly due to the residual contamination from global fallout and the Chernobyl accident. Apart from tritium, the influence of the Temelín plant on the concentration of the activation and fission products in the hydrosphere has been negligible. Maximum annual released activity of activation and fission products excluding tritium was 0.46 GBq, which is still completely overlapped by the persisting impact of the deposition after the accident in Chernobyl NPP and atmospheric test of nuclear weapons in the last century.

Natural processes, residual contamination from atmospheric tests of nuclear weapons in the last century and discharges from nuclear facilities are the main sources of tritium concentrations in the environment. In terms of the tritium quantities, the residual contamination from the tests is dominating, however, this component is gradually diminishing consequently to the tritium radioactive decomposition. Effective half-life calculated for the period 1977 – 2008 was 8.1 years. For the period 1990 – 2008, the half-life was 12.3 years or 8.4 years if we subtract natural tritium component and tritium originating from the atmospheric transfer from nuclear facilities worldwide.

An increasing role is presently played by local tritium sources, specifically by outflows of waste waters from nuclear facilities. The results of tritium monitoring downstream from the outflow of waste waters from the Temelín plant showed that the annual tritium concentrations did not exceed an indicative limit of 100 Bq/l specified in a Decree of the State Institute for Nuclear Safety No. 307/2002.

Annual tritium outflows that have been derived from data from tritium monitoring in the Vltava River at Solenice are in harmony with the values derived from the data provided by the operator of the Temelín plant. These results therefore also substantiate the fact that the pollution data from the independent monitoring can affectively be used for verification of the pollution outflows from the Temelín plant.

For two time periods (1990-1994 and 1995-2008), the concentrations of ^{137}Cs were analysed in surface water and fish and for one period (1990-2008) in sediments. The effective ecological half-lives in water in individual tributaries and outflow from Orlick Reservoir were evaluated in the range 1.1 – 2.2 years for the period 1990 – 1994 and 5.9 – 10.4 years for the period 1995 – 2008. The results showed that in the first period (close to the accident in Chernobyl) the concentrations of ^{137}Cs were rapidly decreasing while slow decline was detected for the second period (after 1995). For ^{137}Cs in sediments the effective half-life was 6.2 years for the period 1990-2008. Evaluated effective ecological half-lives for fish were 1.0 y for the period 1986 – 1990 and 6.1 years for the period 1994 – 2008. Concentrations of ^{137}Cs in water and fish were decreasing approximately with the same rate. Temporal changes of the ^{90}Sr concentrations in water samples taken from Orlick Reservoir and its tributaries were studied for period 1993 – 2008. The effective ecological half-lives in water in individual tributaries and outflow from Orlick Reservoir were evaluated in the range 6.8 – 12.4 y.

Temporal changes of the ^{134}Cs and ^{137}Cs concentrations in sediments were studied for period 1990 – 1998 and 1990 – 2008 respectively. The assessment of ^{134}Cs was stopped in 1998 because from this year all observed values were below the MDA. The effective half-life was 1.6 y for ^{134}Cs (for the period 1990-1998). For ^{137}Cs the effective half-life was 6.2 y for the period 1990-2008.

Data on river flows and concentrations of suspended solids, ^{90}Sr and ^{137}Cs were used to assess possible impacts of the reservoir on monitored matters. It was derived that the annual deposition of suspended solids ranged between 71% – 95% (with the average value of 86 %) of the inflow of the suspended solids. The annual deposition of ^{137}Cs was derived

between 36% and 76% with the average value of 61 %. The annual deposition of ^{137}Cs was decreasing in time consequently to half life of 7.1 years (in the period 1990 – 2008). The analysis of ^{90}Sr concentrations showed that the outflow from the reservoir exceeds that of the inflow from the tributaries and the inter-basin area. The percentage outflow of ^{90}Sr was detected in the range from -37% to 72% with the average value of 20%.

During the period 1990 – 2008, the ^{137}Cs concentration factor calculated from fish samples ranged from 92 to 671 l/kg with the average value of 338 l/kg. Committed effective dose by ^{137}Cs via ingestion of 10 kg fish (by adult) within the first few months after the Chernobyl accident was 4.9 μSv and since 2004 it is smaller than 0.1 $\mu\text{Sv}/\text{y}$.

In surface water, river bottom sediments and also fish samples from the Temelín vicinity, the ^{137}Cs and ^{90}Sr concentrations show a decreasing trend, including the samples taken downstream from the waste water outflow from the Temelín plant.

Acknowledgement

The chapter was prepared from the results of projects MZP 0002071101 and SP/2e7/229/07 sponsored by Czech Ministry of Environment.

12. References

- Bennet, B.G. (1973): Environmental tritium and the dose to man, In Proceedings of 3th International Congress of the International Radiation Protection Association, Washington, pp. 1047-1053
- Bogen, D.C.; Welfrod, G.A. & White, C.G. (1979): Tritium distribution in man and his environment, In: Behaviour of Tritium in the Environment, Proceedings of an International Atomic Energy Agency conference, Vinna, IAEA, IAEA-SM-232/74, pp. 567-574
- Brittain, J.E.; Storrust, A. & Larsen, E. (1991): Radiocaesium in Brown Trout (*Salmo trutta*) from a subalpine lake ecosystem after the Chernobyl reactor accident, *Journal of Environmental Radioactivity*, 14, pp. 181 - 191
- Čapková, A. (1993): Guidelines for determination of water pollution parameters, Ministry of the Environment, Prague (in Czech)
- ČSN EN 25667-1 (75 7051) (1994): Water quality. Sampling, Part 1: Guidance on the design of sampling programmes, Czech Standard Institute (in Czech)
- ČSN EN 25667-2 (75 7051) (1994): Water quality, Sampling, Part 2: Guidance on sampling techniques, Czech Standard Institute (in Czech)
- ČSN EN ISO 5667-3 (75 7051) (1996): Water quality, Sampling, Part 3: Guidance on the preservation and handling of samples, Czech Standard Institute (in Czech)
- ČSN EN ISO 5667-4 (75 7051) (1994): Water quality, Sampling, Part 4: Guidance on sampling from lakes, natural and man-made, Czech Standard Institute (in Czech)
- ČSN EN ISO 5667-6 (75 7051) (1994): Water quality, Sampling, Part 6: Guidance on sampling of rivers and stress, Czech Standard Institute (in Czech)
- ČSN EN ISO/IEC 17025 (2001): General requirements for the competence of testing and calibration laboratories, Czech Standard Institute (in Czech)
- ČSN ISO 9698 (75 7635) (1996): Water quality, Determination of tritium activity concentration, Liquid scintillation counting method, Czech Standard Institute (in Czech)

- ČSN ISO 10703 (75 7630) (1999): Water quality – Determination of the activity concentration of radionuclides by high resolution gamma-ray spektrometry, Czech Standard Institute (in Czech)
- Decree of the State Institute for Nuclear Safety No. 307/2002 Col., on Radiation protection as amended by Decree No. 499/2005 Col.
- Council Directive on the quality of water intended for human consumption (98/83/EC)
- Fechtnerová, M. (2002): Annual report about environment 2001, CEZ Group, Temelín (in Czech)
- Fechtnerová, M. (2003): Annual report about environment 2002, CEZ Group, Temelín (in Czech)
- Fechtnerová, M. (2004): Annual report about environment 2003, CEZ Group, Temelín (in Czech)
- Fechtnerová, M. (2005): Annual report about environment 2004, CEZ Group, Temelín (in Czech)
- Fechtnerová, M. (2006): Annual report about environment 2005, CEZ Group, Temelín (in Czech)
- Flamm, E.J.; Lingenfelter, R.E.; Mac Donald, J.F. & Libby, W.F. (1962): Tritium and helium-3 solar flares and loss of helium from the earth's atmosphere, *Science*, Vol. 138, No. 3536, pp. 48-50
- Guidance document to Resolution of the Czech Government No. 229/2007 Coll., Ministry of the Environment of the Czech Republic, pp. 58 (in Czech)
- Hanslík, E. & Mansfeld, A. (1983): Tritium in wastes from nuclear fuel cycle and options for its disposal. *Works and Studies*, Vol. 159, Water Research Institute, SZN, Prague (in Czech)
- Hanslík, E. (1995): Impact of Temelín Nuclear Power Plant on hydrosphere and other components of environment, Final report T. G. Masaryk Water Research Institute, Prague (in Czech)
- Hanslík, E. (1998): Impact of nuclear devices on environment, Final report T. G. Masaryk Water Research Institute, Prague (in Czech)
- Hanslík, E. (1999a): Assessment of surface and groundwater quality in connection with construction and operation Temelín Nuclear Power Plant on surrounding environment, Report T. G. Masaryk Water Research Institute, Prague (in Czech)
- Hanslík, E.; Budská, E.; Sedlářová, B. & Šimonek, P. (1999b): Time changes of radionuclides activity in hydrosphere in vicinity Temelín Nuclear Power Plant, In: XVI. Conf. Radionuclides and ionizing radiation in water management, ČSVTVS, České Budějovice, pp. 32-39, ISBN 80-02-01336-0 (in Czech)
- Hanslík, E. (2000): Assessment of surface and groundwater quality in connection with construction and operation Temelín Nuclear Power Plant on surrounding environment, Report T. G. Masaryk Water Research Institute, Prague (in Czech)
- Hanslík, E. (2001a): Assessment of surface and groundwater quality in connection with construction and operation Temelín Nuclear Power Plant on surrounding environment, Report T. G. Masaryk Water Research Institute, Prague (in Czech)
- Hanslík, E.; Budská, E.; Placáková, N.; Sedlářová, B.; Šimonek, P. & Ivanovová, D. (2001b): Reference stage of hydrosphere and prognosis of Temelín Nuclear Power Plant impact, In: XVII. Conf. Radionuclides and ionizing radiation in water management, ČSVTVS, České Budějovice, pp. 13-23, ISBN 80-02-01468-5, (in Czech)
- Hanslík, E. (2002): Assessment of surface and groundwater quality in connection with construction and operation Temelín Nuclear Power Plant on surrounding environment, Report T. G. Masaryk Water Research Institute, Prague (in Czech)
- Hanslík, E. (2003): Assessment of surface and groundwater quality in connection with construction and operation Temelín Nuclear Power Plant on surrounding environment, Report T. G. Masaryk Water Research Institute, Prague (in Czech)

- Hanslík, E. (2004a): Assessment of surface and groundwater quality in connection with construction and operation Temelín Nuclear Power Plant on surrounding environment, Report T. G. Masaryk Water Research Institute, Prague (in Czech)
- Hanslík, E. & Ivanovová, D. (2004b): Concentrations of radioactive substances in Orlický Reservoir and its tributaries after beginning of the operation of Temelín NPP, Report T. G. Masaryk Water Research Institute (in Czech)
- Hanslík, E. (2005a): Assessment of surface and groundwater quality in connection with construction and operation Temelín Nuclear Power Plant on surrounding environment, Report T. G. Masaryk Water Research Institute, Prague (in Czech)
- Hanslík, E.; Jedináková-Křížová, V.; Ivanovová, D.; Kalinová, E.; Sedlářová, B. & Šimonek, P. (2005b): Observed half-lives of ^3H , ^{90}Sr and ^{137}Cs in hydrosphere in the Vltava River basin (Bohemia). *Journal of Environmental Radioactivity*, Vol. 81, pp. 307-320
- Hanslík, E. (2006a): Assessment of surface and groundwater quality in connection with construction and operation Temelín Nuclear Power Plant on surrounding environment, Report T. G. Masaryk Water Research Institute, Prague (in Czech)
- Hanslík, E.; Ivanovová, D.; Juranová, E. & Šimonek, P. (2006b): Impact of nuclear power plant waste water on tritium concentration in the Vltava and Elbe Rivers, In: T. G. Masaryk Water Research Institute Collection of papers, T. G. Masaryk Water Research Institute, Prague, pp. 47-60, ISBN 80-85900-64-5
- Hanslík, E. (2007): Assessment of surface and groundwater quality in connection with construction and operation Temelín Nuclear Power Plant on surrounding environment, Report T. G. Masaryk Water Research Institute, Prague (in Czech)
- Hanslík, E. (2008): Assessment of surface and groundwater quality in connection with construction and operation Temelín Nuclear Power Plant on surrounding environment, Report T. G. Masaryk Water Research Institute, Prague (in Czech)
- Hanslík, E.; Ivanovová, D.; Jedináková-Křížová, V.; Juranová, E. & Šimonek, P. (2009a): Concentration of radionuclides in hydrosphere affected by Temelín nuclear power plant in Czech Republic, *Journal of Environmental Radioactivity*, 100, No. 7, pp. 558-563. ISSN 0265-931X
- Hanslík, E.; Ivanovová, D.; Juranová, E.; Šimonek, P. & Jedináková-Křížová, V. (2009b): Monitoring and assessment of radionuclide discharges from Temelín Nuclear Power Plant into the Vltava River (Czech Republic), *Journal of Environmental Radioactivity*, 100, No. 2, pp. 131-138, ISSN 0265-931X
- Hanslík, E.; Ivanovová, D. & Kluganostová, M. (2009c): Balances of suspended matter and radionuclides in inflow and outflow waters of Orlický Reservoir, Vltava River (Czech Republic), *Radioprotection*, 44, No. 5, pp. 321-326. ISSN 0033-8451
- Ivanovová, D. & Hanslík, E. (2009a): Bioaccumulation of ^{137}Cs in fish in Orlický reservoir (South Bohemia) during the period 1990 - 2007. In: *Trace Elements in the Environment as a Risk of Health*, Budapest, Hungary, pp. 177-181, ISBN 978-963-7067-19-8
- Ivanovová, D. & Hanslík, E. (2009b): Impact of nuclear power plant Temelín on tritium concentration in the Vltava and Elbe Rivers, *VTEI*, 51, No. 6, pp. 1–5, ISBN 0322-8916 (in Czech)
- IAEA (1996): Evaluation of water resources monitoring, Report on assessment of analytical methods for radioactivity monitoring, RU-6172 (CZR/8/002), Vienna
- IAEA (2003): International Basic Safety Standards for Protection against Ionizing Radiation and for the Safety of Radiation Sources (CD-ROM Edition), Safety Series No. 115/CD

- Libby, W.F. (1946): Atmospheric helium-3 and radiocarbon from cosmic radiation, *Physical Review* - 1946, 69 (11-12), pp. 671-672
- Lysáček, F. (2007): Annual report about environment 2006, CEZ Group, Temelín (in Czech)
- Lysáček, F. (2008): Annual report about environment 2007, CEZ Group, Temelín (in Czech)
- Lysáček, F. (2009): Annual report about environment 2008, CEZ Group, Temelín (in Czech)
- NCRP (1979): Tritium in the environment environment: recommendations of the National Council on Radiation Protection and Measurements, NCRP Report, No. 62, Washington
- Nir, A.; Kager, S.T.; Lingenfelter, R.E. & Flamm, E.J. (1966): Natural tritium. Review of Geophysics and Space Physics, Vol. 4, pp. 441-456
- Palomo, M.; Penalver, A.; Aguilar, C & Borrull, F. (2007): *Applied radiation and isotopes*, 65, pp. 1048-1056
- Permit on Water Management (2007) No. 18378/20/2005 OZZL, České Budějovice, 22.1.2007 (in Czech)
- Permit issued by the State Agency for Nuclear Safety (2009) No. SÚJB/OROPC/26161/2009, Prague, 1.12.2009 (in Czech)
- Smith, J.T.; Leonard, D.R.P.; Histon, J. & Applty, P.G. (1997): Towards a generalised model for the primary and secondary contamination of lakes by Chernobyl-derived radiocaesium, *Health Physics*, 72, 880
- Smith, J.T.; Kudelsky, A.V.; Ryabov, I.N. & Haddingh, R.H. (2000): Radiocaesium concentration factors of Chernobyl contaminated fish: a study of influence of potassium and „blind“ testing of a previously developed model, *Journal of Environmental Radioactivity*, 48, pp. 359 - 369
- Smith, J.T. & Beresford, N.A. (2005): *Chernobyl Catastrophe and Consequences*, Praxis Publishing Ltd, Chichester, UK, ISBN 3-540-23866-2
- UNSCEAR (1993): Sources and effects of ionizing radiation, Report to the General Assembly with Scientific Annexes, UNSCEAR
- Vakulovky, S.M.; Nikotin, A.I.; Chumichev, V.B.; Katrich, I.Yu.; Voitsekhovith, O.A.; Medinets, V.I.; Pisarev, V.V.; Bovkum, L.A. & Khersonsky, E.S. (1994): Cs-137 and Sr-90 contamination of water bodies in the area affected by releases from the Chernobyl Nuclear Power Plant accident: An overview, *Journal of Environmental Radioactivity*, 23, 103
- Zibold, G.; Kaminski, S.; Klemm, E. & Smith, J.T. (2001): Time-dependency of the ¹³⁷Cs activity concentration in fresh lakes, measurement and prediction, *Radioprotection*, Vol. 37, C1, 2002, Proceeding of the International Congress ECORAD 2001, Aix-en-Provence, France, pp. 75-80

Fatigue, sleep disorders, and excessive sleepiness: important factors for nuclear power shift workers

Marco Túlio de Mello^{1, 2, 3}

Samantha Lemos Paim¹

Sérgio Tufik^{1, 2, 3}

¹Universidade Federal de São Paulo

²Centro de Estudo Multidisciplinar em Sonolência e Acidentes – CEMSA
(Multidisciplinary Study Center in Sleepiness and Accidents)

³Pesquisador CNPq (CNPq researcher)

In current urban societies, it is estimated that approximately 20% of the population does not work traditional working hours, and this percentage is tending to increase due to economic, demographic, and technological changes that have occurred in the last decades (Presser, 1999; Rajaratnam, 2001).

From the middle of last century, researchers have reported (Bjerner, 1948; Andersen, 1970; Akerstedt, 1981) that working in shifts affects the health of workers; even then, it was shown that shift workers complained about fatigue and sleepiness. Around 81% of the workers complained about night shifts in contrast to only 4% for afternoon shifts (Bjerner, 1948).

Production and distribution of electrical power from nuclear stations requires 24 h operation. Therefore, as in other sectors, the security of the whole operational system depends on the efficiency and the ability of the worker to execute tasks with remarkable accuracy and attention. However, because this type of energy is government-controlled, access to research in this area is mostly difficult; therefore, there is a scarcity of scientific publications related to the health of these shift workers.

The objective of this chapter is to describe aspects related to sleepiness, particularly excessive day sleepiness, with respect to its origins and consequences as well as the forms of minimization and preventive strategies that can be adopted by companies that use shifts and night work. Such practices may reduce the number of accidents related to fatigue and sleepiness that occur inside and outside the work environment.

1. Sleep and shift work

Although sleep functions are not completely known yet, it was assumed for several decades that brain activity was widely reduced or absent during sleep (Saper, 2005; Tufik et al. 2009). However it is important to emphasize that even during sleep, the brain is 80% active, such

that sleep is an active process of neuronal reorganization rather than just a process of diminishing wakefulness (Hobson, 2007).

Currently, it is accepted that the wakefulness-sleep cycle in human beings is coordinated by two processes that interact among themselves: the homeostatic process (process S) and the circadian process (process C) (Borbely, 1982; Borbely, 1999). The homeostatic process reflects the duration of wakefulness and can be monitored by slow-wave activity (Dijk, 1990), while the circadian process occurs during a 24-hour time frame and sets the rhythms of several physiological activities. Both processes interact to consolidate sleep (Czeisler, 1980).

The first systematic classification of sleep stages was described in the Standard Manual organized by Rechtschaffen and Kales (1968), where sleep was divided into NREM sleep (stages 1, 2, 3, and 4) and REM sleep. REM sleep alternates with NREM in intervals of 70 to 110 minutes that are repeated 4 to 6 times a night, depending on the total time slept (Silva, 1996). The duration of REM sleep episodes in humans progressively increases over a sleeping period, with longer episodes occurring closer to the awakening time (Siegel, 2007). Shift or night work, characterized as being performed outside regular working hours, i.e., from 8 or 9 am to 5 or 6 pm (Fischer, 2003), is part of the professional experience of an increasing number of workers around the world (Smith et al., 2005).

According to research by the European Union (2000), only 24% of the population works within regular working hours. Countries like the United States of America (USA) estimate that approximately 20 to 25% of their workers are engaged in some type of shift work (U.S. Congress, 1991).

Consequently there is an increasing number of people constantly changing their sleep times. This means that they never sleep in a fixed period, resulting in adaptation problems and an inability to sleep for a long or sufficient period (Rutenfranz et al., 1989). Moreover, due to sleep time irregularity, other problems can also occur, such as decreased professional performance, social and marital conflicts, mood changes, serious traffic or work accidents, increased cardiovascular disease/systemic high blood pressure, and even serious psychiatric diseases and disorders (Moore Ede, 1993; Presser, 1999; Smith et al., 2005).

The adverse effects of shift work can individually vary according to age and gender as well as to the performed activities. Younger people can better tolerate shift work than older people, principally due to the sleep architecture and pattern change (Akerstedt, 2003).

Sleepiness is a biological function defined by an increased probability to sleep (Bittencourt, 2005), and excessive sleepiness (ES), or hypersomnia, refers to an increased propensity to sleep with a subjective compulsion to sleep, i.e., to take involuntary naps and have sleep attacks, when inappropriate (Bassetti, 2000).

ES is also referred to in terms of a decreased capacity for physical and/or mental work as well as incomplete rest after insufficient sleep, and is generally associated with sleep disorders (Bakshi, 2003).

The first laboratory studies that simulated work conditions and tried to use EEG and EOG to identify the moment when workers began to doze off and sometimes even sleep were from the 1960s and focused, among other things, on telephone switchboard operators, nurses (Folkard, 1978), truck drivers, and airplane pilots (Lille, 1982).

To investigate ES, some procedures, such as clinical evaluation, sleep diaries, subjective and objective measures (scales, specific questionnaires and polysomnography, Sleep Multiple Latencies Test and the Wakefulness Maintenance Test, respectively) can be used. Other methods of accident risk evaluation are also specifically recommended for accident

prevention. These include the FAID "Fatigue Audit InterDyne" (Roach, 2004), the CAS "Circadian Alertness Simulator" (Moore-Ede, 2004), and the "Risk Index" (Folkard, 2004).

2. Shift workers and sleepiness

The most important consequences of sleepiness for shift workers are related to quality of life, decreased production, and increased potential risk of accidents and injuries during working hours (Dinges, 1995).

According to Akerstedt (2001), women present a lower peak of sleepiness than men in the night shift. According to this study, the risk of being involved in an accident provoked by sleepiness during night work is doubled for men compared to women.

Fischer et al. observed a reduction in the total sleep time after a night shift that resulted in lower sleep efficiency. In the evaluated workers, this reduction in sleep could have contributed to a reduction in alertness after the sixth to tenth continuous hours of work. Thus, a decrease of the sleep period can lead to sleepiness during the day or the night, jeopardizing efficiency during working hours.

Several studies showed an increase in the frequency of complaints related to sleep disorders in shift workers, including insomnia, excessive sleepiness, breathing and movement disorders; all of these could contribute in a substantial way to decreased life quality of the workers (Mello et al., 2000; Ohayon et al., 2002; Sallinen et al., 2003; Akerstedt, 2003; Howard et al., 2004; Menezes et al., 2004; Pandi-Perumal et al., 2006; Akerstedt, 2007).

Mathias et al. (2004) verified a significant reduction of the sleep latency (SL) in resident anesthesiologists on duty after 24 or 30 hours without sleeping. In this study, values of SL below 5 min (considered pathological) were observed, reflecting the extreme fatigue that these professionals are submitted to. These data obtained are important for determining the total working time and break times between shifts.

Carvalho & Vieira (2002) reviewed the literature to analyze medical errors. Although barely mentioned in the scientific literature, the statistics indicate that many incidences of medical errors are due to fatigue and sleepiness; this rate increases according to the level of complexity and frequency of the procedure. Most incidents occur during the night shift and are related to cognitive aspects, although environmental (noise, heat), psychological (depression, anxiety, stress), and physiological factors (fatigue, sleep) also contribute to the occurrence of errors. The authors verified that after working 24 h without sleeping, the psychomotor performance of a health professional is similar to one subject legally intoxicated.

A Brazilian study interviewed 400 professional interstate bus drivers from 20 transportation companies, aiming to evaluate the more common complaints of sleep among this type of worker. Important data were obtained related to sleepiness, as it was verified that 16% of the surveyed drivers had dozed off when driving, with an average of 8 such events per trip (Mello et al., 2000). Another Brazilian study of professional drivers diagnosed 38% of these workers with Sleep Apnea and Hypopnea Syndrome (Santos et al., 2004).

Moreno et al. (2004) analyzed the risk of sleep apnea in 10,101 drivers and verified that 26% of them met the criteria for high risk for SA. However, scientific publications related to worker health in nuclear power plants are scarce. Smith and Folkard (1993) used questionnaires to study the impact of shift work on the general aspects of health, sleep, and social problems for shift workers of nuclear stations. In general, it was demonstrated that

with night shifts, alertness and the duration and quality of sleep decrease, generating problems related to health and influencing social and family dynamics.

Continuing this study, Smith and collaborators (1995) investigated the level of alertness, the cognitive performance and the work load of shift workers in nuclear stations. Sleep duration and quality were analyzed for 35 days and the work load was kept stable during that period. The authors confirmed that night shift workers presented sleep of lower duration and quality as well as a significant decrease in alertness and performance levels, especially during the first hours of the day.

Takahashi et al. (2005) investigated the adaptation to shift work among Japanese nuclear station workers in relation to several variables, including sleep. In comparison to workers considered to be little-adapted to shift and night work, those classified as adapted had day sleep (before the night shift) of better quality and also took some naps during the night work. In continuation of this study, the same group (Smith et al., 2005) demonstrated that factors related to sleep and fatigue directly influence the tolerance to shift work: workers who present a higher flexibility for sleep at different times, as required for shift workers, report less complaints related to sleepiness and fatigue.

However, except for the studies of Smith's and Takahashi's groups, little is known about the complaints and possible sleep disorders in nuclear power plant shift workers.

3. Sleepiness and Nuclear Power Plant shift workers

Paim et al. (2008) study described the sleep complaints and polysomnographic results for shift workers in nuclear stations using the Unifesp Sleep Questionnaire (Pires et al., 2007) and polysomnography, respectively.

According to the criteria established by Pires et al. (2007), 113 (35%) of workers presented subjective complaints of insomnia, excessive sleepiness, snoring and leg movements. The frequency of insomnia was less than that found by Pires et al. (2007) in 1995 in the city of São Paulo. In the survey, 13.1% of the male population reported difficulties in initiating sleep (versus 8.8% among night shift workers), 24.6% presented difficulties in maintaining sleep (versus 17.1% of shift workers), and 11.3% complained about early morning awakening (versus 8.2% in the Paim et al. study).

The data found are closer for the frequency of complaints related to excessive sleepiness at 3.9% and 3.3% for Pires et al. (2007) and Paim et al. (2008), respectively. Similar figures were also found for the two studies with regard to snoring frequency or wakening with a suffocating sensation at 26.3% and 23.5%, respectively.

Even though it was expected, based on the literature (Mello et al., 2000, Akerstedt, 2003; Menezes et al., 2004; Santos et al., 2004), that the rate of sleep complaints would be higher among shift workers compared to the general population, that expectation was not confirmed.

As this specific population does not present a wide diversity with respect to social, cultural, and educational aspects and because it has good access to medical care, it was considered important to identify the factors involved in sleep complaints.

Some studies show that aging is associated with a more fragmented and superficial sleep that results in subjective complaints related to sleep (Young et al., 1993; Dijk et al., 1999; Buysse et al., 2005). Paim and colleagues (2008) found that workers with subjective sleep complaints were older, supporting with the aforementioned studies.

Polysomnographic recording of the nuclear power plant shift workers (Paim et al., 2008) characterized the frequency and the severity of the breathing events and periodic limb movement. Of the ninety workers that presented polysomnographic alterations, 18 (20%) met the criteria for periodic limb movement, 30 (33%) had sleep apnea, and 42 (47%) had both conditions; however, the disorders were observed to be mild in the great majority of the workers. Because the combination of sleep disorders can be a consequence of a respiratory disorder that secondarily generates leg movements, the task force of 2006 (WASM-2006) suggested that apnea treatment should be offered first, after which the presence of periodic leg movement should be verified. Considering that the great majority of workers presented a light degree of sleep disorder, the use of measures such as physical activity, appropriate eating habits, and sleep hygiene could help to reduce the consequences of these disorders, their worsening and decreasing the risk of accidents (De Mello et al., 2000).

In reference to the study of Paim and colleagues (2008), the limitations we can identify include the inability to correlate the collected and presented data with work schedules or workdays, as all data were collected in the work environment and during shifts. However, it is important to highlight that the objective of this study was to verify and describe the presence of sleep disorders in this specific population. Thus, the identified limitations did not affect the analysis; even though a circadian variation could affect the observation of the frequency of some sleep disorders, this would be identified with any type of methodology used.

Paim and colleagues (2008) verified that among 327 shift workers, 35% reported some kind of subjective sleep complaint, 12% sought out a physician for sleep problems, and 12% confirmed that had already taken sleeping pills. Ninety workers presented polysomnographic alterations, where 18 (20%) had MPP, 30 (33%) had SA, and 42 (47%) had both alterations. Although the results obtained represent a preliminary evaluation, they are expected to contribute to a better comprehension of the sleeping patterns of shift workers and of the factors that influence such patterns, with the aim of establishing corrective and preventive measures to promote worker health.

4. Sleep deprivation and its costs

Several studies point to a higher number of accidents during the night compared to the day period (Akerstedt, 2004; Costa, 1996, Ingre, 2004; Knutsson, 2004). A possible explanation might be that night shift workers have other jobs or other activities during the day, resulting in a double workday, with insufficient time for sleep (Rosa, 1993). Another explanation might be that the night shift has an increased risk for accidents (Costa, 1996) or that the risk of workers being involved in accidents is related to an increase in continuous working time, as many of these workers have long working periods, performing the same work without breaks (Akerstedt, 2001; Santos et al. 2002; Folkard, 2004). Therefore, this risk would increase after about around 9 hours of work; after 12 hours it would double, and after 14 hours the risk would triple.

Pinho et al. (2006), studied a sample of 300 professional drivers and observed that 46% presented excessive sleepiness associated, in the case of younger drivers, with snoring and working periods of more than 10 consecutive hours, often without breaks. This excessive sleepiness was also associated with reports of accidents for long working periods.

Another factor that contributes to increased accident rates is the presence of sleep disorders. People with sleep disorders have a higher risk of being involved in accidents. The main sleep disorder, apnea syndrome and obstructive sleep hypopnea (ASOSH), which generally occurs in obese and sedentary individuals, increases the possibility of being involved in car accidents by two- or three-fold in comparison to the population without this syndrome (Folkard, 2004).

Epidemiologic studies carried out in the city of São Paulo by the Department of Psychobiology of the Paulista Medicine School showed variations in the sleep complaints of the general population. In 1987, Del Giglio demonstrated that 76% of the population presented some complaint related to sleep; in 1997, Palma (1997) found that this proportion increased to around 82%. In a more recent study by Bittencourt et al. (2009), 63% of the population presented at least one subjective sleep complaint.

The number of road accidents involving commercial and private vehicles is increasing annually, and is it concern for authorities and respective agencies in the entire world. Studies relating these accidents to sleepiness have been garnering special attention in recent years (Hakkanen, 2000).

According to Caldwell (2001), problems related to fatigue cost the USA approximately US \$18 billion a year in terms of productivity. Sleepiness on the roads provokes/causes more than 1,500 deaths, 100,000 automobile crashes and 76,000 injuries a year.

Statistics show that from 26 to 32% of the automobile accidents are caused by sleepiness and fatigue when driving. Studies carried out in other countries, such as France, also revealed that around 31% of fatal car accidents can be due to sleepiness or dozing when driving. The same study found that sleep deprivation, long working periods, and (mainly) sleep disorders were the factors that contributed the most to these fatal accidents, as they directly affect psychomotor function and alertness. These factors were also attributed to work schedules that, in several cases, were inappropriate for the drivers' wakefulness/sleep pattern.

According to data obtained from the Denatran Yearbook (National Traffic Department) in Brazil, a total of 394,596 and 337,190 traffic accidents occurred in 2001 and 2002, respectively, distributed as shown in Table 1 (DENATRAN 2005).

Comparison of traffic accidents in the years 2001 and 2002				
	Accidents with victims	Fatalities	Non-fatal injuries	TOTAL NUMBER OF VICTIMS
2001	307,287	20,039	374,557	394,596
2002	251,876	18,877	318,313	337,190

Table 1. Comparative data of traffic accidents in the years 2001 and 2002

A reduction in the total number of victims and accidents may have been a result of the great number of traffic education campaigns that the government is promoting; however, a study carried out by the IPEA (Economic Researches Institute -2003), demonstrated that the costs related to traffic accidents in Brazil are still very high and distributed as follows:

- Average cost of a traffic accident: US \$4,878
- Average cost of a traffic accident with injury: US \$19,520
- Average cost of a traffic accident with fatality: US \$80,080

In a simple analysis, it was observed that the financial cost of accidents with fatalities (not considering other types of accidents and victims) was approximately US \$3,116,371,660 in

2001-2002. This represents a very high cost for any country; a strategy to minimize the costs of accidents and deaths that involves educational and preventive projects could reduce both this cost and the number of fatalities.

5. Minimizing the problem of sleepiness

Knauth (1996) mentioned Guidelines (see Table 2) for planning working hours in accordance with psycho-physiological criteria; such guidelines could improve or minimize the negative effects of night/shift work and reduce the incidence of work accidents.

An epidemiologic survey on physical activity and sleep complaints carried out by Mello et al. in 2000 in the city of São Paulo, Brazil demonstrated that physically active people presented less complaints related to sleep and excessive sleepiness during the day, suggesting that physical activity was a favorable factor for the sleep quality. This study suggested that the psychosocial factors, lifestyle, sleep location, and the living conditions of the individual directly influenced the quality of life and physical performance. Therefore, the implementation of physical activity for that population is highly important for consolidation and improvement of sleep efficiency.

Guidelines	Effect
1. Quick rotation shift systems	• Less interference in circadian rhythms
2. Clockwise rotation	• Allow longer resting periods
3. Avoid early morning shifts	• Reduce sleep fragmentation
4. Avoid long journeys (9-12 h), or adjust the breaks	• Minimize fatigue
5. Regular shift systems	• Guaranteed free weekend; make the most of leisure; minimize social impact
6. Scheduled night work only for special situations	

Table 2. Guidelines for the planning of work hours (Knauth, 1996).

6. Brazilian Legislation

Recently, the National Traffic Council (CONTRAN) (de Mello et al., 2009) approved the inclusion of clinical evaluation of sleep disturbances for Brazilian drivers who will be submitted for the first evaluation to obtain, renew, or alter the category (to categories C, D, and E) of their driver's license. This new approach and evaluation for professional drivers in Brazil could also be applied to shift workers and nuclear energy station workers, as evaluation of sleep disturbance is essential for minimizing the risks of fatigue and accidents.

Acknowledgments

Centro de estudo Multidisciplinar em Sonolência e Acidentes - CEMSA; Centro de estudos em Psicobiologia e exercício - CEPE Conselho Nacional em Pesquisa - CNPq Associação Fundo de Incentivo à Psicofarmacologia - AFIP Fundação de Amparo a Pesquisa do Estado de São Paulo - FAPESP Projeto CEPID/Sono - FAPESP

7. References

- Akerstedt T, Gilberg M. Sleep disturbances and shiftwork. In: Reinberg A, Vieux N, Andlauer P, eds. *Night and shift work: biological and social aspects*. Oxford: Pergamon Press, 127-38, 1981.
- Akerstedt T, Kecklund G. Age, gender and early morning highway accidents. *J Sleep Res* 10(2):105-10, 2001.
- Akerstedt T, Kecklund G, Jonhasson S. Shift work and mortality. *Chronobiol Int* 1:1055-61, 2004.
- Akerstedt T. Shift work and disturbed sleep/wakefulness. *Sleep Med Rev* 2:117-128, 1998.
- Akerstedt, T. Work hours, sleepiness and the underlying mechanisms. *J Sleep Res* 4(2): 15-22, 1995.
- Andersen FE. *Three-shift work*. Copenhagen: Socialforskningsintituter, 1970.
- Arnold W, Eysenck H, Meili R. *Dicionário de psicologia*. São Paulo: Loyola, 1982.
- Bakshi R. Fatigue Associated with Multiple sclerosis: diagnosis, impact and management. *Mult Scler* 9(3):219-27, 2003.
- Bassetti C, Gugger M. Hypersomnia: etiology, clinic, diagnosis and therapy of excessive sleepiness. *Ther Umsch* 57(7): 421-9, 2000.
- Bittencourt LRA, Silva RS, Santos RF, Pires MLN, De Mello MT. Sonolência Excessiva. *Rev Bras Psiquiatria* 27(supl:1):16-21, 2005.
- Bittencourt LRA; Santos-Silva R; Taddei JA; Andersen ML; de Mello MT; Tufik S. Sleep complaints in the adult brazilian population:a national survey based on screening questions. *J Clin Sleep Med* 5(5):459-463, 2009.
- Bittencourt LRA et al. Chronobiological Disorders: Current and Prevalent Conditions. *J Occup Rehabil.*, 20:21-32, 2010.
- Bjerner B, Holm A, Swensson A. *Natt och skiftarbete (Night and shif work)*. Stockholm: Statens Offentliga Utredningar, 1948.
- Borberly AA, Achermann P. Concepts and models of sleep regulation: an overview. *J Sleep Res.* 1992;1:63.
- Borberly AA, Achermann P. Sleep homeostasis and models of sleep regulation. *J Biol Rythms.* 1999;14:557.
- Browne RC. The day and night performance of teleprinter switchboard operator. *Occup Psychol* 23:121-6, 1949.
- Caldwell JA. The impact of fatigue in air medical and other types of operations: a review of fatigue facts and potential countmeasures. *Air Med J* 20(1): 25-32, 2001.
- Carvalho M, Vieira AA. Medical errors in hospitalized patients *J Pediatr* 78(4): 261-8, 2002.
- Connor J, Norton R, Ameratunga S, Robinson E, Civil I, Dunn R, Bailey J, Jackson R. Driver sleepiness and risk of serious injury to car occupants: population based case control study. *BMJ* 324(7346):1125, 2002
- Connor J, Norton R, Ameratunga S, Robinson E, Wigmore B, Jackson R. Prevalence of driver sleepiness in a random population-based sample of car driving. *Sleep* 24(6): 688-94, 2001.
- Costa G. Effects on health and well-being. In: Colquhoun WP, Costa G, Folkard S, Knauth P. *Shift work. Problems and solutions*. Arbeitswissenschaft in der betrieblichen Praxis. Frankfurt am Main: Peter Lang 7: 113-39, 1996.
- Czeisler CA, Weitzman E, Moore-Ede MC, et al. Human Sleep: Its duration and organization depend on its circadian phase. *Science.*;210:1264, 1980.

- Del Giglio SB. Estudo da ocorrência de queixas de insônia, de sonolência excessiva diurna e das relativas as parassonias na população adulta de São Paulo. Tese (Doutorado). Universidade Federal de São Paulo – Escola Paulista de Medicina, Departamento de Psicobiologia, São Paulo, 1988.
- DENATRAN (Departamento Nacional de Trânsito). Disponível na Internet: <http://www.denatran.gov.br/estatisticas.htm>. (19 maio 2003 e 07 dez. 2005).
- Dinges DF. An overview of sleepiness and accidents. *J. Sleep Res* 4(2):4-14,1995.
- Dijk DJ, Brunner DP, Borbely AA: Time course of EEG power density during long sleep in humans. *AM J Physiol.*;258:650,1990.
- Folkard S, Monk TH, Lobban MC. Short and long-term adjustment of circadian rhythms in 'permanent' night nurses. *Ergonomics* 21(10): 785-99, 1978.
- Findley LJ, Unverzagt ME, Suratt PM. Automobile accidents involving patients with obstructive sleep apnéia. *Am Rev Respir Dis* 138:37-40, 1998.
- Fischer FM, Moreno CRC, Borges FNS, Louzada FM. Implementation of 12-hour shifts in a Brazilian petrochemical plant: impact on sleep and alertness. *Chronobiol Int* 17: 521-37, 2000.
- Folkard S, Lombardi DA. Toward a "Risk Index" to assess work schedules. *Chronobiol Int* 21(6): 1063-72, 2004.
- Folkard S, Monk TH, Lobban MC. Short and long-term adjustment of circadian rhythms in 'permanent' night nurses. *Ergonomics* 21(10): 785-99, 1978.
- Folkard S. Effects on performance efficiency. In: Colquhoun WP, Costa G, Folkard S, Knauth P. Shiftwork. Problems and solutions. *Arbeitswissenschaft in der betrieblichen Praxis*. Frankfurt am Main: Peter Lang 7: 67-87, 1996.
- George CPF, Sliley A. Sleep Apnea e automobile crashes. *Sleep* 22(6): 790-95, 1999.
- Hakkanen H, Summala H. Sleepiness at work among comercial truck drives. *Sleep* 23: 49-57, 2000.
- Hansotia P. Sleep, sleep disorders and motor vehicle crashes. *Wis Med J* 96(5): 42-7, 1997.
- Härmä M. Sleepiness and shift work: individual differences. *J Sleep Res* 4(2): 57-61,1995.
- Hobson, JA. Sleep is of the brain, by the brain and for the brain. *Nature*: 437:1254-1278, 2007.
- Horne J, Reyner L. Vehicle accidents related to sleep: a review. *Occup Environ Med* 56(5): 289-94, 1999.
- Horne JA, Reyner LA. Sleep related vehicle accidents. *Br Med J* 310: 565-67, 1995.
- Horne JA, Reyner LA. Driver sleepiness. *J. Sleep Res* 4 2: 23-29, 1995.
- Ingre M, Kecklund G, Akerstedt T, Kecklund L. Variation in sleepiness during early morning shifts: a mixed model approach to an experimental field study of train drivers. *Chronobiol Int.* 21(6): 973-90, 2004.
- Knauth P. Designing better shift systems. *Appl Ergon* 27(1): 39-44, 1996.
- Knutsson A, Hammar N, Karlsson B. Shift workers mortality scrutinized. *Chronobiol Int* 21(6): 991-1001, 2004.
- Lauber JK, Kayten PJ. Sleepiness, circadian disrhythmia, and fatigue in transportation system accidents *Sleep* 11:503-12, 1988.
- Leger D. The cost of sleep related accidents: a report for the National Commission on Sleep Disorders Research. *Sleep* 17: 84-93, 1994.
- Lille F, Cheliout F. Variations in diurnal and nocturnal waking state in air traffic controllers. *Eur J Appl Physiol Occup Physiol* 49(3): 319-28, 1982.

- Masa Jf, Rubio M, Findley LJ, Habitually sleepy drivers have a high frequency of automobile crashes associated with respiratory disorders during sleep. *Am J Respir Crit Care Med* 162(4 Pt 1): 1407-12, 2000.
- Mathias Last et al. O Plantão noturno em anestesia reduz a latência de sono. *Rev Bras Anesthesiol* 54(5): 693-9, 2004.
- Mello MT, et al. Sleep patterns and sleep-related complains of Brazilian interstate bus drives. *Braz J Med Biol Res* 33: 71-7, 2000.
- Mello MT, et al. Sleep and transit in Brazil: New legislation. *Journal of Clin Sleep Medicine*. Vol 5:2, 2009.
- Mitler MM, Carskadon MA, Czeisler CA, Dement WC, Dinges DF, Graeber RC. Catastrophies, sleep, and public policy. *Consensus Report Sleep* 11:100-9, 1988.
- Mitler MM, Dinges DF, Dement WC. Sleep Medicine, public policy and public health. In : Kryeger MH, Roth T, Dement WC, eds. *Principles and Practice of Sleep Medicine*. 2. ed. Philadelphia: W.B.Saunders & Co, 453-62, 1994.
- Moore-Ede M, Heitmann A, Guttkuhn R, Trutschel U, Aguirre A, Croke D. Circadian alertness simulator for fatigue risk assessment in transportation: application to reduce frequency and severity of truck accidents. *Aviat Space Environ Med* 75(3 Suppl): A107-18, 2004.
- Paim et al. Sleep Complaints and Polysomnographic Findings: A study of nuclear power plant shift workers. *Chronobiology International*, 25(2&3): 321-331, 2008.
- Palma BD, Andersen ML, Mello M, Tufik S. Sleep complaints in São Paulo city: a comparison between the years 1987 and 1995. *Sleep Res* 26: 455, 1997.
- Philip P, Taillard J, Guilleminault C, Quera Salva MA, Bioulac B, Ohayon M. Long distance driving and self induced sleep deprivation among automobile drivers. *Sleep* 22(4):475-80, 1999.
- De Pinho, RSN et al. Hypersomnolence and accidents in truck drivers: a cross-sectional study. *Chronobiology International*, 23(5): 1-9, 2006.
- Powell NB, Kenneth B, Robert W, Kasey LI, Troell R, Guilherminault C. The road to danger: the comparative risks of driving while sleepy. *Laryngoscope* 4:887-93, 2001.
- Presser MB. Toward a 24-hour economy. *Science* 284: 1178-9, 1999.
- Ohayon MM, Lemoine P, Arnaud-Briant V, Dreyfus M. Prevalence and consequences of sleep disorders in a shift worker population. *J Psychosom Res*. 53: 577-583, 2002.
- Rajaratnam SM. Legal issues in accidents caused by sleepiness. *J Hum Ergol D30*(1-2): 107-11, 2001.
- Roach GD, Fletcher A, Dawson D. a model to predict work-related fatigue based on hours of work. *Aviat Space Environ Med* 75(3 suppl): A61-9; discussion A70-4, 2004.
- Rosa RR, Bonnet MH, Warm JS. Recovery of performance during sleep following sleep deprivation. *Psychophysiology* 20:152-9, 1983.
- Rotemberg L, Portela LF, Marcondes WB, Moreno C, Nascimento CP. Gênero e trabalho noturno: sono, cotidiano e vivências de quem troca o dia pela noite. *Cad Saúde Pública* 17: 639-49.2001.
- Rechtschaffen A, Kales A. Manual of standardized terminology, techniques, and scoring system for sleep stages of human subjects. *Brain Information Service/Brain Research Institute, UCLA, Los Angeles*. 1968.
- Rutenfranz J, Knauth P, Fischer F. Trabalho em turnos e noturnos. Tradução. Reinaldo Mestrinel. São Paulo: Hucitec, 135, 1989.

- Sallinen M, Harma M, Mutanen P, et al. Sleep-wake rhythm in a irregular shift system. *J Sleep Res*.12: 103-112, 2003.
- Santos EHR, De Mello MT, Pradella-Hallinan M, Luchesi L, Pires MLN, Tufik S. Sleep and sleepiness among Brazilian shift-working bus drivers. *Chronobiol Int* 21(6): 881-8, 2004.
- Saper CB, Scammell, TE, Lu, J. Hypothalamic regulation of sleep and circadian rythms. *Nature* 437:1257-1263,2005.
- Santos EHR, De Mello MT, Tufik S. Polisomnographic evaluation in interstate bus drivers In: 15th meeting - APSS, 2001, Chicago. *Journal Sleep and Sleep Disorders Research* 24: A282, 2001.
- Siegel, JA. Clues to the functions of mammalian sleep. *Nature* 437:1264-1271, 2007.
- Silva, RS. Introdução ao estagiamento do sono humano. *Braz. J. Epilepsy Clin. Neurophysiol.* 3(2):187-99, 1996.
- Smith L, Tanigawa T, Takahashi M, et.al. Shiftwork Locus of Control, Situational and Behavioral Effects on Sleepiness and Fatigue in Shiftworkers. *Industrial Health.* 43: 151-170, 2005.
- Spielberger CD, Gorshusch RL, Lushene E. Manual for the state-trait anxiety inventory ("Self-Evaluation Questionnaire"). Consulting Psychologist Press, Palo Alto, CA, 1970.
- Tepas et al. Polisomnographic correlates of shift worker performance in the laboratory. In: Reinberg A, Vieux N, Andlauer P, eds. *Night and shift work: biological and social aspects.* Oxford: Pergamon Press, 179-86, 1981.
- Tufik S et al. Paradoxical Sleep Deprivation: neurochemical, hormonal and behavioral alterations. Evidence from 30 years of research. *An Acad.Bras. Cienc.* Vol.3, 2009.
- Tucker P, Sytnik N, Macdonald I, Folkard S. Temporal determinants of accident risk: the "2-4 hour shift phenomenon" In: Hornberger S, Knauth P, Costa G, Folkard S, eds. *Shiftwork in the 21st Century.* New York: Peter Lang, 99-105, 2000.
- Walsh JK, Muehlback MJ, Schweitzer PK. Hypnotics and caffeine as countermeasures for shiftwork related sleepiness and sleep disturbances. *J Sleep Res* 4(2): 80-3,1995.

Benchmark modeling and analysis

Hangbok Choi
General Atomics
United States

1. Introduction

The physics design and analysis of a nuclear reactor includes multiple steps such as nuclear data generation, fuel and fuel assembly modeling, lattice parameter generation, and reactor system modeling and analysis, which inevitably result in uncertainties in simulation results due to imperfectness of nuclear data, geometry modeling, and solution methods. It is however essential that the computational tools and methods should predict the nuclear reactor system accurately so that the nuclear reactor operates safely and economically as designed. The accuracy of the design and analysis is required not only for the nuclear reactor system, but also for the nuclear transportation, waste disposal, experiment, accident analysis, and standard development (Bess et al., 2009). Confidence in the nuclear design and analysis results can only be obtained by comparing calculated results with measurement data. Fortunately a large number of reactor physics experiments have been conducted and the results have been documented as standard benchmark problems for various nuclear fuel and reactor types.

This chapter will describe in general the background and evolution of benchmark problems that have been developed through international cooperation. In order to illustrate how the benchmark problems are used for the reactor design and analysis, examples of detailed benchmark calculations are given for the critical assembly measurement. Though many benchmark problems are available, the benchmark problems that can be used for the new fuel and reactor concepts are limited. In that case, numerical benchmark tests are often performed as an alternative during the research and development stage. This chapter will also provide examples of numerical benchmark models based on a Monte Carlo code.

2. Development of Benchmark Problems

Reactor physics experiments have been performed in parallel with the nuclear fuel and reactor development to validate and support the physics design and analysis activities. Since it is a tedious, time-consuming, and costly process to research, collect, and organize all the experimental results over the world, international cooperative programs were launched to develop benchmark problems that can be effectively used for specific applications (Briggs et al, 2000). These programs identify and verify comprehensive sets of criticality experimental data, evaluate the data, quantify the overall uncertainty, and compile the data into a standardized format. These benchmark data typically include key performance

parameters of the nuclear reactor system such as measurements of reactivity, reaction rates, buckling, flux distribution, reactivity coefficients, and fuel burnup.

2.1 Cross Section Evaluation Working Group

The Cross Section Evaluation Working Group (CSEWG) was organized in 1966 and is now a cooperative effort of the national laboratories, industry, and universities in the United States (US) and Canada. The main mission of the CSEWG is to produce the US Evaluated Nuclear Data File (ENDF), which has been adopted as the international standard in 2001 (CSEWG, 2010). The CSEWG community has utilized integral experiment results as a mechanism for validating ENDF/B data files. In 1973, the CSEWG community has compiled 25 fast reactor and 36 thermal reactor benchmark problems, of which examples are given below (Alter et al., 1974).

JEZEBEL	Bare sphere of plutonium especially suited for testing the plutonium cross sections in the fission source energy range
GODIVA	Bare sphere of enriched uranium especially suited for testing ^{235}U and ^{238}U cross sections in the fission source energy range
TRX-1, 2, 3, 4	H_2O -moderated, fully reflected simple assemblies operated at room temperature with uranium metal (1.3 wt.% ^{235}U) fuel
PNL-1, 2, 3, 4, 5	Five unreflected spheres of plutonium nitrate solution with hydrogen/ ^{239}Pu atom ratios ranging from 131 to 1204
BAPL-1, 2, 3	H_2O -moderated, fully reflected simple assemblies operated at room temperature with high-density UO_2 (1.3 wt.% ^{235}U) fuel

2.2 International Criticality Safety Benchmark Evaluation Project

The International Criticality Safety Benchmark Evaluation Project (ICSBEP) was initiated in 1992 by Department of Energy (DOE) and Idaho National Laboratory (INL) and is operated under Organization for Economic Cooperation and Development (OECD) Nuclear Energy Agency (NEA) and managed by the INL with US participation and leadership sponsored by DOE National Nuclear Security Administration (NNSA) nuclear criticality safety program (ICSBEP, 2010). The ICSBEP working group systematically evaluates and archives data required for validation of criticality safety analyses. Specifically the ICSBEP working group compiles critical and subcritical benchmark experiment data into a standardized format so that criticality safety analysts can easily use the data to validate cross-section libraries, analysis model, and calculation tools (Briggs, 2001).

In 2009, the ICSBEP issued a handbook of evaluated criticality safety benchmark experiments which includes 4,283 critical or subcritical configurations, 24 criticality-alarm/shielding configurations, and four fundamental physics benchmarks with 200 fission rate and transmission measurements. The handbook is divided into seven volumes depending on different type of fissile material such as plutonium, highly enriched uranium ($^{235}\text{U} \geq 60$ wt.%), intermediate and mixed enrichment uranium (10 wt.% $< ^{235}\text{U} < 60$ wt.%), low enriched uranium ($^{235}\text{U} \leq 10$ wt.%), uranium-233, mixed plutonium-uranium and special isotope system. Examples are given below for the mixed plutonium-uranium system with their identification number and description (NEA, 2009)^a.

MIX-MET-FAST-012	ZPPR-21 Phase A, a cylindrical assembly of Pu metal reflected by graphite
MIX-MET-INTER-001	k-infinity experiments in fast/intermediate neutron spectra for various fissile materials
MIX-COMP-FAST-001	ZPR-6 assembly 7, a cylindrical assembly with mixed (Pu,U)-oxide fuel and sodium with a thick depleted-uranium reflector
MIX-COMP-INTER-005	Under-moderated mixed (Pu,U)-oxide (11 wt.% PuO ₂) lattice in the EOLE reactor

2.3 International Reactor Physics Evaluation Project

The International Reactor Physics Evaluation Project (IRPhEP) was initiated in 1999 by the OECD/NEA Nuclear Science Committee (NSC) to provide an extensively peer-reviewed set of reactor physics-related integral data that can be used by reactor designers and safety analysts to validate the analytical tools used to design next-generation reactors and establish the safety basis for operation of these reactors (IRPhEP, 2010). Overall technical coordination of the IRPhEP is directly supported by the US DOE's office of NE. The US participation on the IRPhEP is coordinated by the INL and Argonne National Laboratory (ANL).

The work of the IRPhEP is formally documented in the International Handbook of Evaluated Reactor Physics Benchmark Experiments (NEA, 2009)^b. This handbook contains reactor physics benchmark specifications that have been derived from experiments that were performed at various nuclear experimental facilities around the world. The 2009 Edition contains data from 36 different experimental series that were performed at 21 different reactor facilities. The handbook is organized with seven different reactor types such as the Pressurized Water Reactor (PWR), Water-Water Energetic Reactor (VVER), Liquid Metal Fast Reactor (LMR), Gas-cooled Thermal Reactor (GCR), Light Water Moderated Reactor (LWR), Heavy Water Moderated Reactor (HWR), and fundamental experiments. Sample benchmark problems are given below for the LWR.

DIMPLE-LWR-EXP-001	Light water moderated and reflected low enriched uranium (3 wt.% ²³⁵ U) dioxide rod lattices DIMPLE S01
KRITZ-LWR-RESR-001	KRITZ-2:19 experiment on regular H ₂ O/fuel pin lattices with mixed oxide fuel at temperatures 21.1°C and 235.9°C

3. Critical Assembly Benchmark Analysis

This section describes actual benchmark calculations conducted for conventional Canada Deuterium Uranium (CANDU) reactor physics codes against the Deuterium Critical Assembly (DCA) (Choi and Roh, 2004). The benchmark calculations are carried out for the effective multiplication factor (k_{eff}), void reactivity, local power peaking factor, and power distribution of a uniform core with 1.2 wt.% UO₂ fuel and two-region cores with PuO₂-UO₂ fuel.

3.1 Description of DCA Critical Assembly

The DCA core is deployed in an aluminum tank, of which the diameter and height are 3 m and 3.5 m, respectively. It contains a square lattice of either 121 or 97 fuel assemblies with

lattice pitches of 22.5 cm and 25.0 cm, respectively.

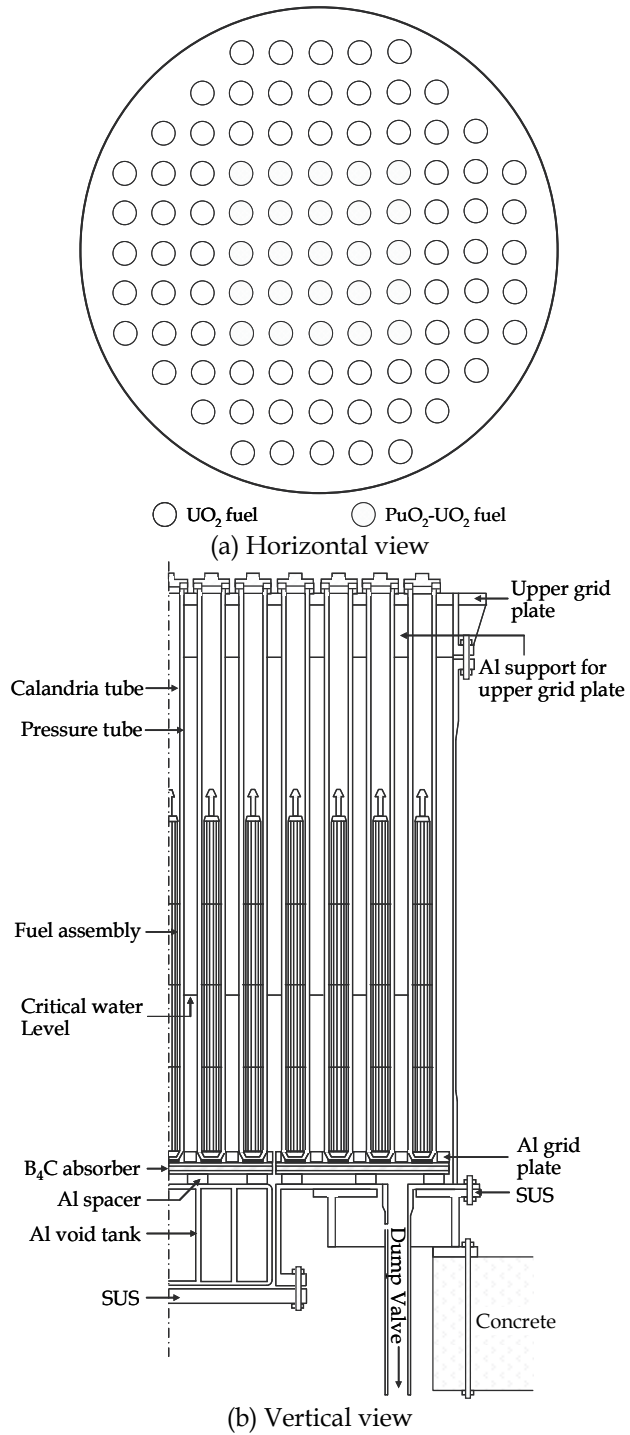


Fig. 1. Configuration of DCA core with a lattice pitch of 25 cm

In this study, the 97-assembly core was chosen, which can constitute a uniform core by loading UO_2 fuel assemblies or a heterogeneous core by loading $\text{PuO}_2\text{-UO}_2$ fuel assemblies in the central core region as shown in Fig. 1(a). In the DCA core, the criticality is adjusted by changing the heavy water moderator level. The light water coolant level in the pressure tube is made nearly equal to the critical level of the moderator. Below and above the fuel region, there are several structural compartments, which are shown in Fig. 1(b).

The standard DCA fuel assembly has 28 fuel rods and consists of three concentric rings of fuel rods. The fuel assembly is loaded in a pressure tube and the calandria tube surrounds the pressure tube, which physically separates the heavy water moderator from the light water coolant. Aluminum is used for both the pressure and calandria tube material. The dimensions of the DCA fuel lattice are given in Table 1 along with the core characteristics. The cluster geometry of the fuel assembly is shown in Fig. 2. Both the UO_2 and $\text{PuO}_2\text{-UO}_2$ fuel assemblies have the same active fuel height (2 m) and configuration except for the fuel rod size. The fuel rod size and composition are summarized in Table 2. The $\text{PuO}_2\text{-UO}_2$ fuel is a mixture of natural uranium oxide and standard plutonium oxide.

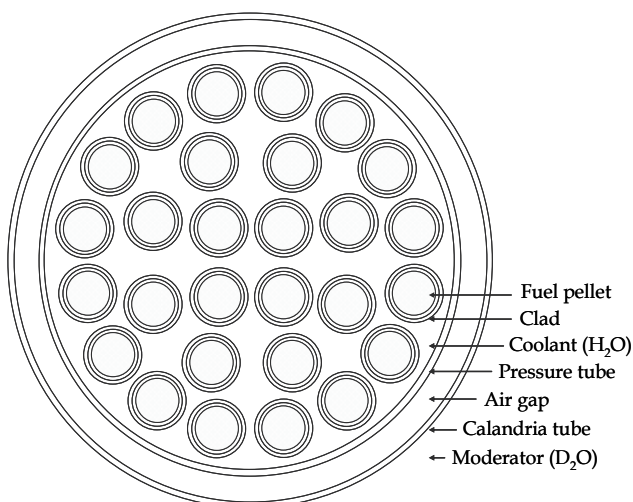


Fig. 2. Cross-sectional view of a 28-rod fuel assembly

Radius of fuel cluster ring		Core tank	Aluminum
Inner/Middle/Outer	13.13/30.0/ 47.58	Inner/Outer diameter	3005.0/3035.0
Fuel cluster length	2223.0	Height	3500.0
Fuel meat length	2000.0	Grid plates	Aluminum
Pressure tube	Aluminum	Moderator	D_2O
Inner/Outer diameter	116.8/121.0	Purity	99.4 mol%
Calandria tube	Aluminum	Temperature	$\sim 22^\circ\text{C}$
Inner/Outer Diameter	132.5/136.5		

Table 1. Dimensions of the DCA fuel lattice and core (dimensions in mm)

Fuel type	0.54 wt. % PuO ₂ -UO ₂	0.84 wt. % PuO ₂ -UO ₂	1.2 wt. % UO ₂
Fuel pellet			
Density (g/cm ³)	10.17	10.17	10.36
Diameter (mm)	14.69	14.72	14.80
Enrichment (wt.%)	5SPu*	8SPu**	1.203
Composition (wt.%)			
U-235	0.6214	0.6194	1.057
U-238	86.782	86.503	86.793
Pu-238	0.000102	0.000145	
Pu-239	0.4304	0.6849	
Pu-240	0.04115	0.06584	
Pu-241	0.004359	0.006960	
Pu-242	0.000303	0.000510	
O	12.12	12.12	12.15
Fuel pin (mm)			
Clad material	Zircaloy-2	Zircaloy-2	Al
Clad inner diameter	15.06	15.06	15.03
Clad outer diameter	16.68	16.68	16.73
Gap material	He gas	He gas	Air

*5SPu: PuO₂ weight fraction in PuO₂-UO₂ = 0.542 wt%

**8SPu: PuO₂ weight fraction in PuO₂-UO₂ = 0.862 wt%

Table 2. Characteristics of experimental fuel assemblies

3.2 Computer Codes and Analysis Model

The DCA core was analyzed by the WIMS and RFSP codes for lattice parameter generation and core calculation, respectively (Donnelly, 1986; Jenkins and Rouben, 1991). The WIMS code is a multi-group transport code, which was originally developed by United Kingdom Atomic Energy Authority (UKAEA) Winfrith and updated by Atomic Energy of Canada Limited (AECL). It performs a detailed calculation for a single lattice cell, providing flux distributions, eigenvalues, reaction rates and lattice parameters. The calculation methods used for the generation of lattice parameters are as follows:

- The transport calculation is performed by the collision probability (PIJ) method using the 89-group ENDF/B-V cross-section library.
- The main transport calculation is performed using full energy group.
- The mesh size is set to 5 mm for the coolant and moderator region.
- The B1 method is used for the effective cell flux calculation by condensing the lattice parameters.
- The Benoist diffusion constant model is used to generate the cell average diffusion coefficients.

The cell-average lattice parameters are collapsed into two energy groups using effective cell-average neutron fluxes obtained by critical buckling. Because the effective fuel section (moderated by heavy water) is about one half of the active fuel height, axial leakage effect is much greater than the radial one in the DCA core. For example, the radial and the axial geometric bucklings are approximately 2.56×10^{-4} and 8.61×10^{-4} cm⁻², respectively. Therefore importance is given to the axial leakage when generating the cell-average diffusion constants using critical buckling.

The two-group lattice parameters are used for core calculation by the RFSP code. The RFSP is a CANDU reactor fuel management code specifically developed by the AECL. Its main function is to calculate neutron flux and power distributions based on the two-group three-dimensional neutron diffusion theory. In order to determine the reference RFSP model, sensitivity calculations were performed for the mesh size and boundary condition, and the results are as follows:

- The reference fuel type is 1.2 wt.% UO₂. The perturbed fuel type (PuO₂-UO₂, voided and bare fuel) and structural materials are represented by the incremental cross-section, which is defined as the difference of the macroscopic cross-sections of the nominal and perturbed lattices, $\Delta\Sigma = \Sigma_{\text{pert}} - \Sigma_{\text{ref}}$.
- The reference mesh sizes of the active core region are 12.5 cm and 10 cm in the radial (XY) and axial (Z) directions, respectively. In the Z-direction, the mesh size of the lower half of the fuel is subdivided into 5 cm sections.
- The aluminum tank, which is the radial boundary of the core, is modeled in a rectangular geometry by conserving the total volume.

3.3 Benchmark Calculation of DCA

Since the design of DCA by the Japan nuclear cycle development institute in 1960, a series of critical experiments have been performed to study the core physics for the heavy water moderated, light water cooled, and pressure-tube type research facility (Hachiya and Hatakenaka, 1972; Hachiya et al., 1976; Wakabayashi and Hachiya, 1977; Fukumura, 1981; Kowata and Fukumura, 1988; Aihara et al., 1991). In this study, benchmark calculations are performed for the CANDU reactor physics codes using criticality measurement data of the uniform and two-region DCA cores with a lattice pitch of 25 cm. The uniform core is loaded with 1.2 wt.% UO₂ fuels, while the two-region core has both the UO₂ and PuO₂-UO₂ fuels. The two-region core calculations were carried out for two PuO₂-enriched fuels: 0.54 wt.% PuO₂-UO₂ (5SPu) and 0.84 wt.% PuO₂-UO₂ (8SPu) fuels. The effective multiplication factor and void reactivity are estimated for the uniform core and the two-region core with six different configurations, of which the number of PuO₂-UO₂ fuel assemblies are 1, 5, 9, 13, 21, and 25.

3.3.1 Effective Multiplication Factor

The effective multiplication factors of the critical core are summarized in Table 3 for 13 cases. The root-mean-square (RMS) error of the k_{eff} estimated by the WIMS/RFSP is 0.57% δk . The WIMS/RFSP consistently overestimates the criticality for all cases, which can be attributed to the approximation of the WIMS multi-group treatment in the resonance energy range (4 eV - 9 keV). Though the WIMS generally produces results in good agreement with measurements over a range of light and heavy water moderated lattices when used with ENDF/B-V cross-section library, it is known that the WIMS under-predicts resonance captures in ²³⁸U by up to ~4% for under-moderated light water lattices (Donnelly, 1992). The effect of resonance cross-sections of the WIMS library was assessed by replacing them with multi-group cross-sections generated by a Monte Carlo code MCNP (Briesmeister, 1997). The MCNP calculation also used the ENDF/B-V cross-sections for consistency. The adjustment of WIMS resonance cross-sections results in an average k_{eff} value of 1.00376, which is a reduction of RMS error by 0.17% δk .

Core type	WIMS/RFSP	Adjusted	Core type	WIMS/RFSP	Adjusted
97-UO ₂	1.00548	1.00395	1-8SPu 96-UO ₂	1.00477	1.00313
1-5SPu 96-UO ₂	1.00519	1.00354	5-8SPu 92-UO ₂	1.00527	1.00360
5-5SPu 92-UO ₂	1.00601	1.00431	9-8SPu 88-UO ₂	1.00588	1.00417
9-5SPu 88-UO ₂	1.00553	1.00386	13-8SPu 84-UO ₂	1.00449	1.00276
13-5SPu 84-UO ₂	1.00534	1.00361	21-8SPu 76-UO ₂	1.00498	1.00320
21-5SPu 76-UO ₂	1.00627	1.00426	25-8SPu 72-UO ₂	1.00574	1.00398
25-5SPu 72-UO ₂	1.00628	1.00446	Average	1.00548	1.00376

Table 3. Summary of the effective multiplication factor

3.3.2 Coolant Void Reactivity

The coolant void reactivity is calculated by replacing the coolant with air, which is written as the difference of $1/k_{\text{eff}}$ for the nominal and the voided core, given in Table 4. The calculation has shown that the plutonium reduces the void reactivity more than uranium in the DCA core. As the UO₂ fuel is replaced by PuO₂-UO₂ fuel in the central core region, the void reactivity becomes more negative. As for the enrichment of the PuO₂-UO₂ fuel, the void reactivity also decreases as the plutonium content increases. This trend is consistent in both the experimental and calculation results, which can be explained by a large resonance near 0.3 eV of the fissile isotopes such as ²³⁹Pu and ²⁴¹Pu. In other words, the spectrum hardening due to the coolant voiding increases neutron resonance absorption at ~0.3 eV for the plutonium fuel when compared to the uranium fuel.

Core type	Experimental value	WIMS/RFSP		WIMS/RFSP (adjusted)	
		Calculated	C-E	Calculated	C-E
97-UO ₂	-0.044±0.015	-0.001	0.043	-0.361	-0.317
1-5SPu 96-UO ₂	-0.441±0.102	-0.156	0.285	-0.506	-0.065
5-5SPu 92-UO ₂	-0.928±0.169	-0.637	0.291	-1.004	-0.076
9-5SPu 88-UO ₂	-1.410±0.224	-1.122	0.288	-1.514	-0.104
13-5SPu 84-UO ₂	-1.791±0.258	-1.475	0.316	-1.831	-0.040
21-5SPu 76-UO ₂	-2.306±0.297	-2.012	0.294	-2.349	-0.043
25-5SPu 72-UO ₂	-2.406±0.307	-2.181	0.225	-2.536	-0.130
1-8SPu 96-UO ₂	-0.629±0.135	-0.348	0.281	-0.698	-0.069
5-8SPu 92-UO ₂	-1.918±0.258	-1.674	0.244	-2.025	-0.107
9-8SPu 88-UO ₂	-3.165±0.351	-2.900	0.265	-3.212	-0.047
13-8SPu 84-UO ₂	-3.786±0.395	-3.599	0.187	-3.948	-0.162
21-8SPu 76-UO ₂	-4.836±0.493	-4.598	0.238	-4.946	-0.110
25-8SPu 72-UO ₂	-4.980±0.500	-4.825	0.155	-5.188	-0.208
RMS error			0.250		0.136

Table 4. Summary of the void reactivity calculation

The RMS error of the void reactivity is 0.25% $\delta(1/k)$. For about one half of the cases that have relatively higher plutonium content, the calculation error is smaller than the measured uncertainty. Considering that the prediction error of the k_{eff} is 0.57% δk for the nominal core, the reduction of the error for the void reactivity calculation indicates that the WIMS/RFSP

consistently overestimate the k_{eff} even for the voided core. However if the lattice parameters are generated based on the adjusted cross-sections, the calculation error decreases, resulting in 0.14% $\delta(1/k)$. In fact, the calculation error is within the measured uncertainty for all cases except for the uniform UO_2 fuel core.

3.3.3 Assembly Power Distribution Across Scattered Core

The accurate prediction of power distribution is very important for the precise understanding of the nuclear characteristics such as the fuel burnup distribution. In the DCA core, the assembly power was measured for the scattered core configuration, which simulates postulated fuel distribution with different fuel burnup. In the scattered core, the PuO_2 - UO_2 fuels are deployed in 13 positions as shown in Fig. 3. The critical condition of the scattered core to measure the assembly power distribution is summarized in Table 5 where two kinds of coolant conditions (nominal and voided) are considered for two different fuel types (5SPu and 8SPu). As shown in Table 5, the criticality condition is satisfied within the RMS errors of 0.54% δk . It is worth to note here that the prediction error of the k_{eff} is smaller for the voided core when compared to the nominal one, which was expected from the analysis of the void reactivity.

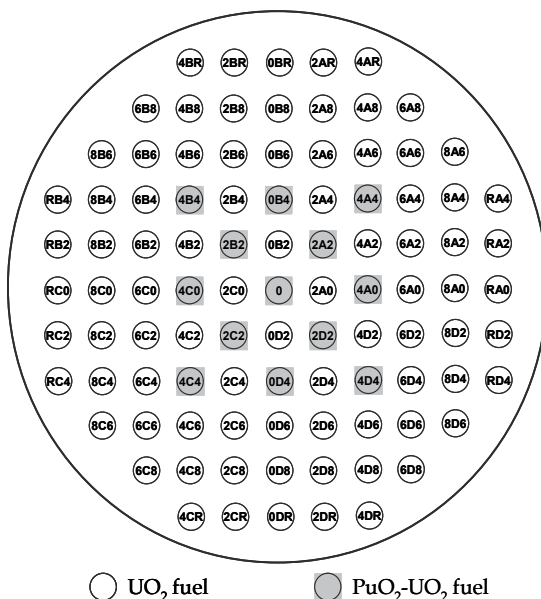


Fig. 3. Channel identification of a scattered DCA core

Fuel type	Lattice	H_c (cm)	k_{eff}
13-5SPu 84- UO_2	Nominal	98.95	1.00704
	Voided	100.69	1.00204
13-8SPu 84- UO_2	Nominal	90.28	1.00713
	Voided	95.13	1.00327

H_c : Critical water level

Table 5. Results of criticality for the scattered core

Position	Experiment	Nominal		Experiment	Voided	
		Calculation	C-E (%)		Calculation	C-E (%)
UO ₂ 0DR	0.2701±0.0074	0.2761	2.22	0.3584±0.0470	0.3395	-5.27
UO ₂ 0D8	0.5449±0.0061	0.5701	4.63	0.6436±0.0462	0.6519	1.28
UO ₂ 0D6	0.8525±0.0205	0.8795	3.17	0.9668±0.0684	0.9595	-0.75
5SPu 0D4	1.3121±0.0143	1.2617	-3.84	1.3735±0.0040	1.3328	-2.96
UO ₂ 0D2	1.3220±0.0139	1.3730	3.86	1.3774±0.0214	1.4111	2.45
5SPu 0	1.6083±0.0334	1.5550	-3.31	1.5986±0.0196	1.6030	0.27
UO ₂ 0B2	1.3280±0.0287	1.3730	3.39	1.3813±0.0723	1.4121	2.23
5SPu 0B4	1.3150±0.0452	1.2618	-4.05	1.3444±0.0081	1.3347	-0.73
UO ₂ 0B6	0.8647±0.0173	0.8795	1.72	0.9470±0.0471	0.9615	1.53
UO ₂ 0B8	0.5825±0.0134	0.5702	-2.10	0.6542±0.0313	0.6536	-0.10
UO ₂ 0BR	-	0.2761	-	0.3549±0.0301	0.3405	-4.06
RMS error			3.35			2.51

Table 6. Normalized power distribution with 5SPu and UO₂ fuels

Position	Experiment	Nominal		Experiment	Voided	
		Calculation	C-E (%)		Calculation	C-E (%)
UO ₂ 0DR	0.2598±0.0034	0.2422	-6.78	0.3335±0.0175	0.2959	-11.28
UO ₂ 0D8	0.5564±0.0085	0.5184	-6.82	0.6386±0.0149	0.5802	-9.15
UO ₂ 0D6	0.8940±0.0106	0.8520	-4.70	-	0.8831	-
8SPu 0D4	1.3240±0.0211	1.4718	11.16	1.3123±0.0117	1.4271	8.75
UO ₂ 0D2	1.5659±0.0180	1.4674	-6.29	1.4461±0.0188	1.3733	-5.04
8SPu 0	1.7732±0.0321	1.8955	6.90	1.6365±0.0192	1.7636	7.76
UO ₂ 0B2	1.5740±0.0102	1.4675	-6.77	1.4002±0.0530	1.3734	-1.92
8SPu 0B4	1.3403±0.0351	1.4720	9.83	1.3052±0.0049	1.4272	9.35
UO ₂ 0B6	0.8934±0.0128	0.8522	-4.61	0.9528±0.0126	0.8832	-7.31
UO ₂ 0B8	0.5568±0.0052	0.5186	-6.86	0.6485±0.0207	0.5803	-10.53
UO ₂ 0BR	0.2623±0.0025	0.2424	-7.57	0.3262±0.0112	0.2960	-9.26
RMS error			7.35			8.45

Table 7. Normalized power distribution with 8SPu and UO₂ fuels

The measured and calculated assembly power distributions for the 5SPu and 8SPu fuels are given in Tables 6 and 7, respectively. The calculated assembly power distributions are in general consistent with the measured values. The RMS errors of the nominal and the voided cores are 3.4% and 2.5%, respectively, for the 5SPu fuel core. Compared to the case of 5SPu core, the RMS error increases a little in the 8SPu core, which has higher plutonium content. The RMS errors of assembly power for the nominal and the voided core are 7.4% and 8.5%, respectively, for the 8SPu fuel core. The effect of resonance cross-sections for the WIMS/RFSP calculation is negligible as far as the assembly power distribution is concerned.

3.4 Summary

The measurement data of the DCA experiments were used to benchmark physics codes WIMS/RFSP, cross-section libraries, and analysis models. The benchmark calculation and sensitivity analysis have shown the following facts:

- The criticality and the void reactivity are estimated within 0.6% δk and 0.3% $\delta(1/k)$, respectively,

which could be further reduced if a fine mesh model is used and the resonance absorption cross-section of ^{238}U is adjusted.

- It is appropriate to use critical buckling when calculating the effective neutron flux for the group constant collapsing. Importance should be given to the axial diffusion constant when generating the cell-average diffusion constant to effectively describe the axial leakage effect.
- The power distribution generally matches measured value within 9%. It was found that the resonance cross-sections have a negligible effect on the prediction of power distribution, while it directly affects the criticality and the void reactivity.

4. Numerical Benchmark Model and Analysis

There are continuous research and development activities for advanced nuclear fuel and reactors. In the area of advanced fuel development, for example, various fuel materials have been considered such as recovered uranium, low enriched uranium, mixed plutonium-uranium oxide, and direct use of spent PWR fuel in CANDU reactors (DUPIC). In the area of reactor development, Generation-IV reactor systems are being studied for six reactor concepts: Supercritical Water Reactor (SCWR), Very High Temperature Reactor (VHTR), Sodium-cooled Fast Reactor (SFR), Gas-cooled Fast Reactor (GFR), Lead-cooled Fast Reactor (LFR), and Molten-salt Reactor (MSR). However, the criticality experiment data that can be used for benchmarking such advanced fuel and reactor designs are not readily available and new physics measurement activities require a large investment in terms of infrastructure, expertise and cost. From this aspect, the Monte Carlo method has been used as an alternative way of benchmarking because of its superiority over other physics methods such as handling continuous-energy nuclear data, capability of modeling very complex geometry and realistic simulation of neutron and photon interactions in the medium. So far the MCNP code has been the most widely used as a numerical benchmarking tool for various reactor systems such as PWR fuel Doppler constant, Boiling Water Reactor (BWR) fuel lattice, and the DUPIC fuel analyses (Mosteller and Eisenhart, 1991; Rahnama and Ilas, 1997; Roh and Choi, 2000).

4.1 MCNP Library Generation

The public MCNP cross-section libraries have a limited number of isotopes and temperature data, which is not sufficient to analyze non-conventional fuels and reactors. New MCNP cross-section library can be generated from ENDF using processing codes that convert the evaluated data into the appropriate ACE format for the MCNP code. The NJOY nuclear data processing system is widely used to produce working libraries for the transport codes, including MCNP (MacFarlane and Muir, 1994). The NJOY system consists of many independent modules such as RECONR, BROADR, UNRESR, HEATR, THERMR, GROUPR, ACER, etc. The data processing procedure is composed of three steps: reconstruction after reading ENDF into the point-wise ENDF (PENDF), production of the group-wise ENDF (GENDF) using PENDF and the weighting spectrum, and recompilation of PENDF and GENDF into an appropriate library format for the transport code.

In this study, in order to assess the performance of an MCNP model, new cross-section libraries were generated for seven temperature points: 293, 298, 342, 561, 673, 960 and 1473 K. Using the MAKXSF cross-section processor, which is included in the MCNP code package, the cross-section libraries were combined and named. For the thermal scattering

law data, since the MCNP cross-section library was not made for a specific temperature, two temperature data were generated using the nearest temperature data and interpolated to the specific temperature needed. The NJOY input parameter for the fractional tolerance was set to be 0.001.

4.2 Test of MCNP Library

The accuracy of the newly generated cross-section libraries was assessed for the typical benchmark problems such as TRX-1, 2, BAPL-1, 2, 3 pin-cell lattices and KENO criticality safety benchmark problems (CSEWG, 1974; Petrie and Landers, 1984). Both the pin-cell lattice and criticality safety benchmark calculations have shown to be consistent with the existing MCNP library and in good agreement with the experimental data, which are described in the following sections.

4.2.1 Pin Cell Problems

The TRX and BAPL lattices are light-water-moderated, fully reflected, simple assemblies reduced from a whole reactor operating at room temperature. The fuel materials of the TRX and BAPL lattices are 1.3 wt.% enriched uranium metal and uranium oxide, respectively. The moderator-to-fuel volume ratios of TRX-1 and TRX-2 lattice are 2.35 and 4.02, respectively. The moderator-to-fuel ratios of BAPL-1, BAPL-2 and BAPL-3 are 1.43, 1.78 and 2.40, respectively. These lattices are modeled in a two-dimensional geometry with hexagonal sides using the reflective boundary condition on the radial boundary of the pin cell. For all cases, the fuel gap is homogenized with the cladding material.

The MCNP calculations for all the pin-cell lattices were done with 1000 particles per cycle and 1000 active cycles after 100 inactive cycles; the results of the k_{∞} calculations are given in Table 8. For comparison, the reference calculations were also performed using the ENDF60 library provided by Los Alamos National Laboratory (LANL) and the results were compared to those of the new library, which is based on ENDF/B-VI release 3. The comparison shows a maximum difference of k_{∞} is 0.22% δk . The difference in k_{∞} between these two MCNP calculations could be due to the NJOY input parameter used to generate the library. The ENDF60 library was processed with NJOY and thinned with a flat weighting function so that most nuclides have no more than 400,000 words (Hendricks et al., 1994). On the other hand, the new library was processed with NJOY, but the thinning option of the ACER module was not used in order to improve the accuracy, even though the file sizes are large.

Case	ENDF6 (LANL)	NEW
TRX-1	1.17933±0.00053	1.18151 (0.00218)
TRX-2	1.16453±0.00044	1.16636 (0.00183)
BAPL-1	1.13978±0.00057	1.14152 (0.00174)
BAPL-2	1.14447±0.00050	1.14654 (0.00207)
BAPL-3	1.13098±0.00045	1.13292 (0.00194)
Average	1.15182±0.00022	1.15377 (0.00195)

() difference computed as $k^{\text{NEW}} - k^{\text{ENDF6}}$

Table 8. Comparison of k_{∞} for infinite pin-cell lattice

Reaction rate ratios were also calculated and compared from each other for the ENDF6 and new libraries as summarized in Table 9. The reaction rate ratios are defined as follow:

ρ^{28} : the ratio of capture reactions in ^{238}U above 0.625 eV to those below 0.625 eV,

δ^{25} : the ratio of fission reactions in ^{235}U above 0.625 eV to those below 0.625 eV,

δ^{28} : the ratio of fission reactions in ^{238}U to those in ^{235}U ,

C^* : the ratio of capture reactions in ^{238}U to fission reactions in ^{235}U .

For all cases, δ^{25} has shown good agreement with the reference values with a maximum differences of 1.4%. The maximum differences of δ^{28} (fast fission factor) and ρ^{28} are 1.0% and 2.1%, respectively, from the reference value. In general, the results of the MCNP calculation with the new library are lower than those of the reference. Particularly, the discrepancies come from the capture reaction rates of ^{238}U . Compared with the reference calculation, the low value of C^* with the new library is consistent with the high value of k_{∞} .

Case	Source	ρ^{28}	δ^{25}	δ^{28}	C^*
TRX-1	ENDF6	1.3278±0.175%	0.0966±0.156%	0.0918±0.175%	0.7913±0.127%
	NEW	(-1.665%)	(-1.201%)	(-0.359%)	(-1.009%)
TRX-2	ENDF6	0.8331±0.219%	0.0594±0.175%	0.0662±0.179%	0.6398±0.120%
	NEW	(-1.469%)	(-1.212%)	(-0.266%)	(-0.768%)
BAPL-1	ENDF6	1.4013±0.184%	0.0819±0.149%	0.0723±0.175%	0.8097±0.127%
	NEW	(-2.074%)	(-1.014%)	(-0.387%)	(-1.297%)
BAPL-2	ENDF6	1.1569±0.192%	0.0667±0.142%	0.0623±0.175%	0.7350±0.127%
	NEW	(-1.831%)	(-1.439%)	(-0.963%)	(-1.046%)
BAPL-3	ENDF6	0.9106±0.215%	0.0514±0.158%	0.0516±0.179%	0.6580±0.120%
	NEW	(-2.015%)	(-1.188%)	(-0.736%)	(-1.055%)
Average	ENDF6	1.1259±0.088%	0.0712±0.070%	0.0688±0.079%	0.7268±0.056%
	NEW	(1.811%)	(1.211%)	(0.542%)	(1.035%)

() relative difference computed as (NEW-ENDF6)/ENDF6 × 100

Table 9. Comparison of reaction rates for infinite pin-cell lattice

4.2.2 Criticality Safety Problems

In order to further verify the accuracy of the new MCNP library, criticality safety benchmark calculations have been performed for 25 sample problems used for the KENO Monte Carlo code. The sample problems constitute the KENO standard benchmark set and represent a relatively wide variety of criticality problems. The input parameters and detailed geometry descriptions are given in the Criticality Safety Benchmark Problems (Wagner et al., 1992).

The results of the MCNP benchmark calculations are given in Table 10. Compared with the experimental data, the new library produces results which are as good as ENDF60 generated by LANL, though there is a slight increase of error. Even when the same library version is used, there could be differences in the calculation results. For example, when KENO benchmark No. 3 was run with the ENDF50 (RMCCS) library, the k_{eff} was 0.9977 ± 0.0010 , while it was 0.9990 ± 0.0011 and 0.9993 ± 0.0011 in Wagner et al. (1992) and Hendricks et al. (1994), respectively. However, such differences are small enough to be attributed to the difference of the MCNP version and the computational environment.

No.	MCNP calculation				Difference from experiment	
	ENDF60		NEW		ENDF60	NEW
	k_{eff}	STD	k_{eff}	STD		
1	0.99513	±0.00081	0.99483	±0.00087	-0.00487	-0.00517
2	0.99513	±0.00081	0.99483	±0.00087	-0.00487	-0.00517
3	1.00134	±0.00107	0.99963	±0.00101	0.00134	-0.00037
4	0.99866	±0.00268	0.99769	±0.00318	-0.00134	-0.00231
5	1.00075	±0.00300	1.00332	±0.00275	0.00075	0.00332
6	0.74257	±0.00053	0.74210	±0.00065	*	*
7	0.99506	±0.00082	0.99566	±0.00083	-0.00494	-0.00434
8	0.93879	±0.00071	0.93633	±0.00078	*	*
9	2.25974	±0.00226	2.25645	±0.00101	*	*
10	0.99513	±0.00081	0.99483	±0.00087	-0.00487	-0.00517
11	0.99513	±0.00081	0.99483	±0.00087	-0.00487	-0.00517
12	0.99944	±0.00124	0.99695	±0.00123	-0.00056	-0.00305
13	0.99236	±0.00082	0.99011	±0.00081	-0.00764	-0.00989
14	0.99717	±0.00089	0.99483	±0.00077	-0.00283	-0.00517
15	1.00053	±0.00106	0.99966	±0.00099	0.00053	0.00034
16	0.99551	±0.00101	0.98944	±0.00089	*	*
17	0.99689	±0.00146	0.99589	±0.00145	*	*
18	1.02736	±0.00134	1.02569	±0.00126	*	*
19	0.99944	±0.00124	0.99695	±0.00123	-0.00056	-0.00305
20	0.99960	±0.00146	0.99264	±0.00137	-0.00040	-0.00736
21	0.99283	±0.00086	0.99194	±0.00090	-0.00717	-0.00806
22	0.99404	±0.00084	0.99719	±0.00087	-0.00596	-0.00281
23	0.99513	±0.00081	0.99483	±0.00087	-0.00487	-0.00517
24	0.99521	±0.00078	0.99762	±0.00079	-0.00479	-0.00238
25	0.99516	±0.00088	0.99537	±0.00088	-0.00484	-0.00463
Average	0.98425	±0.00030	0.98320	±0.00030	0.00358	0.00436

* Experimental values of k_{eff} could not be located for these problems

STD: one standard deviation due to statistical uncertainty

Table 10. KENO criticality safety benchmark calculation

In order to further investigate the dependence of k_{eff} on the ENDF version and the thinning option of the NJOY processing system, additional calculations have been performed for two cases; the first case uses the same thinning option as was used for ENDF60 (ENDF/B-VI Release 2) and the second case uses 0.001 as the tolerance. The average differences for these two cases are 0.00408 and 0.00370, which are very close to the result of the reference calculation done by the ENDF60 library (0.00358). This comparison has shown that the new MCNP library was generated in a consistent way with the references and the differences are residing in the ENDF version. In general, the results are more consistent with the experimental data when a tight tolerance (0.001) is used for the NJOY process.

4.3 DCA Numerical Benchmark Model

Based on the description given in Section 3.1, an MCNP model was developed for the DCA

and the results were compared to the experimental data. The simulation was performed using a fully heterogeneous core model that explicitly describes the individual fuel rod and channel. The criticality calculation has shown an excellent agreement for the k_{eff} ; the average k_{eff} is 0.99898 and the RMS error is 0.14% δk . The code has shown a strong credibility in the prediction of an integral parameter such as the k_{eff} , which can be attributed to the robust solution method as well as the capability of exact modeling of the fuel assembly and the reactor core.

For the void reactivity, the calculation error was defined as the difference of the calculation and experimental results (C-E), because the experimental value is very small for some cases, and the RMS error is 0.40% $\delta(1/k)$ for 13 cases. Though the MCNP has predicted the k_{eff} of the nominal core with excellent accuracy, the error of the void reactivity is a little larger than the RMS of measured uncertainty ($\sim 0.30\%$). If the error of the k_{eff} for the voided core is assumed to be the same as that for the nominal core, a simple error propagation formulation will give an error of 0.20% $\delta(1/k)$ for the void reactivity. However the results in Table 11 indicate that the accuracy drops a little for the k_{eff} calculation if the coolant channel is voided.

The RMS error of the local power peaking factor (LPPF), defined as the ratio of the power density of an individual fuel ring over the average power density of a fuel assembly, was estimated by weighting ring-wise LPPF error with the number of fuel rods in each ring as given in Table 12. The simulation has shown that the RMS error of the LPPF is a little higher for the voided fuel assembly compared with the nominal one. For the fuel types considered here (5SPu and 8SPu in central 25 fuel channels), the RMS errors of the LPPF are 0.39% and 1.1% for the nominal and the voided assemblies, respectively. It is worth to note that the LPPF measurements were made for central 25 fuel assemblies of the DCA, and the average value was taken for each fuel ring. The LPPFs estimated by the MCNP are also from the core calculation that explicitly describes individual fuel rod.

Core type	k_{eff}	Void reactivity		
		Experiment	Calculated	C-E
97-UO ₂	0.99851±0.00020	-0.044±0.015	0.243	0.287
1-5SPu and 96-UO ₂	0.99772±0.00019	-0.441±0.102	0.143	0.584
5-5SPu and 92-UO ₂	0.99858±0.00020	-0.928±0.169	-0.436	0.492
9-5SPu and 88-UO ₂	0.99919±0.00021	-1.410±0.224	-0.933	0.477
13-5SPu and 84-UO ₂	0.99873±0.00020	-1.791±0.258	-1.343	0.448
21-5SPu and 76-UO ₂	1.00026±0.00020	-2.306±0.297	-1.838	0.468
25-5SPu and 72-UO ₂	1.00005±0.00021	-2.406±0.307	-2.048	0.358
1-8SPu and 96-UO ₂	0.99728±0.00019	-0.629±0.135	-0.078	0.551
5-8SPu and 92-UO ₂	0.99818±0.00020	-1.918±0.258	-1.532	0.386
9-8SPu and 88-UO ₂	0.99994±0.00021	-3.165±0.351	-2.845	0.320
13-8SPu and 84-UO ₂	0.99841±0.00021	-3.786±0.395	-3.596	0.190
21-8SPu and 76-UO ₂	0.99952±0.00021	-4.836±0.493	-4.786	0.050
25-8SPu and 72-UO ₂	1.00041±0.00021	-4.980±0.500	-4.998	-0.018
Average	0.99898±0.00021			0.396

Table 11. Summary of the effective multiplication factor and void reactivity

Fuel type	Ring	Nominal			Voided		
		Experiment	Calculated	C/E-1 (%)	Experiment	Calculated	C/E-1 (%)
5SPu	1	0.64±0.01	0.643±0.002	0.52	0.76±0.01	0.770±0.001	1.32
	2	0.82±0.01	0.813±0.001	-0.82	0.86±0.01	0.856±0.001	-0.43
	3	1.18±0.01	1.183±0.001	0.22	1.13±0.01	1.129±0.001	-0.06
8SPu	1	0.61±0.01	0.613±0.001	0.48	0.71±0.01	0.726±0.001	2.27
	2	0.79±0.01	0.791±0.001	0.11	0.81±0.01	0.823±0.001	1.57
	3	1.20±0.01	1.201±0.001	0.11	1.17±0.01	1.157±0.001	-1.10
RMS error				0.39			1.10

Table 12. Comparison of the local power peaking factor

5. Conclusion

This chapter has described the current status of international activities of benchmark problem development, examples of practical benchmark calculations of a critical assembly, and the feasibility of applying numerical benchmark models when the measurement data are not available. The results of benchmark calculations have shown that the current nuclear data, computer code system and the conventional design and analysis approach have a good confidence level in predicting integral parameters of the critical assembly and power reactor. It was also found that the numerical benchmark models developed by the Monte Carlo code can be used to validate the advanced nuclear fuel and reactor design and analysis during the earlier stage of the development.

The international community has systematically collected and processed reactor physics measurement data that provide the basis for recording, development and validation. These results became a valuable asset that can be used for research and development today and in the future as well. In conclusion the importance of the benchmark modeling and analysis can be summarized as follows (Sartori, 2000):

- The experimental benchmarks are required to validate the physics models used in computer codes in conjunction with the associated nuclear data used to describe the microscopic phenomena underlying the macroscopic behavior.
- The benchmark analysis can be used as a training tool for the users to understand how a well-defined problem is modeled in a computer. Even though the best nuclear data and computer codes are used for the analysis, the quality of the results depends on the modeling capability of the users and therefore it is essential to train the users based on validated and verified problems.
- The benchmark problems need to be continuously developed and expanded to comply with the requirements of licensing design and analysis tools. Especially the measurement data for the safety-related parameters such as fuel temperature coefficient and coolant void reactivity are limited. More physics measurement data are also required for the gas-cooled reactor system which is currently being developed as a next generation nuclear plant.

6. Acknowledgement

This research has been carried out by the Korea Atomic Energy Research Institute (KAERI) under the fund of the Nuclear Research and Development Program of the Korea Ministry of Education, Science and Technology. The author would like to thank G. H. Roh of KAERI for conducting the code simulations. The author is also grateful to J. Crosier of General Atomics for editing manuscript.

7. References

- Aihara, N.; Fukumura, N.; Kadotani, H.; Hachiya, Y. (1991). Axial Dependence of Partial Void Reactivity in a Light Water-Cooled, Heavy Water-Moderated, Pressure-Tube Reactor, *Nuclear Science and Engineering*: **109**, pp.158-170.
- Alter, H.; Kidman, R.; LaBauve R.; Protsik R. & Zolotar B. (1974). Cross Section Evaluation Working Group Benchmark Specifications, BNL-19302 (ENDF-202), Brookhaven National Laboratory.
- Bess, J.; Briggs, J. & Nigg, D. (2009). Providing Nuclear Criticality Safety Analysis Education through Benchmark Experiment Evaluation, *Proc. ANS Winter Meeting and Young Professionals Congress*, Washington D.C., U.S.A.
- Briggs, J.; Dean, V. & Pešić, M. (2000). The International Criticality Safety Benchmark Evaluation Project, INEEL/CON-00-01184, Idaho National Engineering and Environmental Laboratory.
- Briggs, J. (2001). The Activities of the International Criticality Safety Benchmark Evaluation Project (ICSBEP), INEEL/CON-01-00049, Idaho National Engineering and Environmental Laboratory.
- Brismester, J. ed. (1997). MCNP- A General Monte Carlo N-Particle Transport Code, Version 4B, LA-12625-M, Los Alamos National Laboratory.
- Choi, H. and Roh, G. (2004). Benchmarking MCNP and WIMS/RFSP Against Measurement Data-I: Deuterium Critical Assembly, *Nucl. Sci. Eng.*, **146**, pp.188-199.
- Cross Section Evaluation Working Group (1974). Cross-Section Evaluation Working Group Benchmark Specifications, BNL-19302 (ENDF-202), Brookhaven National Laboratory.
- Cross Section Evaluation Working Group (2010). www.nndc.bnl.gov.
- Donnelly, J. (1986). WIMS-CRNL: A User's Manual for the Chalk River Version of WIMS, AECL-8955, Atomic Energy of Canada Limited.
- Donnelly, J. (1992). Description of the Resonance Treatment in WIMS-AECL, AECL-10550, Atomic Energy of Canada Limited.
- Fukunura, N. (1981). Measurement of Local Power Peaking Factors in Heavy-Water Moderated Plutonium Lattices, *Journal Nuclear Science and Technology*, **18** [4], pp.285-399.
- Hachiya, Y. and Hatakenaka, H. (1972). Neutron Behavior in Cluster-Type Fuel Lattices, (I) Experimental Method and Results, *Journal of Nuclear Science and Technology*, **9** [11], pp.629-641.
- Hachiya, Y.; Fukumura, N.; Nishi, A.; Iijima, K.; Sakata, H. (1976). Lattice Parameter Measurements on Cluster-Type Fuel for Advanced Thermal Reactor, *Journal of Nuclear Science and Technology*, **13** [11].
- Hendricks, J.S.; Frankle, S.C. and Court, J.D. (1994). ENDF/B-VI Data for MCNP, LA-12891, Los Alamos National Laboratory.
- International Criticality Safety Benchmark Evaluation Project (2010). icsbep.inel.gov.

- International Reactor Physics Evaluation Project (2010). irpheap.inel.gov.
- Jenkins, D. and Rouben, B. (1991). Reactor Fuelling Simulation Program - RFSP: User's Manual for Microcomputer Version, TTR-321, Atomic Energy of Canada Limited.
- Kowata, Y. and Fukunura, N. (1988). Study on Coolant Void Reactivity of Pressure-Tube-Type Heavy Water Lattice by the Substitution Method, *Nuclear Science and Engineering*, **99**, pp.299-312.
- MacFarlane, R.E. and Muir, D.W. (1994). The NJOY Data Processing System Version 91, LA-12740-M, Los Alamos National Laboratory.
- Mosteller, R. and Eisenhart, L. (1991). Benchmark Calculations for the Doppler Coefficient of Reactivity, *Nucl. Sci. Eng.*, **107**, 265.
- Nuclear Energy Agency (2009)^a. *International Handbook of Evaluated Criticality Safety Benchmark Experiments*, NEA/NSC/DOC(2006)1, Nuclear Energy Agency.
- Nuclear Energy Agency (2009)^b. *International Handbook of Evaluated Reactor Physics Benchmark Experiments*, NEA/NSC/DOC(95)03, Nuclear Energy Agency.
- Petrie, L.M. and Landers, N.F. (1984). KENO V.a An Improved Monte Carlo Criticality Program with Supergrouping, Section F11, Vol. 2, NUREC/CR-0200, U.S. Nuclear Regulatory Commission.
- Rahnema, F. and Ilas, D. (1997). Boiling Water Reactor Benchmark Calculations, *Nucl. Technol.*, **117**, 184.
- Roh, G. and Choi, H. (2000). Benchmark Calculations for Standard and DUPIC CANDU Fuel Lattices Compared with the MCNP-4B Code, *Nuclear Technology*, **132** (1), pp.128-151.
- Sartori, E. (2000). Basic Data, Computer Codes and Integral Experiments: The Tools for Modelling in Nuclear Technology, Workshop on Nuclear Data and Nuclear Reactors: Physics, Design and Safety, Trieste, France.
- Wagner, J.C.; Sisolak, J.E. and McKinney, G.W (1992). MCNP: Criticality Safety Benchmark Problems, LA-12415, Los Alamos National Laboratory.
- Wakabayashi, T. and Hachiya, Y. (1977). Thermal-Neutron Behavior in Cluster-Type Plutonium Lattices, *Nuclear Science and Engineering*: **63**, pp.292-305.

Nuclear Plants and Emergency Virtual Simulations based on a Low-cost Engine Reuse

Carlos Alexandre F. Jorge^{1,2}, Antônio Carlos A. Mól^{1,3},
Pedro Mól Couto¹ and Cláudio Márcio N.A. Pereira^{1,3}

¹*Comissão Nacional de Energia Nuclear, Instituto de Engenharia Nuclear*

²*Universidade Federal do Rio de Janeiro*

³*Universidade Gama Filho
Brazil*

1. Introduction

Our industrialised society comprises many industrial processes that are very important for everyone, in a wide range of fields. Activities related to these industrial processes, though, involve, in higher or lower degrees, some risk for personnel, – besides risk for the general public in some cases. Therefore, efficient training programs and simulations are highly required, to improve the processes involved, increasing safety for people. To cite an example, nuclear plants pose high safety requirements in operational and maintenance routines, to keep plants in safe operation conditions and reduce personnel exposure to radiation dose.

Besides operational and maintenance in nuclear plants, there are also other situations where efficient training is required, as in evacuation planning from buildings in emergency situations. Also, rescue tasks play similar role. These apply specially for nuclear sites.

Another situation that requires efficient training is security, what has special meaning for plants that involve dangerous materials, such as nuclear plants. Nuclear materials must be kept under high security level, to avoid any misuse.

With these problems in hand, personnel such as supervisors, trainers and planners, traditionally make use of training programs that may involve both theoretical and hands-on stages. However, computer-based training can help training, if performed before the hands-on training stage, for example, so people can face the specific problem they are being trained for, first in a safe environment, before going to the real ones. Computer-based simulations can thus reduce personnel exposure to risky factors, as radiation dose in the nuclear plant example, during the first training experiments. In some cases, training in the real plants or sites can be very dangerous, – if not impracticable –, as in simulations dealing with fire or nuclear contamination avoidance. In these cases, computer-based simulations may be the only means of training and evaluation.

Many publications span through the use of computer-based simulation for training. For the present R&D, two main application-specific problems can be emphasised: (a) computer-based simulation for training of personnel in operational and maintenance tasks, as

exemplified by the following references (Moltenbrey, 1999; Lee et al., 2001; Sebok et al., 2002; Badler et al., 2002; Bluemel et al., 2003; Bluemel et al., 2009; Bloomfield et al., 2003; Ohga et al., 2005; Ródenas et al., 2004; Ródenas et al., 2005; Nystad, 2005; Rindahl et al., 2006, Lebedev et al., 2007; Meyer, 2007); and (b) training for emergency preparedness and response, exemplified by (Louka & Balducelli, 2001; Jain & McLean, 2003; Jain & McLean, 2005; Sanders & Lake, 2005; Shendarkar et al., 2006; Van de Walle & Turoff, 2007).

Virtual reality-based simulations find an important role in computer-based simulations due to their immersive and interactive characteristics (Burdea & Philippe, 1994; Pimentel & Teixeira, 1995; Vince, 1995; Stuart, 1996).

In this work, the interest falls into a more specific use of virtual reality-based simulation, through the reuse of low-cost computer game engines. In particular, one of them was chosen, which is free for academic use, and flexible enough for adaptation to a diversity of application-specific problems.

Game engines reuse for serious applications has become a strong tendency in research (Lewis & Jacobson, 2002; Rosenbloom, 2003; Zyda, 2007; Threnholme & Smith, 2008), being part of the research field known as "serious games". Application-specific problems range from a diversity of areas, as military training (Manijlovich et al., 2003a; Manijlovich et al., 2003b; Prasithsangaree et al., 2003; Prasithsangaree et al., 2004; Zyda et al., 2003; Chatam, 2007), and rescue simulations in emergency situations (Wang et al., 2003a; Wang et al., 2003b; Wang et al., 2003c; Carpin et al., 2009), just to cite some high safety- and security-related ones.

This work deals specifically with the reuse of a game engine for the following simulation problems: (a) dose exposition evaluation for workers in nuclear plants, (b) evacuation from buildings in emergency situations, (c) security threat counteraction in nuclear sites.

2. Related work

This Section gives a brief introduction to R&D work by other research groups, related to the present one, either in the approaches adopted or in the problems to be solved. Some R&D groups adopt more similar or quite different approaches in which virtual reality-based simulations are used, including game engines reuse. This bibliographical research helped making choices among the different approaches found in the literature.

2.1 Emergency and security related simulation

Emergency situations may occur in a broad range of scenarios, as in industrial plants, buildings, or public places. Emergencies may also involve different hazardous factors, as fire and smoke, a diversity of contaminants – as nuclear, chemical or biological ones–, or other related security threats. Here it becomes clear the possible co-occurrence of emergencies and security threats.

To counteract these situations, training is required, what is carried out, in general, in the real places, with people who occupy them. For example, it is common practice to perform building evacuation training with those people who occupy it, so as they can learn how to escape from the building in an appropriate manner, in the case of real emergencies. Also, staffs responsible for planning evacuation and rescue tasks, benefit from these training, as better strategies can be tested and evaluated.

As mentioned in Section 1, though, computer-based training can improve training performance, since people can evaluate different scenarios and conditions first in a safe and flexible environment.

There are different approaches for computer-based evacuation training, that may comprise communication functionalities to improve people's skills, or the use of autonomous avatars (virtual persons) guided through some specific rule, to evaluate crowded situations.

2.2 Radiation dose simulation in nuclear plants

Different research groups have proposed this type of simulation, for personnel training. Operational and maintenance tasks can be tested and evaluated first in such a safe environment, before people enter the real plants. Based on the simulation results, supervisors can perform better planning of working activities. Thus, unnecessary radiation dose is avoided in the first training stages, fulfilling the As Low As Reasonably Achievable (ALARA) principle (ICRP, 1991), which states, in other words, radiation dose for people must be minimised.

Researchers have proposed different approaches for dose simulation (Brissaud & Ridoux, 1992; Knight et al., 1995; Knight et al., 1997; Vermeersch & Van Bosstraeten, 1998; Vermeersch & Van Bosstraeten, 2000; Lee et al., 2001; Nystad et al., 2002; Sebok et al., 2002; Hajek et al., 2004; Ródenas et al., 2004; Ródenas et al., 2005; Ohga et al., 2005; Kim & Park, 2005; Xu & Bushart, 2006). From these R&D, basically two approaches can be summarised: (a) dose rates collected from measurements in the corresponding real plants, (b) dose rates computed by simulation codes.

In all cases, it is common practice to compute and present users the dose received by the avatars according to the time spent in each location within the plant. One important aspect is that, the more accurate is the dose rate representation, the more accurate will be the received dose computation.

2.3 Serious games

Researchers who intend to perform computer-based simulation could make use of commercial simulation software, or develop their own platforms. The former approach may involve high costs, while developing codes may be a hard work itself. But in the last years, researchers noticed that some first-person computer game engines are very suitable for scientific and technological applications. Game engines comprise the core of computer games, which encompass some functionalities that are independent of the specific application for which they were designed, and are very desirable for other non-game simulations (Lewis & Jacobson, 2002). These functionalities are: (a) physics representation – such as Gravity effect and collision handling, (b) efficient graphical rendering capabilities, (c) networking capabilities. The later enable multi-user interactive simulation.

As long as some of these game engines are free or have low-cost for academic use, and are flexible enough to be adapted and reused (Lewis & Jacobson, 2002), researchers can concentrate in their own fields of application and research, taking advantage of all those embedded functionalities.

Among the available game engines suitable for R&D, two of them are recommended as very good choices (Lewis & Jacobson, 2002): Unreal from Epic Games, and Quake from ID Software. Unreal was chosen as platform for this R&D from the beginning, but Quake

Unreal Engine comes with a scenario editor, – named UnrealEd –, originally intended for gamers to design their own playing scenarios. This editor can be used by researchers to design any desired scenarios to be simulated, as plants or buildings. This is done by importing to Unreal Engine scenarios built on CAD software, and generating textures from photos taken in the real places to be simulated.

This R&D work was implemented by personnel of Instituto de Engenharia Nuclear, Comissão Nacional de Energia Nuclear – IEN, CNEN (Nuclear Engineering Institute, a R&D Institution of Brazilian Commission of Nuclear Energy). Therefore, the virtual environments implemented correspond to or are based on some existing buildings within this Institution.

Both male and female avatars are used, from modification of existing ones that had unrealistic dimensions. Users can choose avatars' dressing colours, to differentiate among users.

Unreal Engine source code is not available in this free version used, but the Engine enables code implementation through a scripting language similar to Java, – named UnrealScripting. Original code follows object oriented philosophy, with classes and hierarchical structure. Thus, a class inherit functionality from higher level ones, besides adding their own functionality. Researchers cannot modify existing classes, but can instead replicate them, and perform modification in these new created classes. Therefore, researchers have, in principle, broad possibilities to implement their own desired functionalities.

Fig. 1 shows current classes' structures, with original and created classes. A colour legend enables class identification: (a) in blue: original classes, (b) in orange: general purpose created classes, (c) in green: evacuation simulation-related created classes, (d) in purple: security simulation-related created classes, (e) in red: dose simulation-related created classes, (f) in yellow: other interface-related created classes.

3.1 Modifications for evacuation and security related simulation

The virtual environment for evacuation simulation corresponds to a real building of IEN, with its three floors, rooms and laboratories, designed virtually from its architectural design data. Furniture was also added. Fig. 2 shows the design stage in UnrealEd for this virtual building. In fact, two buildings were designed, the one used for this simulations was the one shown at the right side (in the upper left frame of Fig. 2).

The original avatars' velocities were not realistic, so they had to be changed to more realistic ones. Walking velocity is the important one for emergency and other related serious simulation, since people are supposed to walk in these situations, because running can lead to more serious consequences. Also, within nuclear plants, people execute their tasks walking or standing, but not running. Thus, walking velocity was fixed to a typical value of 1.5 m.s^{-1} .

A time counter was implemented to compute time spent by each avatar, during evacuation simulations. Each user sees his or her own elapsed time on screen.

One user is needed to control each avatar. There is no rule for guide autonomous avatars for now, it is under implementation currently. An advantage of this approach is that users' natural cognition plays an important role, since anyone can make decisions from what he or she sees relatively to other avatar's behaviour. For example, in evacuation simulation, a user can decide to get back when sees other avatars coming from a locked exit. Thus, people behave in a way similar to that they would do in real situations, making their own decisions

through reasoning. Results of this part of the R&D were published earlier, describing implementation details (Mól et al., 2008a).

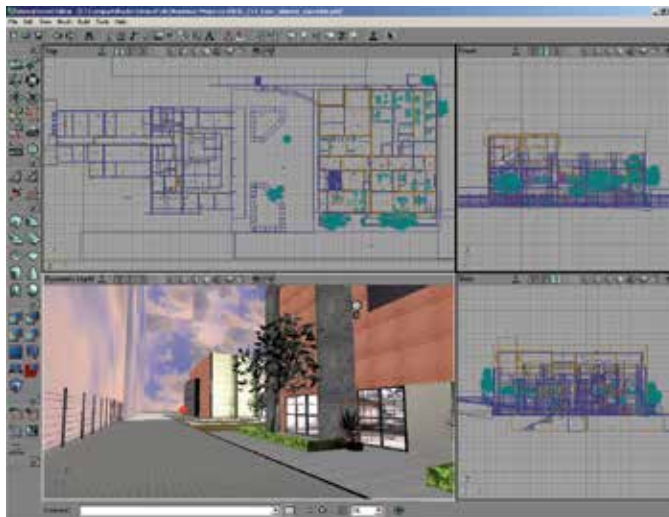


Fig. 2. IEN building's design in UnrealEd

For the security related simulation, a hypothetical scenario was designed, in part considering the real IEN campus, but introducing a virtual nuclear material deposit that would be subject to threat. IEN's campus is supposed to be invaded by intruders to steal nuclear material in that deposit. They must be detected and caught by responders. Fig. 3 shows the developed scenario, where the hypothetical deposit is shown to the left side (in the upper left frame of Fig. 2). Comparing Fig. 3 with Fig. 2, it can be noticed that this hypothetical deposit was designed to the left of the building previously used for the evacuation simulation (in place of the other formerly existing virtual building). Results of this part of the R&D were published, describing implementation details (Augusto et al., 2009).

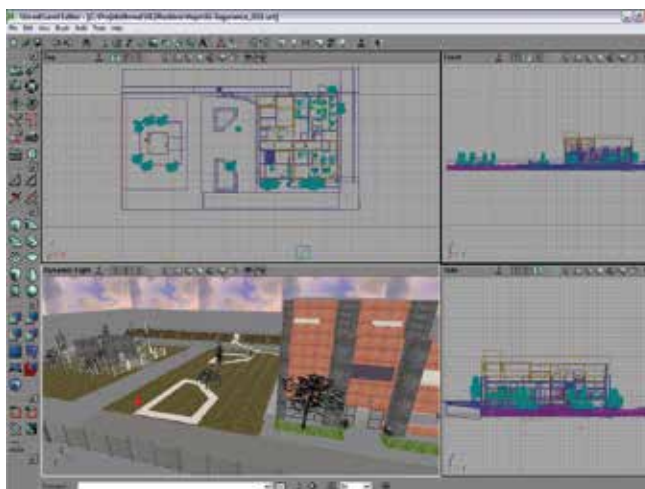


Fig. 3. Hypothetical security-threat scenario

3.2 Modifications for radiation dose simulation in nuclear plants

For this application, an existing nuclear plant at IEN was virtually modelled: Argonauta research reactor. This reactor have been in operation since 1965, used mainly for R&D in nuclear applications. These later span from non-destructive evaluation of materials using radiation, – such as radiography with gammas or neutrons –, to radioisotope production for industrial applications. It is also used as support for the experimental activities of the graduate course of IEN itself, – which as its own graduate program in nuclear engineering and technology –, besides graduate courses of other universities of Rio de Janeiro State, as Universidade Federal do Rio de Janeiro (Federal University of Rio de Janeiro) and Instituto Militar de Engenharia (Brazilian Army's Military Engineering Institute). Some operational tasks, as for example non-destructive evaluation, require that personnel enter and stand or walk through Argonauta's room. Maintenance tasks also require that personnel enter that room. In both cases, they receive dose, what is unavoidable. Simulation can help though optimising tasks planning, to fulfil ALARA requirements.

In this case, the virtual environment was also designed from its architectural design data, thus the virtual environment corresponds to the real one, to evaluate working activities in the safe environment. Fig. 4 shows the design stage in UnrealEd for this nuclear plant.

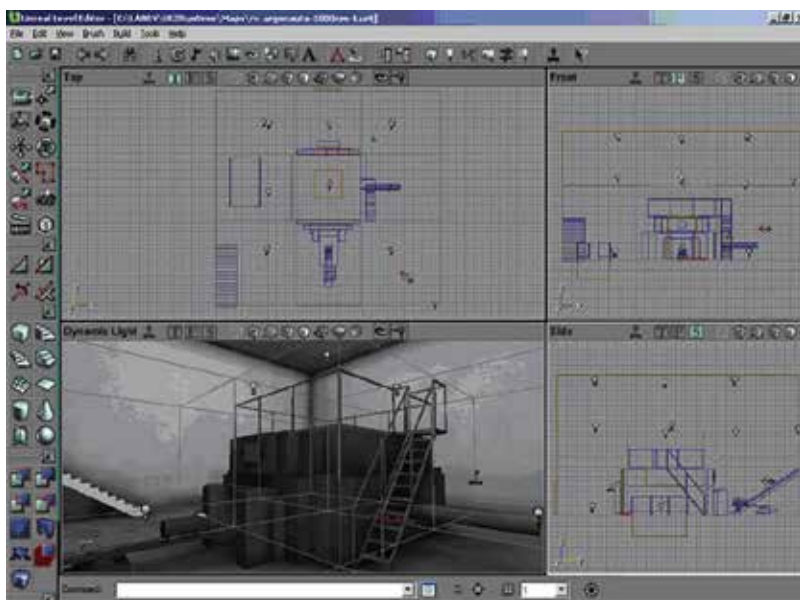


Fig. 4. Argonauta reactor's design in UnrealEd

3.2.1 Offline dose rate

This application specific problem was solved following the approach of using measured dose rates, instead of dose rate computing. There were measurements available, previously collected by the radiological protection service of IEN, during operational routines, which could be readily imported into Unreal Engine. The idea is similar to that used by another research group (Ródenas et al., 2004; Ródenas et al., 2005), which implemented a grid of points corresponding to dose rate measurements. At the time this R&D began, only scarce

data were available, so a gross grid of points was implemented, but the idea could be demonstrated. A more detailed data distribution would have to be obtained later by other means.

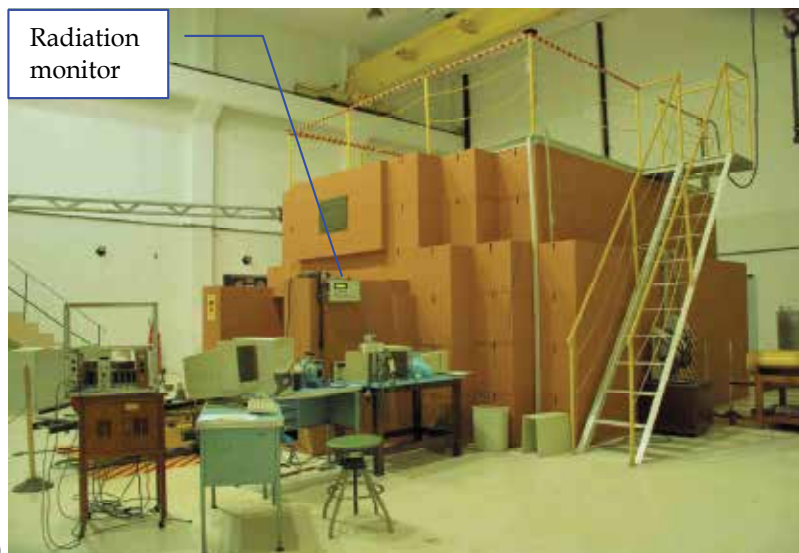
The dose received by the avatars is computed by the dose rate value at its location, considering the time spent there. This was implemented through the use of volumes, in fact prisms with rectangular bases, each one assigned to a constant dose rate value, to represent the hot regions within Argonauta's room. The Engine is able to identify the collision between an avatar and any of these volumes, assigning to the avatar the corresponding dose rate value, for received dose computation. The application informs users on the screen either the dose rate value at his or her position, or the total received dose up to the present time. These prisms can be noticed in Fig. 4 (in the lower left frame). Results of this part of the R&D were published earlier, (Augusto et al., 2007; Mól et al., 2009a).

3.2.2 Online dose rate

The following R&D stage improved simulation through the use of online dose rates, collected by radiation monitors installed in the real plant. Dose rate may vary during operational or maintenance routines, in the former case due to operational power level modification, and in the later one due to opening of any barrier to access the fuel rods in the reactor core or auxiliary radiation sources. This cannot be considered in the former approach, but can be taken into account with this second one. Thus, this is a clear advantage of the online measurement approach.

IEN's staff had for long term developed electronics instrumentation for the nuclear field, what resulted in a diversity of radiation monitors, both portable, to be handled by radiological protection service supervisors during activities, and others to be installed in hot locations (as within nuclear plants' rooms). Those monitors span different types of radiation detection capabilities with the appropriate probes. Some of them were patented and licensed to manufacturing industries.





(b)

Fig. 5. (a) Argonauta reactor's output channel; (b) One radiation monitor installed near Argonauta's output channel

This R&D made use of one monitor to be installed within nuclear plants rooms, named MRA 7027, for gamma or neutron measurement (Oliveira et al., 1997; Oliveira et al., 2000). Two of them were installed within Argonauta's room, at key locations: (a) one near the entrance, (b) and the other near the output radiation channel, in front of which materials to be tested are put for evaluation, and where dose rates achieve higher levels. Many other monitors could be networked, to collect online data from different locations, depending only on manufacturing and installation of new MRAs, but the main principle could be demonstrated.

Fig. 5a shows Argonauta reactor's output channel, while Fig. 5b shows one of the installed monitors.

This radiation monitor may be networked through RS-485 local network or TCP/IP protocol. The later enables its remote use through Internet. In general, networking is performed with a supervisory computer that presents data for users on screen. In this R&D, measured data was imported into Unreal Engine for avatar's received dose computation.

Three processes were developed for this purpose, in a scheme known as Man in the Middle (MiM): (a) one process collects and publishes data from the monitors, (b) another process feeds these data to Unreal Engine, (c) an intermediate process performs communication (and optionally some processing) between the two former ones.

These three processes can reside in the same computer, or in separate computers. This MiM process was developed with the macro language AutoIt (www.autoitscript.com/autoit3), and communication make use of HTTP protocol version 1.1. Fig. 6 shows the MiM scheme.

Results of this part of the R&D were published earlier, (Mól et al., 2008b; Mól et al., 2009b).

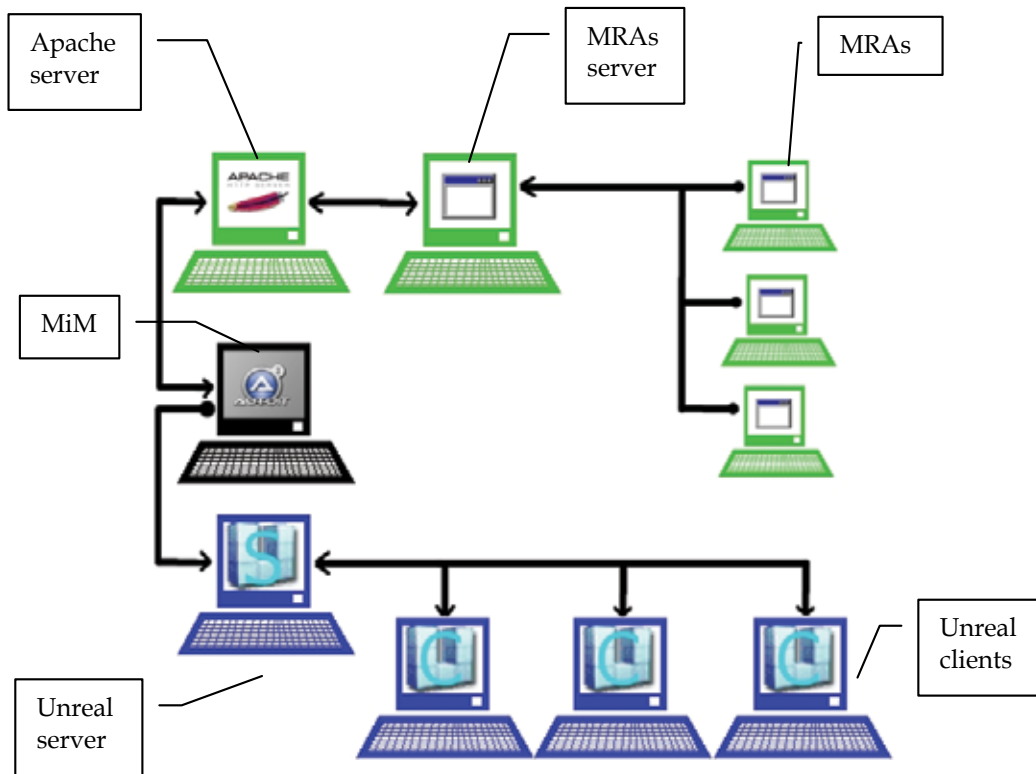


Fig. 6. Networking the monitors with Unreal Engine through MiM scheme

3.2.3 Interpolated dose rate

The later achievement in this R&D, relatively to the dose simulation problem involved two aspects: (a) obtain radiation dose measurements in a finer grid of points within Argonauta's room, for different operating power levels, (b) combine both the offline measurements referred above and online data collected by the radiation monitors to interpolate dose rate for different power levels.

For the former purpose, a measurement campaign was carried out, using portable radiation monitors at a finer grid of points, in a region in the frontal part of Argonauta, meaning to the output radiation channel side. This was so because this region is subject to higher dose rates, and other regions' measurements resulted in dose rate levels around background level, and as such, was not considered in this stage. The region was subdivided into three subareas, comprising the one just in front of the output channel, and two other ones to the sides. Fig. 7a, Fig. 7b and Fig. 7c show the considered areas, named respectively: Area 1, Area 2 and Area 3. Area 2 is the hottest one. Fig. 7d shows the remaining areas not considered, grouped in the so-called Area 0.



Fig. 7. a), b) and c) The areas considered for finer grid of measurements; d) The area not considered

For the later purpose, an intelligent interpolation system was developed using neural networks, to take into account unknown nonlinear effects in dose rate distribution due to power level variation. General regression neural networks (GRNN), (Specht, 1991; Schøler & Hartmann, 1992; Caudill, 1993) were trained, and results showed the system is performing well. Aim is to predict dose rate values for cases not measured, which may occur during tasks execution and can be detected by the radiation monitors installed within Argonauta's room. Results of this part of the R&D were published earlier, describing implementation details (Freitas et al., 2009).

4. Results

4.1 Results for evacuation and security simulation

Relatively to the evacuation simulation, both real and virtual tests were performed for comparative analysis, aiming to evaluate if the later one could really be used as preliminary simulations before the real ones. First tests considered just one person evacuating the building at a time, and later ones considered more people evacuating the building simultaneously. Two runs were performed: (a) one considering only one person, (b) another considering three persons evacuating simultaneously, and results showed the virtual simulations agreed with the real ones.

Fig. 8 shows a simulation screen shot for a third-person view, within the simulated building. In third-person view a user sees his or her own avatar, while for first-person view user does not see the avatar, but rather sees the virtual environment as he or she would do from the avatar's position. The time counter for this avatar is shown in the lower left screen's corner.



Fig. 8. An evacuation simulation screen shot within the building and the time counter

As mentioned in Section 3.1, users' natural cognition plays an important role, and people behave in a way similar to that they would do in real situations, making their own decisions through reasoning. Thus, each user tends to control his or her own avatar for walking through corridors and stairs in a very natural way, searching for the shortest paths. Avatars do not walk, in general, in prescribed paths, as for example in straight lines in the middle of corridors or stairs. Users guide them to freely walk through general curved paths to shorten distances. That is the way people walk in real situations.

Also, as mentioned in Section 3.1, users can make decisions from what they see relatively to other avatars' behaviour. For example, in evacuation simulation, people can decide to get back and search for another exit when see other avatars coming from a locked one, or when see a crowded exit. An example of a crowded exit is shown in Fig. 9. In this situation, an user's avatar may be unable to escape, and have to wait the others get out before going through that exit.



Fig. 9. An example of a crowded exit

Figure 10 shows an avatar escaping through an automatic sliding door. In this case, user has just to get closer to the door to open it. In other cases, for conventional doors that must be pulled, an user's avatar must get close to that door and get back just a bit to give space for the door open. Therefore, preliminary training must be performed so users get familiar with gaming itself, to control the avatars.

Fig. 10 shows another interesting detail. Outdoor environments can be simulated too, but in a rather different way. While indoor environments is designed with CAD software, considering all architectural details, before being imported into Unreal Engine, outdoor environments are designed also with textures obtained from photos taken in the real locations. Fig. 10 shows another campus, external to IEN (in fact the campus of Universidade Federal do Rio de Janeiro), took by photo. But it does not influence simulation, since it only takes part within IEN's campus, it only gives a more visual realism for users. For more details see (Mól et al., 2008a).



Fig. 10. Avatar escaping through a door with outdoor texture-based view



Fig. 11 The hypothetical virtual building of nuclear material deposit, used for the security threat simulation

For the security threat simulation, avatars can run. During simulations, intruders invade the IEN's campus and also the deposit, to steal nuclear material. An avatar of the intruders' team steal material by getting close to it. Then, the intruder can left place running carrying the stolen material. Fig. 11 shows the hypothetical virtual building of nuclear material deposit, used for the security threat simulation.

Four virtual cameras were implemented in Unreal Engine, to simulate surveillance video cameras that would be installed in a real situation. Those virtual cameras' displays are shown in Fig. 12. A supervisor is supposed to monitor any suspect behaviour and inform it to security staff responders, that must immediately catch the intruders. In the virtual simulation, an intruder is caught when an avatar of the responders' team get close to an avatar of the intruders' team, and the later cannot move anymore.



Fig. 12 The four virtual cameras' displays to monitor and detect suspect behaviour

In Fig. 12 it is possible to notice each camera is directed towards strategic views. From left to right: (a) the first camera focuses IEN's campus terrain limit, to detect any invasion; (b) the second one focuses the deposit building, where it is possible to see an avatar of the intruders team trying to invade it; (c) the third camera focuses the deposit building interior, showing the nuclear materials to be monitored; (d) the last one shows also another view of IEN's campus terrain. Other virtual cameras could be implemented, but simulations were performed with these four, to demonstrate the idea. For more details see (Augusto et al., 2009)

4.2 Results for dose simulation

Results for offline radiation dose rate measurements comprise both gammas and neutrons, because routine measurement involves both types of radiation. Fig. 13 shows a screen shot of such a simulation, viewed in the 2 m × 3 m projection screen available at the Virtual Reality Lab. of IEN, CNEN. This is one option for users, besides the view on PC screen. In both cases, perspective or stereo view can be chosen. It can be noticed both received dose for both radiation types (gammas and neutrons), and also the total received dose, sum of the

two. Received dose is shown in nSv, although its is usually shown in μSv , for the following reason: in μSv , the dose value increasing would take long term, while in nSv users can see clearly the increasing dose value, what gives them a better notion about the ambient dose rate at their position. For more details see (Augusto et al., 2007; Mól et al, 2009a).

Fig. 14 shows results for online measurements. A in this case only gamma data is available, the neutrons column is null. This lacking data could be presented too, if the installed radiation monitors measured dose rate for both types of radiation. Thus, it is only a matter of using different probes, if needed. In Fig. 14a results are shown for radiation dose rate for the two monitors, – for which the virtual ones are indicated –, installed in Argonauta. In Fig. 14b, though, results are shown for received dose for each avatar present in the simulation. Users can switch between both views. For more details see (Mól et al, 2008b; Mól et al., 2009b).



Fig. 13 Offline radiation dose simulation.

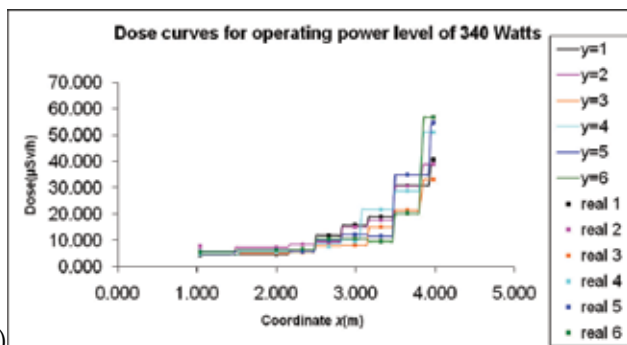


(a)

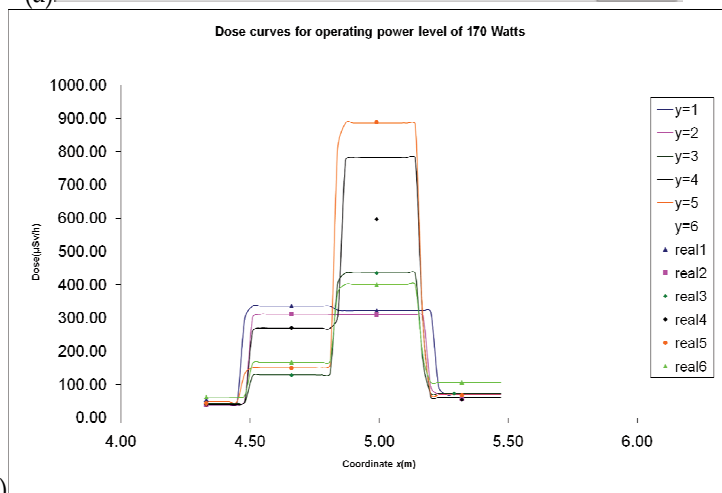


(b)

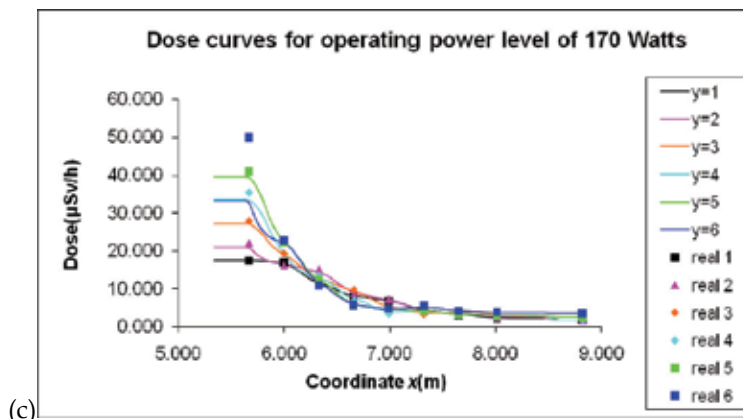
Fig. 14. Online radiation dose simulation: (a) radiation dose rates collected by the two real monitors; (b) radiation doses received by each avatar.



(a)



(b)



(c) Fig. 15. Interpolated radiation dose rates: (a) Area1, operating power level of 340 W; (b) Area2, 170 W; (c) Area3, 170 W.

Results for the interpolated dose rate R&D stage are shown in Fig. 15. Fig. 15a shows interpolation dose rate curves for the operating power level of 340 W, for Area 1, for each x coordinate value; Fig. 15 b shows similar results for 170 W in Area 2 (in front of Argonauta's radiation output channel, see Fig. 7b); while Fig. 15c show results for 170 W in Area3. The points are the values measured during the campaign, while the curves were interpolated by the GRNN. There are many other curves, for the other operating power levels, and also for Area 1 and Area 3, but these three were chosen as example. For more details see (Freitas et al., 2009).

5. Concluding remarks and perspectives

This R&D has been supplying interesting results up to the present, for a diversity of application-specific problems: evacuation simulation in emergency situations, security threat counteraction and received radiation dose simulation, all as support to improve safety for people and security relatively to hazardous materials.

IEN's staff plans to continue and expand this R&D, either improving simulations through more detailed implementations, or directing it towards other application-specific problems. One possibility is to improve interaction between avatars, as with text or voice transmission through computer networking. Another possibility under development is the development and implementation of combined image and video processing and pattern recognition for people tracking within nuclear plants, to assign dose rate values online and dynamically, according to their movement. Other application field of these tracking and recognition techniques is security, for people tracking and identification, as well as suspect behaviour identification.

The reuse of computer game engines have proved to be a very flexible and time-saving platform for serious applications, what encourage us to continue this bridging between consumer graphics and simulation.

8. References

- Augusto, S.C.; Mól, A.C.A.; Jorge, C.A.F.; Couto, P.M.; Cunha, G.G. & Landau, L. (2007). Use of virtual reality to estimate radiation dose rates in nuclear plants. *Proceedings of the 2007 International Nuclear Atlantic Conference (INAC 2007)*, DVD-ROM, ISBN 978-85-99141-02-1, Santos, SP, Brazil, September 30 to October 05 2007, ABEN, Rio de Janeiro
- Augusto, S.C.; Mól, A.C.A.; Couto, P.M. & Sales, D.S. (2009). Using virtual reality in the training of security staff and evaluation of physical protection barriers in nuclear facilities, *Proceedings of the 2009 International Nuclear Atlantic Conference (INAC 2009)*, DVD-ROM, ISBN 978-85-99141-03-8, Rio de Janeiro, RJ, Brazil, September 27th to October 02, ABEN, Rio de Janeiro
- Badler, N. I. (2002). LiveActor: a virtual training environment with reactive embodied agents, *Workshop on Intelligent Human Augmentation and Virtual Environments (WIHAVE)*, University of North Carolina at Chapel Hill, Chapel Hill, NC, October 2002,
- Bloomfield, A.; Deng, Y.; Rondot, P.; Wampler, J.; Harth, D.; McManus, M. & Badler, N. (2003). A taxonomy and comparison of haptic actions for disassembly tasks, *Proceedings of the IEEE Virtual Reality*, pp. 225–231, ISBN 0-7695-1882-6, LA, CA, March 2003, IEEE
- Bluemel, E.; Hintze, A.; Schulz, T.; Shumann, M. & Stuering, S. (2003). Virtual environments for the training of maintenance and service tasks, *Proceedings of the 2003 Winter Simulation Conference (WSC'03)*, pp. II-2001–II-2007, ISBN 0-7803-8131-9, New Orleans, Louisiana, December 2003, IEEE
- Bluemel, E.; Termath, W. & Haase, T. (2009). Virtual reality platforms for education and training in industry. *International Journal of Advanced Corporate Learning*, Vol. 2, No. 2, 2009, 4–12, ISSN 1867-5565
- Brissaud, A. & Ridoux, P. (1992). PANTHERE RP: a tool for prevision of dose rates, *Proceedings of the 8th International Congress of the International Radiation Protection Association (IRPA 8)*, pp. 2-1677–2-1680, Montreal, Quebec, Canada, May 1992, IRPA
- Burdea, G. & Philippe, C. (1994). *Virtual Reality Technology*, John Wiley & Sons, ISBN 0-471-36089-9, New York
- Carpin, S.; Lewis, M.; Wang, J.; Balakirsky, S. & Scrapper, C. (2007). USARSim: a robot simulator for research and education, *Proceedings of the 2007 IEEE International Conference on Robotics and Automation (ICRA'07)*, pp. 1400–1405, ISBN 1-4244-0601-3, Rome, Italy, April 2007, IEEE
- Carpin, S.; Lewis, M.; Wang, J.; Balakirsky, S. & Scrapper, C. (2009). Bridging the gap between simulation and reality in urban search and rescue. *Lecture Notes in Computer Science (Robocup 2006: Robot Soccer World Cup X)*, Vol. 4434, 1–12, ISBN 978-3-540-74023-0
- Caudill, M. (1993). GRNN and bear it. *AI Expert*, Vol. 8, No. 5, May 1993, 28–33, ISSN 0888-3785
- Chatam, R.E. (2007). Games for training. *Communications of the Association for Computing Machinery (CACM) – Special Issue on 'Creating a Science of Games'*, Vol. 50, No. 7, July 2007, 36–43, ISSN 0001-0782
- Francis, G.A. & Tan, H.S. (1999). Virtual reality as a training instrument. *The Temasek Journal* 7, 4–15
- Freitas, V.G.V.; Mól, A.C.A. & Pereira, C.M.N.A. (2009). Real time determination of dose radiation through artificial intelligence and virtual reality, *Proceedings of the 2009 International Nuclear Atlantic Conference (INAC 2009)*, DVD-ROM, ISBN 978-85-99141-03-8, Rio de Janeiro, RJ, Brazil, September 27th to October 02, ABEN, Rio de Janeiro

- Hajek, B.; Kang, K.; Lee, Y. & Shin, Y.J. (2004). Internet virtual reality environment for simulating, predicting, and minimizing worker radiation exposure, *Proceedings of the American Nuclear Society's 4th International Topical Meeting on Nuclear Power Plant Instrumentation and Human Machine Interface Technologies (NPIC & HMIT 2004)*, ISBN 0-89448-688-8, Columbus, Ohio, September 2004, ANS
- ICRP Publication 60 (1991). Recommendations of the International Commission on Radiological Protection
- Jain, S. & McLean, C. (2003). A framework for modeling and simulation for emergency response, *Proceedings of the 2003 Winter Simulation Conference*, pp. 1-1068-1-1076, ISBN 0-7803-8131-9, New Orleans, Louisiana, December 2003, IEEE
- Jain, S. & McLean, C. (2005). Integrated simulation and gaming architecture for incident management training, *Proceedings of the 2005 Winter Simulation Conference*, pp. 904-913, ISBN 0-7803-9519-0, Orlando, Florida, December 2005, IEEE
- Kim, Y.H. & Park, W.M. (2005). Use of simulation technology for prediction of radiation dose in nuclear power plant. *Lecture Notes in Computer Science*, Vol. 3314, 2005, 413-418, ISBN 978-3-540-24127-0
- Knight, T.W.; Dalton, G.R. & Tulenko, J.S. (1995). Virtual radiation fields for ALARA determination. *Transactions of the American Nuclear Society*, Vol. 72, 1995, 105-107, ISSN 978-3-540-24127-0
- Knight, T.W.; Dalton, G.R. & Tulenko, J.S. (1997). Virtual radiation fields – a virtual environment tool for radiological analysis and simulation. *Nuclear Technology*, Vol. 117, No. 2, 255-266, ISSN 0029-5450
- Lebedev, V.; Mitrofanov, S.; Slonimsky, V.; Aliev, A.; Borsky, Y.; Malkin, S.; Rakitin, I.; Schukin, A.; Gramotkin, I.; Bilik, A.; Medintsov, V.; Kuchunsky, V.; Illichov, A.; Bratteli, J.; Edvardsen, S. T.; Johnsen, T.; Louka, M. N.; Mark, N.-K.; Meyer, G.; Rekvinn, S. & Øwre, F. (2007). VR technology used in planning, training, and presentation of operations, maintenance, and decommissioning at ChNPP and LNPP RBMKs, *Proceedings of the Man-Technology-Organisation Sessions at the 2007 Enlarged Halden Programme Group Meeting*, Storefjell, Norway, 2007
- Lee, D.J.; Salve, R.; Antonio, A.; Herrero, P.; Perez, J.M.; Vermeersch, F. & Dalton, G. (2001). Virtual reality for inspection, maintenance, operation and repair of nuclear power plants (VRIMOR), *Mid-term Symposium on Shared-Cost and Concerted Actions (FISA 2001) – EU Research in Reactor Safety*, EC, Luxembourg, November 12-15 2001
- Lewis, M. & Jacobson, J. (2002). Introduction. *Communications of the Association for Computing Machinery (CACM) – Special Issue on 'Game Engines in Scientific Research'*, Vol. 45, No. 1, January 2002, 27-31, ISSN 0001-0782
- Louka, M.N. & Balducci, C. (2001). Virtual reality tools for emergency operation support and training, *Proceedings of The International Emergency Management Society (TIEMS) 2001*, Oslo, June 2001, TIEMS
- Manijlovich, J.; Prasithgaree, P.; Hughes, S.; Chen, J. & Lewis, M. (2003a). UTSAF: a multi-agent-based framework for supporting military-based distributed interactive simulations in 3D environments, *Proceedings of the 2003 Winter Simulation Conference*, pp. 1-960-1-968, ISBN 0-7803-8131-9, New Orleans, Louisiana, December 2003, IEEE

- Manijlovich, J.; Prasithgaree, P.; Hughes, S., Chen, J. & Lewis, M. (2003b). UTSAF: getting the best of consumer graphics into military simulations, *Proceedings of the 47th Annual Meeting of the Human Factors and Ergonomics Society (HFES)*, pp. 2123–2127, ISSN 0-945-289-22-7, Santa Monica, CA, 2003, HFES
- Mathieu, R.; Contassot-Vivier, S.; Guillerminet, C.; Gschwind, R.; Makovicka, L. & Bahi, J. (2003). Prospective de la planification des traitements radiothérapeutiques basée sur les réseaux de Neurones, *Journées SFRP-SFPM-FIRAM (Codes de calcul en radioprotection, radiophysique et dosimétrie)*, pp., ISBN, Sochaux, October 2003, Publisher, City
- Mathieu, R., Gschwind, R., Martin, E., Makovicka, L., Contassot-Vivier, S., Bahi, J., 2004. Use of the neural networks in external radiotherapy. *Current Topics in Monte Carlo Treatment Planning, Advanced Workshop*, May 3–5, Montréal
- Meyer, G. (2007). Three-dimensional simulation of maintenance activities for planning and evaluation, *Proceedings of the Man-Technology-Organisation Sessions at the 2007 Enlarged Halden Programme Group Meeting*, Storefjell, Norway, 2007
- Mól, A.C.A.; Jorge, C.A.F. & Couto, P.M. (2008a). Using a game engine for VR simulations in evacuation planning. *IEEE Computer Graphics and Applications*, Vol. 28, No. 3, May-June 2008, pp. 6–12, ISSN 0272-1716
- Mól, A.C.A.; Aghina, M.A.C.; Jorge, C.A.F. & Couto, P.M. (2008b). Virtual simulations of nuclear plants for dose assessment with on-line measurements collected by networked radiation monitors. *Proceedings of the 11th IEEE International Conference on Computational Science and Engineering – Workshops (CSE 2008)*, pp. 367–372, ISBN 987-0-7695-3257-8, São Paulo, SP, Brazil, July 2008, IEEE
- Mól, A.C.A.; Jorge, C.A.F.; Couto, P.M.; Augusto, S.C.; Cunha, G.G. & Landau, L. (2009a). Virtual environments simulation for dose assessment in nuclear plants. *Progress in Nuclear Energy*, Vol. 51, No. 2, March 2009, 382-387, ISSN 0149-1970
- Mól, A.C.A.; Aghina, M.A.C.; Jorge, C.A.F.; Lapa, C.M.F. & Couto, P.M. (2009b). Nuclear plant's virtual simulation for on-line radioactive environment monitoring and dose assessment for personnel. *Annals of Nuclear Energy*, Vol. 36, No. 11-12, November-December 2009, 1747-1752, ISSN 0306-4549
- Moltenbrey, K. (1999). Extreme visualization—a prototype VR system for viewing hazardous environments expands the boundaries of 3D scientific and engineering visualization. *Computer Graphics World*, Vol. 22, No. 1, January 1999, 42–46
- Nystad, E.; Drøivoldsmo, A. & Sebok, A. (2002). Use of radiation maps in a virtual training environment for NPP field operators, *Halden Work Report HWR-681*
- Nystad, E. (2005). Improved human performance in maintenance by using virtual reality tools: experimental results and future applications, *CSNI Workshop 'Better Nuclear Plant Maintenance: Improving Human and Organisational Performance'*, pp. 3–5, Ottawa, Canada, October 2005
- Ohga, Y.; Fukuda, M.; Shibata, K.; Kawakami, T. & Matsuzaki, T. (2005). A system for the calculation and visualisation of radiation field for maintenance support in nuclear power plants. *Radiation Protection Dosimetry*, Vol. 116, No. 1-4, December 2005, 592-596, Online ISSN 1742-3406 Print ISSN 0144-8420
- Oliveira, M.V.; Aghina, M.A.C. & Soares, M. (1997). Sistema de monitoração de radiação 7027, *Proceedings of the 4th Brazilian National Meeting on Nuclear Applications and 11th Brazilian National Meeting on Reactor Physics and Thermal Hydraulics*, pp. 473–476, Poços de Caldas, MG, Brazil, ABEN, Rio de Janeiro

- Oliveira, M.V.; Aghina, M.A.C. & Mól, A.C.A. (2000). Sistema de monitoração de radiação 7027 do reator Argonauta, *Proceedings of the 5th Brazilian National Meeting on Nuclear Applications, 8th General Congress on Nuclear Energy and 12th Brazilian National Meeting on Reactor Physics and Thermal Hydraulics*, pp. 473–476, Rio de Janeiro, RJ, Brazil, ABEN, Rio de Janeiro
- Pimentel, K. & Teixeira, K. (1995). *Virtual Reality: Through the New Looking Glass*, 2nd edition, McGraw-Hill, ISBN 10: 0070501688 ISBN 13: 978-0070501683, New York
- Prasithsangaree, P.; Manojlovich, J.; Chen, J. & Lewis, M. (2003). UTSAF: a simulation bridge between OneSAF and the Unreal Engine, *Proceedings of the 2003 IEEE International Conference on Systems, Man, and Cybernetics*, pp. 1333–1338, ISSN 1062-922X, Washington, DC, October 2003, IEEE
- Prasithsangaree, P.; Manojlovich, J.; Hughes, S. & Lewis, M. (2004). UTSAF: a multi-agent-based software bridge for interoperability between distributed military and commercial gaming simulation. *Simulation*. Vol. 80, No. 12, 2004, 647–657, ISSN 0037-5497, SCS
- Rindahl, G.; Johnsen, T.; Øwre, F. & Iguchi, Y. (2002). Virtual reality technology and nuclear decommissioning, *Proceedings of the International Conference on Safe Decommissioning for Nuclear Activities*, pp. 223–238, ISSN 0774-1884, IAEA, Berlin, 2002, IAEA
- Ródenas, J.; Zarza, I.; Burgos, M.C.; Felipe, A. & Sánchez-Mayoral, M.L. (2004). Developing a virtual reality application for training nuclear power plant operators: setting up a database containing dose rates in the refuelling plant. *Radiation Protection Dosimetry*, Vol. 111, No. 2, September 2004, 173–180, Online ISSN 1742-3406 Print ISSN 0144-8420
- Ródenas, J.; Zarza, I.; Felipe, A. & Sánchez-Mayoral, M.L. (2005). Generation of dose databases for an operator training application in nuclear facilities, *Proceedings of the 3rd International Conference on Education and Training in Radiological Protection (ETRAP 2005)*, Brussels, Belgium, November 2005
- Rosenbloom, A. (2003). Introduction. *Communications of the Association for Computing Machinery (CACM) – Special Issue on ‘A Game Experience in Every Application’*, Vol. 46, No. 7, July 2003, 28–31, ISSN 0001-0782
- Sanders, R.L. & Lake, J.E. (2005). Training first responders to nuclear facilities using 3-D visualization technology, *Proceedings of the 2005 Winter Simulation Conference*, pp. 914–918, ISBN 0-7803-9519-0, Orlando, Florida, December 2005, IEEE
- Sebok, A.; Nystad, E. & Drøivoldsmo, A. (2002). Improving safety and human performance in maintenance and outage planning through virtual reality-based training systems, *Proceedings of the IEEE 7th Conference on Human Factors and Power Plants*, pp. 8-14–8-22, ISBN 0-7803-7450-9, Scottsdale, Arizona, 2002, IEEE
- Schløler, H. & Hartmann, U. (1992). Mapping neural network derived from the parzen window estimator. *Neural Networks*, Vol. 5, No. 6, 1992, 903–909, ISSN 0893-6080
- Shendarkar, A.; Vasudevan, K.; Lee, S. & Son, Y.-J. (2006). Crowd simulation for emergency response using BDI agent based on virtual reality, *Proceedings of the 2006 Winter Simulation Conference*, pp. 545–553, ISBN 1-4244-0500-9, Monterey, California, December 2006, IEEE
- Specht, D.F. (1991). A Generalized Regression Neural Network. *IEEE Transactions on Neural Networks*, Vol. 2, No. 6, November 1991, 568–576, ISSN 1045-9227.
- Stuart, R. (1996). *The Design of Virtual Environments*, McGraw-Hill, ISBN 10: 0770632995 ISBN 13: 978-0070632998, New York

- Threnholme, D. & Smith, S. P. (2008). Computer game engines for developing first-person virtual environments. *Virtual Reality*, Vol. 12, No. 3, September 2008, 181–187, ISSN Print 1359-4338 ISSN Online 1434-9957
- Van de Walle, B. & Turoff, M. (2007). Emergency response information systems: emerging trends and technologies. *Communications of the Association for Computing Machinery (CACM) – Special Section ‘Emergency response information systems: emergina trends and technologies’*, Vol. 50, No. 3, March 2007, 28–31, ISSN 0001-0782
- Vermeersch, F. & Van Bosstraeten, C. (1998). Development of the VISIPLAN ALARA planning tool, *Proceedings of the International Conference on Topical issues in Nuclear Radiation and Radioactive Waste Safety*, Vienna, Austria, August 31 to September 04 1998
- Vermeersch, F. & Vanbosstraeten, C. (2000). Software VISIPLAN: a powerful tool for optimisation, *Proceedings of the 2nd European Workshop on Occupational Exposure Management at NPPs*, Tarragona, Spain, April 2000
- Vince, J. (1995). *Virtual Reality Systems*, Addison-Wesley, ISBN 0-201-87687-6, Cambridge
- Wang, J.; Lewis, M. & Gennari, J. (2003a). USAR: a game-based simulation for teleoperation, *Proceedings of the 47th Annual Meeting of the Human Factors and Ergonomics Society (HFES)*, pp. 493–497, ISSN 0-945-289-22-7, Santa Monica, CA, 2003, HFES
- Wang, J.; Lewis, M. & Gennari, J. (2003b). A game engine based simulation of the NIST urban search and rescue arenas, *Proceedings of the 2003 Winter Simulation Conference*, pp. 1-1039–1-1045, ISBN 0-7803-8131-9, New Orleans, Louisiana, December 2003, IEEE
- Wang, J.; Lewis, M. & Gennari, J. (2003c). Interactive simulation of the NIST USAR arenas, *Proceedings of the 2003 IEEE International Conference on Systems, Man, and Cybernetics*, pp. II-1327–II-1332, , ISSN 1062-922X, Washington, DC, October 2003, IEEE
- Wu, X. & Zhu, Y. (2000). A neural network regression model for relative dose computation. *Physics in Medicine and Biology*, Vol. 45, No. 4, 2000, 913–922, Online ISSN 1361-6560 Print ISSN 0031-9155
- Xu, X.G. & Bushart, S. (2006). Virtual-reality dose simulation for nuclear power plant. *Proceedings of the The American Nuclear Society’s 14th Biennial Topical Meeting on Radiation Protection and Shielding (RPS 2006)*, pp. 449–451, Carlsbad, New Mexico, April 2006, ANS
- Zyda, M.; Hiles, J.; Mayberry, A.; Wardynski, C.; Capps, M.; Osborn, B.; Shilling, R.; Robaszewski, M. & Davis, M. (2003). Entertainment R&D for defense. *IEEE Computer Graphics and Applications*, Vol. 23, No. 1, January-February 2003, 28–36, ISSN 0001-0782
- Zyda, M. (2007). Introduction. *Communications of the Association for Computing Machinery (CACM) – Special Issue on ‘Creating a Science of Games’*, Vol. 50, No. 7, July 2007, 26–29, ISSN 0001-0782



Edited by Pavel Tsvetkov

The world of the twenty first century is an energy consuming society. Due to increasing population and living standards, each year the world requires more energy and new efficient systems for delivering it. Furthermore, the new systems must be inherently safe and environmentally benign. These realities of today's world are among the reasons that lead to serious interest in deploying nuclear power as a sustainable energy source. Today's nuclear reactors are safe and highly efficient energy systems that offer electricity and a multitude of co-generation energy products ranging from potable water to heat for industrial applications. The goal of the book is to show the current state-of-the-art in the covered technical areas as well as to demonstrate how general engineering principles and methods can be applied to nuclear power systems.

Photo by FooTToo / iStock

IntechOpen

